



UNIVERSITY OF THE
WITWATERSRAND,
JOHANNESBURG

Synthetic, Mechanistic and Biological
Studies of Novel
Metal-Imidazo[1,2-*a*]pyridines and
Xanthenes

Jean Dam

Supervised by C B de Koning and M L Bode

A thesis submitted to the Faculty of Science, University of the Witwatersrand,
Johannesburg, in fulfilment of the requirements for the Degree of Doctor of Philosophy
Submitted June 2016

Declaration

I declare that this Thesis is my own, unaided work. It is being submitted for the Degree of Doctor of Philosophy at the University of the Witwatersrand, Johannesburg. It has not been submitted before for any degree or examination at any other University.

A handwritten signature in black ink, appearing to read 'Jean Dam', enclosed within a hand-drawn circle.

Jean Dam

23rd day of September 2016

Abstract

The work detailed in this PhD involves two distinct, separate areas of research. The first project involved an investigation into the synthesis, characterisation and metal-chelation of pyridoimidazo[1,2-*a*]pyridines in the search for new compounds for the treatment of cancer.

Previously in our laboratories at the University of the Witwatersrand a small library of imidazo[1,2-*a*]pyridines were synthesized that showed significant activity (IC_{50} values between 6.57-21.98 μ M) against Caco-2 and HT-29 colorectal cancer cell lines while showing little cytotoxicity towards white blood cells; significantly less than camptothecin the 'golden standard'. In an attempt to improve the overall activity of the imidazo[1,2-*a*]pyridines methodology was developed to coordinate zinc, copper and platinum to the imidazo[1,2-*a*]pyridines to generate novel metal-imidazo[1,2-*a*]pyridine complexes. These novel compounds were characterised by NMR spectroscopy (where possible) and Single Crystal X-ray Diffraction (SCXRD) and tested against colorectal (Caco-2 and HT-29), leukemic (K562 and HL-60) and breast (MCF-7 and MDA-MB231) cancer cell lines, where the copper-containing compounds showed the most significant activity. A library of 11 copper complexes screened showed excellent activity in all the cell lines tested, some of which were more active than camptothecin.

The second part of this PhD involved a detailed investigation into novel methodology to synthesize xanthenes and related diones, for example such as 4*a*-methoxy-2*H*-xanthene-2,9(4*aH*)-dione, discovered in our laboratory. Initially this reaction was reported to be mediated by ceric ammonium nitrate (CAN), however it was determined during the course of this investigation that the novel reaction was actually mediated by ceric ammonium sulfate (CAS) and that different products were isolated depending on which reagent (CAN or CAS) was used. In this thesis, the mechanism of the reaction was probed and it was determined that the electronic nature of the starting benzophenone (e.g. (2-hydroxyphenyl)(2,4,6-trimethoxyphenyl)methanone) plays a crucial role in the outcome of the reaction. In addition to the furnishing of xanthenes (e.g. 4-methoxy-9*H*-xanthen-9-one) and spirofurans (such as 2',6'-dimethoxy-3*H*-spiro[benzofuran-2,1'-cyclohexa[2,5]diene]-3,4'-dione) using this CAS-mediated reaction, novel biaryl-fused dimers (e.g. (4,4'-dihydroxy-[1,1'-biphenyl]-3,3'-diyl)bis((2,4-dimethoxyphenyl)methanone)) were also isolated and these results were explained by the mechanisms detailed in this work. Reliable methodology was developed using a sodium dithionite-mediated method for the conversion of dione products (such as 4*a*-methoxy-2*H*-xanthene-2,9(4*aH*)-dione) to hydroxy-containing xanthenes (such as 7-hydroxy-9*H*-xanthen-9-one).

Finally, as a proof of concept, this novel CAS-mediated methodology was extended to the synthesis of the nitrogen-containing derivatives, the acridones, and a single acridone, 10-benzyl-2-methoxyacridin-9(10*H*)-one, was successfully synthesized using CAS as the reagent, albeit in a low yield.

Acknowledgements

An African proverb says that it takes a village to raise a child. I have been incredibly blessed by the village that as a scientist I've been raised in and to whom I owe a great deal of thanks.

First and foremost, to my supervisors Prof Charles de Koning and Dr Moira Bode, thank you. Charles thank you for seeing something in me that I hadn't seen in myself and for taking a risk on a young, green girl and growing her into a half-way decent scientist. Moira, thank you for your impeccable attention to detail and research standards, it truly has made me a better scientist. As supervisors, I cannot thank you enough for your generosity with your time, patience, integrity and mentorship both personally and professionally.

Thank you to the National Research Foundation (NRF) and Southern African Biochemistry and Informatics for Natural Products (SABINA, a SIG-RISE network) for the generous financial support of both myself and my research and for giving me opportunities for personal and professional growth.

Dr Amanda Rousseau and Prof Manuel Fernandes - thank you for your invaluable contributions to my research and for always making time for a laugh or a vent.

Kennedy Ngirwa and Hendrik Henning thank you for being my chemistry siblings. You guys have made my PhD a special experience and the input you made to my project with our natural fun dynamic is something I'll always cherish. To the rest of my lab mates; Myron, Priya, Hannah, Jimmy, Memory, Charles, Peter, Donald, Kamogelo and Fatima thank you for your advice, friendship, dancing and laughter. Thank you for putting up with me!

A very big thank you to all the staff and postgraduates that have helped me with all the data collection needed to complete this PhD. Prof Lawrence Carlton, Dr Richard Mampa, Dr Myron Johnson and Dr Izak Kotze thank you for your endless assistance with NMR. Prof Andreas Lemmerer, Prof Manuel Fernandes and Dr Sanaz Khorasani thank you for granting me temporary Loonie status and for all your help with my extensive crystal structure collection. Thank you to Prof Helder Marques and Dr Christopher Perry for being brave enough to help me tackle the pK analysis of my compounds. Thank you Dr Stuart Miller for rescuing my second project with your PXRD analysis – you really were a lifesaver!

I'd like to extend thanks to Dr Leonie Harmse, Taurai Kurebwa, Zeenat Ismail and Somayya Ragie at the WITS School of Pharmacology for the extensive biological testing performed on my compounds. Thank you for such a fruitful collaboration!

Special mention needs to be made to the Cake and Wine club – Bronwyn, Monika, Amy, Robyn, Loren and Jesse – and for the constant reminder that there is always time for cake or wine (or both).

On a personal note, I'd like to thank Ed and my Cell Group for their constant support, encouragement and prayers throughout my PhD. Thank you to Shaun, Rachael, Bianca and my siblings, Logan, Claire and Riaan (as well as the little people) for commiserating with me on statue days, celebrating with me on pigeon days and for walking with me all the days in between. Mom and Dad thank you for teaching me to dream big and for supporting me throughout every crazy endeavour I've undertaken. Your love has been invaluable! 234

Finally I'd like to thank the Lord for bringing me to this particular village and guiding me through it. Thank you for lighting my path every step of the way and for calling me to greater things than I could have dreamt of for myself.

Table of Contents

Abstract	iii
Acknowledgements	v
Table of Contents	vii
At the End of My Tether	1
Introduction	2
1.1. Cancer	2
1.1.1. Colorectal Cancer	3
1.1.2. Breast Cancer	4
1.1.3. Leukemia	6
1.1.4. Commonly Used Chemotherapies	7
1.2. The Future of Chemotherapy	12
1.2.1. Hybrid Compounds	12
1.2.2. Organic Hybrid Compounds	13
1.2.3. Metal-Containing Hybrids	14
1.3. Imidazo[1,2- <i>a</i>]pyridines	29
1.3.1. Synthetic History	29
1.3.2. Biological applications and further development	33
1.3.3. Metal imidazo[1,2- <i>a</i>]pyridine complexes	38
1.4. Project Introduction	42
Results and Discussion	44
2.1. Synthesis and development of imidazo[1,2- <i>a</i>]pyridine library	44
2.2. Attempts at modification of the imidazo[1,2- <i>a</i>]pyridine	51
2.2.1. Using the Suzuki-Miyaura Cross Coupling Reaction to build the tether	52
2.2.2. Heck coupling reactions	57
2.2.3. Attempted modification using arylation-type reactions	59
2.3. Results from Biological Testing	61

2.4. Introducing metals to imidazo[1,2- <i>a</i>]pyridines.....	65
2.4.1. Combining imidazo[1,2- <i>a</i>]pyridines with ferrocene	65
2.4.2. Chelation approach to the synthesis of metal hybrids	67
2.4.3. Synthesis of isocyanides	73
2.4.4. The R ₃ substituent effect library.....	74
2.4.5. Complex Stability Studies	80
2.4.6. Biological Results for the R ₃ substituent library	86
2.4.7. A more focused Structure-Activity study library	89
2.4.8. Results from Biological Testing.....	94
Conclusions and Future Work	98
3.1. Imidazo[1,2- <i>a</i>]pyridine synthesis and biological activity	98
3.2. Attempts at modifying the imidazo[1,2- <i>a</i>]pyridines and attempted tether syntheses.....	99
3.3. Introducing metals to the imidazo[1,2- <i>a</i>]pyridines	101
3.3.1. Introducing ferrocene to the imidazo[1,2- <i>a</i>]pyridine.....	101
3.3.2. Synthesis of isocyanides to generate a wider variety of imidazo[1,2- <i>a</i>]pyridines	101
3.3.3. Adding metals directly to the imidazo[1,2- <i>a</i>]pyridine.....	101
3.3.4. Complex Stability Studies	102
3.3.5. Anticancer activity of the metal complexes	102
3.3.6. Investigation into the Structure-Activity relationship	103
Plot Twist.....	105
Introduction	106
4.1. The use of Ceric Ammonium Nitrate in Organic Synthesis	106
4.1.1. CAN as an oxidant.....	107
4.1.2. CAN as a nitrating agent	113
4.1.3. Removal and addition of protection groups using CAN	115
4.1.4. Other uses of CAN in organic synthesis	123
4.2. The use of Ceric Ammonium Sulfate in Organic Synthesis	127
4.2.1. CAS in polymerization reactions.....	127
4.2.2. CAS in the solid state	128

4.2.3. Using CAS in Organic Synthesis.....	129
4.3. The use of CAN/CAS in the WITS Laboratories	139
4.3.1. Project Origin.....	139
4.3.2. Development by Johnson	143
4.3.3. Development of CAN reaction by Omolo	146
4.4. Aims of this project.....	151
Results and Discussion	154
5.1. Repetition of work by Johnson	154
5.2. Initial attempts towards the synthesis of acridones.....	157
5.3. Irreproducible results and confusing catalysts	160
5.3.1. Irreproducibility of Johnson's results	160
5.3.2. Analysis of the CAN samples	163
5.4. When life gives you CAS.....	168
5.4.1. Repetition of the chlorine-containing reactions performed by Johnson using CAS...170	
5.4.2. Conversion of diones to xanthenes	173
5.5. Investigation of the mechanism of the CAS-mediated ring closure reactions.....	176
5.5.1. Synthesis of (2-hydroxyphenyl)(2-methoxyphenyl)methanone 312.....	176
5.5.2. Synthesis of dimethoxybenzophenone substrates.....	177
5.5.3. Subjection of substituted benzophenones to CAS	180
5.5.4. A deeper look at the proposed mechanisms.....	184
5.6. Revisiting the acridone synthesis.....	190
Conclusions and Future Work	194
6.1. CAN vs. CAS.....	194
6.1.1. Conclusion	194
6.1.2. Future work	195
6.2. Mechanistic investigations.....	196
6.2.1. Conclusions from the mechanistic investigations	196
6.2.2. Future work from the results from the mechanistic investigations	197
6.3. Extension of the methodology to the formation of Acridones.....	198

6.3.1. Conclusions.....	198
6.3.2. Future work	198
Experimental	200
7.1. General Experimental Procedures	200
7.1.1. Purification of solvents and reagents	200
7.1.2. General laboratory techniques and equipment	200
7.1.3. Chromatographic Separations.....	201
7.1.4. Spectroscopic Techniques	201
7.1.5. Melting Points	202
7.1.6. Elemental Analysis.....	202
7.1.7. Single Crystal X-ray Diffraction	202
7.1.8. pH measurements	203
7.1.9. UV-vis Spectroscopy	203
7.1.10. Data Analysis	203
7.2. Experimental Procedures for At the End of My Tether	205
7.2.1. General Procedure and Experimental details for the Groebke-Blackburn-Bienaymé MCR reactions	205
7.2.2. Tether synthesis	216
7.2.3. Suzuki-Miyaura Cross Coupling reactions.....	217
7.2.4. Knoevenagel condensation reaction	222
7.2.5. General Procedure for Heck Reactions.....	223
7.2.6. Synthesis of ferrocene-containing imidazo[1,2- <i>a</i>]pyridines.....	225
7.2.7. General procedure for the synthesis of isocyanides used in the Groebke-Blackburn- Bienaymé multicomponent coupling reaction	227
7.2.8. Synthesis of pyridyl-containing imidazo[1,2- <i>a</i>]pyridines for metal complexation reactions.....	229
7.2.9. General procedure for the synthesis of metal-imidazo[1,2- <i>a</i>]pyridine complexes....	232
7.2.10. Synthesis of pyridyl imidazo[1,2- <i>a</i>]pyridines for the SAR study	239
7.2.11. Synthesis of Copper Complexes	243

7.3. Experimental Procedures for the preparation of xanthenes and related compounds.....	247
7.3.1. General procedure for the benzyl protection of salicylic acids and salicylaldehyde..	247
7.3.2. Reduction of naphthoquinone	249
7.3.3. General procedure for the bromination of substituted benzenes and naphthalenes	250
7.3.4. Grignard Reaction for the synthesis of 310	253
7.3.5. Method for Pyridinium Chlorochromate (PCC) oxidation	254
7.3.6. General procedure for the lithiation reactions to form benzophenones.....	255
7.3.7. General procedure for the debenylation of organic compounds using palladium on carbon.....	262
7.3.8. General Procedure for the novel CAS-mediated ring closure	268
7.3.9. CAN-mediated formation of spirofuran 300	280
7.3.10. General procedure for the conversion of diones to xanthenes	281
7.4. Experimental Procedures for the preparation of acridones.	284
7.4.1. Benzyl Protection of Anthranilic acid	284
7.4.2. Synthesis of Weinreb amide	285
7.4.3. Lithium mediated coupling reactions.....	286
7.4.4. Benzyl protection of 2-aminobenzophenone derivative	289
7.4.4. CAS mediated ring closure.....	290
Appendices.....	291
A1 - ^1H and ^{13}C NMR Spectra for selected imidazo[1,2- <i>a</i>]pyridines	292
A2 - Crystallographic Information for selected imidazo[1,2- <i>a</i>]pyridines.....	303
A3 - An example of the UV-vis spectra and Data Analysis obtained in this project.....	307
A4 - ^1H and ^{13}C NMR Spectra for selected compounds.....	312
A5 - Crystallographic Data obtained for Plot Twist crystal structures	324
References.....	326

At the End of My Tether

At the end of my tether:

Introduction

1.1. Cancer

While homeostasis carefully controls changes to the body, some changes such as mutations to the cells are not always controlled. These mutated or abnormal cells often grow uncontrollably, resulting in tumours. Contributing to this rapid growth is an increase in blood supply around to the tumour.¹ These tumours can detach from the surrounding healthy cells, allowing abnormal cells to spread, taking over healthy organs resulting in severe illness and, if untreated, death. While there are different types of this disease, they are collectively known as cancer.²

In healthy cells, a process known as apoptosis occurs that causes a cell to die when harmful mutations occur in the cell. This process is more commonly known as intracellular suicide or programmed cell death.³ Apoptosis causes the release of proteases (mainly caspases) and nucleases which destroys the proteins, lipids and DNA of the cell when an abnormal change in the cell is detected. The cell shrinks, becomes lobed and is quickly ingested by neighbouring cells without damage to the surrounding area. This process is considered to be essential for human development as it prevents the replication of any unwanted changes in a cell. In cells where irreparable damage has occurred – especially DNA damage – an internal signal that is controlled by caspases is normally generated to trigger apoptosis, preventing the spread of the mutation.¹ In cancerous cells, the release of these caspases is inhibited, preventing apoptosis and allowing the mutated cells to multiply rapidly in an uncontrolled fashion leading to a cancerous tumour.

Introduction

Significant advances in the understanding of cancer, early detection and the treatment thereof has dramatically increased the average cancer survival rate from an estimated 35 % in 1953 to 68 % in 2005.⁴ However, the rates of incidence and treatment resistance is on the rise indicating the need for further research and discovery.⁵

Obtaining accurate, updated cancer statistics is difficult for numerous reasons, however there are a few reports estimating current cancer statistics. The World Health Organisation has outlined the cancer mortality data revealed in a Globocan 2012 report. Figure 1 illustrates the contribution of various cancer types towards cancer related deaths. Of particular interest to this PhD, it can be seen that breast, colorectal and leukemic cancers accounted for nearly a quarter of all cancer related deaths globally in this year.⁶⁻⁷

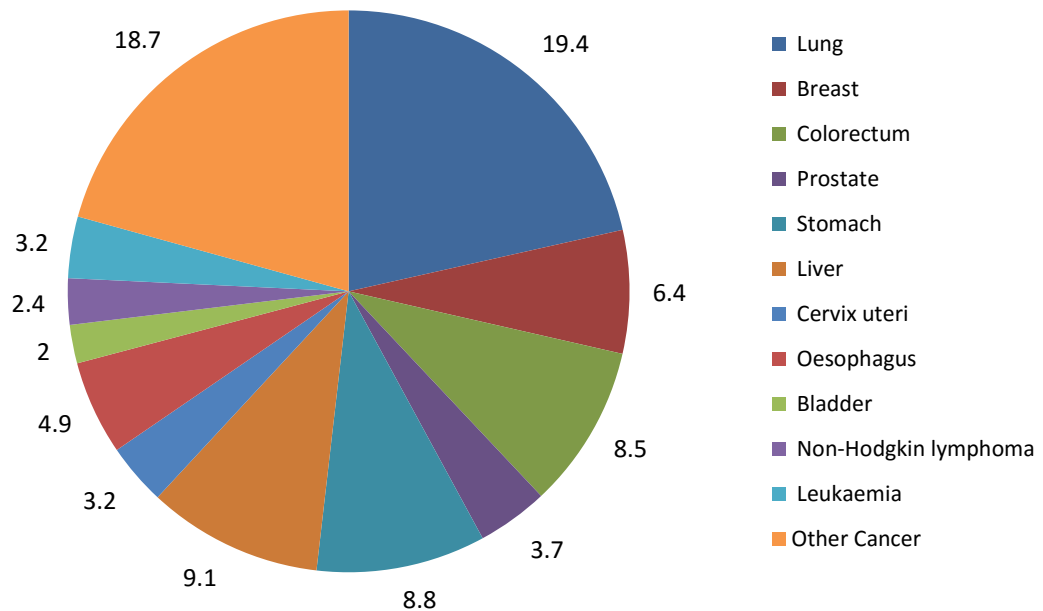


Figure 1 – World Cancer Mortality Rates (%) for 2012

1.1.1. Colorectal Cancer

Colorectal cancer, as the name suggests, is cancer of the colon and/or rectum. It begins as a benign polyp in the lining of the colon or rectum, following which the cancer cells continue to multiply, forming a tumour. The tumour is considered to be malignant once multiple significant changes have taken place on a DNA level, typically indicated by the presence of at least one active oncogene and a loss of tumour suppressor genes.¹ According to a report released in 2014 specifically on colorectal cancer statistics, the majority of colorectal cancers occur in the proximal

colon (comprising of the cecum, the ascending and transverse colon), the remaining cases being shared nearly evenly between the distal colon (the descending and sigmoid) and the rectum.⁸

There are currently several methods for the detection of colorectal cancer in South Africa. More invasive but more definitive methods include biopsy, colonoscopy and sigmoidoscopy while less invasive measures such as barium enemas may be used as a form of early detection.⁹ The conventional treatment for colorectal cancer is removal by surgical ablation, and depending on the degree to which the cancer has spread, the treatment may be supplemented with radiation and/or chemotherapy. Unfortunately there is a 40% chance of developing metastases after surgery and in more highly metastasized cancers these conventional approaches tend to have very little effect on the cancer.¹⁰

1.1.2. Breast Cancer

Breast cancer is thought to originate in the cells that line the breast ducts and spread from there. However, there are also reported cases where the cancers start in the lobules or the breast tissue itself.¹¹ The danger in this type of cancer is that the cells can easily metastasize (spread rapidly) to the nearby lymph nodes. Once there they can easily be spread to other parts of the body via the lymphatic system, making this a particularly dangerous form of cancer if not diagnosed in time. According to the World Health Organisation, breast cancer is the leading type of cancer in women, making up 25% of the global cancer diagnoses in women.¹² Due to early detection methods and significant advances in treatment only 14 % of these cases result in death.⁶ Breast cancer is not limited to woman, and can also occur in men, although significantly less common. While the majority of cancers are the result of a seemingly random set of mutations, it has been found that in the case of breast cancer there is a genetic link. Those that test positive for breast-related cancer antigens 1 and 2 (BRCA-1 and BRCA-2) have a 50-85% chance of developing breast cancer at some point in their life.¹³

Unlike most other cancers that require a medical professional's examination and side effects to detect cancer, women are strongly encouraged to do regular self-examinations in order to detect any lumps or irregularities in their breasts. This campaign has resulted in early diagnosis and treatment of breast cancer before it can spread and become more serious. The Cancer Association of South Africa has released an infographic (Figure 2) outlining what woman should look out for and to quash common myths.¹⁴

Once an abnormality has been detected, a doctor typically confirms the presence of the abnormality and, should the doctor feel it is warranted, send for further tests. Typical tests include mammograms (X-ray of the breast), breast ultrasound and MRI and these are used to

Introduction

show the nature of the abnormality. From these results, a biopsy may be used to confirm the presence and stage of the cancer and potentially whole body scans may be done to confirm that the cancer hasn't spread to other parts of the body.¹¹

Treatment for breast cancer is determined depending on the stage of the cancer as well as the age and the health of the individual. Surgery to remove the abnormal mass is the normal approach. Depending on the size and type of tumour, this is either a lumpectomy (removal of the tumour and a small amount of surrounding tissue) or mastectomy (removal of the entire breast) followed by reconstructive surgery. All of these treatments are often followed up with radiation and/or chemotherapy to ensure that no cancer cells are left behind, preventing the cancer from reoccurring.¹¹

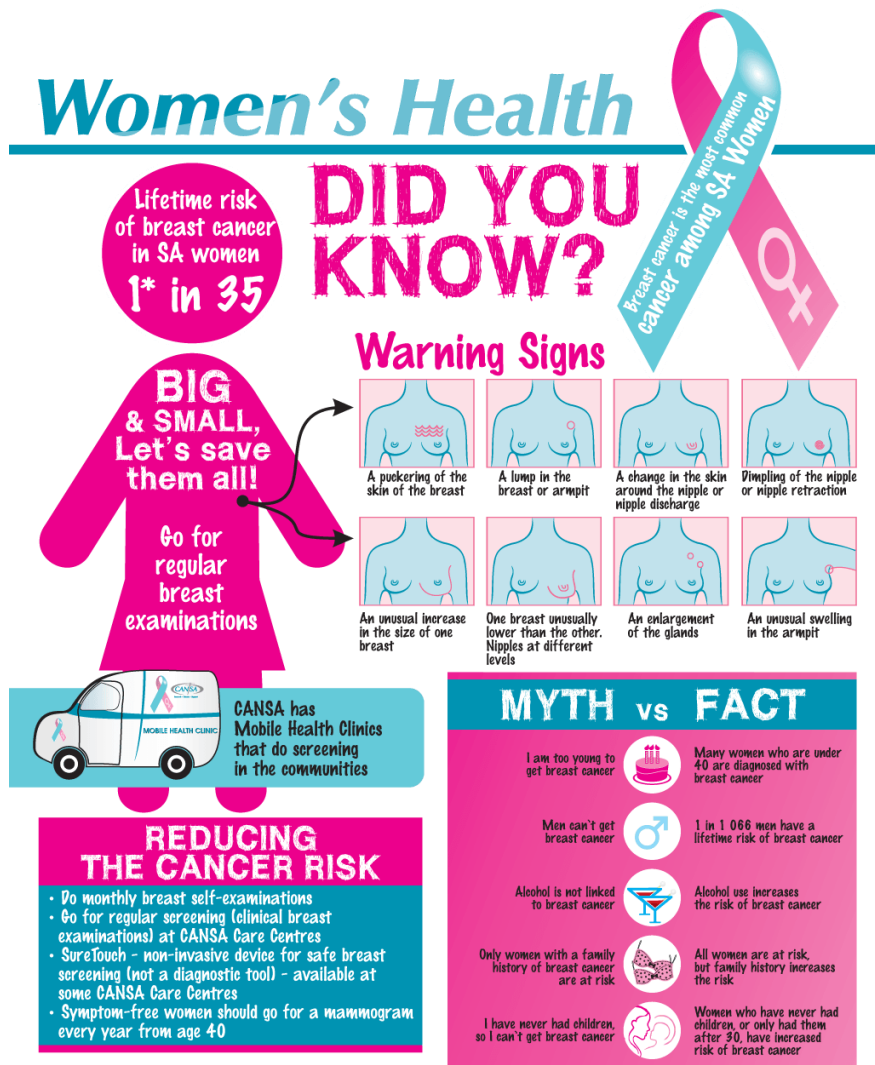


Figure 2 – Breast Cancer Infographic courtesy of the CANSA Association¹⁴

1.1.3. Leukemia

Perhaps one of the most difficult cancers to treat is leukemia. A broad description for this type of cancer is cancer of the blood and bone marrow. The bone marrow contains blood stem cells which are responsible for producing red blood cells (erythrocytes), white blood cells (leucocytes) and platelets which make up a large proportion of blood. The blood stem cells produce myeloid and lymphoid stem cells. The myeloid stem cells produce erythrocytes, platelets and granulocytes (certain types of leucocytes) while the lymphoid stem cells produce the rest of the leucocytes. Leukemia originates when the bone marrow produces abnormal white blood cells (commonly referred to as leukemia cells). These abnormal cells accumulate in the marrow and blood making it significantly harder to circulate healthy blood to the tissues, control bleeding and fight infections. Since blood circulates around the entire body, it is easy for the leukemic cells to spread (often to the lymph nodes, spleen and brain).¹⁵

While for most cancers the likelihood of developing cancer increases with age, leukemia is prevalent in both children and adults. Leukemia accounted for approximately 31 % of all childhood cancers, and 12 % of adolescent cancers in a study on childhood cancers in 2014.¹⁶

There are four major types of leukemia:

- Acute myeloid leukemia (AML)
- Chronic myeloid leukemia (CML)
- Acute lymphocytic leukemia (ALL)
- Chronic lymphocytic leukemia (CLL)

The myeloid/lymphocytic term refers to where the abnormality occurs. Acute cancers are the more aggressive, fast growing and metastatic type of cancers where the affected individual experiences fatigue, bruises easily and contracts infections easily, forcing them to seek medical attention. The leukemic cells typically collect in the bone marrow and blood. Chronic cancers are slow growing and spreading, and are often only discovered as a result of routine checks. They are characterised by an increase in the number of leucocytes in the blood.¹⁵ Diagnosis of leukemia can be confirmed by blood tests and/or bone marrow aspiration and biopsy. Other tests such as contrast CT scans and MRI's may be done to detect if the cancer is localised to an area or if it has spread to other tissues. Unlike many other types of cancers, leukemia does not form a solid tumour. Surgery is therefore not an effective form of treatment, making treatment fully reliant on chemotherapy and/or radiation.¹⁷

1.1.4. Commonly Used Chemotherapies

Since there is still very little known about the origins of cancer in the body, designing targeted treatment for each particular cancer is difficult. As a result, there are a host of chemotherapies that are currently employed in the treatment of cancer. Discussed in this section is a selection of commonly used chemotherapies in the treatment of leukemia, colorectal and breast cancers. It should be noted that many of the chemotherapeutic agents are used for a variety of different cancers and may extend past what is mentioned here. These agents may also be used in conjunction with each other in an individual's treatment plan, depending on the severity of the cancer.

For the treatment of colorectal cancer, one or more of the following chemotherapeutic agents (as illustrated in Figure 3) are often used:

- fluorouracil, **1** (marketed as 5-FU or Adrucil®)¹⁸
- the prodrug of fluorouracil, capecitabine, **2** (marketed as Xeloda®)¹⁹
- oxaliplatin, **3** (marketed as Eloxatin)²⁰
- irinotecan, **4** (marketed as Camptostar)²¹

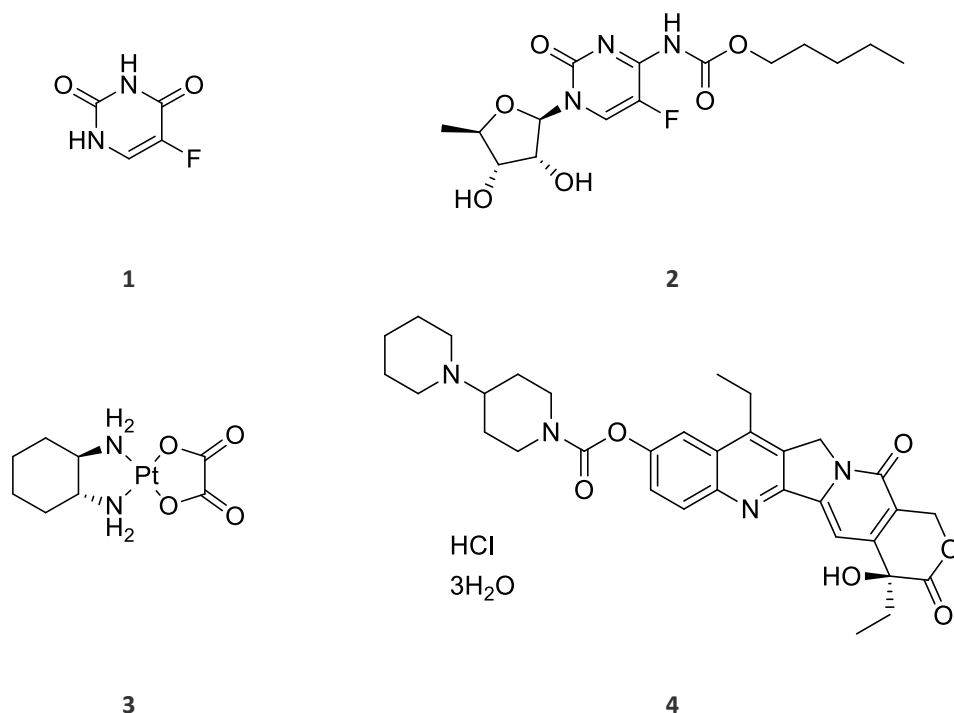


Figure 3 – Currently used chemotherapies for colorectal cancer

Certain classes of compounds have inherent anticancer activity, where differing substituents show better activity against particular cancers. Several of these families will also be discussed in

Introduction

this section. Camptostar (**4**) is a derivative of camptothecin (**5**) shown in Figure 4. Camptothecin was first isolated by M. E. Wall in the early 1960's from the *Camptotheca acuminata*, Nyssaceae tree, which is native to China. The extracts were screened and found to contain high anti-tumour activity. It was found that only the (*S*)-camptothecin enantiomer was biologically active.²² Camptothecin was developed into **4** and approved by the Food and Drug Administration (FDA) for the treatment of colorectal cancer.²¹ A further slight variation of **5** results in the derivative **6**, another drug known as topotecan (marketed as Hycamtin® and shown in Figure 4) although this is used more for the treatment of leukemia and small cell lung cancer.²³ This family of compounds acts by binding to the topoisomerase I DNA during the unwinding of the DNA helix, preventing the DNA from recombining after transcription.²²⁻²³

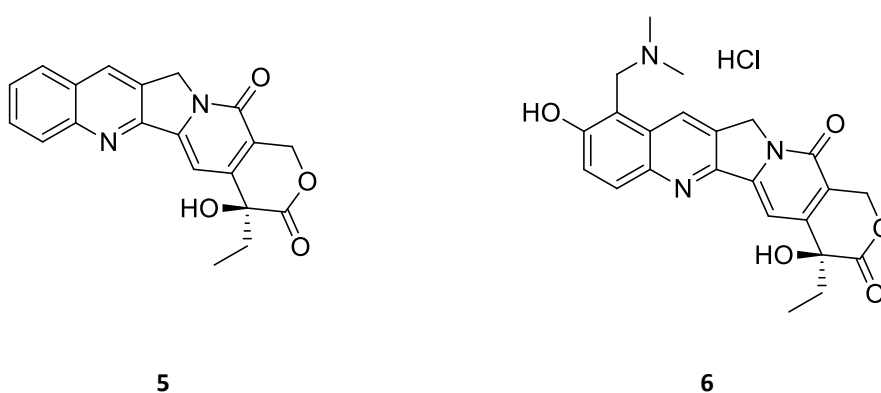


Figure 4 – Camptothecin (5) and its prodrug, topotecan (6)

Another family of cancer fighting compounds are the platinum-containing drugs. As previously mentioned, oxaliplatin (**3**) is a drug used to treat colon cancer. Considered to be the third generation derivative of the platinum-containing drug, cisplatin (**7**, Figure 5),²⁴ this is an example of the platinum-containing complexes of significant interest to this project.

Cisplatin was first reported in 1965 to inhibit cell division and was approved for drug use by the FDA in 1978.^{25,26} To date it has been used to successfully treat a variety of human cancers. One such example of the success of cisplatin can be seen in the increase in the cure rate of testicular cancer, which was about 10% in the late 1970's and increased to almost 90% after the introduction of the cisplatin treatment.^{27,28} However, metastatic colorectal cancer has developed drug resistance to cisplatin, making it an ineffective treatment.²⁹ The development of **7** led to the formation of a second generation drug, carboplatin (**8**, Figure 5) which has significantly lower toxicity compared to cisplatin and was approved by the FDA for the treatment of ovarian, lung, head and neck cancers. More recently the third generation of cisplatin, oxaliplatin (**3**) (in combination with 5-fluorouracil (**1**) and/or leucovorin) was approved for use in Europe in 1996 and in the US in 2002 for treatment of metastatic colorectal cancer.^{8,30} Over 50% of all cancer

Introduction

patients worldwide are treated using these platinum-containing compounds either alone or supplemented by other drugs.

Once in the body, these platinum compounds are hydrolysed inside the cell. The hydrolysed product reacts rapidly with nitrogen donor ligands in DNA.³¹ This binding leads to distortion of the overall helical shape of the DNA, preventing replication and transcription from occurring.³²



Figure 5 – First and second generation platinum based chemotherapy

Drugs that are commonly used in the treatment of breast cancer include:

- platinum group therapies such as cisplatin (**7**) and carboplatin (**8**)³³
- capecitabine, **2** (marketed as Xeloda®)¹⁹
- docetaxel, **9** (marketed as Taxotere® shown in Figure 6)³⁴
- paclitaxel, **10** (marketed as Taxol shown in Figure 6)³⁵

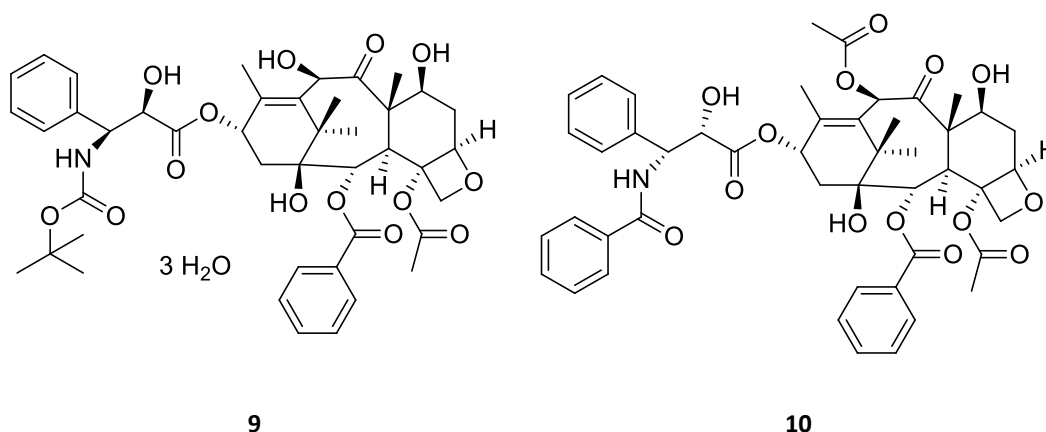


Figure 6 – docetaxel (**9**) and paclitaxel (**10**) used in the treatment of breast cancer

Capecitabine (**2**) has two modes of action. Firstly it prevents uracil from converting into thymidine (important for the synthesis of DNA) by binding to thymidylate synthase, thus inhibiting cell division. Secondly, after the metabolism by the cancer cell to the triphosphate

Introduction

analogue, it can be incorporated into the RNA during its synthesis, preventing further RNA processing and protein synthesis.¹⁹

Paclitaxel (**10**) was originally isolated by Wall and co-workers in 1966 from the bark of *Taxus brevifolia*, a tree typically found in Washington State. The structure was determined a few years later by means of X-ray crystallography in combination with infrared and mass spectrometry.²² Since then, a number of syntheses of paclitaxel have been described and a variety of other biologically active analogues such as docetaxel have been developed. The mode of action of these compounds is considered to be tubulin binding. The taxel analogues are thought to promote the assembly of, and stabilise the stacking of, the microtubules and prevents the disassembly of these polymer type structures, preventing mitosis from occurring in the mutated cells.^{34,35}

Considering the limited treatment options for leukemia, chemotherapeutic agents used are of particular importance. Some of the drugs currently administered (outlined in Figure 7) include:

- Topotecan, **6** (marketed as Hycamtin®)²³
- Cladribine, **11** (marketed as Leustatin®)³⁶
- Fludarabine, **12** (marketed as Fludara®)³⁷
- Etoposide, **13** (marketed as Etopophos®)³⁸

Introduction

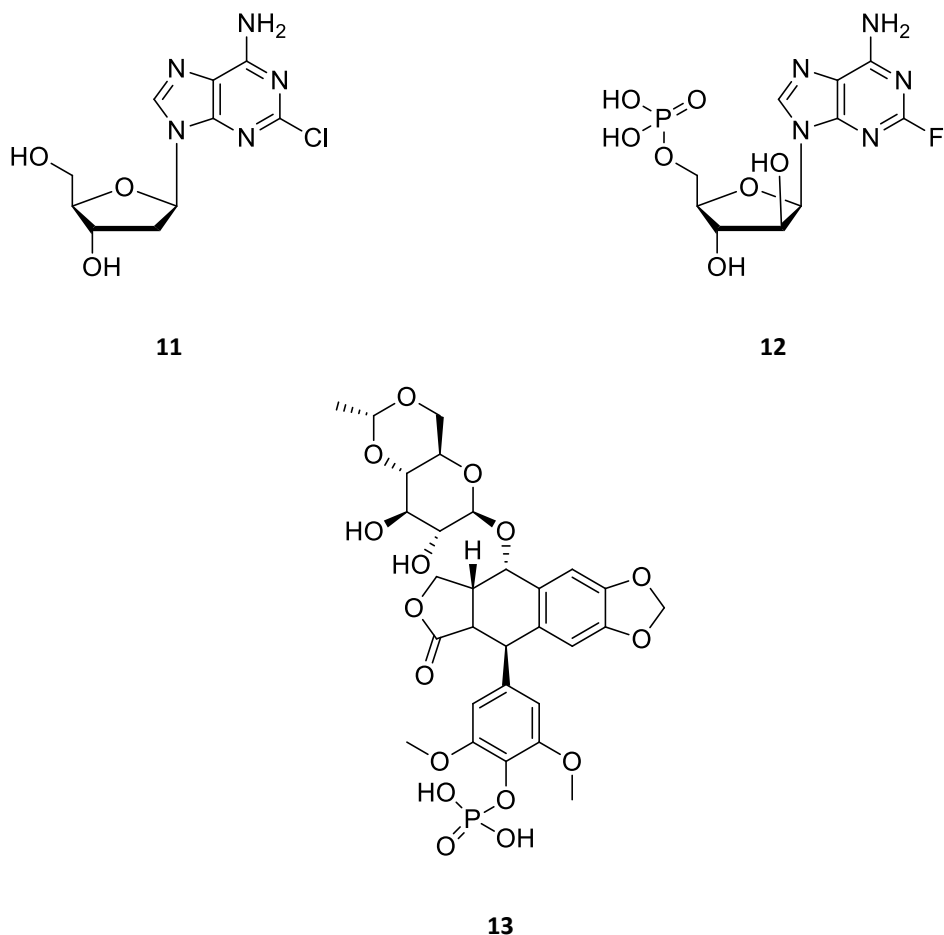


Figure 7 – Cladribine (11), Fludarabine (12) and Etoposide (13) used in the treatment of leukemia

The mode of action of cladribine (**11**) and fludarabine (**12**) is still under investigation, however it is thought that the drugs are metabolised and converted into the active triphosphorylated species which inhibit DNA polymerase and primase and ribonucleotide reductase. This prevents the synthesis of cancerous DNA.^{36,37} Etoposide (**13**), on the other hand, is considered to interact with the topoisomerase-II-DNA complex preventing replication of the mutated DNA.³⁸

On a more interesting note, while the cause of leukemia is still not known, medical professionals are beginning to notice an increase in patients developing leukemia who were previously treated with the platinum-containing chemotherapies for other types of cancer.³³

1.2. The Future of Chemotherapy

1.2.1. Hybrid Compounds

Despite significant advances in currently used chemotherapies and the on-going search for new chemotherapeutic agents to introduce to the market, cancer continues to plague society. Aside from the high toxicity and severe side effects of currently used chemotherapies,³⁹ several cancer cell lines are becoming treatment resistant, especially in recurring cancers.²⁹

With the high cost of drug development, researchers are continually investigating new ways to reduce the cost of development. One such strategy that is of current interest is the development of hybrid molecules/drugs. In a review by Meunier, hybrid molecules are defined to be chemical moieties with different biological functionalities that form part of the same compound.⁴⁰ The biologically active moieties on the hybrid molecule do not necessarily need to be acting on the same target site. There are several modes of interaction possible with hybrid molecules as shown in Figure 8. These include 'double-edged' hybrids, as shown in **A**, where the active components of the molecule both act on the same target, hybrids where each active moiety acts on independent targets (**B**), and finally hybrids where each active part acts on related targets simultaneously (as in **C**).⁴⁰

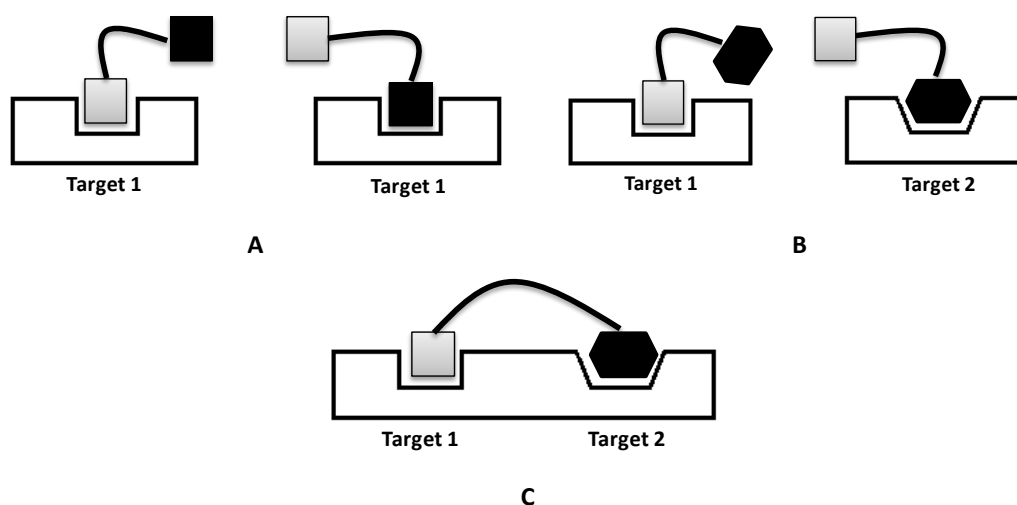


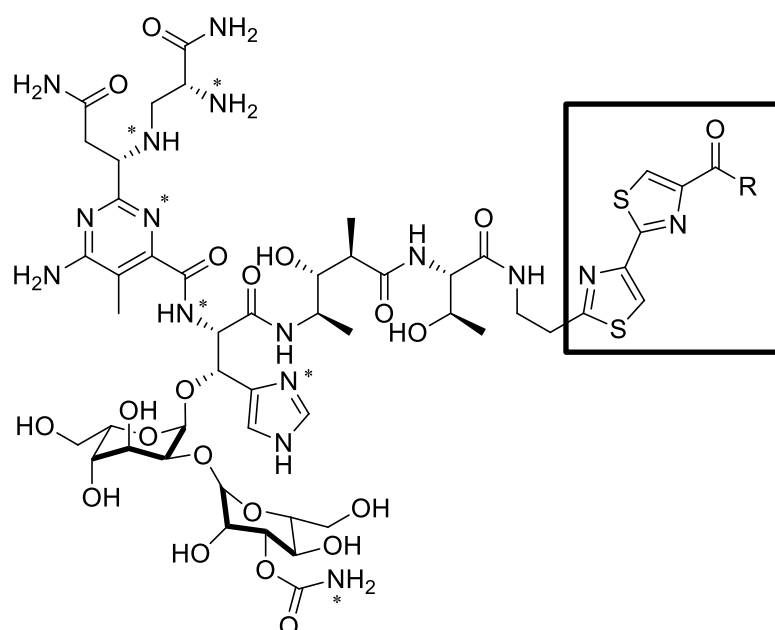
Figure 8 – The different types of hybrid molecules as described by Meunier⁴⁰

The overall activity of the compounds can be significantly increased when one pharmacophore is linked to another by either a covalent or coordination bond. The activity of the hybrid is often much higher than the additive activity of both pharmacophores. Significant other advantages of hybrid compounds were highlighted in Meunier's review, including better absorption of certain active pharmacophores (for example, a low solubility pharmacophore might be better absorbed if

tethered to a significantly more soluble compound). It is also easier to administer a hybrid compound than a combination of separate pharmacophores and the pharmacodynamic properties are more predictable.⁴⁰

1.2.2. Organic Hybrid Compounds

One of the most successful hybrid compounds available on the market is Bleomycin – an anticancer agent. Effectively a prodrug until administered, it is administered metal free. Once in the body it chelates with free iron through the nitrogen atoms indicated by the asterisks (*) in **14** (Figure 9).⁴¹



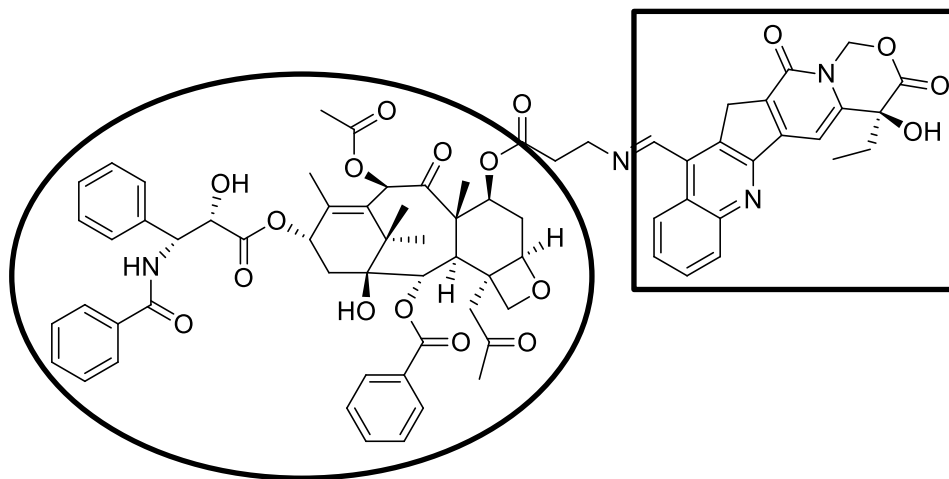
14

Figure 9 – the structure of Bleomycin with * indicating the iron coordination sites

Derivatives of hybrid **14** have three main areas of activity. Aside from the metal binding domain (indicated by *), the molecule also contains a DNA binding domain (highlighted by the square in Figure 9) and the sugar/carbohydrate domain which improves cell penetration.⁴¹ This is an example of type C of the hybrids discussed in Figure 8. However, the synthesis of bleomycin is troublesome⁴² and unfortunately while bleomycin shows good biological activity they also show significant toxicity.

Nakagawa-Goto *et al.* investigated the feasibility of tethering paclitaxels (such as **9** and **10**) with other antitumor agents such as camptothecin (**5**) and epipodophyllotoxin by means of an ester, imine, amine or amide bond. Hybrid **15** in Figure 10 is an example of the type of compounds that

were investigated, where paclitaxel (in the circle) has been tethered to camptothecin (in the square). It was found that these hybrid compounds showed significantly better activity than the unmodified paclitaxel compounds in prostate cancer cell lines.⁴³



15

Figure 10 – A paclitaxel-camptothecin hybrid

The hybrid approach to drug discovery is being investigated in many areas of medicinal chemistry aside from the treatment of cancer. Dos Santos *et al.* reported their preparation of phthalimide derivatives containing furoxanyl moieties for potential use as a treatment for sickle cell disease symptoms.⁴⁴ Saadeh, Mosleh and Mubarak synthesized hybrid compounds combining metronidazole, chloroquine and 5-nitrofuracrylic acid in an attempt to improve their activity against parasites, specifically malaria, after they were inspired by work by Peyton and co-workers.^{45,46} Noted in this study was that the hybrid compounds were better absorbed into the desired areas of activity in relation to the conventionally active drugs.⁴⁵ This highlights the significant advantage of the pharmacological properties being improved in hybrid molecules.

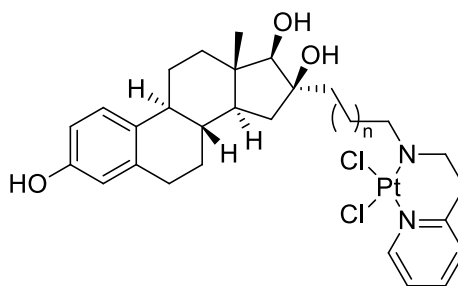
1.2.3. Metal-Containing Hybrids

1.2.3.1. Platinum

Up until this point in this thesis, the covalent linking of multiple organic molecules to afford organic hybrids has been discussed. However; metals can also be combined with biologically active organic pharmacophores to afford hybrid molecules. Since platinum is currently used in chemotherapies, this is an important area of research to consider and is currently a ‘hot’ research topic. Significant research is being done into creating platinum-hybrid compounds specifically to target cancer cell lines.

Introduction

In hormone-dependent cancers, a high oestrogen receptor count has been noted making them potential targets for drug design. Gagnon *et al.* synthesized a variety of platinum-containing hybrids that combine cisplatin with oestrogen. Compared to cisplatin, hybrids such as **16** (Figure 11) where $n = 6$ or 8 were found to be up to 7 times more active. In addition to this, these compounds were also active against cisplatin resistant cell lines.³⁹ Figure 11 is an example of the hybrids shown in Figure 8B, the oestrogen component directs the drug to the cancer cells (due to the high oestrogen receptor count) and once there enables the platinum moiety to serve as a DNA intercalator.

**16****Figure 11 – An oestrogen/cisplatin hybrid**

Another promising example of platinum hybrids are platinum-acridines (Figure 12) however, while the second generation platinum-acridines (**17**) show promising results, it was noted that the pharmacological properties of this generation of hybrids needed some improvement. Graham *et al.* looked at the effects of the addition of a carboxylic acid ester group to acridine (**18**).⁴⁷

Introduction

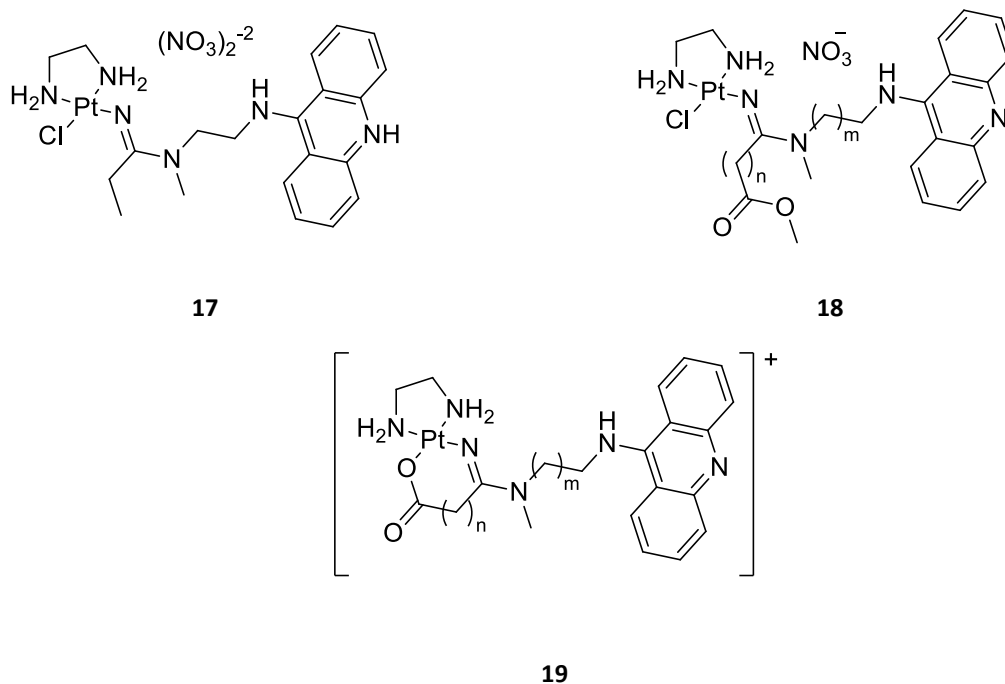


Figure 12 – platinum-acridine hybrids

In the article it was proposed that in an aqueous environment, the ester would be converted into a chelated carboxylato ligand (**19**). Also proposed was that since these modified platinum-acridines still showed anticancer activity, adding a receptor targeted component to the end of this ester could be a potential method for making these anticancer compounds more selective – and potentially more active. This targeted method of action is outlined briefly in Figure 13 and serves as an example of targeting hybrid molecules where there are 3 active pharmacophores (the targeted receptor, the acridine and the platinum DNA intercalator). In Figure 13, the targeted receptor is denoted as R, the moiety attracted to the target (as T) with the platinum binding to nitrogen bases in the DNA once in the cell.⁴⁷

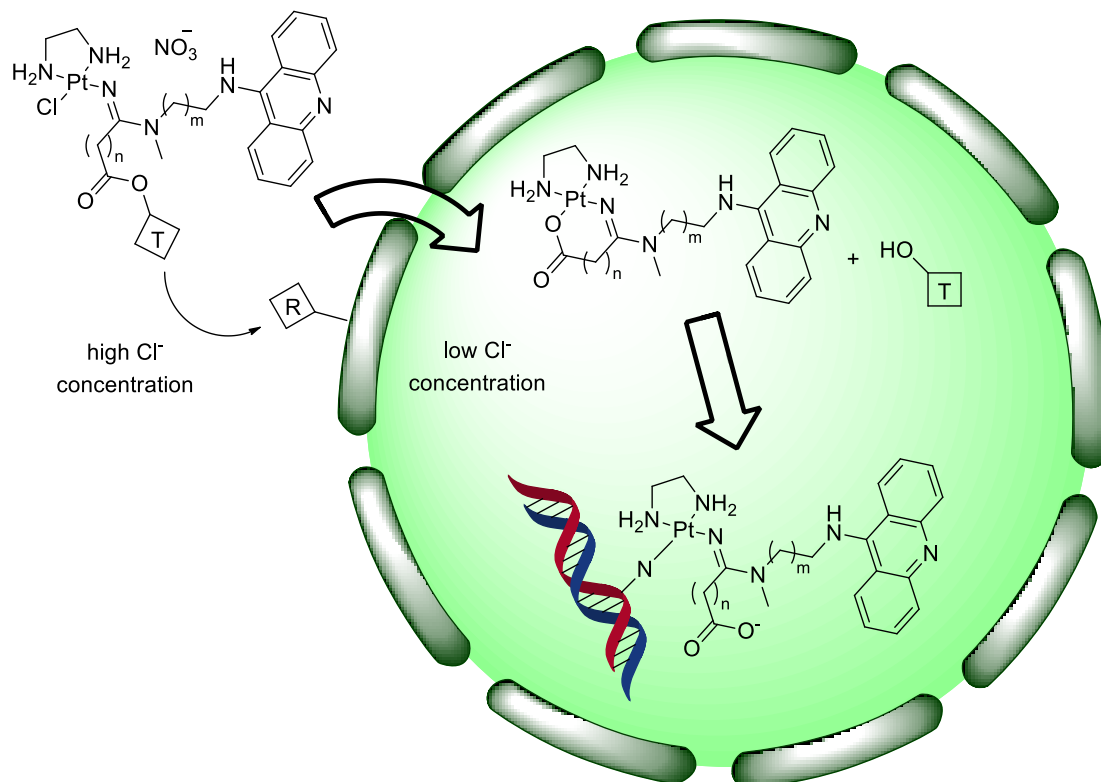


Figure 13 – Proposed mode of action of targeted platinum based complexes⁴⁷

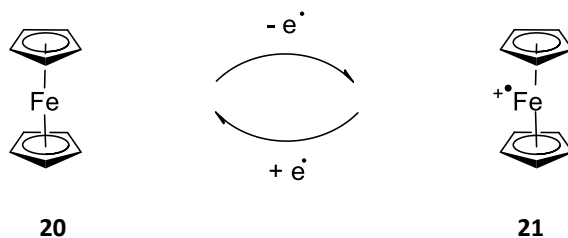
While the chemistry and biology of platinum is well established, it is not the only metal that shows anticancer activity or, for that matter, the only metal looked at for hybrid compound development. There is a vast amount of research into using transition metals (not just platinum group metals) in chemotherapy. Historically all metals incorporated into drugs were thought to behave like platinum – binding to DNA – however recently discoveries are showing that different metals tend to have their own individual modes of action. Alessio and co-workers summarised the different possible modes of action of metals to be used in anticancer drugs as *functional* (i.e. the metal binds to the target), *structural* (metals have particular binding geometries which lend their structure to the overall shape of the molecule), *carrier* (delivers active ligands *in vivo*), *catalysis* (speeding up naturally occurring reactions) and *photo-sensitive* (the metal compound acts as a photo-sensitizer).⁴⁸

1.2.3.2. Iron and ferrocene based hybrids

Iron is another metal of interest for the development of hybrid drugs, often in the form of ferrocene. Ferrocene, **20** (Scheme 1) in its simplest form is a Fe^{2+} metal atom sandwiched between two cyclopentadiene molecules. Not to be outdone by the significant redox potential of

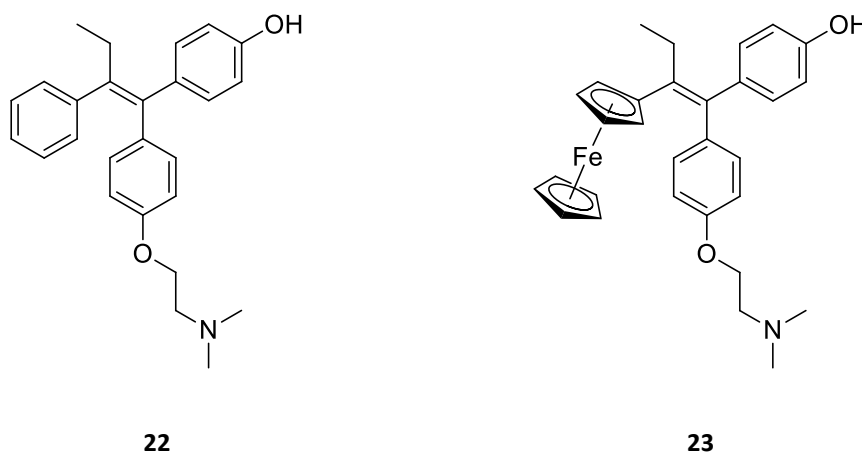
Introduction

iron ($\text{Fe}^{3+} + \text{e}^- \rightarrow \text{Fe}^{2+}$), ferrocene can just as easily be oxidized to ferrocenium (**21**) as shown in Scheme 1. Under biological conditions, **20** can be oxidized to **21**, which can then act as an electron (or free radical) scavenger and be reduced back to **20**. In cancerous cells, there is a build-up of superoxide and secondary radicals (such as $\cdot\text{OH}$) in the cells which bind to DNA causing damage during DNA replication. In theory, **21** can act as a free radical scavenger and thus 'mop-up' the excess superoxide and free radicals thereby reducing the damage done to the DNA and preventing the spread of cancerous cells.⁴⁹



Scheme 1 – The redox activity of ferrocene

The use of ferrocene on its own has not found any medical use, however there are many examples of ferrocene hybrid molecules, where the presence of ferrocene greatly enhances the activity of the organic component that it is linked to by a covalent bond. A particularly surprising example of this success was the tethering of ferrocene to tamoxifen derivatives such as hydroxytamoxifen (**22**, Figure 14).⁴⁸ Tamoxifen, as shown in Figure 14, being an oestrogen receptor targeting molecule was found to be active on hormone dependent cancerous tumours.⁵⁰ Jaouen and co-workers found that by the replacement of a benzene ring with ferrocene to this class of therapeutic agents, resulting in the hybrid, ferrocifen (**23**), was active not just to hormone dependent tumours but also to hormone independent tumours.⁵¹

Figure 14 – Hydroxytamoxifen (**22**) and its ferrocene-containing derivative ferrocifen (**23**)

1.2.3.3. Zinc-containing Hybrids

Aside from iron, there has been an increase in the amount of research being put into investigating the use of other transition metals in cancer treatment. Zinc is perhaps one of the less documented metals, however is of significant importance to this project. Zinc pyrithione (**24**, Figure 15) is a complex originally added to shampoo as an antidandruff agent,⁵² but has subsequently been investigated for its anticancer properties. Carraway and Dobner found that zinc pyrithione induces necrotic cell death in prostate cancer cell lines.⁵³ Liguori *et al.* also noted that their synthesized zinc complexes showed significant anticancer activity in three different prostate cancer cell lines, especially in comparison to cisplatin. Two of these complexes (**25** and **26**) are shown in Figure 15 and were found to induce apoptosis.⁵⁴

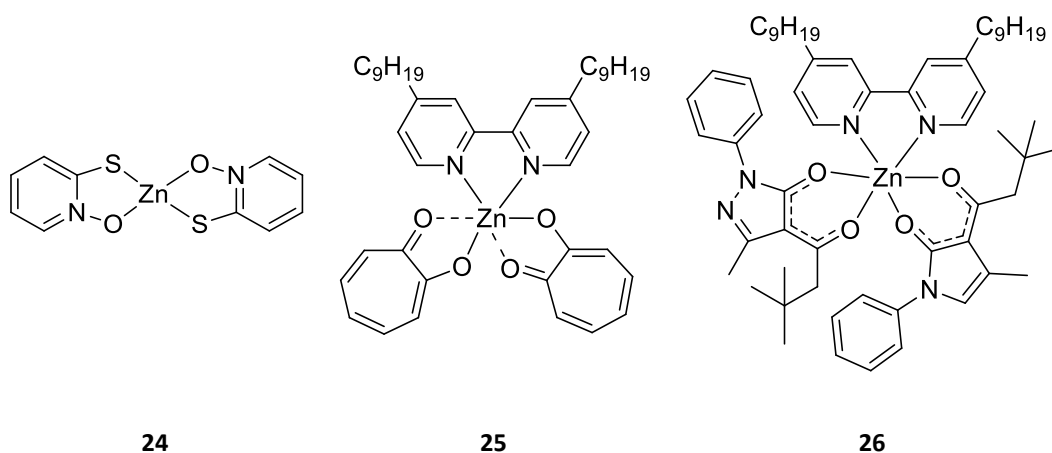
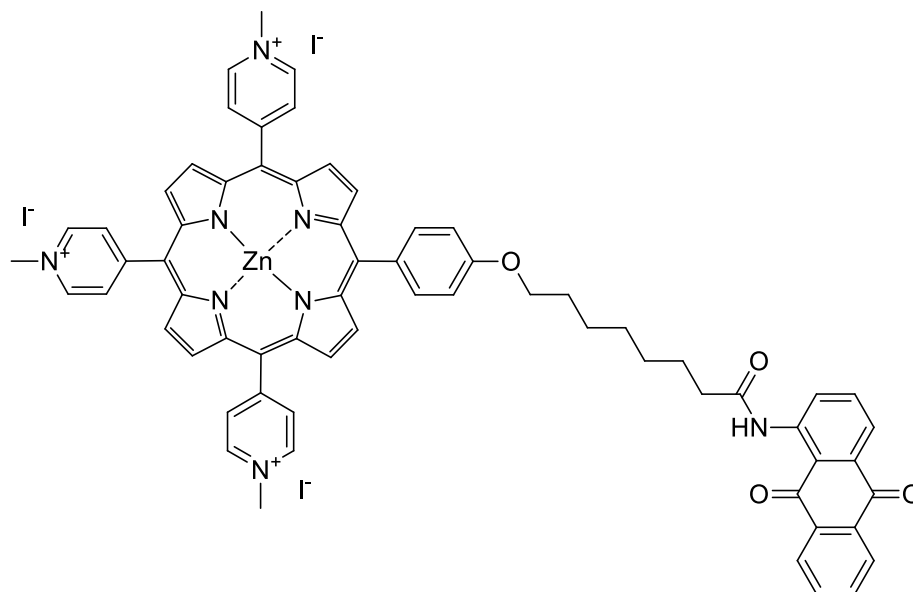


Figure 15 – Zinc-containing hybrids

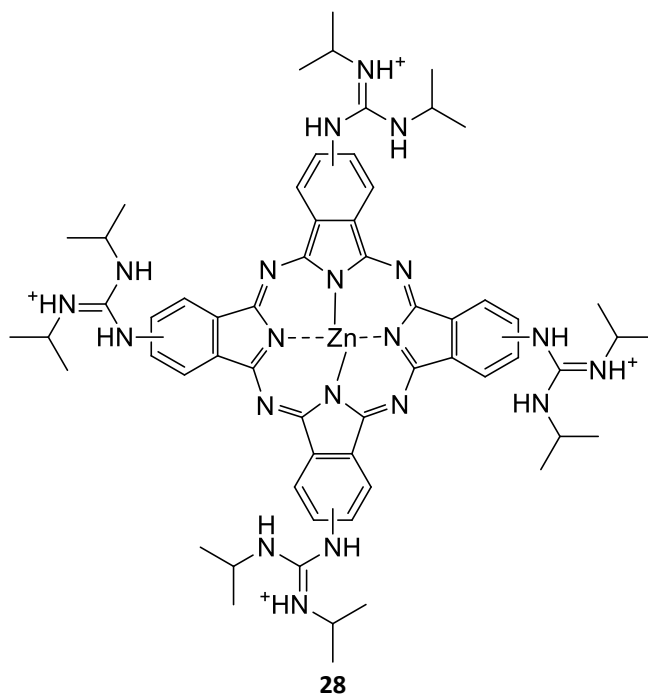
Zinc can easily be incorporated into macrocycles such as porphyrins and phthalocyanines. Zhao *et al.* synthesized a variety of metal-containing porphyrins, such as **27** in Figure 16, that were tethered to anthraquinone in order to investigate the DNA intercalating and photocleaving abilities of the hybrid. The anthraquinone section serves as a DNA intercalator that shows some specificity for cancer cells, while the porphyrin portion is responsible for the photocleavage of DNA.⁵⁵



27

Figure 16 – A zinc-containing porphyrin tethered to anthraquinone

While the previous zinc-containing compounds took advantage of the ability of zinc to bind to DNA, zinc also has photoluminescence properties making zinc-containing compounds particularly suitable for their use in photodynamic therapy.⁵⁶ Alzeer *et al.* designed luminescent probes which target *c-myc*, an enzyme that is overexpressed in cancer cells. This involved the coordination of zinc to a phthalocyanine with a guanidinium modification such as **28** in Figure 17.⁵⁷



28

Figure 17 – A photoluminescent zinc-containing porphyrin

1.2.3.4. Copper in Chemotherapy

Arguably one of the best kept secrets in the field of anticancer research is the use of copper-based compounds. Copper is a transition metal that is naturally occurring in many biological systems. Nature takes advantage of its significant redox potential to transfer single electrons by cycling copper between its 2+ and 1+ oxidation states.⁵⁸ There are a variety of human enzymes that are copper-containing, including amine oxidases (that oxidize primary amines), ceruloplasmin and haphaestin (in blood plasma and essential for iron and copper transport), cytochrome c oxidase (essential in the mitochondrial respiratory chain), dopamine β -hydroxylase (involved in catecholamine metabolism), lysyl oxidase (cross-linking of collagen and elastin and keratin), superoxide dismutase (destroys superoxide radicals) and tyrosinase (catalyses pigment production) amongst others.⁵⁹ While the reactivity of copper is clearly of great importance, the body strictly regulates copper levels to prevent any unwanted redox reactivity. Copper is absorbed into the body from the stomach and small intestine and is processed through the liver, where excess copper is excreted through bile back into the gut.⁶⁰ While there are several diseases associated with significant changes in copper levels (such as Wilsons disease, Menkes disease and Alzheimers disease)⁶⁰ a significant amount of research is being done into investigating copper's use in cancer treatment. Cancer cells have been found to contain significantly larger amounts of copper than their healthy cell equivalents.^{58,61} This abnormal metabolism process provides significant selectivity and is something that could be exploited of for the treatment of cancer.

The nature of the ligands used has been extensively considered. The coordination of copper to the ligand needs to be strong enough to survive physiological conditions to get the copper to its active site in the cell, however once there the ligand needs to be labile enough to allow the copper to act once in the active site.⁶¹ Sulfur, nitrogen, oxygen, phosphorus and carbon donor atoms have all been considered by a variety of different research groups, however for the purposes of this project mainly nitrogen donor ligands will be reviewed.

Belicchi-Ferrari *et al.* embraced the metal hybrid concept by building a thiosemicarbazidic tether onto a uracil moiety (based on fluorouracil **1**) in order to house a copper atom. Following the synthesis of the uracil based ligands (such as **29**, Figure 18), they synthesized a variety of tridentate Cu²⁺ complexes using CuNO₃·3H₂O and CuCl₂·2H₂O. While their characterisation of these complexes did not include any crystal structures to determine absolute configuration of the complexes, they made use of infrared and electronic spectra to propose the coordination structure, for example compound **30** (Figure 18). Their study found that both the free ligands and the copper complexes showed significant DNA binding. They also found that varying the substituent on the end of the thiocarbazidic chain has an effect on the uptake of the compound into the cells, but has little effect on the DNA binding ability.⁶²

Introduction

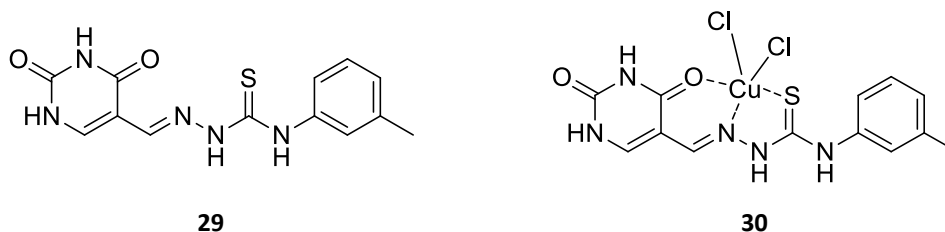


Figure 18 – Examples of uracil based hybrids

Bis(thiosemicarbazone) copper complexes were investigated by Palanimuthu *et al.* Of particular relevance to this project, they investigated both zinc and copper complexes against a variety of cancer cell lines. One of the most active complexes in their study was **31** (Figure 19) which exhibited growth inhibition (GI_{50}) of $0.17 \mu\text{M}$ in MCF7 breast cancer cell lines and IC_{50} values of $1.45 \mu\text{M}$ and $1.23 \mu\text{M}$ in MDA-MB-231 breast and HCT116 colorectal cancer cell lines respectively. These values are comparable to that of adriamycin and are also significantly lower than its zinc equivalent, which displayed a good GI_{50} value of $2.27 \mu\text{M}$ in the MCF7 cancer cell line. A variety of other copper analogues also showed significant activity against cancer cell lines and after further studies in the HCT116 cell lines these workers concluded that the complexes partially intercalate with DNA, preventing further DNA synthesis thus inducing apoptosis.⁶³

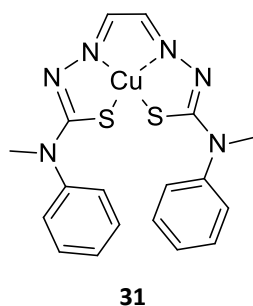


Figure 19 – Copper-containing bis(thiosemicarbazone) hybrid

The detailed mode of action of copper complexes is still under investigation, but most have been shown to induce apoptosis. There are, however, examples where the copper complexes induce neither apoptosis nor necrosis, but rather another form of programmed cell death known as paraptosis.⁵⁸ Dallavalle *et al.* investigated copper and palladium coordination complexes for their activity against fibrosarcoma (HT1080) and human fibroblast (HF) cancer cell lines. As shown in Figure 20, the copper complexes (**32** and **33**) showed significantly greater activity than the palladium complex **34** which was virtually inactive. Complex **32** showed the most promising activity overall.⁶⁴ Tardito *et al.* continued the investigation of **32** that was then shown to have comparable activity to cisplatin. Investigation of the mode of action of the complex revealed that

Introduction

it does not induce apoptosis. Instead large cytoplasmic vesicles form, swell and become large, coalescent vacuoles, eventually filling the cytoplasmic space with these vacuolar formations. After ruling out autophagy as the mode of action and having performed a variety of other tests it was concluded that **32** most likely acts by means of paraptosis – thus providing a potential new target for apoptosis resistant cell lines.⁶⁵

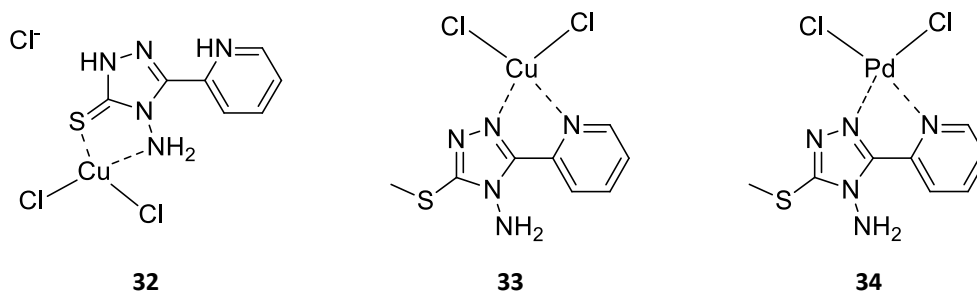


Figure 20 – Examples of copper coordinated hybrid compounds currently under investigation

A variety of copper-containing compounds were synthesized by Ranford *et al.* where they combined a series of substituted phenanthrolines and salicylates. Depending on the conditions the reactants were subjected to, the formation of different complexes was possible. Most of the compounds synthesized in this series showed comparable anticancer activity to cisplatin in the L1210 leukemic, ADJ/PC6 murine plasmocytoma and CH1 human ovarian cancer cell lines. These complexes were also investigated as potential HIV inhibitors, however none of them showed any significant activity. Three of the most active metal complexes (**35**, **36** and **37**) are shown in Figure 21. It is thought that the salicylate ligands are important for the transportation of the complex to the nucleus, while the phenanthroline moiety is necessary for DNA intercalation.⁶⁶

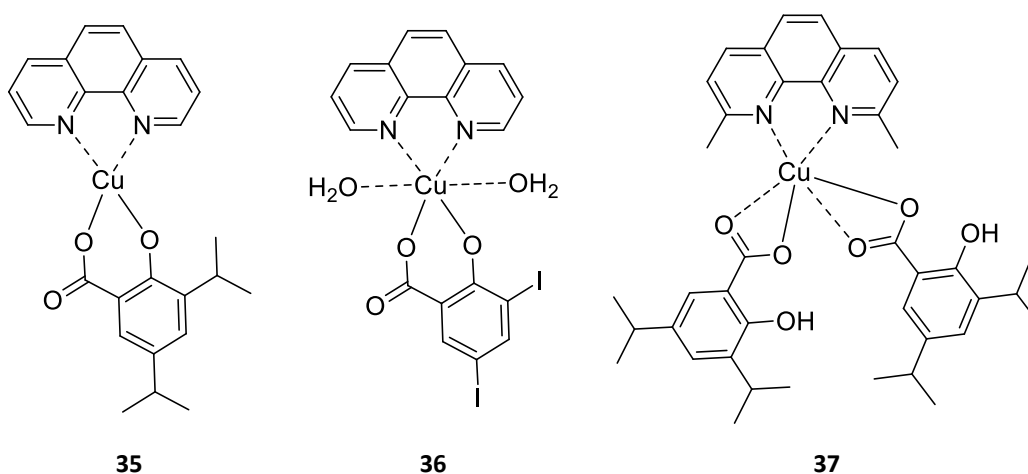


Figure 21 – Copper-containing phenanthrolines and salicylates

Introduction

A more complex type of phenanthroline, 2-(naphthalen-1-yl)-1H-imidazo[4,5-*f*][1,10]phenanthroline was investigated by Bhat *et al.* as shown in Figure 22. Of particular interest to this study was the fluorescent nature of both the free ligand and the copper complexes which were used in fluorescence studies to monitor the activity of the complexes in DNA. When tested against MCF7 and HL-60 cancer cell lines, compounds **38** and **39** showed significant, selective anticancer activity, with **39** showing better activity (IC_{50} of 1522 nM) than the paclitaxel standard (IC_{50} of 1635 nM) in the HL-60 cell lines.⁶⁷

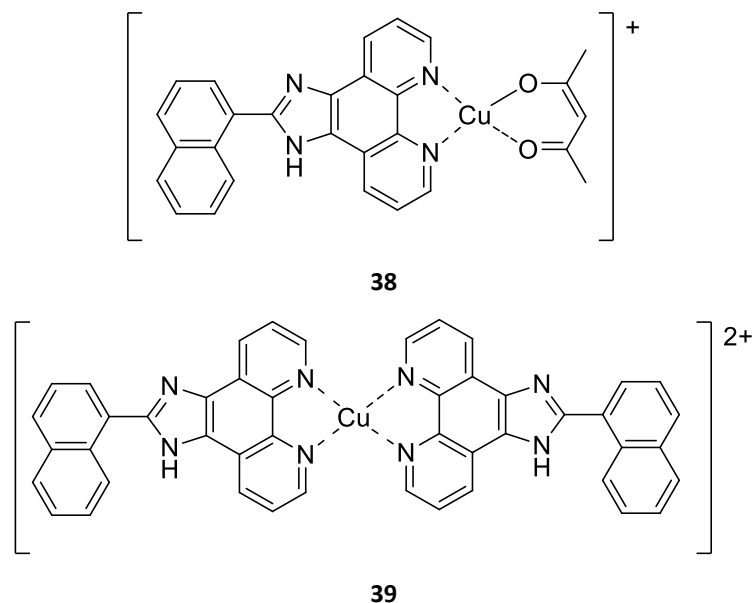


Figure 22 – Mono (38) and di (39) phenanthroline copper complexes

Pitié and co-workers have done extensive investigations into using bisphenanthroline copper complexes in order to oxidatively cleave DNA. Amongst the many notable outcomes of their research, they concluded that the bisphenanthroline complexes (such as **40** in Figure 23) that were linked by a serinol bridge showed significantly more activity than the unlinked counterparts.⁶⁸ Their research was further expanded into the hybrid complex domain by tethering a bisphenanthroline copper complex to a cisplatin moiety at the end of the tether (**42**, where $n=6$ or $n=10$). Both **40** and **42** were tested to investigate their anticancer ability in comparison to cisplatin as well as the bisphenanthroline platinum complex without the presence of copper (**41**). The results of these tests were mixed; in some cell lines **40** showed the most notable anticancer activity (in the WIDR, EVSA-T, H226 and IGROV cell lines) while in the A549 cell line the only compound with any activity of interest was **41** where $n=10$ (showing greater activity than cisplatin). In the M19 cell line, both the $n=6$ and $n=10$ complexes of **42** showed better activity than cisplatin by a full order of magnitude. Complexes **41** where $n=6$ and $n=10$ both showed the most notable activity in the MCF7 breast cancer cell lines.⁶⁹ This study suggests

that there is some selectivity in cancer cell lines to different metals and is an important aspect to consider in the synthesis of metal-containing hybrid compounds.

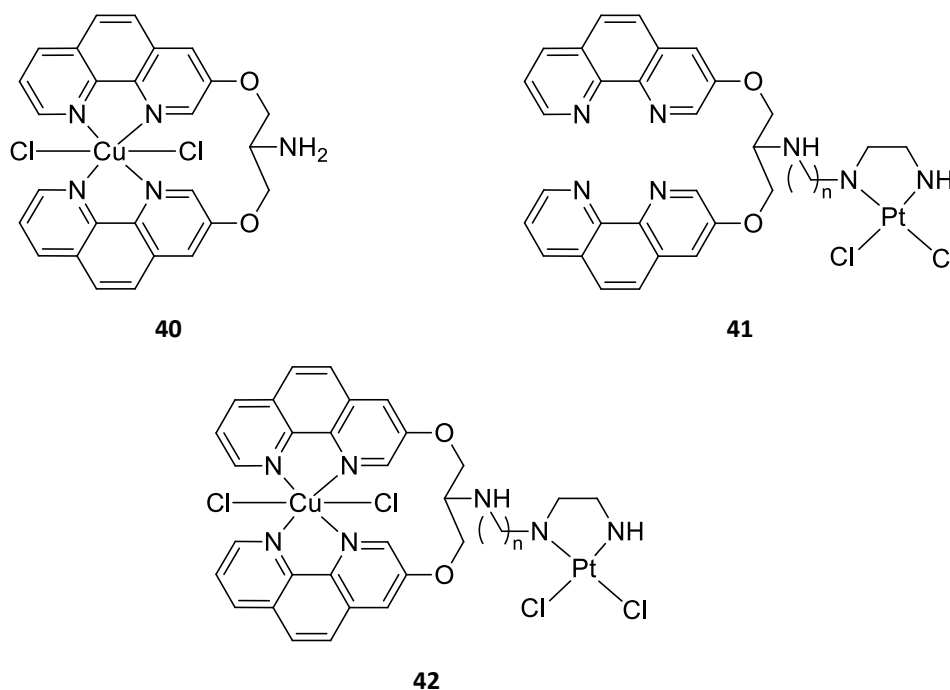


Figure 23 – Copper and platinum-containing phenanthroline compounds

Trávníček *et al.* investigated how the substitution pattern around a purine ring, the ratio in which the ligand and metals are added and the solvent system affected the copper complex formed. In this study it was found that the 6-(2-chlorobenzylamino)purine and the 6-(3-chlorobenzylamino)purine ligands resulted in the formation of different metal complexes such as **43** and **44** (Figure 24). The complexes formed were tested against mouse melanoma (B16-F0), human malignant melanoma (G361), human osteogenic sarcoma (HOS) and human breast cancer (MCF7) cell lines, with **43** and **44** showing moderate activity.⁷⁰

Introduction

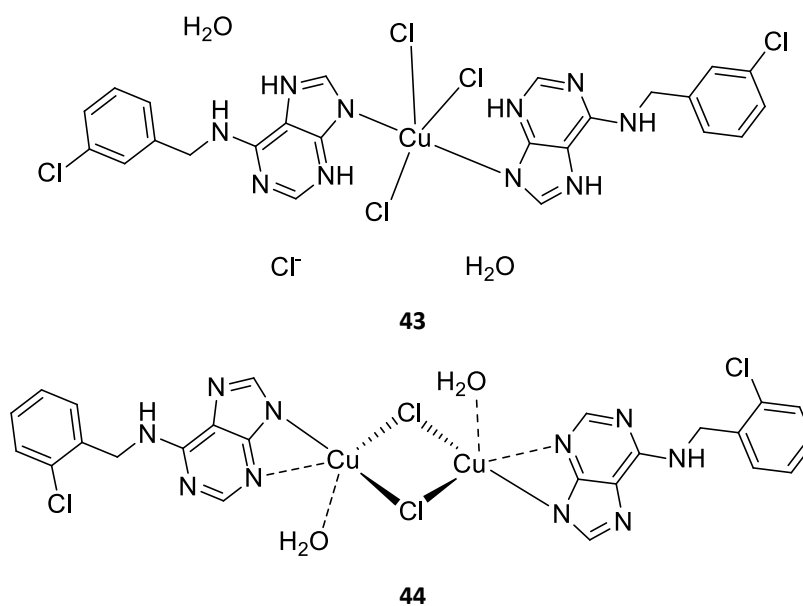


Figure 24 – Purine based copper complexes

Figure 25 illustrates another example of DNA intercalating copper complexes by Zhang *et al.* where they investigated the complexation of $\text{Cu}(\text{ClO}_4)_2$ and $\text{Zn}(\text{ClO}_4)_2$ with a novel 1-[3-(2-pyridyl)pyrazol-1-ylmethyl]naphthalene ligand. Yet again it was found that the copper-containing compound (**45**) showed superior anticancer activity when compared to the zinc complex (**46**) and free ligand when tested against the HL-60, BGC-823 (human stomach) and MDA-MB-435 (human breast) cancer cell lines.⁷¹

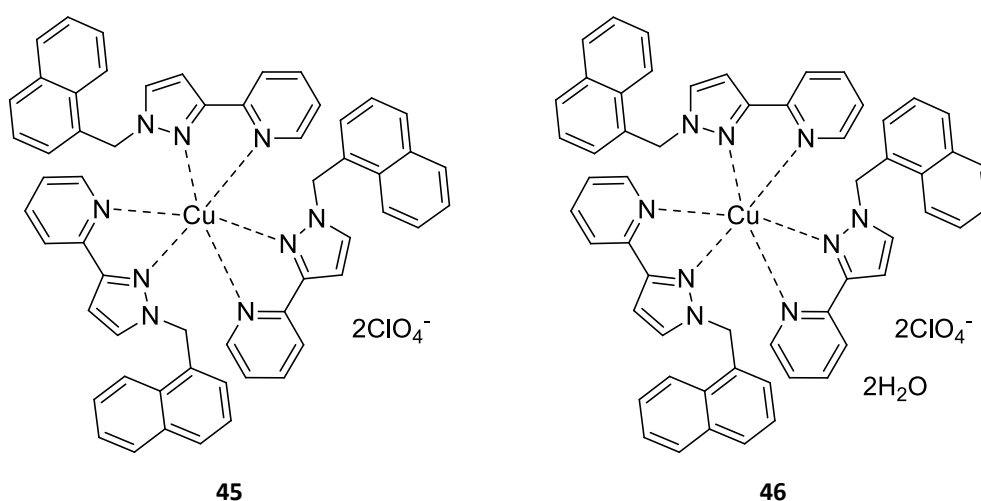


Figure 25 – Examples of DNA intercalating copper complexes

The work on copper-containing complexes mentioned thus far represents a small selection of the vast amount of research that has been done. Iakovidis *et al.* compiled a review of copper in medicine.⁶⁰ Santini, Tisato and their co-workers have also published two comprehensive reviews on the recent advances in copper-containing complexes as anticancer treatments. In these reviews, both Cu(I) and Cu(II) complexes and their coordination geometries are investigated. What can be concluded from these reviews is that depending on the nature of the donor ligands, the copper complexes can act as DNA intercalators, or generate radical oxygen species (ROS) which then degrade the affected cell by inducing apoptosis or inhibiting proteasomes.⁶⁰ There are also a few examples where paraptosis has been evident.⁶⁵ The types of donor ligands used increase the lipophilicity of the complexes and control where they act. Also highlighted in the reviews is the lack of testing in animal models, making it difficult to identify what exactly is needed to develop these 'lead' copper complexes into marketable drugs.⁶¹

1.2.3.5. Ruthenium based Hybrids

One of the 'hottest' metals currently under investigation for potential chemotherapy is ruthenium. This transition metal is a d^4 (for a 3+ oxidation state), d^5 (for the 2+ oxidation state) or a d^6 metal (for the 1+ oxidation state) that is proving to behave rather interestingly in biological systems in that its behaviour can be fine-tuned by changing the ligands – and in turn binding – around the metal centre. There are numerous examples of ruthenium based anticancer metallocenes, arenes, carbonyls and carbenes showing the diversity of ruthenium,⁷² but the most successful of these are NAMI-A (**47**), KP1019 (**48**) and RAPTA-T (**49**) as shown in Figure 26. These compounds did not show significant *in vivo* activity, however clinically was found to induce apoptosis.⁵⁰ Of particular interest with ruthenium is its significant photoluminescent ability. Ruthenium is being investigated extensively for its use in solar cells,⁷³ however is also gaining interest in photodynamic therapy as a theranostic agent where it can be used both for imaging purposes (being UV-active) as well as having anticancer properties itself.⁵⁶ The advantage of this type of therapy is that the chemotherapy and contrast agents are combined thus the progression of the treatment can easily be monitored without the need for additional contrast compounds being added to the patient.

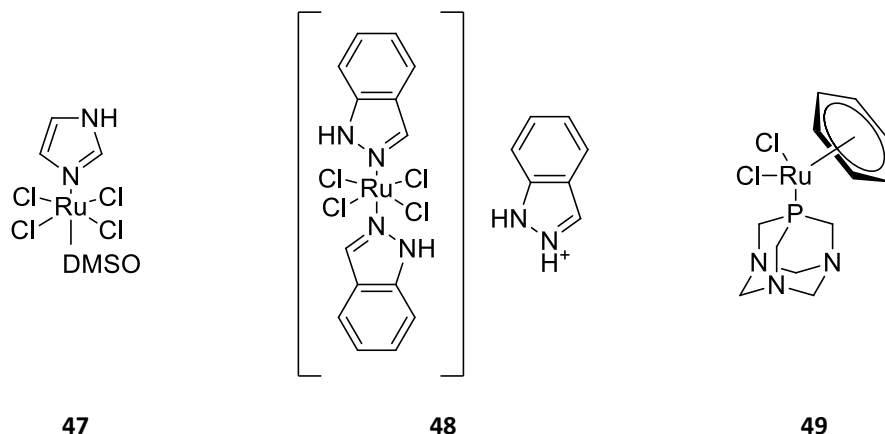


Figure 26 – Examples of ruthenium based complexes

1.2.3.6. Other metals under investigation

Other metals currently being investigated for their use in cancer treatment include gold (as structural, DNA binding and antimetastatic functions),⁷⁴ osmium (structural and photoluminescence mode of action),^{72,75} titanium (in the form of titanocene),⁷² iridium and rhodium (which in their half sandwich form are DNA intercalators as well as show structural activity)⁷² and cobalt (in the form of cobalt carbonyls, typically used as a carrier).⁷² While platinum, ruthenium, gold and iridium are expensive metals, there is potential for developing more active and significantly less expensive chemotherapies by using metals such as iron, zinc and copper. This also shows that there is still much to be discovered about hybrid compounds – in particular metal-containing hybrids.

1.3. Imidazo[1,2-*a*]pyridines

1.3.1. Synthetic History

A class of compounds that have sparked interest in the medicinal chemistry field are imidazo[1,2-*a*]pyridines (Figure 27). Structurally this ring system is fully aromatic, using the lone pair of electrons on nitrogen at position 4 to complete the aromaticity. They show significant biological activity, most notably as enzyme inhibitors, receptor ligands and anti-infectious agents.⁷⁶ Imidazo[1,2-*a*]pyridines are easily accessible through synthesis and can be customised to suit their intended biological function.⁷⁷

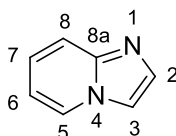


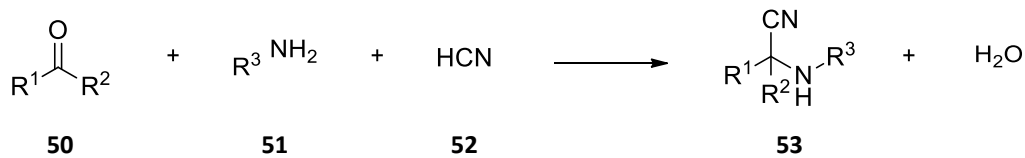
Figure 27 – The imidazo[1,2-*a*]pyridine ring and its numbering

The imidazo[1,2-*a*]pyridine ring system can be synthesized using a variety of approaches. These include condensation reactions (from α -halo, α -diazo and α -tosyloxyketones), tandem reactions (coupling 2-aminopyridines and nitroolefins or nitroalkenes), intramolecular C-H amination and multicomponent coupling reactions (commonly referred to as MCRs). A recent review by Bagdi *et al.* details these various approaches.⁷⁸ As the name suggests, multicomponent reactions consists of the combination of three or more reagents to form a product in such a way that the majority of the atoms of the starting materials can be found in the product. The starting materials do not react simultaneously, but as a sequence of reactions, the most favourable of which has an irreversible step which drives product formation. MCRs are also one-pot reactions that are simple to perform and since they are highly atom economical, can be performed under environmentally friendly conditions and generate fairly complex molecules in a single step make MCR's close to being an 'ideal' reaction. Using MCRs a wide variety of fairly complex compounds can be synthesized easily in essentially a single step.⁷⁷

Isocyanides have been found to be a particularly useful reagent in MCRs due to their α -acidity (which can be increased by the addition of electron-withdrawing groups in the α -position) and their ability to form radicals easily. Most importantly though, they react with nucleophiles and electrophiles at the isocyanide carbon atom resulting in an α -adduct product (a property only shared by carbon monoxide and carbenes).⁷⁷

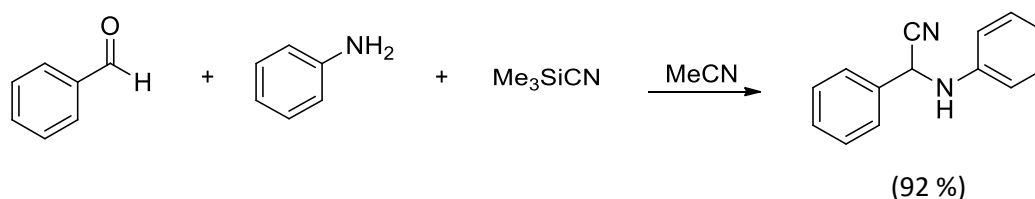
Introduction

The first published example of an MCR was reported by Strecker in 1850. Since this discovery, the coupling of an amine (**51**), a carbonyl (**50**) and a cyanide (hydrogen cyanide, **52**, or alkaline metal cyanides) to form α -amino-nitriles (**53**) has been named the Strecker reaction (Scheme 2).⁷⁹



Scheme 2 – The first type of MCR developed by Strecker

Over the years, the Strecker reaction has been modified to prevent the use of hydrogen cyanide (which is highly toxic); however, the new conditions meant that strong Lewis-acid catalysts were needed. More recently, the Strecker reaction has been further modified to make the reaction conditions both less harsh and safer to perform. An example of the more recent Strecker reaction is by Martinez *et al.* and is outlined in Scheme 3.⁷⁹

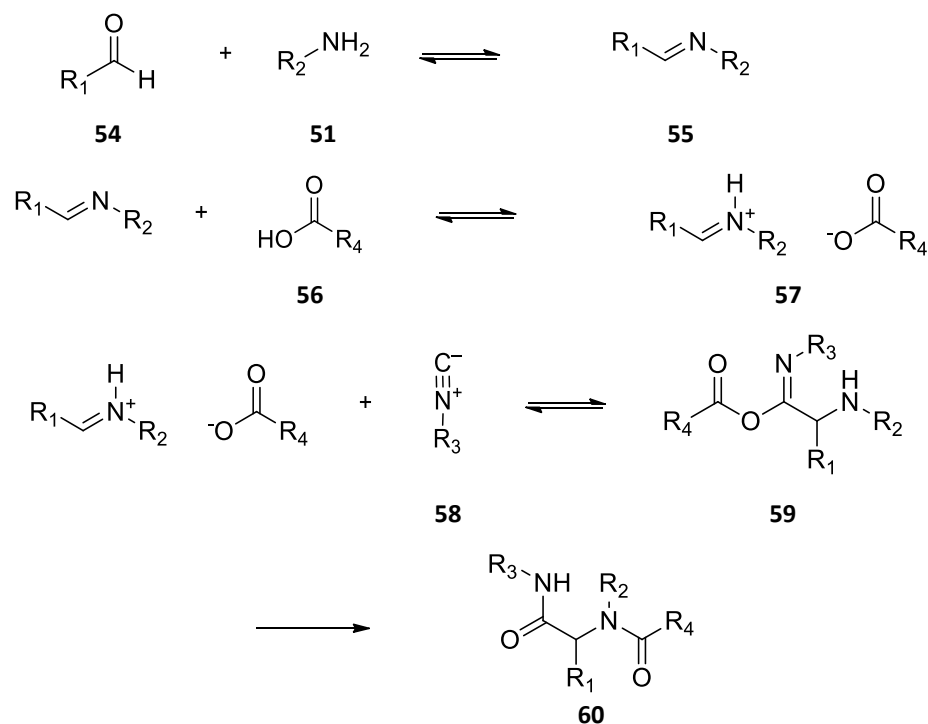


Reaction conditions: MeCN, 25 °C, 1-3 h.

Scheme 3 – A more recent example of the Strecker reaction

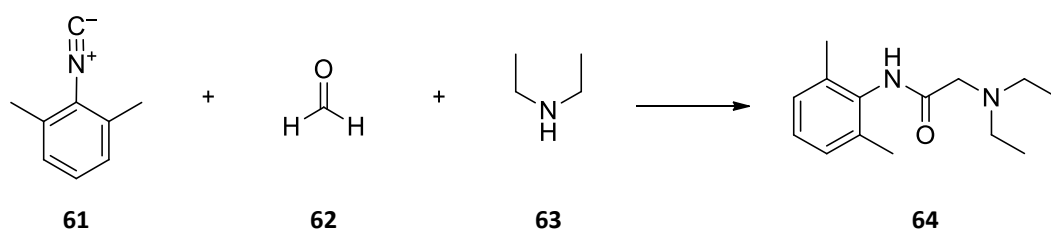
Another important type of MCR was discovered by Ugi in 1959.⁸⁰ Now commonly referred to as U-4CR, the reaction consists of four components; a primary amine, an aldehyde or ketone, an isocyanide and a carboxylic acid, which react to form an α -amino acylamide. Scheme 4 shows a simplified mechanism of the U-MCR, where the oxo component (**54**) and the amine (**51**) condense, via a hydroxyl aminal, to form the imine, (**55**, a Schiff base). While the formation of the Schiff base is not always necessary, the reaction works better if the base is activated. The activation occurs where the carboxylic acid (**56**) protonates the nitrogen atom of the Schiff base resulting in **57**, which increases the electrophilicity of the C=N bond. From there, the protonated imine and the nucleophilic acid anion (**57**) react with the isocyanide carbon atom (**58**) resulting in **59**, the α -adduct product. The stable Ugi product is obtained from an intramolecular acylation from a hydroxylamine to the more stable amide rearrangement, **60**.⁷⁷

Introduction



Scheme 4 – The Ugi multicomponent coupling reaction

The first important application of this was the single step synthesis of the anaesthetic xylocain (also referred to as lidocaine), **64** shown in Scheme 5, from 2,6-dimethylphenyl isocyanide (**61**), formaldehyde (**62**) and diethylamine (**63**). The reaction was performed in methanol with sodium formate (being a substitute for the carboxylic acid and not incorporated into the final structure).⁷⁷



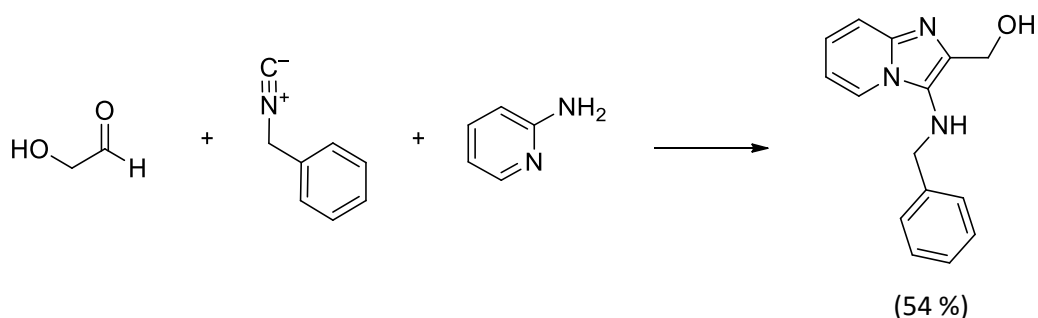
Reaction conditions: HCOONa, MeOH, reflux.

Scheme 5 – The MCR synthesis of xylocain (**64**)

Of interest for this PhD project is the Groebke-Blackburn-Bienaymé multicomponent reaction. Groebke and co-workers first published a novel one-pot synthesis of imidazo-annulated pyridines, pyrazines and pyrimidines in 1998. The Groebke-Blackburn-Bienaymé reaction involves the reaction of amino-pyridines, amino-pyrazines and amino-pyrimidines with aldehydes and

Introduction

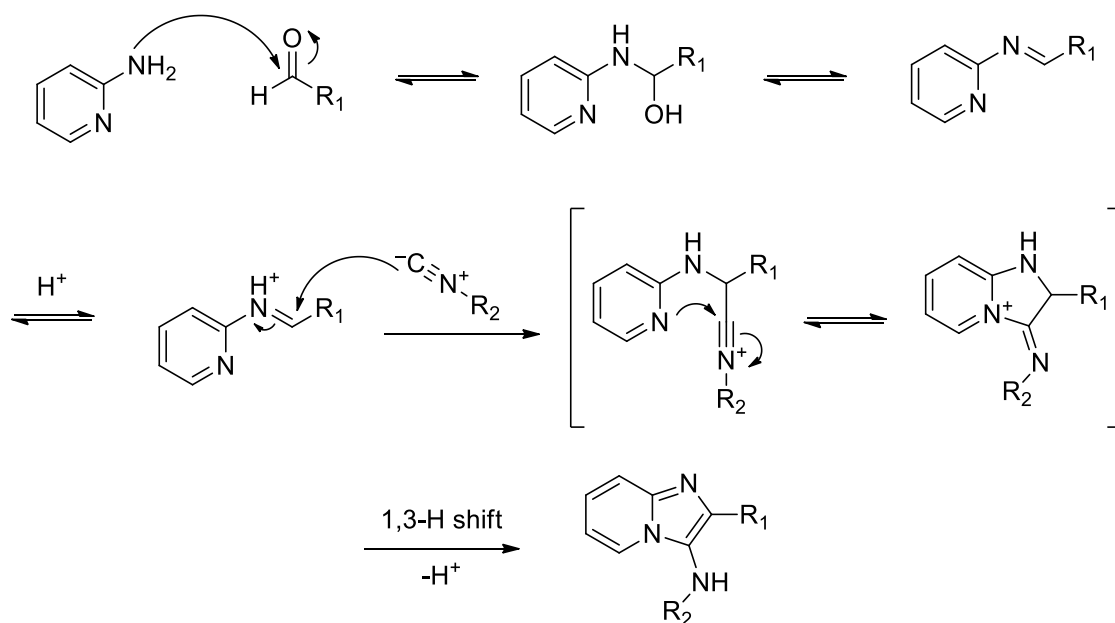
isocyanides. An example of the Groebke-Blackburn-Bienaymé reaction with amino pyridines is outlined in Scheme 6.⁸¹



Reaction conditions: AcOH (1-2eq), MeOH, rt, 18 h.

Scheme 6 – An example of the Groebke-Blackburn-Bienaymé multicomponent coupling reaction

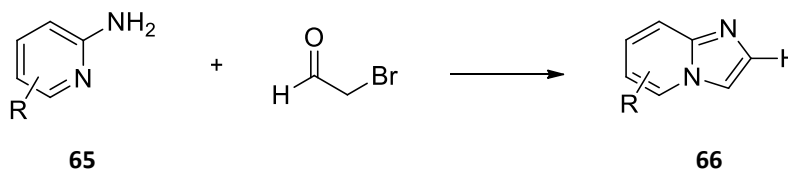
Groebke also proposed a mechanism for the assembly of imidazo[1,2-*a*]pyridines which is shown in Scheme 7. In a similar manner, imidazo[1,2-*a*]pyrazines and imidazo[1,2-*a*]pyrimidines can be formed from 2-aminopyrazines and 2-aminopyrimidines respectively.⁸¹



Scheme 7 – Proposed mechanism for the Groebke-Blackburn-Bienaymé MCC reaction

Following this initial synthesis, these compounds have been investigated for a host of potential biological applications. Published examples relevant to this project include those by Geuiffer *et al.* who investigated the use of imidazo[1,2-*a*]pyridines for treatment of cytomegalovirus and

varicella zoster virus which is especially dangerous in new-born babies and immune-suppressed patients. They reported the formation of imidazo[1,2-*a*]pyridine **66** from the condensation of a 2-aminopyridine derivative (**65**) with an R-halogenocarbonyl compound (such as bromoacetaldehyde, chloroacetone or phenacyl bromide) in ethanol (a general scheme for the reactions investigated is shown in Scheme 8).⁷⁶



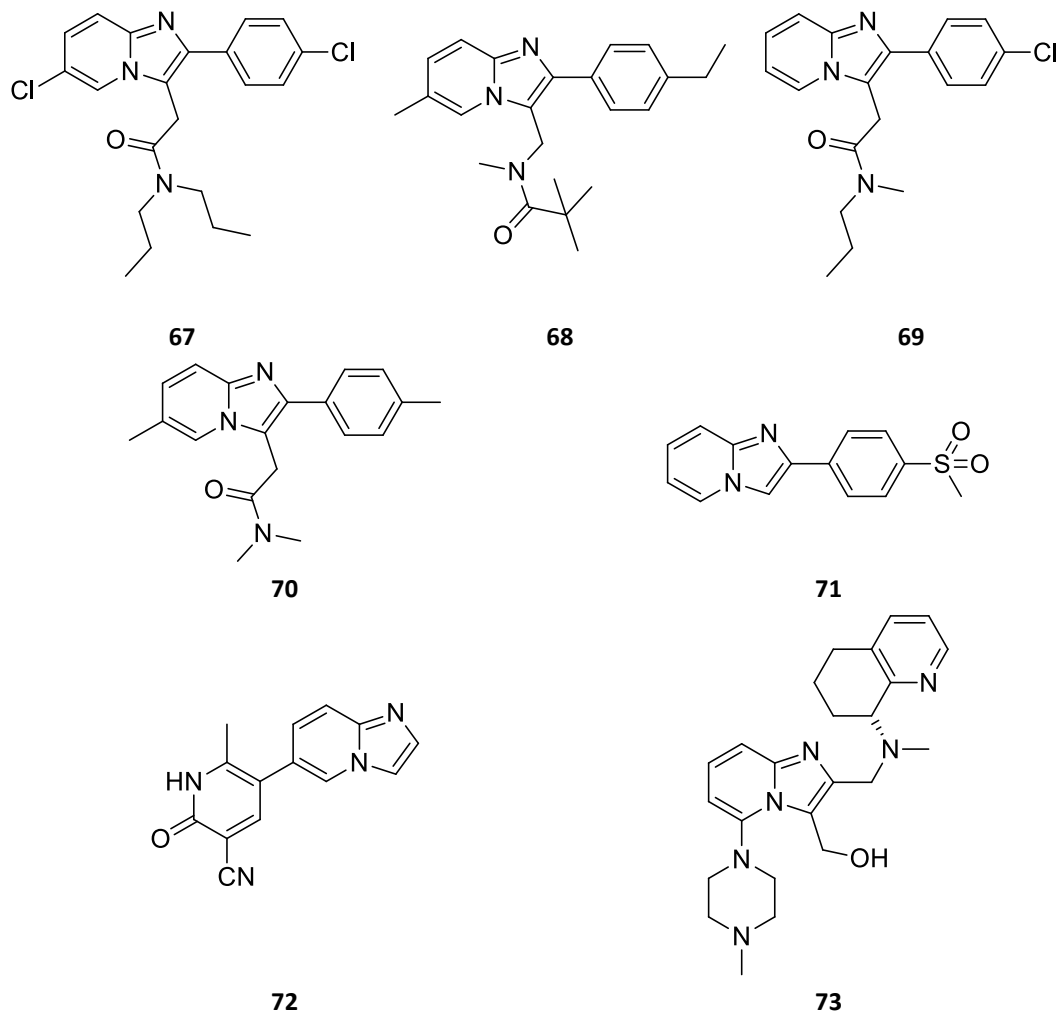
Reaction conditions: EtOH, reflux, 4 h.

Scheme 8 – An alternative one pot synthesis of imidazo[1,2-*a*]pyridines

1.3.2. Biological applications and further development

Given the significant biological activity exhibited by these compounds, it is not surprising that some imidazo[1,2-*a*]pyridines have been developed into commercially available drugs. Figure 28 below shows a selection of currently available drugs that are used to treat anxiety (**67**, **68** and **69**),^{82,83} insomnia (**70**),⁸² peptic ulcers (**71**),⁸⁴ acute heart failure (**72**)⁸⁵ and potentially to treat HIV (GSK812397, **73**).⁸⁶ It is interesting to note is that these compounds are mostly substituted with aryl groups at C-2, amide type chains at C-3 and that if there are any other substituents, they are typically at C-6. This could be an important biological feature to consider when designing new imidazo[1,2-*a*]pyridine drugs.

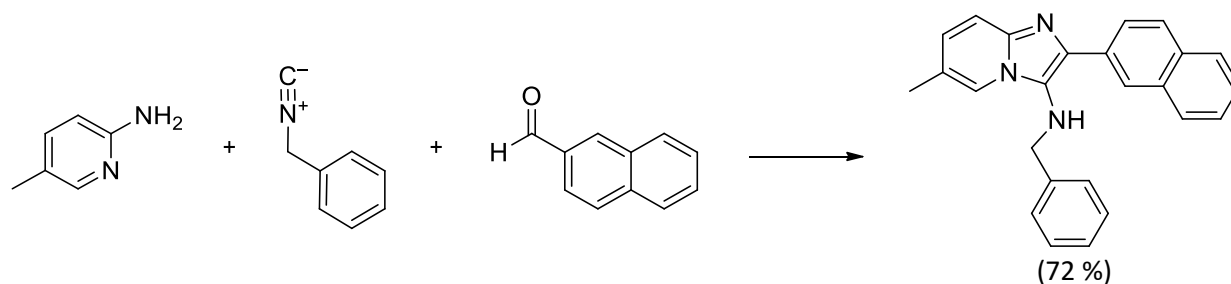
Introduction

Figure 28 – Commercially available imidazo[1,2-*a*]pyridines

Rousseau *et al.* also made use of the Groebke-Blackburn-Bienaymé MCR in their synthesis of imidazo[1,2-*a*]pyridines.⁸⁷ They reported that the conventional catalyst, scandium(III) triflate,⁸⁸ could be replaced with zinc(II) chloride or Montmorillonite K10 clay,⁸⁹ both of which are significantly more affordable than scandium(III) triflate. They did note, however, that zinc(II) chloride was not suitable for use with aminated aldehydes as the zinc forms stable complexes with the imine intermediate. Also investigated was the use of microwave irradiation to perform the MCR instead of utilizing conventional reflux reactions.⁸⁷

This was not the first mention of using microwave irradiation to perform one-pot MCR's. Ireland *et al.* performed Ugi-type MCR's under microwave conditions using scandium(III) triflate in methanol, an example of which is given in Scheme 9.⁹⁰

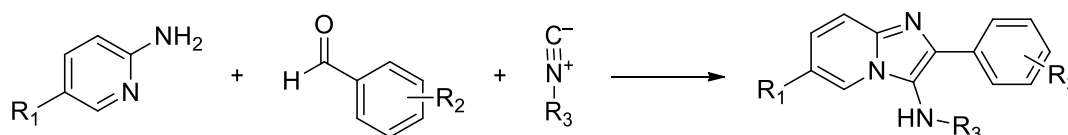
Introduction



Reaction conditions: $Sc(OTf)_3$ (5 mol % eq), MeOH, microwave, 200 W, 160 °C, 10 min.

Scheme 9 – Groebke-Blackburn-Bienaymé MCR using scandium(III) triflate in methanol

The Groebke-Blackburn-Bienaymé MCC reaction has also been investigated in our laboratory at the University of the Witwatersrand. A series of 6-substituted imidazo[1,2-*a*]pyridines were synthesized from 6-substituted 2-aminopyridines, substituted benzaldehydes and commercially available isocyanides in dioxane using Montmorillonite K10 clay as a catalyst. Scheme 10 outlines the general synthesis previously employed in our labs.⁹¹



$R_1 = NO_2, Br, Me$ or H

$R_2 = 2,4$ -dihydroxy, 3,4-dimethoxy, 2,5-dimethoxy, 3,4-dibenzyloxy, 2,4-dimethoxy

$R_3 =$ cyclohexyl, xylyl or benzyl

Reaction conditions: Montmorillonite K10 clay (1 mass eq), dioxane, reflux, 4-18 h.

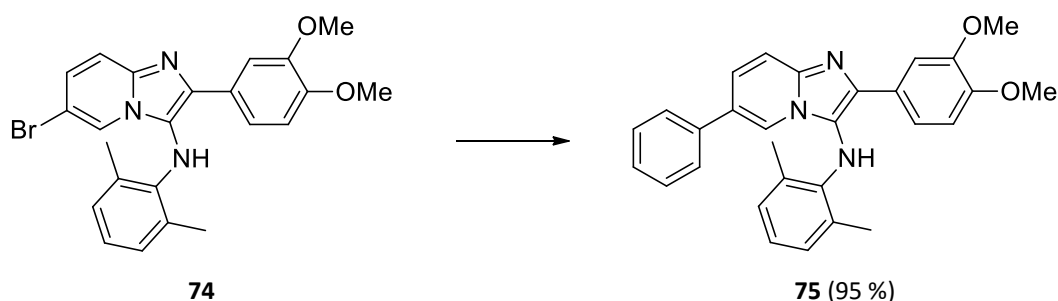
Scheme 10 – General synthesis for the imidazo[1,2-*a*]pyridines previously investigated in our laboratory

Of importance to this PhD, was that a number of imidazo[1,2-*a*]pyridines synthesized previously in our labs showed good activity against colon cancer cell lines HT-29 ($IC_{50} = 6.6$ -22.0 μM) and Caco-2 ($IC_{50} = 6.4$ -20.3 μM). Additionally these compounds showed little toxicity towards white blood cells – significantly better than camptothecin which it was compared to. This made these compounds of particular interest and their activity was described in a Full Patent Specification (PCT Int. Appl. (2010), WO 2010116302 A1 20101014).⁹² Further biological assays showed that the imidazo[1,2-*a*]pyridines trigger the process of apoptosis in the cancer cell lines HT-29 and Caco-2, causing the cancerous cells to die thus preventing the spread of the cancerous DNA mutations as well as destroying the cancer cells.⁹¹ This suggested that further development of these novel 6-substituted imidazo[1,2-*a*]pyridines may lead to compounds that could be used as

Introduction

potential anticancer agents and reduce the resistance to current chemotherapeutic regimens of the colorectal cancer cells.

Also noted in this study was that if there was a bromine substituent on the synthesized imidazo[1,2-*a*]pyridine ring, it provided a potential handle to further functionalise the ring by making use of Suzuki-Miyaura cross coupling with boronic acids as shown in Scheme 11 below. Making use of microwave irradiation, **74** was coupled to a simple phenyl boronic acid resulting in imidazo[1,2-*a*]pyridine **75**. It was found that this particular substituent change did not have a significant effect on the activity of the compound, with compounds **74** (HT-29 $IC_{50} = 7 \pm 2 \mu M$ and Caco 2 $IC_{50} = 6 \pm 1 \mu M$) and **75** (HT-29 $IC_{50} = 9 \pm 1 \mu M$ and Caco 2 $IC_{50} = 9 \pm 1 \mu M$) showing comparable IC_{50} values.⁹¹

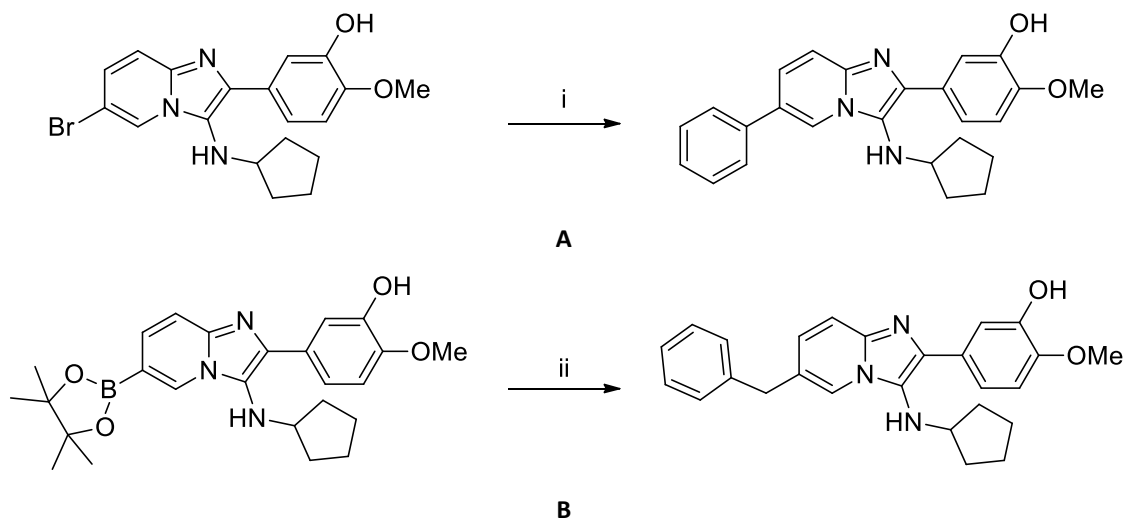


Reaction conditions: $Pd(PPh_3)_4$ (10 mol % eq), $PhB(OH)_2$ (1eq), CsF (2.5 eq), DME, microwave, 150 °C, 150 W, 20 min.

Scheme 11 – Suzuki-Miyaura coupling reaction to functionalise the imidazo[1,2-*a*]pyridine at the 6-position

The idea of functionalising the imidazo[1,2-*a*]pyridine was not novel. Odell *et al.* reported functionalization of the 6-position on imidazo[1,2-*a*]pyridines in their attempt to develop better *M. tuberculosis* glutamine synthetase (*MtGS*) inhibitors. They investigated Suzuki-Miyaura reactions using brominated imidazo[1,2-*a*]pyridines with various boronic acids (Scheme 12A) as well as converting the imidazo[1,2-*a*]pyridines into boronic acids and reacting them with benzyl bromides (Scheme 12B). These reactions were performed using microwave conditions. Although they did not successfully generate more active *MtGS* inhibitors, it is an example of functionalised imidazo[1,2-*a*]pyridines.⁹³

Introduction

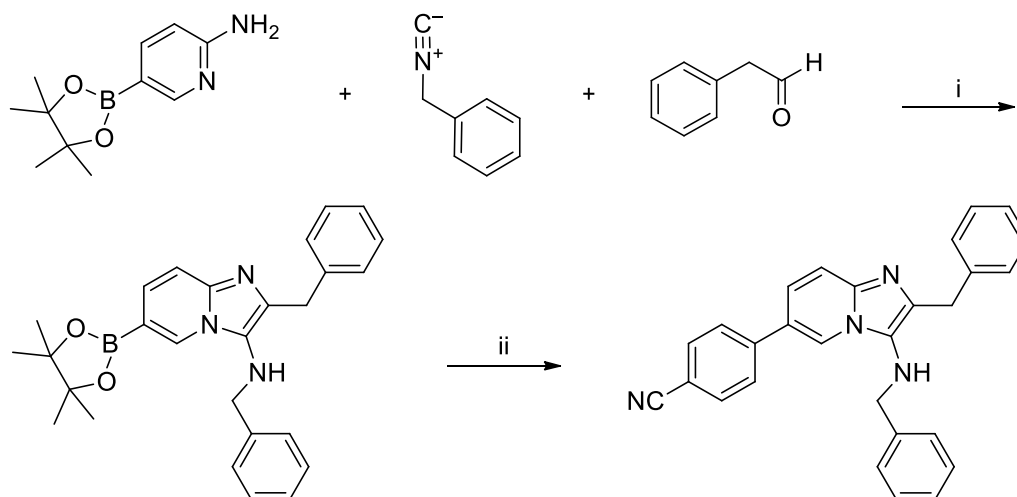


Reaction conditions: i) $\text{Ph}(\text{B}(\text{OH})_3)$ (3 eq), $\text{Pd}(\text{PPh}_3)_4$ (7 mol %), Cs_2CO_3 (3.5 eq), DMF, microwave, 120 °C, 20 min; ii) benzyl bromide (0.8 eq), $\text{Pd}(\text{dppf})\text{Cl}_2$ (10 mol %), K_2CO_3 (3 eq), EtOH, H_2O , microwave, 130 °C, 30 min.

Scheme 12 – An example where the imidazo[1,2-*a*]pyridine was functionalised using boronic acids (A) as well as where it can be made into a boronic acid (B)

Di Mauro and Kennedy made use of an interesting one pot microwave-assisted four-component coupling. They investigated the synthesis of substituted imidazo[1,2-*a*]pyridine-type boronic acids using microwave irradiation and then performing Suzuki-coupling with aromatic bromides in the same reaction vessel, an example of which is shown in Scheme 13. The remarkable stability of the pinacol ester was noted, even under the harsh conditions experienced in a microwave. With ethanol or methanol as the solvent, magnesium chloride was used as the catalyst in the Groebke-Blackburn-Bienaymé reaction (Scheme 13) while the Suzuki-Miyaura reaction was catalysed by [1,1'-bis(diphenylphosphino)ferrocene]dichloropalladium(II) ($\text{Pd}(\text{dppf})\text{Cl}_2$) instead of the traditionally used tetrakis ($\text{Pd}(\text{PPh}_3)_4$).⁹⁴

Introduction



Reaction conditions: i) MgCl_2 (4 mol %), MeOH, microwave, 160 °C, 10 min; ii) aq K_2CO_3 , $\text{Pd}(\text{dppf})\text{Cl}_2$ (10 mol %), microwave, 90 °C, 30 min.

Scheme 13 – An aminopyridine-containing boronic acid in the MCR (i) and then it being used in a Suzuki-Miyaura coupling reaction (ii)

A recent review on metal-catalysed functionalization of imidazo[1,2-*a*]pyridines highlights a variety of different possibilities for further functionalization. These include well known palladium catalysed reactions such as Heck, Sonogashira and Suzuki-Miyaura cross coupling reactions, Stille cross coupling reactions, copper mediated Buchwald reactions and arylation reactions amongst others.⁹⁵ This suggests that there are numerous approaches that could be used to install a variety of different functionalities onto the imidazo[1,2-*a*]pyridine post ring formation. There are two main advantages to this in that firstly it allows for a much larger library of compounds to be synthesized with the aim of investigating small libraries for biological activity. Secondly, of interest to this project was that it provides a unique opportunity to build a tether/linker onto the ring which could potentially be used to form hybrid type compounds.

1.3.3. Metal imidazo[1,2-*a*]pyridine complexes

A relatively unexplored feature of the imidazo[1,2-*a*]pyridines is the potential reactivity of the free lone pair on nitrogen 1 (see Figure 29). This aspect of the imidazo[1,2-*a*]pyridines is of significance to this project and there are only a handful of reports of metal coordination to this nitrogen, most of these investigated for their potential use in new materials rather than for medicinal properties.

Forniés *et al.* were amongst some of the first to report the synthesis of a metal-imidazo[1,2-*a*]pyridine complex. They reported the synthesis of several platinum imidazo[1,2-*a*]pyridine complexes (such as **76**, **77** and **78** in Figure 29) in order to study their luminescence properties for

potential applications in materials chemistry. Only compounds **77** and **78** showed significant luminescence and perhaps more interestingly, **77** shows luminescent thermochromism; phosphorescing green at 77 K but orange-red at 298 K.⁹⁶

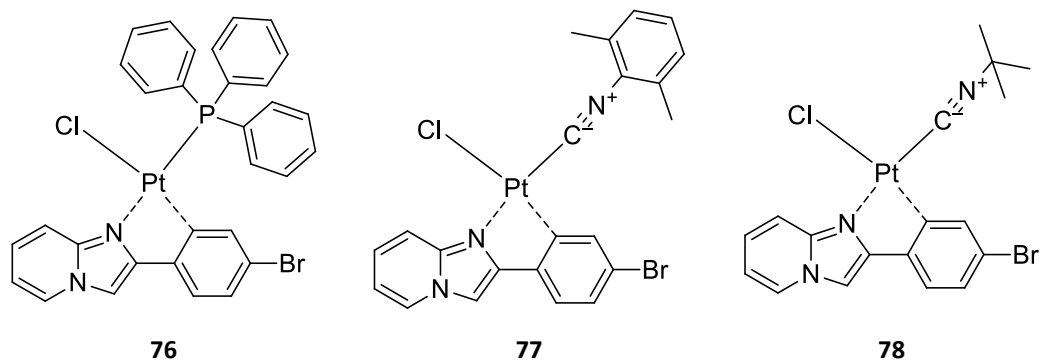


Figure 29 – Platinum-containing imidazo[1,2-*a*]pyridines

Another early example of metal-imidazo[1,2-*a*]pyridine complexes was provided by Yong *et al.* where they synthesized a zinc coordination polymer with imidazo[1,2-*a*]pyridines (such as Figure 30). This polymer showed significant antiferromagnetic coupling between the radicals and red-yellow-green fluorescence emission that could be taken advantage of in LED's or as part of an electroluminescence device.⁹⁷ This was later expanded to include cobalt derivatives as well as to vary the counter ion and incorporate a 1,4-benzenedicarboxylate coordination in the polymer. The cobalt derivatives showing a change in magnetic phase transition at 344 K.⁹⁸

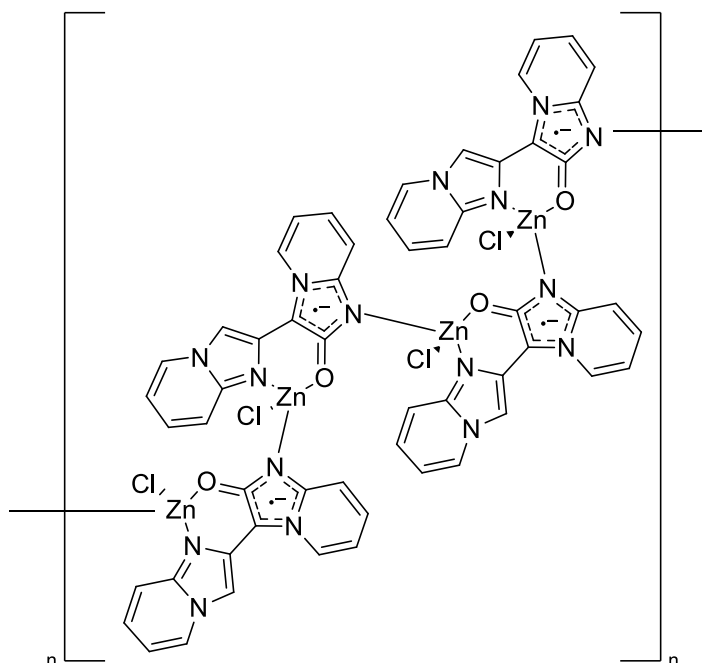


Figure 30 – An example of a zinc-imidazo[1,2-*a*]pyridine polymer

Introduction

Liu *et al.* investigated zinc and nickel coordinative metal imidazo[1,2-*a*]pyridine polymers in a similar manner to Yong *et al.* They incorporated 1,3-benzenedicarbonate and 1,3,5-benzenetricarbonate into the polymers in addition to the 1,4-benzenedicarbonate used by Yong *et al.* Resulting from this study was that reaction temperature influenced the type of polymer formed and that the zinc compounds also showed fluorescent properties.⁹⁹

A computational and crystallographic study by Malecki compared the coordination energies of **79** (Figure 31) to **80**. They found that the donation of the ligands to the Pd(II) was greater than the back donations from the metal to the ligand. Complex **80** was also calculated to be a stronger ligand than **79**, and **79** not exhibiting any fluorescent properties.¹⁰⁰

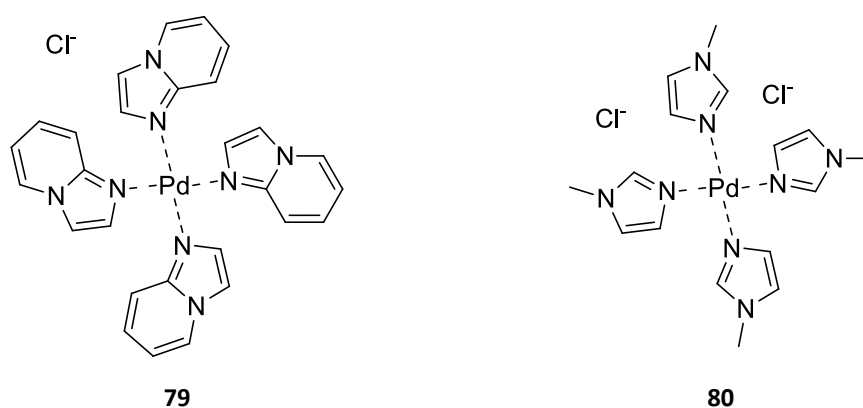


Figure 31 – Palladium-containing imidazo[1,2-*a*]pyridine and imidazole derivatives

An unusual reported application of metal imidazo[1,2-*a*]pyridine coordination complexes was reported by Li *et al.* where they synthesized ruthenium(II) based complexes to be used as catalysts for the transfer hydrogenation of ketones. After synthesising imidazo[1,2-*a*]pyridine **81**, they formed a neutral catalyst, **82** as well as a charged catalyst, **83** (Figure 32). Catalyst **83** was found to be the most efficient catalyst, where a variety of ketones could be reduced to secondary alcohols by refluxing them in isopropyl alcohol with a 0.1 mol % catalyst loading.¹⁰¹

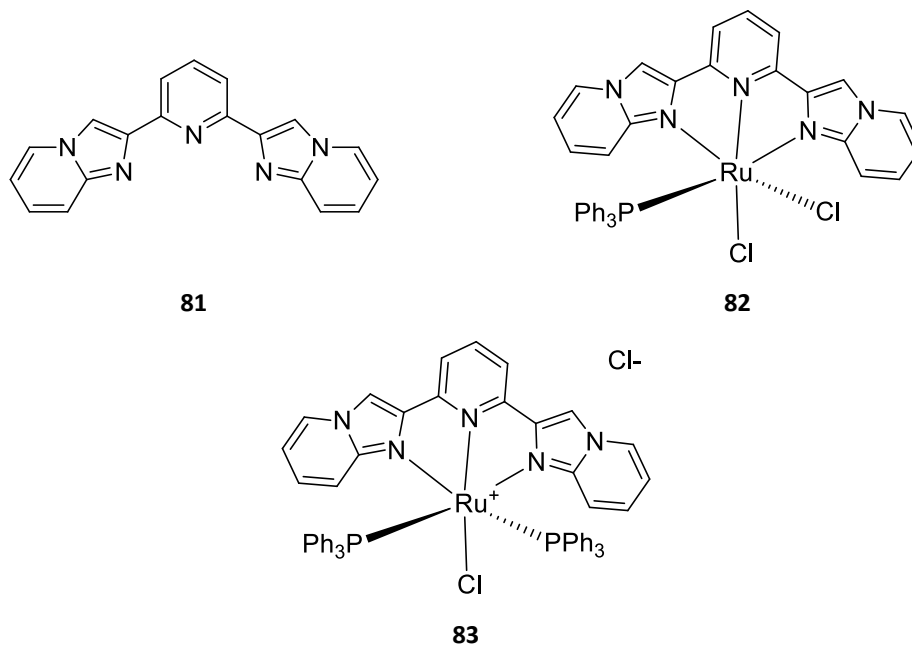


Figure 32 – Examples of ruthenium-containing imidazo[1,2-*a*]pyridines

1.4. Project Introduction

The broad aim of this project was to improve and develop the novel imidazo[1,2-*a*]pyridine derivatives synthesized in our laboratories that showed good activity against cancer cell lines, while attempting to inflict as little damage to healthy cells as possible.

The imidazo[1,2-*a*]pyridines previously investigated had substituents at the 2 and 3 positions, with most also having substituents at the 6-position. All the compounds had aromatic substituents at the 2-position while the 3-position typically contained xylamine or cyclohexylamine substituents. The most biologically active imidazo[1,2-*a*]pyridines from the previous study in our laboratory were **84** and **75** (Figure 33), with IC_{50} values of 6.57 ± 1.91 and $8.56 \pm 1.22 \mu\text{M}$, respectively, against HT-29 colorectal cells and 6.43 ± 1.01 and $8.73 \pm 1.28 \mu\text{M}$, respectively, against Caco-2 colorectal cancer cells.⁹¹

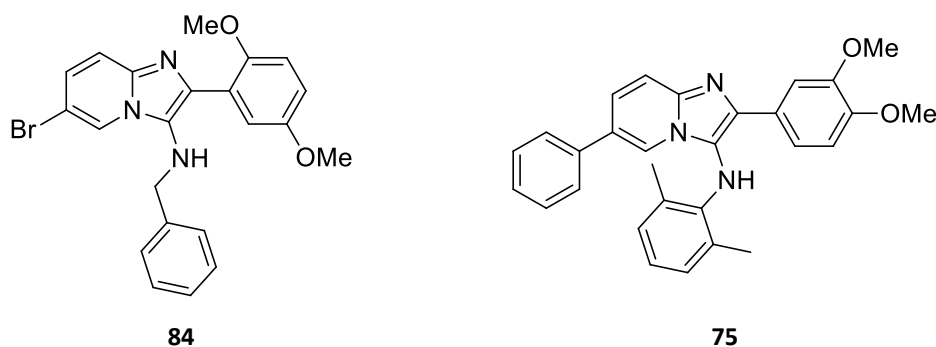


Figure 33 – Examples of imidazo[1,2-*a*]pyridines synthesized by de Koning and co-workers

This project aimed at expanding the compound library tested against the colorectal cell lines to determine if there is some selectivity of these compounds towards cancer cell lines. The first aim of this research was to use the Groebke-Blackburn-Bienaymé MCC synthetic methodology used previously⁹¹ to generate an expanded library, optimizing⁹¹ the reaction conditions and purification protocol.

Given the lack of research into the synthesis of metal imidazo[1,2-*a*]pyridine complexes, particularly for biological applications, in this project a second major aim was to develop methods for synthesis of such compounds with a variety of different metals, such as platinum, zinc and copper. The approach proposed was to form a new “hybrid” molecule containing both an active imidazo[1,2-*a*]pyridine ring as well as an active metal centre. There have been few reports of the preparation of bifunctional hybrid compounds containing platinum-based molecules as anticancer drugs,⁴⁷ however it has not been satisfactorily explored. It is this area of research we proposed to explore by combining our anticancer imidazo[1,2-*a*]pyridines with metal-containing compounds (e.g. cisplatin) to form the bifunctional hybrid adducts. Finally, a third aim, also of

Introduction

interest to this project was to see if metals other than platinum can improve the activity of the imidazo[1,2-*a*]pyridines not just for colorectal cancer, but other cancer cell lines (such as breast cancer and leukemia) where traditional metal-based chemotherapies are lacking.

While there has been some research done on investigating the synthesis of metals coordinated to imidazo[1,2-*a*]pyridines, the examples are limited to platinum,⁹⁶ zinc¹⁰² and nickel.⁹⁹ To the best of our knowledge, there are no reported platinum complexes of imidazo[1,2-*a*]pyridines specifically as anticancer agents, or other reported metal hybrid imidazo[1,2-*a*]pyridines that exhibit anticancer properties.

Of key importance to this project was to establish if the formation of these hybrid molecules would result in lower toxic side effects as compared to traditional platinum derived drugs for anticancer treatment.

From a chemistry standpoint, two approaches were considered in this project. The first was to take advantage of the free lone pair of electrons on the N1 of the imidazo[1,2-*a*]pyridine ring and coordinate the metal directly to the imidazo[1,2-*a*]pyridine core. The second approach was to investigate methods for adding a tether to the imidazo[1,2-*a*]pyridines and coordinate the metal to the tether compounds. To the best of our knowledge, there have been only a few reports to modify the imidazo[1,2-*a*]pyridine structure,^{93,94} and no examples of these modifications to be used as tethers.

At the end of my tether:

Results and Discussion

2.1. Synthesis and development of imidazo[1,2-*a*]pyridine library

The research done by de Koning and co-workers was limited in scope with a small library of compounds, making it impossible to determine any structure-activity relationships.⁹¹ Also considering that the exact target of these compounds was unknown, a larger library of compounds needed to be synthesized and investigated in order to draw any conclusions about structure-activity relationships. We determined that there were three main substituent areas that could be varied (shown in Figure 34) – the R₁ substituent resulting from the 2-aminopyridine, the R₂ substituent derived from the aldehyde and the R₃ from the isocyanide used.

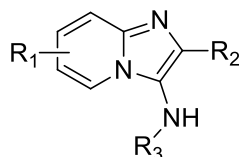


Figure 34 – The three main areas for modification of the imidazo[1,2-*a*]pyridine nucleus

Nearly all of the compounds in the previous study contained a R₁-substituent in the 6-position on the imidazo[1,2-*a*]pyridine ring (See Figure 27). Thus the first series of imidazo[1,2-*a*]pyridines investigated in this PhD also needed to contain a substituent in this 6-position and the focus was placed on varying the substituents at the R₂ and R₃ positions. A bromide substituent at this 6-

position was settled on largely because it could later be modified utilizing well-known chemical reactions. Using the methodology outlined by de Koning and co-workers, commercially available 5-bromo-2-aminopyridine was refluxed in dioxane with other commercially available isocyanides and aldehydes with Montmorillonite K10 clay as a catalyst, a library of imidazo[1,2-*a*]pyridines was synthesized. Figure 35 shows the compounds synthesized using this methodology along with their corresponding yields.

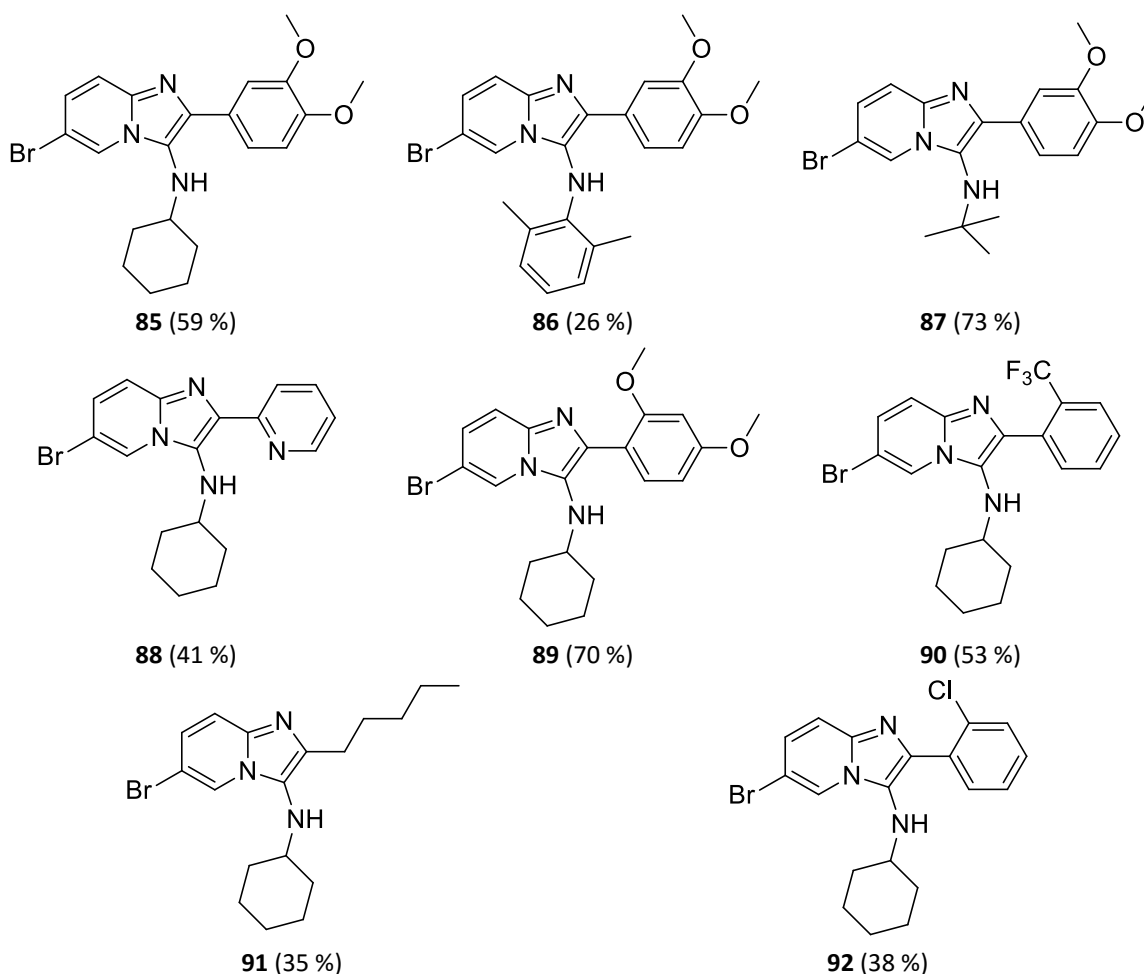
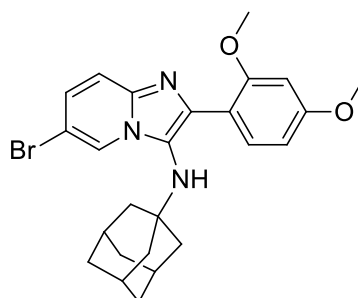


Figure 35 – The first series of imidazo[1,2-*a*]pyridines synthesized (85 - 92)

Recently it has been shown that the addition of adamantyl substituents to biologically active molecules notably improves the overall activity of the compound.¹⁰³ With this in mind we decided to introduce an adamantyl moiety onto the imidazo[1,2-*a*]pyridine nucleus. The simplest strategy to do so would be from the R₃ substituent stemming from adamantyl isocyanide. While adamantyl isocyanide is commercially available, its high cost led to us synthesising it from adamantylamine (discussed later). Once synthesized it was used in the Groebke-Blackburn-Bienaymé multicomponent coupling reaction to result in imidazo[1,2-*a*]pyridine **93** in an excellent yield of 93% as shown in Figure 36 below.

**93 (93 %)****Figure 36 – An adamantane-containing imidazo[1,2-*a*]pyridine (93)**

Filtering all of the reaction mixtures directly through a Celite/flash silica gel plug in a glass frit funnel was found to successfully remove both the K10 clay as well as most of the dark brown sticky by-product that formed during the course of the reaction. After concentration *in vacuo* most of the resulting products solidified. All of the compounds except **91** were purified by recrystallization from an appropriate solvent. Compound **91** was a liquid and so was purified by means of column chromatography as the reaction was performed on a much smaller scale. Compound **93** was also purified by column chromatography. The varying yields obtained are unfortunately characteristic of this reaction. Throughout literature it has been noted that the yields are notoriously unpredictable and substrate and catalyst dependant.⁸⁷

NMR spectroscopic analysis of these compounds revealed characteristic imidazo[1,2-*a*]pyridine signals for each of the compounds in Figure 35 and Figure 36. The absence of any aldehyde signals and the presence of N-H signals along with the relevant substituent peaks confirmed the structure of these compounds. Of particular interest to highlight is the ¹³C NMR spectral shift of the bromine substituted C6 at approximately 106 ppm; the presence of bromine in the imidazo[1,2-*a*]pyridines was also confirmed by the characteristic bromine isotopes (⁷⁹Br and ⁸¹Br) in the HRMS spectra. A few unusual splitting patterns were noted, one of which is the coupling of the amine N-H proton for certain compounds (**85**, **88**, **90** and **92**) to the methine C-H on the cyclohexyl ring.

During the recrystallization process it was noted that large volumes of boiling solvent were required to completely dissolve the compounds. Once dissolved, the solvent volume was then greatly reduced before the solution reached saturation point and compounds could crystallize out of solution. This suggested that strong intra- and intermolecular bonding existed between the molecules. Single Crystal X-ray Crystallography (SCXRD) was then used to investigate how selected compounds behaved in the solid state to try to rationalise what was seen in the laboratory.

Interestingly, during the recrystallization of **85** both block and needle crystals were isolated from the recrystallization. NMR spectroscopic analysis of these compounds did not show a significant difference, bar the presence of what appeared to be a small water signal in the ^1H NMR spectrum in the block crystals. From SCXRD it was discovered that the block crystals formed a hydrate crystal, where a water molecule was hydrogen bonded to **85** through $\text{O3w}-\text{H3b}\cdots\text{N1}$ ($d = 1.97 \text{ \AA}$) and $\text{C11}-\text{H11}\cdots\text{O3w}$ ($d = 2.56 \text{ \AA}$) as shown in Figure 37A. Of additional importance in this structure is the presence of an intramolecular hydrogen bond, $\text{C15}-\text{H15}\cdots\text{N24}$ ($d = 2.62 \text{ \AA}$). In contrast, Figure 37B shows the crystal structure for the needles collected. This structure only contains the intramolecular $\text{C11}-\text{H11}\cdots\text{N24}$ hydrogen bond ($d = 2.48 \text{ \AA}$). This distance is shorter than that of the hydrate and suggests that this particular hydrogen bond is weakened slightly when the molecule is involved in hydrogen bonding elsewhere in the molecule.

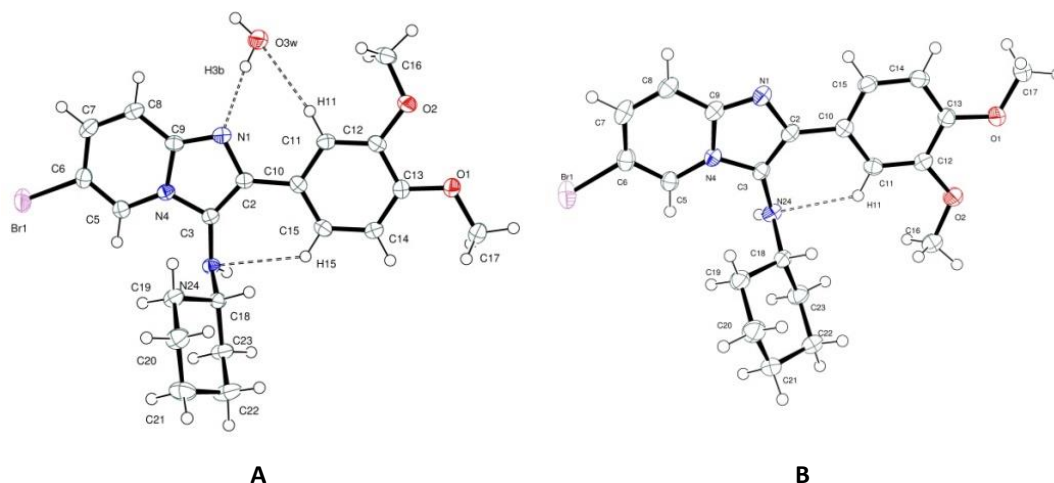


Figure 37 – The asymmetric units of the block and needle crystals of **85**

The crystal structure of imidazo[1,2-*a*]pyridine **89** showed hydrogen bonding between $\text{N24}-\text{H24}\cdots\text{O1}$ ($d = 2.19 \text{ \AA}$). In Figure 37A and B the imidazo[1,2-*a*]pyridine core and the aryl R_2 substituent were in the same plane allowing for π stacking in the unit cell. As can be seen in Figure 38, however, there is a torsion angle of $42.7(1)^\circ$ between the imidazo[1,2-*a*]pyridine ring and the R_2 aryl substituent in **89** which prevents any π stacking. Most likely this is the reason that **89** shows better solubility than that of **85** in organic solvents.

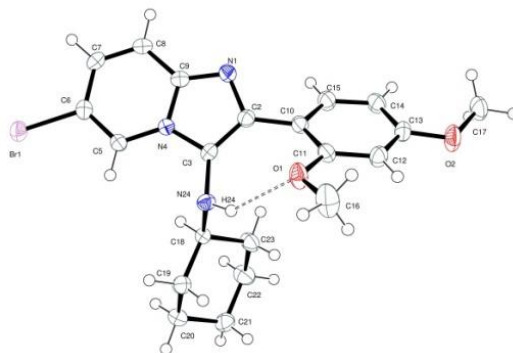


Figure 38 – The asymmetric unit of **89**

Looking at a considerably different imidazo[1,2-*a*]pyridine, **90** in Figure 39, the only intramolecular hydrogen bonding occurs between C17—H17a···F1 ($d = 2.55 \text{ \AA}$). The imidazo[1,2-*a*]pyridine ring and the R_2 fluorinated aryl group are at an angle of $107.3(1)^\circ$ to each other. This is most likely attributed to the bulky nature of the CF_3 group and consequently prevents significant π stacking from occurring, making the imidazo[1,2-*a*]pyridine the most soluble of all.

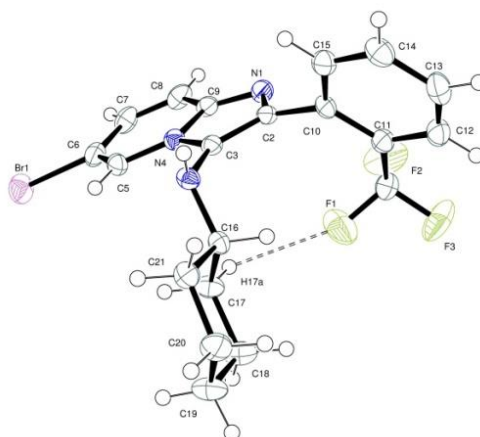


Figure 39 – The asymmetric unit of **90**

Naturally we also needed to investigate compounds with in positions other than 6, as well as compounds without any R_1 substituents. In order to address this, the first series was expanded by synthesizing imidazo[1,2-*a*]pyridines from commercially available 2-aminopyridine, 2-amino-6-bromopyridine and 2-amino-3-bromopyridine. Completely removing the bromine atom from the molecule was not favourable as it would prevent further modification post imidazo[1,2-*a*]pyridine formation. For this reason moving the bromine atom to a position on the R_2 aryl substituent was also investigated. Making use of bromobenzaldehyde derivatives allows this feature to be retained. The next series of compounds and yields are shown in Figure 40.

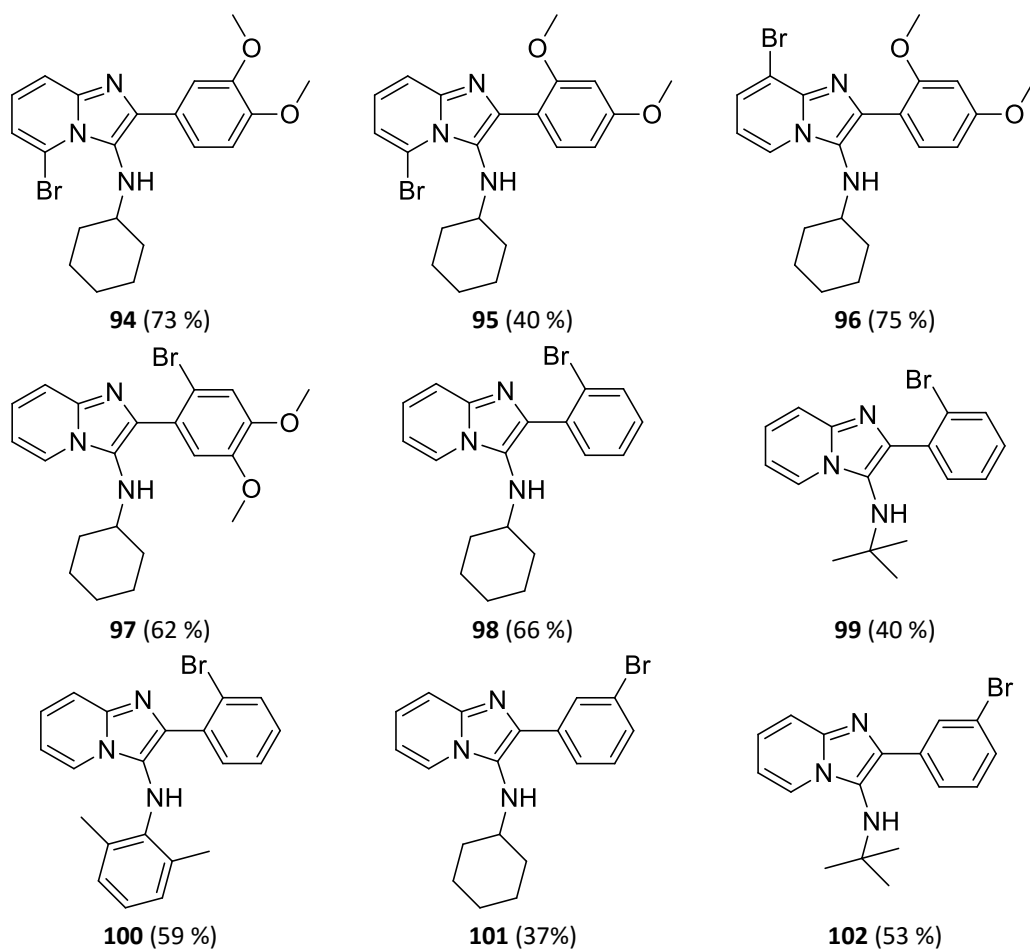


Figure 40 – Imidazo[1,2-*a*]pyridines varying the R₁ substituent (94 - 102)

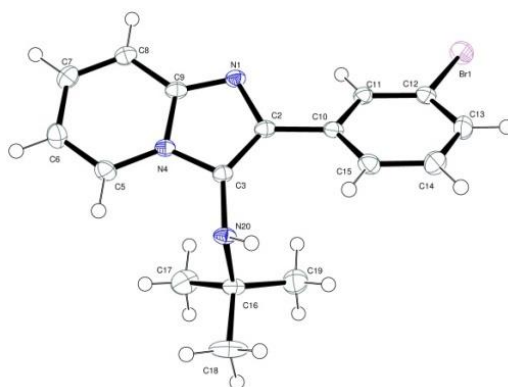
It is quite evident that the yields for many of the reactions were unsatisfactory, especially if these compounds were to be used in a further series of reactions. In an attempt to increase the yields of the reactions the products were purified by column chromatography to determine if the low yields were a result of the recrystallization process. Unfortunately, the method of purification did not appear to have an effect on the yield. While many articles have also noted the unpredictability of yields, the type of solvent used has been shown to have an effect. In order to investigate this, the synthesis of **102** was repeated using water and ethanol. Results from this are shown in Table 1 where it was noted that using ethanol resulted in the best yield and additionally the reaction was found to be much cleaner and easier to recrystallize. All further reactions were then carried out in this solvent system.

Table 1 – Resulting yields from varying the solvent in the formation of 102

Solvent	Yield
Dioxane	53 %
Ethanol	63 %
Water	50 %

The structures of the compounds in Figure 40 were again confirmed largely by NMR spectral analysis. Characteristic imidazo[1,2-*a*]pyridine signals were observed for these compounds, the ^1H and ^{13}C NMR spectral signals shifted appropriately with the variation in the position of the bromine substitution. In compounds **95**, **96**, **97**, **98** and **101** the N-H signals were observed as doublets, suggesting that the N-H couples to the methine C-H on the cyclohexyl ring. High resolution ESI-MS again revealed the presence of bromine on these molecules showing the characteristic isotopic peaks.

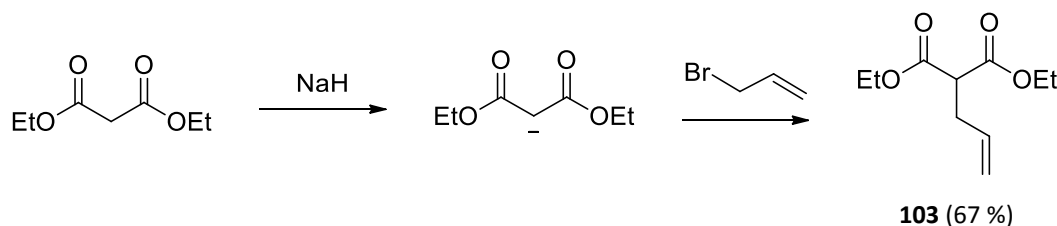
The crystallization of **102** from ether resulted in the formation of block crystals which were analysed using SCXRD. Figure 41 shows that in this structure there are no intramolecular hydrogen bonds. However, in the unit cell there is intermolecular hydrogen bonding between C15—H15...N1 ($d = 2.66 \text{ \AA}$) and N20—H20...N-1 ($d = 2.47 \text{ \AA}$). This compound was significantly more soluble than those described in Figure 35, and the lack of notable intramolecular bonding interactions seen in Figure 41 may account for this change in solubility.

**Figure 41 – The asymmetric unit of 102**

2.2. Attempts at modification of the imidazo[1,2-*a*]pyridine

In order to use these imidazo[1,2-*a*]pyridines as part of a hybrid molecule, we envisaged that a tether needed to be added to the imidazo[1,2-*a*]pyridine in order to house the platinum (or another metal) atom. The 'house' would need to consist of atoms that would favour metal chelation – such as oxygen or nitrogen atoms – and these atoms arranged in a manner that would allow for favourable geometry once coordinated. The 'house' would be linked to the imidazo[1,2-*a*]pyridine by a carbon linker of different chain lengths and this linker could be attached using a variety of different reactions. We believed the best type of 'house' to introduce would be a 1,3-diol or a 1,3-diamine.

The most convenient way to introduce the 1,3-diol or the 1,3-diamine was by reduction of a diethyl malonate or malononitrile derivative. While in some instances the diethyl malonate and malononitrile could be used directly, the 1,3-dicarbonyl needed to be functionalised further to include an alkene. Using a procedure by Ahmed *et al.*, the diethyl malonate was converted into diethyl 2-allylmalonate (**103**) after the addition of sodium hydride and allyl bromide as outlined in Scheme 14.¹⁰⁴ Unfortunately, **103** was found to polymerise easily and so had to be freshly prepared and distilled right before use in further reactions.



Reaction conditions: NaH (1.1 eq), allylbromide (1.5 eq), THF, 0 °C.

Scheme 14 – Synthesis of tether 103

¹H and ¹³C NMR spectroscopy was used to confirm the formation of compound **103**, where extensive coupling resulted in complicated spectra. Distinctive ethoxy signals were observed at approximately 4.2 ppm (OCH₂) and 1.2 ppm (CH₃) in the ¹H NMR spectrum as well as 61 ppm (OCH₂) and 14.12 ppm (CH₃), respectively, in the ¹³C NMR spectrum. The presence of an ester carbonyl signal was also observed at 169 ppm. Typical ester-type stretches were also noted on the IR spectrum at 1730 and 1643 cm⁻¹.

We attempted to synthesize 2-allylmalononitrile (**104** in Figure 42) using a similar procedure, however none of **104** was isolated, instead the diallylmalononitrile (**105** in Figure 42) formed even when reducing the reaction time and the equivalents of NaH added.



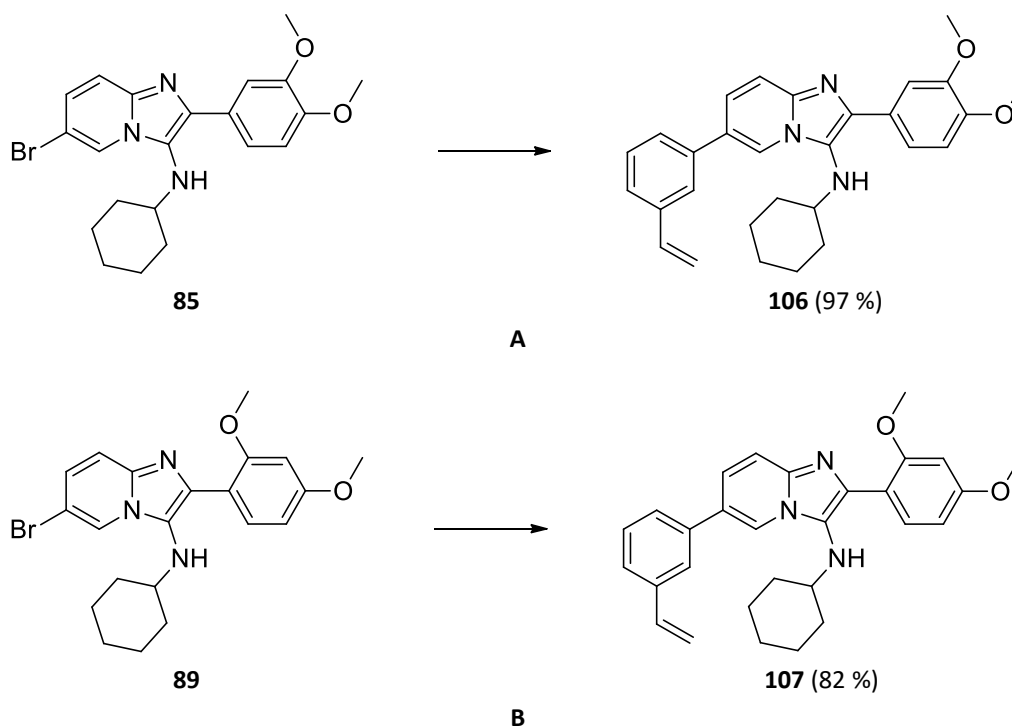
Figure 42 – 2-allylmalononitrile (**104**) and diallylmalononitrile (**105**)

2.2.1. Using the Suzuki-Miyaura Cross Coupling Reaction to build the tether

At the commencement of this project, there was little literature supporting modifications being made to an imidazo[1,2-*a*]pyridine ring after synthesis. One of these was reported by de Koning and co-workers, using Suzuki-Miyaura cross coupling to introduce a phenyl substituent at the 6-position.⁹¹ This concept was expanded upon during this PhD, where substitutions were made at the bromine on the imidazo[1,2-*a*]pyridines with a variety of commercially available boronic acids. The use of substituted phenylboronic acids provides the addition of functional groups that could be further be built upon.

Suzuki-Miyaura cross coupling reactions have been used extensively in our laboratories, and reliable methods for both conventional and microwave synthesis have been developed.¹⁰⁵ Using microwave irradiation, the Suzuki-Miyaura coupling reaction was performed on the relevant imidazo[1,2-*a*]pyridines using catalytic amounts of Pd(PPh₃)₄ in dimethoxyethane (DME) using cesium fluoride (CsF) as the base. Reaction conditions were typically 150 °C at 120 Watts for 15-20 minutes. While this is a quick and easy method it is limited by the scale of the reaction (only applicable for reactions on a 100-300 mg scale). Conventionally, the reactions were performed under inert reflux conditions with catalytic Pd(PPh₃)₄ and 2M Na₂CO₃ in DME overnight.

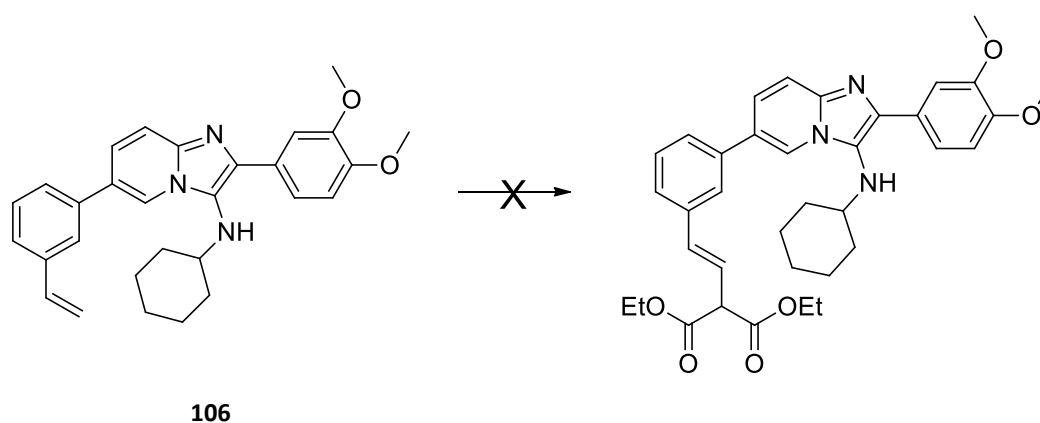
The first boronic acid of interest was 3-vinylphenylboronic acid which was conducted using microwave conditions. Using two different imidazo[1,2-*a*]pyridines, the reactions were highly successful in yields of 97 % for **106** and 82 % for **107** (Scheme 15). Spectroscopically, the aromatic region was found to be significantly more complicated than for the starting materials, with the addition of 4 more aromatic protons. In addition to this, the most significant changes on the ¹H NMR spectrum were the appearance of the three alkene protons at 6.81, 5.79-5.91 and 5.33 ppm for **106** and 6.80, 5.84 and 5.32 ppm for **107**. Similarly the presence of 6 additional aromatic carbon signals on the ¹³C NMR spectrum further indicated the presence of the vinyl phenyl group as well as the alkene carbon signals at 114.75 and 136.70 ppm for **106** and 114.57 and 136.59 ppm for **107**.



Reaction conditions: 3-vinylphenylboronic acid (1.5 eq), CsF (2.5 eq), Pd(PPh₃)₄ (10 mol %), DME, 150 °C, 150 W, 20 min.

Scheme 15 – Suzuki-Miyaura cross coupling reactions to form 106 (A) and 107 (B)

Attaching 3-vinylphenylboronic acid to the imidazo[1,2-*a*]pyridine ring allowed for the addition of a terminal alkene that could then be reacted with **103** by means of cross metathesis using the Grubbs II catalyst. An example of what we hoped to achieve is outlined in Scheme 16, but unfortunately these reactions were unsuccessful, despite extensive investigation.



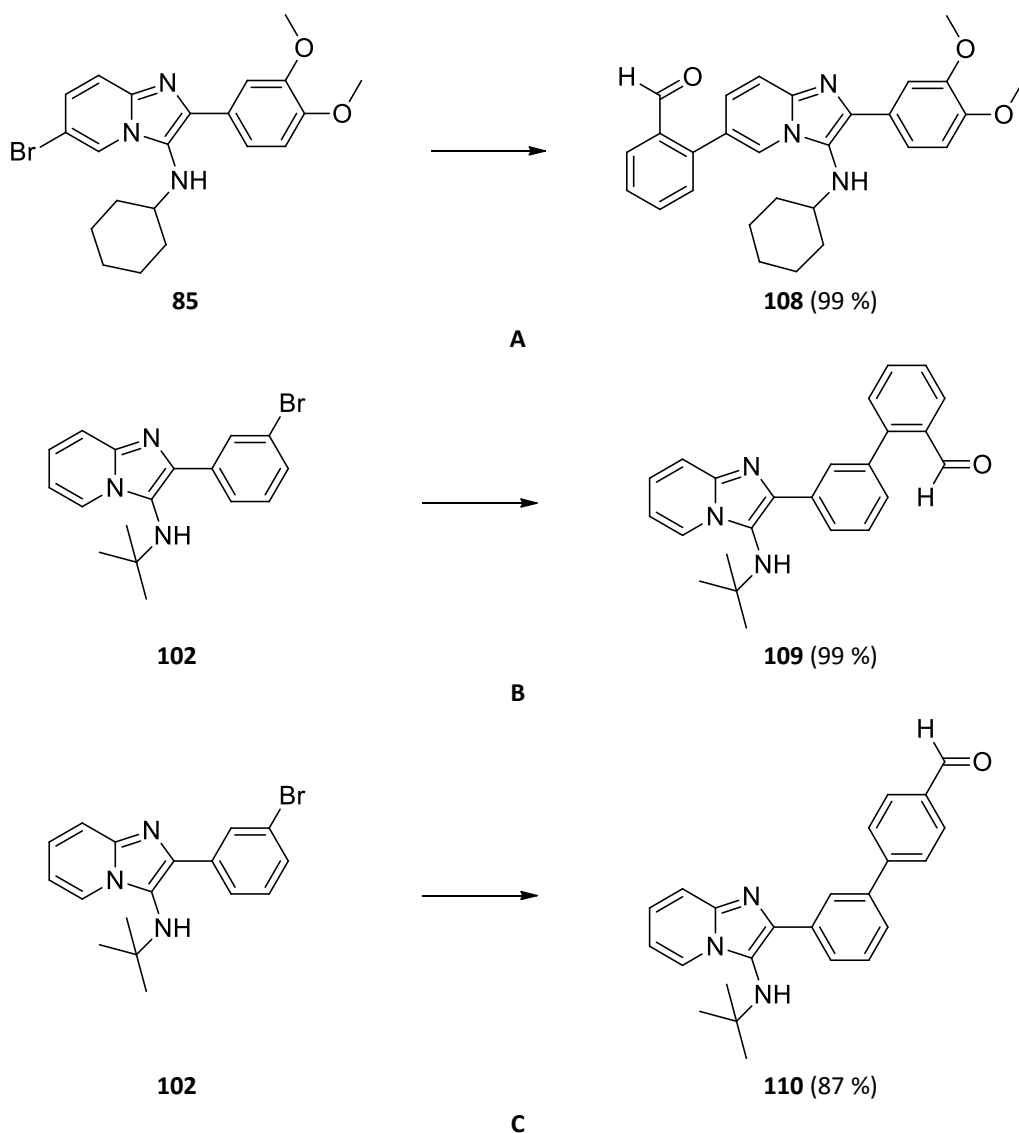
Reaction conditions: **103** (2 eq), Grubbs II (5-15 mol %), toluene or DCM or DCE, reflux, 24 h; **103** (2 eq), Hoveyda Grubbs (10 mol %), toluene, 24 h.

Scheme 16 – An example of the cross metathesis attempted during this project

Given the failure of cross metathesis to occur on the already formed imidazo[1,2-*a*]pyridine, cross metathesis was attempted on the aldehyde precursor for the reaction. The Suzuki-Miyaura coupling reaction of 2-vinylphenyl boronic acid with 3-bromobenzaldehyde was successful, however the product was not isolated due to the compound rapidly polymerizing once purified.

Since the cross metathesis attempts were unsuccessful, another approach needed to be sought. The next attempt was made by using 2- and 4-formylphenylboronic acid. Substitution at the 6-position (Scheme 17A) as well as on the bromophenyl substituent at the 2-position (Scheme 17, B and C) were investigated for these reactions. Conventional methods were used for the synthesis of **108**, which, after purification by column chromatography, was afforded in a quantitative yield. Both **109** and **110** were also synthesized using conventional heating methods and obtained in excellent yields.

Characterisation of these compounds was done spectroscopically, with an increase of 4 aromatic signals being observed in the ^1H and ^{13}C NMR spectra. Also evident are the aldehyde protons at 10.09 (**108**), 10.04 (**109**) and 10.03 (**110**) ppm in the ^1H NMR spectrum and the aldehyde carbonyl signal at 191.5 (**108**), 192.5 (**109**) and 191.9 (**110**) ppm in the ^{13}C NMR spectrum. This was further supported by the presence of carbonyl stretches for each compound on the IR spectra; 1691 cm^{-1} on compound **108**, 1681 cm^{-1} on **109** and 1711 cm^{-1} on compound **110**.



Reaction conditions: 2- or 4-formylphenylboronic acid (1.5 eq), 2M Na₂CO₃ (5 eq), Pd(PPh₃)₄ (10 mol %), DME reflux, 18 h.

Scheme 17 – Suzuki-Miyaura cross coupling reactions performed using conventional methods

The structure of aldehyde **108** was also confirmed by SCXRD (Figure 43), where an intramolecular C11—H11···N18 hydrogen bond ($d = 2.56 \text{ \AA}$) as well as an intermolecular N18—H18···O1 hydrogen bond ($d = 2.31 \text{ \AA}$) was noted. The imidazo[1,2-*a*]pyridine ring and the dimethoxyphenyl substituent at the R₂ position are arranged in a similar plane (at an angle of 19.3(1)° to each other) while the formylphenyl C₆ substituent is twisted at 52.3(1)° to the main ring structure. The torsion in this molecule prevents π stacking and probably as a consequence of this the general solubility of **108** was vastly improved in comparison to the starting material, **85**.

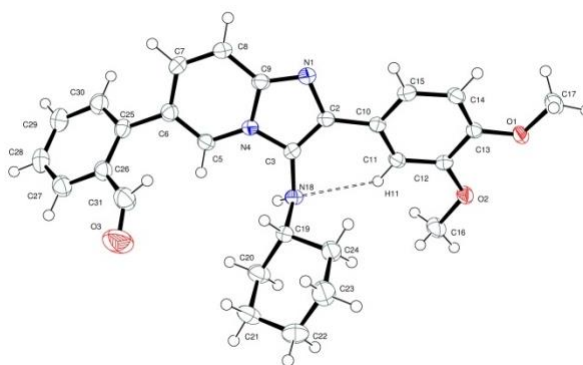
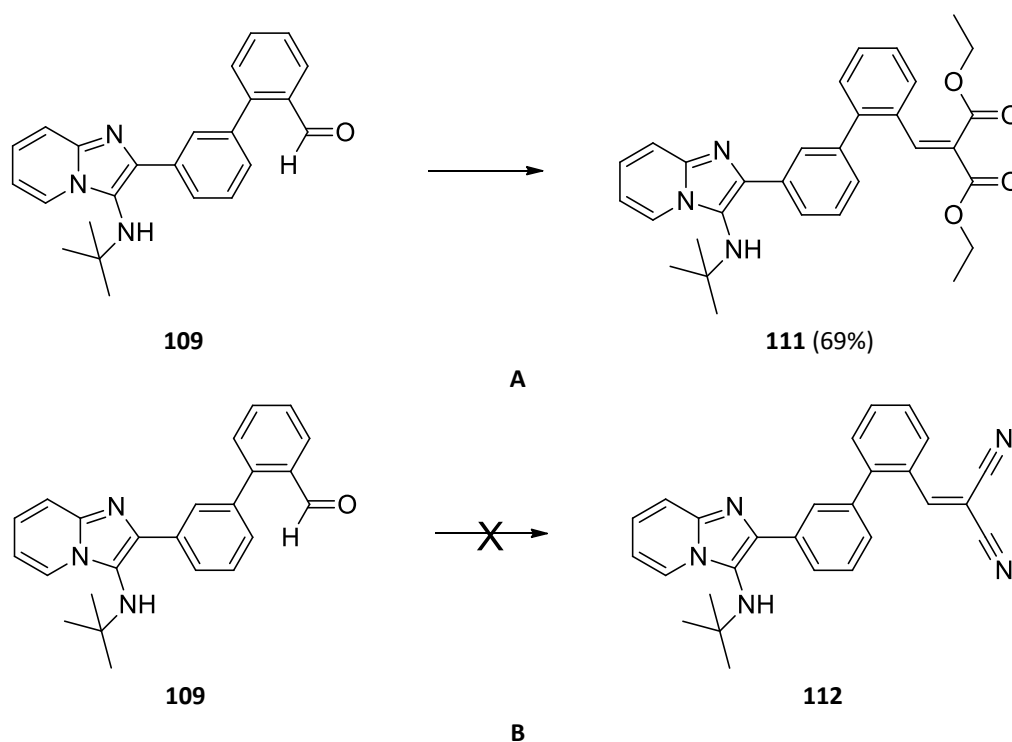


Figure 43 – The asymmetric unit of **108**

Diethyl malonate and malononitrile could then be reacted with the benzaldehyde substituent of **109** by means of a Knoevenagel condensation as shown in Scheme 18A. The method for this condensation was adapted from work by Gu and Holland,¹⁰⁶ where **109**, either diethyl malonate (Scheme 18A) or malononitrile (Scheme 18B), piperidine and benzoic acid were combined in toluene under inert Dean-Stark conditions. This resulted in the successful formation of compound **111** with diethyl malonate in a yield of 89 %. However the Knoevenagel condensation using malononitrile to form **112** was not successful.

The ¹H NMR spectrum for **111** shows a conjugated alkene proton signal at 8.0 ppm along with the OCH₂CH₃ signals at 4.28 (2H), 4.12-4.23 (2H) and 1.14-1.27 ppm (6H). The ¹³C NMR spectrum also showed the corresponding changes, where the alkene carbon signals were observed at 143.4 and 127.3 ppm, and the OCH₂CH₃ carbon signals at 61.4, 61.3, 14 and 13.9 ppm. Also noted were the ester carbonyl signals at 166.4 and 163.8 ppm.



Reaction conditions: Diethyl malonate (1.5 eq), piperidine (0.2 eq), benzoic acid (0.1 eq), toluene, Dean-Stark, reflux, 18 h.

Scheme 18 – Knoevenagel condensation reactions for the successful synthesis of 111 (A) and the unsuccessful synthesis of 112 (B)

The final step in the synthesis was to reduce **111** to the corresponding diol. In theory, this reduction could be performed using lithium aluminium hydride (LiAlH_4), however these reductions were unexpectedly unsuccessful, bringing this approach to another dead end.

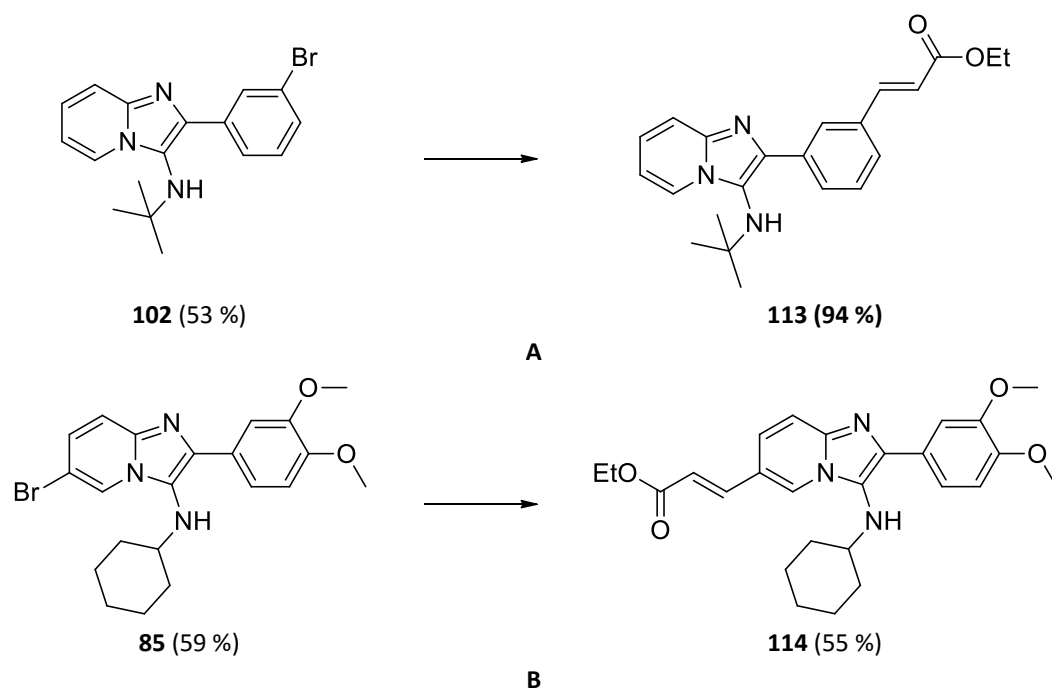
2.2.2. Heck coupling reactions

Changing tack slightly, we opted to make use of a Heck coupling reaction in an attempt to add a slightly shorter tether to the imidazo[1,2-*a*]pyridine. The method for this synthesis was adapted from previous work done in our lab by Riaan Petersen, where palladium(II) acetate ($\text{Pd}(\text{OAc})_2$) and *tri(o-tolyl)phosphine* were combined with the brominated and alkene-containing reagents in an acetonitrile/dimethylformamide/water solvent mixture.¹⁰⁷ However, it was found that in order for the reaction to occur, the formation of the active palladium catalyst from $\text{Pd}(\text{OAc})_2$ (which is reduced to Pd^0) and *tri(o-tolyl)phosphine* in the solvent mixture under inert conditions at 40 °C was essential before any of the reactants could be added. Once the catalyst had formed, the imidazo[1,2-*a*]pyridine (either **85** or **102**) was dissolved in more acetonitrile and added to the mixture along with ethyl acrylate, triethylamine and additional dimethylformamide. This was left to react at 78 °C under inert conditions overnight. Temperature control was very important to

this reaction; too low and the reaction would not go to completion, when above 80 °C the active catalyst decomposed.

An unforeseen problem with this synthesis was the significant coordination of the tri(*o*-tolyl)phosphine to the imidazo[1,2-*a*]pyridine ring. The reactions were monitored by TLC and only a single new spot appeared, however despite numerous attempts at purification using column chromatography the tri(*o*-tolyl)phosphine remained visible in the ¹H and ¹³C NMR spectra. It was found that the best method to purify these compounds was in fact to use a modification of the work up procedure. After quenching the reaction, the organic layer was washed several times with 1M hydrochloric acid. The imidazo[1,2-*a*]pyridine was found in the acidic layer while the tri(*o*-tolyl)phosphine remained in the organic layer. Neutralization of the acid with solid sodium bicarbonate forced the imidazo[1,2-*a*]pyridine out of the water layer and extraction with ethyl acetate, drying and concentration *in vacuo* resulted in pure **113** (Scheme 19A).

The reaction shown in Scheme 19B did not go to completion, and so even post acid extraction **114** was separated from the starting material (**85**) by flash column chromatography. Ester **114** was isolated in a mediocre yield of 55 %. The presence of the vinylic protons was evident at 7.76 and 6.54 ppm for **113** and 7.65-7.70 and 6.40 ppm for **114**. Additionally, the ester CH₂ quartet and CH₃ triplet protons were evident at 4.27 and 1.33 ppm for **113** and 4.29 and 1.36 ppm, respectively, for **114**. The presence of the ester carbonyl signals at 166.8 and 167.0 ppm in the ¹³C NMR spectra and the carbonyl stretches (1707 cm⁻¹ for **113** and 1709 cm⁻¹ for **114**) in the IR spectra for each compound further support the successful formation of the desired compounds.



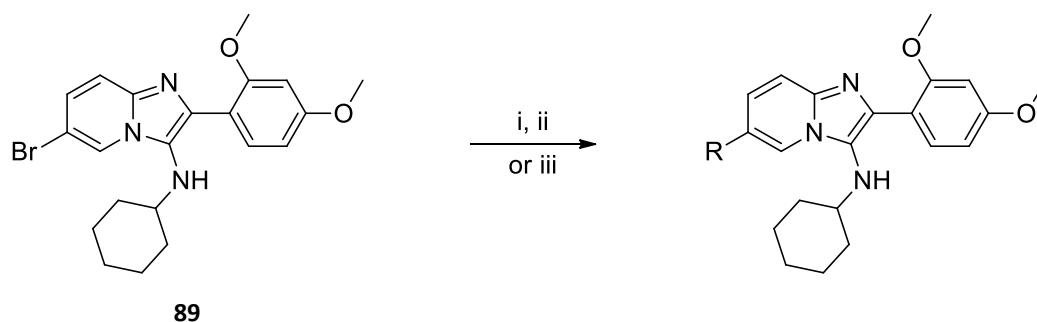
Reaction conditions: Ethyl acrylate (1 eq), Pd(OAc)₂ (0.4 eq), P(*o*-tolyl)₃ (1.6 eq), NEt₃ (10 eq), MeCN/DMF/H₂O, 70 °C, 18 h.

Scheme 19 – Heck cross coupling reactions to form 113 and 114

Following the addition of an ester based tether, the next objective was to hydrolyse the ester to an acid and attempt to chelate the acid to a metal. The hydrolysis of the ester to the carboxylic acid appeared to be successful, however the resulting product was significantly insoluble such that further development, of this idea along these lines was not possible.

2.2.3. Attempted modification using arylation-type reactions

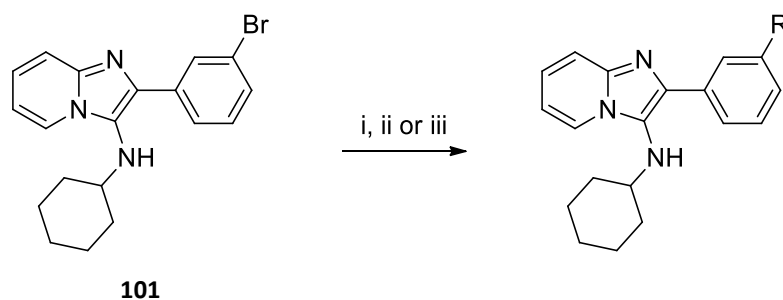
Considering that we had no information about the mechanism of the action or the biological target of the active site of the imidazo[1,2-*a*]pyridines we thought it prudent to investigate building tethers of shorter length than those previously synthesized. In order to do so, we investigated adding shorter tethers onto the imidazo[1,2-*a*]pyridine using arylation-type reactions. Using diethyl malonate or malononitrile and attaching it directly to the imidazo[1,2-*a*]pyridine, as shown in Scheme 20, would allow for such a tether.



Reaction conditions: i) Malononitrile (1.1 eq), NaOBu^t (3 eq), PCy₃ (3 mol %), PdCl₂ (1 mol %), THF, reflux; ii) diethyl malonate (1.1 eq), K₃PO₄ (1.5 eq), [Pd(PPh₃)₄Cl₂] (5 mol %), THF, reflux; iii) Malononitrile (1.1 eq), NaH (1.5 eq), [Pd(PPh₃)₄Cl₂] (5 mol %), THF, reflux.

Scheme 20 – Conditions for arylation reactions at the 6-position considered in this project

At the time of synthesis, again there was little literature available for performing these reactions on imidazo[1,2-*a*]pyridines so a variety of methods were investigated based on arylation reactions performed on pyridine rings.¹⁰⁸ Despite extensive investigation, none of the methods were successful and starting material was recovered in each case. We considered that substitution directly on the imidazo[1,2-*a*]pyridine directly might be problematic and so, as we did with the Suzuki-Miyaura and Heck reactions, we attempted to add the tether to a bromine substituent at onto the substituent benzene ring (as shown in Scheme 21). Unfortunately once again starting material was recovered from these reactions.



Reaction conditions: i) malononitrile (1.1 eq), NaH (1.5 eq), [Pd(PPh₃)₄Cl₂] (5 mol %), THF, reflux; ii) Diethyl malonate (1.1 eq), NaH (1.1 eq), Pd(OAc)₂ (5 mol %), dppf (7 mol %), THF, reflux; iii) Diethyl malonate (1.1 eq), Cs₂CO₃ (1 eq), CuI (25 mol %), 2-phenylphenol (0.5 eq), THF, 50 °C.

Scheme 21 - Conditions for arylation reactions on the R₂ aryl substituent considered in this project

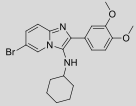
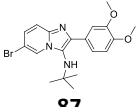
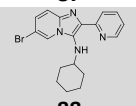
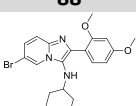
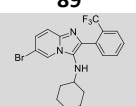
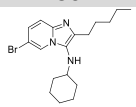
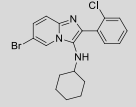
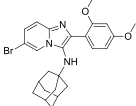
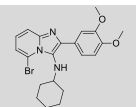
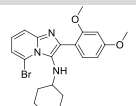
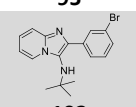
2.3. Results from Biological Testing

The imidazo[1,2-*a*]pyridines (Figure 35, Figure 36 and Figure 40) synthesized thus far were sent to Dr Leonie Harmse at the Pharmacology Department at WITS Medical School for biological testing and formed the basis for the Master of Science in Medicine (Pharmacology) for Somayya Ragie¹⁰⁹ and Taurai Kurebwa¹¹⁰ and current MSc student Zeenat Ismail.¹¹¹ All of the biological results reported in this thesis were generated by Ragie, Kurebwa and Ismail and details of the experiments performed investigating the mode of action of these compounds can be found in their dissertations.

Firstly, the Caco-2 and HT-29 colorectal cancer cell lines were investigated by Ragie¹⁰⁹ as in the previous study by de Koning and co-workers⁹¹ but additional cell lines were also tested to investigate the full potential of the synthesized imidazo[1,2-*a*]pyridine. The new cell lines include MCF-7 and MDA-MB231 (breast cancer cell lines investigated by Kurebwa¹¹⁰) and leukemic cell lines, K562 and HL-60 investigated by Ismail.¹¹¹ All the compounds were initially screened at a fixed dose of 200 μ M in each cancer cell line using an 3-(4,5-dimethylthiazol-2-yl)-2,5-diphenyltetrazolium bromide (MTT) assay. Only the compounds that resulted in a >20% cell viability after dosing for 48 hours were carried through to obtain IC₅₀ values. Imidazo[1,2-*a*]pyridines **85** to **102** and **113** were considered for the initial testing. Compounds for which IC₅₀ values were obtained are shown in Table 2, with a comparison to the 'golden standard' camptothecin.

Results and Discussion

Table 2 – IC₅₀ values in μM obtained for compounds in colorectal (HT-29 and Caco-2), breast cancer (MCF7 and MDA-MB231) and Leukemia (K562 and HL-60) cell lines

Compound	Colorectal Cancer Lines		Breast Cancer Lines		Leukemia Lines	
	HT-29	Caco-2	MCF7	MDA-MB231	K562	HL-60
Camptothecin	5.0 \pm 0.7	11 \pm 2	0.32 \pm 0.01	0.33 \pm 0.04	2.6 \pm 0.2	0.005 \pm 0.003
 85	-	-	42 \pm 2	-	11 \pm 2	-
 87	-	-	71 \pm 3	-	13 \pm 2	11 \pm 2
 88	-	-	35.4 \pm 0.4	-	36 \pm 4	-
 89	-	-	-	-	-	13.0 \pm 0.2
 90	-	-	32 \pm 2	33 \pm 3	-	-
 91	-	14.0 \pm 0.8	43 \pm 4	-	51 \pm 6	-
 92	10.7 \pm 0.4	-	-	-	-	-
 93	28.2 \pm 0.9	34 \pm 3	18 \pm 2	30 \pm 2	15 \pm 3	15.0 \pm 0.1
 94	-	-	-	-	21 \pm 1	-
 95	8 \pm 2	-	35 \pm 2	-	24.9 \pm 0.9	18 \pm 2
 102	4.1 \pm 0.4	15 \pm 2	32.6 \pm 0.9	-	27 \pm 1	13 \pm 3

Imidazo[1,2-*a*]pyridine **86** had featured in the previous study by de Koning and co-workers. In their study the IC₅₀ values for **86** were reported as 9 ± 1 μM in the HT-29 cell line and 9 ± 1 μM in the Caco-2 cell line.⁹¹ Interestingly, in this study **86** was not considered to be active enough to obtain an IC₅₀ value in any of the cell lines investigated. Not many of the compounds in this first library showed significant activity in the colorectal cancer cell lines, however compounds **92**, **95** and **102** showed activity similar to that seen in the de Koning study,⁹¹ where imidazo[1,2-*a*]pyridine **102** showed the best activity in both HT-29 and Caco-2 cell lines. The imidazo[1,2-*a*]pyridines in this first study showed significantly more activity in the leukemic and breast cancer cell lines than the colorectal lines, however none of these compounds showed activity comparable to that of the camptothecin.

One of the most positive aspects of the imidazo[1,2-*a*]pyridines from the de Koning study was the low toxicity of the compounds towards leucocytes.⁹¹ In order to verify these results, leucocytes were dosed with the imidazo[1,2-*a*]pyridines from this first compound library. These tests were again performed using an 3-(4,5-dimethylthiazol-2-yl)-2,5-diphenyltetrazolium bromide (or MTT) assay, where the leucocytes were dosed with the relevant imidazo[1,2-*a*]pyridine for 24 hours at their respective IC₅₀ values for the K562 and the HL-60 cell lines. Figure 44 shows the results obtained for these experiments.

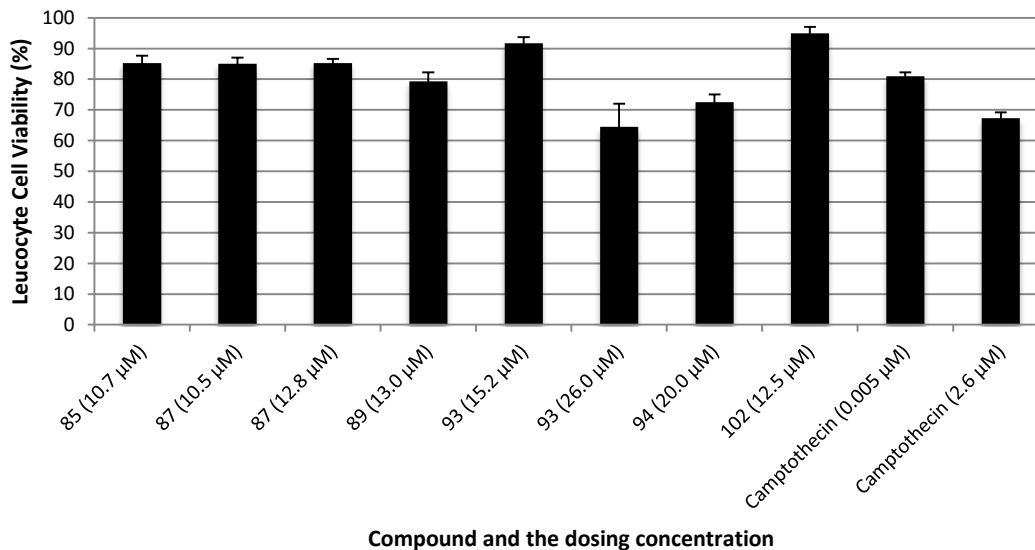


Figure 44 – Leucocyte cell viability after 24 hours of exposure to selected imidazo[1,2-*a*]pyridines at their IC₅₀ concentrations

The camptothecin that was used as a standard showed significant toxicity at relatively low concentrations (67.3 % at 2.6 μM). A similar level of toxicity was only noted in imidazo[1,2-

a]pyridine **93** at 26.0 μM (tenfold more concentrated than that of the camptothecin). The imidazo[1,2-*a*]pyridines showed significantly less toxicity than camptothecin towards the leucocytes. This correlates with what was previously observed and suggests the imidazo[1,2-*a*]pyridines show some selectivity towards cancer cells.

While the IC_{50} values in the cancer cell lines may not have been as low as we had initially hoped, the relatively low toxicity of the imidazo[1,2-*a*]pyridines was promising and prompted further investigation.

2.4. Introducing metals to imidazo[1,2-*a*]pyridines

2.4.1. Combining imidazo[1,2-*a*]pyridines with ferrocene

Being unable to successfully tether the imidazo[1,2-*a*]pyridine to a metal using the traditional linker approach, a few methods were investigated in order to achieve a different type of hybrid. The first of these was to introduce a metal directly to the imidazo[1,2-*a*]pyridine during the Groebke-Blackburn-Bienaymé coupling reaction. This was found to be possible using commercially available ferrocenecarbaldehyde, resulting in the formation of **115** to **117** as shown in Figure 45.

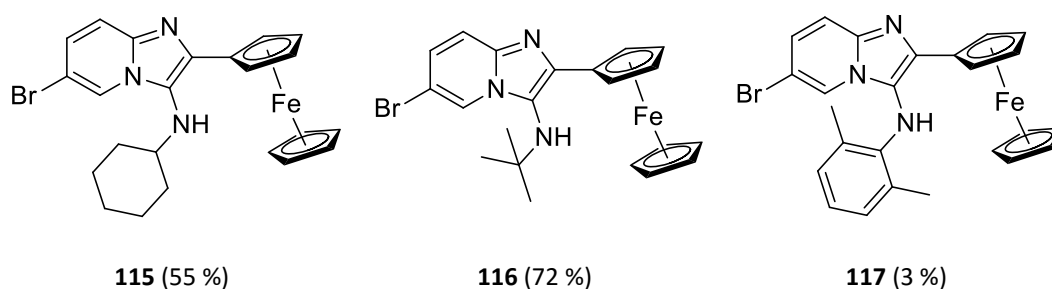


Figure 45 – Ferrocene-containing imidazo[1,2-*a*]pyridines **115** to **117**

These reactions were performed with varying degrees of success. The best yielding reaction was **116** with 72 %, while **115** formed in a mediocre yield of 55 % and **117** in a very poor yield of 3 %. These compounds were characterised mainly by ^1H and ^{13}C NMR spectroscopy with characteristic substituted ferrocene proton signals in a 2:2:5 ratio in the ^1H NMR spectra along with the three imidazo[1,2-*a*]pyridine protons. The ^{13}C NMR spectrum corroborates this with a quaternary ferrocenyl carbon at approximately 78-79 ppm followed by the remaining three carbon signals between 65-70 ppm. Unfortunately compound **117** was found to be significantly insoluble in organic solvents so much so that it was not possible to obtain a ^{13}C NMR spectrum for this compound even in d_6 -DMSO.

Crystals suitable for SCXRD were grown and so the exact structure of these compounds could be obtained. This resulted in some unexpected interactions. Ferrocene **115** (Figure 46A) was found to crystallize with methanol forming intermolecular hydrogen bonds with O1—H1 \cdots N1 ($d = 2.01$ Å) and N26—H26 \cdots O1 ($d = 2.12$ Å) to form dimer type crystal packing. Interestingly, while **116** also included methanol in the crystal structure the same dimer type pattern was not observed. Hydrogen bonding through O1—H1 \cdots N1 ($d = 2.82$ Å) as shown in Figure 46B, binds the methanol to the imidazo[1,2-*a*]pyridine and no obvious π stacking was noted.

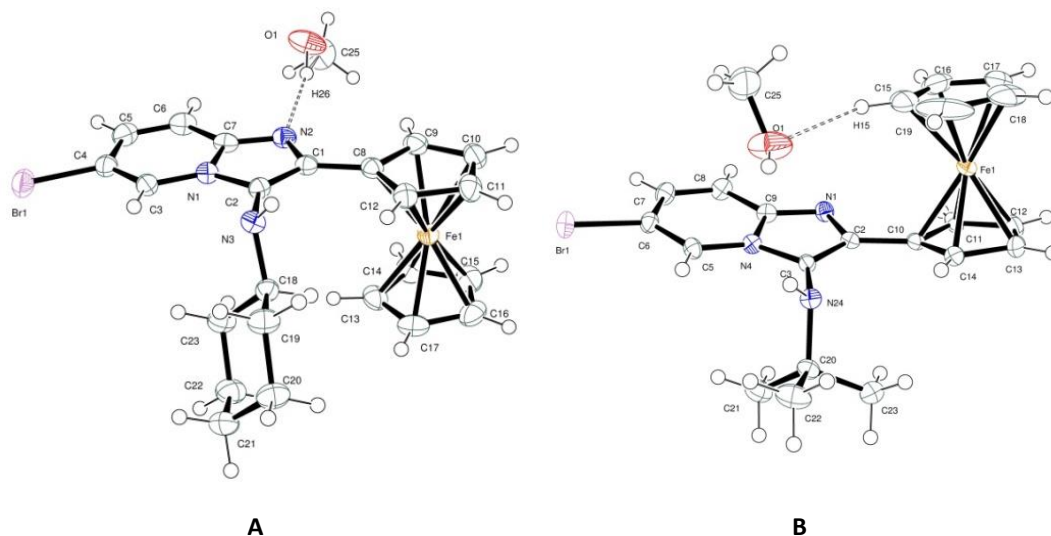


Figure 46 – The asymmetric units of **115** and **116**

In a stroke of fortune, the insoluble **117** was crystallized from ethanol. Figure 47 gives us a clear indication of why this compound is so insoluble, as there is intermolecular hydrogen bonding between C27b—H27e...N1a ($d = 2.90 \text{ \AA}$), C27—H27c...N1b ($d = 2.78 \text{ \AA}$), C28b—H28b...N1a ($d = 2.57 \text{ \AA}$) and N28a—H28a...N1b (2.53 \AA). Additionally the small torsion angle of $11.8(1)^\circ$ between the imidazo[1,2-*a*]pyridine ring and the top cyclopentene ring of the ferrocene ring allowed for significant $\pi \cdots \pi$ interactions between the centrosymmetric pair. The π stacking continues throughout the crystal packing.

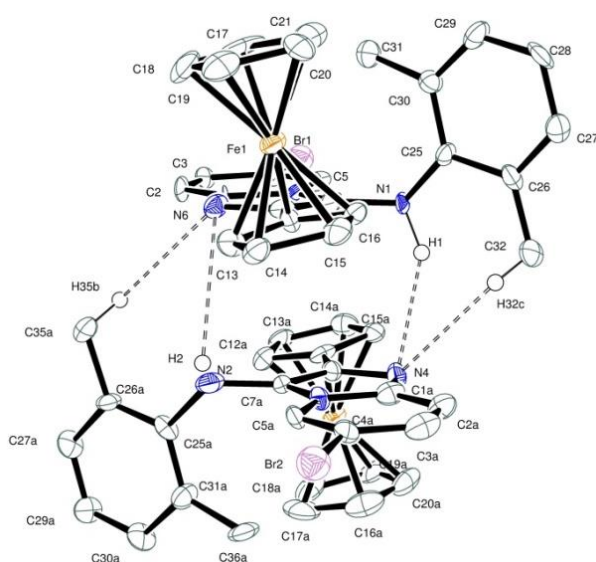


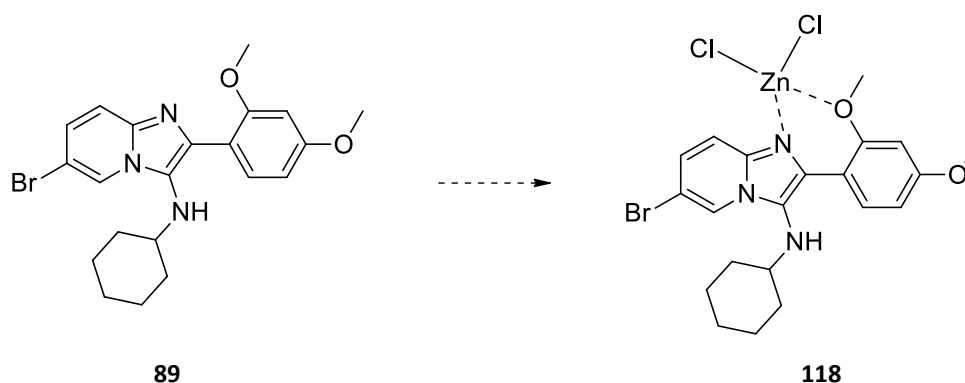
Figure 47 – The asymmetric unit of **117** (hydrogen atoms not involved in hydrogen bonding are omitted for clarity)

The compounds shown in Figure 45 were the first successful examples of the types of hybrid compounds we were interested in synthesising and were sent for biological testing. Unfortunately compound **117** was not soluble under the conditions required for anticancer testing and so could not be tested. Compounds **115** and **116** showed no significant biological activity despite being soluble in a water-dimethylsulfoxide medium.

2.4.2. Chelation approach to the synthesis of metal hybrids

The final approach considered in the synthesis of hybrid compounds was based on using the inherent electron rich properties of the imidazo[1,2-*a*]pyridine itself. When considering the imidazo[1,2-*a*]pyridine ring core, the lone pair of electrons on N4 are tied up in the overall aromaticity of the compound while the lone pair on N1 are free and could serve as possible sites for chelation to a metal ion. The coordinative ability of N1 has already been seen in Figure 37A and Figure 46 where water and methanol respectively were included in the crystal structures through hydrogen bonding to N1 and suggested that this could be a good starting point.

Given that there has been very little work done in this particular area of research and metal chelation was not common practise in our laboratory we decided to do initial investigations with zinc-based compounds before attempting to introduce platinum as originally proposed. Using a procedure by Forniés *et al.*, the first attempted synthesis of chelated zinc imidazo[1,2-*a*]pyridine was performed as shown in Scheme 22, chelating imidazo[1,2-*a*]pyridine **89** and zinc chloride in an attempt to form a 6 membered chelate ring (**118**).⁹⁶ This experiment produced a cream solid as a product that showed limited solubility in organic solvents. It was immediately evident that characterisation of the product would prove tricky and the use of NMR spectroscopy would be fairly limited. NMR spectroscopy could confirm the presence of the imidazo[1,2-*a*]pyridine in the compound collected, and show the expected peak shifts, however it would not give the exact position of the chelation or how many organic units were chelated to the zinc. The use of SCXRD in the characterisation of these compounds in this project was therefore imperative.



Scheme 22 – Proposed synthesis of a 6 membered chelate coordination compound

The crystallization of the cream powder by slow evaporation using methanol resulted in the formation of wafer thin colourless plates that were suitable for SCXRD. This showed that the product from the reaction was not **118** as expected but an unexpected chelation product **119** shown in Figure 48. This chelate structure preserved the intramolecular hydrogen bonding that was initially seen in Figure 38, the crystal structure of the free ligand **89**. This suggests that this intramolecular bonding is significant and more energetically favourable than the chelate ring would be. Aside from this, Figure 48 is conclusive proof that chelation to N1 is possible and preferable, however results in the formation of this zinc-organic ligand complex of relatively high molecular mass was not ideal in terms of drug discovery. In addition to this, a single chelation may not be strong enough to withstand physiological conditions.

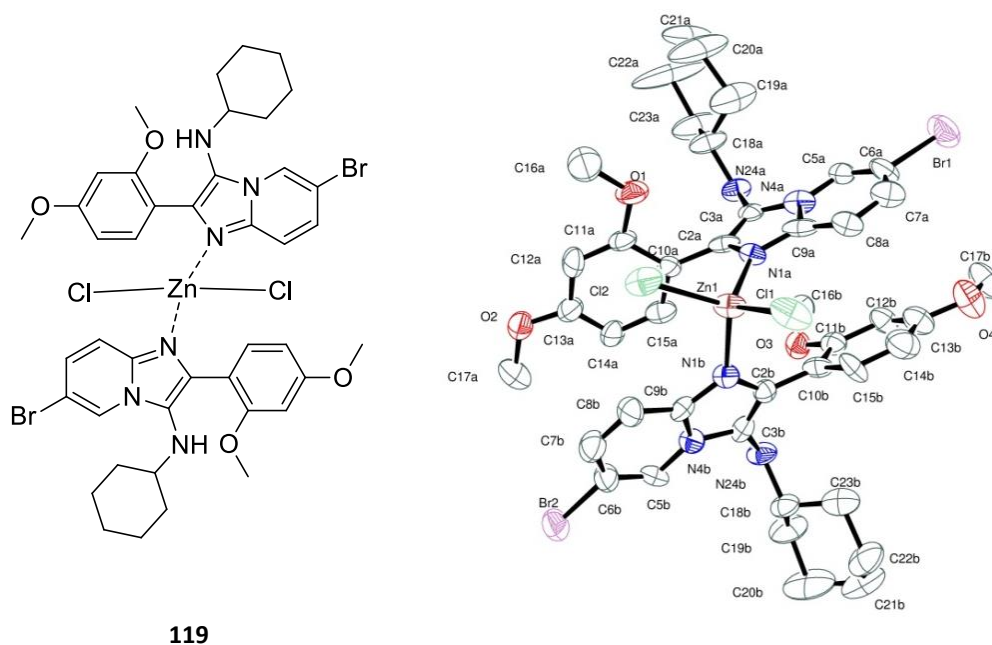
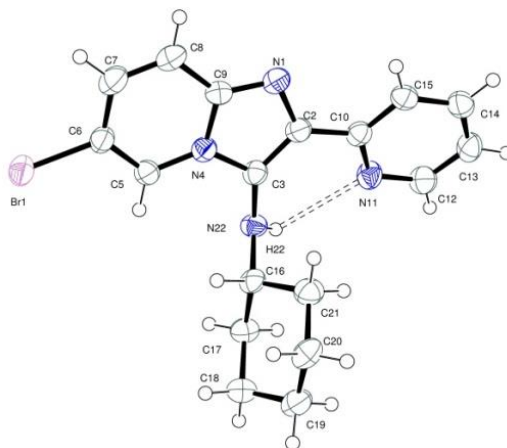
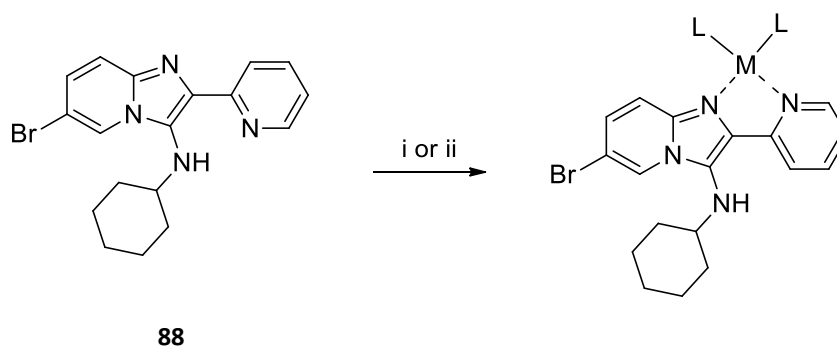


Figure 48 – The structure and asymmetric unit of 119 (hydrogen atoms are omitted for clarity)

In an attempt to address this, imidazo[1,2-*a*]pyridine **88** was revisited. In this particular imidazo[1,2-*a*]pyridine, the presence of a second pyridyl group in the R₂ position creates the potential for the formation of a more stable metal 5-membered chelate ring. The crystal structure of **88**, Figure 49, revealed that there is significant intramolecular hydrogen bonding between N22—H22...N-11 (2.54 Å). This hydrogen bonding would need to be overcome in order for any metal chelation to occur.

Figure 49 – The asymmetric unit of **88**

Exposing compound **88** to a variety of different metal salts, as shown in Scheme 23, resulted in the successful formation of metal complexes. A procedure from Steffen and Palenik that was heavily modified¹¹² was used to generate the metal-imidazo[1,2-*a*]pyridines as shown in Figure 50 in varying yields. A variety of different methods were used to characterise these complexes, depending on their nature.



Reaction conditions: i) $ZnCl_2$, $Zn(OAc)_2$ or $Cu(OAc)_2$ (0.9 eq), diethyl ether, rt, 18 h; ii) $PtCl_2$ (0.9 eq), DMF, reflux, 18 h.

Scheme 23 – General synthesis to form metal chelated imidazo[1,2-*a*]pyridines

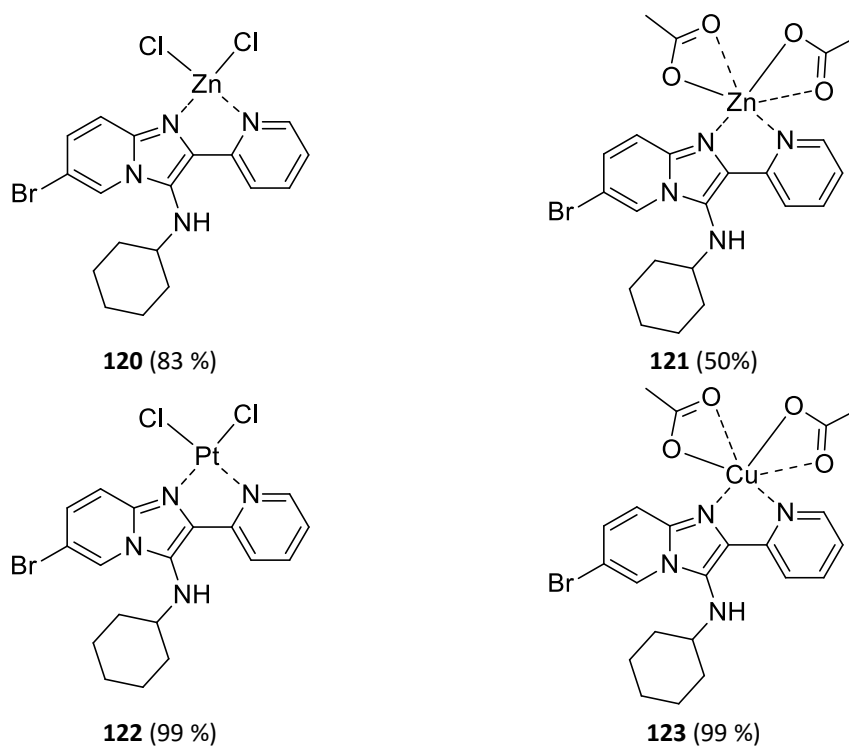


Figure 50 – The first metal complex library

These compounds were found to be unstable under the conditions for Mass Spectroscopy and so this method could not be used as an analytical technique for characterisation of these compounds.

Initial investigations were conducted using the inexpensive zinc chloride salt. This resulted in the formation of zinc-imidazo[1,2-*a*]pyridine complex **120** as a cream coloured powder in an excellent yield of 83%. Characterisation proved problematic due to the relative insolubility of the compound. This compound was not soluble enough to perform NMR spectroscopic analysis, however suitable crystals for SCXRD analysis (Figure 50) were grown by slow evaporation from isopropyl alcohol. From the crystal structure, it was evident that the pyridyl R₂ substituent and the imidazo[1,2-*a*]pyridine ring become planar once chelated to the zinc. This allows for significant π -stacking to occur in the crystal lattice, possibly explaining the low solubility of the compound.

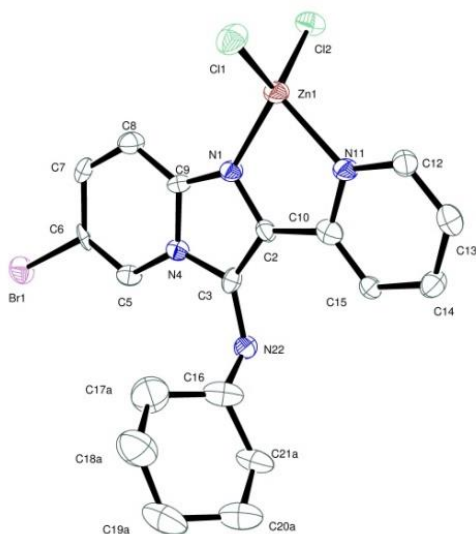


Figure 51 – The asymmetric unit of 120 (hydrogen atoms are omitted for clarity)

Using $\text{Zn}(\text{OAc})_2$ instead of ZnCl_2 dramatically improved the solubility of the complex and this complex - **121** – could be characterised by NMR spectroscopy as well as SCXRD. From the NMR spectra it could be seen that there were significant changes to the chemical shifts of both the ^1H and ^{13}C NMR signals. It was also noted that the signals were significantly broader than in the free ligand **88**. The additional CH_3 peaks due to the acetate were observed at 2.10 ppm in the ^1H NMR spectrum and at 22.14 ppm in the ^{13}C NMR spectrum, and the acetate carbonyl signals was present at 180.60 ppm. While this significant signal shifting and the acetate signal presence confirmed the formation of a complex, it did not provide an exact location for the chelation of the zinc. Slow evaporation of the complex from CDCl_3 resulted in colourless crystals confirming the structure of **121** by SCXRD as shown in Figure 52. Intramolecularly, hydrogen bonding between $\text{C15}—\text{H15}\cdots\text{N22}$ ($d = 2.66 \text{ \AA}$) was noted. On an intermolecular level, these molecules tended to form dimers through noteworthy hydrogen bonds between $\text{N22}—\text{H22}\cdots\text{O-4}$ at distances of 2.15 and 2.23 Å respectively. These crystals were found to include the CDCl_3 solvent which was between the voids in the crystal lattice.

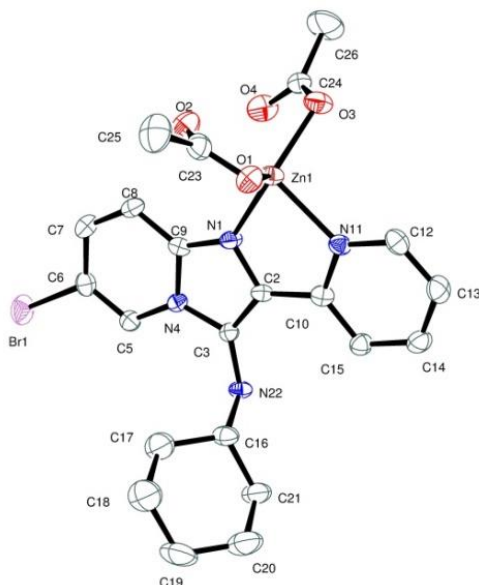


Figure 52 – The asymmetric unit of 121 (hydrogen atoms are omitted for clarity)

Given the success of the complexation reactions, this was then attempted using platinum chloride. However, due to the insoluble nature of platinum compounds, the reaction was performed in dimethylformamide under reflux conditions overnight. This resulted in the formation of an insoluble mustard yellow powder that was determined to be **122**. Unfortunately no crystal structure for this compound could be obtained, however NMR spectroscopy could be used to characterise this compound. From this it could be clearly seen that the imidazo[1,2-*a*]pyridine signals that were present in the ligand, had shifted appropriately and showed significantly reduced splitting. The most significant change in the ^1H NMR spectrum was the shifts of the cyclohexyl ring signals. The appropriate signal shifts were also noted in the ^{13}C NMR spectrum.

In order for the compounds to be considered for biological application, the solubility of the compounds was of vital importance. Given the large amount of research into the use of copper medicinally,⁶¹ copper acetate was also considered. In the event, stirring **88** with copper acetate produced a green powder, **123**, that showed significantly improved solubility in organic solvents over the zinc and platinum compounds. Due to the paramagnetic properties of copper, **123** could not be analysed using NMR spectroscopy. Thankfully the improved solubility made analysis of **123** by SCXRD significantly easier (Figure 53) after crystallization by vapour diffusion of hexane into dichloromethane. Interestingly, the crystal packing of **123** was very similar to that of **121**, where there is intramolecular C8—H8 \cdots O2 hydrogen bonding ($d = 2.52 \text{ \AA}$) and in the unit cell the complex forms a dimer through intermolecular hydrogen bonding (C-22—H-22 \cdots O-4, $d = 2.13 \text{ \AA}$).

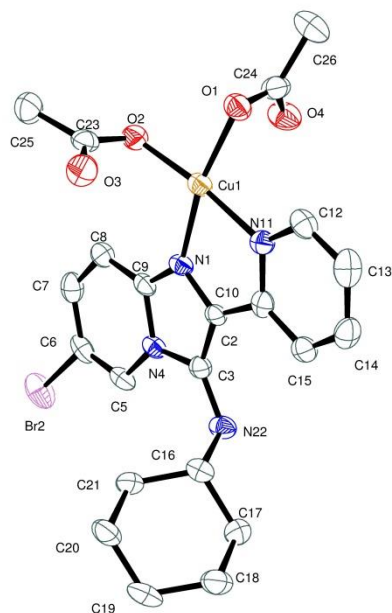


Figure 53 – The asymmetric unit of 123 (hydrogen atoms are omitted for clarity)

Initial anticancer biological assays indicated that the **121** and **123** showed good activity against a few of the cancer cell lines. This is discussed in greater detail later on, however it did prompt the idea of expanding the library to include more zinc and copper-imidazo[1,2-*a*]pyridine complexes. Since the imidazo[1,2-*a*]pyridine ring core and the pyridyl R₂ substituent were necessary, it was decided that an investigation into the R₃ substituent provided by the isocyanide component would be important.

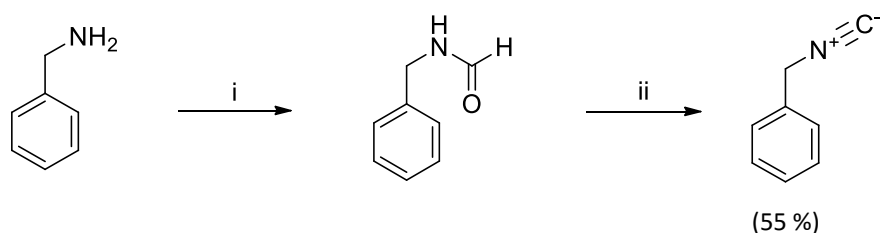
2.4.3. Synthesis of isocyanides

In order to investigate the biological effect of the R₃ substituent the nature of the isocyanides needed to have substantial differences. The xylol isocyanide used previously resulted in very poor yields and products with low solubility in organic solvents. Taking this into account, as well as the substantial cost of the isocyanide it was excluded from the series. The use of *t*-butyl isocyanide resulted in the most soluble compounds previously, however the reaction was unsuccessful with the pyridyl R₂ substituent and so this was not further explored.

Since the cyclohexyl ring is relatively non polar, it was decided that a polar substituent, from commercially available ethyl isocyanoacetate, should be included in this study. In the initial de Koning study, an imidazo[1,2-*a*]pyridine with a benzyl R₃ substituent showed promising results⁹¹ and so the benzyl substituent was reconsidered for this study. Additionally we remained interested in the adamantyl cage and how this would affect the biological activity of the complex.

While both benzyl and adamantyl isocyanide are commercially available, due to a change in shipping regulations and significant cost both needed to be synthesized.

The synthesis of isocyanides has become of interest to our research lab in recent years¹¹³ and the favoured synthesis is outlined in Scheme 24 demonstrating the synthesis of benzyl isocyanide. This involved the formylation of benzylamine followed by dehydration under basic conditions using phosphorus oxychloride.¹¹⁴



Reaction conditions: i) formic acid, acetic anhydride, rt, N₂, 18 h; ii) NEt₃ (10 eq), POCl₃ (3 eq), DCM, 0 °C, 2 h.

Scheme 24 – Synthesis of benzyl isocyanide from benzyl amine

Interestingly, the ¹³C NMR spectrum of the benzyl isocyanide showed a triplet of the isocyanide C (157.7 ppm) as well as the benzylic CH₂ carbon at 45.6 ppm as a result of the C-N coupling. The same splitting was not seen with the adamantyl isocyanide.

The nature of benzyl isocyanide meant that it was synthesized only when absolutely necessary and reacted as soon as possible to prevent any storage of the noxious substance. A similar synthesis of adamantyl isocyanide resulted in a product that was significantly more tolerable to work with, but proved to be a significantly more volatile reaction.

2.4.4. The R₃ substituent effect library

Following all that we had learnt from the previous libraries, the R₃ library compounds were synthesized using the Groebke-Blackburn-Bienaymé multicomponent coupling reaction in ethanol. The imidazo[1,2-*a*]pyridines shown in Figure 54 form the ligands which were used to assemble this library.

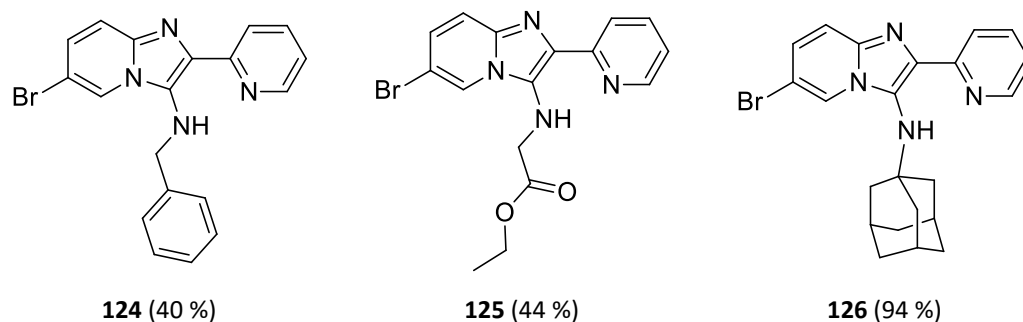


Figure 54 – Pyridyl imidazo[1,2-*a*]pyridines synthesized for the R₃ substituent library

Spectroscopic analysis provided confirmation of the structure of these compounds, where distinguishing features such as the benzyl CH₂ for **124** at 4.24 ppm in the ¹H NMR spectrum, the ester carbonyl signal at 170.6 ppm on the ¹³C NMR spectrum and the ethoxy group for **125** with a quartet at 4.18 ppm and a triplet at 1.19-1.25 ppm in the ¹H NMR spectrum and the adamantyl peaks for **126** at 1.96-2.00 (integrating for 3H), 1.17 (integrating for 6H) and 1.58 ppm (integrating for 3H) in the ¹H NMR spectrum were noted. The amine N-H signal for both **124** and **125** appeared as triplets, suggesting there is coupling to the CH₂ (which appear as doublets). SCXRD analysis revealed that the preferred conformation of these structures is similar to that of **88**, where there is intramolecular hydrogen bonding that effectively locks the structure in a twisted conformation. Figure 55 shows the crystal structures of the compounds in Figure 54, along with the intramolecular hydrogen bonding.

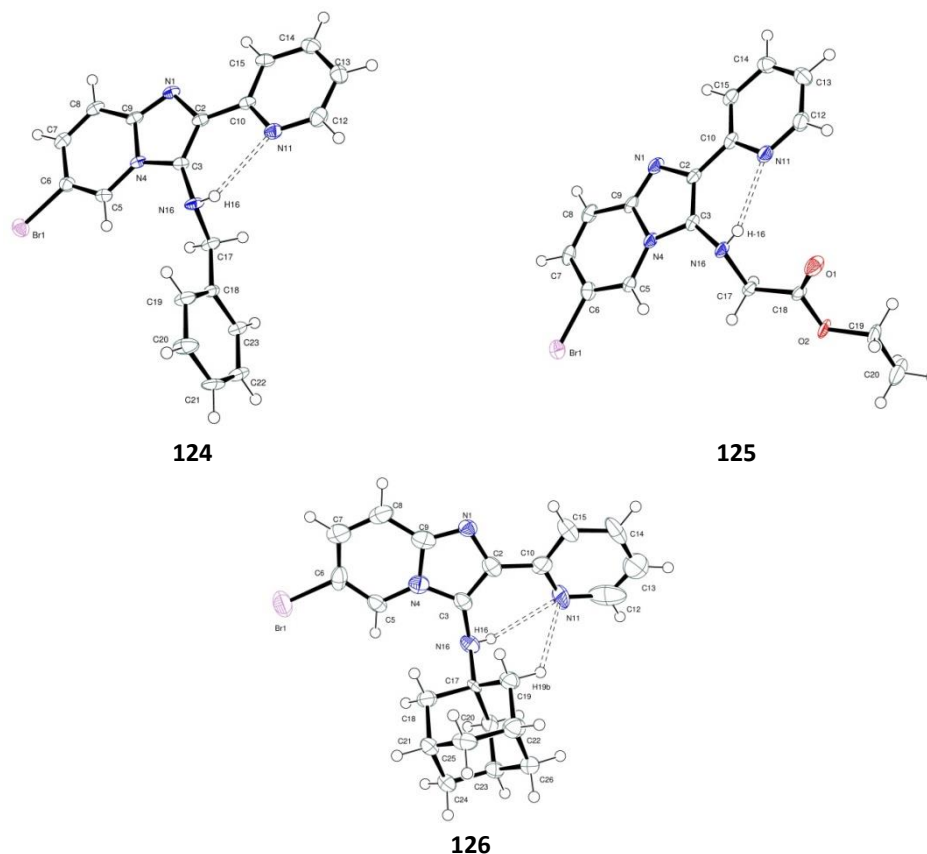


Figure 55 – The asymmetric units of **123, **124** and **125** (hydrogen atoms are omitted for clarity)**

Using these ligands as a starting point, zinc and copper complexes were easily synthesized as before and characterised using similar methods (Figure 56). We attempted to form platinum complexes of **125** and **126** but the reactions formed highly insoluble complexes that were not able to be characterised. The complexation reaction of **124** with platinum chloride resulted in a yellow powder. This powder was found to be complex **129** after being successfully characterised using both NMR spectroscopy as well as SCXRD.

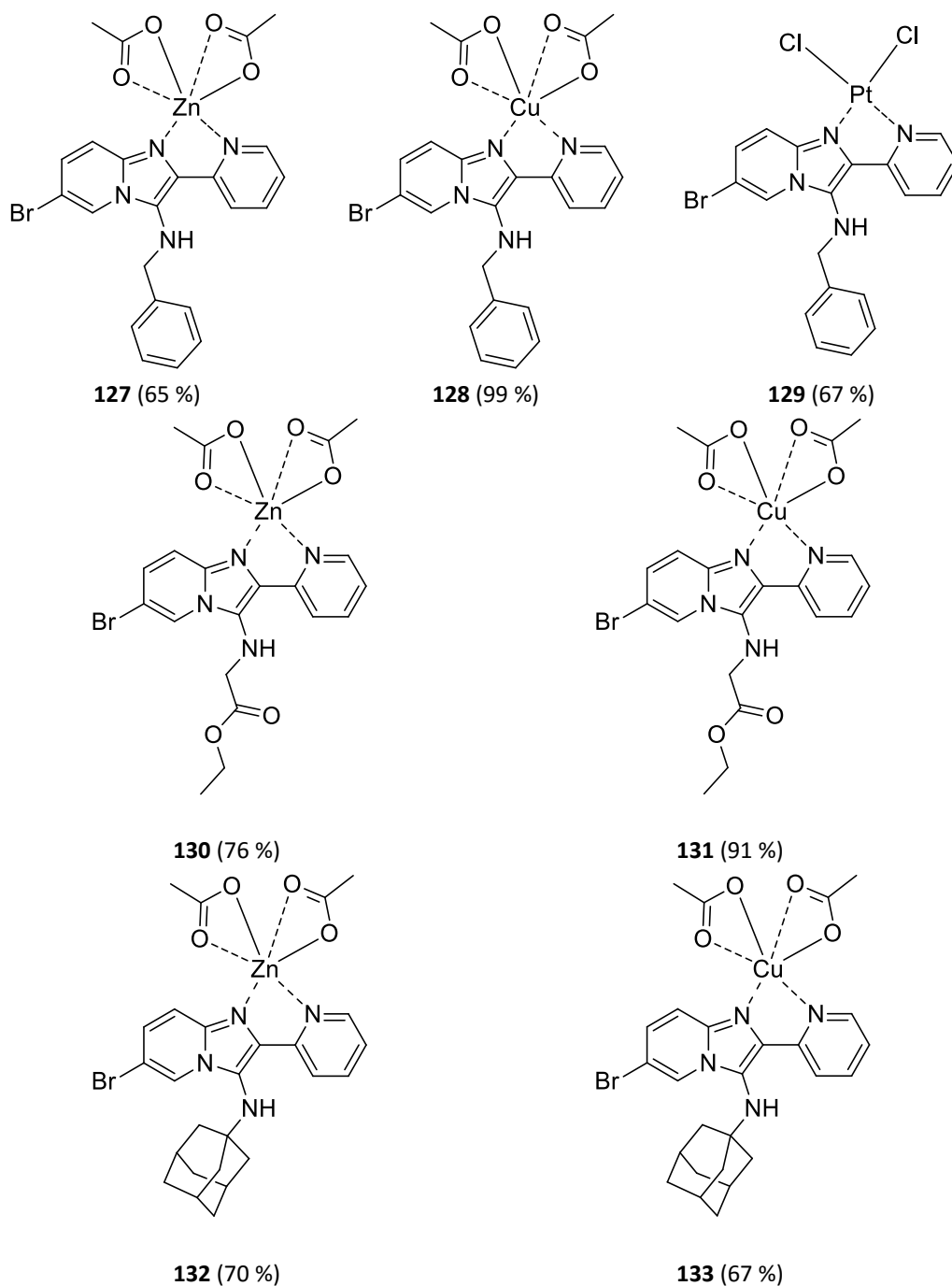


Figure S6 – Zinc, platinum and copper complexes synthesized using the imidazo[1,2-*a*]pyridines synthesized in the R₃ library

NMR spectroscopy of the zinc compounds **127**, **130** and **132** revealed significant shifting of the signals in both the ¹H and ¹³C NMR spectra compared to the ligands. Reduced splitting in the ¹H NMR spectra suggested that the complexation reaction was successful. This was further supported by the presence of the acetate CH₃ in the ¹H NMR spectrum and the acetate carbonyl signal in the ¹³C NMR spectrum. The structures were also confirmed by SCXRD analysis as shown

in Figure 57. Interestingly, in the crystal packing of both **127** and **130** the compounds form dimers through hydrogen bonding, while **132** didn't show any intermolecular hydrogen bonding. The dimer in **127** forms through intermolecular N16—H16...O4 ($d = 2.14 \text{ \AA}$) hydrogen bonding, and similarly in **130** through N16—H16...O6 ($d = 2.06 \text{ \AA}$).

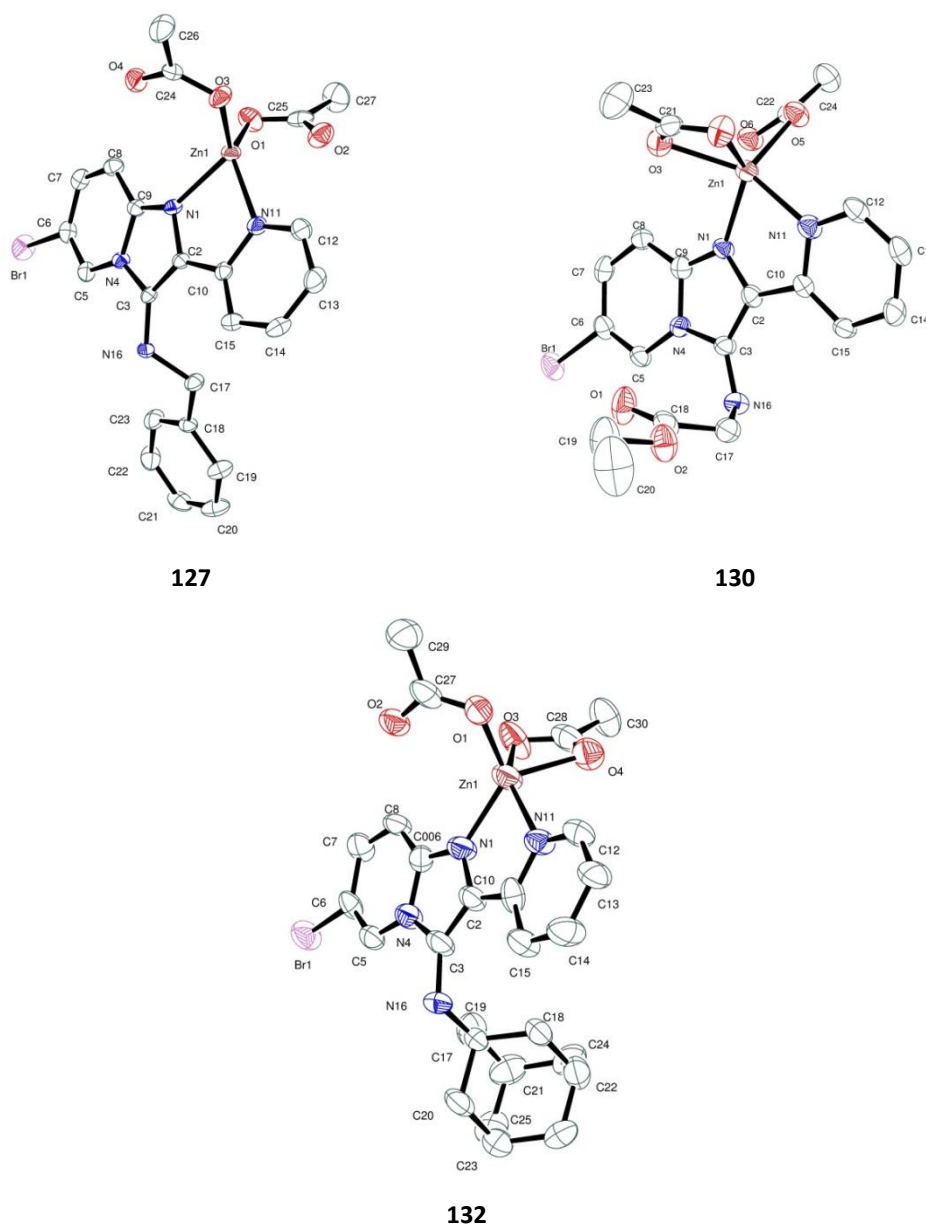


Figure 57 – The asymmetric units of 127, 130 and 132 (hydrogen atoms are omitted for clarity)

The platinum compound **129** was found to be significantly soluble in d_6 -DMSO and using NMR spectroscopy, characteristic imidazo[1,2-*a*]pyridine signals were observed on both the ^1H and ^{13}C NMR spectra with appropriate signal shifting and peak broadening. On standing, yellow crystals formed in the NMR tube and these were analysed using SCXRD to confirm the structure as shown

in Figure 58. The confirmation of this structure lends support to the structure of **122** proposed earlier.

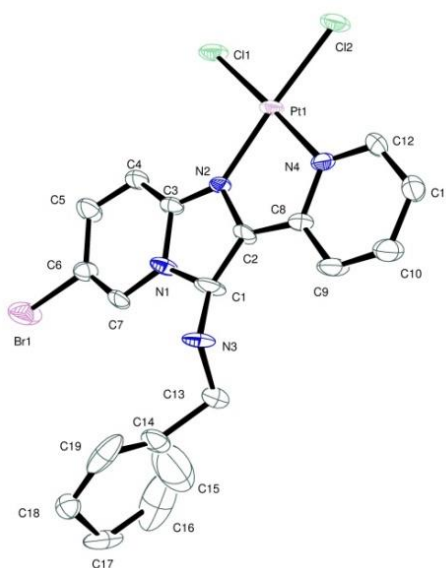


Figure 58 – The asymmetric unit of 122 (hydrogen atoms are omitted for clarity)

The structures of copper complexes **128** and **133** were confirmed by SCXRD. Green crystals were grown from d_4 -MeOD by slow evaporation and the resulting structures are shown in Figure 59. Unfortunately no crystals of complex **131** suitable for SCXRD could be grown. However, given that the crystal structure for the zinc complex **130** was obtained and all the previous crystal structures tend to form in the same manner, the structure of **131** can be deduced. Elemental analysis of compounds **128**, **131** and **133** further supported the structures shown.

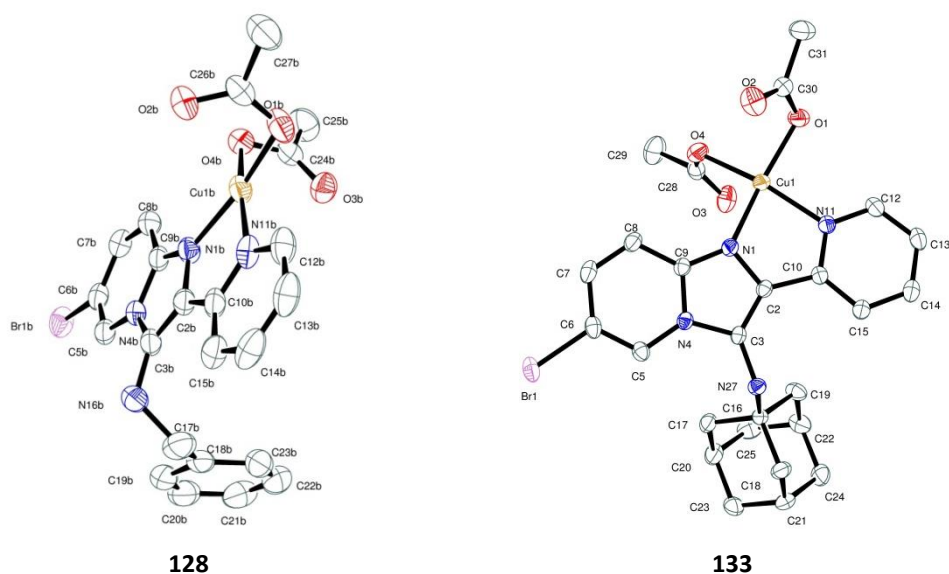


Figure 59 – The asymmetric units of 128 and 133 (hydrogen atoms are omitted for clarity)

2.4.5. Complex Stability Studies

Considering that the complexes synthesized so far were novel, that there are very few reports of metal imidazo[1,2-*a*]pyridine complexes and that these complexes were intended for medicinal use, it was important to determine the stability of the metal complexes. A literature search did not result in significant insight into the p*K* value of the imidazo[1,2-*a*]pyridine ring itself. The only reported values and experimental details are summarised in Table 3.

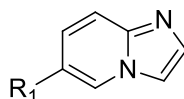


Table 3 – Reported literature values for the p*K* of imidazo[1,2-*a*]pyridine

Reference	Substituents	Solvent System	Temperature	p <i>K</i>
Paulder ¹¹⁵	R ₁ = H	90% EtOH/H ₂ O	-	5.06
Paulder ¹¹⁵	R ₁ = Me	90% EtOH/H ₂ O	-	5.33
Catalan ¹¹⁶	R ₁ = H	Water	25 °C	6.49
Humphries ¹¹⁷	R ₁ = H	-	-	6.9

The lack of significant detail in experimental conditions as well as substituent effects on the p*K* value made it of particular importance for us to independently determine the p*K* values of the free imidazo[1,2-*a*]pyridines before we considered that of the metal complexes. The common practise for the determination of the p*K* values for compounds in our school was by means of a closed cell p*K* titration. We hoped to employ this method in our study, however once set up we found the absorbance spectra obtained from the solution of **88** degraded significantly while circulating through the closed flow cell setup. This suggested that there was a reaction occurring during the circulation of the compound through the apparatus. Having ruled out the choice of buffer system and contaminants in the apparatus setup as the cause of the degradation to the compounds, it was proposed that the compounds were reacting with the silicone tubing.

In order to determine if the tubing was in fact the cause of the problem, a quick study was conducted. A 50% methanol/water solution containing zinc complex **120** was divided into three separate sample vials in 10 ml aliquots. The first sample vial was kept as the control sample. Into the other two sample vials a length of water washed silicon tubing (the same as that used in the closed flow cell setup) was placed into the second sample vial and acid and water washed silicon tubing to the second was added and the solutions left to stand overnight. Both lengths of tubing were dried before being placed into each solution. Obtaining the absorbance spectra for the solutions the following morning revealed some interesting results. The control solution showed two significant absorption bands at 265 and 356 nm respectively. The two solutions exposed to silicone tubing overnight showed significant degradation of these absorption bands (Figure 60).

The solution containing water washed tubing showed significant degradation, while the solution that had the acid washed tubing showed not only degradation, but also a shift in the 356 nm absorption band. Thus it can be concluded that the imidazo[1,2-*a*]pyridines undergo a reaction with the silicone tubing.

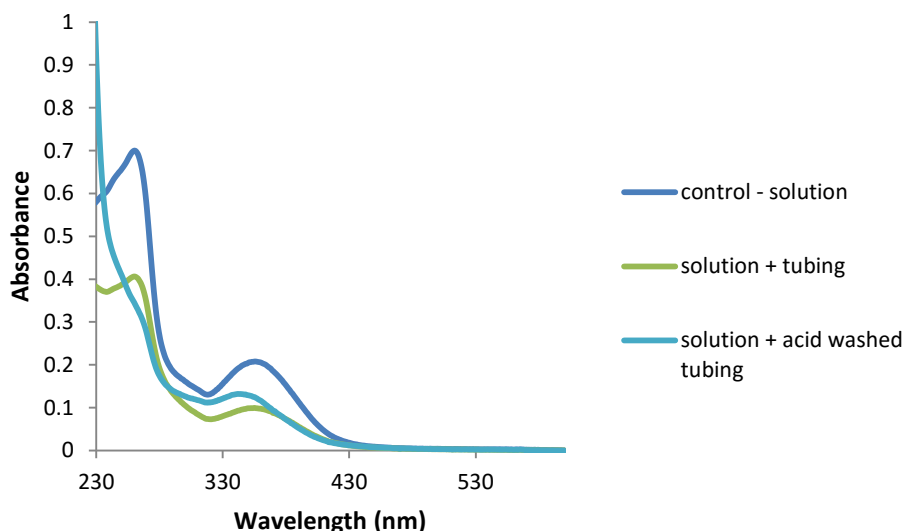


Figure 60 – Changes in the absorbance spectra of 120 when exposed to silicone tubing overnight

Thus it was determined that the traditional closed cell *pK* titration would not be suitable for our purposes. This meant that an out-of-cell *pK* titration procedure needed to be employed instead. This involved dividing a bulk solution of the desired compound into individual glass vials, and adjusting each vial independently to the desired *pH* and obtaining the absorbance spectrum for each vial.

Considering the apparent reactivity of the imidazo[1,2-*a*]pyridines, and the significant potential for them to form complexes the type of buffer system used for these experiments needed to be carefully considered. Using a combination of NaH_2PO_3 and 2-(*N*-morpholino)ethanesulfonic acid (MES) at a final concentration of 1 mM was finally settled upon. In order to ensure complete dissolution of both the free ligands and the metal complexes, a 50% methanol/water bulk solution was used. A 5 ml concentrated stock solution for each compound was made up in methanol or methanol/water. This stock solution was used firstly to determine the appropriate concentration for the *pK* titration by adding 1 μl of the stock solution at a time to 2.5 ml of 50% methanol/water and monitoring the absorbance spectrum. Once at the appropriate concentration, concentrated hydrochloric acid and sodium hydroxide was added consecutively in order to monitor the maximum changes in the absorbance spectra and to determine which

wavelengths would be appropriate to monitor in order to accurately determine the pK of the solution, as well as to determine the appropriate wavelength for the source change over.

The stock solution was then used to form the diluted bulk solutions for the pK titrations. The bulk solutions were made by dissolving the NaH_2PO_3 and MES in water and further diluting to a total volume of 125 ml of water purified using the Millipore system. This was then introduced to a 250 ml volumetric flask and the appropriate volume of stock solution added. The solution was then made up to 250 ml with methanol, the solution thoroughly shaken and then left to equilibrate for 18 hours at 23 °C. The bulk solution was then divided into the individual glass vials in 10 ml aliquots and the pH of each solution was adjusted using concentrated hydrochloric acid or sodium hydroxide with a pulled capillary tube. The solution was then added to a cuvette and the UV-vis absorption spectrum obtained at that pH. In between each sample, the cuvette was washed with water and acetone and dried before the next solution was added. The pK titration was repeated in triplicate for each ligand and each experiment monitored at 2-3 wavelengths between 200 and 600 nm. Figure 61 shows examples of the typical absorbance spectra obtained for the ligands (A), the zinc complexes (B) and the copper complexes (C).

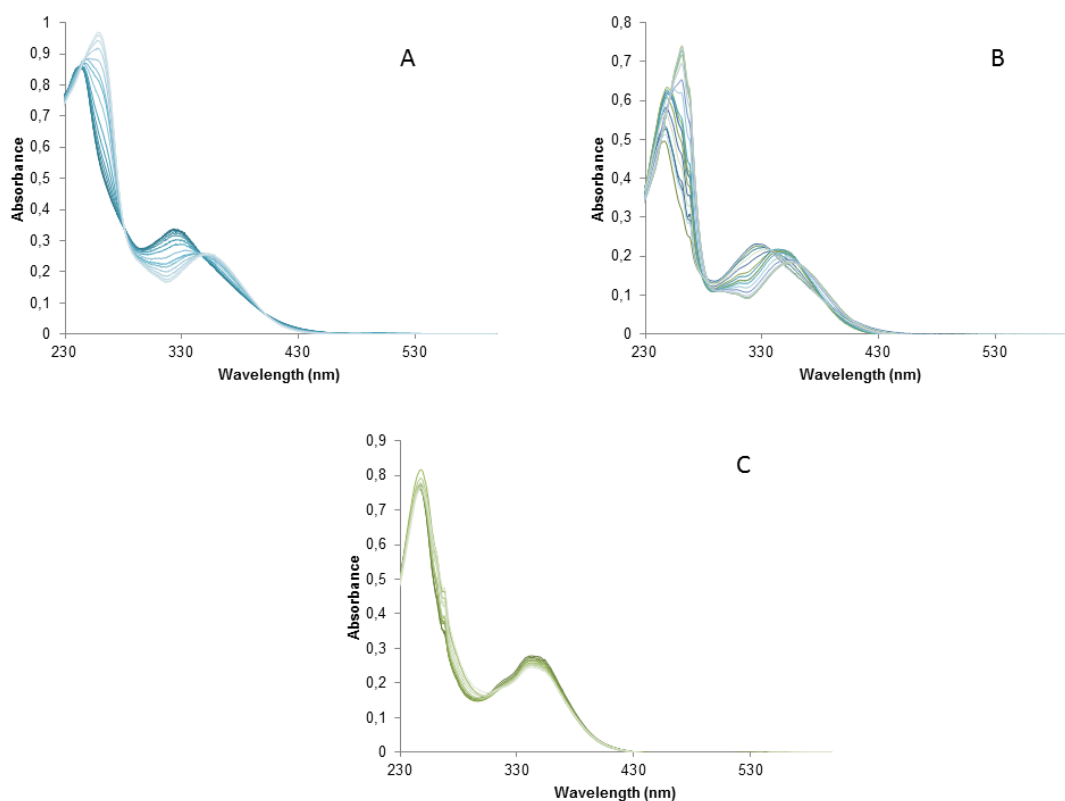


Figure 61 – Changes in the absorbance spectra for compounds 123 (A), 126 (B) and 127 (C) over a 2-10 pH range

The data collected from these experiments were then analysed using SigmaPlot¹¹⁸ where the total absorbance at the monitoring wavelength A_T , is given by Equation 1 (if there is a single pK) or Equation 2 (for two pK_a values) where A_i is the absorbance due to the i^{th} species. The derivation of these equations along with the absorption data for the compounds analysed are available in the Digital Appendix, while an example from one compound can be found in Appendix A3. An example of the SigmaPlot fits of the changes in the absorbance can be seen in Figure 62.

$$A_T = \frac{A_1[H^+] + A_2K_1}{K_1 + [H^+]} \quad \text{Equation 1}$$

$$A_T = \frac{A_1[H^+]^2 + A_2K_1[H^+] + A_3K_1K_2}{[H^+]^2 + K_1[H^+] + K_1K_2} \quad \text{Equation 2}$$

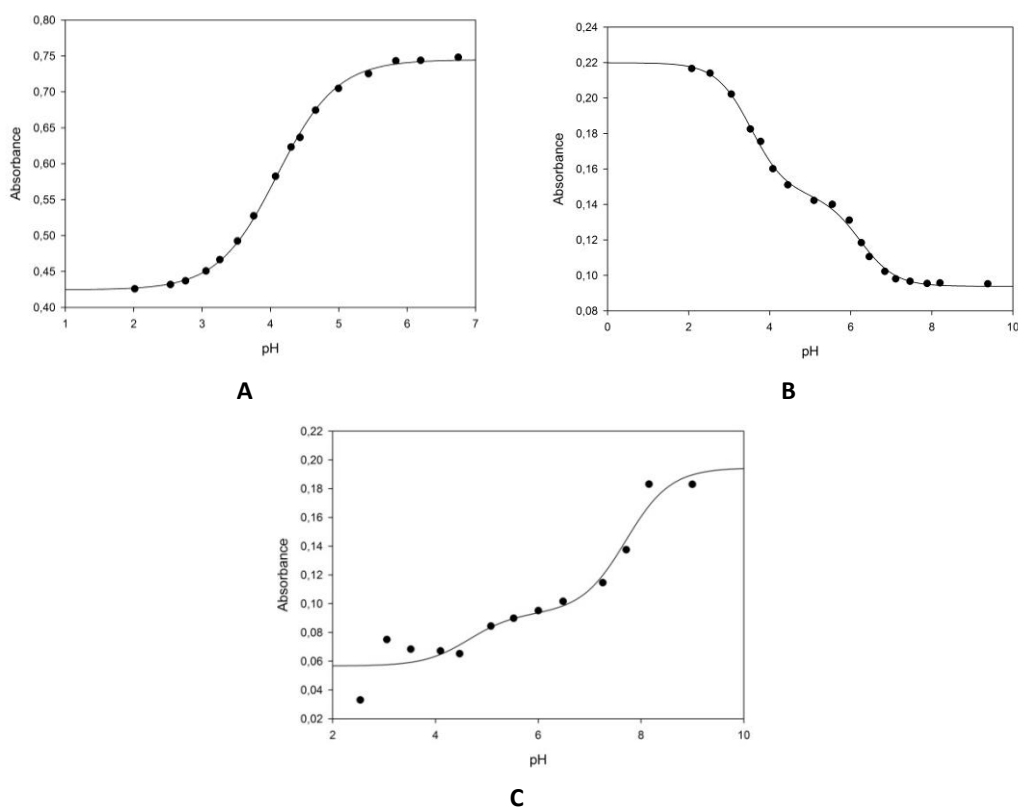


Figure 62 – Examples of SigmaPlot fits for 123 (A), 126 (B) and 127 (C). A shows a single pK fit while B and C show a two pK fit

The pK values for each wavelength of each run were then used to determine the average K value, the standard deviation in the average K value and consequently, the average pK value, with the error calculated using Equation 3 in Microsoft Excel.

$$\text{error} = pK + \log_{10}(\text{Average } K + \text{Standard Deviation}) \quad \text{Equation 3}$$

The pK values for ligands **88**, **124**, **125** and **126**, zinc complexes **120**, **121**, **127**, **130** and **132** and copper complexes **123**, **128**, **131** and **133** were determined using the method described above. The concentration of the solutions and the pK values for each compound are outlined in Table 4.

Table 4 – pK values for selected compounds evaluated in the out-of-cell pK titration

Compound	pK ₁	pK ₂	Concentration (μM)
88	3.9 ± 0.1	-	32.32
120	3.5 ± 0.1	6.73 ± 0.08	22.07
121	3.2 ± 0.1	6.76 ± 0.08	33.73
123	3.6 ± 0.1	8.8 ± 0.2	31.06
124	4.11 ± 0.05	-	34.09
127	3.5 ± 0.1	6.30 ± 0.06	24.85
128	3.5 ± 0.3	5.6 ± 0.3	30.67
125	4.00 ± 0.07	-	45.41
130	2.81 ± 0.08	7.5 ± 0.2	26.69
131	3.6 ± 0.2	5.6 ± 0.3	35.27
126	3.9 ± 0.1	-	65.61
132	3.50 ± 0.07	6.35 ± 0.07	49.65
133	4.4 ± 0.2	5.2 ± 0.3	58.49

Despite having two 'free' nitrogen atoms in the molecule, the ligands **88**, **124**, **125** and **126** only showed a single pK value. While unexpected, this can be explained using the hydrogen bonding seen in the crystal structures of the ligands where the pyridyl N11 pyridine experiences hydrogen bonding with the amine N-H (Figure 49 and Figure 55). In an attempt to confirm this, crystals of the ligand **88** were grown from HBr. Figure 63 is the crystal structure from the crystals grown by slow evaporation of HBr, where the N22—H22···N11 hydrogen bonding is preserved as it was in Figure 49, while the imidazo[1,2-*a*]pyridine hydrogen bonds to the HBr acid through Br6—H6···N1 (*d* = 3.21 Å). If even under concentrated acidic conditions, the pyridyl—amine hydrogen bonding is preserved then this explains why only a single pK value is seen in the imidazo[1,2-*a*]pyridines shown in Table 4.

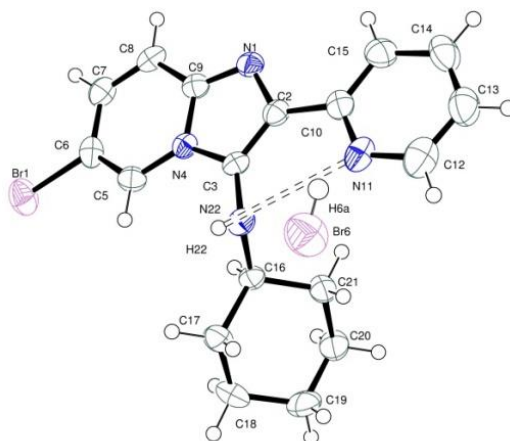


Figure 63 – The asymmetric unit of 88 under acidic conditions

The zinc complexes **120**, **121**, **127**, **130** and **132** showed significant spectroscopic changes that were successfully modelled using Equation 2. In all the complexes, the pK_1 value was significantly lower than that of the corresponding free ligand, while the pK_2 value varied depending on the ligand used. Of all the compounds analysed complex **130** showed pK values that were notably different from all the other compounds tested, and currently there is no reasonable explanation for this although it could serve as an area to expand on in the future.

Copper complexes **123**, **128**, **131** and **133** were more difficult to analyse than the other complexes and had to be approached on an individual basis. Since copper complexes form $\text{Cu}(\text{OH})_2$ after pH 10, the titrations were only performed between pH 2 and pH 9.5. Complexes **123** and **128** could be successfully fitted using a two pK model (Equation 2). The spectroscopic changes for pK_1 and pK_2 were not always visible at the specific wavelength being monitored for complexes **131** and **133**. This meant that the pK 's for these compounds had to be considered individually using a single pK model (Equation 1) for each pK . The absorbance of the imidazo[1,2- α]pyridine portion of the molecules was so large in comparison to that of the copper, at the concentration required to monitor the changes in the imidazo[1,2- α]pyridine, that the characteristic d-d copper absorption bands were not visible. They were however confirmed to be present using the stock solutions and found to appear around 670 nm.

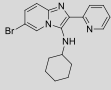
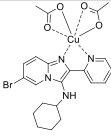
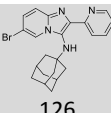
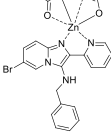
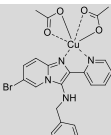
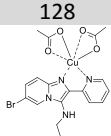
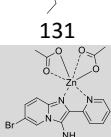
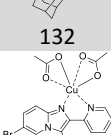
Looking at the data obtained from this study as a whole, we can conclude that these compounds can be expected to be stable under physiological conditions (approximately pH 7.35). The significant hydrogen bonding seen in the ligands is overcome when exposed to a metal salt to form the chelated products, evident by the presence of the second pK observed in the metal complexes. The pK_1 values for all the imidazo[1,2- α]pyridines are similar and change slightly to significantly depending on the metal it is chelated to. The pK_2 value shows a much more metal dependent correlation.

2.4.6. Biological Results for the R₃ substituent library

The isocyanide derived R₃ substituent library sent for anticancer testing comprised of ligands **124-126** as well as metal complexes **120-123** and **127-133**. Biological testing of the ligands and the compounds was again performed by Dr Leonie Harmse and her team as previously described. IC₅₀ values for active compounds are outlined in Table 5 with the results for **88** are included for ease of comparison.

Results and Discussion

Table 5 - IC₅₀ values obtained for the most active metal-containing compounds in colorectal (HT-29 and Caco-2), breast cancer (MCF7 and MDA-MB231) and leukemia (K562 and HL-60) cell lines

Compound	Colorectal Cancer Lines		Breast Cancer Lines		Leukemia Lines	
	HT-29	Caco-2	MCF7	MDA-MB231	K562	HL-60
Camptothecin	5.0 ± 0.7	11 ± 2	0.32 ± 0.01	0.33 ± 0.04	2.6 ± 0.2	0.005 ± 0.003
 88	-	-	35.4 ± 0.4	-	36 ± 4	-
 123	8.0 ± 0.4	12.2 ± 0.6	0.62 ± 0.03	28 ± 2	1.9 ± 0.9	2.2 ± 0.5
 126	-	-	-	49 ± 5	27 ± 2	-
 127	-	-	-	90 ± 8	-	-
 128	3.9 ± 0.6	9.6 ± 0.4	3.7 ± 0.5	30 ± 1	7.7 ± 0.5	6.5 ± 1
 131	11 ± 1	6 ± 2	2.2 ± 0.1	29 ± 1	8.7 ± 0.8	3.8 ± 0.7
 132	9.2 ± 0.5	12 ± 2	-	38.3 ± 0.5	-	-
 133	5.9 ± 0.8	-	*	*	-	-

*Complex **133** was not found to be soluble enough for testing in the MCF7 and MDA-MB231 cell lines

The compounds shown in Table 5 showed significantly better activity than those that of the first library (Table 2). Aside from **88** which only showed moderate activity in two anticancer cell lines, the only other imidazo[1,2-*a*]pyridine that showed any notable activity was **126**. The platinum complexes tested (**122** and **129**) were highly insoluble and showed little activity against the

cancer cell lines. Of the zinc complexes tested, only **132** showed any activity. It was immediately evident that the most active compounds to date were the copper-containing complexes (**123**, **128**, **131** and **133**) that showed activity comparable to that of camptothecin. The only difference between these imidazo[1,2-*a*]pyridines was the nature of the substituent at C-3, with different substituents showing slightly better activity in different cancer cell lines. Complex **128** showed the most significant activity in the colorectal cancer cell lines. Complex **123** showed the most significant activity in the leukemic and breast cancer cell lines. None of the complexes in this study showed activity comparable to camptothecin in the triple negative MDA-MB231 cell line. For the sake of comparison the raw metal salts that were used to make the complexes ($\text{Cu}(\text{OAc})_2$, $\text{Zn}(\text{OAc})_2$ and ZnCl_2) were also tested against these cancer cell lines and found to show no significant activity.

Given that these metal complexes were the first of their kind no toxicity data was available for them. As previously described, leucocytes were treated with the imidazo[1,2-*a*]pyridine complexes at a concentration of 20 μM for 24 hours and the results are shown in Figure 64.

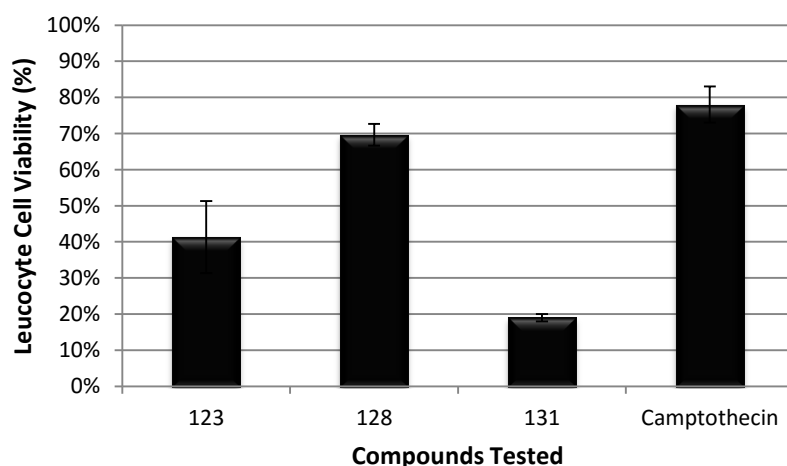


Figure 64 – Leucocyte viability when exposed to selected metal complexes at 20 μM for 24 hours

Unsurprisingly, from Figure 64, it can be seen that these metal complexes show significantly greater toxicity than that of the metal free imidazo[1,2-*a*]pyridines seen earlier. Complex **128** showed toxicity comparable to that of camptothecin, while complexes **123** and **131** showed greater toxicity, with **131** showing the most significant toxicity of all. The toxicity of these compounds is an important feature to monitor as the greater the toxicity seen, the more harsh the side effects that can be expected from the ultimate treatment, going against the broader aim of this project.

Considering that the free metal salts did not show any significant activity in the cell lines and the imidazo[1,2-*a*]pyridine ligands only showed moderate activity, as well as the pK data obtained from the previous section, it can be concluded that the significant improvement in the IC_{50} values for these metal complexes compared to compounds previously tested is due to the hybrid effect of the compounds. This proved our initial project aims – albeit with a different metal than was initially envisaged and prompted further investigation.

2.4.7. A more focused Structure-Activity study library

Given the significant activity of **123** across several cell lines, it was fairly clear that the cyclohexyl substituent was important for activity. From there it was decided that the other substituents on the imidazo[1,2-*a*]pyridine ring needed to be investigated in order to further enhance our understanding of these compounds. Using the general procedure the imidazo[1,2-*a*]pyridines outlined in Figure 65 were synthesized. This series includes compounds where the halogen substituent was absent (**134**), the position of the bromine substituent has been changed (**135** and **136**), the R_1 substituent has been changed to a chlorine atom (**137**) as well as where the halogen substituent has been moved to the R_2 pyridyl ring (**138** and **139**).

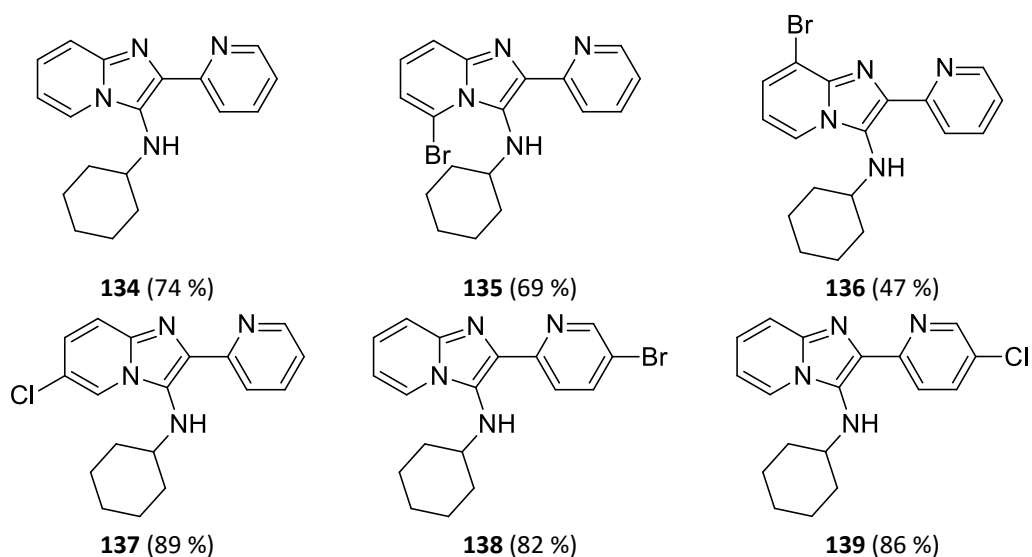


Figure 65 – Pyridyl-containing imidazo[1,2-*a*]pyridines **134** to **139**

These compounds were characterised using 1H and ^{13}C NMR spectroscopy where the characteristic chemical shifts for the compounds were as expected. The N-H signals for compounds **138** and **139** appeared as doublets, while for the other imidazo[1,2-*a*]pyridines **134** to **137** they appeared as singlets. Given the conformation of imidazo[1,2-*a*]pyridine **88**, crystal structures were obtained for all the compounds in this new library (with the exception of **135** which was collected as a golden oil) after growing crystals by slow evaporation from appropriate

solvents. These crystal structures are shown in Figure 66. In these structures, the same twisted conformation as that in **88** can be seen. This suggests that for these types of structures, this is the most energetically favourable conformation for this particular ring system, regardless of the substituents on the imidazo[1,2-*a*]pyridine.

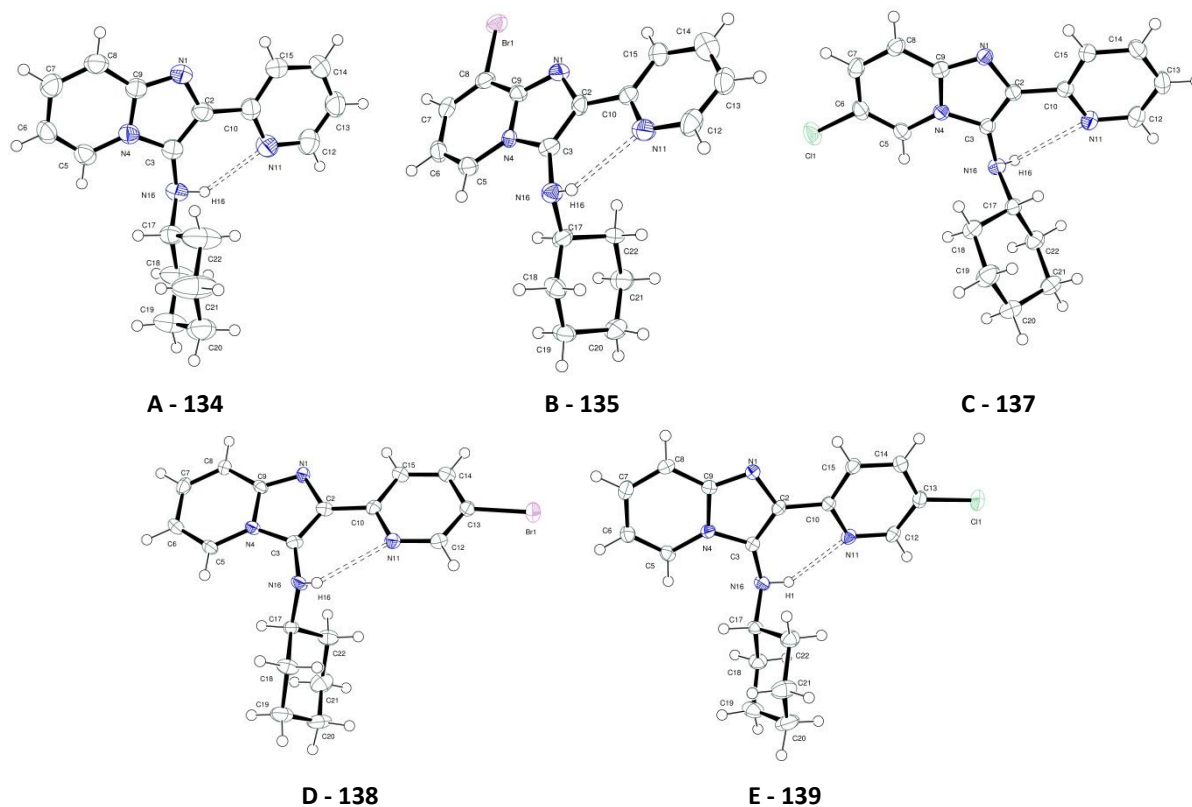


Figure 66 – The asymmetric units of **134**, **135**, **137**, **138** and **139**

Using imidazo[1,2-*a*]pyridines **134** to **139**, a series of copper acetate complexes were formed in a similar manner to those previously described. These complexes form the final series of compounds investigated in this study and the expected complexes are shown in Figure 67, along with copper chloride and copper nitrate complexes of **88** to investigate the effect of the counter ion on the anticancer activity of the complex.

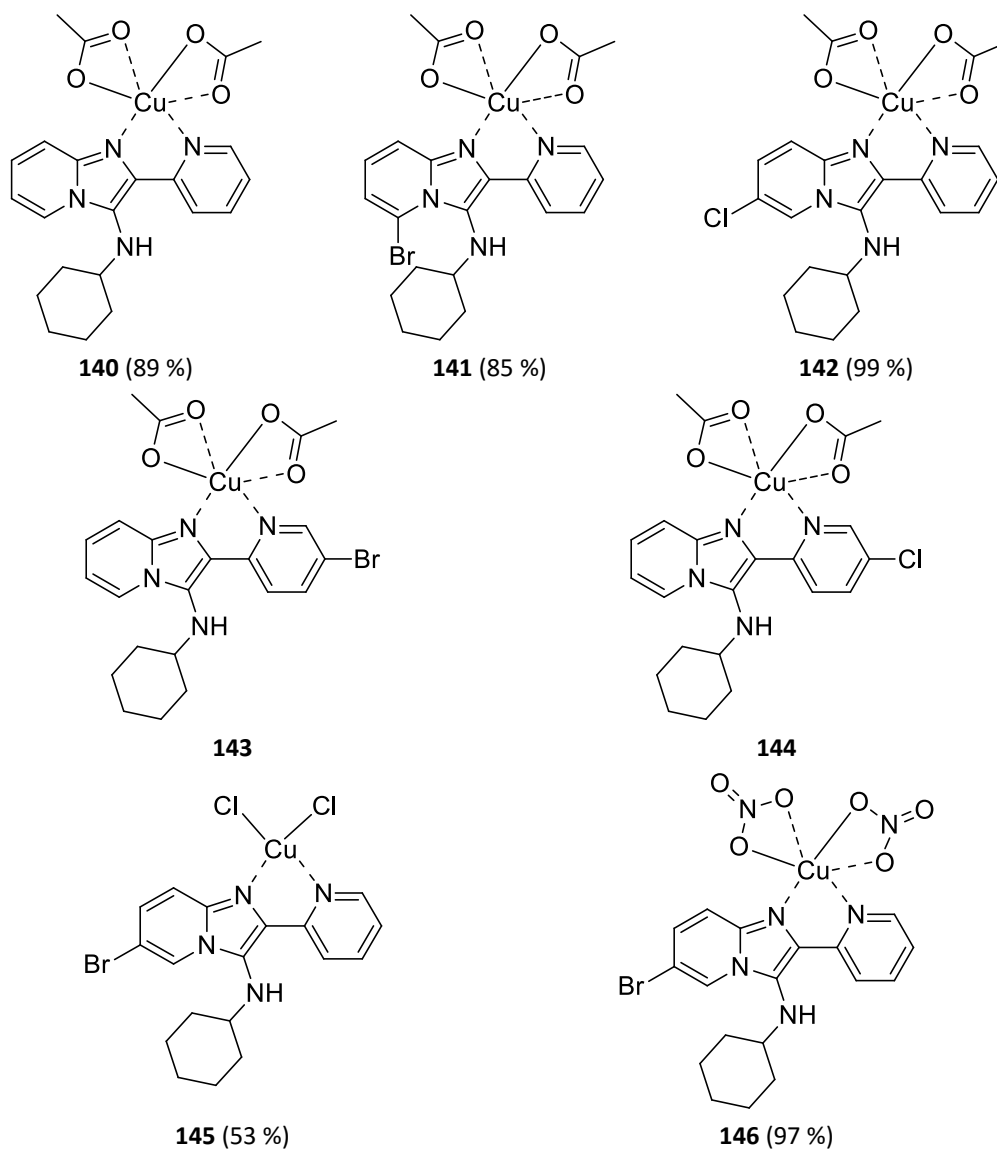


Figure 67 – Copper complexes (140 to 146) synthesized to for the SAR study

This series of compounds highlighted the importance of using crystallography in this project. Suitable crystals of all of the complexes synthesized for this series were grown from the appropriate solvents. Figure 68 shows the ORTEP diagrams for complexes **140** to **142**, showing the resulting complexes were as expected. Unfortunately the complexation reaction of imidazo[1,2-*a*]pyridine **136** with copper acetate was unsuccessful as determined by ESI mass spectroscopy where no ligand could be detected.

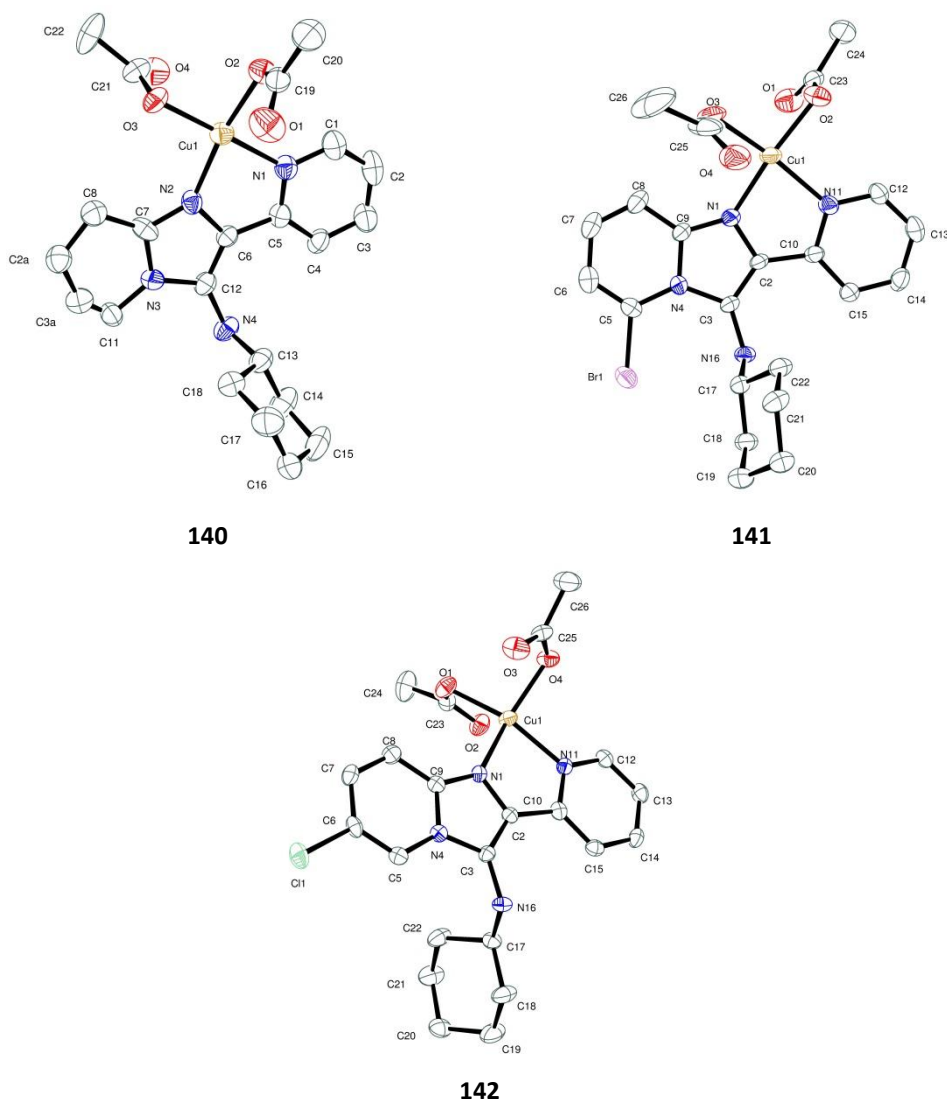


Figure 68 – The asymmetric units of 140, 141 and 142 (hydrogen atoms are omitted for clarity)

While we expected that the complexes generated from **138** and **139** would form the monomer complexes **143** and **144** as all the previous metal complexes had, SCXRD showed that reactions do not always go as expected. The complexes generated were in fact **147** (A) and **148** (B) shown in Figure 69.

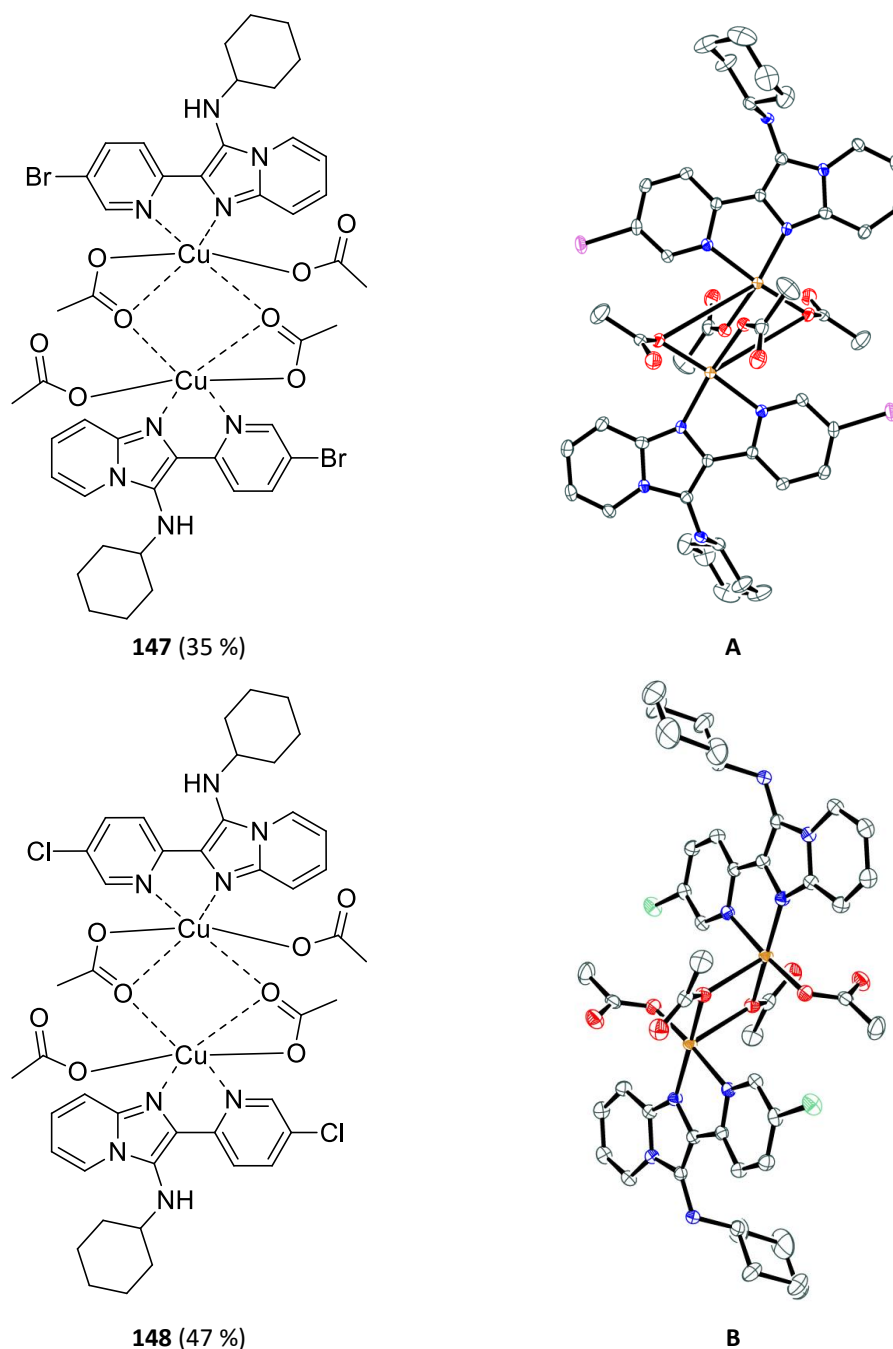
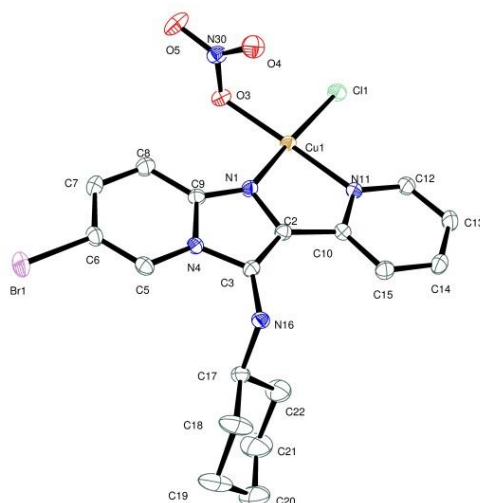


Figure 69 – The structures and asymmetric units of 147 and 148 (hydrogen atoms are omitted for clarity)

Given that all the copper complexes had acetate moieties as counterions, it was deemed important to investigate other types of counterions, in this case chloride and nitrate. Preparation of the copper sulfate derivative of **88** was attempted, however this was found to be unsuccessful also using ESI mass spectroscopy. Complex **145** was crystallized by slow evaporation from a $\text{CDCl}_3/d_4\text{-MeOD}$ mixture, explaining why one nitrate group was replaced by a chlorine atom. The resulting crystal structure for **145** is given in Figure 70.



145

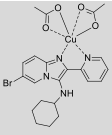
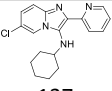
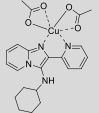
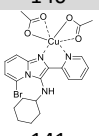
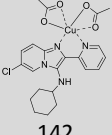
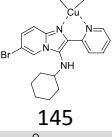
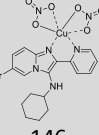
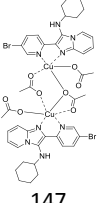
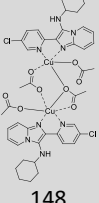
Figure 70 – The asymmetric unit of 145 (hydrogen atoms are omitted for clarity)

2.4.8. Results from Biological Testing

On the back of the success seen in the anticancer activity of copper complex **123**, we hoped to gain some insight into the structurally important features in the complex, if not to further improve the anticancer activity of the copper complexes. Imidazo[1,2-*a*]pyridines **134** to **139** and copper complexes **140** to **146** were sent for testing at Wits School of Pharmacology with Dr Harmse and her team for the same testing that was done on the other small library. The results from these tests are shown in Table 6, where complex **123** has been included for ease of comparison.

Results and Discussion

Table 6 - IC₅₀ values (μM) obtained for the active compounds in the SAR study in colorectal (HT-29 and Caco-2), breast cancer (MCF7 and MDA-MB231) and leukemia (K562 and HL-60) cell lines

Compound	Colorectal Cancer Lines		Breast Cancer Lines		Leukemia Lines	
	HT-29	Caco-2	MCF7	MDA-MB231	K562	HL-60
Camptothecin	5.0 ± 0.7	11 ± 2	0.32 ± 0.01	0.33 ± 0.04	2.6 ± 0.2	0.005 ± 0.003
 123	8.0 ± 0.4	12.2 ± 0.6	0.62 ± 0.03	28 ± 2	1.9 ± 0.9	2.2 ± 0.5
 137	67 ± 5	-	23 ± 3	-	-	29.2 ± 0.7
 140	3 ± 1	11 ± 1	1.1 ± 0.6	-	3 ± 1	3 ± 1
 141	6 ± 1	10.94 ± 0.06	1.20 ± 0.08	2.4 ± 0.4	6.0 ± 0.4	2.1 ± 0.3
 142	14 ± 2	48 ± 3	3.8 ± 0.9	19 ± 1	3.0 ± 0.4	5 ± 2
 145	10 ± 3	1.6 ± 0.4	1.0 ± 0.5	14 ± 1	11.1 ± 0.8	3.6 ± 0.1
 146	14 ± 4	24.6 ± 0.3	1.1 ± 0.3	19 ± 1	9 ± 1	12 ± 4
 147	-	-	8.2 ± 0.4	23 ± 4	4 ± 2	13 ± 3
 148	14 ± 4	20 ± 1	9.2 ± 0.9	18 ± 2	10.6 ± 0.7	14 ± 2

All of the copper complexes (**140** to **146**) submitted for testing showed significant anticancer activity. In the colorectal cancer cell lines it can be seen that moving the bromine substituent from the 6-position to the 5-position (as in **141**) significantly increases the activity of the compound. However, compound **142** also showed better activity than **123**, suggesting that a chlorine substituent may be more favourable than the bromine atom in the same position. The activity of these compounds are comparable to and slightly better than that of the camptothecin standard. In the Caco-2 cell line, changing the counterion from the acetate groups in **123** to the chloride ions in **145** results in a ten-fold improvement in the activity of the compound.

In the MCF7 breast cancer cell line all of the complexes showed good to excellent activity. In this study copper complex **123** continued to show the greatest activity in the library. Considering how low the IC₅₀ value for camptothecin is, to have complexes showing similar activity is an excellent result. Copper complexes **140**, **141**, **145** and **146** also show excellent activity against this cancer cell line. This suggests that having a halogen substituent on the imidazo[1,2-*a*]pyridine ring improves the activity while the counterion has little effect on the overall activity. In the MDA-MB231 cell line, only **141** showed any significant activity. Considering this showed good activity in the MCF7 cell lines as well, this makes complex **141** of particular interest for the possible treatment of breast cancer.

The K562 leukemic cell line was also particularly susceptible to the imidazo[1,2-*a*]pyridine—copper complexes. Again complex **123** had the best activity, showing a greater activity than that of camptothecin. Complexes **140**, **142** and **143** also showed comparable activity to that of camptothecin. Changing the counterion from the acetate groups decreased the activity of the compounds substantially. Unfortunately none of the complexes tested showed any activity comparable to camptothecin, however, several complexes showed IC₅₀ values below 3 μM in the HL-60 leukemic cell line - **123**, **140**, **141** and **145**. Copper complexes **123** and **140** showed significant anticancer activity in both leukemic cell lines and could be developed further in the treatment of leukemia.

The final series of compounds was used to test the toxicity of these compounds towards leucocytes. Leucocytes were dosed at 20 μM for 24 hours and analysed using an MTT assay as before. From Figure 71 it can be seen that the imidazo[1,2-*a*]pyridines **134** to **139** show little toxicity in the leucocytes. The copper complexes (**140** to **146**) in general showed a greater toxicity than that of the imidazo[1,2-*a*]pyridines and the camptothecin, with complex **145** exhibiting the most toxicity and complex **143** the least, being comparable to that of the imidazo[1,2-*a*]pyridines and camptothecin.

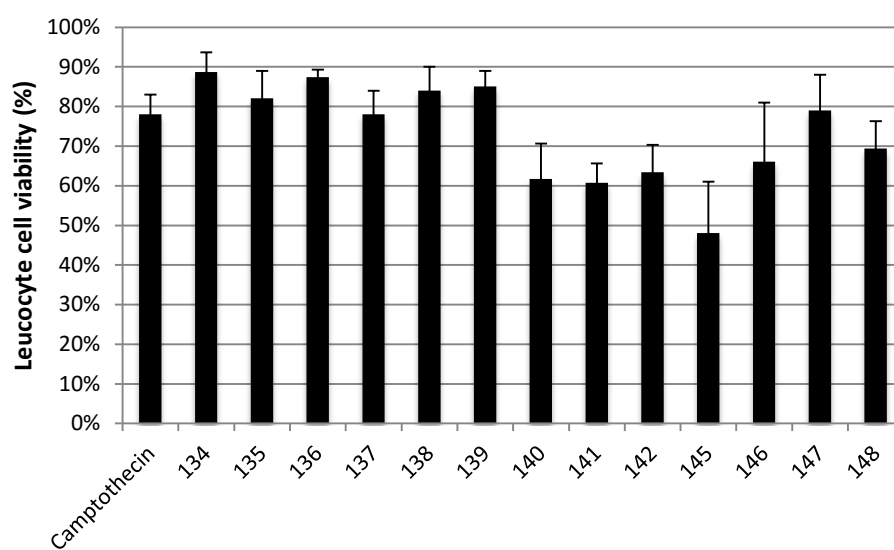


Figure 71 - Leucocyte viability when exposed to selected imidazo[1,2-*a*]pyridines and imidazo[1,2-*a*]pyridine-metal complexes at 20 μ M for 24 hours

At the end of my tether:

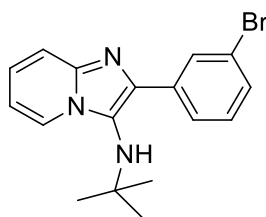
Conclusions and Future

Work

3.1. Imidazo[1,2-*a*]pyridine synthesis and biological activity

Over the course of this project, the library of available imidazo[1,2-*a*]pyridines synthesized by our laboratory was expanded upon significantly (imidazo[1,2-*a*]pyridines **85** to **102**). This was done using previously developed methodology,⁹¹ as well as modified methodology using ethanol as a solvent. The use of ethanol as a solvent resulted in reactions with fewer side products and were higher yielding overall. The yields for the Groebke-Blackburn-Bienaymé multicomponent coupling reaction were notoriously unpredictable and could potentially be further investigated to optimize each individual reaction. The type of acid catalyst used in the coupling reaction could be another avenue for further investigation.

Testing this imidazo[1,2-*a*]pyridine library against leukemic (K562 and HL-60), breast (MCF-7 and MDA-MB231) and colorectal (Caco-2 and HT-29) cancer cell lines only resulted in one compound that showed significantly better activity than those previously investigated by de Koning and co-workers.⁹¹ Imidazo[1,2-*a*]pyridine **102** (Figure 72) showed significant activity in the HT-29 colorectal cancer cell line ($IC_{50} = 4.1 \pm 0.4 \mu\text{M}$).¹⁰⁹ Additionally, these compounds did verify that the imidazo[1,2-*a*]pyridines show significantly lower toxicity towards leucocytes than the camptothecin standard they were tested against (Figure 44 and Figure 71).



102

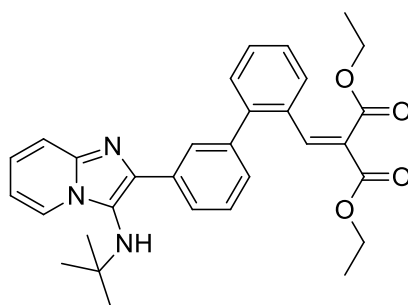
Figure 72 – Imidazo[1,2-*a*]pyridine showing the greatest anticancer activity

3.2. Attempts at modifying the imidazo[1,2-*a*]pyridines and attempted tether syntheses

With the intention of synthesizing metal-imidazo[1,2-*a*]pyridine complexes, we initially envisaged that a tether (or linker) would have to be built onto the imidazo[1,2-*a*]pyridine in order to house the metal. This was to come from diethyl malonate or malononitrile directly or from the tether derivatives (**103**) being added to the imidazo[1,2-*a*]pyridine.

The use of Suzuki-Miyaura coupling reactions in modifying the bromine-containing imidazo[1,2-*a*]pyridine was found to be successful using a variety of substituted phenyl boronic acids, using both conventional and microwave conditions and using Pd(PPh₃)₄ as a catalyst.¹⁰⁵ The reactions were successful regardless of the position of the bromine on the imidazo[1,2-*a*]pyridine.

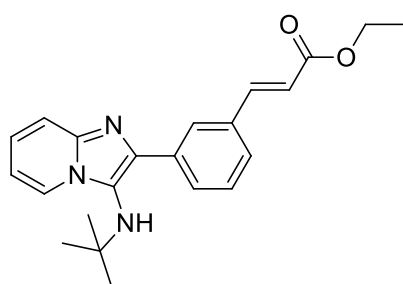
The addition of a vinyl group to the imidazo[1,2-*a*]pyridine was successful using Suzuki-Miyaura cross coupling, resulting in the formation of both **106** and **107**. Unfortunately using a cross metathesis reaction to add **103** to the imidazo[1,2-*a*]pyridine was unsuccessful despite extensive investigation. A benzaldehyde substituent was also successfully added to the imidazo[1,2-*a*]pyridine using 2- or 4-formylphenylboronic acid (**108** to **110**). Using **109** in a Knoevenagel reaction with diethyl malonate was successful under Dean Stark conditions to afford **111** (Figure 73), however the compound was not successfully reduced to the diol required to house the metal.



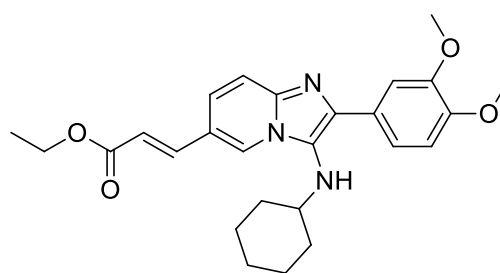
111

Figure 73 – The product from the successful Knoevenagel condensation reaction

The imidazo[1,2-*a*]pyridines resulting from the Suzuki-Miyaura coupling reactions were very large. This made adding small molecules (like the tethers) onto the large imidazo[1,2-*a*]pyridine troublesome. The Heck reaction was then investigated to add a shorter, more flexible tether onto the imidazo[1,2-*a*]pyridine. Using a previously developed method for Heck coupling reactions,¹⁰⁷ ethyl acrylate was successfully coupled to the aromatic bromide containing imidazo[1,2-*a*]pyridines **85** or **102** resulting in **114** and **113** respectively (as shown in Figure 74). The reaction was higher yielding when the bromide was on the R₂ substituent (**102**) which went to completion, rather than directly on the ring itself (**85**) where starting material was recovered from the reaction. The ester (**113**) was reduced to the carboxylic acid using potassium hydroxide, however this resulted in a compound that was insoluble and could not be used in further chelation attempts.



113



114

Figure 74 – Products from the Heck coupling reactions

To add diethyl malonate or malononitrile directly onto the molecule, arylation reactions were also investigated. Scheme 25 and Scheme 26 outline the attempts at the arylation reactions using a wide variety of catalysts and reaction conditions, however none of these reactions were successful.

Unfortunately no tethered complexes were successfully synthesized over the course of this project and could serve as an area for potential further development.

3.3. Introducing metals to the imidazo[1,2-*a*]pyridines

3.3.1. Introducing ferrocene to the imidazo[1,2-*a*]pyridine

The first attempt to add metals to the imidazo[1,2-*a*]pyridine was made by using ferrocenecarbaldehyde to introduce it directly onto the imidazo[1,2-*a*]pyridine in the Groebke-Blackburn-Bienaymé coupling reaction. This resulted in the formation of compounds **115** to **117** in varying yields. These compounds were found to exhibit significant π stacking, making these compounds insoluble. Due to this insolubility, the anticancer activity of these compounds could not be determined.

3.3.2. Synthesis of isocyanides to generate a wider variety of imidazo[1,2-*a*]pyridines

In order to use the Groebke-Blackburn-Bienaymé coupling reaction to generate imidazo[1,2-*a*]pyridines, substituted isocyanides are required. Over the course of this project it was noted that there were several limitations to the isocyanides that could be commercially obtained, leading to benzyl and adamantyl isocyanide being synthesized using methodology used extensively in our laboratory.¹¹⁴ Both the benzyl and adamantyl isocyanides were synthesized in good yields and used to generate imidazo[1,2-*a*]pyridines **124** and **126** along with a commercially available ethyl isocyanoacetate to form **124**.

3.3.3. Adding metals directly to the imidazo[1,2-*a*]pyridine

Having been unsuccessful in adding a tether to the imidazo[1,2-*a*]pyridine, we attempted to add metals directly onto the imidazo[1,2-*a*]pyridine ring using imidazo[1,2-*a*]pyridine **88**. This was found to be successful using a variety of metal salts (ZnCl_2 , Zn(OAc)_2 , Cu(OAc)_2 and PtCl_2), resulting in the formation of compounds **120** to **123**. The general description for the types of metal complexes synthesized is given in Figure 75. It was found that the zinc acetate and platinum chloride complexes could be characterised using NMR spectroscopy; the imidazo[1,2-*a*]pyridine signals could be identified in the ^1H NMR spectrum even with the significant shifting and reduced signal splitting. All of the compounds could only be conclusively characterised using single crystal x-ray diffraction and elemental analysis.

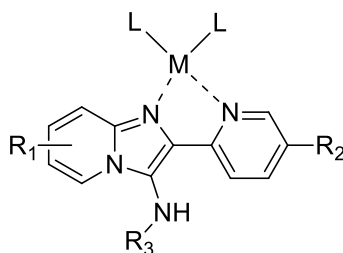


Figure 75 – General scaffold for the metal complexes synthesized

This library was expanded to include metal complexes generated from the imidazo[1,2-*a*]pyridines **124-126**. The resulting complexes were outlined in Figure 56 and were intended to investigate the biological importance of the nature of the R₃ substituent.

3.3.4. Complex Stability Studies

Given that the types of complexes in Figure 50 and Figure 56 were novel, investigation into the stability of the compounds was paramount. Having ruled out the usual closed cell titration setup due to the imidazo[1,2-*a*]pyridines reacting with the silicone tubing (Figure 60), out-of-cell p*K* titrations in 50% methanol/water with a 1 mM MES and NaH₂PO₃ buffer system were performed. Imidazo[1,2-*a*]pyridines **88**, **124**, **125** and **126**, zinc complexes **120**, **121**, **127**, **130** and **132** and copper complexes **123**, **128**, **131** and **133** were investigated. The p*K* values were calculated using SigmaPlot and are summarised in Table 4. The imidazo[1,2-*a*]pyridines were found to exhibit only a single p*K* value instead of the 2 which were expected for each coordinating nitrogen, this was attributed to the significant hydrogen bonding that was seen in the crystal structures for the molecules (Figure 49 and Figure 55). This hypothesis was further supported by the hydrogen bond being preserved in a crystal grown from HBr (Figure 63). The metal complexes showed the expected 2 p*K* values. All of the compounds investigated in this study showed p*K* values below pH 7.35 (except for **130**) and thus can be expected to be stable under physiological conditions.

3.3.5. Anticancer activity of the metal complexes

Testing these compounds against leukemic, colorectal and breast cancer cell lines resulted in the copper-imidazo[1,2-*a*]pyridine complex **123** (Figure 76) showing the greatest activity in the leukemic and breast cancer cell lines and **128** in the colorectal cancer cell lines. The zinc and platinum complexes that were tested showed little to no significant activity in any of these lines. These results earmarked **123** as a potential lead compound that could be further developed. The copper complexes in this study were shown to have comparable toxicity to that of camptothecin in leucocytes, with **131** showing the greatest toxicity in the series (Figure 64).

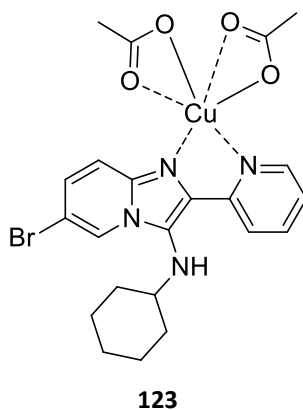


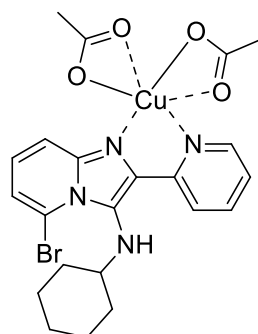
Figure 76 – Potential lead copper complex 123

In general it was found that crystals suitable for SCXRD could be grown using d_4 -MeOD for zinc complexes and $CDCl_3$ for the copper-containing compounds.

3.3.6. Investigation into the Structure-Activity relationship

In order to do a more detailed structure-activity study, the metal complex library was further expanded to investigate the importance of the halogen as well as position on the imidazo[1,2-*a*]pyridine, as well as the effect of the counterion on the metal salt used. In order to investigate the significance of the halogen in this study imidazo[1,2-*a*]pyridines **134** to **139** were synthesized using the general procedure and copper complexes **140** to **144** were made from these compounds. Additionally compounds **145** and **146** were synthesized from **88** in order to investigate the counterion effect on the activity of the molecule. Testing the anticancer activity of these compounds resulted in significant activity being observed in all the copper complexes tested. In the colorectal cancer cell lines (HT-29 and Caco-2) complex **140** was found to be the most active complex, suggesting that the position of the halogen was significant. In the Caco-2 cell line it was noted that changing the counterion from acetate groups to chloride ions (as in **145**) showed a significant change in activity.

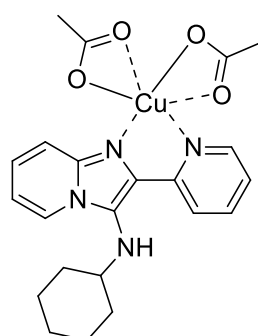
In the MCF7 breast cancer cell line, copper complex **123** showed the most significant activity of all the complexes tested. Complexes **140**, **141**, **145** and **146** showed excellent activity that should also be noted. The MDA-MB231 cell lines were mostly resistant to the imidazo[1,2-*a*]pyridines tested in this study, however complex **141** (Figure 77) showed the most significant activity. Combining this with the activity of **141** seen in MCF7 cells this compound should be further investigated for its use in the fight against breast cancer.



141

Figure 77 – Most active compound in breast cancer cell lines

In the K562 leukemic cell lines, copper complex **123** showed greater activity than that of camptothecin. In this cell line it was noted that changing the counterion from acetate groups to chloride or nitrate ions dramatically decreased the activity of the compounds. None of the complexes showed activity comparable to camptothecin in the HL-60 cancer cell line, however, several showed anticancer activity at concentrations below 3 μ M. Copper complexes **123** and **140** (Figure 78) showed notable activity in both the K562 and HL-60 cell lines which could be further developed as a treatment for leukemia.



140

Figure 78 – A copper complex showing significant anticancer activity in K562 and HL-60 cancer cell lines

Having obtained these excellent anticancer results, further testing on these active compounds is required. Testing these compounds in an animal model would give far more information on how successful these compounds would be as potential drug candidates. It would also help us gain a better understanding of how these compounds behave in the body and what the potential side effects could be. Since the exact target of these molecules is not known, testing in an animal model could also help narrow down the exact target.

Plot Twist

Plot Twist:

Introduction

The choice of reagent used to perform a particular reaction is invariably key in organic synthesis. The reaction conditions (solvent, temperature, atmosphere etc.) often govern the reaction that a particular reagent can mediate – especially when the reagent can facilitate multiple transformations. Two related reagents of particular importance to this section of this PhD are ceric ammonium nitrate (CAN) and ceric ammonium sulfate (CAS) and their novel use in organic synthesis. Before discussing their use in these novel reactions, it is important to revisit the existing uses of CAN and CAS. The review below details the previous transformations made possible by both CAN and CAS.

4.1. The use of Ceric Ammonium Nitrate in Organic Synthesis

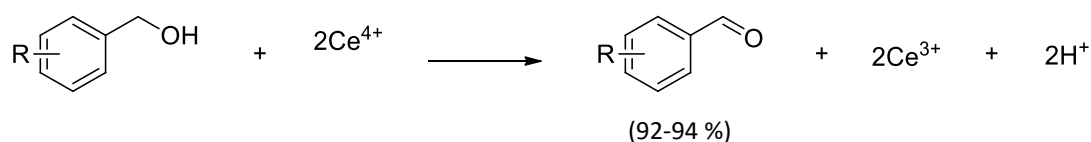
Found on the shelves of nearly every organic chemistry lab is ammonium cerium(IV) nitrate, commonly referred to as ceric ammonium nitrate or CAN. Commercially available as dark orange crystals or a light orange powder, it is considered to be a typical example of a cerium salt in the 4+ oxidation state. Smith *et al.* were of the first research groups to synthesize and make use of CAN in 1936. Before this point, ceric sulfate had been used as an oxidative standard in titrations. Obtaining analytically pure ceric sulfate proved problematic at the time with high concentrations of other lanthanide species remaining present in the salt. They reported a highly efficient synthesis of CAN in high purity even from the highly impure cerium sulfate starting material. Additionally this new salt showed significantly improved solubility and stability in water and

organic solvents and since then has been widely used in analytical testing and organic synthesis.¹¹⁹

It wasn't until 1968 that the crystal structure was reported by Beineke and Delgaudio that confirmed the structure proposed by Smith *et al.* – $(\text{NH}_4)_2\text{Ce}(\text{NO}_3)_6$.¹²⁰ In the decades that have followed, CAN has been found to efficiently transfer a single electron, reducing the Ce^{4+} to the equally stable Ce^{3+} and as a result making it suitable for many different applications. It has also been noted that the solvent choice can influence the behaviour of the CAN in the reaction, allowing for a variety of different types of reactions to occur.¹²¹

4.1.1. CAN as an oxidant

One of the first reported uses of CAN for synthetic purposes was in the Physical Chemistry laboratories at Oxford by J. Shorter where it was found that alcohols and ketones containing α -hydrogen atoms could be oxidized to carbon dioxide, formic acid or acetic acid.¹²² Shortly after Shorter's findings were published Trahanovsky and Young further developed the methodology to make it more suitable for synthetic oxidations of organic molecules. Additionally they showed that these oxidations can be applied to the oxidation of benzyl alcohols to benzaldehydes in excellent yields. Scheme 25 outlines this synthesis that was performed in a 50% aqueous acetic acid solution containing a 0.5 M CAN solution at room temperature (or slightly warmed) for a few minutes before being extracted with ether and washed with 1.5 M potassium hydroxide solution.¹²³



Reaction conditions: 0.5 M CAN 50 % AcOH/H₂O, rt.

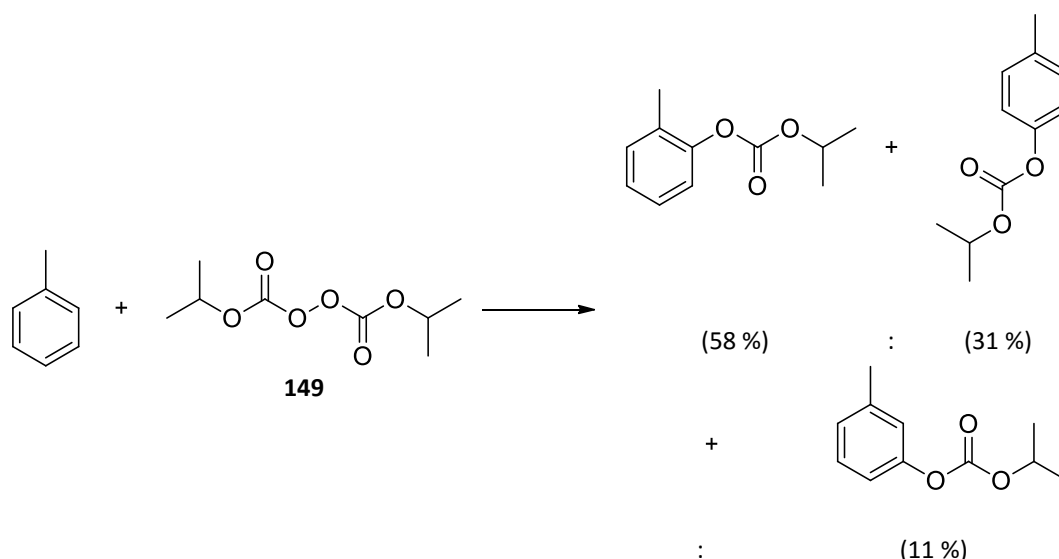
Scheme 25 – CAN-mediated oxidation of benzyl alcohols to benzaldehydes, where R = H, OMe, NO₂ or Br

A few years after, they extended their work to the oxidation of cyclopropylmethanol to cyclopropanecarbaldehyde in water at 75 °C. What made this work of particular importance was that it was a relatively high yielding reaction where all other reported yields for this oxidation with other oxidants tended to be low or as a by-product of another reaction.¹²⁴

Following these initial reports, the use of CAN as an oxidant became increasingly popular. The first review on the use of CAN in organic synthesis was published in 1973 by Ho. In this review he

highlighted that while exposing primary alcohols to CAN generates aldehydes (as in Scheme 25), similarly secondary alcohols could be oxidized to ketones.¹²⁵

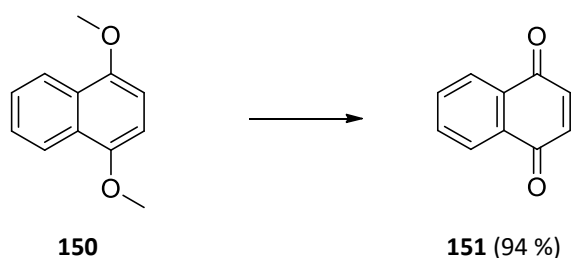
Using CAN, Kurz *et al.* found that dicarbonates could be introduced to a toluene molecule from various peroxide sources (such as **149** in Scheme 26). They found that the carbonate could be added in a variety of different positions as shown in Scheme 26.¹²⁶



Reaction conditions: CAN (2.25 eq), MeCN, 60 °C, 24 h.

Scheme 26 – Oxidative dicarbonate additions to toluene using CAN

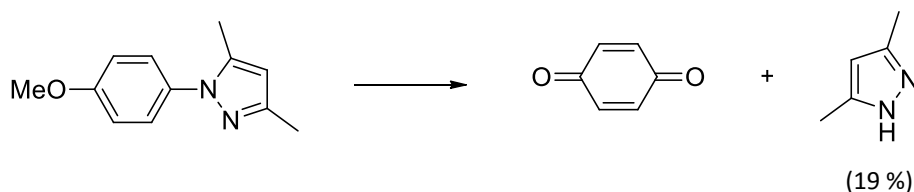
One of the most important examples of the use of CAN as an oxidant for this project was described by Jacob *et al.* where CAN was used to oxidize 1,4 dimethoxybenzenes to their corresponding quinones. These reactions were performed in acetonitrile with the addition of 2-3 equivalents of CAN as an aqueous solution at room temperature for 30 minutes. During this study it was also noted that 1,4-dimethoxynaphthalene (**150**) could be oxidized to naphthoquinone (**151**) exclusively using the conditions shown in Scheme 27.¹²⁷ This particular method can also be applied to 1,4-dihydroxybenzene systems as well as highly substituted 1,4-dimethoxynaphthalene derivatives.¹²¹



Reaction conditions: CAN aq (2-3 eq), MeCN, rt.

Scheme 27 – CAN-mediated oxidation of 1,4-dimethoxynaphthalene to naphthoquinone

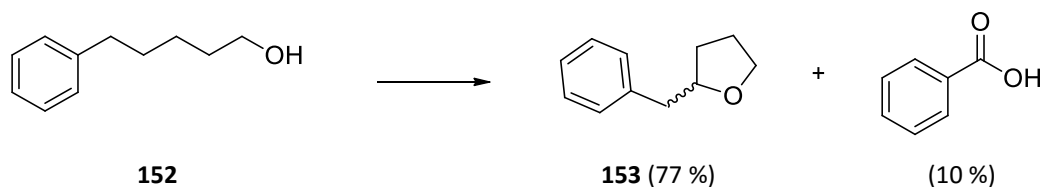
This reaction has since become a staple in the synthetic chemist's handbook and is common practise in our laboratories.¹²⁸ The oxidative abilities is not only limited to dimethoxy or dihydroxy substituents, but can also be applied to asymmetrical molecules. Butler *et al.* found that CAN could be used to oxidize *N-p*-anisylazoles to quinones and pyrazoles as shown in Scheme 28 where both products could be successfully isolated. Their study found similar results with triazoles, tetrazoles and pentazoles (which decomposes spontaneously to azide and nitrogen gas). Additionally it was found that the C–O and C–N bonds were oxidized preferentially to C–C bonds.¹²⁹



Reaction conditions: CAN (2.1 eq), MeOH/H₂O, rt, 24 h.

Scheme 28 – Oxidation of *N-p*-anisylazole to quinone and pyrazole using CAN

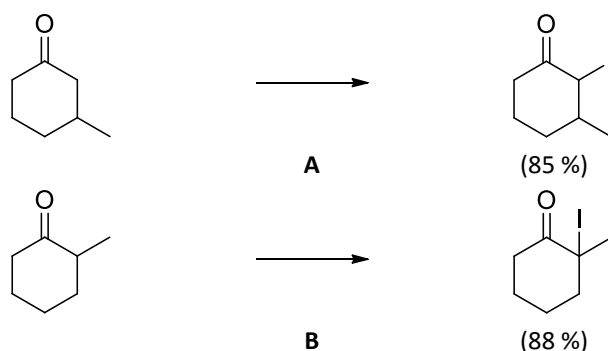
Aside from just a basic oxidation, it has been found that the oxidative conditions could prompt further reactions. Doyle *et al.* found that exposing substituted alkyl alcohol chains (such as **152**) with a phenyl substituent to CAN resulted in the formation of furan type rings, such as **153** outlined in Scheme 29 with minimal formation of side products (such as benzoic acid).¹³⁰



Reaction conditions: CAN (2 eq), MeCN/H₂O, 75 °C.

Scheme 29 – CAN-mediated oxidation of alkyl alcohol to form a furan ring

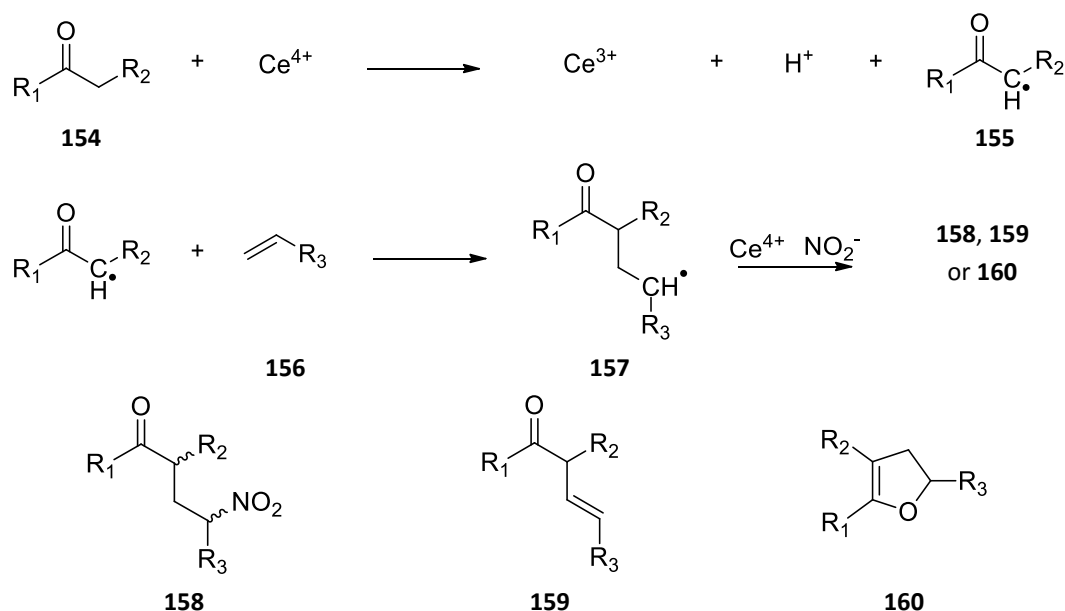
Horiuchi and Kiji found that in the presence of CAN, oxidative iodination could be performed on cyclic and acyclic ketones selectively at the α -position (Scheme 30A). They found that, given the choice, iodination occurs at the more highly substituted position as shown in Scheme 30 in high yields.



Reaction conditions: CAN (0.5 eq), I_2 (0.5 eq), AcOH/H₂O, 50 °C, 8 h.

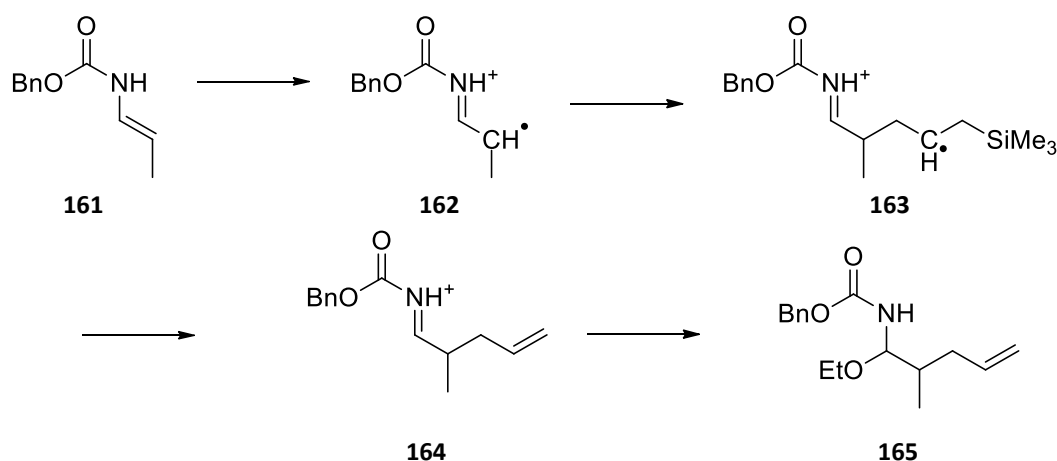
Scheme 30 – α -position iodination of cyclohexanones

The research group of Baciocchi has done extensive investigations into the use of CAN as an oxidant. Amongst their substantial research was the 1,2- and 1,4-addition of aldehydes/ketones (**154**, Scheme 31) with alkenes enabled by CAN. In this report, a mechanism for the addition was proposed where CAN was used to generate an α -ketoalkyl radical on the aldehyde/ketone (**155**) which could add to the alkene (**156**) to generate radical **157**. On exposure to a further equivalent of CAN, and the presence of a counterion (ONO_2^-) three products would be possible – nitroketoalkane **158**, the unsaturated adduct **159** and the dihydrofuran **160**. They concluded surprisingly that **158** tended to be the major product out of the reactions, and the that R_3 substituent was unaffected by the reaction regardless of its degree of saturation. They made no mention of the resulting stereochemistry in nitroketoalkane **158**.¹³¹



Scheme 31 – 1,2- and 1,4-oxidative additions of alkenes to ketones

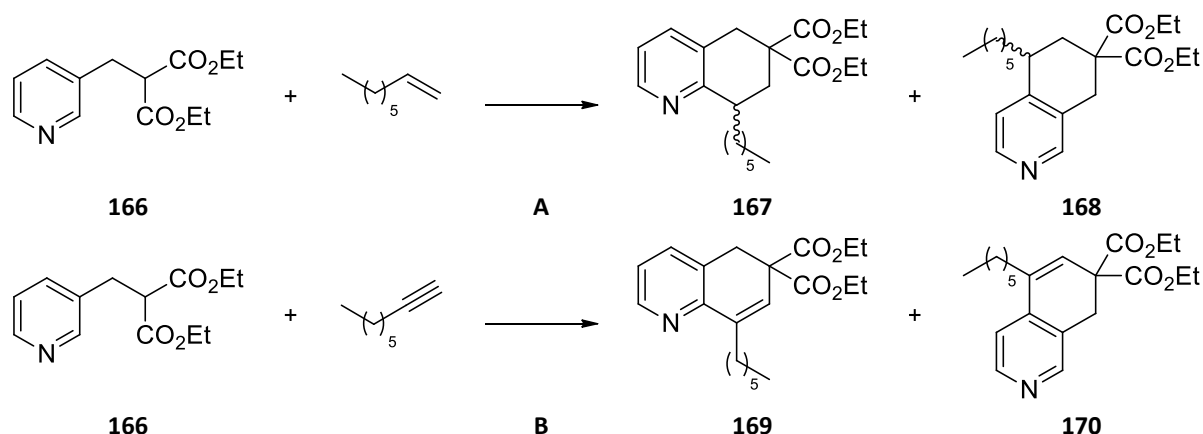
In molecules where there is no α -carbon, CAN can still be used to perform other vinylic and alcoholic coupling reactions with carbonyl-containing compounds (e.g. carbamates). A recent example of such a reaction was published by Bekkaye and Masson. They postulated a mechanism for the reaction where CAN oxidizes carbamate **161** to generate radical **162** (Scheme 32). This radical reacts with allyltrimethylsilane to form intermediate **163** which would be immediately oxidized by a further equivalent of CAN, in the process removing the trimethylsilyl (TMS) group to form **164**. The alcohol (such as EtOH in the example given in Scheme 32) can then add nucleophilically to the imine to form the desired product **165** in a single pot. Bekkaye and Masson generated a library of about 20 compounds using this method with other highly substituted carbamates, allyltrimethylsilanes and a few simple alcohols making this a method that could be widely used to generate β -allylated α -carbamido ethers under relatively mild conditions.¹³²



Reaction conditions: CAN (2.5 eq), allyltrimethylsilane (1 eq), EtOH (1 eq), MeCN, -15 °C, 1 h.

Scheme 32 – Multicomponent coupling reaction using CAN in the formation of complex vinyl carbamates

Citterio *et al.* used CAN to add alkene and alkyne substituents to diethyl (pyridylmethyl)malonate (such as **166**) as shown in Scheme 33. This resulted in the formation of cyclic products **167-170** in relatively high yields. Interestingly, for the alkene addition (Scheme 33A) the formation of the *ortho* product **167** and *para* product **168** was in a nearly equal ratio, with the *para* product being in slight excess when the reaction was performed in methanol. Conversely, the reaction with the alkyne (Scheme 33B) resulted in the substantial major product being the *ortho* product **169** under similar conditions.¹³³

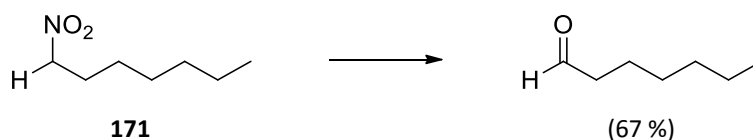


Reaction conditions: CAN (2.2 eq), MeOH, N_2 , rt, 1-6 h.

Scheme 33 – Alkene and alkyne addition to diethyl (pyridylmethyl)malonate facilitated by CAN oxidation

In the presence of mole equivalents of CAN, benzylic alcohols could be oxidized to the corresponding benzaldehydes. Mehdi *et al.* investigated performing these reactions in ionic liquids. When substituted benzyl alcohols were exposed to 2 mol equivalents of CAN in 1-alkyl-3-methylimidazolium triflate at 100-125 °C for 6-8 hours the alcohols were oxidized to their benzaldehyde in near quantitative yields. What was interesting to note was that no nitrated product or benzoic acid was collected when this ionic liquid was used.¹³⁴

Another use of CAN in an oxidative role is as an alternative to the Nef reaction in generating ketones and aldehydes from nitro compounds. Scheme 34 is an example of the reactions investigated by Olah and Gupta where the nitro alkane **171** was oxidized to heptaldehyde using a single equivalence of CAN (aqueous) in triethylamine and acetonitrile. In this study they found their method applicable to primary or secondary nitro alkyl (or alkyl aryl) compounds. A similar procedure can be performed on silyl nitronates as well as some unsaturated nitro compounds.¹³⁵

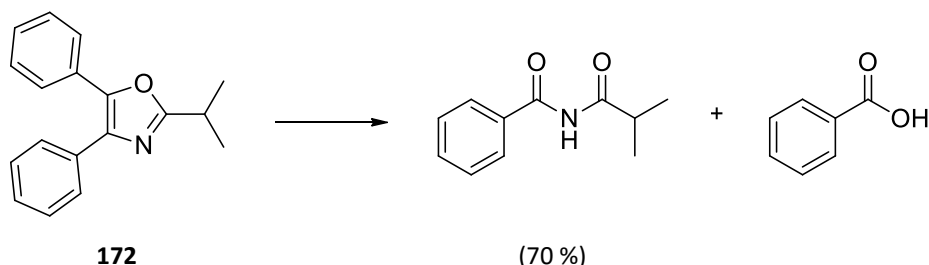


Reaction conditions: NEt_3 , aqueous CAN (1 eq), MeCN, 50 °C, 1.5 h.

Scheme 34 – An example of the use of CAN to oxidize nitro compounds to aldehydes

Of course the oxidation is not limited to ring forming reactions, but can also oxidize heterocycles into open ring analogues. Evans *et al.* provide an excellent example of this where they made use of CAN to oxidize oxazoles in moderate to good yields. They investigated this reaction with a wide variety of substituted oxazoles (such as **172** in Scheme 35) and found it to be widely applicable.

Performing the same reaction with other oxidants did not result in the same outcome. Only partial conversion was achieved using KMnO_4 and $\text{Ce}(\text{OTf})_4$, however none to the excellent extent that was achieved with CAN. Interestingly, not all cerium based oxidants could be used for this transformation.¹³⁶

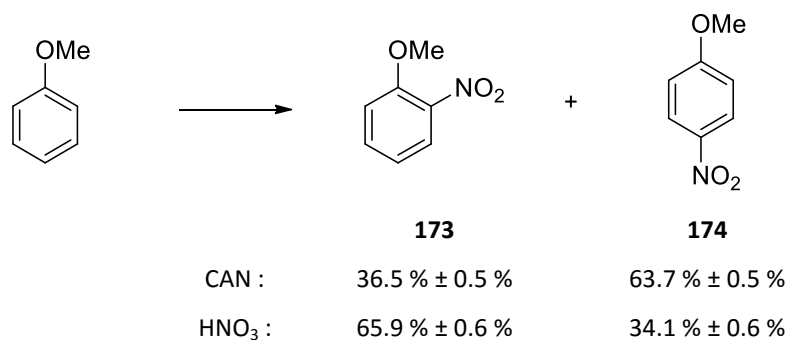


Reaction conditions: CAN (3.8 eq), MeCN/ H_2O , rt.

Scheme 35 – Oxidation of oxazoles to form imides and carboxylic acids

4.1.2. CAN as a nitrating agent

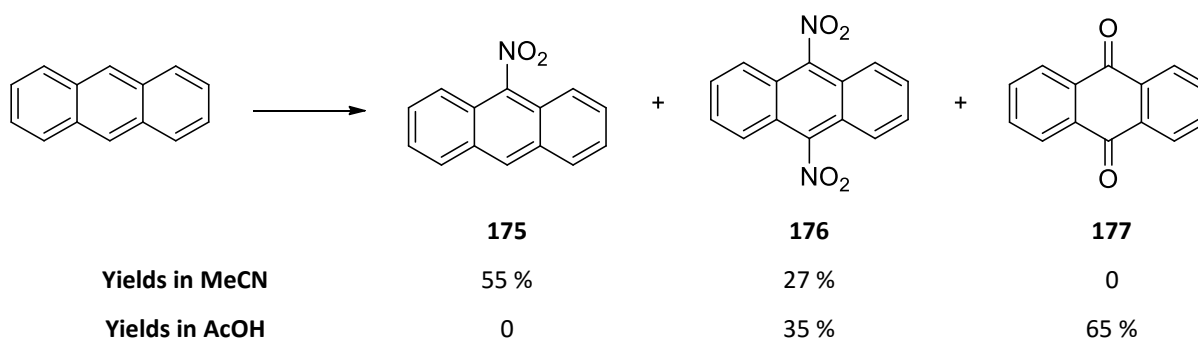
Aside from oxidations, CAN has been used in the nitration of organic compounds. One of the first reports of this particular feature of CAN was by Ridd and his co-worker Dinçtürk where they nitrated several substituted benzene derivatives in acetonitrile. They compared their results to the standard method for nitration using concentrated nitric acid. Their results showed no significant difference between CAN and nitric acid in the ratio of the products (*ortho* or *para*) formed with the exception of with anisole where with CAN the major product formed was *para* product **174** (Scheme 36) while with nitric acid, *ortho* product **173** was the major resulting product. Additionally they found that the addition of water to the reaction suppressed nitration. The anisole reaction is shown in Scheme 36 outlining the differences in ratios between the nitric acid and the CAN-mediated reaction.¹³⁷



Reaction conditions: CAN or HNO_3 (1 eq), MeCN, 84 °C, 2 min.

Scheme 36 – Nitration of anisole using CAN and HNO_3

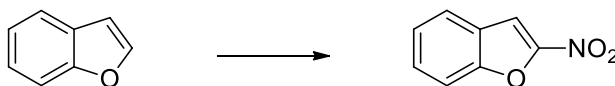
Chawla and Mittal used CAN on a silica gel support to nitrate fused aromatic rings such as naphthalene, anthracene (used as an example in Scheme 37) and phenanthrene. They found that when only acetonitrile as a solvent was included in the reaction mononitrated (such as **175**) and dinitrated products (such as **176**) resulted. When the reaction was performed in acetic acid the resulting products were dinitrated aromatics (such as **176**) as well as quinones (e.g. **177**) further highlighting the importance of the role of the solvent in the nature of reactions that occur.¹³⁸



Reaction conditions: CAN (1.1 eq), SiO₂ (1 g), 60-65 °C, 1 h.

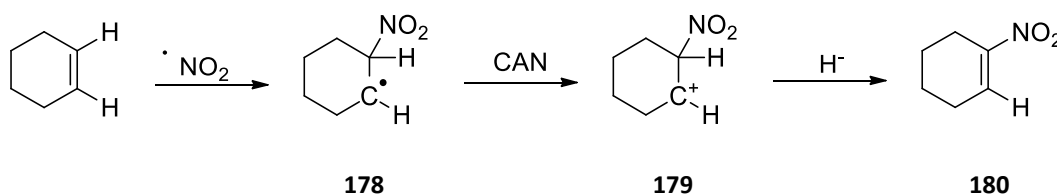
Scheme 37 – CAN-mediated oxidation of anthracene under controlled conditions

In the years that followed, the research group of Hwu *et al.* did extensive research into the use of CAN to generate α,β -unsaturated nitroalkenes. This can be done by the sonication of the alkene, sodium nitrite (10 eq) and CAN (2 eq) in acetic acid in a sealed tube. This methodology could be used on a wide variety of alkenes, including alkyl, cyclic and silyl and heterocyclic containing alkenes as shown in Scheme 38. They also proposed a mechanism for the nitration (Scheme 39) which again involves the generation of a radical on the alkene (**178**) after the nitro radical has attacked one end of the double bond. This radical can be transferred to the Ce⁴⁺ in the CAN, leaving a cation behind (**179**). Elimination of hydrogen then results in the regeneration of the alkene (**180**).^{139, 140}



Reaction conditions: CAN (2 eq), NaNO₂ (10 eq), AcOH (12 eq)/CHCl₃, 25-73 °C, 2.5 – 4 hours

Scheme 38 – Nitration of benzofuran



Scheme 39 – Proposed mechanism for the nitration of alkenes

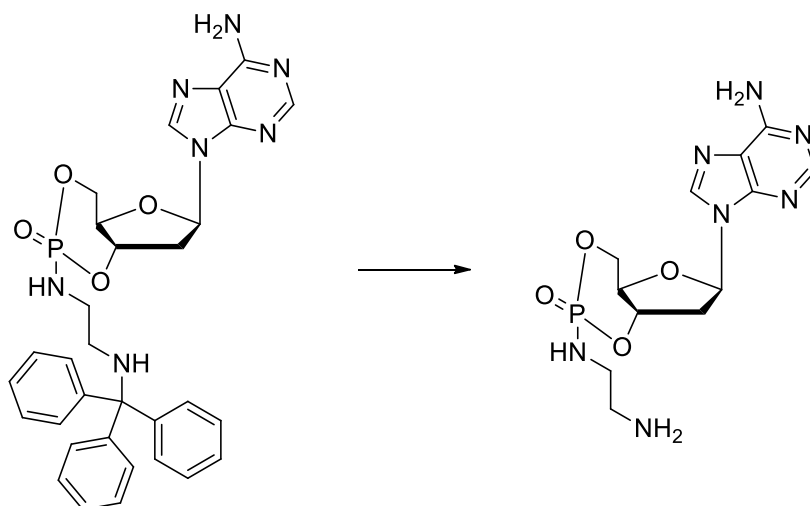
Given the importance of the choice of solvent in nitration reactions with CAN, Deleersnyder *et al.* investigated using ionic liquids as the solvent. Their study focused on using 1-ethyl-3-methylimidazolium triflate as the solvent as all of the substrates of interest were found to be soluble in this ionic liquid. When naphthalene was exposed to CAN in this particular ionic liquid, the major product from the reaction was 1-nitronaphthalene (90 %) with only trace amounts of 2-nitronaphthalene (8 %), naphthoquinone (1 %) and phthalic acid (1 %) noted. The more water was introduced to the reaction the more naphthoquinone was formed, however significant quantities of 1-nitronaphthalene were isolated regardless of the volume of water added to the reaction.¹⁴¹ The use of ionic liquids in CAN based reactions is an interesting avenue of research and something that could be of potential use in other reactions.

4.1.3. Removal and addition of protection groups using CAN

4.1.3.1. Removal of protection groups

Protection groups are widely used in organic synthesis, however once they have performed their function they can be problematic to remove. Methods for removal of protection groups often require harsh acidic conditions. CAN has been found to have substantial success removing a number of protection groups using mild catalytic conditions.¹⁴²

One of the first reported CAN-mediated deprotections was by the Hwu research group where they found that with CAN the trityl protection group could easily be removed from nucleotides and nucleosides. After stirring the protected nucleotide in an acetonitrile/dimethylformamide/water solvent mixture at room temperature for 1-15 hours with 0.1 equivalents of CAN resulted in the formation of the deprotected nucleotide exclusively with no damage to the sugar moiety or phosphate chain. An example of this work is given in Scheme 40. They also found that the mono *p*-methoxytrityl group could also be successfully removed under the proposed conditions.¹⁴³



Reaction conditions: CAN (0.1 eq), MeCN/DMF/H₂O, 25 °C, 10 h.

Scheme 40 – Trityl protection group removal using catalytic amounts of CAN

Not long after, the same research group found that the *tert*-butoxycarbonyl (or BOC) protection group could successfully be removed from nitrogen, oxygen or sulfur atoms and making it particularly useful for the removal of BOC groups from protected amino acids. Examples of the compounds that were successfully deprotected are shown in Figure 79. These reactions were performed in acetonitrile under reflux conditions with 0.2 equivalents of CAN.¹⁴⁴

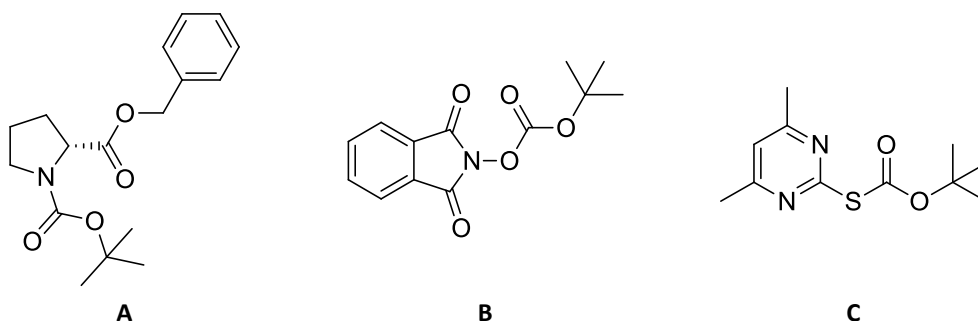
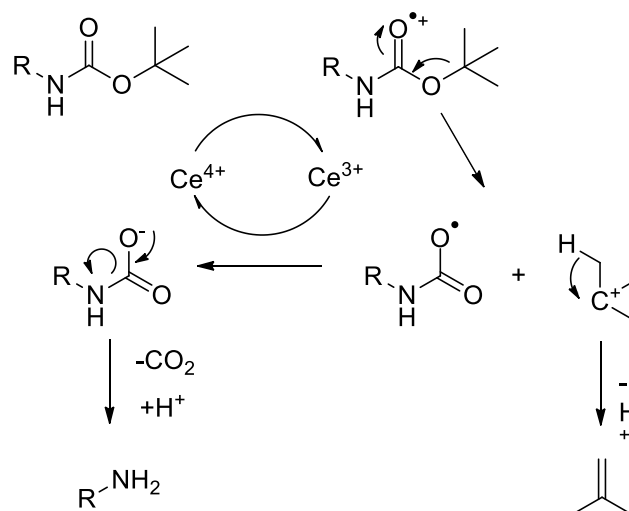


Figure 79 – N-protected (A), O-protected (B) and S-protected (C) BOC-containing compounds successfully deprotected using CAN

Hwu proposed a mechanism for the protection group removal which accounted for how CAN could be used in catalytic amounts. Scheme 41 outlines the proposed mechanism for the removal of the BOC group from an amine, however a similar mechanism was proposed for the removal of the trityl group, in which the CAN oxidizes the heteroatom (O, N or S) and later the Ce³⁺ reduces the amide during the removal of the BOC protection group to regenerate the Ce⁴⁺, resulting in the formation of the alcohol/amine/thiol.¹⁴⁴



Scheme 41 – Proposed mechanism for the catalytic deprotection of BOC from an amine

Another research group – Markó *et al.* – did extensive research into the use of CAN in the removal of ketals and acetals to regenerate alcohols. They also noted that while many methods exist for the removal of such groups, the typical acidic conditions could not be used for molecules containing sensitive moieties. The CAN procedure they developed allowed for the removal of the protecting groups using mild, neutral conditions with catalytic amounts of CAN (3 mol %) where no racemization or additional oxidation of the compounds they tested was noted. This procedure could be applied to a variety of acetals and ketals however was unsuccessful for the pinacol derived ketal. Figure 80 shows a selection of sensitive molecules that were successfully deprotected using their methodology in acetonitrile with a borate/hydrochloric acid buffer (pH 8) at 60 °C for 0.3 – 2.5 hours in excellent yields.¹⁴⁵

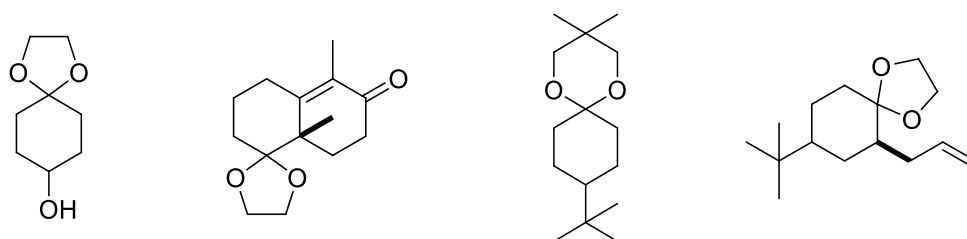


Figure 80 – Deprotection of ketals and acetals using mild, neutral conditions described by Markó *et al.*

They also found that this methodology could be extended to the deprotection of tetrahydropyranyl (THP) and tetrahydrofuranyl (THF) ethers under the same conditions as described above. Again under these conditions the CAN was found to behave as a Lewis acid rather than an oxidant, resulting in only the removal of the ether moieties and no further

reactions occurred, allowing for the deprotection of highly sensitive alcohols. Examples of the types of molecules that were investigated and were successfully deprotected in good yields are depicted in Figure 81.¹⁴⁶

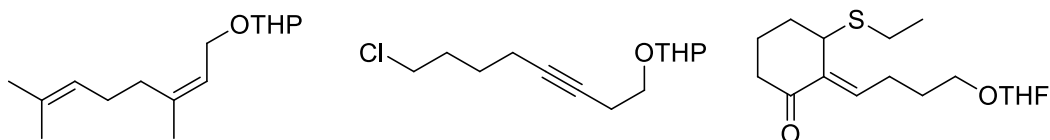
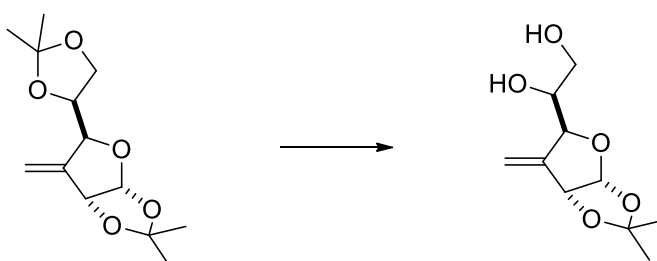


Figure 81 – A selection of compounds that were successfully deprotected using catalytic amounts of CAN

Markó *et al.* found that this method was sensitive enough to be used in the deprotection of a single dioxolane moiety in bis protected sugars such as **181** in Scheme 42.¹⁴⁷

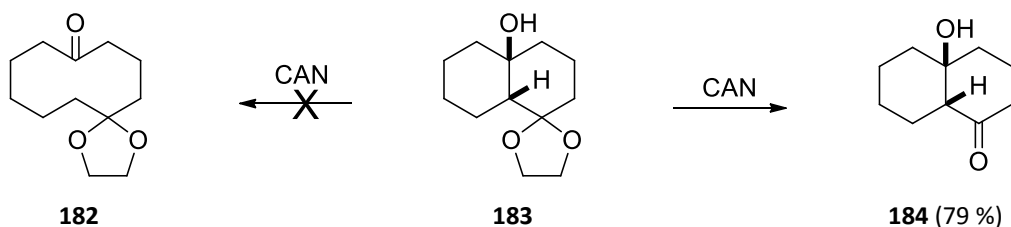


181

Reaction conditions: CAN (3% mol), NaBrO₃ (1.5 eq), MeCN/H₂O, 60 °C, 1.2 h.

Scheme 42 – Deprotection of a sensitive sugar using catalytic amounts of CAN

Even when mole equivalents of CAN was added to the reaction mixture, the deprotection of ketals was still found to be favourable over the oxidation of other parts of the molecule. For example exposing **183** (Scheme 43) to CAN (2.5 eq) in acetonitrile/water could be expected to result in protected ketone **182** (given the significant oxidative ability of CAN), however the research group of Markó found that exclusively **184** was formed instead in a 79 % yield.¹⁴⁷



182

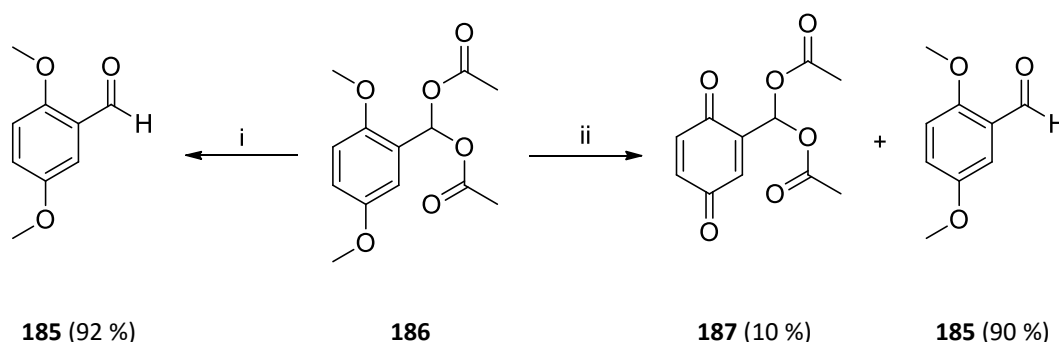
183

184 (79 %)

Reaction conditions: CAN (2.5 eq), MeCN/H₂O, 70 °C.

Scheme 43 – Selective acetal deprotection of **183** even when exposed to mole equivalents of CAN

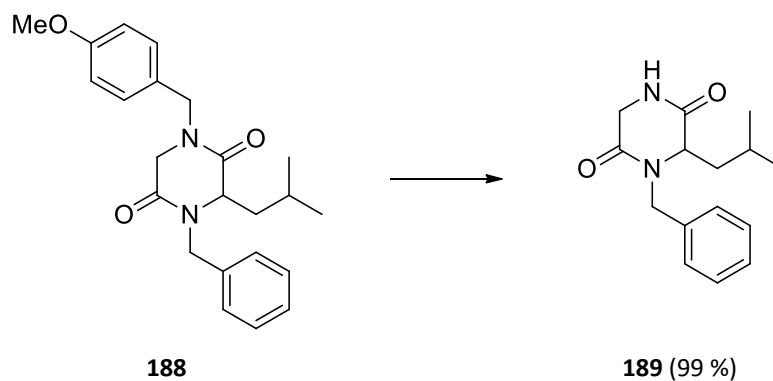
Cotelle and Catteau investigated the use of CAN in the removal of benzylic acetal substituents. They found that CAN adsorbed onto SiO₂ in dichloromethane resulted in the successful removal of the acetate groups, resulting in the regeneration of benzaldehydes. Interestingly, in diacetate-protected benzaldehydes containing an aryl acetate functionality, the aryl acetate remained intact after the reaction. Particularly of interest was that **186** on exposure to CAN/Silica in dichloromethane formed benzaldehyde **185**. When the same reaction was performed but with an addition of a small amount of water/methanol further oxidation to the quinone **187** was collected along with **185** (shown in Scheme 44). The acetal groups could not be removed from quinone **187** using this methodology.¹⁴⁸



Reaction conditions: i) CAN/SiO₂ (1 eq), DCM, rt, 92 %; ii) CAN/SiO₂ (1eq), DCM/H₂O, rt.

Scheme 44 – Deacetylation and oxidation of diacetal protected aldehydes

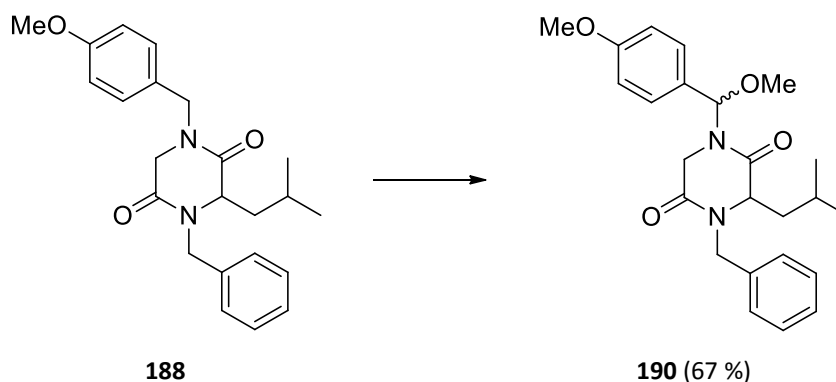
The use of CAN to remove the protection groups discussed up until now tends to be used more as an alternate method when the more conventional methods prove unsuccessful. Yoshimura *et al.* were amongst the first to discover that CAN could be used to remove the *para*-methoxybenzyl (or PMB) group. During the course of their research they found that PMB could be selectively removed from diketopiperazine derivatives (such as **188**, Scheme 45), even in the presence of other methoxy substituents.¹⁴⁹ On further development, it was discovered that PMB could be removed from a wide variety of analogues, such as **188** resulting in **189** in moderate to good yields. They investigated the use of CAN in 2-7.6 mol equivalents and in acetonitrile/water and methanol/water mixtures.¹⁵⁰



Reaction conditions: CAN (3.8 eq), MeCN/H₂O, rt, 2 h.

Scheme 45 – CAN-mediated removal of PMB protection group from diketopiperazine

When the reaction was performed without the addition of water, it was found that a methoxy substituent was introduced to the benzylic position of the PMB group and **190** (Scheme 46) was the major product isolated.¹⁵⁰

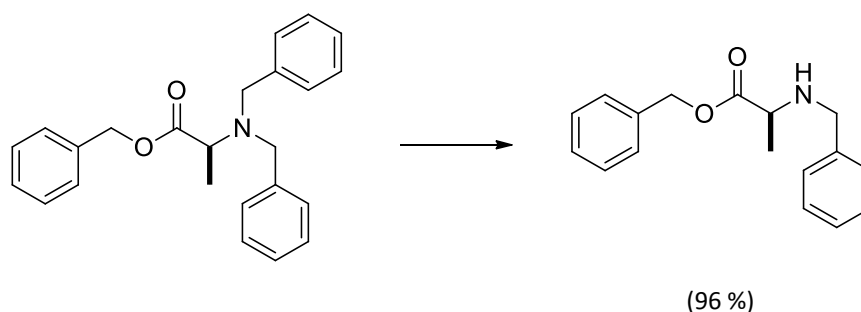


Reaction conditions: CAN (3.8 eq), MeOH, rt, 3 h.

Scheme 46 – CAN-mediated addition of methanol to the benzylic position of the PMB group on diketopiperazine 188

In the examples given by Yoshimura *et al.* the benzyl group appeared to remain intact after exposure to CAN. The research group of Davies at Oxford reported that on tertiary amines where both a benzyl group and a PMB group is present and exposed to CAN, two products were isolated (one where the PMB group was removed and one where the benzyl group was removed) in a 1:1 ratio. In tertiary amines that contained two benzyl groups, they found that with 2.1 equivalents of CAN at room temperature in aqueous acetonitrile a single benzyl group could be removed. However, it was also noted that the third substituent in the tertiary amine impacted whether the benzyl group could be removed or not; the reactions were only successful with propyl, butyl,

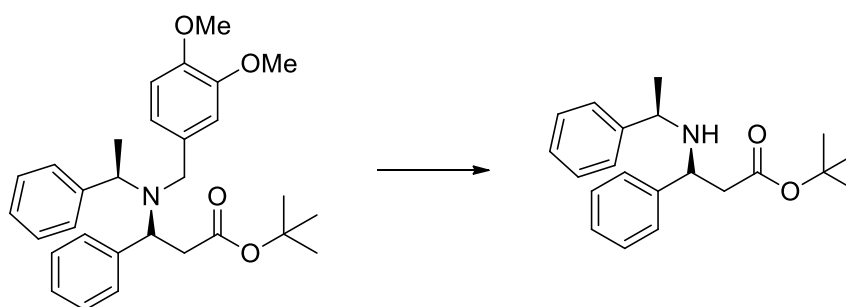
hexyl and *t*-butyl amines. It was also possible with other, more highly substituted alkyl chains as shown in Scheme 47 below.¹⁵¹



Reaction conditions: CAN (2.1 eq), MeCN/H₂O; rt, 10 min.

Scheme 47 – Benzyl deprotection from a tertiary amine using CAN

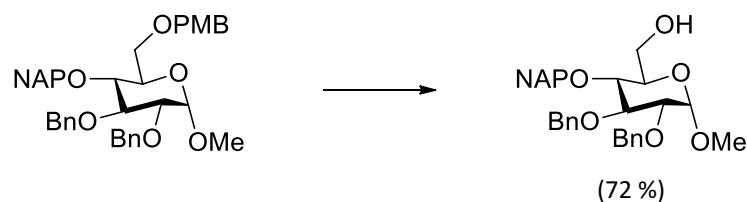
A slightly different version of the PMB group – 3,4-dimethoxybenzyl group could also be removed using CAN. Davies and Ichihara made use of this in their synthesis of β -lactams and *N*-(α -methylbenzyl)- β -amino esters, an example of which is shown in Scheme 48.¹⁵²



Reaction conditions: CAN, MeCN/H₂O, rt.

Scheme 48 – CAN-mediated removal of the 3,4-dimethoxybenzyl group from a tertiary amine

Further highlighting the sensitivity and selectivity of this deprotection method, Wright *et al.* found that PMB groups could selectively be removed from monosaccharides in an acetone/water solution, even in the presence of other protection groups as shown in Scheme 49.¹⁵³



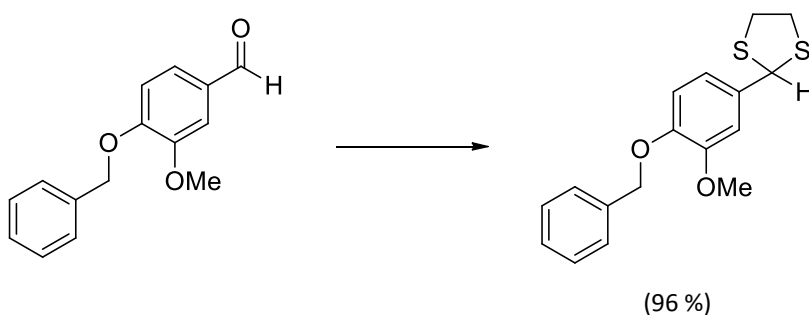
Reaction conditions: CAN (4.2 eq), acetone/H₂O, rt, 85 min.

Scheme 49 – PMB removal from monosaccharides

The use of CAN in the removal of the PMB protection group has become widely accepted as the standard methodology because of its high efficiency and mild conditions. So much so that it has played a crucial role in the synthesis of several highly complex natural products such as the synthesis of (+)-18-epi-latrunculol A,¹⁵⁴ lactacystin,¹⁵⁵ (±)-lepadiformine A¹⁵⁶ and latrunculin A¹⁵⁷ to name a few. Greater detail on the use of CAN in the removal of protection groups can be found in a review by Maulide *et al.*¹⁴²

4.1.3.2. Addition of protection groups

Interestingly, CAN can also be used to add protecting groups to heteroatoms in selected examples. The research group of Roy *et al.* found that the addition of catalytic amounts of CAN could be used to chemoselectively protect aldehydes with 1,2-ethanedithiol in chloroform at room temperature as shown in Scheme 50. Additionally, under reflux conditions alicyclic ketones could also be selectively protected.¹⁵⁸



Reaction conditions: 1,2-ethanedithiol (2.1 eq), CAN (0.2 eq), CHCl_3 , rt, 18 h.

Scheme 50 – Chemoselective thioacetalization of aldehydes

A wide variety of alcohols can also be protected using 3,4-dihydro-2H-pyran and CAN adsorbed on silica in acetonitrile at room temperature for 5-15 minutes. Pachamuthu and Vankar developed this method and found that it could be applied to highly sensitive molecules. A selection of sensitive molecules that were successfully THP protected are shown in Figure 82. It should be noted that the reaction was not enantioselective and both enantiomers of each product were isolated.¹⁵⁹

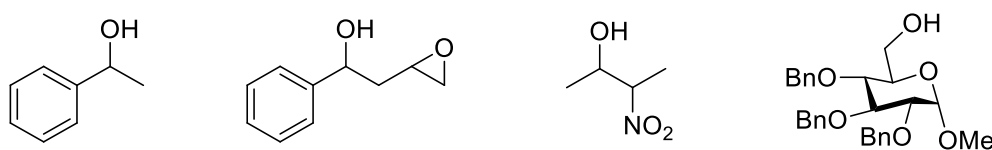
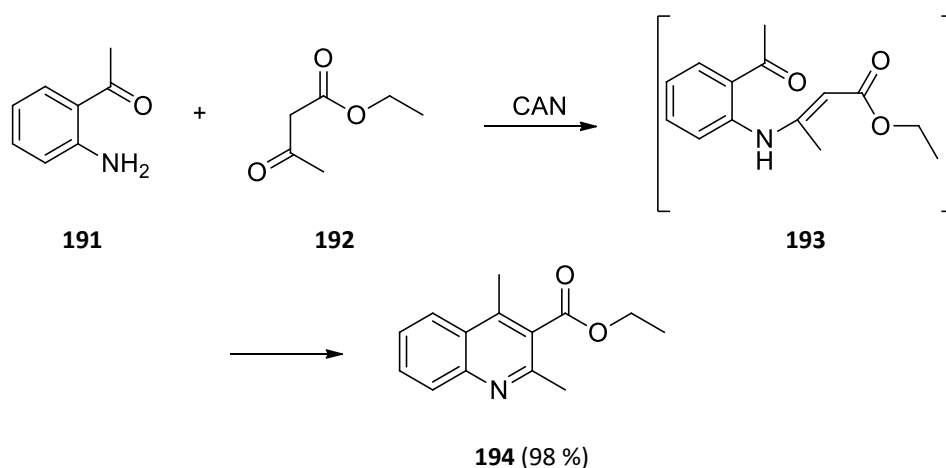


Figure 82 – A selection of alcohols that were successfully THP protected using CAN adsorbed on SiO_2

4.1.4. Other uses of CAN in organic synthesis

CAN has been used to facilitate a variety of other reactions. CAN has been used in a multicomponent coupling reaction, reported by Sridharan *et al.* where CAN was used in Friedländer and Friedländer-Borsche annulations for the synthesis of luotonin A. The reactions were performed in ethanol where CAN behaves as a Lewis Acid. Scheme 51 details one of the reactions investigated, where the substituted aniline **191** and ethyl 3-oxobutanoate **192** condense to form intermediate **193** in the presence of CAN that can then cyclize resulting in the formation of **194**.¹⁶⁰

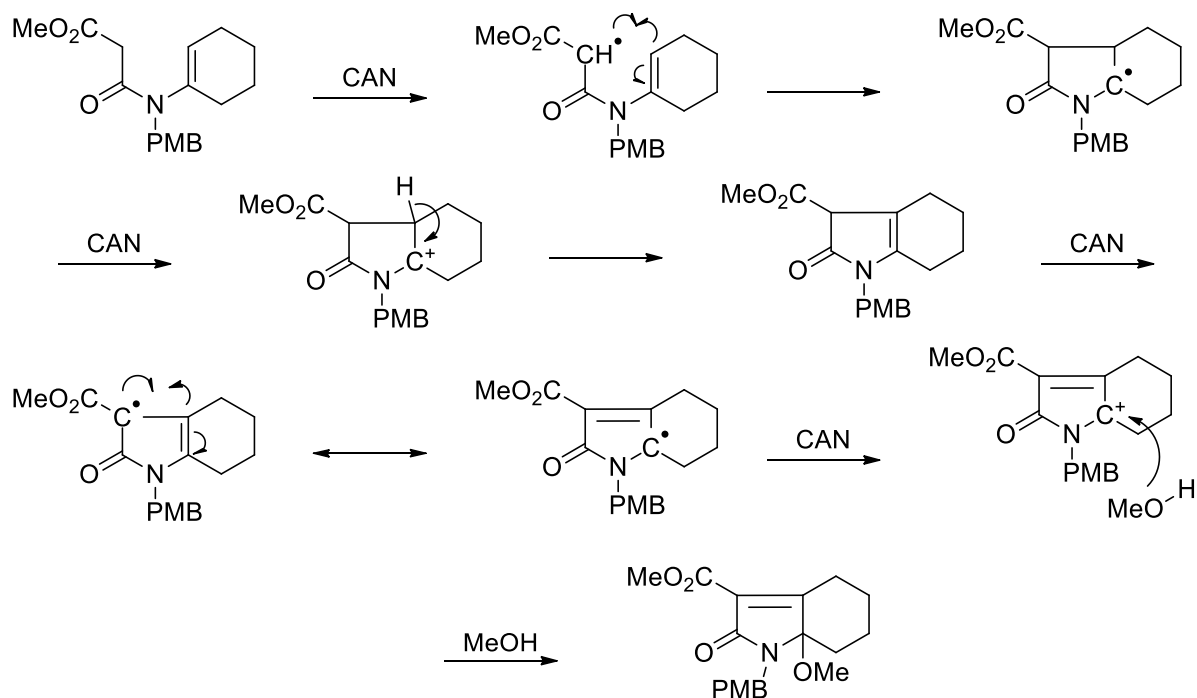


Reaction conditions: CAN (15 mol %), EtOH, reflux, 8 hours.

Scheme 51 – Friedländer annulation catalysed using CAN

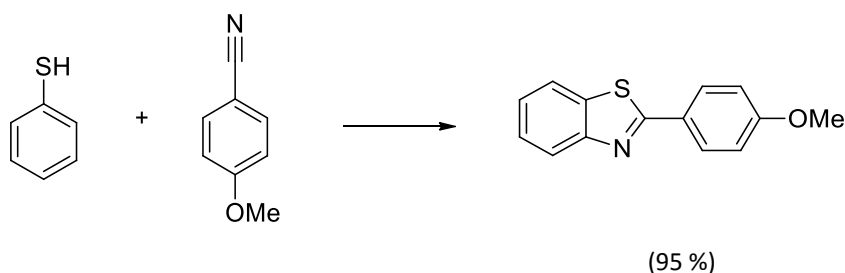
Clark *et al.* reported the use of CAN as a radical initiator in the oxidative 5-*endo* cyclization of enamides in average yields. This was performed in methanol and the reaction proposed to proceed as outlined in Scheme 52. The choice of solvent was determined by the nature of the ester present in the molecule to prevent nucleophilic attack of the solvent at the ester.¹⁶¹

Introduction



Scheme 52 – Proposed mechanism for the CAN-mediated cyclization of enamides

An article was published by Tale in *Organic Letters* in 2002 that outlined the use of CAN to generate 2-arylbenzothiazoles from thiophenols and aromatic nitriles. The reaction was performed in acetonitrile with 2 equivalents of CAN and solid sodium bicarbonate as shown in Scheme 53.¹⁶²



Reaction conditions: CAN (2 eq), NaHCO₃, MeCN, rt, 30 min.

Scheme 53 – Reported CAN-mediated formation of 2-arylbenzothiazoles by Tale

The following year Nair and Augustine found that the work published by Tale was irreproducible under the reported conditions and that the only product that was isolated from the reactions were disulfides (such as **195** in Figure 83) or thiosulfonates (such as **196**). They achieved the same results even without the addition of the aromatic nitrile and rationalized what was seen by the generation of radicals on the thiols which can quench by reacting with themselves resulting in the disulfides (such as **195**), the presence of more CAN could further oxidize the disulfides to

thiosulfonates (such as **196**). Alternatively the thiol radical could be oxidized further with atmospheric oxygen which could then react further to give the thiosulfonates.¹⁶³



Figure 83 – An example of the disulfides and thiosulfonates generated when thiols are exposed to CAN

There have been several reports of diaryl sulfides oxidized by CAN to sulfoxides which supports this theory.^{125,164} A more recent example of this oxidation was by Hajipour *et al.* where sulfides were successfully oxidized to sulfoxides using CAN in 1-hexyl-3-methylimidazolium bisulfate (an ionic liquid) at 80 °C. This reaction was successful even without the addition of water to the reaction. Figure 84 shows some examples of some of the sulfides that were successfully oxidized using CAN.¹⁶⁵

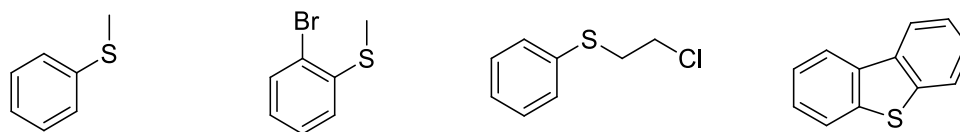
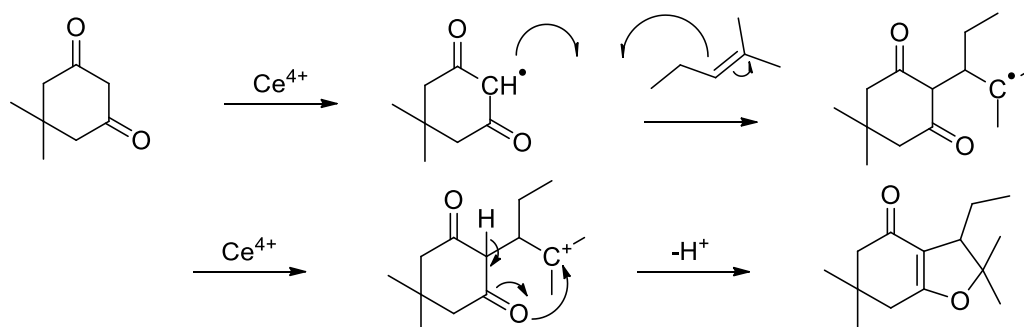


Figure 84 – A selection of sulfides that can be oxidized to sulfoxides when exposed to CAN

A more unusual example of the reactivity of CAN was published by Nair and Mathew where dihydrofurans were synthesized from 1,3-dicarbonyl compounds and alkenes. A mechanism for this unusual reaction was postulated and is outlined in Scheme 54. This methodology was applied to two 1,3-dicarbonyl compounds (dimedone and acetylacetone) and a variety of different alkenes and showed superior reactivity over a similar reaction being performed using manganese acetate. In order for this reaction to occur it was found that a methanolic solution of the dicarbonyl and the alkene (in a 2.5:3 ratio) needed to be cooled to 0 °C over an ice bath before CAN (4.6 mmol equivalents) dissolved in methanol was added. The reaction was deemed complete after 15 minutes. The reactions were less successful with dienes than with alkenes and there were no reports of regioisomers collected.¹⁶⁶



Scheme 54 – Proposed mechanism for the synthesis of dihydrofurans from 1,3-dicarbonyls and alkenes

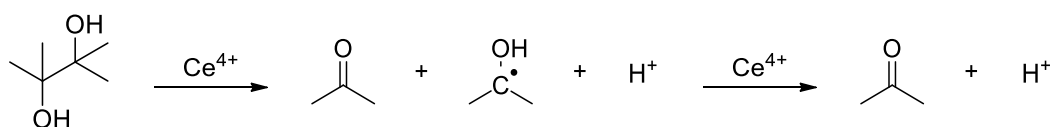
The mild conditions required for reactions with CAN have allowed for its use in a variety of other unusual reactions; for example as a radical initiator for polymerization reactions¹⁶⁷ or to modify protein residues.¹⁶⁸ Greater detail on the use of CAN in organic synthesis can be found in one of several different reviews by Ho,¹²⁵ Sridharan and Menéndez,¹⁶⁹ Nair *et al.*¹⁷⁰ and Hwu and King.¹⁷¹

4.2. The use of Ceric Ammonium Sulfate in Organic Synthesis

Ceric ammonium sulfate (or CAS) is the significantly less famous older brother of CAN. It was initially developed to prevent the cumbersome fresh preparation of ceric sulfate from an impure ceric oxide (which was used as a reference standard in oxidimetry). In the report by Smith *et al.* that described the first proposed synthesis and use of CAN, they noted that while CAS was commercially available and readily soluble in dilute sulfuric acid, the solution composition of sulfate and ammonia was highly variable and formed a highly hygroscopic salt making it unsuitable for use as a reference standard.¹¹⁹ Physically, CAS $((\text{NH}_4)_4\text{Ce}(\text{SO}_4)_4 \cdot 2\text{H}_2\text{O})$ is markedly similar in appearance to the better known CAN and is commercially available as orange powder/crystals. CAS also tends to behave as a single electron transfer agent. The major difference between the two being the solubility of the ceric salts in water and organic solvents – CAN is readily soluble in both while CAS is significantly less so. Perhaps consequently, very little literature exists on the use of CAS in synthetic reactions. The literature review below details the few reports of CAS in organic synthesis.

4.2.1. CAS in polymerization reactions

One of the first reports of the use of CAS was by Mino *et al.* in 1958 where they investigated the oxidation of pinacol using CAS. The use of CAS (in 1N sulfuric acid) was used to determine the effect of the presence of acrylamide in the reaction mixture would have on the oxidation of pinacol. When no acrylamide was added to the reaction, it was found that CAS successfully oxidizes pinacol to acetone as shown in Scheme 55.¹⁷²



Scheme 55 – CAS mediated oxidation of pinacol

When acrylamide (a monomer) was introduced to the reaction, significantly less acetone was formed along with the appearance of a polymer. It was determined that the radical alcohol generated by the oxidation of pinacol served as an initiator for the polymerization of acrylamide. The polymerization was terminated when the radical polymer was quenched by a further equivalent of Ce^{4+} .¹⁷²

Several years later, Subramanian and Santappa also used CAS as a radical initiator for the polymerization of acrylonitrile, methyl acrylate and methyl methacrylate using malonic acid or cyclohexanone to complete the redox systems. Their study confirmed that while the rate of

initiation was slower than what would be obtained using CAN, the chain length of the polymer that resulted was longer.¹⁷³

Since then, CAS has been used as a polymerization initiator. Due to CAS being a single electron transfer agent, it became vital that CAS be used as part of a redox pair to be able to use CAS in catalytic amounts and to prevent the formation of large amounts of homopolymer formation. An example of more recent polymerization work was published by Chowdhury *et al.* in 2001 where they used CAS and dextrose as a redox pair in the graft polymerization of methyl methacrylate onto guar gum. They investigated the optimal parameters for this particular reaction but found that polymethyl methacrylate could easily be found using the CAS/dextrose redox pair initiator in water.¹⁷⁴

4.2.2. CAS in the solid state

Due to the tendency of the CAS to hydrolyse in an aqueous environment – growing crystals suitable for SCXRD analysis was found to be very difficult. Shan and Huang managed to use hydrothermal methods to grow crystals of CAS as a dimeric unit.¹⁷⁵ CAS has also been used as a raw material to generate a variety of other cerium (IV) based complexes. Abrahams *et al.* used CAS and 2,5-dihydroxybenzoquinone (dhbq) in a 1:2 ratio to generate a Ce^{3+} complex ($Ce_2(dhbq)_3 \cdot 24H_2O$) regardless of ratio of reactants were added. The dhbq serves as a chelating bridge between two cerium metal centers which, along with the 8-coordinate geometry of the cerium metal centers, form cages that can trap large amounts of water molecules.¹⁷⁶

Singh and Singh investigated the complexation of coumarins to a variety of metals. It was thought that the hydroxyl group on coumarins was the main reason for the significant biological activity shown as it could form complexes. Singh and Singh took the opportunity to investigate how different metals (Mn^{2+} , Fe^{3+} , Cu^{2+} , Ti^{4+} , Zr^{4+} , Ce^{4+} , Th^{4+} and UO_2^{2+}) would coordinate to 4-methyl-7,8-dihydroxycoumarin and 4-methyl-6,7-dihydroxycoumarin. CAS was dissolved in an aqueous ethanolic solution before the coumarins were added and once the solution was adjusted to pH 5 the precipitates that were collected were found to be complexes **197** and **198** in Figure 85.¹⁷⁷

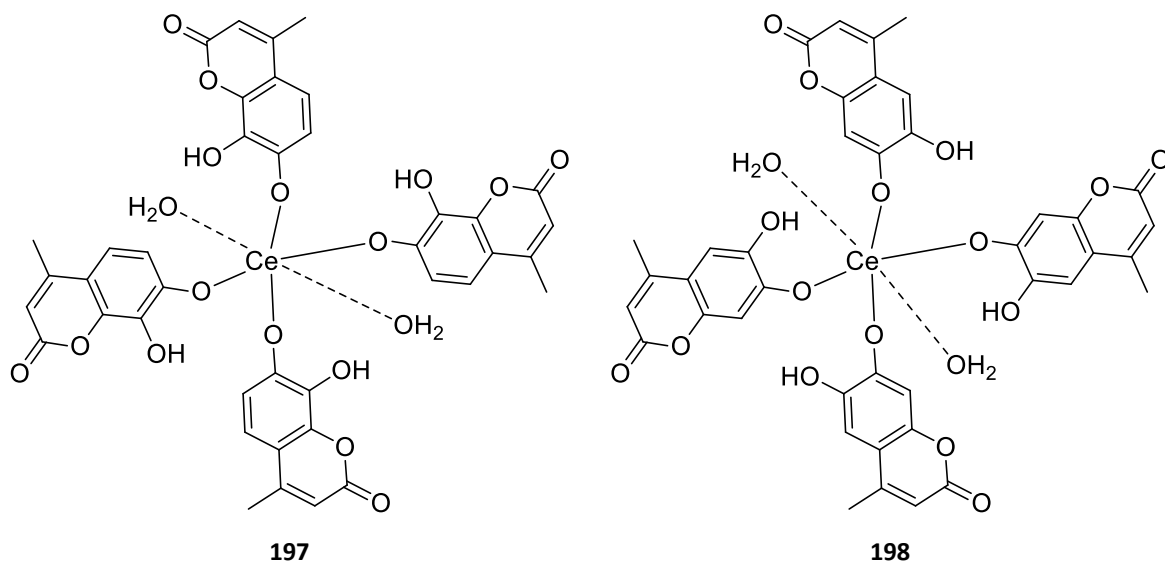
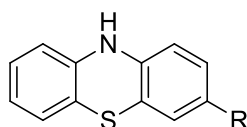


Figure 85 – Ceric complexes generated from exposing CAS to coumarins

4.2.3. Using CAS in Organic Synthesis

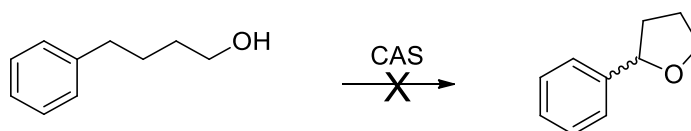
In the 1950's Tozer and Tuck used CAS to generate semiquinone free radicals in phenothiazines (Figure 86). Their aim was to investigate the lifetime (and hence stability) of the free radicals generated and was performed under acidic conditions allowing the CAS to be readily soluble throughout their experiment.¹⁷⁸



R = OMe, Me, Ph, Cl, Br or I

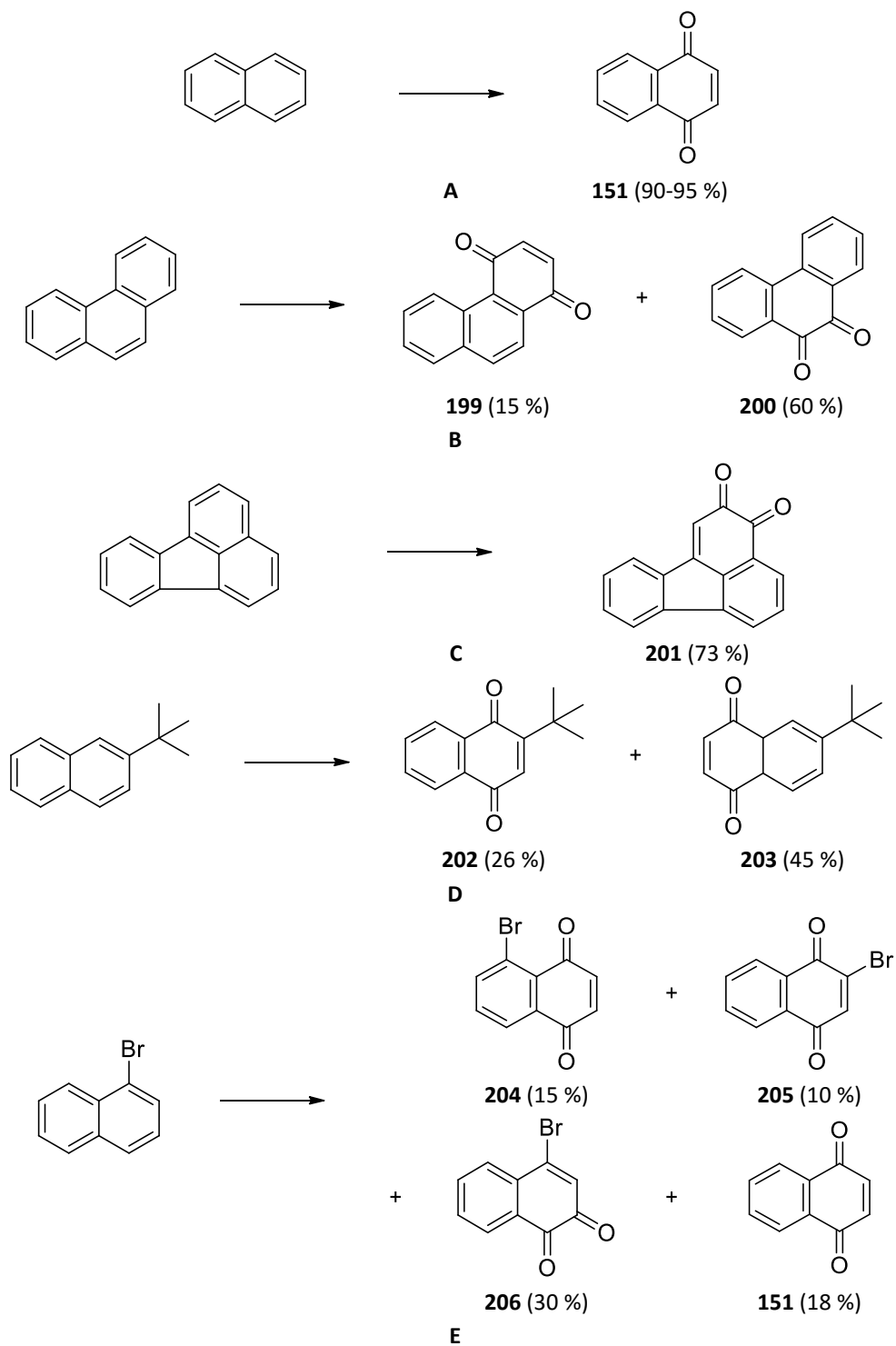
Figure 86 – Phenothiazine scaffold that was oxidized to semiquinones using CAS

As previously mentioned, Doyle *et al.* used CAN to generate furan rings from alkyl alcoholic chains containing an aryl substituent (Scheme 29). Included in their research, they investigated using CAS instead of CAN to mediate the reaction and found that only starting material was obtained from the reaction (Scheme 56). It was also noted that while the CAN formed the characteristic ceric-complex red colour when added to the alcohol, the same observation was not noted when CAS was used. Given that the reactions were performed in 7:1 acetonitrile : water it is possible that no reaction occurred due to a lack of solubility.¹³⁰



Scheme 56 – Attempted CAS mediated oxidative cyclization of alkyl alcohols

One of the first synthetic uses for CAS was by Periasamy and Bhatt. They found that CAS could be used to oxidize polycyclic aromatic hydrocarbons to quinones. Given that this was the first official report of the use of CAS and the general lack of literature surrounding using CAS in organic synthesis, a detailed investigation into their work is outlined in Scheme 57. The reactions were performed in acetonitrile with dilute sulfuric acid with 6 mol equivalents of CAS at temperatures ranging between 25-50 °C for 4-6 hours. The results of these reactions resulted in several surprises – the first of which being the formation of *ortho*-quinones **200** (B), **201** (C) and **206** (E). The naphthalene in Scheme 57D showed that either aromatic ring could be oxidized (**202** and **203**), however the non-substituted aromatic ring oxidation (**203**) was produced in higher yields. Finally when 1-bromonaphthalene was exposed to CAS a variety of products were isolated. The first of which being the most predictable brominated naphthoquinone (**204**), surprisingly a 1,2-bromine shift during the oxidation of the naphthalene affording **205**, the formation of *ortho*-quinone **206** as mentioned previously as well as the isolation of *para*-naphthoquinone (**151**) where the bromine atom was absent.¹⁷⁹

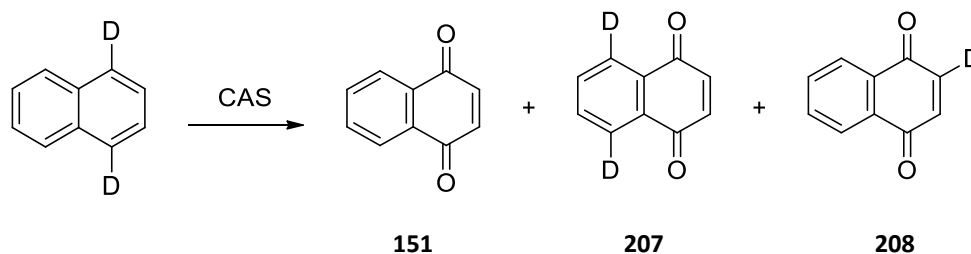


Reaction conditions: CAN (6 eq), 4N H₂SO₄, 25-50 °C, 4-6 h.

Scheme 57 – CAS mediated oxidation of polycyclic aromatic hydrocarbons

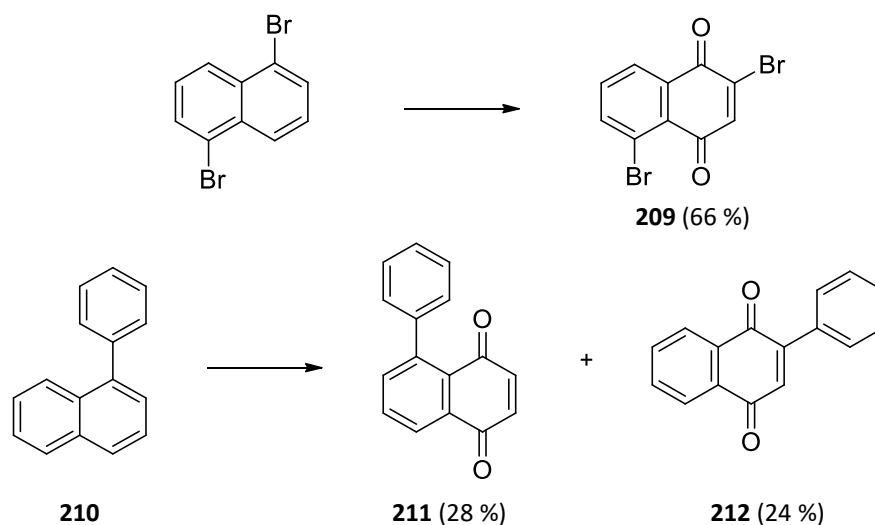
The 1,2-shift of the naphthalene substituent was highly unexpected and prompted further investigation by this research group. To confirm the oxidation products, they exposed 1,4-*d*₂naphthalene to CAS and found that at least 3 products (Scheme 58) were formed; **151** (where

the oxidation occurred at the deuterium atoms), **207** (where the alternate aromatic ring was oxidized) and **208** where a 1,2-shift occurs on oxidation. These products were determined by mass spectroscopy and no mention was made regarding yields.¹⁸⁰



Scheme 58 – Oxidation of deuterium labelled naphthalene using CAS

In order to investigate the extent of the 1,2-shift Periasamy and Bhatt furthered their investigations to include the reactions outlined in Scheme 59 below. Exposing 1,5-dibromonaphthalene to CAS resulted in the exclusive formation of the 1,2-shift oxidation product, **209** in a respectable yield of 66%. Perhaps more interestingly, when **210** was oxidized by CAS both the oxidation to quinone (**211**) had occurred in addition to the 1,2-shift oxidation product **212** in almost equal proportions.¹⁸⁰

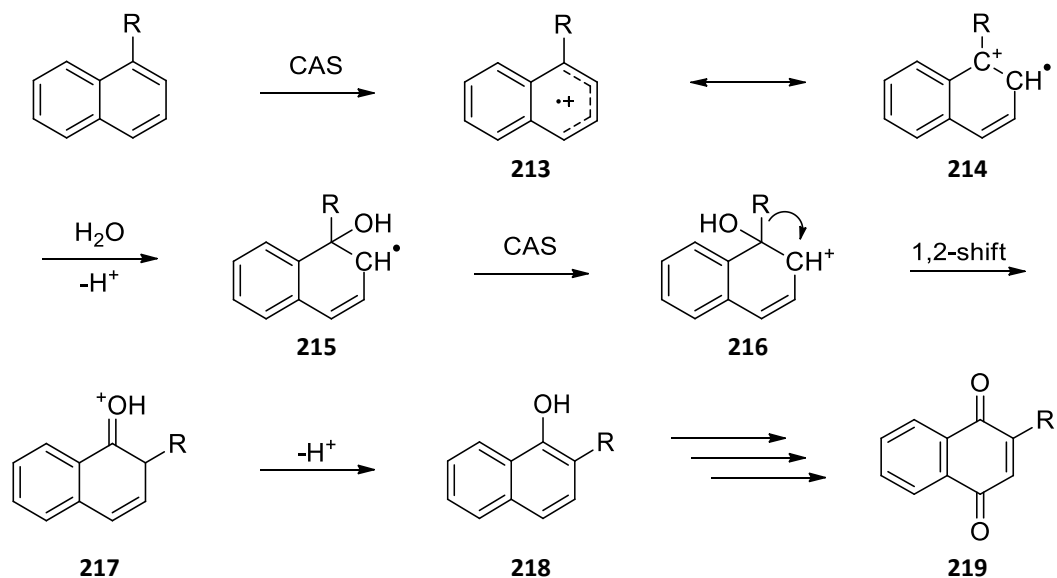


Reaction conditions: CAN (4 eq), MeCN/4N H₂SO₄, 50-60 °C, 4-5 h.

Scheme 59 – Investigation of the 1,2-substituent shift in other substituted naphthalenes

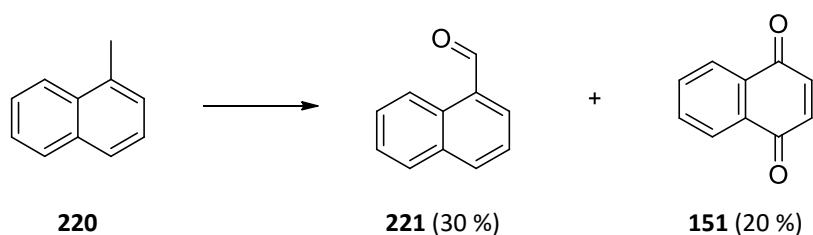
The presence of **212** is highly significant as this was the first example of a C–C bond shift that occurs exclusively in oxidation reactions using CAS – so much so that it was highlighted in a review on the effects of transition metal salts on hydrocarbons.¹⁸¹ A mechanism was proposed by Periasamy and Bhatt (Scheme 60), where the naphthalene is oxidized to radical cation **213** which would exist in equilibrium with **214**. From there water can add to the carbocation to give **215**. On

further oxidation of **215** a carbocation is generated (**216**) and from there the 1,2-shift occurs to give **217**. Following the removal of a proton to give rise to **218** and the further oxidation and further addition of water affords the naphthoquinone **219**.¹⁸⁰ Decades later, they noted that the 1,2-shift could occur after the first hydroxy group was introduced to the naphthalene.¹⁸²



Scheme 60 – Proposed mechanism for the 1,2-shift during the oxidation of naphthalenes

The oxidation of 1-methyl naphthalene (**220**, Scheme 61) resulted in the formation of 1-naphthaldehyde (**221**) and naphthoquinone (**151**). Furthermore, when 1-naphthaldehyde **221** (or 1-naphthoic acid) was exposed to CAS under the same conditions the only product isolated from the reaction was naphthoquinone (**151**) in average yields of 42-50 %. A similar observation was noted with 1-naphthol, however naphthoquinone (**151**) was only isolated in a poor yield (20 %) and the remainder of the majority of the reaction produced polymeric, oxidative material.

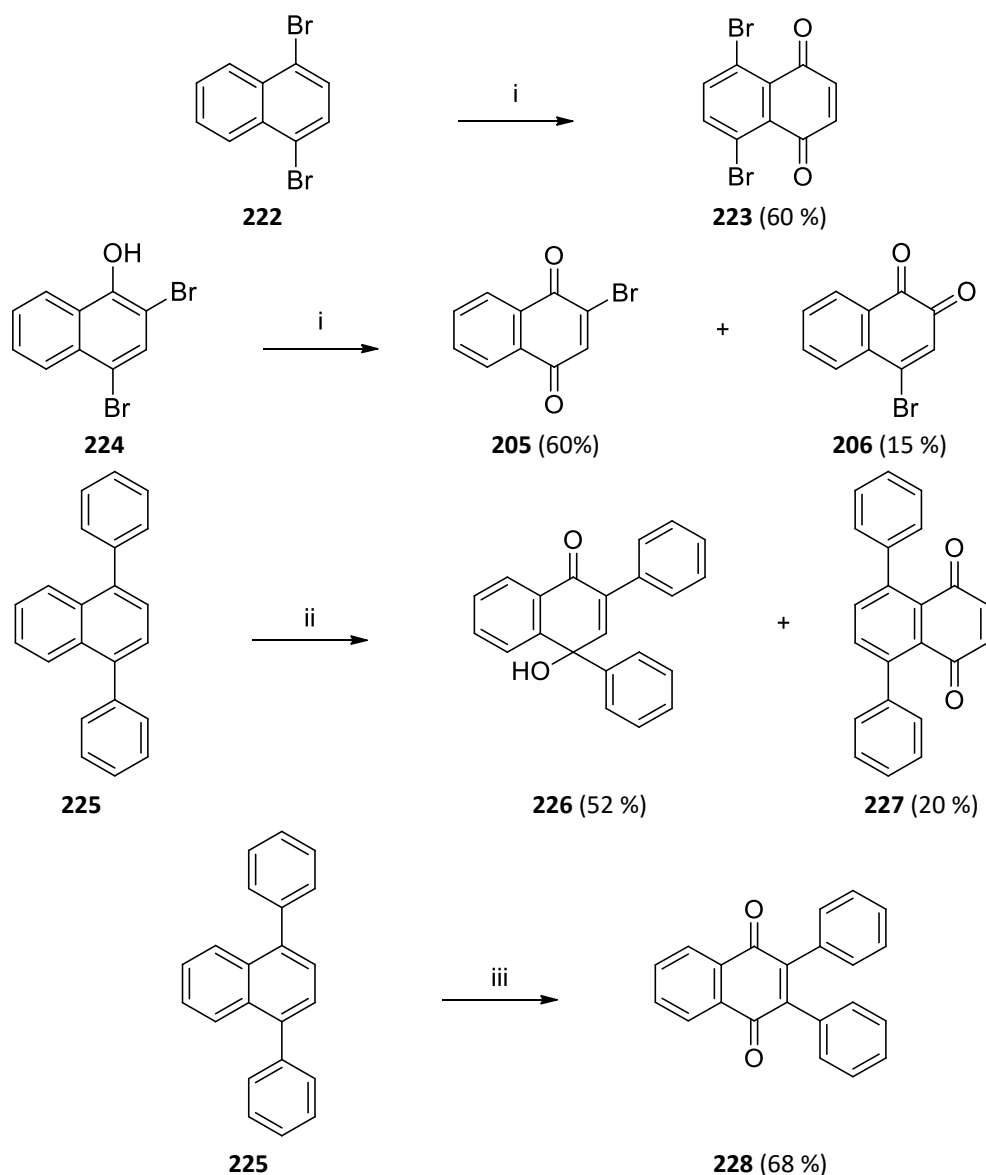


Reaction conditions: CAN (6 eq), MeCN/2M H₂SO₄, 25 °C, 24 h.

Scheme 61 – CAS mediated oxidation of 1-methyl naphthalene

They also exposed naphthalenes **222** and **224** (Scheme 62) to CAS under similar conditions resulting in **223** in a respectable yield (from **222**) and in the formation of **205** and **206** (from **224**). Interestingly, when **225** was exposed to CAS in a solution containing dilute acid two products

were isolated – an unexpected **226** being the major product along with a small amount of **227** formed. In a reaction with more concentrated sulfuric acid, only **228** was isolated. This was the only example of a double 1,2-substituent shift in their research. Bhatt and co-workers also found that similar 1,2-substituent shifts during the oxidation of naphthalenes (such as those in Scheme 62) could be achieved using manganese(III) sulfate.¹⁸²

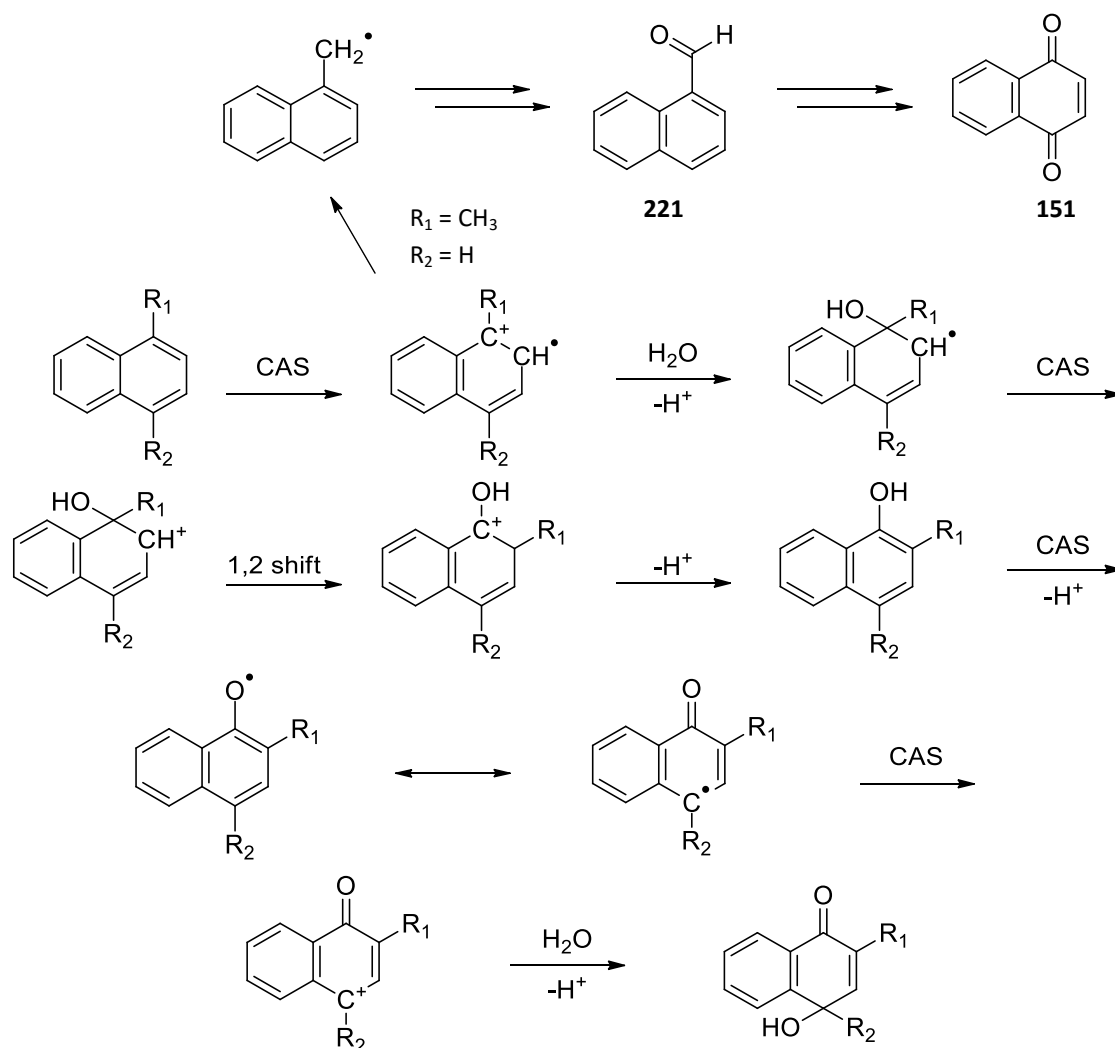


Reaction conditions: i) CAN (4 eq), MeCN/2M H₂SO₄, 25 °C, 2 h; ii) CAN (6 eq), MeCN/0.5M H₂SO₄, 50 °C, 3 h; iii) CAN (6 eq), MeCN/6M H₂SO₄, 50 °C, 4 h.

Scheme 62 – CAS oxidation of 1,4-disubstituted naphthalenes

In order to explain the results seen in Scheme 62, a new mechanism was proposed and this is outlined in Scheme 63.¹⁸² Similar to the mechanism in Scheme 60, the new mechanism also incorporates how naphthoquinone **151** is obtained from naphthalenes containing a methyl,

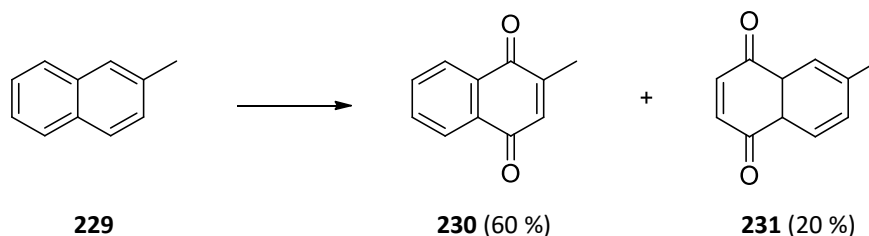
formyl or acid substituent (R_1). The isolation of compound **226** showed a key intermediate in the 1,2-shift of the substituents.



Scheme 63 – Proposed mechanism for the oxidation and 1,2-substituent shifts of substituted naphthalenes

In the early 80's Skarzewski developed a redox system that would allow for the use of CAS in catalytic quantities. He reported that the addition of silver(I) nitrate, sodium dodecyl sulfate and ammonium persulfate added to the reaction with CAS in order to oxidize the cerium from Ce^{3+} back to Ce^{4+} after it has oxidized the naphthalene. The reactions were successful even when the sodium dodecyl sulfate and ammonium persulfate were excluded from the reaction but resulting in a significantly lower yield. When the silver(I) nitrate was excluded from the reaction, the yield from the reaction was entirely dependent on the amount of CAS that was added. Skarzewski was concerned with the extent to which his methodology could be applied and found that the methodology was unsuccessful (or very poor yielding) in compounds where 1,4-dimethoxy

substituents were present as well as alcohol substituents anywhere in the molecule (the alcohol formed a complex with the ceric ion instead of reacting further). An example of the compounds investigated in this study is demonstrated in Scheme 64, where 2-methyl naphthalene (**229**) was oxidized by CAS to **230** as the major product and **231** as a minor product.¹⁸³

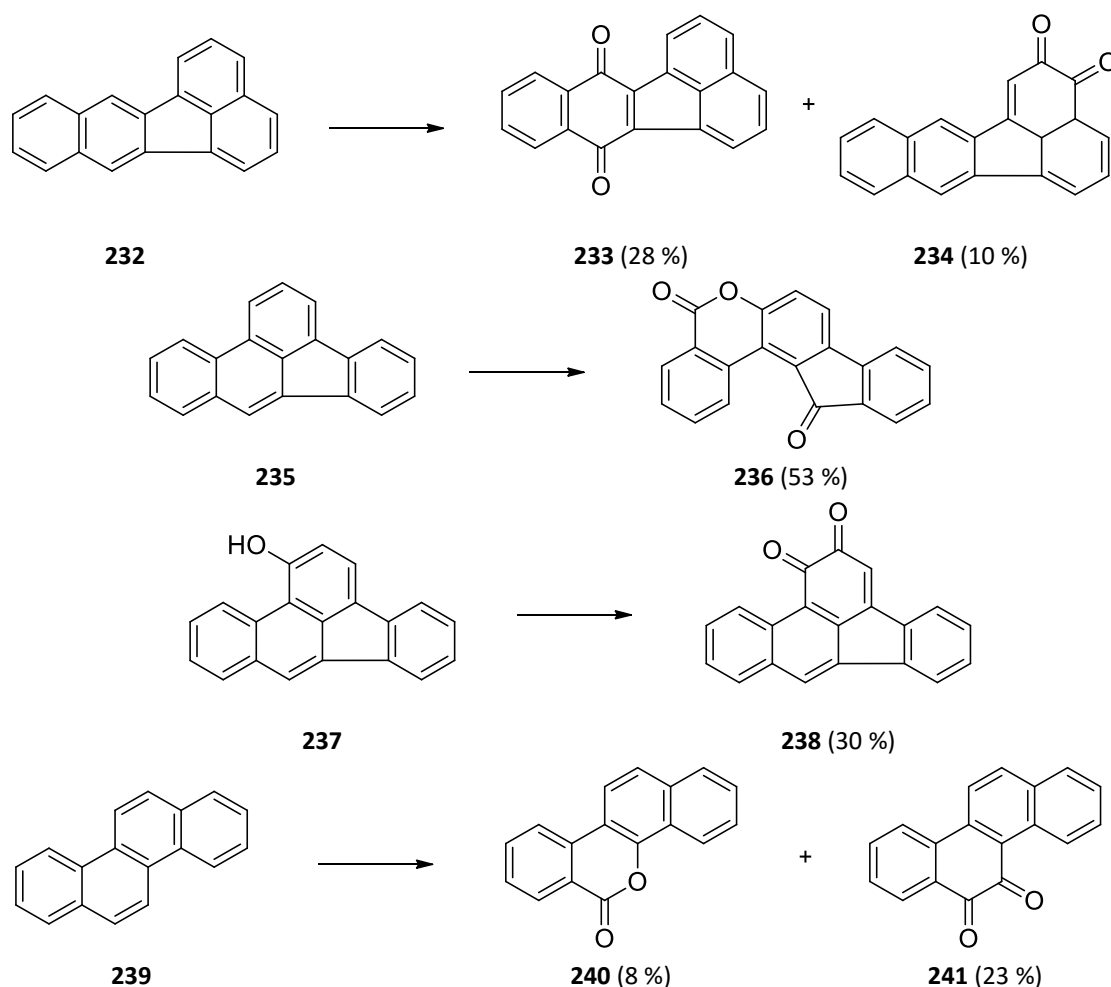


Reaction conditions: CAN (0.1 M), $(\text{NH}_4)_2\text{S}_2\text{O}_8$ (3.5 g), AgNO_3 (0.03 M), SDS (0.001 M), 0.55 M H_2SO_4 , 50 °C, 5 h.

Scheme 64 – An example of the oxidations investigated using the Skarzewski CAN redox method

Inspired by the work done by Bhatt and co-workers, Balanikas *et al.* explored the oxidation of more polynuclear aromatic hydrocarbons using CAS. In acetonitrile/4N sulfuric acid, 2 mol equivalents of CAS was added to the relevant polyaromatic compound and stirred at room temperature for 5 hours (selected examples shown in Scheme 65). The oxidation of benzo[*k*]fluoranthene (**232**) resulted in the formation of *para*-quinone **233** and *ortho*-quinone **234**. Interestingly, when benzo[*b*]fluoranthene (**235**) was exposed to CAN, lactone **236** was formed exclusively in a mediocre yield. When there was a hydroxy substituent present on the 1-position of benzo[*b*]fluoranthene (**237**) an *ortho*-quinone, **238** was formed instead. When chrysene (**239**) was oxidized using CAS, both lactone **240** (minor) and *ortho*-quinone **241** (major) were isolated in poor yields. The formation of lactones **236** and **240** are particularly noteworthy as one of the aromatic rings was oxidized and a ring closing cyclization occurred.¹⁸⁴

Introduction



Reaction conditions: CAN (2 eq), MeCN/4N H₂SO₄, rt, 5 h.

Scheme 65 – Polyaromatic compounds oxidized using CAS

The most recent example of the use of CAS in organic synthesis was by Lawrence *et al.* where instead of adding a reagent to oxidize the Ce³⁺ back to Ce⁴⁺, this was performed using electrolysis for the oxidation of alcohols to their corresponding benzaldehydes in a biphasic system. The relevant benzyl alcohol was dissolved in dichloromethane, the CAS (0.23 equivalents) was dissolved in a 1.3M solution of perchloric acid and carefully placed on top of the dichloromethane solution. Two types of experiments were performed; one where the dichloromethane layer was mixed exclusively and the electrodes (2.5 F/mol and 30 mA/cm² current density) were placed in the aqueous acidic layer close to the interface between the layers but without touching it and the second one where the two phases were stirred together for 90 minutes. They found that the biphasic electrolysed method resulted in higher yields for the biphasic system than when the biphasic system was mixed. Figure 87 below shows the benzaldehydes that were successfully generated using their methodology.¹⁸⁵

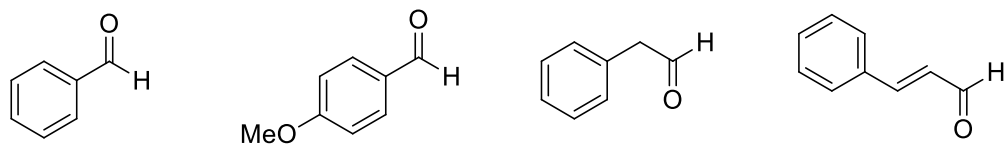


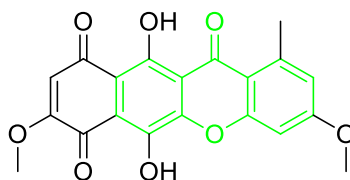
Figure 87 – Benzaldehydes generated using the electrolytic biphasic system by Lawrence *et al.*

4.3. The use of CAN/CAS in the WITS Laboratories

4.3.1. Project Origin

As previously stated, CAN is currently used in the WITS Laboratories to remove *para*-methoxybenzyl protecting groups from heteroatoms, but mainly for the oxidation of aromatic *para*-dimethoxy ethers to quinones.¹²⁸ It has also become of interest to our laboratories for the synthesis of xanthenes where we developed novel methodology based on the use of CAN, as will be outlined later in this section.

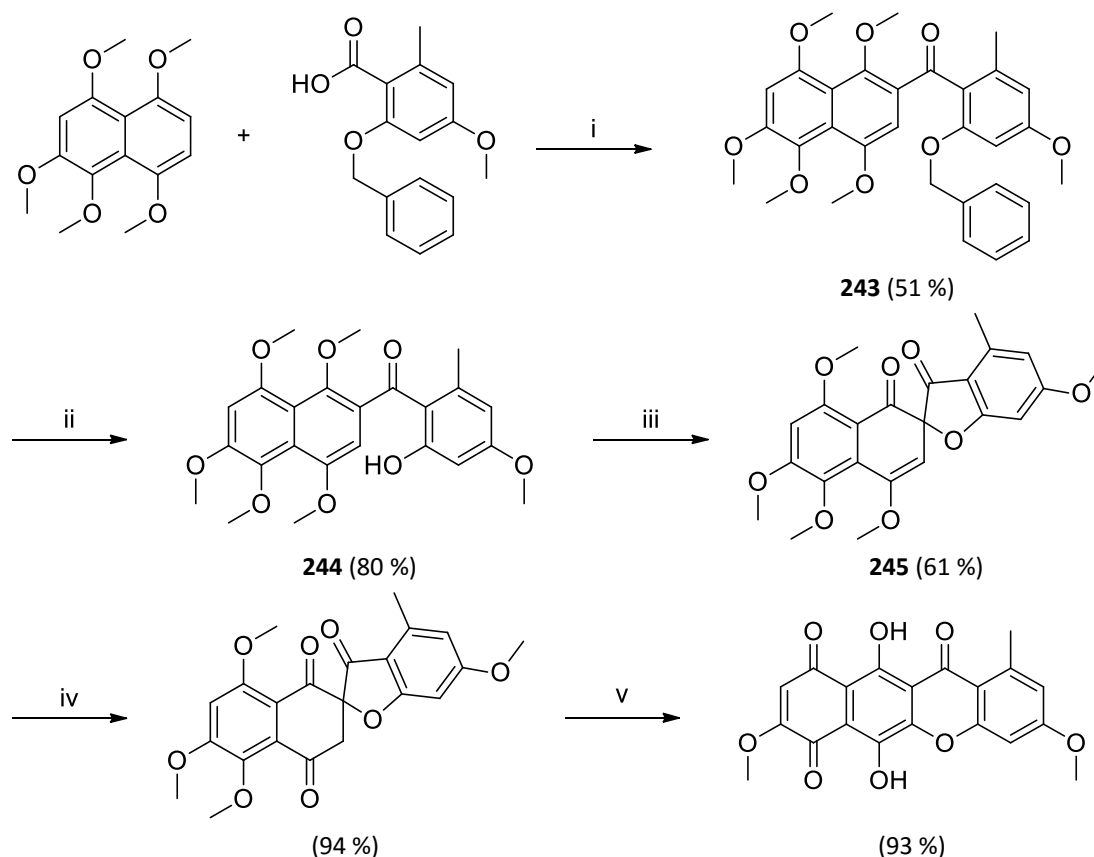
However, our interest in the synthesis of xanthenes began in 1988 where my supervisor, Charles de Koning, and Giles developed methodology for the synthesis of the xanthone bikaverin (**242**) shown in Figure 88. The xanthone core is highlighted in green in Figure 88.¹⁸⁶



242

Figure 88 – The structure of bikaverin with the xanthone ring core highlighted in blue

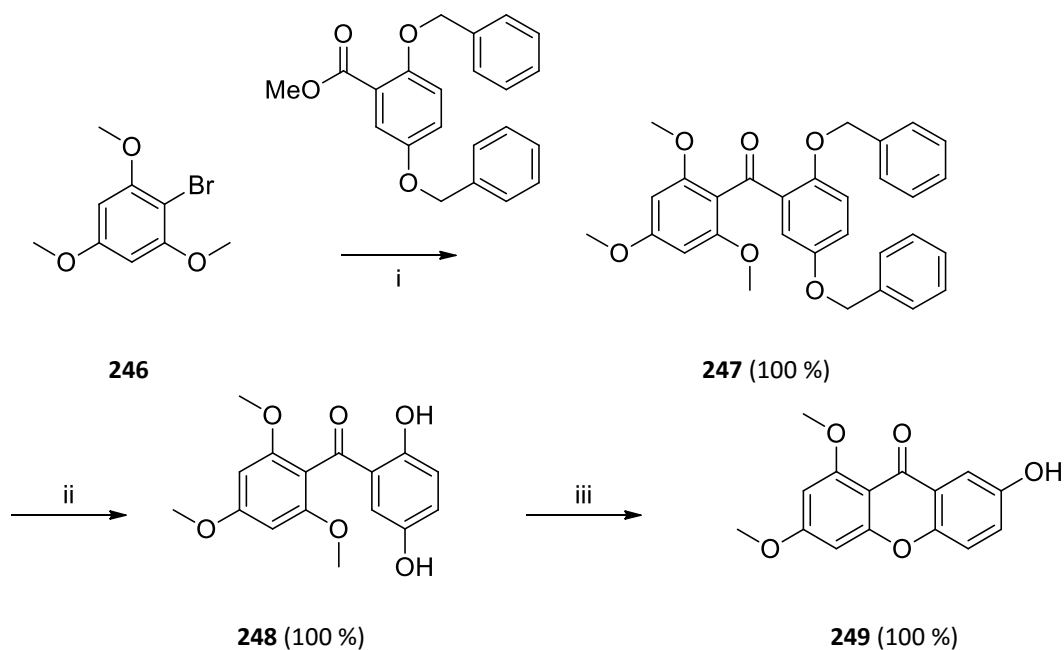
Scheme 66 outlines the synthetic route used, where a Friedel Crafts reaction mediated by trifluoroacetic anhydride (TFAA) resulted in the formation of benzophenone **243**. In this synthesis, it is also important to highlight the unexpected synthesis of spiroketal **245** which was formed from the 2,3-dichloro-5,6-dicyano-1,4-benzoquinone (DDQ) oxidation of **244**, probably mediated by a radical process.¹⁸⁶



Reaction conditions: i) TFAA, DCM, rt, 90 h; ii) 10 % Pd/C, H₂, 5 bar, 1 h; iii) DDQ, benzene, rt, 68 h; iv) TFA (aq), CH₂Cl₂, rt, 5 min; v) 200 °C, 1.1 bar, 1 h.

Scheme 66 – Synthetic route employed by de Koning and Giles in the synthesis of bikaverin

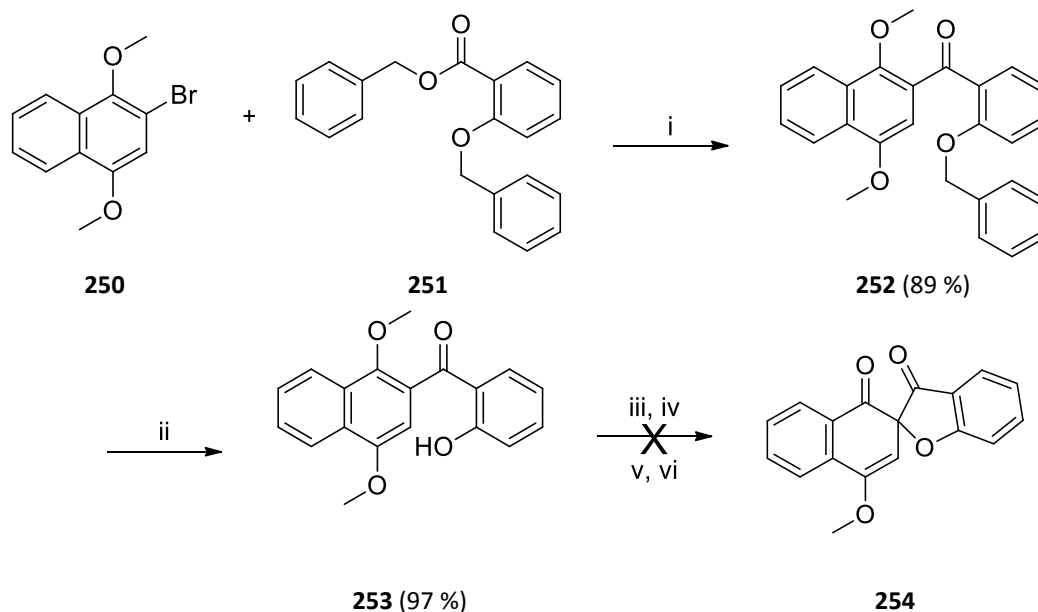
More recently, an attempt was made to expand this methodology to other naturally occurring xanthenes. However the use of this route proved to be unsuccessful, in part due to the Friedel Crafts reaction to form the benzophenone which resulted in products formed in very low yields. However, when Mondal *et al.* changed the synthetic approach a new method was reported. The key features of their synthesis is outlined in Scheme 67, where the benzophenone (**247**) was installed using a lithiation reaction; 1-bromo-2,3,5-trimethoxybenzene (**246**) was treated with *n*-butyllithium (*n*-BuLi) and reacted with a benzyl protected ester at -78 °C. Following the removal of the benzyl groups from **247** using 10% palladium on carbon (Pd/C), the xanthone **249** was formed quantitatively by the treatment of **248** under basic conditions (potassium hydroxide at reflux in methanol) by means of an oxa-Michael addition followed by elimination to furnish **249**.¹⁸⁷



Reaction conditions: i) *n*-BuLi (1 eq), THF, -78 °C, 75 min; ii) 10 % Pd/C, H₂, MeOH, rt, 6 h; iii) KOH (5 eq), MeOH, reflux, 12h.

Scheme 67 – Synthetic route employed by Mondal *et al.* to synthesize xanthones

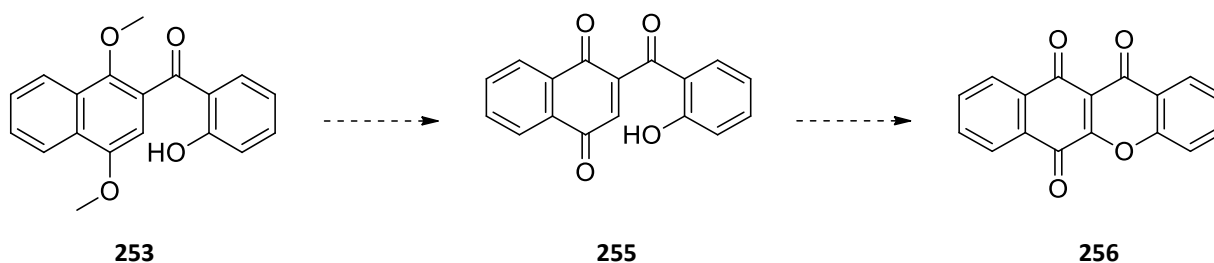
While the base catalysed oxa-Michael addition to form xanthones was successful for Mondal *et al.*, it was not of interest to our research group. The *n*-butyl lithium facilitated formation of the substituted ketone was synthetic methodology we wished to utilize. In previous research in our laboratories, this formed a key step of Jeremy Naidoo's MSc. Combining the synthetic methodologies by de Koning and Mondal, he attempted to form spirofuran **254** using the synthetic route outlined in Scheme 68. The lithiation reaction between 2-bromo-1,4-dimethoxynaphthalene (**250**) and the benzyl protected ester (**251**) resulted in the successful formation of the benzophenone compound **252** in a good yield. The deprotection of **252** to form the phenol **253** was also high yielding. Unfortunately the formation of **254** using DDQ was unsuccessful regardless of the conditions used.¹⁸⁸



Reaction conditions: i) *n*-BuLi, THF, -78 C, 90 min; ii) 5 % Pd/C, H₂, 5 atm, 18 h; iii) DDQ, benzene, rt, 72 h; iv) DDQ, benzene, reflux, 72 h; v) DDQ, CHCl₃, rt, 72 h; vi) DDQ, CDCl₃, reflux, 72 h.

Scheme 68 – Synthetic route employed by Naidoo in an attempt to form the spirofuran 254

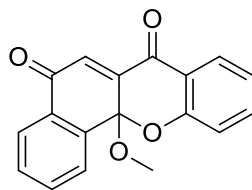
Naidoo then had to change tack in the synthesis, they envisaged that **253** could be oxidized to **255** which could then undergo a Michael addition reaction to form xanthone **256** – potentially all in a single step using CAN as shown in Scheme 69.¹⁸⁸



Reaction conditions: CAN, MeCN/H₂O, rt, 1.5 h.

Scheme 69 – Proposed CAN oxidation of 253

On exposure of **253** to CAN in acetonitrile/water the expected oxidation did not occur, however an unexpected product was isolated instead. The dione product (**257**) shown in Figure 89 was isolated in a reproducible yield of 72 %.¹⁸⁸

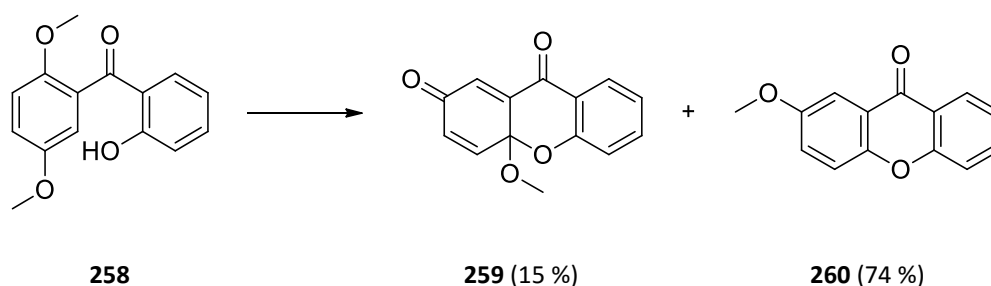


257

Figure 89 – Unexpected product when 253 was exposed to CAN

There was some literature precedence for the generation of such diones under oxidative conditions – Franck and Zeidler reported the generation of similar diones as well as xanthenes and spirofuran type compounds when exposing benzophenones which contain an alcohol substituent to potassium ferrocyanate ($K_3[Fe(CN)_6]$) and later by Ellis *et al.* using the same catalyst.^{189,190}

Given how unexpected this product was, Naidoo repeated this synthesis, this time using the substrate derived from 1,4-dimethoxybenzene. When this benzophenone (**258**) was exposed to CAN, two products resulted; dione **259** (15 %) and xanthone **260** (74 %) as shown in Scheme 70.¹⁸⁸

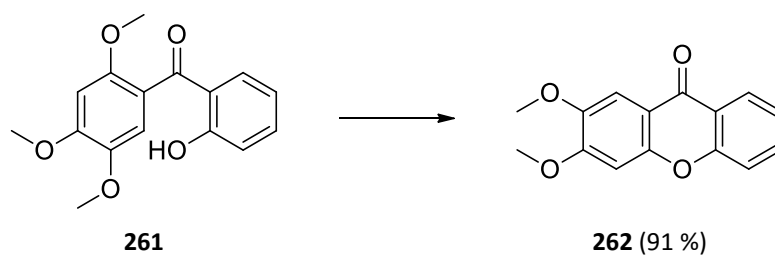


Reaction conditions: CAN, MeCN, rt, 1.5 h.

Scheme 70 – CAN oxidation of substituted benzophenone 258

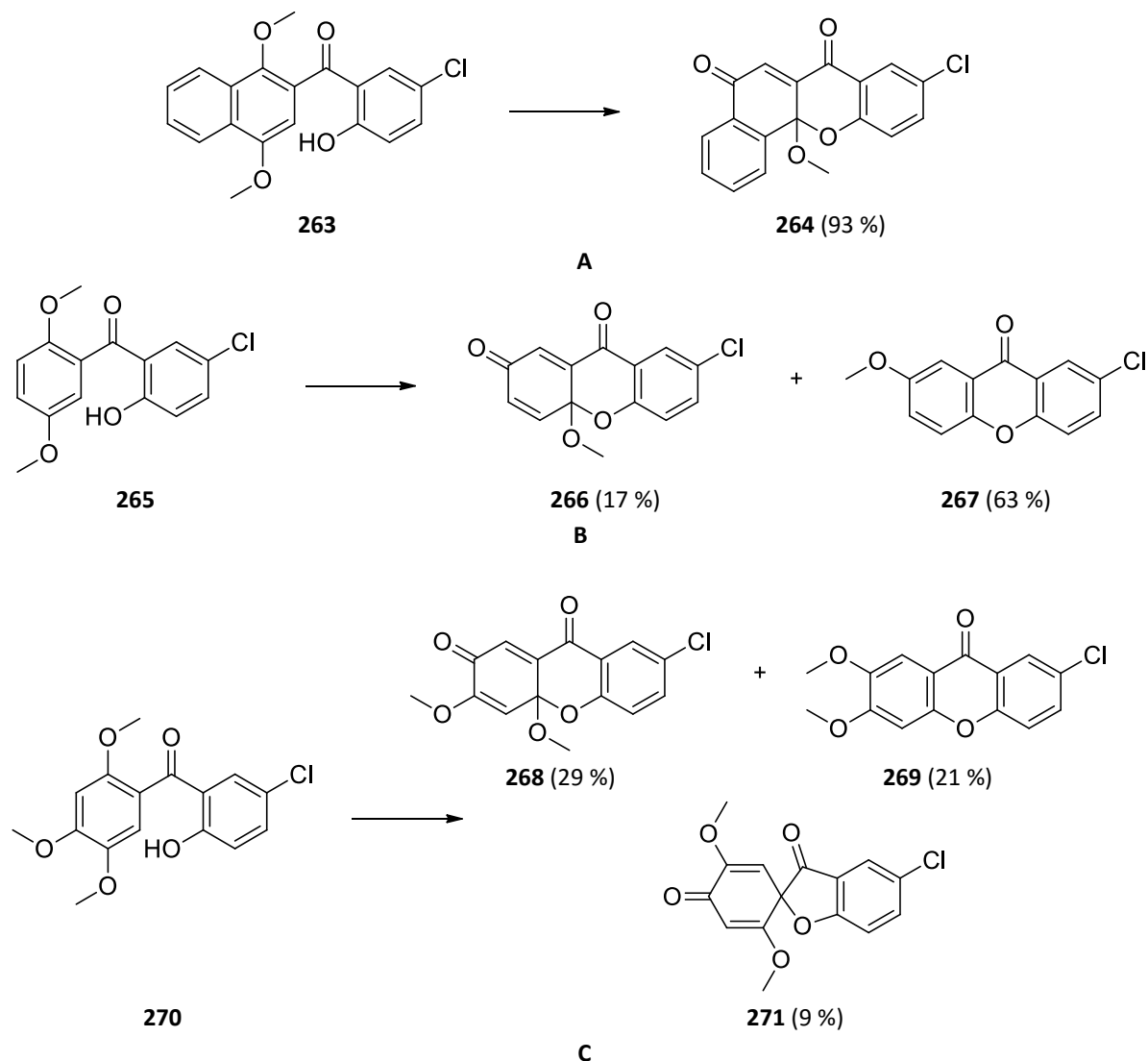
4.3.2. Development by Johnson

These interesting results also formed the basis of Myron Johnson's MSc at this university where he further investigated this CAN-mediated reaction. To confirm the results obtained by Naidoo, Johnson repeated the CAN oxidations of **253** and **258** and found the same products were generated in similar yields. Furthermore, when the trimethoxybenzophenone (**261**, Scheme 71) was exposed to CAN he found that only a single product, xanthone **262**, was collected in an excellent yield (91 %).¹⁹¹



Scheme 71 – CAN oxidation of trimethoxybenzophenone 261

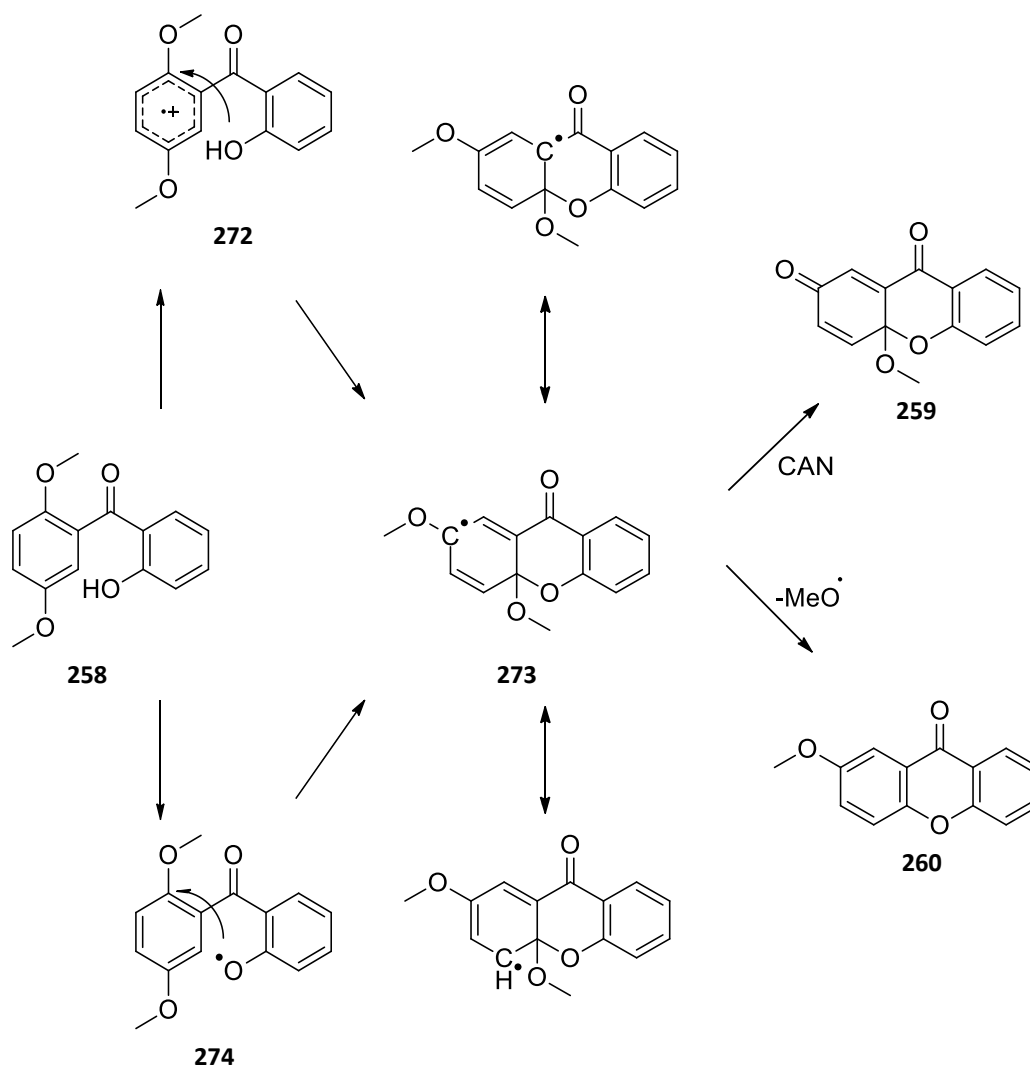
In order to determine how general this CAN-mediated reaction was, it was further expanded to include the chlorine-containing substrates as shown in Scheme 72. The results obtained for Scheme 72A and B show similar results to that obtained without the chlorine; phenol **263** was oxidized exclusively to novel dione **264**, while dimethoxybenzophenone **265** was oxidized afforded dione **266** and xanthone **267**. When trimethoxybenzophenone **270** was exposed to CAN dione **268** and xanthone **269** resulted, along with trace amounts of unexpected spirofuran-containing product, **271**.¹⁹¹



Reaction conditions: CAN (5 eq), MeCN/H₂O/CHCl₃, rt, 10 min.

Scheme 72 – CAN-mediated oxidation of chlorine-containing benzophenones

These results were novel and were published as a *Note* in the *Journal of Organic Chemistry* in 2010, along with a proposed mechanism for the reaction (Scheme 73). We postulated that the substituted benzophenone (such as **258**) could either be oxidized by CAN to generate a radical cation on the dimethoxybenzene ring as shown in intermediate **272** (Scheme 73) which could then succumb to nucleophilic attack from the phenol to give radical intermediate **273**. Alternatively, CAN could generate an oxygen centered radical on the phenol (**274**) which could then add to the dimethoxybenzene ring, also generating radical intermediate **273**. This radical can be stabilized by resonance and can then either be quenched by further oxidation of **273** resulting in the formation of dione (such as **259**) or could eliminate methanol resulting in xanthone **260**.¹⁹²

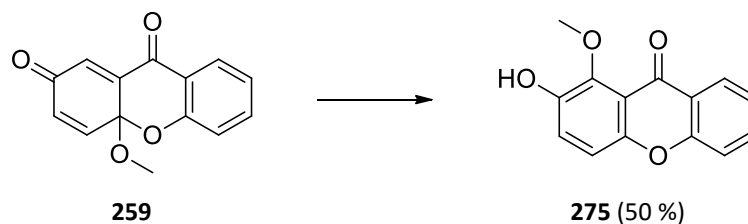


Scheme 73 – Proposed mechanism for the CAN oxidation of substituted benzophenones to form diones and xanthenes

4.3.3. Development of CAN reaction by Omolo

From these results, and aiming to use this new methodology to synthesize naturally occurring xanthenes, Justin Omolo during the course of his PhD at the University of the Witwatersrand explored this methodology further. He began by repeating Scheme 70 and Scheme 71, however this time in his hands he exclusively isolated **259** from **258** in a 72 % yield (no xanthone **260** was isolated) and **262** from **261** in a slightly lower yield of 63 %.

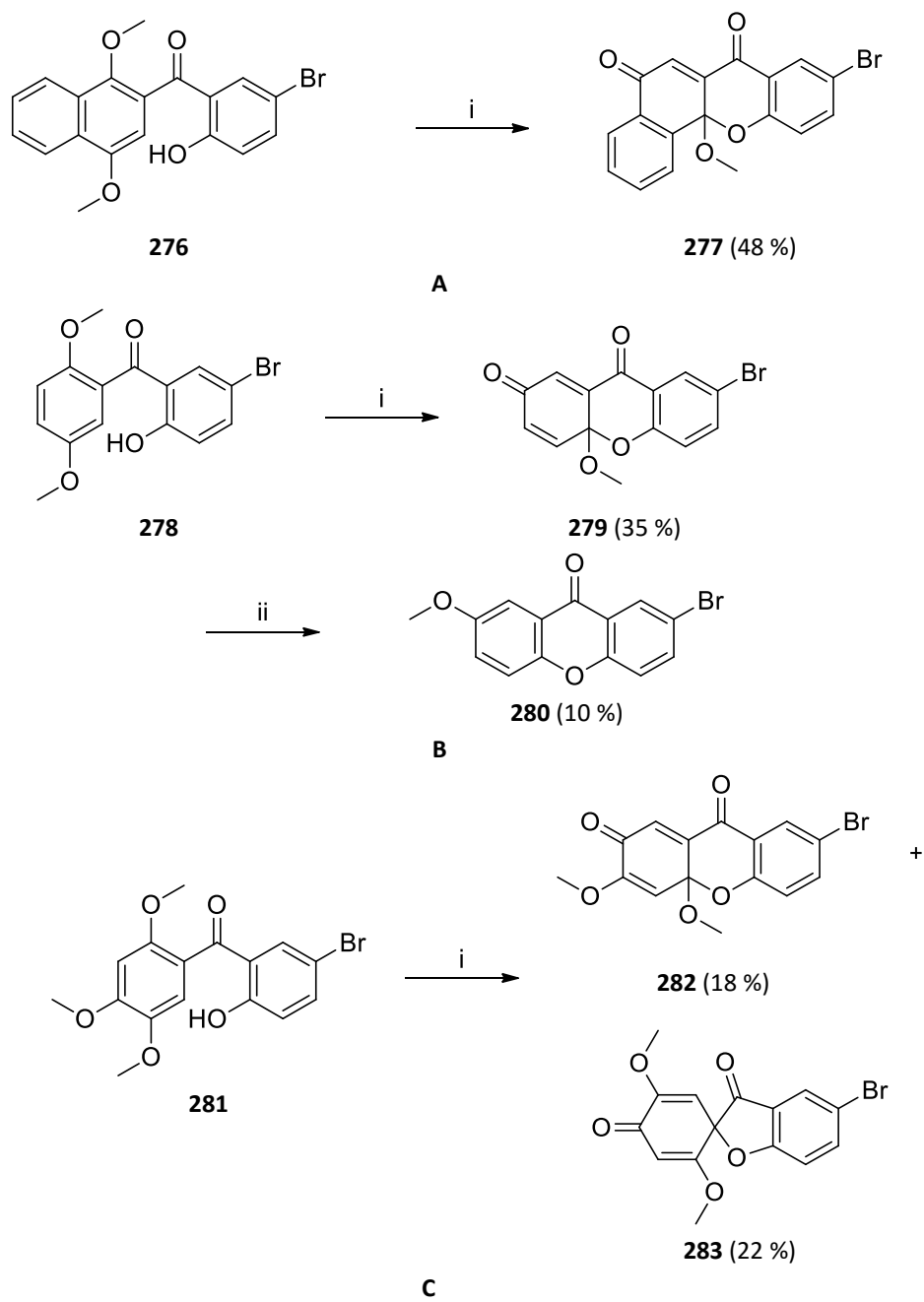
It was completely unexpected that Scheme 70 would result exclusively in dione **259** – especially when it was previously only isolated as a minor product. Thus Omolo investigated methods to convert these diones into xanthenes. He found that subjecting the dione **259** to microwave irradiation in DME resulted in the desired transformation. For example, Scheme 74 where **259** was converted into **275** in a 50 % yield.¹⁹³



Reaction conditions: DME, microwave, 10 min, 150 °C, 120 W.

Scheme 74 – Conversion of dione to xanthone

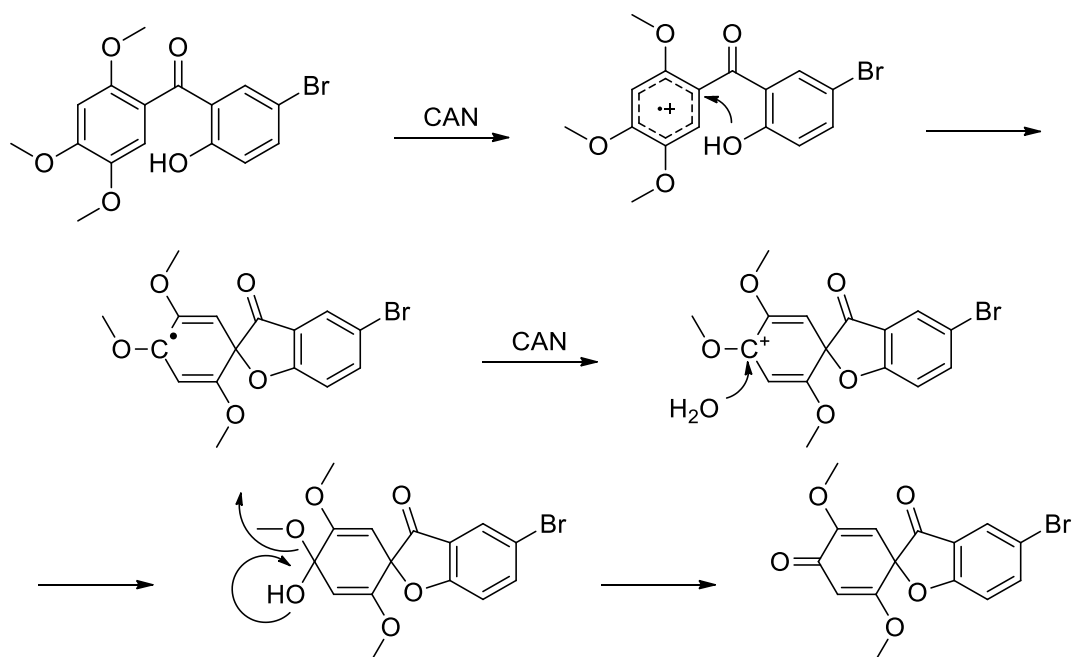
Omolo expanded the series of reactions performed by investigating the CAN-mediated reaction of benzophenones with aromatic bromides. He wished to obtain substrates containing aromatic bromides as these could be used in transition metal cross coupling reactions. The results from these reactions are reported in Scheme 75 where naphthalene **276** resulted in the formation of dione **277** in a mediocre yield of 48 %. The dimethoxybenzophenone substrate **278** resulted in the exclusive formation of **279** in a low yield and this could be converted to xanthone **280** in a poor yield. Following the same procedure, trimethoxybenzophenone **281** resulted in the formation of both dione **282** and spirofuran **283** in low yields when exposed to CAN.¹⁹³ Although these reactions were novel, the outcome of the reactions in Scheme 75 was markedly different from what was obtained in the hands of Johnson and Naidoo.



Reaction conditions: i) CAN, MeCN/H₂O/CHCl₃, rt, 10 min; ii) DME, microwave, 10 min, 150 °C, 120 W.

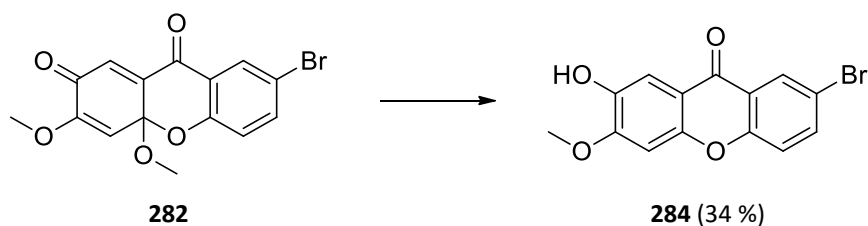
Scheme 75 – CAN-mediated oxidation reactions performed by Omolo

The mechanism proposed by Omolo for the formation of spirofurans under the CAN oxidative conditions is outlined in Scheme 76 and follows the one proposed in the JOC 2010 paper.¹⁹³



Scheme 76 – Proposed mechanism for the CAN-mediated formation of spirofurans

Even though formed from low yielding reactions, the presence of the bromine atom on these diones, xanthenes and spirofurans allowed further manipulation using the Suzuki-Miyaura cross coupling reaction – a well-developed reaction used extensively in the WITS laboratories. Initially attempted using dione **282**, Omolo found that the Suzuki-Miyaura reaction (which was performed using microwave conditions) was unsuccessful, resulting in the formation of xanthone **284** (Scheme 77).¹⁹³



Reaction conditions: 2-formylphenyl boronic acid, CsF, Pd(PPh₃)₄, DME, microwave, 10 min, 150 °C, 120 W.

Scheme 77 – Resulting product from the attempted Suzuki-Miyaura coupling reaction under microwave conditions

The Suzuki-Miyaura coupling reaction was then attempted using spirofuran compound **283** and was found to be successful using Pd(PPh₃)₄ under microwave conditions using a variety of aromatic boronic acids in moderate to good yields. A selection of the compounds formed and their yields are detailed in Figure 90.

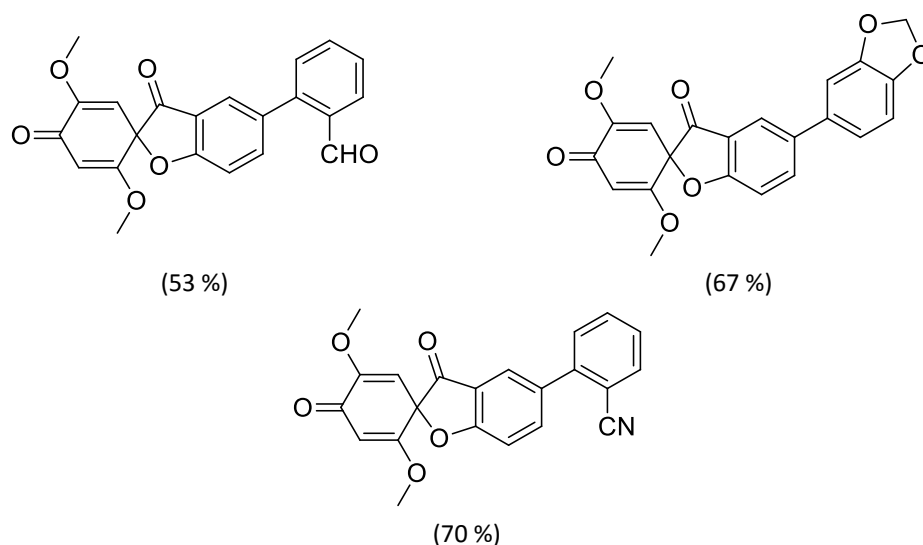


Figure 90 – Spirofuran compounds altered using Suzuki-Miyaura coupling reactions

The spirofuran compounds synthesized bore a striking similarity to a commercial antifungal agent, griseofulvin (Figure 91) and so the spirofurans (and selected xanthenes and diones from both Omolo and Johnson's work) were tested for antimicrobial and antifungal activity. The results were published in *Bioorganic and Medicinal Chemistry Letters* in 2011 where the spirofurans showed good activity against the *Cryptococcus neoformans* yeast. Additionally, dione **259** showed the best antifungal activity of all the compounds screened in both the *Cryptococcus neoformans* and the *Candida albicans* yeast cell lines and was comparable to the activity exhibited by the amphotericin B standard.¹⁹⁴ This suggested that the use of this novel synthetic methodology could be useful in the development of new antifungal agents.

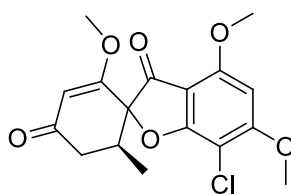
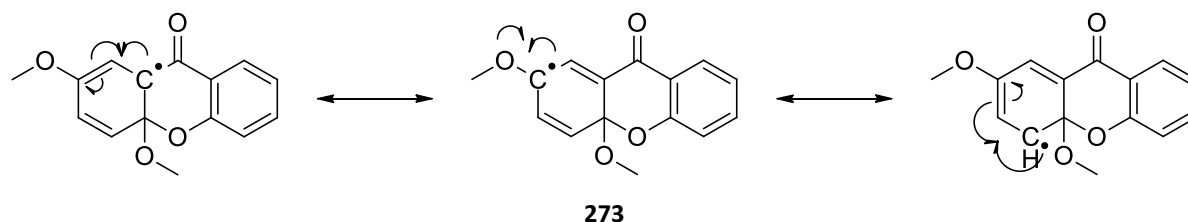


Figure 91 – The structure of commercially available antifungal griseofulvin

4.4. Aims of this project

Given the potential of developing new synthetic methodology for new antifungal agents as well as the discrepancy between the results obtained by Johnson and Omolo, it was deemed that further exploration of the novel CAN reaction was necessary. This aim formed one of the major objectives for this PhD project.

In the paper published by Johnson *et al.* in 2010 a mechanism was proposed that relied on the fact that a *para*-methoxy substituent was necessary to stabilize the radical cation. The proposed radical generated, once cyclisation has occurred (**273**), has the potential to be resonance stabilized as shown in Scheme 78.¹⁹² From the proposed mechanism, the presence of methoxy groups in these positions would stabilise the radical intermediate and hence allow for the formation of xanthenes or diones. However, no experiments had been conducted to support this hypothesis.



Scheme 78 – Resonance stabilization of the radical intermediate of 273

This project aimed at probing this mechanism by using the methodology developed by Johnson to generate benzophenone derivatives with methoxy substituents in other varying positions on the benzene rings that could be exposed to CAN. We were also interested in the effect of removing or adding additional methoxy groups to these substrates.

An additional aim of this project is to determine if this novel synthetic methodology could be adapted to the synthesis of the nitrogen-containing derivatives, the biologically active acridones. Figure 92 shows examples of acridones isolated from the root of *Thamnosma rhodesica*.¹⁹⁵

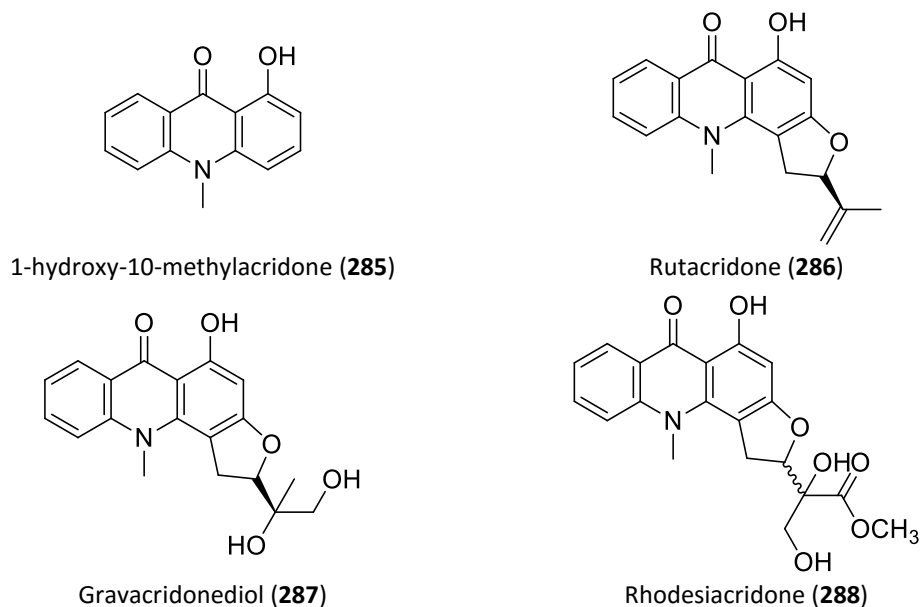
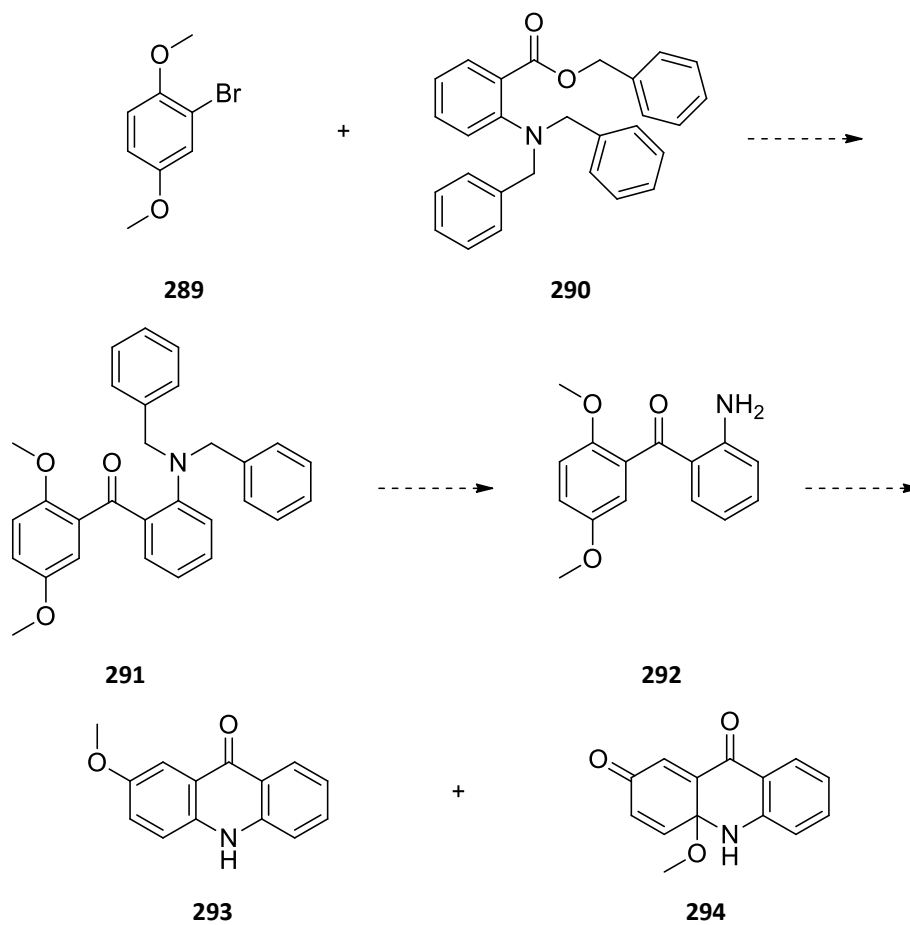


Figure 92 – Examples of naturally occurring acridones showing biological activity

We hypothesised that the synthesis of the acridone ring core could be achieved by using the CAN-mediated ring closure methodology as outlined in Scheme 79 from commercially available anthranilic acid and 1,4-dimethoxybenzene. After a series of transformations akin to the xanthone methodology we would obtain benzophenone **291**. Following deprotection of **291**, **292** could then be exposed to CAN to hopefully obtain either **293** or **294** (or a combination of both).



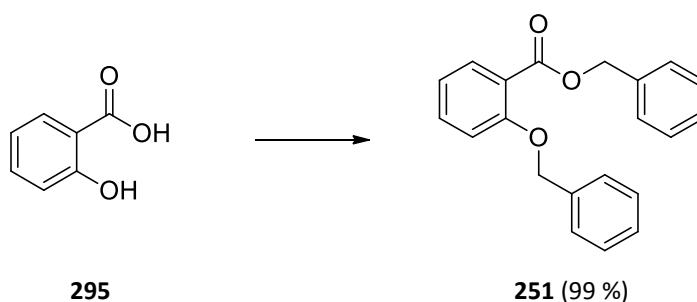
Scheme 79 – Proposed synthesis of acridones using the CAN-mediated methodology

Plot Twist:

Results and Discussion

5.1. Repetition of work by Johnson

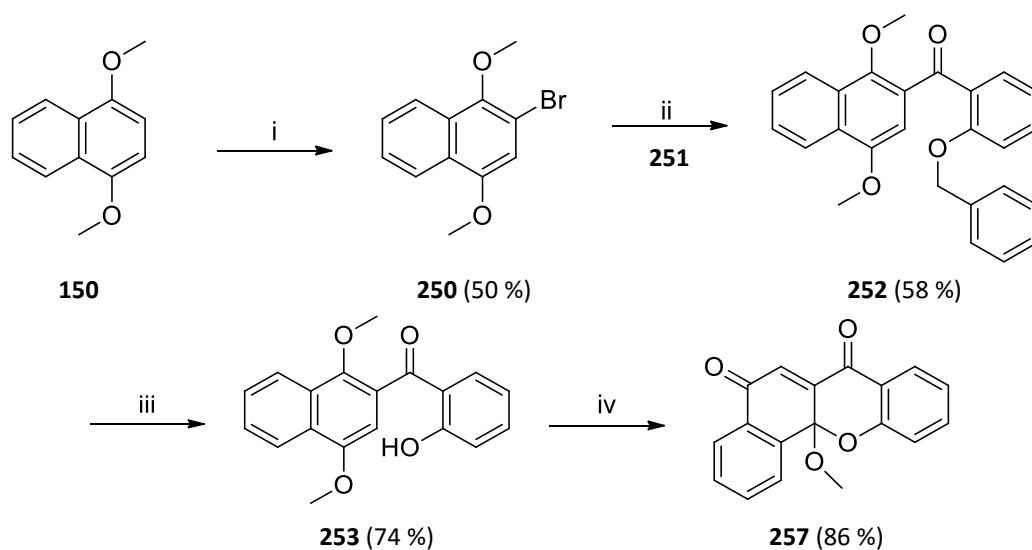
Given the promising antifungal testing results obtained previously, some of the xanthenes and related compounds needed to be resynthesized to conduct further biological assays. Following literature precedent, salicylic acid was easily converted to the corresponding *O*-benzyl protected ester **251** as shown in Scheme 80.



Reaction conditions: Benzyl bromide (2.1 eq), K₂CO₃ (3 eq), acetone, reflux, 18 h.

Scheme 80 – Benzyl protection of salicylic acid

Since the following reactions were repeated exactly as described in Johnson's MSc,¹⁹¹ the reactions are summarized in Scheme 81 below. 1,4-Dimethoxynaphthalene **150** was easily converted into **253** via the intermediates of **250** and **252**.

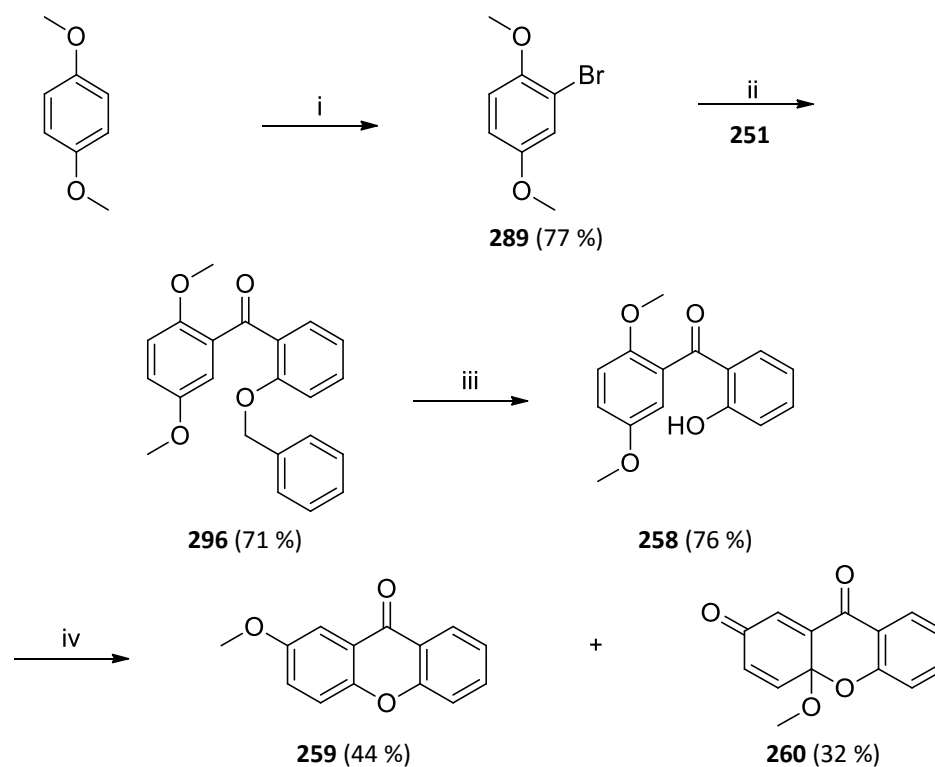


Reaction conditions: i) NBS (1 eq), CHCl_3 , reflux, 2 h; ii) *n*-BuLi (1.28 M, 1 eq), **251** (0.9 eq), THF, -78°C , 2 h; iii) 5 % Pd/C (10 mass %), MeOH, rt, 18 h; iv) CAN (5 eq), MeCN/ H_2O / CHCl_3 , rt, 18 h.

Scheme 81 – Synthesis of dione 257

The final step of this synthesis involved the key CAN-mediated oxidative cyclization of **253**, which occurred as expected resulting in the formation of **257** in a similar yield to what was previously obtained. The structure of dione **257** was confirmed by ^1H and ^{13}C NMR spectroscopy and, along with COSY and HSQC experiments, the spectra were fully assigned.

Similarly, dione **259** and xanthone **260** were synthesized using the same methodology employed by Johnson as shown in Scheme 82. Commercially available 1,4-dimethoxybenzene could be brominated to afford **289**, subjected to lithiation and reacted with **251** to generate benzophenone compound **296**. Finally, debenzoylation to produce **258** resulted in a substituted benzophenone that could be used in the CAN-mediated cyclization reaction. All of these reactions occurred in good yields and the NMR spectra obtained matched Johnson's results.¹⁹¹



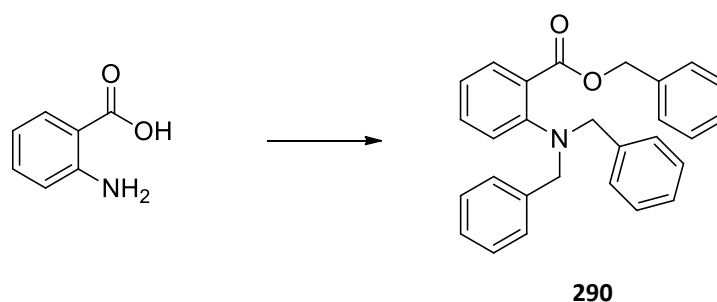
Reaction conditions: i) NBS (1 eq), CHCl_3 , reflux, 3 d; ii) *n*-BuLi (1.4 M, 1 eq), **251** (0.9 eq), THF, -78°C , 2 h; iii) 5 % Pd/C (10 mass %), MeOH, rt, 18 h; iv) CAN (5 eq), MeCN/ H_2O / CHCl_3 , rt, 18 h.

Scheme 82 – Synthetic route utilized in the synthesis of dione **259 and xanthone **260****

While both **259** and **260** were isolated from the oxidation of **258** with CAN, a disturbing aspect was that they were isolated in markedly different yields to those reported by both Johnson and Naidoo (**259** in a 15 % yield and **260** in a 74 % yield).¹⁹¹ As the purpose of the synthesis was to generate more xanthenes and diones for biological testing it was performed on a significantly larger scale than that performed by Johnson. We initially attributed the difference in yields to the difference in reaction scale. As will be discussed later, this was not the case.

5.2. Initial attempts towards the synthesis of acridones

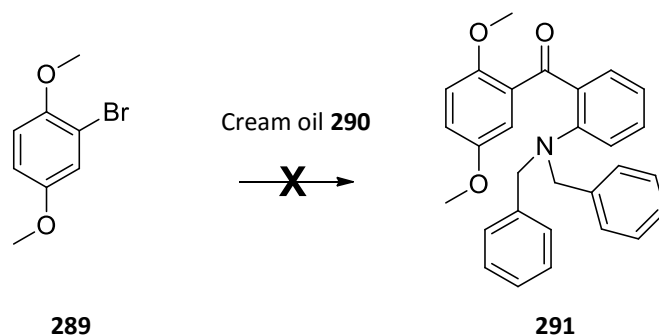
With more confidence gained in the synthetic methodology to be used in this project, the synthesis of acridones was then attempted, as outlined in Scheme 79, using the same synthetic methods. Starting from commercially available anthranilic acid, we began with the benzyl protection as before. As detailed in Scheme 83, the combination of anthranilic acid, potassium carbonate and benzyl bromide with heating under reflux conditions, resulted in the formation of a sticky cream oil of **290** after purification by column chromatography. The ^1H NMR spectrum of the product collected showed the presence of methylene benzyl groups which would be indicative of what we assumed were three benzyl groups attached to the anthranilic acid.



Reaction conditions: Benzyl bromide (3.1 eq), K_2CO_3 (3.5 eq), acetone, reflux, 12 h.

Scheme 83 – First attempted benzyl protection of anthranilic acid

The presumed **290** was used in the lithiation reaction (Scheme 84), and this resulted in the formation of a luminous yellow reaction mixture. Purification of this yellow product resulted in a yellow solid that was determined to be mono-*N*-benzylated benzophenone **297** (Figure 93) in a very low yield (12 %). The structure was determined from the ^1H and ^{13}C NMR spectra, where the benzylic CH_2 signal was evident at 4.53 ppm and the N-H signal at 9.40 ppm in the ^1H NMR spectrum and the ketone carbonyl signal at 198.5 ppm and the benzylic methylene carbon at 46.9 ppm in the ^{13}C NMR spectrum. This suggested that the sticky cream coloured oil which we assumed to be **290** was actually a mixture of benzylated products.



Reaction conditions: *n*-BuLi (1.4 M, 1 eq), **290** (0.9 eq), THF, -78 °C, 2 h.

Scheme 84 – Lithiation reaction using the sticky cream oil thought to be 290

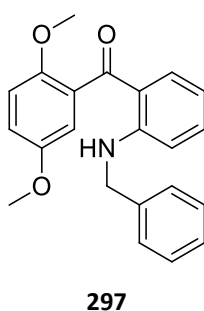
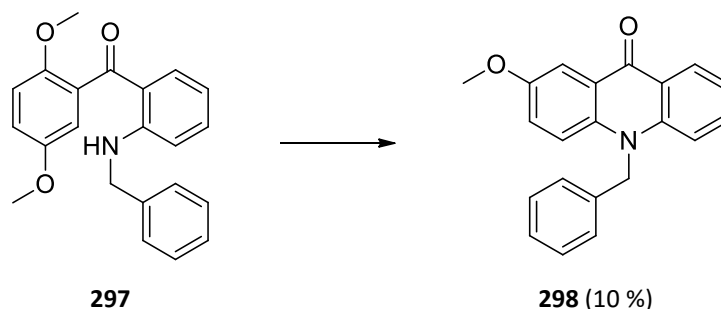


Figure 93 – Product isolated from the lithium mediated coupling of 1,4-dimethoxybenzene and the sticky cream oil

While **297** was not the desired product, it could potentially be a suitable candidate for attempting the CAN-mediated ring closure reaction and Scheme 85 outlines our first attempt at the formation of acridones using this method. The reaction was performed as before in an acetonitrile/water/chloroform solvent system at room temperature overnight. After purification by column chromatography, mostly starting material was isolated from the reaction (50 %), although acridone **298** was isolated in a 10 % yield as a yellow solid. Characterisation was made primarily using NMR spectroscopy where only a single methoxy signal was noted at 3.95 ppm, along with the presence of the benzylic CH₂ at 5.61 ppm in the ¹H NMR spectrum. Furthermore, the absence of the N-H signal suggested that the ring closure had in fact occurred. The ¹³C NMR spectrum (and relevant 2D experiments) along with high resolution ESI-MS further supported this structure ([M+H]⁺ for C₂₁H₁₈NO₂ calculated 316.1338 and found to be 316.1338). It was also observed that the solution of **298** fluoresced blue under natural light – another characteristic feature of acridones.¹⁹⁶



Reaction conditions: CAN (5 eq), MeCN/H₂O/CHCl₃, rt, 18h.

Scheme 85 – The first attempt at acridone formation using the CAN-mediated methodology

While wondering about the discrepancy in yields between our work and that of Johnson in our labs, it is of significance to highlight that up until this point, the CAN used was the same container of CAN that Johnson had used in his project. This container was hand-labelled, contained both orange and yellow crystals and was almost finished at this point of the project (shown in Figure 94 and Figure 95).



Figure 94 – The ‘Old CAN’ container with the faded labels

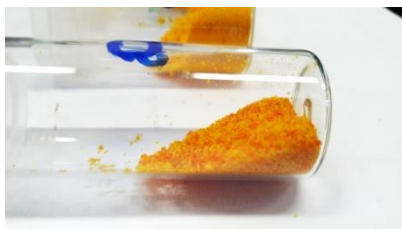


Figure 95 – The physical appearance of the ‘Old CAN’

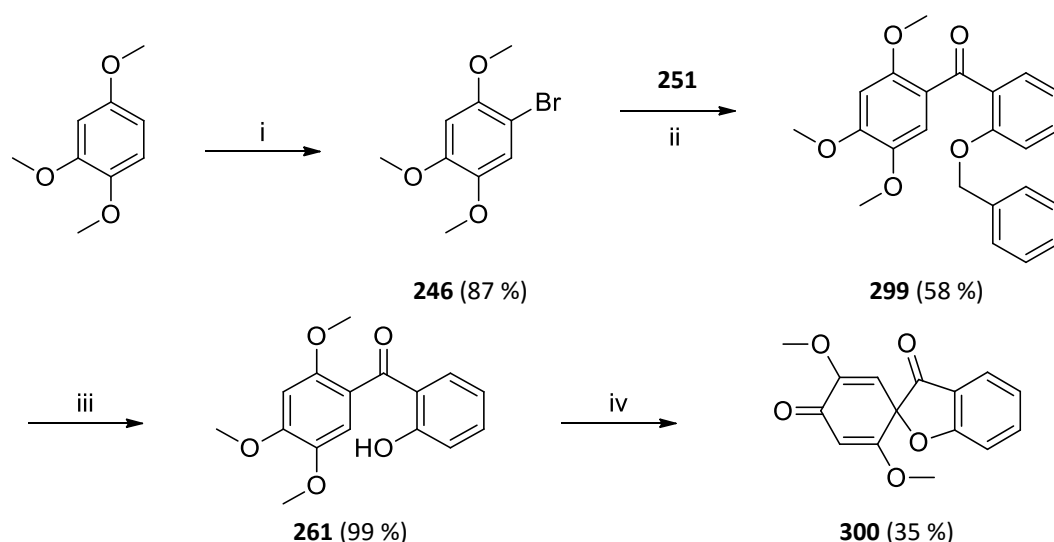
Given that a large amount of starting material was returned from Scheme 85, the reaction was repeated with the collected **297** but this time with the addition of CAN from a new bottle obtained from Sigma-Aldrich. After leaving the repeated reaction overnight (as previously done) no starting material remained. Unfortunately, no acridone **298** was isolated either. Albeit an accidental synthesis, this was a promising start for this project and was proof of concept that at least one acridone could be synthesized using the CAN methodology. Unfortunately, despite numerous attempts to repeat this synthesis using the Sigma-Aldrich CAN, no acridone was formed.

5.3. Irreproducible results and confusing catalysts

5.3.1. Irreproducibility of Johnson's results

After the disappointment of not being able to reproduce the synthesis of acridones, we returned to the work performed in Johnson's MSc dissertation to test if we could reproduce the results obtained using the new CAN obtained from Sigma-Aldrich.

Bromination of 1,2,5-trimethoxybenzene was found to be spontaneous at room temperature when it was added to a stirring suspension of recrystallized *N*-bromosuccinimide in dichloromethane. The lithiation of **246** and subsequent reaction with ester **251** was successful, although in a mediocre yield (also noted by Johnson¹⁹¹). Debenzylation of **299** was quantitative using 5 % Pd/C under a hydrogen atmosphere, resulting in the formation of **261** as shown in Scheme 86. The NMR spectroscopic data matched well with Johnson's reports for compounds **246**, **299** and **261**. When Johnson exposed **261** to CAN he isolated xanthone **262** in a 91 % yield,¹⁹¹ however, repetition of the same reaction (as shown below in Scheme 86) resulted in the isolation of an unexpected spirofuran **300** albeit in a low yield. No starting material or any other products were isolated from this reaction and **300** was isolated even after repeating the reaction numerous times.



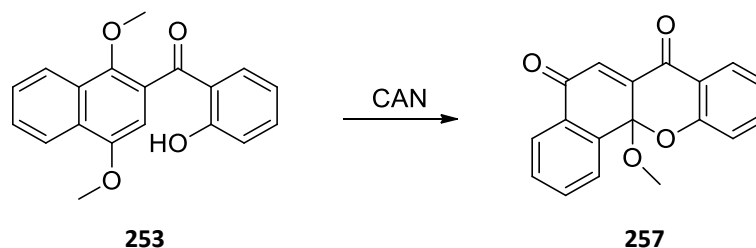
Reaction conditions: i) NBS (1 eq), DCM, rt, 20 min %; ii) *n*-BuLi (1.2 M, 1 eq), **251** (0.9 eq), THF, -78 °C, 2 h; iii) 5 % Pd/C (10 mass %), MeOH, rt, 18 h; vi) CAN (3 eq), MeCN/H₂O, rt, 10 min.

Scheme 86 – Synthetic route utilized in the repeated synthesis of the trimethoxy series

Concerned that there was a contaminant in the new bottle of CAN purchased from Sigma-Aldrich that was resulting in the difference in the products obtained we recrystallized the CAN purchased from Sigma-Aldrich following the methodology prescribed by Perrin in the *Purification of*

Results and Discussion

*Laboratory Chemicals.*¹⁹⁷ Scheme 81 and Scheme 82 were repeated using the recrystallized CAN. This time CAN was added portion-wise to a solution of substrate **253** and the reaction monitored by TLC. After the addition of only 2 equivalents of the new CAN (and after only about 10 minutes) no further starting material could be visualized on the TLC plate. After purification of the reaction mixture, dione **257** was collected, unfortunately in a very poor yield. Table 7 shows a comparison between the results obtained using the old hand-labelled bottle of CAN and the new bottle purchased from Sigma-Aldrich, as well as in comparison with results previously obtained.



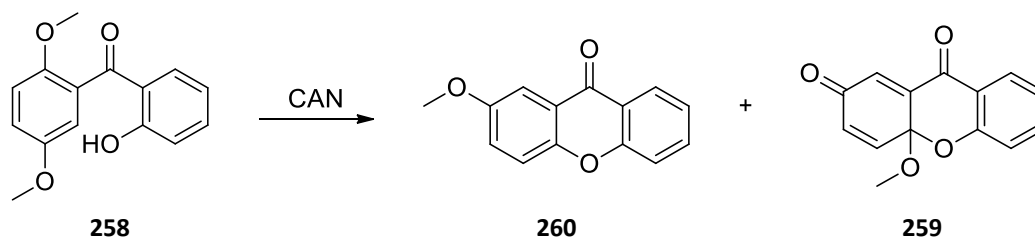
Scheme 87 – Repeated synthesis of 257 using the recrystallized CAN

Table 7 – Comparison of the attempted synthesis of 257 using two different sources of CAN

Experiment	Catalyst	Reaction conditions	Yield of 257
Naidoo ¹⁸⁸	Old CAN (5 eq)	MeCN/H ₂ O/CHCl ₃ , r.t., overnight	72 %
Johnson ¹⁹¹	Old CAN (5 eq)	MeCN/H ₂ O/CHCl ₃ , r.t., overnight	72 %
Dam	Old CAN (5 eq)	MeCN/H ₂ O/CHCl ₃ , r.t., overnight	86 %
Dam	New CAN (2 eq)	MeCN/H ₂ O, r.t., 10 min	26 %

As concerned as we were by this outcome, even more concerning results were obtained when the reaction was repeated using substrate **258** (Scheme 88). With the new bottle of CAN no xanthone **260** was isolated, and only dione **259** was isolated in a very poor yield. Using fewer equivalents of the new CAN and changing the temperature of the reaction (to reflux or to 0 °C) did not affect the outcome of the reaction. Changing the solvent mixture to a methanol/water solution resulted in the same observation – all the starting material was consumed almost immediately and only **259** was isolated in a poor yield. These results are outlined in Table 8.

Results and Discussion



Scheme 88 – Repeated oxidation of 258 using the new CAN

Table 8 – Comparison of the results obtained when 258 was exposed to different CAN sources

Experiment	Catalyst	Reaction Conditions	Yield of 260	Yield of 259
Johnson ¹⁹¹	Old CAN (5 eq)	MeCN/H ₂ O/CHCl ₃ , r.t., overnight	74 %	15 %
Dam	Old CAN (5 eq)	MeCN/H ₂ O/CHCl ₃ , r.t., overnight	32 %	44 %
Dam	New CAN (5 eq)	MeCN/H ₂ O, r.t., 10 min	0	3 %
Dam	New CAN (2.5 eq)	MeCN/H ₂ O, reflux, 10 min	0	30 %
Dam	New CAN (2.5 eq)	MeCN/H ₂ O, 0 °C, 10 min	0	24 %
Dam	New CAN (5 eq)	MeOH/H ₂ O, r.t., 10 min	0	16 %

Even when the reaction was performed with a single equivalent of new CAN, the starting material was consumed within 10 minutes and only dione **259** formed in a poor yield. Since, from the proposed mechanism (Scheme 73), two equivalents of CAN were required to generate the dione species and dione was exclusively formed even with the addition of 1 equivalent of CAN, it was thought that the Ce⁴⁺ ion was being regenerated during the reaction. Repeating this reaction under completely inert conditions where CAN was added in 0.1 mol equivalents and monitoring the reaction by TLC showed some interesting results. On the TLC plate the xanthone **260** appeared as a fluorescent blue spot at a higher R_f than the starting material **258** (which was a dark spot), the dione **259** also appeared as a dark spot on the TLC plate but at a similar R_f value (just slightly higher than the starting material). After the addition of the 0.2 equivalents of CAN, the TLC showed the presence of a fluorescent blue spot at the same R_f as xanthone **260** along with starting material. This fluorescence spot increased in sized as the reaction proceeded with further additions of CAN and the starting material spot decreased in size slowly. After 0.6 equivalents of CAN had been added, the appearance of a third spot – with the same R_f as dione **259** – was observed. As more equivalents of CAN were slowly added the dione spot increased dramatically and the fluorescent blue spot, as well as the starting material spot, reduced slowly until only trace amounts were found by the time a full equivalent of CAN had been added. These traces had completely disappeared after the reaction had been worked up. Figure 96 below is a graphical representation of what was noted on the TLC plate. Although not a quantitative representation, the graph is given for clarity.

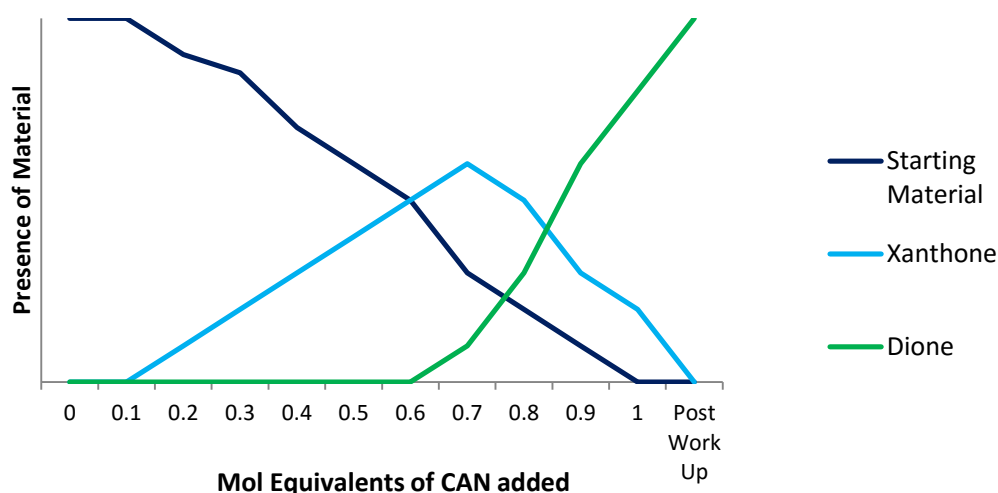


Figure 96 – TLC observations of the addition of CAN in 0.1 mol equivalents under inert conditions

5.3.2. Analysis of the CAN samples

Hence, it was proposed that there must be a contaminant present either in the old CAN that facilitated the reaction or in the new CAN preventing the reaction from occurring. Therefore, the contents of the two bottles of CAN needed to be investigated.

Powder X-ray diffraction (PXRD) analysis was performed on both the old CAN used by Johnson (and the author at the start of this project) and the new CAN obtained from Sigma-Aldrich. PXRD analysis was performed by Dr Stuart Miller at the University of the Witwatersrand on a Bruker D2 diffractometer on a silicon wafer zero background sample holder with a cobalt X-ray source (step size 0.16°). The powder patterns that were obtained were compared with the files for CAN (and variations thereof) in the Joint Committee on Powder Diffraction Standards (JCPDS) database using the search/match algorithm on the EVA Bruker X-ray data evaluation package. The PXRD pattern of the CAN obtained from Sigma-Aldrich agreed well with a monoclinic CAN powder pattern from the database (Figure 97). The recrystallized CAN showed a similar pattern to that of the commercially available CAN (Figure 98) and also fitted well with the monoclinic CAN pattern in the JCPDS database.

Plot Twist
Results and Discussion

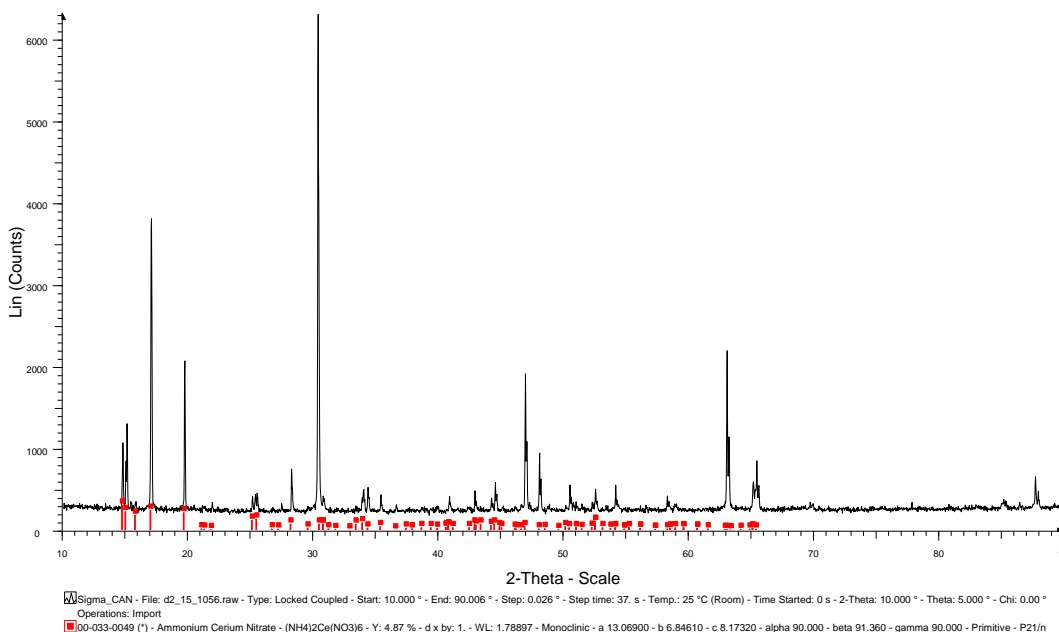


Figure 97 – PXRD pattern for the CAN purchased from Sigma-Aldrich with the database CAN superimposed in red

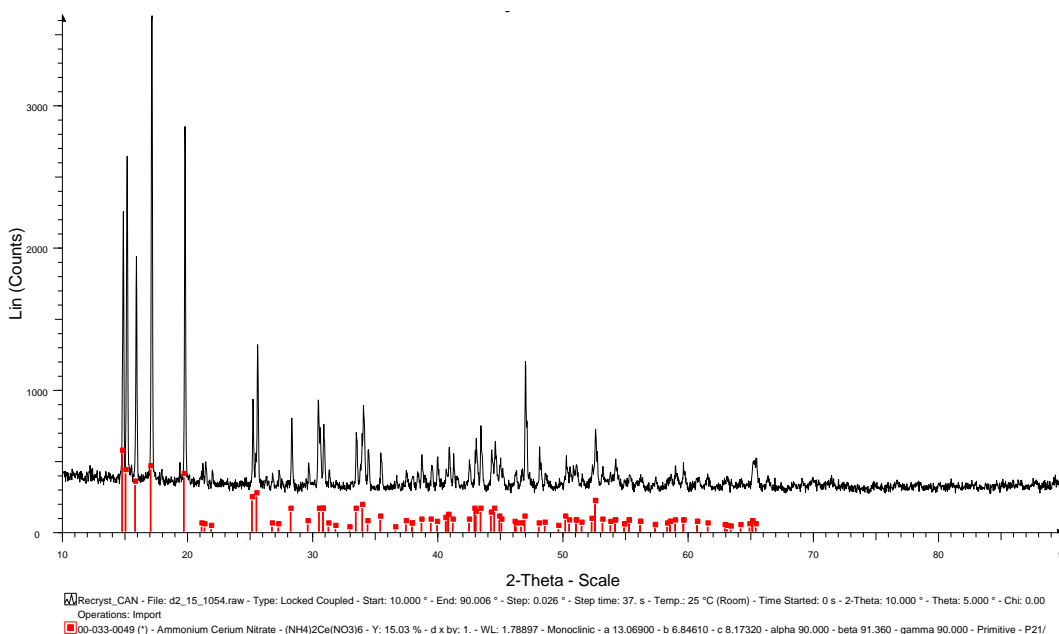


Figure 98 – PXRD pattern for the recrystallized Sigma-Aldrich CAN and its match from the database overlaid in red

The sample from the old CAN container gave a PXRD pattern that did not match with any cerium nitrate or any cerium oxide salt present in the database. This wasn't completely surprising as the old container appeared to contain a mixture of yellow and orange crystals. It was found that the orange crystals were soluble in water while the yellow crystals were insoluble and thus could be

separated by filtration after the orange crystals were dissolved in the water. The filtrate was concentrated *in vacuo* to furnish the orange crystals. Both the yellow and orange crystals were dried separately in a desiccator overnight before attempting any further analysis. The PXRD of the yellow crystals showed a more amorphous structure that appeared to be a mixture of cerium oxides (Figure 99).

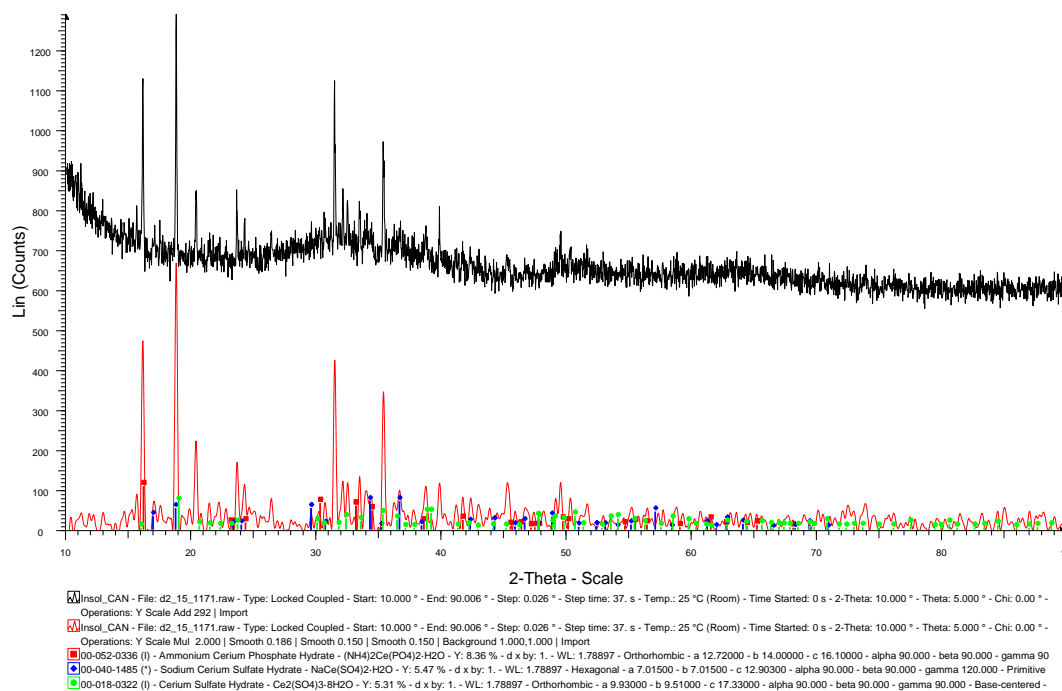


Figure 99 – PXRD pattern of the insoluble yellow crystals from the Old CAN container

The water soluble orange crystals on the other hand gave a good diffraction pattern that indicated the presence of a single compound. This pattern did not match any of the powder patterns in the JCPDS database for any ceric ammonium nitrate compound – even with different hydration or varying the oxides of CAN as shown in Figure 100.

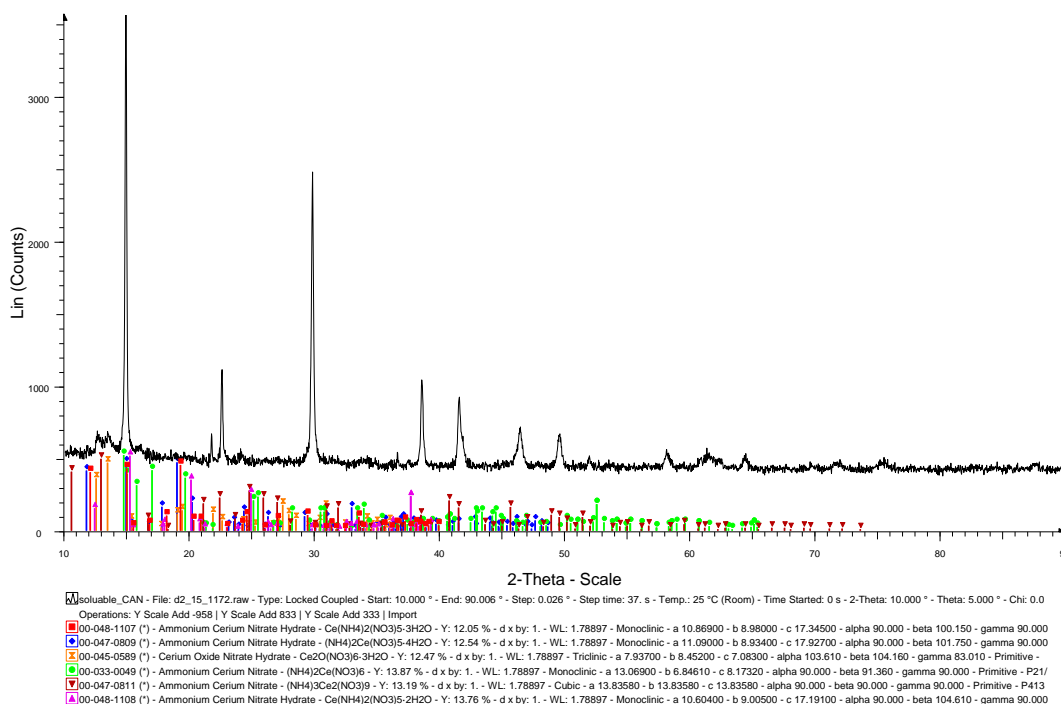


Figure 100 – PXR D pattern of the orange crystals from the old CAN compared to the CAN (and CAN variation) patterns from the PXR D database

Thankfully Dr Miller expanded the search of the database to include any cerium based compounds and an exact match was found. Figure 101 shows the PXR D pattern for the water soluble orange crystals compared with the PXR D pattern of ammonium cerium sulfate (or CAS). The spectra were almost identical. This meant that the catalyst in the old CAN container which was responsible for the ring closure reaction that resulted in xanthenes and diones was in fact CAS not CAN. Considering that the physical properties of CAN and CAS are very similar, and that CAS is hardly ever used in organic synthesis while the use of CAN is common practice, it is easy to see how the container was mislabelled. Figure 102 shows the distinct physical similarity between the water soluble orange crystals (which is CAS), commercially obtained CAS and recrystallized CAN. The commercially obtained CAN appears as a darker orange, however is still not very different from the orange crystals of CAS analysed.

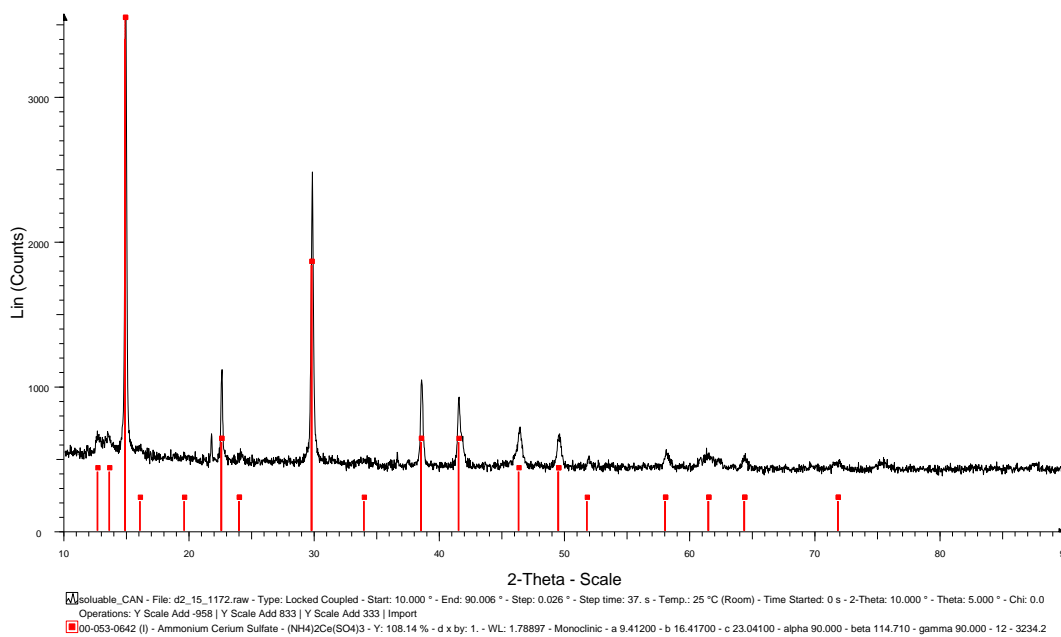


Figure 101 – PXRD pattern of the orange crystals from the old CAN and the comparison to ammonium cerium sulfate from the database superimposed in red



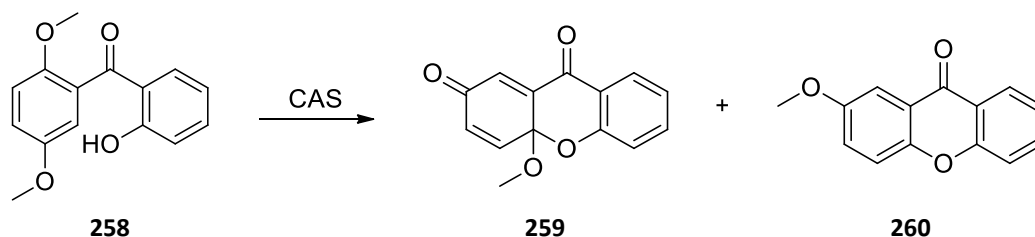
Figure 102 – Ceric ammonium sulfate, the water soluble portion of the 'Old CAN', recrystallized CAN and ceric ammonium nitrate obtained from Sigma-Aldrich (left to right) showing the distinct similarities in physical properties of CAS and recrystallized CAN.

5.4. When life gives you CAS

This surprising turn of events sparked new interest in the novel xanthone forming reaction that was developed in our labs. The first step going forward was to confirm that the results published by our group in the *Journal of Organic Chemistry* were in fact correct, just with a change in reagent (and hence catalyst ratio). Johnson reported the addition of 5 equivalents of 'CAN' to the reactions, which when recalculated this was found to be 4.3 equivalents of CAS. The synthesis (Scheme 89) was repeated with known amounts of CAS. Additionally we decided to change the reaction conditions to fully understand the effects of the different components in the reaction. When the reaction was performed with 4 equivalents of CAS in an acetonitrile/water/chloroform solution at room temperature both dione **259** and xanthone **260** were isolated after column chromatography – after repeating this reaction in triplicate it was found that dione **259** formed in an average yield of 30 % and **260** in an average yield of 45 %. This ratio was significantly different than the ratio obtained by Johnson, however since the reaction showed a similar product ratio every time it was repeated, we deemed these results reliable. It was found that under these conditions, at least 3 equivalents of CAS was required for the reaction to go to completion. When the chloroform was not included in the solvent mixture the reaction went to completion, however the two products were isolated in very low yields even when performed under reflux conditions. Changing the solvent system to a methanol/water solution resulted in the exclusive formation of xanthone **260** in low to average yields, depending on the temperature at which the reaction was performed. These results – along with the corrected results previously obtained – are detailed in

Table 9. The reaction was also performed in a chloroform/water solvent system and it was found that despite the formation of some of **259** (determined by TLC) the reaction did not go to completion regardless of how much CAS was added to the reaction or the temperature at which the reaction was performed.

Results and Discussion



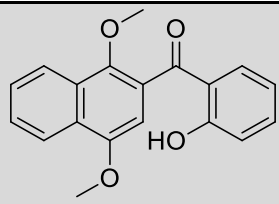
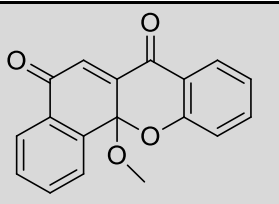
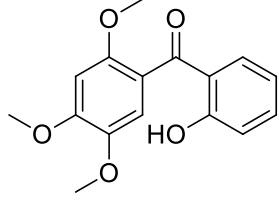
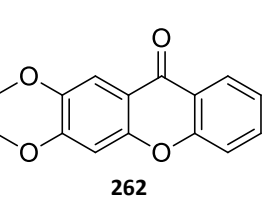
Scheme 89 – CAS mediated oxidation of 258

Table 9 – Results from the CAS mediated cyclization of 258 as well as the corrected results obtained previously

Author	Catalyst	Reaction Conditions	Yield 259	Yield 260
Johnson ¹⁹¹	CAS (4.3 eq)	MeCN/H ₂ O/CHCl ₃ , r.t., overnight	15 %	74 %
Dam	CAS (4.3 eq)	MeCN/H ₂ O/CHCl ₃ , r.t., overnight	44 %	32 %
Dam	CAN (5 eq)	MeOH/H ₂ O, r.t., 10 min	16 %	0
Dam	CAS (5 eq)	MeCN/H ₂ O, r.t., overnight	32 %	10 %
Dam	CAS (4 eq)	MeCN/H ₂ O/CHCl ₃ , r.t., overnight	Ave = 45 %	Ave = 30 %
Dam	CAS (3 eq)	MeCN/H ₂ O, r.t., overnight	8 %	21 %
Dam	CAS (2 eq)	MeOH/H ₂ O, reflux, 1 hour		54 %
Dam	CAS (5 eq)	MeOH/H ₂ O, reflux, 1 hour		31 %
Dam	CAS (5 eq)	MeCN/H ₂ O, reflux, 1 hour		20 %

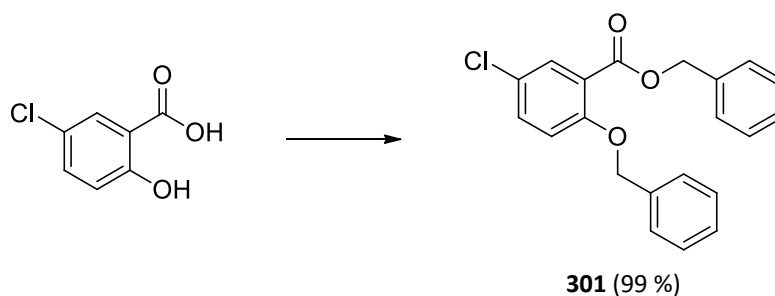
Excited by these results we determined that the optimal reaction conditions were 4 equivalents of CAS in an acetonitrile/water/chloroform solvent system combined in a 4:2:1 ratio, stirring at room temperature for 18 hours. Based on these results, we repeated the reaction on the other substrates reported in the *JOC* paper using these conditions and the results are shown in Table 10. These results matched well with what was reported in the *JOC* note.¹⁹²

Table 10 – CAS reaction performed on benzophenones previously reacted with CAN

Starting Benzophenone	Product	Johnson Yield ¹⁹¹	Product Yield
 <p style="text-align: center;">253</p>	 <p style="text-align: center;">257</p>	72 %	81 %
 <p style="text-align: center;">261</p>	 <p style="text-align: center;">262</p>	91 %	70 %

5.4.1. Repetition of the chlorine-containing reactions performed by Johnson using CAS

Realising that we needed to correct the *JOC* note, the rest of the reactions on all the substrate precursors needed to be repeated to ensure that the correct products were obtained in the yields reported in the *JOC* paper. Given that the synthesis was reported in detail by Johnson, the reaction schemes will only briefly be discussed. Commercially available 5-chlorosalicylic acid was successfully *O*-benzylated to obtain **301** as shown in Scheme 90.

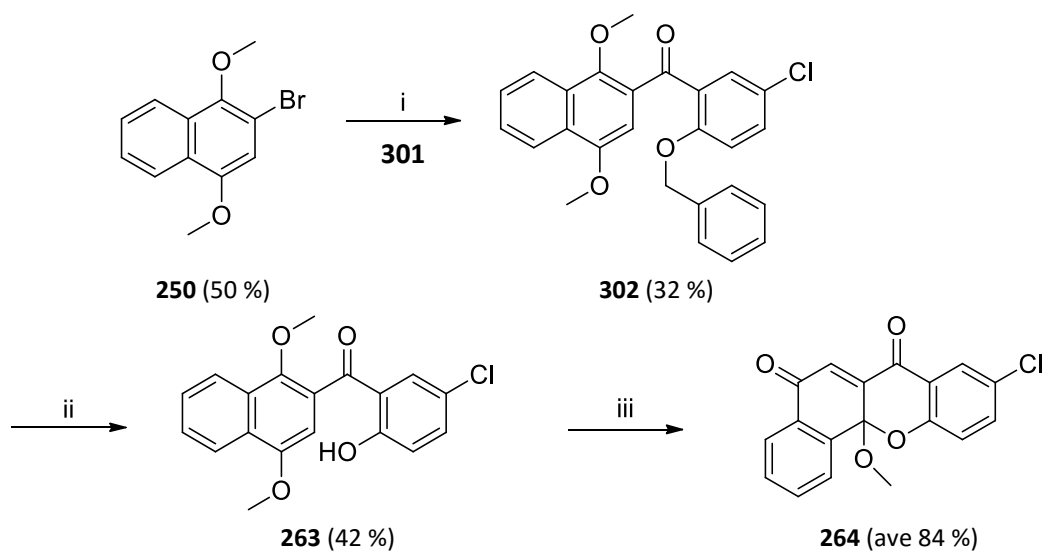


Reaction conditions: Benzyl bromide (2.1 eq), K_2CO_3 (3 eq), acetone, reflux, 18 h.

Scheme 90 – Benzyl protection of 5-chlorosalicylic acid

5.4.1.1. The chlorine-containing dimethoxynaphthalene series

As before, **250** was lithiated using *n*-BuLi and reacted with the benzyl protected salicylic acid **301** to generate benzophenone **302** (Scheme 91). Benzophenone **302** was significantly insoluble in methanol and so the debenzylation reaction needed to be performed in ethyl acetate. The reaction needed to be closely monitored to make sure that the reaction was stopped before the chlorine atom was reduced after the removal of the benzyl group (accounting for the relatively low yielding reaction). The debenzylated compound **263** was then exposed to CAS resulting in the formation of dione **264** in a high yield. The spectroscopic data obtained for these compounds concurred with the data reported by Johnson.¹⁹¹

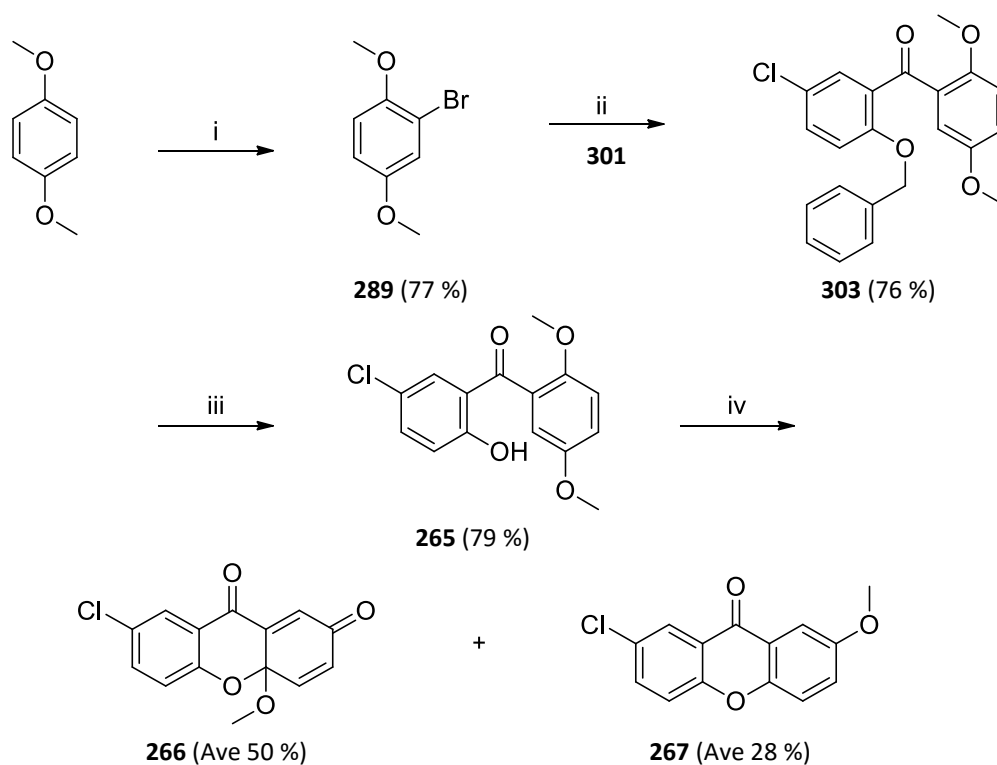


Reaction conditions: i) *n*-BuLi (1.28 M, 1 eq), **301** (0.9 eq), THF, -78 °C, 2 h; ii) H₂, 5 % Pd/C (10 mass %), EtOAc, rt, 1 h; iii) CAS (4 eq), MeCN/H₂O/CHCl₃, rt, 18 h.

Scheme 91 – Synthesis of dione 264

5.4.1.2. The chlorine-containing 1,4-dimethoxybenzene series

Following the synthesis outlined in Scheme 92, benzophenone **303** was isolated in a 76 % yield. Debenzylation of **303** under a hydrogen atmosphere was successful to afford **265**. The reaction had to be closely monitored to prevent the removal of the chlorine substituent as well under the reductive conditions. Finally, the CAS reaction resulted in the formation of both dione **266** and xanthone **267** from benzophenone **265**. Repetition of the reaction in triplicate resulted in the formation of dione **266** in an average yield of 50 % and 28 % xanthone **267**. This too is markedly different from the ratio reported by Johnson (17 % **266** and 63 % **267**).¹⁹¹

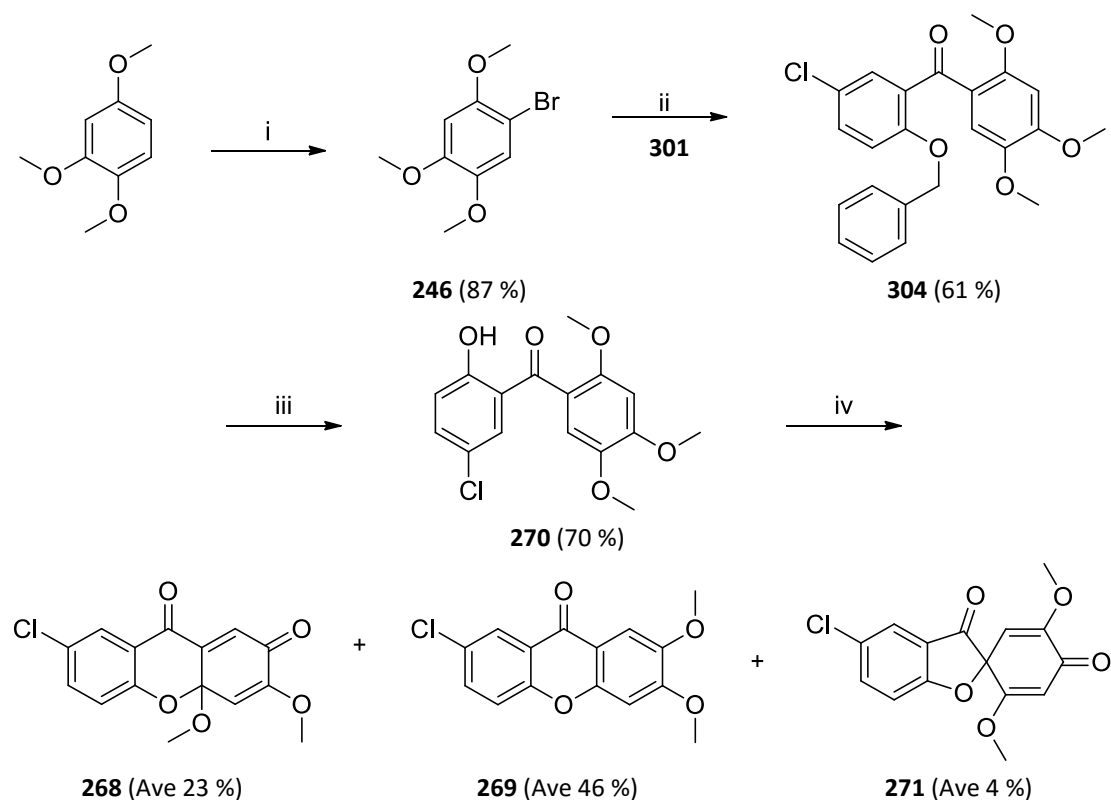


Reaction conditions: i) NBS (1 eq), CHCl_3 , reflux, 3 d; ii) *n*-BuLi (1.28 M, 1 eq), **301** (0.9 eq), THF, $-78\text{ }^\circ\text{C}$, 2 h; iii) 5% Pd/C (10 mass %), MeOH, rt, 4 h; iv) CAS (4 eq), MeCN/ H_2O / CHCl_3 , rt, 18 h.

Scheme 92 – Synthetic route utilized in the synthesis of dione 266 and xanthone 267

5.4.1.3. The chlorine-containing trimethoxybenzene series

The synthetic route as outlined in Scheme 93 was successful. The lithiation of **246** and subsequent reaction with **301** resulted in the furnishing of **304** in a reasonable yield. Removal of the benzyl group resulted in **270** being isolated in a good yield. This reaction occurred fast and was complete after an hour with dechlorinated compound **261** isolated also. The CAS mediated oxidation of **270** resulted in the visualization of three new spots on the TLC plate. These products were isolated using flash column chromatography and found to be dione **268**, xanthone **269** and spirofuran **271**. This reaction was repeated in triplicate and the yields reported are reported as average yields. Again, the ratio of the products collected was somewhat different to that obtained by Johnson (**268** reported yield 28 %, **269** 21 % and **271** 9 %).¹⁹¹



Reaction conditions: i) NBS (1 eq), DCM, rt, 20 min; ii) *n*-BuLi (1.2 M, 1 eq), **301** (0.9 eq), THF, -78 °C, 2 h; iii) 5 % Pd/C (10 mass %), MeOH, rt, 2 h; iv) CAS (4 eq), MeCN/H₂O, rt, 18 h.

Scheme 93 – Synthetic route employed in the synthesis of the chloro-trimethoxy series

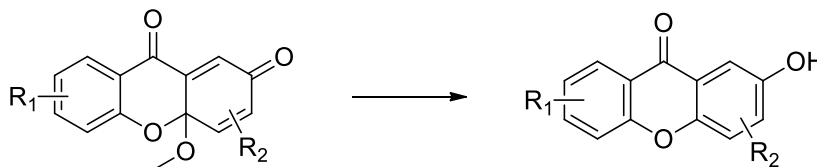
Overall, these reactions show that the outcomes published in the *JOC* Note were indeed true. Given that the oxidant that Johnson used contained a mixture of cerium oxides in addition to CAS, this could explain the difference in ratios between the products obtained in this project and what was previously determined. It also confirms the PXRD findings that the initial catalyst used was CAS and not CAN.

5.4.2. Conversion of diones to xanthenes

Amongst the results reported by Omolo, he noted that diones could successfully be converted to xanthenes using microwave irradiation. Using this procedure, Omolo obtained xanthone **275** (Scheme 74) from dione **259**.¹⁹³ When the same reaction was repeated by the author no conversion was found to occur and only starting material (**259**) was recovered from the reaction. Increasing the temperature, reaction time or wattage applied to the reaction did not have any influence on the reaction.

Hoping to find another method for the conversion of diones to the naturally occurring xanthenes, we considered that the structure of the diones contained a quinone acetal functionality. Since

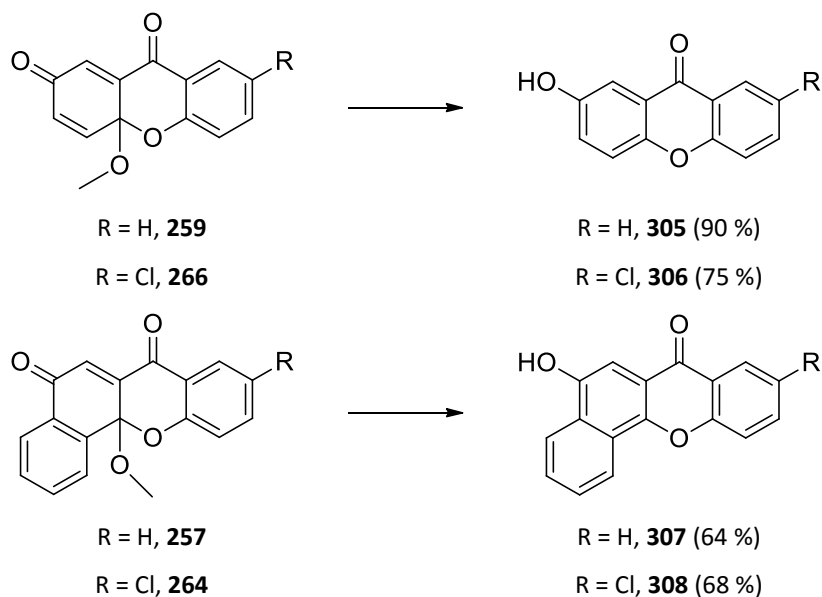
sodium dithionite is used to reduce quinones to their aromatic-hydroquinone equivalents,¹²⁸ we postulated that in applying similar conditions to diones, the dione could be reduced to its hydroxy-aromatic equivalent, as shown in Scheme 94.



Reaction conditions: $\text{Na}_2\text{S}_2\text{O}_4$ (3 eq), THF/ H_2O , rt, 10 min.

Scheme 94 – Conversion of diones to xanthones using sodium dithionite

This reaction was found to be remarkably successful under the given conditions and diones **257**, **259**, **264** and **266** were successfully converted to novel hydroxy-containing xanthones (**305** to **308**) shown in Scheme 95. As soon as the sodium dithionite was added to the rapidly stirring yellow dione/THF/water mixture the solution turned bright green, when the solution returned to a yellow colour (or a light yellow precipitate formed) the reaction was deemed over. These reactions were performed on a small scale (under 100 mg) so the addition of a phase transfer catalyst (such as TBAI) was not beneficial, however on a larger scale it may be advisable to add TBAI to the reaction. Purification of the reaction mixture was performed without the need for column chromatography as the phenolic-xanthone could be deprotonated under strongly basic conditions during the work up (making it soluble in the aqueous layer) while any unreacted starting material remained in the organic layer. After adjusting the pH of the aqueous layer to near neutral with solid ammonium chloride, the xanthone precipitated out of solution and was filtered off, washed with water and dried in a desiccator. Characterisation of these compounds showed significant shifting of the signals in the ^1H NMR spectrum in the aromatic region in comparison to the dione precursors. The xanthones generated were also significantly less soluble than the dione precursors and hence NMR samples had to be made up in d_4 -MeOD and d -DMSO preventing the O-H signal from being observed in the ^1H NMR spectrum. Moreover, only a single carbonyl carbon was observed for each of the compounds (where the starting diones contained two) in the ^{13}C NMR spectrum along with a new aromatic C–O type signal around 150 ppm. The IR spectra for these compounds revealed the tell-tale O–H stretches between $3300\text{--}3400\text{ cm}^{-1}$ confirming the presence of a phenol in the xanthones.



Reaction conditions: $\text{Na}_2\text{S}_2\text{O}_4$ (3 eq), THF/ H_2O , rt, 10 min.

Scheme 95 – Conversion of dione compounds to hydroxy-containing xanthenes

The successful development of this method meant that regardless of whether diones or xanthenes were obtained from the reaction or the ratio they were obtained in, xanthenes could still be generated in good yields – albeit with a hydroxy substituent rather than the methoxy substituent present in previous xanthenes.

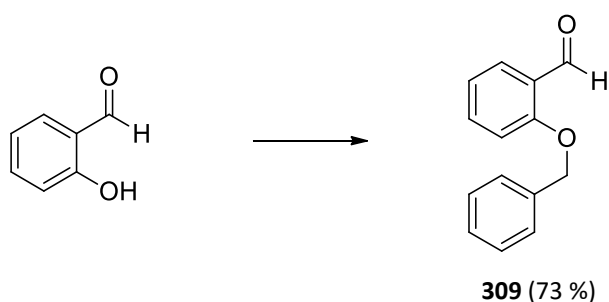
5.5. Investigation of the mechanism of the CAS-mediated ring closure reactions

Having optimized the reaction conditions for the CAS-mediated oxidation reaction, the next focus was to probe the mechanism of the reaction. Johnson *et al.* proposed a mechanism for the reaction (Scheme 73) which relied on the stabilization effects from the dimethoxy substituents arranged *para* to each other to stabilize the radical intermediate **273**. This radical intermediate could further be resonance stabilized as previously shown in Scheme 78.

To investigate this, we needed to synthesize suitable benzophenones containing methoxy substituents in a variety of positions. We were also interested in the effects of the second methoxy substituent, so a benzophenone with only a single methoxy substituent was also deemed necessary. In this section the synthesis of the various benzophenone precursor substrates will be discussed individually and then the results from subjecting these benzophenones to CAS discussed together at the end of the section.

5.5.1. Synthesis of (2-hydroxyphenyl)(2-methoxyphenyl)methanone **312**

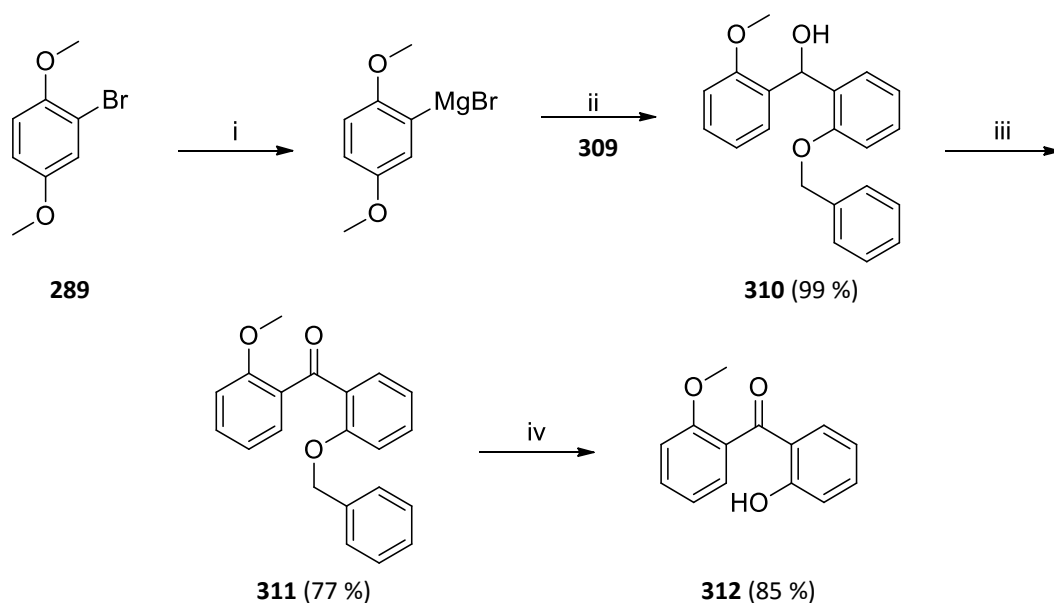
As detailed in Scheme 96, *O*-benzyl protection of salicylaldehyde was performed in the same manner as that for the salicylic acids however with the addition of only 1.1 equivalents of benzyl bromide resulting in aldehyde **309**.



Reaction conditions: Benzyl bromide (1.1 eq), K_2CO_3 (2 eq), acetone, reflux, 18 h.

Scheme 96 – Benzyl protection of salicylaldehyde

Exposure of the Grignard reagent of **289** (Scheme 97) to **309** afforded alcohol **310**. PCC oxidation of **310** resulted in benzophenone **311**, which after debenzylation furnished the desired substrate **312**.



Reaction conditions: i) Mg (eq), THF, rt, 1 h; ii) **309** (eq), THF, 0 °C, 2 h; iii) PCC (eq), silica, DCM, rt, 1 h; iv) 5 % Pd/C (10 mass %), MeOH, rt, 18 h.

Scheme 97 – Synthetic scheme employed to synthesize substituted benzophenone **312**

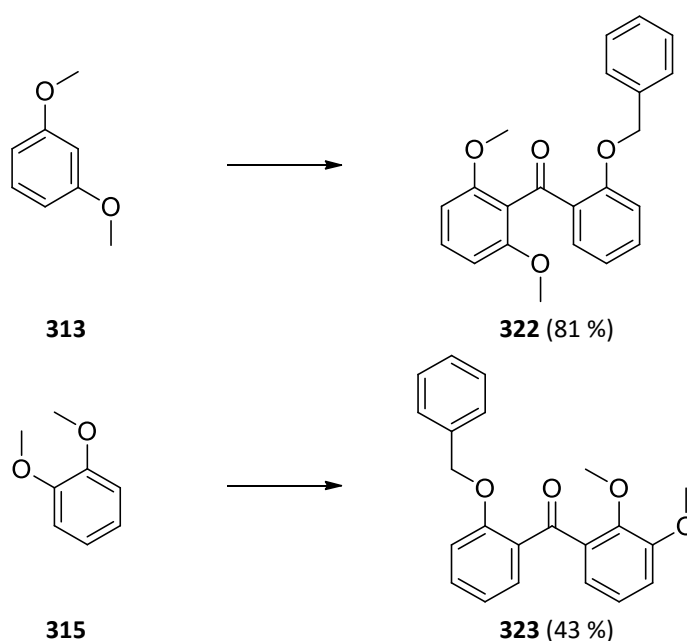
5.5.2. Synthesis of dimethoxybenzophenone substrates

5.5.1. Bromination of dimethoxybenzenes **313**, **315** and **317**

The first step in attempting to generate a variety of di- and tri-methoxy-substituted benzophenones was the bromination of dimethylresorcinol (**313**), veratrole (**315**) and 1,3,5-trimethoxybenzene (**317**) as shown in Scheme 98. The brominations occurred exclusively to afford the monobrominated benzenes **314** and **316**. For benzene **314**, the aromatic region in the ^1H NMR spectrum contained three signals – a doublet at 7.73 ppm with a coupling constant (J) of 8.7 Hz, a doublet ($J = 2.7$ Hz) at 6.46 ppm and a doublet of doublets ($J = 8.7$ and 2.7 Hz). These signals were indicative of the structure of **314**. Similar splitting patterns were observed in the ^1H NMR spectrum of **316**; a doublet of doublets ($J = 8.5$ and 2.3 Hz) at 6.99 ppm and two doublets at 6.94 ppm ($J = 2.3$ Hz) and 6.68 ppm ($J = 8.5$ Hz). From the coupling constants, both *meta* and *ortho* coupling were indicated, confirming the structure of **316**.

5.5.3. Directed Ortho-metalation Reactions

In order to access more benzophenones that would contain methoxy substituents on the benzene ring we considered using directed-orthometalation reactions (or DOM reactions) using dimethoxyresorcinol (**313**) and veratrole (**315**) as starting materials. The same lithiation procedure (using *n*-BuLi and the same reaction conditions) as previously mentioned was used, except with lithiation occurring on the benzene rings without being positioned by the presence of the bromine atom. The reactions and resulting products are outlined in Scheme 99. The preferential position for the DOM lithiation was between the two methoxy substituents on **313**, and hence **322** was furnished as a peach coloured solid in a good yield. The tell-tale symmetry of this compound was seen on the ^1H NMR spectrum; there was a single methoxy signal integrating for 6 protons at 3.55 ppm and a distinct doublet integrating for 2 protons at 6.42 ppm. This symmetry was also seen in the ^{13}C NMR spectrum. The structure of **323** was less easily determined due to the number of aromatic signals present in the ^1H NMR spectrum. This spectrum did look significantly different to that of **320**, suggesting that the proposed structure was correct.



Reaction conditions: *n*-BuLi (1 eq), ester (0.9 eq), THF, -78 °C, 90 min.

Scheme 99 – Products from DOM reactions with substituted benzenes

5.5.4. Debenzylation of the protected benzophenones

Using the 5 % Pd/C catalysed debenzylation reactions under a hydrogen atmosphere as previously outlined, the five benzophenones **324** - **328** were successfully synthesized as shown in Figure 104.

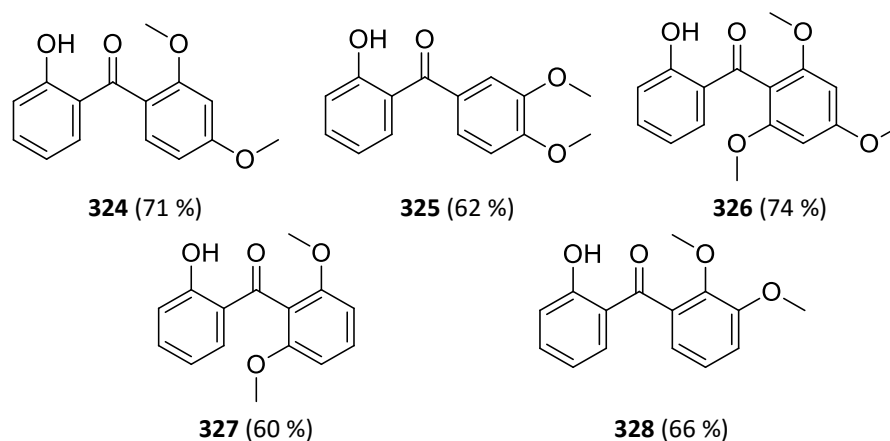
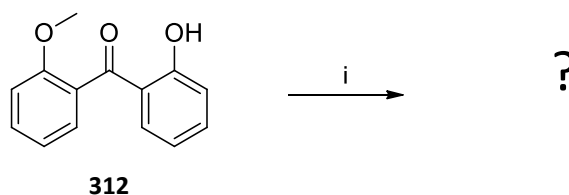


Figure 104 – Substituted benzophenones generated after debenylation

5.5.3. Subjection of substituted benzophenones to CAS

Having synthesized a series of substituted benzophenones, we were then in a position to expose each one to CAS under the optimized reaction conditions. Since we were exploring the scope of this novel reaction, the reactions were closely monitored by TLC, and any new spots that were identified were isolated and where possible characterised. Each reaction was repeated in triplicate (or more) to ensure that any result obtained was reproducible.

When monomethoxybenzophenone **312** (Scheme 100) was exposed to CAS no starting material was noted. Unfortunately no compound could be successfully isolated from the reaction. This result tentatively suggested that the presence of the second methoxy substituent on the anisole benzene was necessary for the cyclization to occur.

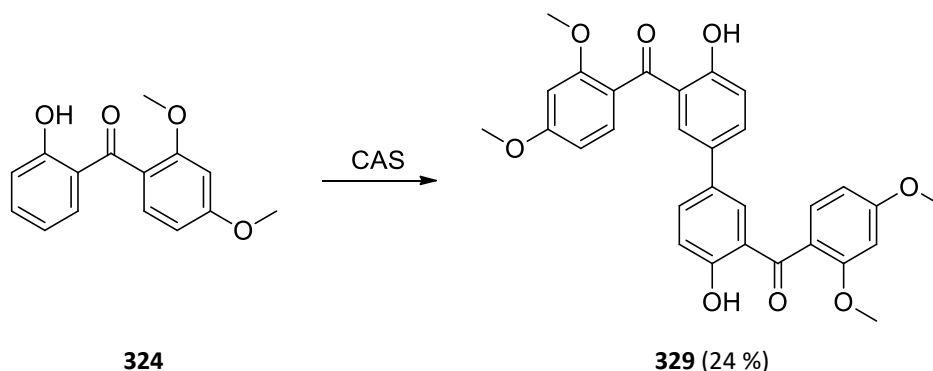


Reaction conditions: CAS (2-4 eq), MeCN/H₂O/CHCl₃, rt, 18 hours.

Scheme 100 – Exposure of **312** to CAS

The next step was to conduct the CAS-mediated reactions on the dimethoxy-benzophenones **324** - **328**. An interesting result was obtained when **324** was exposed to CAS. Multiple spots were observed on the TLC plate, however only a single compound isolated could be characterised. We were surprised to find that in the ¹H NMR spectrum of this compound the phenolic signal remained present at 12.15 ppm along with both methoxy signals at 3.91 and 3.61 ppm. Additionally, only six aromatic signals were present where the starting material (**312**) contained

seven. From the NMR spectral data it was determined that substitution had occurred *para* to the phenol. One possible explanation for this result was that the benzophenone **324** had dimerized as shown in Scheme 101. The same product was isolated with each repetition of the reaction, and this was the major product isolated from the reaction – despite the relatively low yield.



Reaction conditions: CAS (2-4 eq), MeCN/H₂O/CHCl₃, rt, 18 hours.

Scheme 101 – Proposed dimerization of 324 when exposed to CAS

High resolution mass spectroscopy agreed with the dimer structure. Crystals suitable for SCXRD were grown from diethyl ether, and the structure of **329** confirmed, as shown in Figure 105.

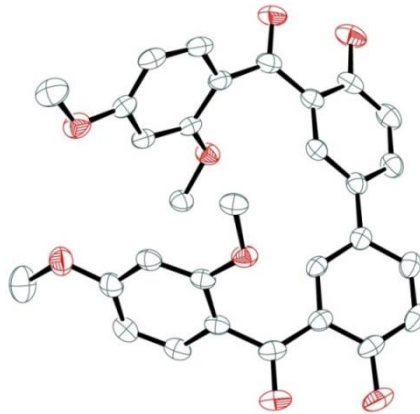
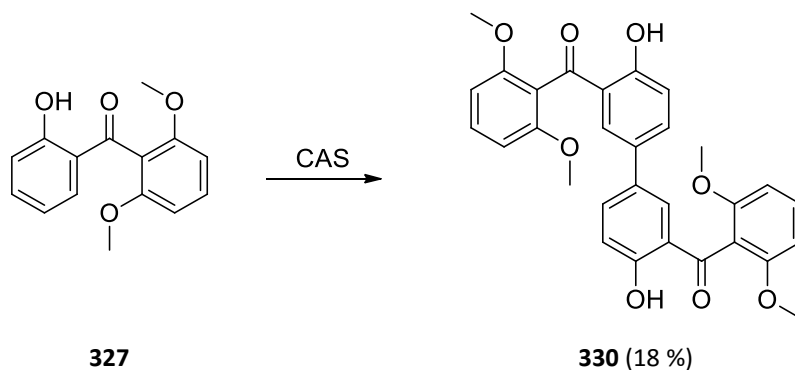


Figure 105 – The asymmetric unit of 329 (hydrogen atoms are omitted for clarity)

Of course we could not rule out the possibility that other dimeric products could be formed in the reaction, however we were unable to isolate and characterise any other products. This reaction does show that CAS has the potential to form biaryl C–C bonds through an oxidative process. A report by Chwala found that when selected phenols (with at least one methyl group positioned *ortho* to the hydroxyl group) were exposed to CAN in acetic acid and hydrogen peroxide, similar dimer-type compounds were isolated in minor quantities. Their particular work

focused on the synthesis of phenol derivatives using CAN, however these unexpected dimer products were noted – the new biaryl bond forming in the *para*-position to the hydroxyl group.¹⁹⁸

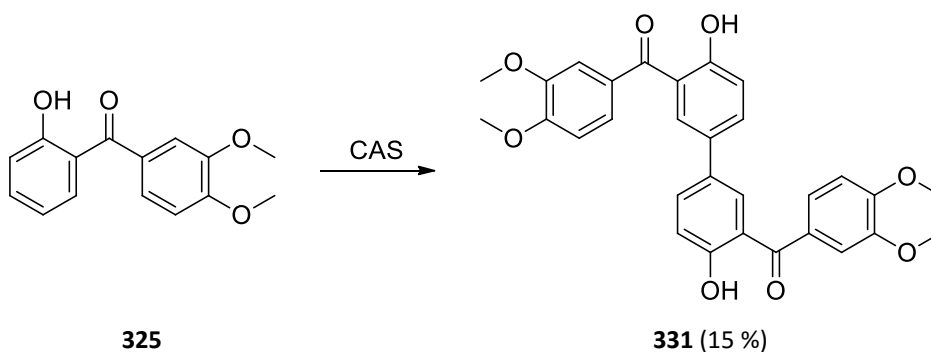
When benzophenone **327** was subjected to the same conditions as **324** a similar observation was made as shown in Scheme 102. The structure of **330** was elucidated from the ¹H and ¹³C NMR spectra (along with supporting 2D experiments) which again suggested that substitution occurred at a position that was *para* to the phenol substituent.



Reaction conditions: CAS (2-4 eq), MeCN/H₂O/CHCl₃, rt, 18 hours.

Scheme 102 – CAS-mediated oxidation of benzophenone 327

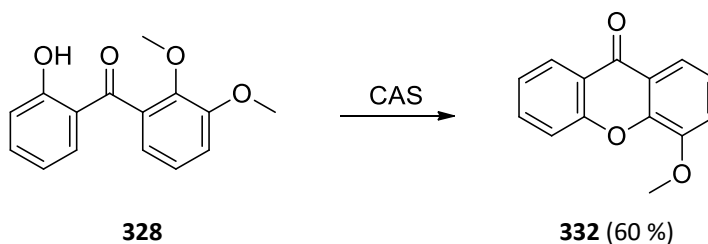
Interestingly, exposing compound **325** to CAS also furnished the dimer **331** (Scheme 103). The structure of **331** was determined using NMR spectroscopy as before, as well as by high resolution ESI mass spectroscopy. This result suggests that for the CAS-mediated ring closure reaction to occur, a methoxy substituent in an *ortho*-position to the ketone is essential.



Reaction conditions: CAS (2-4 eq), MeCN/H₂O/CHCl₃, rt, 18 hours.

Scheme 103 – CAS-mediated oxidation of benzophenone 325

Benzophenone **328** contained two methoxy substituents *ortho* to each other. When **328** was subjected to CAS oxidation (Scheme 104), xanthone **332** was formed in a 60 % yield.



Reaction conditions: CAS (4 eq), MeCN/H₂O/CHCl₃, rt, 18 hours.

Scheme 104 – CAS mediated oxidation of benzophenone 328

Characterisation of the compound showed the presence of only a single methoxy signal at 4.04 ppm and the absence of the phenol signal in the ¹H NMR spectrum. The ¹³C NMR spectrum further supported the ring closed structure. Conclusive proof was obtained from SCXRD, where suitable crystals for analysis were grown from methanol and the results are shown in Figure 106.

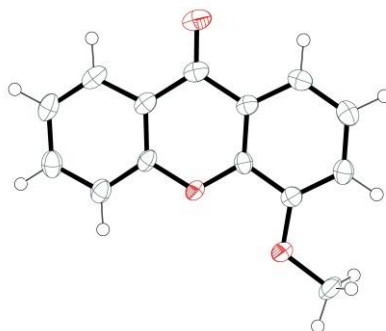
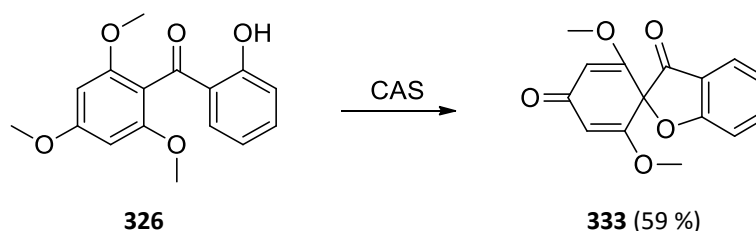


Figure 106 – The asymmetric unit of 332

Finally, the trimethoxybenzophenone **326** was subjected to CAS. This compound was of interest as the compound has a methoxy substituent *ortho* to the ketone as well as two additional methoxy substituents that could theoretically be able to stabilize the radical intermediate. As shown in Scheme 105, spirofuran **333** was isolated in a 50 % yield when **326** was exposed to CAS.



Reaction conditions: CAS (2-4 eq), MeCN/H₂O/CHCl₃, rt, 18 hours.

Scheme 105 – CAS mediated formation of spirofuran 333

The structure of **333** was determined by NMR spectroscopy. From the ^1H NMR spectrum it could be seen that the hydroxyl signal as well as one methoxy signal was no longer present. The presence of four aromatic ring protons showed that the phenol side of the benzophenone remained intact. Two more singlet signals were present – one at 5.64 integrating for 2H and one at 3.64 integrating for 6H. This suggested that there was symmetry in the molecule and that the aromaticity of the second aromatic ring had been disrupted. Additionally from the ^{13}C NMR spectrum two carbonyl signals were evident in the product (at 194.4 and 186.8 ppm), but most distinctively a quaternary carbon at 84.3 ppm (determined along with HSQC). The presence of the two carbonyls and the quaternary carbon around 80 ppm was a feature characteristic to spirofurans and hence structure **333** was proposed. Crystals suitable for SCXRD analysis were grown and after analysis, the structure of **333** confirmed as shown in Figure 107.

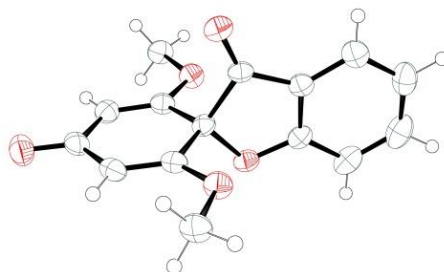
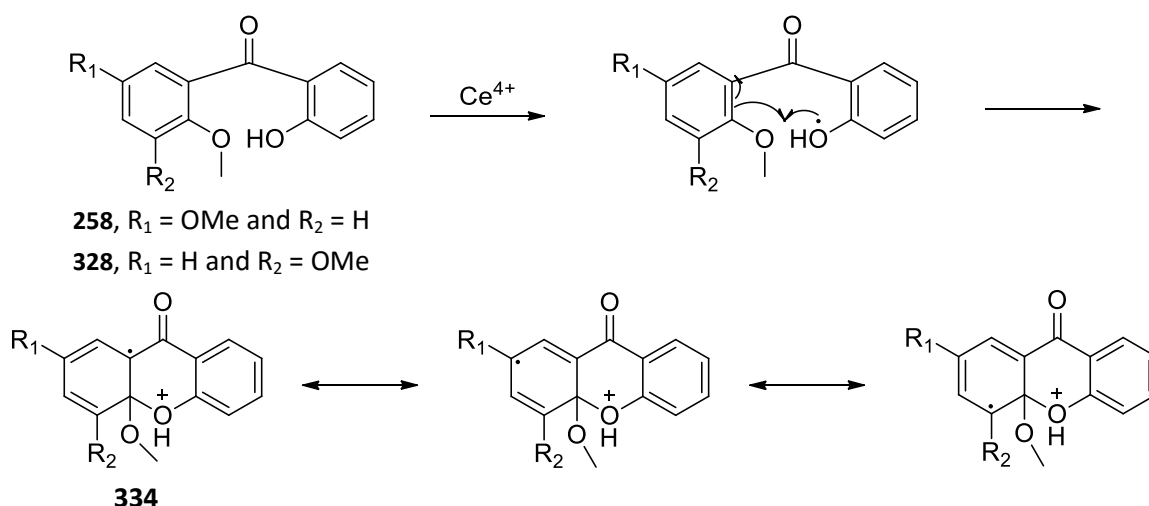


Figure 107 – The asymmetric unit of **333**

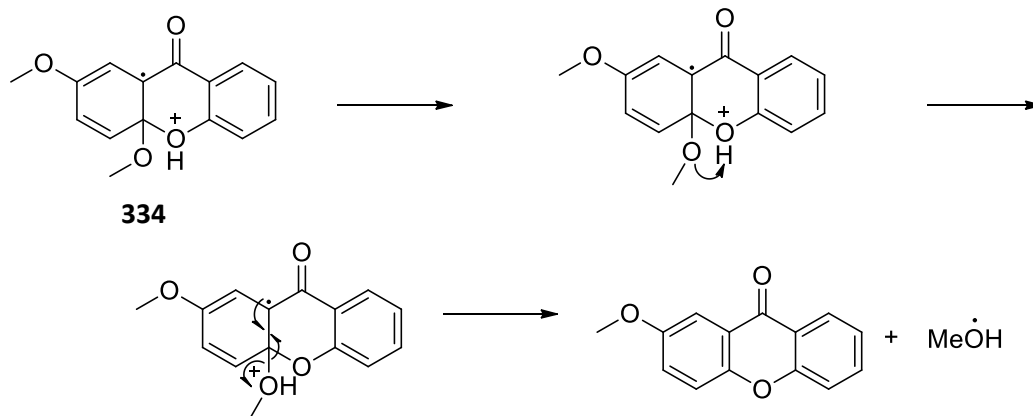
5.5.4. A deeper look at the proposed mechanisms

The *JOC* paper outlined general proposed mechanism (Scheme 73). Using the results previously obtained as well as the new results outlined above a more detailed mechanism could be proposed. An important distinction that needed to be made was the site for the first oxidation – was the first radical generated on an aromatic ring or on one of the oxygen atoms (and if so which one)? Since it has been established that phenol's preferentially coordinate strongly to cerium atoms,^{176,177} it would be safe to assume this would also happen with these phenolic-containing benzophenones with the result of generating a radical on the phenol rather than elsewhere on the molecule. Depending on the nature of the other benzene ring several different pathways leading to the products would then be possible. For example as shown in Scheme 106, the phenol radical can add to the adjacent benzene ring which would generate radical **334** that would be stabilized by the methoxy substituents at positions R_1 and R_2 .



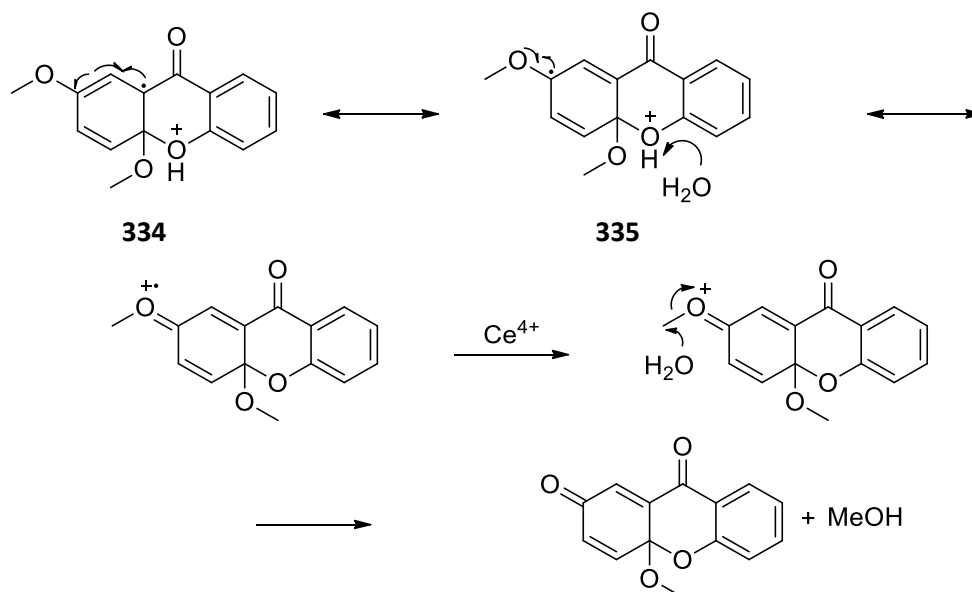
Scheme 106 – Radical generation on the phenol and how it is stabilized once addition has occurred

From the intermediate **334** shown in Scheme 106, both xanthenes and diones could then be generated. Xanthenes could be generated as shown in Scheme 107 where the driving force of rearomatization would force the elimination of a methanol radical which would be quenched as the reaction proceeds.



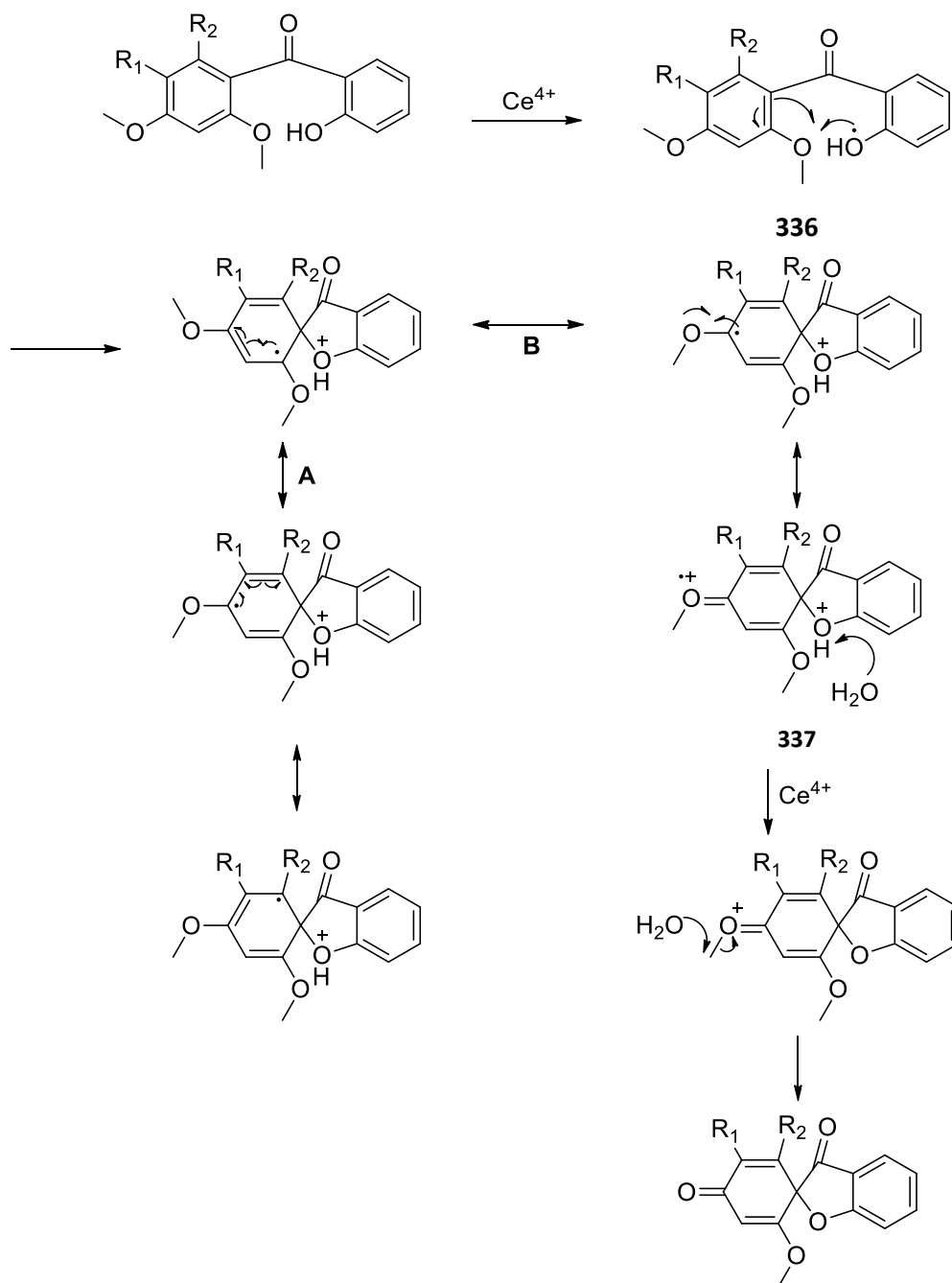
Scheme 107 – Proposed mechanism for the formation of xanthenes

The resonance stabilization of the radical intermediate **334** as shown in Scheme 106 could result in the formation of intermediate **335** (Scheme 108) which is further stabilized by the methoxy oxygen. A further oxidation at this position would facilitate the elimination of methanol generating the diones as are formed in some of the reactions and shown in Scheme 108.



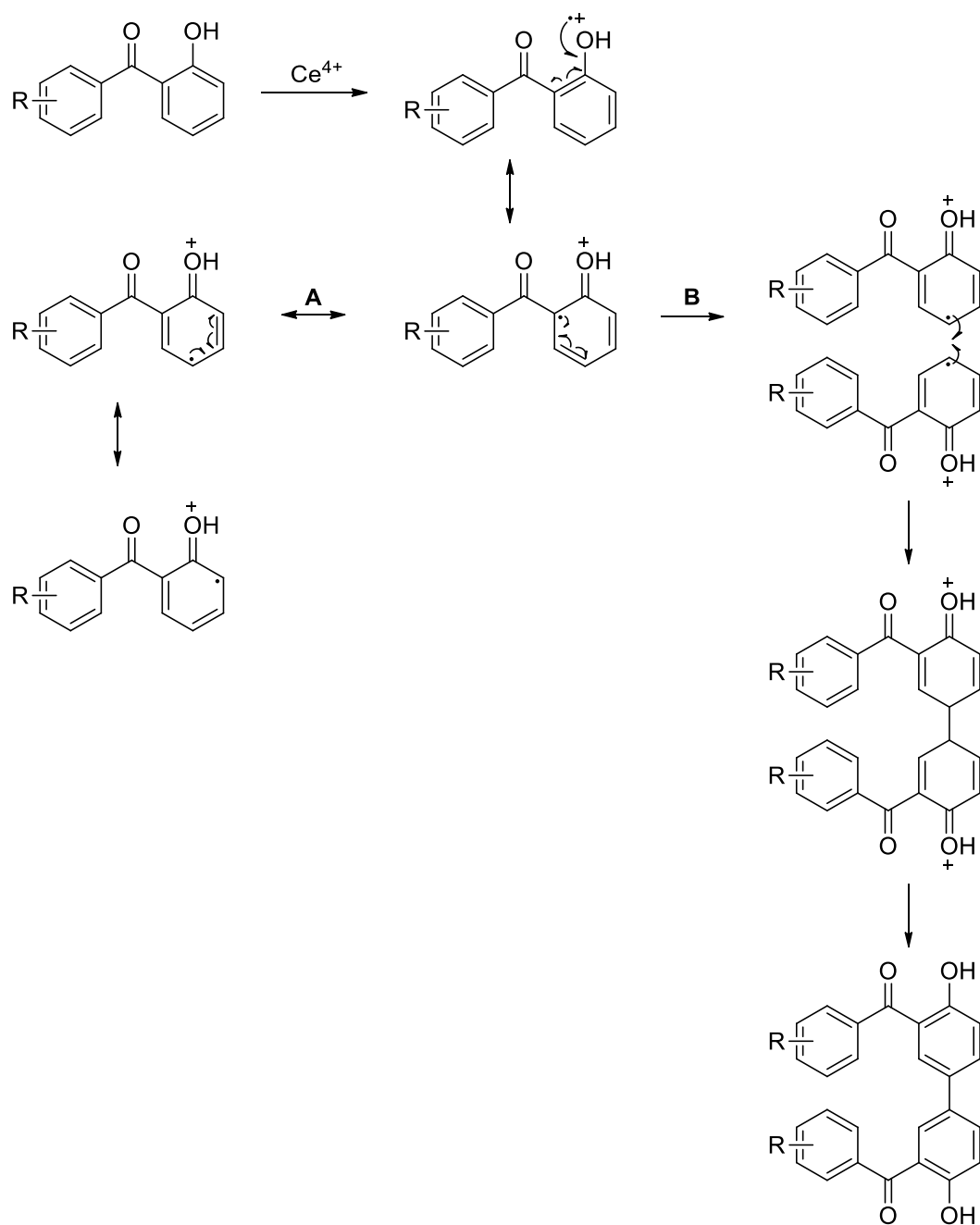
Scheme 108 – Proposed mechanism for the formation of diones

The phenolic radical addition to the benzene ring in Scheme 106 saw the addition of the phenol to the carbon attached to a methoxy substituent. Theoretically the phenol radical could add to the other side of the double bond of the benzene ring as shown in **336** (Scheme 109). In this scenario the methoxy substituent would stabilize the radical intermediate. This could be further stabilized as shown by pathway A (Scheme 109) especially where substituent R_2 is an electron donating substituent such as a methoxy group. Pathway B would also serve in stabilizing the radical intermediate however **337** could further be oxidized by the CAS, eliminating methanol to form the spirofuran product. It is interesting to note that spirofuran products were only isolated where at least 3 methoxy substituents (i.e. R_1 or $R_2 = \text{OMe}$) were present on the starting benzophenone. While benzophenone **324** would also fit this proposed mechanism no spirofuran product was isolated when exposed to CAS suggesting that for this particular mechanism to apply the stabilization through pathway A is crucial and that R_1 and/or R_2 needs to contain an electron donating groups.



Scheme 109 – Proposed mechanism for the formation of spirofurans

Finally the generation of the phenolic radical can also be used to explain the formation of the oxidative dimers **329**, **330** and **331**. In benzophenones where the radical intermediates in Scheme 106 to Scheme 109 were not stabilized the phenolic radical would be able to perform other reactions. Scheme 110 outlines the proposed mechanism for the formation of the novel dimers where the phenolic radical is stabilized as shown by pathway A, however two molecules with radicals in the *para* position to the phenol could combine as shown in pathway B. With the driving force of aromaticity, the molecule can rearrange to form the dimers that were isolated.



Scheme 110 – Proposed mechanism for the formation of dimers

Pathway A in Scheme 110 outlines that in the stabilization of the phenol radical there are several different positions at which the the radical monomers could combine. Depending on how these radicals combine different products are theoretically possible (Figure 108) however only the *para*-substituted dimers were isolated in this work.

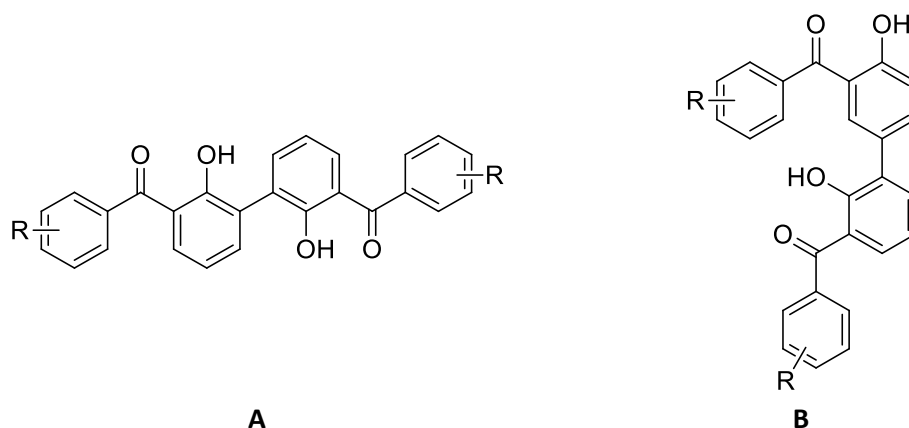


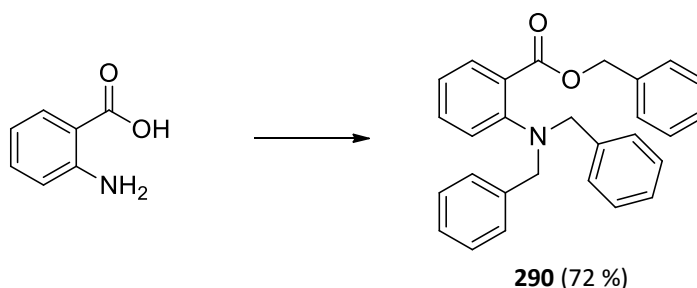
Figure 108 – Other theoretically possible dimers where A represents the coupling of two benzophenones at the *ortho* positions while B represents the coupling at the *para* position of one benzophenone and the *ortho* position of the other

These new proposed mechanisms differ from what was previously proposed, however the generation of a single phenolic radical performing different reactions depending on the electronics of the system far better explains the results the results detailed in this work than several seemingly isolated reactions as previously proposed.

5.6. Revisiting the acridone synthesis

The noticeable difference between CAN and CAS as a reagent for synthesis was one explanation for why the synthesis of acridone **298** was only successful once (when unknowingly CAS was used) and then never again (when CAN was used). Therefore we wished to attempt the synthesis with commercial CAS to confirm this result.

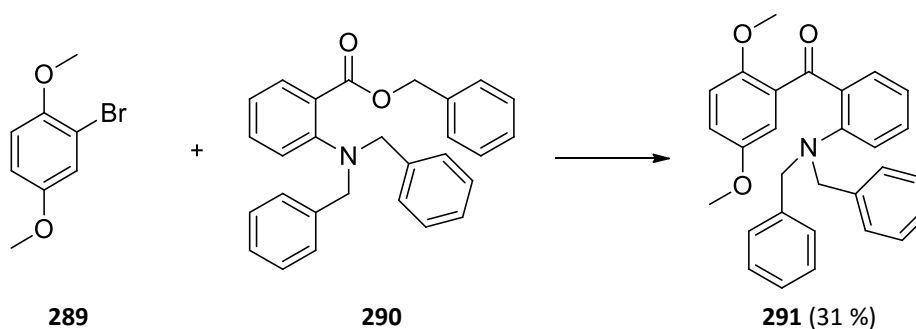
Revisiting the benzyl protection of anthranilic acid, a paper by González-Morales *et al.* reported that anthranilic acid could be protected in a similar manner as we had performed however in a 5:1 methanol:water ratio.¹⁹⁹ Using the González-Morales methodology anthranilic acid was successfully tri-benzyl protected to generate **290** in a 72 % yield (Scheme 111 with the new reaction conditions).



Reaction conditions: Benzyl bromide (3.1 eq), K_2CO_3 (3.8 eq), 5:1 MeOH:H₂O, reflux, 18 h.

Scheme 111 – Successful benzyl protection of anthranilic acid

Coupling of **290** with brominated compound **289** using *n*-BuLi (as shown in Scheme 112) resulted in benzophenone **291** in a very low yield of 31 %. Unfortunately subsequent attempts to remove the benzyl protection groups from the amine proved unsuccessful.



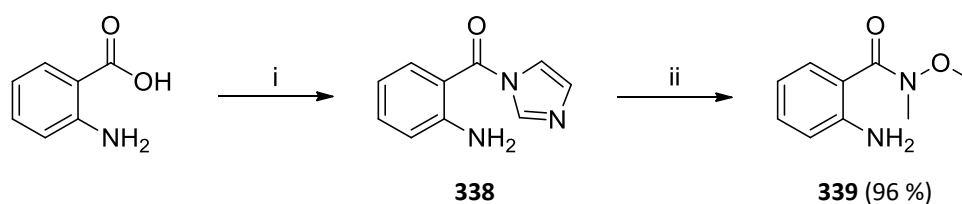
Reaction conditions: *n*-BuLi (1.6 M, 1 eq), THF, -78 °C, 2 h.

Scheme 112 – Lithiation reactions to generate amine-containing benzophenone 291

Having had trouble with forming the desired benzophenone we searched for a different method to construct the desired 2-aminobenzophenones. Frye *et al.* reported a one-pot procedure for the synthesis of a variety of substituted 2-aminobenzophenones using *n*-BuLi, substituted

bromobenzenes and unprotected Weinreb amides. They found that the addition of *n*-BuLi dropwise to a cold (-78 °C) rapidly stirring solution of the substituted bromobenzenes and Weinreb amides in THF resulted in the formation of 2-aminobenzophenones in average yields.²⁰⁰

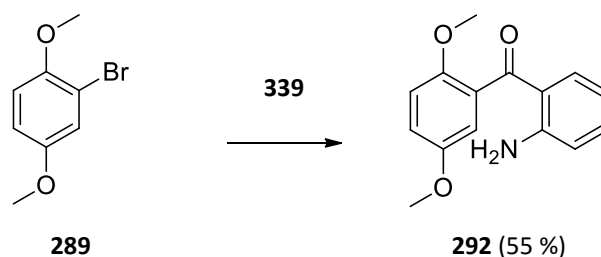
In order to apply the Frye methodology, we first needed to synthesize Weinreb amide **339**. This methodology had been well developed in our labs¹¹³ and involved the reaction of an acid with 1,1'-carbonyldiimidazole (CDI) followed by the addition of *N*-*O*-dimethylhydroxylamine hydrochloride to generate the Weinreb amide such as **339** illustrated in Scheme 113. While these reactions are typically performed in dichloromethane, the poor solubility of the CDI-anthranilic acid complex **338** prevented the addition of the hydroxylamine hydrochloride. It was found that the reaction could either be performed in dry dimethylformamide or in a dichloromethane solution with the addition of small quantities of dimethylformamide to ensure solubility at each stage of the reaction. The sole use of dimethylformamide allowed for complete solubility of the compound throughout the synthesis but it was difficult to remove during the work up. Performing the reaction in dichloromethane with additional dimethylformamide meant that each stage of the reaction needed to be monitored and additional dimethylformamide added if necessary to solubilize the reaction mixture. The brown oil resulting from the reaction was determined to be **339** by NMR spectroscopy.



Reaction conditions: i) CDI (1.2 eq), DMF, rt, 1 h; ii) *N*-*O*-dimethylhydroxylamine HCl (1.2 eq), rt, 18 h.

Scheme 113 – Synthesis of Weinreb amide 339

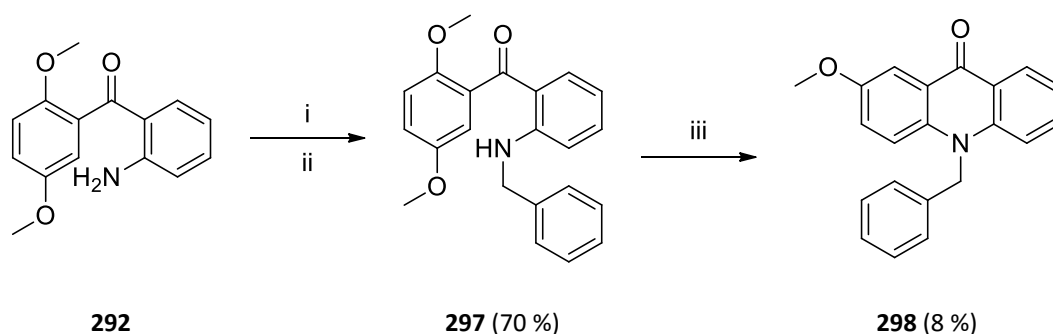
Following the Frye approach, bromo-dimethoxybenzene **289** (Scheme 114) and Weinreb amide **339** were condensed using *n*-BuLi, and 2-aminobenzophenone **292** was synthesized in a 55 % yield.



Reaction conditions: *n*-BuLi (2 eq), ester **339** (1 eq), THF, -78 °C, 90 min.

Scheme 114 – Synthesis of 2-aminobenzophenone 292 using Frye methodology

Since we had previously achieved some success with the CAS reaction using a single benzyl group on the amine (as in compound **297**), we decided to return to this approach. Using reductive amination with benzaldehyde, it was found that **297** (Scheme 115) could be formed from **292** under microwave conditions using sodium cyanoborohydride (NaCNBH₄) in ethanol. Irradiation of **292** with benzaldehyde in ethanol allowed for the formation of an imine (facilitated by the presence of anhydrous sodium sulfate) before the reduction by NaCNBH₄, resulting in **297** in a 70 % yield. The NMR spectra obtained for **297** corresponded with the previously obtained spectra using the alternative synthetic methodology. Exposure of benzophenone **297** to 4 equivalents of CAS resulted in the visualization of a fluorescent blue spot on the TLC plate along with the starting material (**297**) spot. After purification by column chromatography, the fluorescent blue spot was separated from the starting material (36 % collected) and determined to be acridone **298** in a yield of 8 %. Returning the collected starting material to the CAS reaction under reflux conditions resulted in the decomposition of the starting material.



Reaction conditions: i) benzaldehyde (1 eq), Na₂SO₄, EtOH, μW, 100 °C, 150 W, 10 min; ii) NaCNBH₄ (2 eq), EtOH, μW, 100 °C, 150 W, 25 min; iii) CAS (4 eq), MeCN/H₂O/CHCl₃, rt, 18 h.

Scheme 115 – Reductive amination and CAS mediated ring closure reaction to form acridone 298

A potential reason for the low yield of the reaction could be due to the significant hydrogen bonding present in **297** (shown in Figure 109). The N-H proton in the ¹H NMR spectrum was a broad triplet at 9.40 ppm. This downfield chemical shift further supports the hypothesis of

hydrogen bonding, especially since without the benzyl protection group (i.e. **292**) the amine NH₂ showed a chemical shift of 6.39 ppm.

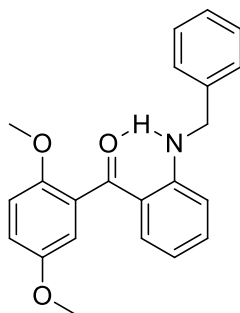


Figure 109 – The hydrogen bonding present in 297

Unfortunately due to time constraints, this project could not be further investigated. However, this result shows a proof of concept – that the CAS mediated ring closure methodology could be applied to the formation of acridones.

Plot Twist:

Conclusions and Future

Work

6.1. CAN vs. CAS

6.1.1. Conclusion

Perhaps the most significant outcome of this project was the discovery that the oxidant reported for the formation of xanthenes and diones in *JOC* was in fact ceric ammonium sulfate (CAS) and not ceric ammonium nitrate (CAN). CAS is significantly less soluble in the acetonitrile/water/chloroform solvent system than CAN and this may play a role in why the reaction works preferentially with CAS rather than CAN. However, we cannot ignore the role the counterion could be playing in the reaction as the nitrate (being a softer ligand than the sulfate) would dissociate from the cerium metal centre faster than the sulfate ion in CAS.

Regardless of this, when hydroxy-containing benzophenones such as **253**, **258** and **261** are exposed to CAN only dione and/or spirofuran compounds (Figure 110) were obtained in very low yields. This correlates well with what was observed by Omolo.¹⁹³

Conclusions and Future Work

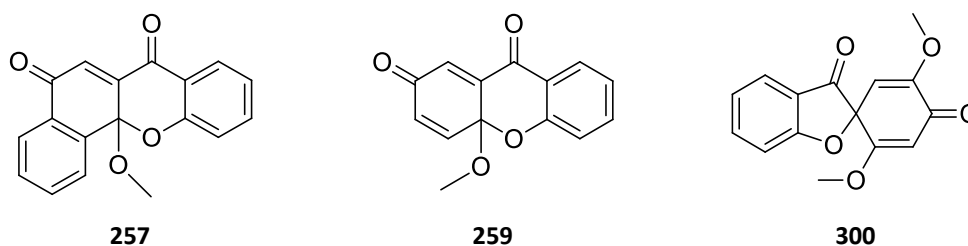


Figure 110 – Dione and spirofuran compounds that resulted from the CAN-mediated reactions

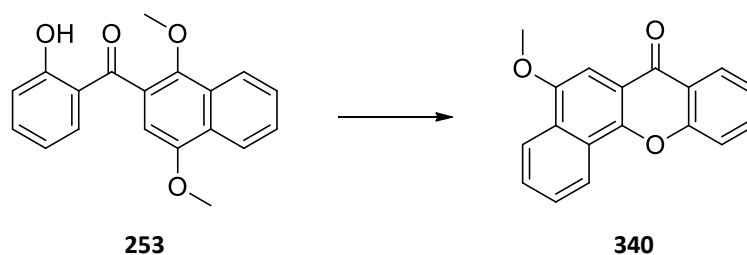
When the reactions were performed using CAS, the results reported by Johnson *et al.* were verified. The same products isolated by Johnson were also obtained in this project, however the ratio of products (when multiple products were collected) were different. We are confident in the ratio of the products reported here as the reactions were performed under controlled conditions in triplicate (or more) and reported as average yields.

Extensive investigation has found that an acetonitrile/water/chloroform solvent system in a 4:2:1 ratio was essential for this novel xanthone or dione reaction to occur and temperature plays no role in the rate of, or the type of products formed during, the reaction. When chloroform was excluded from the reaction, the products were isolated in low yields. When acetonitrile was excluded from the reaction, the reaction did not go to completion (regardless of CAS equivalents or temperature). Changing the solvent system to a methanol/water solution resulted in the exclusive formation of xanthone **260** when benzophenone **258** was subjected to the CAS conditions.

A reliable, quick method for the conversion of dione compounds to xanthenes was also developed over the course of this project (Scheme 94). Novel xanthenes **305**, **306**, **307** and **308** were generated in good yields using this methodology to show the versatility of this reaction.

6.1.2. Future work

While extensive work has gone into understanding the novel CAS reaction, the exclusive formation of xanthone **260** from benzophenone **258** under the aqueous methanol conditions serves as an interesting result that could further be developed. For example it would be interesting to see if naphthalene **253** in Scheme 116 (which forms dione **257** exclusively under ‘normal’ conditions) would still result in dione **257** exclusively in an aqueous methanol environment or if a xanthone (such as **340**) could be generated from the reaction.



Proposed reaction conditions: CAS (4 eq), MeOH/H₂O, rt.

Scheme 116 – Proposed xanthone formation using CAS in a methanol solution

Furthermore, in the reactions presented in this thesis CAS was used in mole equivalents to facilitate the reaction. Since there have been a few reports of using CAS under catalytic conditions by the addition of compounds (such as silver(I) nitrate, sodium dodecyl sulfate and ammonium persulfate as used by Skarzewski)¹⁸³ to reoxidize the cerium, future work could include the development of the reaction further to be performed under catalytic conditions.

6.2. Mechanistic investigations

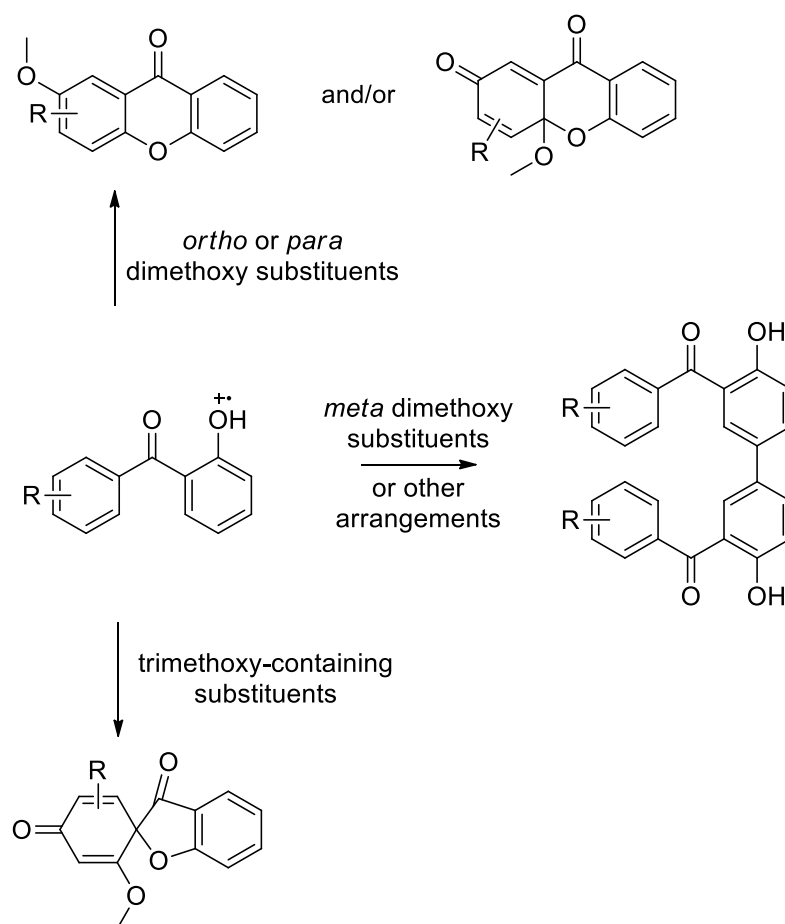
6.2.1. Conclusions from the mechanistic investigations

In order to further understand the mechanisms behind this novel reaction, a series of substituted benzophenones were synthesized. When methoxybenzophenone **312** was exposed to CAS no compounds were successfully isolated from the reaction. This suggests that a second substituent with electron donation abilities was necessary for any reactions to occur.

A variety of different products were isolated depending on the electronic nature of the benzophenone starting material. The exposure of benzophenones that contained *ortho* or *para* dimethoxy substituents (**253**, **258**, **261**, **263**, **265**, **270** and **328**) to CAS resulted in the formation of xanthone and/or dione products. Benzophenones that had a *meta* dimethoxy substitution pattern (**324** and **327**) or where no methoxy substituent *ortho* to the keto-bridge was present (**325**) resulted in the formation of novel dimers under similar conditions. These compounds were characterised by NMR spectroscopy and the structure confirmed by obtaining a crystal structure for dimer **329**. This result highlights the importance of the position of the electron donating methoxy substituents on the benzophenones in directing the type of reaction which occurs.

Furthermore, when trimethoxy-containing substituent **326** was exposed to CAS a spirofuran **333** was isolated and trace amounts of spirofuran **271** was isolated from trimethoxy-containing **270** further highlighting this finding. Curiously when benzophenone **261** was exposed to CAN was a spirofuran product, **300**, was isolated where with CAS exclusively xanthone **262** was formed.

The previously proposed mechanisms did not adequately account for all the results obtained in this work and hence more detailed mechanisms have been proposed. Scheme 106 to Scheme 110 outline the proposed mechanisms for the synthesis of xanthenes, diones, spirofurans and dimers respectively. These new proposed mechanisms detail how all of the products were generated from the simple oxidation of the phenol substituents on the benzophenones as shown in Scheme 117.



Scheme 117 – General scheme for the potential outcomes of exposing hydroxy-containing benzophenones to CAS

6.2.2. Future work from the results from the mechanistic investigations

The formation of dimers **329**, **330** and **331** were unexpected and unprecedented with CAS. Since we were only interested in the outcome of the reaction, this project did not include optimization of the dimerization reaction conditions and this could serve as an interesting extension to this research. Other procedures to form similar dimers require harsh conditions or complicated catalysts, and optimization of this reaction could result in a procedure that requires mild, near neutral conditions.

Of course we cannot rule out the possibility that dimerization could occur in different positions (particularly in the *ortho* position) or that further oxidation could occur as well and this could also serve as a point for further investigation.

6.3. Extension of the methodology to the formation of Acridones

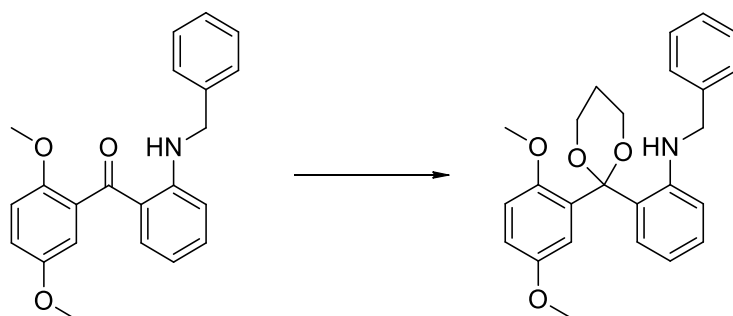
6.3.1. Conclusions

The initial aim of the project was to extend the novel methodology to the synthesis of acridones. Due to the unforeseen use of CAS and not CAN we did not fully explore the potential for the application of this novel reaction to the synthesis of acridones. A proof of concept resulted in the formation of a single acridone, **298**, in a poor yield. The poor yield may be attributed to significant hydrogen bonding in the starting material (**297**) – and the reaction did not go to completion regardless of how much CAS was added to the reaction. No products were successfully isolated when the reaction was performed using CAN.

Reported herein are a selection of synthetic routes which could be used to generate suitable 2-aminobenzophenone precursors that could be used to investigate the potential of the CAS mediated acridone reaction, the most beneficial being the one-pot lithiation reaction with Weinreb amide **339** and bromobenzenes.²⁰⁰ Following this a single benzyl protection of the amine needs to occur before the CAS reaction can be successful.

6.3.2. Future work

Extending the CAS methodology to the synthesis of acridones serves as the largest avenue of future research from this project. The issue of the hydrogen bonding in the precursor for the CAS reaction needs to be addressed. A suggestion would be to protect the ketone as the corresponding acetal to remove/weaken the hydrogen bonding as shown in Scheme 118. Alternatively, the ketone could be reduced to the alcohol before the ring closure is attempted. No research has been done into the necessity of the ketone in the CAS reaction and perhaps this should be investigated with the more established xanthone synthetic series before being applied to the acridone synthesis.



Scheme 118 – Proposed protection of the ketone to facilitate acridone formation

No attempts at removing the benzyl group from acridone **298** were made as only small amounts of the acridone were collected. Once the CAS-mediated ring closure for the formation of acridones has been optimized then methods for the removal of this protection group used needs to be investigated. From there the methodology could be applied in the synthesis of naturally occurring acridones such as those outlined in Figure 91.

Experimental

7.1. General Experimental Procedures

7.1.1. Purification of solvents and reagents

The solvents and reagents used for this project were purchased from ACE Chemicals or Sigma-Aldrich and used without purification unless otherwise stated. Dichloromethane (DCM) and acetonitrile (MeCN) were distilled over calcium hydride under nitrogen gas. Tetrahydrofuran (THF) was distilled over sodium wire and benzophenone under nitrogen gas. Deuterated solvents used for growing suitable crystals for single crystal X-ray diffraction were purchased from Merck.

7.1.2. General laboratory techniques and equipment

During the course of this project, thin layer chromatography (TLC) was performed on aluminium-backed Macherey-Nagel ALUGRAM Sil G/UV₂₅₄ plates that are pre-coated with 0.25 mm silica gel 60. The compounds were detected using ultraviolet light and stained if necessary, using iodine (for the imidazo[1,2-*a*]pyridines) or vanillin (for the acridone synthesis).

Evaporation of solvent under reduced pressure was performed on a Büchi Rotavapor R-3 with a Büchi R-3 heating bath at approximately 50 °C. This is referred to as evaporation/concentration *in vacuo*. Final drying was done using a high vacuum pump at 1 mm/Hg.

Microwave reactions were carried out on a commercial CEM Discover microwave oven.

7.1.3. Chromatographic Separations

Mixtures of products were separated by routine column chromatography, where the silica used was Macherey-Nagel 60, silica gel 60 (particle size 0.063 - 0.200 mm). Flash column chromatography was also performed, using Merck silica gel (particle size 0.035-0.070 mm). In an appropriately sized column, silica of mass approximately 30 times that of the product was packed and the product loaded onto the silica surface and covered with acid washed sand. Elution was achieved using the indicated solvent mixtures that were hexane and ethyl acetate based.

7.1.4. Spectroscopic Techniques

7.1.4.1. NMR Spectroscopy

¹H NMR spectra were recorded using Bruker Advance-500 and Bruker Advance-300 spectrometers operating at 500 MHz and 300 MHz respectively. All spectra were recorded in deuterated chloroform (*CDCl*₃), deuterated methanol (*d*₄-MeOD) or deuterated dimethylsulfoxide (*d*₆-DMSO) with all chemical shift values reported in parts per million referenced against 0.03% tetramethylsilane (TMS) as an internal standard. Coupling constants, *J*, are reported in Hertz (Hz). Commonly used abbreviations in assignments include: s = singlet, d = doublet, t = triplet, q = quartet, m = multiplet.

75.47 MHz and 125 MHz ¹³C NMR (¹H decoupled) spectra were recorded on Bruker Advance-300 and Bruker Advance-500 Spectrophotometers. All spectra were recorded in *CDCl*₃, *d*₄-MeOD or *d*₆-DMSO and the chemical shifts are reported on the δ scale in parts per million (ppm) relative to the central signal of *CDCl*₃ taken as 77.0 ppm, *d*₄-MeOD as 49.0 ppm and *d*₆-DMSO as 39.5 ppm.

All NMR spectroscopic data was processed using the MestReNova software suite licenced to the University of the Witwatersrand.²⁰¹ The ¹H and ¹³C NMR spectra were recorded for all compounds. Additional 2D experiments (COSY, HSQC, HMBC etc.) were recorded for final compounds, novel compounds and for any other compounds where it was deemed necessary. The compounds synthesized in this project were characterised as definitively as the spectra collected would allow, however *,',#,~ and ^ were symbols used to denote interchangeable assignments.

7.1.4.2. Infrared Spectroscopy

Infrared spectra were recorded on a Bruker Tensor 27 Spectrophotometer and all samples were loaded directly onto a diamond cell. All predominant absorptions are reported in terms of wavenumbers (*v/cm*⁻¹). IR spectra were obtained only for compounds where no IR data was available and for final compounds.

7.1.4.3. High Resolution Mass Spectroscopy

High resolution mass spectra (HRMS) were recorded on a Waters Synapt G2. All data was quoted in relative abundance (m/z). HRMS was performed only on novel compounds where no MS data was available as well as for final compounds. The author would like to thank the Mass Spectroscopy Unit at Stellenbosch University for their analysis of the compounds synthesized in this work.

7.1.5. Melting Points

Melting points were recorded using a Stuart SMP10 melting point apparatus. Capillary tubes that were sealed at one end were loaded with small amounts of sample and loaded into the melting point apparatus and observed. The point at which the entire sample had uniformly melted was considered to be the melting point. Melting points are reported without correction.

7.1.6. Elemental Analysis

The author would like to thank the analysis units at the University of Stellenbosch and University of Johannesburg for their elemental analysis of selected samples from this work.

7.1.7. Single Crystal X-ray Diffraction

Single crystal X-ray diffraction was made use of extensively over the course of this project. Suitable crystals were grown and diffraction intensity data collection, crystal structure solution and refinement were conducted by the author of this PhD. The intensity data were collected on a Bruker APEX II CCD area detector diffractometer with graphite monochromated Mo K α -radiation (50kV, 30mA) using the APEX 2 data collection software. The collection method involved ω -scans of width 0.5° and 512x512 bit data frames. Data reduction was carried out using the program *SAINT+* version 6.02.6 software and *SADABS* was used to make empirical absorption corrections.²⁰²

SHELXS-97 was used to solve crystal structures by direct methods.²⁰³ After initial isotropic refinements of non-hydrogen atoms, further anisotropic refinements were done by full matrix least-squares calculations based on F^2 using *SHELXL-97*.²⁰³ C-bound H atoms were first located in the difference map, then positioned geometrically and allowed to ride on their respective parent atoms, with thermal displacement parameters 1.2 times of the parent C atom. Where possible, the coordinates and isotropic displacement parameters of the N-bound and O-bound H atoms involved in the hydrogen bonding interactions were allowed to refine freely. Diagrams and publication material were generated using *WinGX*²⁰⁴ and *ORTEP-3* and the displacement ellipsoids shown at a 50% probability level.²⁰⁵

An example of the crystallographic information along with the ORTEP diagrams for selected compounds can be found in the Appendices, while the crystallographic information for each of the crystal structures obtained in this thesis are available in the Digital Appendix.

7.1.8. pH measurements

A Metrohm High-precision 780 pH meter and Metrohm Unitrode combination pH electrode was used for all pH measurements in the stability study. The electrode was calibrated by means of a 3 buffer calibration at pH 4, 7 and 9 using Metrohm ready-to-use buffer solutions.

7.1.9. UV-vis Spectroscopy

The stability studies were performed using UV-vis spectra that were recorded on either a Cary 100 UV-vis Spectrophotometer or Cary 300 Bio UV-vis Spectrophotometer, fitted with cuvette holders for 1 cm path length cuvettes. Matched Helma standard quartz cuvettes with Teflon stoppers were used for the pK experiments, one of which was used as a reference cell containing a 50% MeOH/H₂O solution. Each spectrum was recorded with a spectral band width of 2 nm, signal averaging time of 0.1 s, data interval of 0.5 nm and a scan rate of 300 nm.min⁻¹.

The scan application of the Cary WinUV software suite was used to facilitate the collection of absorbance spectra.²⁰⁶

7.1.10. Data Analysis

The spectroscopic data collected from the stability study was analysed using SigmaPlot¹¹⁸ to determine the pK of selected compounds. Two models were used to fit the data using equations 1 and 2 below.

$$A_T = \frac{A_1[H^+] + A_2K_1}{K_1 + [H^+]} \quad \text{Equation 1}$$

$$A_T = \frac{A_1[H^+]^2 + A_2K_1[H^+] + A_3K_1K_2}{[H^+]^2 + K_1[H^+] + K_1K_2} \quad \text{Equation 2}$$

The free ligands that showed a single pK were successfully fitted using equation 1. The zinc complexes that showed two distinct pK values were successfully fitted using equation 2. While the copper complexes also showed two pK values, due to the significant spectroscopic differences between pK₁ and pK₂, each pK was fitted separately using equation 1. The derivation of these equations can be found in the Digital Appendix.

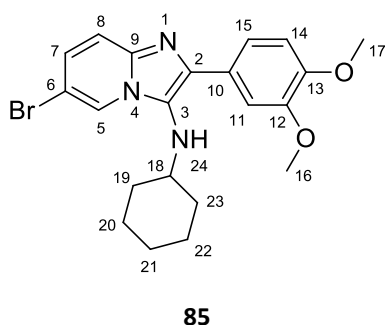
The pK values determined by SigmaPlot was then further analysed in Microsoft Excel to determine the K value for each experiment, the average K value(s) for each compound and the standard deviation. The pK value(s) for each compound was determined using the average K values and the error calculated from the sum of weighted relative percentage error reciprocals.

The raw absorbance data and the reports generated from SigmaPlot are available in the Digital Appendix. An example of the results obtained for one compound is given in Appendix A3.

7.2. Experimental Procedures for At the End of My Tether

7.2.1. General Procedure and Experimental details for the Groebke-Blackburn-Bienaymé MCR reactions

The general procedure for the MCR of imidazo[1,2-*a*]pyridines involved the combination of the appropriate 2-aminopyridine, isocyanide and aldehyde in equal mol ratio's in a round bottomed flask. To this Montmorillonite K10 clay was added (same mass as the 2-aminopyridine that was added) followed by the solvent (dioxane or ethanol). The mixture was stirred under reflux conditions for 4-48 hours, in some cases with additional stirring at room temperature for a further 12 hours. The clay was filtered off through Celite and washed with hot EtOAc or DCM. The filtrate was then concentrated *in vacuo* and the product purified by recrystallization or by column chromatography before being successfully characterised by NMR spectroscopy.

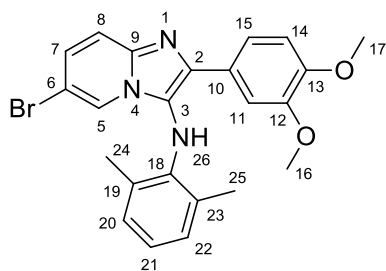


The general procedure was followed using 2-amino-5-bromopyridine (2.00 g, 11.56 mmol), 3,4-dimethoxybenzaldehyde (1.92 g, 11.56 mmol, 1 eq), cyclohexyl isocyanide (1.26 g, 11.56 mmol, 1 eq) and Montmorillonite K10 clay (2.00 g). The product was recrystallized from a large volume of hot ether. Imidazo[1,2-*a*]pyridine **85** was collected as yellow cubes and white crystals (2.94 g, 59 %). $R_f = 0.47$ (50 %

EtOAc/Hexane). **m.p.** = 158-159 °C. $^1\text{H NMR}$ (300 MHz, CDCl_3): $\delta_{\text{H}} = 8.19$ (1H, dd, $J = 2.0$ and 0.9 Hz, H-5), 7.65 (1H, d, $J = 2.0$ Hz, H-11), 7.52 (1H, dd, $J = 8.3$ and 2.0 Hz, H-15), 7.40 (1H, dd, $J = 9.4$ and 0.9 Hz, H-8), 7.15 (1H, dd, $J = 9.4$ and 1.9 Hz, H-7), 6.93 (1H, d, $J = 8.4$ Hz, H-14), 3.97 (3H, s, H-16*), 3.92 (3H, s, H-17*), 3.04 (1H, d, $J = 4.4$ Hz, H-24), 2.97 (1H, m, H-18), 1.78 (2H, d, $J = 9.8$ Hz, H-19a and H-23a), 1.69 (2H, q, $J = 3.8$ Hz, H-20a and H-22a), 1.58 (1H, d, $J = 5.7$ Hz, H-21a), $1.31 - 1.10$ (5H, m, H-19b, H-20b, H-21b, H-22b and H-23b). $^{13}\text{C NMR}$ (75 MHz, CDCl_3): $\delta_{\text{C}} = 149.2$ (C-12*), 148.8 (C-13*), 139.9 (C-9), 137.8 (C-3), 127.2 (C-7), 127.1 (C-10), 124.5 (C-2), 122.9 (C-5), 119.5 (C-15), 117.9 (C-8), 111.2 (C-11), 110.6 (C-14), 106.5 (C-6), 56.9 (C-18), 56.1 (C-16[#]), 56.0 (C-17[#]), 34.3 (C-19 and C-23), 25.8 (C-21), 24.9 (C-20 and C-22). **IR** ($\nu_{\text{m}}, \text{cm}^{-1}$) = 3298, 2928, 2853, 1585, 1504, 1448, 1406, 1361, 1319, 1255, 1224, 1168, 1134, 1026, 941, 891, 862, 798, 760, 715, 671. **ESI-MS** (m/z) calculated for $\text{C}_{21}\text{H}_{25}\text{N}_3\text{O}_2\text{Br}$, $[\text{M}+\text{H}]^+$, 430.3380, found 430.1141.

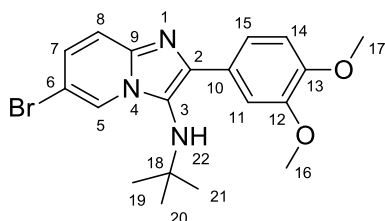
Experimental

The general procedure was followed using 2-amino-5-bromopyridine (2.00 g, 11.56 mmol), 3,4-

**86**

dimethoxybenzaldehyde (1.92 g, 11.56 mmol, 1 eq), xylyl isocyanide (1.52 g, 11.56 mmol, 1 eq) and Montmorillonite K10 clay (2.00 g). The product was recrystallized from hot ether. **86** was collected as a cream powder (1.38 g, 26 %). $R_f = 0.39$ (50 % EtOAc/Hexane). **m.p.** = 202 °C. $^1\text{H NMR}$ (300 MHz, CDCl_3): $\delta_H = 7.85$ (1H, dd, $J = 1.9$ and 0.9 Hz, H-5), 7.54 (1H, dd, $J = 8.4$ and 2.0 Hz, H-15), 7.42 (1H, dd, $J = 9.4$ and 0.9 Hz, H-8), 7.38

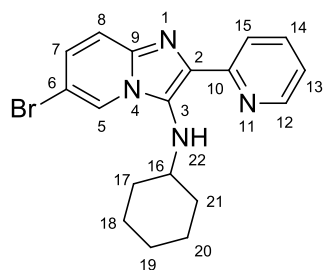
(d, $J = 2.0$ Hz, H-11), 7.17 (1H, dd, $J = 9.4$ and 1.9 Hz, H-7), 6.95 (2H, d, $J = 7.5$ Hz, H-20 and H-22), 6.81 – 6.73 (2H, m, H-14 and H-21), 5.36 (1H, s, H-26), 3.86 (3H, s, H-16*), 3.67 (3H, s, H-17*), 1.97 (6H, s, H-24 and H-25). $^{13}\text{C NMR}$ (75 MHz, CDCl_3): $\delta_C = 148.8$ (C-12 and C-13), 140.4 (C-18*), 139.7 (C-9*), 139.2 (C-3*), 130.1 (C-19 and C-23), 127.6 (C-7), 125.9 (C-2), 124.6 (C-20 and C-22), 122.4 (C-5), 120.9 (C-10), 119.9 (C-21), 119.7 (C-15), 117.8 (C-8), 110.9 (C-11), 109.9 (C-14), 106.9 (C-6), 55.8 (C-12[#]), 55.6 (C-13[#]), 18.5 (C-24 and C-25). **IR** ($\text{v}_m \cdot \text{cm}^{-1}$) = 3363, 3091, 3059, 3045, 3001, 2960, 2947, 2835, 1583, 1504, 1469, 1409, 1375, 1327, 1261, 1259, 1170, 1134, 1026, 947, 850, 806, 756, 730, 678, 642. **ESI-MS** (m/z) calculated for $\text{C}_{23}\text{H}_{23}\text{N}_3\text{O}_2\text{Br}$, $[\text{M}+\text{H}]^+$, 452.0974, found 452.0976.

**87**

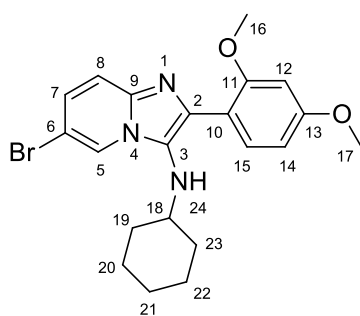
The general procedure was followed using 2-amino-5-bromopyridine (1.50 g, 8.67 mmol), 3,4-dimethoxybenzaldehyde (1.44 g, 8.67 mmol, 1 eq), *t*-butyl isocyanide (0.72 g, 8.67 mmol, 1 eq) and Montmorillonite K10 clay (1.50 g). The mixture was purified by recrystallization from hot EtOAc. Imidazo[1,2-*a*]pyridine **87** was collected as a cream

powder (2.57 g, 73 %). $R_f = 0.31$ (50 % EtOAc/Hexane). **m.p.** = 148 °C. $^1\text{H NMR}$ (300 MHz, CDCl_3): $\delta_H = 8.34 - 8.28$ (1H, m, H-5), 7.53 (1H, 1H, d, $J = 2.0$ Hz, H-8), 7.42 (1H, d, $J = 1.8$ Hz, H-11), 7.41 – 7.37 (1H, m, H-15), 7.16 (1H, dd, $J = 9.4$ and 2.0 Hz, H-7), 6.91 (1H, d, $J = 8.3$ Hz, H-14), 3.97 (3H, s, H-16*), 3.92 (3H, s, H-17*), 3.08 (1H, s, H-22), 1.05 (9H, s, H-19, H-20 and H-21). $^{13}\text{C NMR}$ (75 MHz, CDCl_3): $\delta_C = 149.0$ (C-12*), 148.8 (C-13*), 140.5 (C-9), 140.3 (C-3), 127.7 (C-10), 127.3 (C-7), 123.6 (C-2), 123.4 (C-5), 120.7 (C-15), 117.9 (C-8), 111.5 (C-11), 110.9 (C-14), 106.3 (C-6), 56.6 (C-18), 56.1 (C-16[#]), 55.9 (C-17[#]), 30.5 (C-19, C-20 and C-21). **IR** ($\text{v}_m \cdot \text{cm}^{-1}$) = 3308, 3005, 2966, 2837, 1682, 1584, 1504, 1464, 1386, 1313, 1251, 1209, 1140, 1024, 951, 853, 795, 760, 671. **ESI-MS** (m/z) calculated for $\text{C}_{19}\text{H}_{23}\text{N}_3\text{O}_2\text{Br}$, $[\text{M}+\text{H}]^+$, 404.0974, found 404.0980.

Experimental

**88**

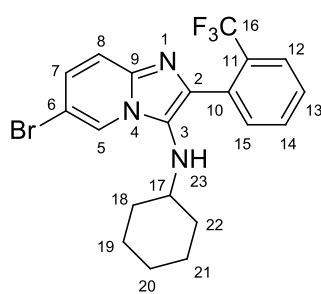
2-Amino-5-bromopyridine (2.00 g, 11.56 mmol), 2-pyridinecarboxaldehyde (1.24 g, 11.56 mmol, 1 eq), cyclohexyl isocyanide (1.26 g, 11.56 mmol, 1 eq) and Montmorillonite K10 clay (2.00 g) were combined and the general procedure followed. The resulting mixture was purified by recrystallization from an ether/methanol mixture to afford imidazo[1,2-*a*]pyridine **88** as yellow needles (1.4 g, 33 %). $R_f = 0.50$ (50 % EtOAc/Hexane). $m.p. = 135 - 136$ °C. 1H NMR (500 MHz, $CDCl_3$): $\delta_H = 8.55$ (1H, ddd, $J = 4.9, 1.9$ and 0.9 Hz, H-12), 8.15 (1H, dt, $J = 8.1$ and 1.1 Hz, H-15), 8.09 (1H, dd, $J = 1.9$ and 0.9 Hz, H-5), 7.75 (1H, td, $J = 7.8$ and 1.8 Hz, H-14), 7.41 (1H, dd, $J = 9.5$ and 0.9 Hz, H-8), $7.17 - 7.09$ (2H, m, H-7 and H-13), 6.21 (1H, d, $J = 9.9$ Hz, H-22), 3.07 (1H, tt, $J = 9.6$ and 5.7 Hz, H-16), $1.93 - 1.84$ (2H, m, H-17a and H-21a), $1.76 - 1.66$ (2H, m, H-18a and H-20a), 1.57 (1H, dd, $J = 9.7$ and 4.4 Hz, H-19a), $1.37 - 1.17$ (5H, m, H-17b, H-18b, H-19b, H-20b and H-21b). ^{13}C NMR (126 MHz, $CDCl_3$): $\delta_C = 154.8$ (C-12), 148.5 (C-9), 139.2 (C-3), 136.7 (C-14), 131.5 (C-2*), 131.4 (C-10*), 126.7 (C-7), 123.1 (C-5), 121.5 (C-13), 120.5 (C-15), 118.6 (C-8), 106.7 (C-6), 55.6 (C-16), 34.2 (C-17 and C-21), 25.9 (C-19), 25.0 (C-18 and C-20). IR (ν_{max}, cm^{-1}) = 3338, 2925, 2918, 2858, 2856, 1612, 1554, 1506, 1456, 1390, 1303, 1298, 1247, 1205, 1159, 1126, 1085, 1024, 912, 887, 844, 779, 736, 702, 667, 634. ESI-MS (m/z) calculated for $C_{18}H_{20}BrN_4$, $[M+H]^+$, 371.0871, found 371.0874.

**89**

2-Amino-5-bromopyridine (2.00 g, 11.56 mmol), 2,4-dimethoxybenzaldehyde (1.92 g, 11.56 mmol, 1 eq), cyclohexyl isocyanide (1.26 g, 11.56 mmol, 1 eq) and Montmorillonite K10 clay (2.00 g) were used and the general procedure followed. The product was recrystallized from an ether/methanol mixture resulting in a yellow powder that was found to be imidazo[1,2-*a*]pyridine **89** (3.50 g, 70 %). $R_f = 0.48$ (50 % EtOAc/Hexane). $m.p. = 164$ °C. 1H NMR (300 MHz, $CDCl_3$): $\delta_H = 8.20$ (1H, d, $J = 1.3$ Hz, H-5), 7.73 (1H, d, $J = 8.5$ Hz, H-15), 7.40 (1H, d, $J = 9.4$ Hz, H-8), 7.13 (1H, dd, $J = 9.4$ Hz and $J = 1.9$ Hz, H-7), 6.66 (1H, dd, $J = 8.5$ Hz and $J = 2.4$ Hz, H-14), 6.57 (1H, d, $J = 2.3$ Hz, H-12), 3.87 (3H, s, H-16*), 3.86 (3H, s, H-17*), 3.85 (1H, s, N-H), $2.67 - 2.59$ (1H, m, H-18), 1.69 (2H, d, $J = 12.6$ Hz, H-19), 1.59 (2H, dd, $J = 9.8$ Hz and $J = 3.3$ Hz, H-20), 1.49 (1H, dd, $J = 8.8$ Hz and $J = 3.6$ Hz, H-21a), $1.16 - 0.96$ (5H, m, H-21b, H-22 and H-23). ^{13}C NMR (75 MHz, $CDCl_3$): $\delta_C = 160.8$ (C-13*), 156.9 (C-11*), 140.0 (C-9), 134.7 (C-3), 132.3 (C-15), 127.0 (C-7), 126.1

Experimental

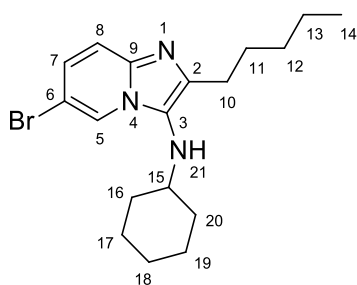
(C-2), 122.7 (C-5), 117.9 (C-8), 116.7 (C-10), 106.1 (C-6), 105.8 (C-14), 99.2 (C-12), 56.4 (C-18), 56.1 (C-16[#]), 55.4 (C-17[#]), 34.1 (C-19 and C-23), 25.7 (C-21), 24.8 (C-20 and C-22). IR ($\nu_{\text{m}}\cdot\text{cm}^{-1}$) = 3340, 2925, 2918, 2858, 2856, 1612, 1558, 1506, 1454, 1392, 1325, 1298, 1247, 1207, 1159, 1126, 1085, 1024, 912, 889, 844, 821, 781, 702, 669, 632. ESI-MS (m/z) calculated for $\text{C}_{21}\text{H}_{25}\text{N}_3\text{O}_2\text{Br}$, $[\text{M}+\text{H}]^+$, 430.1130, found 430.1125.

**90**

Following the general procedure, 2-amino-5-bromopyridine (1.00 g, 5.78 mmol), 2-trifluoromethylbenzaldehyde (1.01 g, 5.78 mmol, 1 eq), cyclohexyl isocyanide (0.63 g, 5.78 mmol, 1 eq) and Montmorillonite K10 clay (1.00 g) were combined and a cream powder resulted after recrystallization from hot EtOAc which was found to be **90** (1.34 g, 53 %). R_f = 0.72 (50 % EtOAc/Hexane). **m.p.** = 160-163 °C. $^1\text{H NMR}$ (300 MHz, CDCl_3): δ_{H} = 8.24 (1H, dd, J = 1.9 and 0.9 Hz, H-5), 7.79 (1H,

dd, J = 7.8 and 1.4 Hz, H-12), 7.61 (1H, td, J = 7.5 and 1.5 Hz, H-14), 7.55 (1H, d, J = 7.7 Hz, H-13), 7.50 (1H, dd, J = 7.4 and 1.4 Hz, H-15), 7.42 (1H, dd, J = 9.4 and 0.9 Hz, H-8), 7.20 (1H, dd, J = 9.5 and 1.9 Hz, H-7), 3.00 (1H, d, J = 5.9 Hz, H-23), 2.66 (1H, m, H-17), 1.76 – 1.44 (5H, m, H-18a, H-19a, H-20a, H-21a and H-22a), 1.04 (5H, m, H-18b, H-19b, H-20b, H-21b and H-22b). $^{13}\text{C NMR}$ (75 MHz, CDCl_3): δ_{C} = 139.5 (C-9), 136.2 (C-3), 133.2 (t, C-11), 132.7 (C-15), 131.4 (C-14), 129.9 (t, C-2), 129.5 (C-10), 129.1 (C-16), 128.5 (C-13), 127.2 (C-7), 126.4 (t, C-12), 123.1 (C-5), 118.4 (C-8), 106.8 (C-6), 56.3 (C-17), 33.8 (C-18 and C-22), 25.6 (C-20), 24.5 (C-19 and C-21). IR ($\nu_{\text{m}}\cdot\text{cm}^{-1}$) = 3248, 2928, 2855, 1555, 1495, 1448, 1408, 1406, 1312, 1231, 1188, 1138, 1107, 1051, 1034, 957, 887, 856, 796, 768, 690, 667, 646. ESI-MS (m/z) calculated for $\text{C}_{20}\text{H}_{20}\text{BrF}_3\text{N}_3$, $[\text{M}+\text{H}]^+$, 438.0793, found 438.0799.

2-Amino-5-bromopyridine (1.50 g, 8.67 mmol), hexanal (0.87 g, 8.67 mmol, 1 eq), cyclohexyl isocyanide (0.95 g, 8.67 mmol, 1 eq) and Montmorillonite K10 clay (1.50 g) were combined and the general procedure followed.

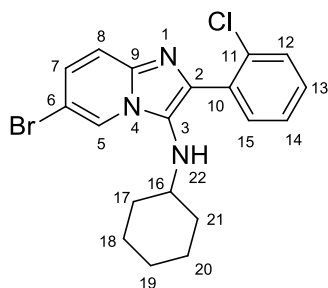
**91**

The product was purified by column chromatography in a 50 % EtOAc/Hexane eluent solution. Imidazo[1,2-*a*]pyridine **91** was collected as a yellow viscous liquid (1.10 g, 35 %). R_f = 0.69 (50 % EtOAc/Hexane). $^1\text{H NMR}$ (300 MHz, CDCl_3): δ_{H} = 8.13 (1H, d, J = 1.8 Hz, H-5), 7.31 (1H, d, J =

Experimental

9.3 Hz, H-8), 7.08 (1H, dd, $J = 9.4$ and 2.0 Hz, H-7), 2.94 – 2.82 (2H, m, H-15 and H-21), 2.74 – 2.64 (2H, m, H-10), 1.91 – 1.82 (2H, m, H-16a and H-20a), 1.82 – 1.70 (4H, m, H-11, H-17a and H-19b), 1.65 – 1.58 (1H, m, H-18a), 1.36 (4H, m, H-12 and H-13), 1.30 – 1.16 (5H, m, H-16b, H-17b, H-18b, H-19b and H-20b), 0.95 – 0.86 (3H, m, H-14). $^{13}\text{C NMR}$ (75 MHz, CDCl_3): $\delta_{\text{C}} = 140.8$ (C-9), 139.6 (C-3), 126.0 (C-7), 124.8 (C-2), 122.5 (C-5), 117.3 (C-8), 105.7 (C-6), 57.1 (C-15), 34.1 (C-16 and C-17), 31.9 (C-13), 29.1 (C-11), 27.3 (C-10), 25.7 (C-18), 24.8 (C-17 and C-19), 22.5 (C-12), 14.0 (C-14). IR ($\text{v}_{\text{m}}\cdot\text{cm}^{-1}$) = 3280, 2928, 2855, 1653, 1564, 1499, 1450, 1402, 1396, 1321, 1261, 1132, 1090, 891, 795, 735. ESI-MS (m/z) calculated $[\text{M}+\text{H}]^+$ for $\text{C}_{18}\text{H}_{27}\text{N}_3\text{Br}$, 364.1388, found 364.1380.

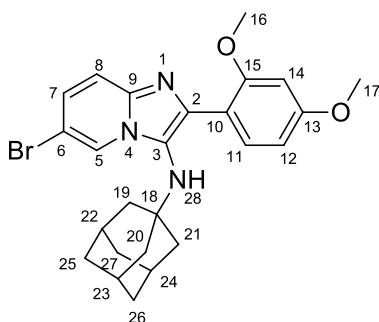
Following the general procedure, 2-amino-5-bromopyridine (1.50 g, 8.67 mmol), 2-



92

chlorobenzaldehyde (1.22 g, 8.67 mmol, 1 eq), cyclohexyl isocyanide (0.95 g, 8.67 mmol, 1 eq) and Montmorillonite K10 clay (1.50 g) were combined and the mixture purified by recrystallization from hot methanol to afford **92** as a cream powder (1.34 g, 38 %). $R_f = 0.62$ (50 % EtOAc/Hexane). **m.p.** = 151 - 152 °C. $^1\text{H NMR}$ (300 MHz, CDCl_3): $\delta_{\text{H}} = 8.26$ (1H, d, $J = 1.7$ Hz, H-5), 7.67 – 7.61 (1H, m, H-15), 7.49 – 7.40 (2H, m,

H-8 and H-12), 7.38 – 7.31 (2H, m, H-13 and H-14), 7.19 (1H, dd, $J = 9.5$, 1.9 Hz, H-7), 3.25 (1H, d, $J = 7.1$ Hz, H-22), 2.64 (1H, dq, $J = 6.4$ and 3.3 Hz, H-16), 1.65 (2H, m, H-17a and H-21a), 1.55 (2H, d, $J = 4.6$ Hz, H-18a and H-20a), 1.52 – 1.41 (1H, m, H-19a), 1.13 – 0.94 (5H, m, H-17b, H-18b, H-19b, H-20b and H-21b). $^{13}\text{C NMR}$ (75 MHz, CDCl_3): $\delta_{\text{C}} = 140.0$ (C-3), 136.2 (C-9), 133.6 (C-2), 132.6 (C-11), 132.5 (C-12), 129.5 (C-14), 129.4 (C-15), 127.1 (C-17), 127.0 (C-7), 126.6 (C-10), 123.0 (C-5), 118.3 (C-8), 106.7 (C-6), 56.4 (C-16), 33.8 (C-17 and C-21), 25.6 (C-19), 24.6 (C-18 and C-20). IR ($\text{v}_{\text{m}}\cdot\text{cm}^{-1}$) = 3354, 2933, 2851, 1557, 1508, 1479, 1448, 1391, 1323, 1261, 1227, 1180, 1109, 1082, 1045, 1029, 931, 889, 831, 785, 734, 711, 652, 601. ESI-MS (m/z) calculated $[\text{M}+\text{H}]^+$ for $\text{C}_{19}\text{H}_{20}\text{N}_3\text{ClBr}$ 404.0529, found 404.0529.



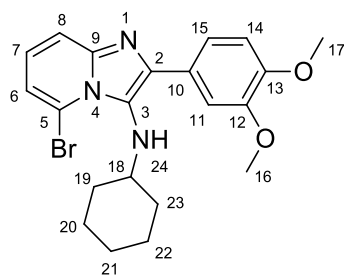
93

2-Amino-5-bromopyridine (0.628 g, 1.55 mmol), 2,4-dimethoxybenzaldehyde (0.258 g, 1.55 mmol, 1 eq), adamantyl isocyanide (0.250 g, 11.56 mmol, 1 eq) and Montmorillonite K10 clay (0.628 g) were used and the general procedure followed. The mixture was purified by column

Experimental

chromatography using a 40 % EtOAc/Hex eluent. The product, **93**, was collected as a peach foam (0.694 g, 93 %). $R_f = 0.69$ (50 % EtOAc/Hexane). **m.p.** = 95 - 97 °C. $^1\text{H NMR}$ (300 MHz, CDCl_3): $\delta_{\text{H}} = 8.43$ (1H, dd, $J = 2.0$ and 0.9 Hz, H-5), 7.72 (1H, d, $J = 8.5$ Hz, H-15), 7.38 (1H, dd, $J = 9.4$ and 0.9 Hz, H-8), 7.12 (1H, dd, $J = 9.4$ and 1.9 Hz, H-7), 6.65 (1H, dd, $J = 8.5$ and 2.4 Hz, H-14), 6.54 (1H, d, $J = 2.4$ Hz, H-12), 3.86 (3H, s, H-16*), 3.85 (3H, s, H-17*) 3.71 (1H, s, H-28), $1.96 - 1.84$ (3H, m, H-22, H-23 and H-24), 1.44 (12H, m, H-19, H-20, H-21, H-25, H-26 and H-27). $^{13}\text{C NMR}$ (75 MHz, CDCl_3): $\delta_{\text{C}} = 160.8$ (C-11*), 156.9 (C-13*), 140.6 (C-9), 137.3 (C-3), 132.3 (C-15), 126.4 (C-7), 124.8 (C-2), 123.7 (C-5), 117.7 (C-8), 117.5 (C-10), 105.8 (C-6), 105.7 (C-14), 99.2 (C-12), 56.1 (C-16[#]), 55.9 (C-17[#]), 55.4 (C-18), 43.5 (C-19, C-20 and C-21), 36.2 (C-25, C-26 and C-27), 29.6 (C-25, C-26 and C-27). **IR** ($\nu_{\text{m}}\cdot\text{cm}^{-1}$) = 3346, 2905, 2847, 1614, 1503, 1456, 1391, 1306, 1285, 1207, 1159, 1163, 1090, 1030, 916, 829, 791, 671, 561. **ESI-MS** (m/z) calculated $[\text{M}+\text{H}]^+$ for $\text{C}_{25}\text{H}_{29}\text{N}_3\text{O}_2\text{Br}$ 482.1443, found 482.1460.

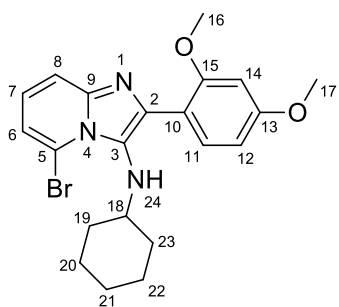
2-Amino-6-bromopyridine (1.50 g, 8.67 mmol), 3,4-dimethoxybenzaldehyde (1.44 g, 8.67 mmol, 1 eq), cyclohexyl isocyanide (0.95 g, 8.67 mmol, 1 eq) and Montmorillonite K10 clay (1.50 g) were combined and the general procedure followed.



94

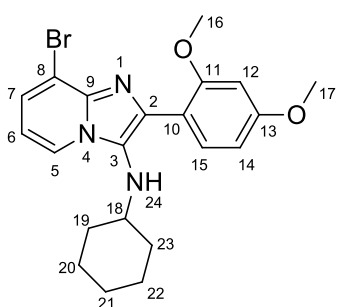
The product was purified by column chromatography using an eluent of 20-80 % EtOAc/Hexane. After concentration *in vacuo*, **94** was collected as a viscous brown oil (2.73 g, 73 %). $R_f = 0.64$ (50 % EtOAc/Hexane). $^1\text{H NMR}$ (300 MHz, CDCl_3): $\delta_{\text{H}} = 7.96$ (1H, d, $J = 2.0$ Hz, H-11), 7.85 (1H, dd, $J = 8.4$ and 2.0 Hz, H-15), 7.51 (1H, dd, $J = 7.2$ and 2.8 Hz, H-8), $6.98 - 6.89$ (3H, m, H-6, H-7 and H-14), 3.98 (3H, s, H-16*), 3.93 (3H, s, H-17*), 3.63 (1H, s, H-24), $3.05 - 2.87$ (1H, m, H-18), 1.70 (2H, d, $J = 11.5$ Hz, H-19a and H-23a), 1.62 (2H, dd, $J = 7.8$ and 2.9 Hz, H-20a and H-22a), 1.54 (1H, d, $J = 4.3$ Hz, H-21a), $1.21 - 1.01$ (5H, m, H19b, H-20b, H-21b, H-22b and H-23b). $^{13}\text{C NMR}$ (75 MHz, CDCl_3): $\delta_{\text{C}} = 148.6$ (C-12 and C-13), 144.1 (C-9), 139.4 (C-3), 127.4 (C-7), 126.4 (C-10), 124.1 (C-2), 120.6 (C-5), 118.5 (C-15), 117.2 (C-8), 111.7 (C-6), 111.1 (C-11), 110.9 (C-14), 59.0 (C-18), 56.0 (C-16*), 55.9 (C-17*), 33.1 (C-19 and C-23), 26.0 (C-21), 25.0 (C-20 and C-22). **IR** ($\nu_{\text{m}}\cdot\text{cm}^{-1}$) = 3352, 2931, 2856, 1708, 1635, 1510, 1452, 1419, 1371, 1311, 1257, 1176, 1139, 1026, 979, 850, 808, 763. **ESI-MS** (m/z) calculated $[\text{M}+\text{H}]^+$ for $\text{C}_{21}\text{H}_{25}\text{N}_3\text{O}_2\text{Br}$ 430.1130, found 430.1132.

Experimental



95

2-Amino-6-bromopyridine (1.50 g, 8.67 mmol), 2,4-dimethoxybenzaldehyde (1.44 g, 8.67 mmol, 1 eq), cyclohexyl isocyanide (0.947 g, 8.67 mmol, 1 eq) and Montmorillonite K10 clay (1.50 g) were combined and the general procedure followed. The mixture was purified by column chromatography using an eluent of 30 % EtOAc/Hexane. The product was further purified by recrystallization from an ether/methanol mixture. Imidazo[1,2-*a*]pyridine **95** was collected as a brown solid (1.498 g, 40 %). $R_f = 0.40$ (50 % EtOAc/Hexane). $m.p = 80 - 81$ °C. $^1\text{H NMR}$ (300 MHz, CDCl_3): $\delta_{\text{H}} =$ $^1\text{H NMR}$ (300 MHz, CDCl_3) $\delta =$ 7.63 (1H, d, $J = 8.5$ Hz, H-11), 7.50 (1H, dd, $J = 8.5$ and 1.4 Hz, H-8), 6.92 (2H, m, H-6 and H-7), 6.66 (1H, dd, $J = 8.5$ and 2.3 Hz, H-12), 6.58 (1H, d, $J = 2.3$ Hz, H-14), 3.87 (3H, s, H-16*), 3.86 (3H, s, H-17*), 3.63 (1H, d, $J = 9.1$ Hz, H-24), 2.88 – 2.72 (1H, m, H-18), 1.73 (2H, d, $J = 12.4$ Hz, H-19a and H-23a), 1.52 (2H, dt, $J = 10.9$ and 5.5 Hz, H-20a and H-22a), 1.47 (1H, s, H-21a), 1.16 – 0.72 (5H, m, H-19b, H-20b, H-21b, H-22b and H-23b). $^{13}\text{C NMR}$ (75 MHz, CDCl_3): $\delta_{\text{C}} =$ 160.9 (C-15[#]), 157.2 (C-13[#]), 143.8 (C-9), 136.5 (C-3), 132.6 (C-5), 129.0 (C-7), 123.2 (C-11), 118.5 (C-8), 116.8 (C-2), 116.7 (C-6), 112.0 (C-10), 105.6 (C-12), 99.1 (C-14), 58.9 (C-18), 56.0 (C-16*), 55.4 (C-17*), 50.2, 33.0 (C-19 and C-23), 25.8 (C-21), 25.0 (C-20 and C-22). IR ($\nu_{\text{m}}\cdot\text{cm}^{-1}$) = 3418, 3341, 2937, 2934, 2843, 1614, 1557, 1506, 1454, 1441, 1400, 1298, 1285, 1259, 1205, 1161, 1123, 1074, 1028, 937, 921, 889, 824, 770, 719, 667, 630. ESI-MS (m/z) calculated $[\text{M}+\text{H}]^+$ for $\text{C}_{21}\text{H}_{25}\text{N}_3\text{O}_2\text{Br}$ 430.1130, found 430.1137.

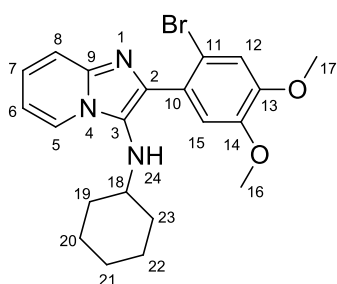


96

2-Amino-3-bromopyridine (1.00 g, 5.78 mmol), 2,4-dimethoxybenzaldehyde (0.961 g, 5.78 mmol, 1 eq), cyclohexyl isocyanide (0.631 g, 5.78 mmol, 1 eq) and Montmorillonite K10 clay (1.00 g) were combined and the general procedure followed. The mixture was purified by column chromatography using an eluent of 40 % EtOAc/Hexane. **96** was found to be the product and was collected as a sticky brown oil (1.866 g, 75 %). $R_f = 0.51$ (75 % EtOAc/Hexane), $^1\text{H NMR}$ (300 MHz, CDCl_3): $\delta_{\text{H}} =$ 8.07 (1H, dd, $J = 6.8$, 0.8 Hz, H-5), 7.83 (1H, d, $J = 8.5$ Hz, H-15), 7.31 (1H, dd, $J = 7.2$ and 0.8 Hz, H-7), 6.66 (1H, dd, $J = 8.5$ and 2.3 Hz, H-14), 6.63 – 6.58 (1H, m, H-6), 6.57 (1H, d, $J = 2.3$ Hz, H-12), 3.96 – 3.87 (1H, m, H-24), 3.84 (3H, s, H-16*), 3.82 (3H, s, H-17*), 2.64 (1H, s, H-18), 1.68 (2H, d, $J = 10.0$ Hz, H-19a and

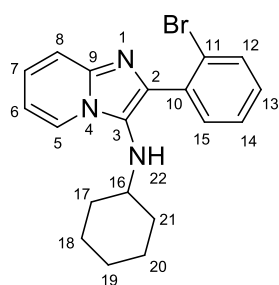
Experimental

H-23a), 1.54 (2H, s, H-20a and H-22a), 1.45 (1H, s, H-21a), 1.01 (5H, m, H-19b, H-20b, H-21b, H-22b and H-23b). $^{13}\text{C NMR}$ (75 MHz, CDCl_3): δ_{C} = 160.8 (C-11*), 156.9 (C-13*), 139.1 (C-9), 134.6 (C-3), 132.7 (C-15), 128.2 (C-2), 125.1 (C-7), 122.0 (C-5), 116.7 (C-8), 111.2 (C-6), 111.1 (C-10), 105.9 (C-14), 99.0 (C-12), 56.3 (C-16[#]), 56.1 (C-18), 55.4 (C-17[#]), 34.0 (C-19 and C-23), 25.6 (C-21), 24.7 (C-20 and C-22). **IR** ($\nu_{\text{m}}\cdot\text{cm}^{-1}$) = 3368, 2932, 2855, 1614, 1580, 1503, 1454, 1447, 1348, 1304, 1263, 1207, 1159, 1088, 1030, 939, 833, 733, 702, 664, 582. **ESI-MS** (m/z) calculated $[\text{M}+\text{H}]^+$ for $\text{C}_{21}\text{H}_{25}\text{N}_3\text{O}_2\text{Br}$ 430.1130, found 430.1136.



97

Following the general procedure 2-aminopyridine (1.50 g, 15.9 mmol), 2-bromo-4,5-dimethoxybenzaldehyde (3.91 g, 15.9 mmol, 1 eq), cyclohexyl isocyanide (1.74 g, 15.9 mmol, 1 eq) and Montmorillonite K10 clay (1.50 g) were combined. The mixture was purified by column chromatography using an eluent of 50 % EtOAc/Hexane. **97** was collected as a mustard foam (4.22 g, 62 %). R_f = 0.31 (50 % EtOAc/Hexane). **m.p.** = 110-112 °C. $^1\text{H NMR}$ (300 MHz, CDCl_3): δ_{H} = 8.13 (1H, d, J = 6.8 Hz, H-5), 7.51 (1H, d, J = 9.1 Hz, H-8), 7.16 – 7.08 (2H, m, H-7 and H-15*), 7.08 (1H, s, H-12*), 6.78 (1H, td, J = 6.8 and 0.9 Hz, H-6), 3.90 (3H, s, H-16*), 3.88 (3H, s, H-17*), 3.27 (1H, d, J = 6.8 Hz, H-24), 2.64 (1H, s, H-18), 1.72 – 1.61 (2H, m, H-19a and H-23a), 1.61 – 1.51 (2H, m, H-20a and H-22a), 1.46 (1H, s, H-21a), 1.15 – 0.96 (5H, m, H-19b, H-20b, H-21b, H-22b and H-23b). $^{13}\text{C NMR}$ (75 MHz, CDCl_3): δ_{C} = 149.5 (C-13*), 148.5 (C-14*), 141.4 (C-9), 136.8 (C-3), 128.5 (C-2), 125.9 (C-5), 123.8 (C-7[#]), 123.0 (C-10), 117.5 (C-12[#]), 115.2 (C-11), 114.9 (C-6), 113.0 (C-8), 111.6 (C-15[#]), 56.5 (C-18), 56.2 (C-16 and C-17), 34.0 (C-19 and C-23), 25.8 (C-21), 24.7 (C-20 and C-22). **IR** ($\nu_{\text{m}}\cdot\text{cm}^{-1}$) = 3346, 2930, 2856, 1657, 1606, 1604, 1503, 1452, 1411, 1342, 1246, 1205, 1169, 1028, 860, 760, 623. **ESI-MS** (m/z) calculated $[\text{M}+\text{H}]^+$ for $\text{C}_{21}\text{H}_{25}\text{N}_3\text{O}_2\text{Br}$ 430.1130, found 430.1133.

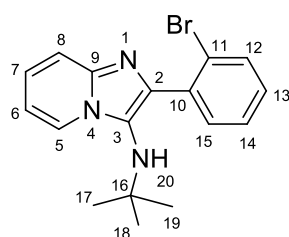


98

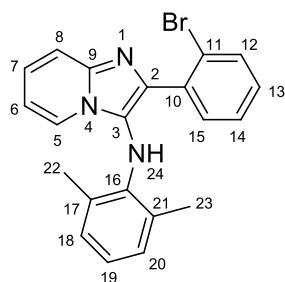
Following the general procedure 2-aminopyridine (2.00 g, 21.25 mmol), 2-bromobenzaldehyde (3.93 g, 21.25 mmol, 1 eq), cyclohexyl isocyanide (2.320 g, 21.25 mmol, 1 eq) and Montmorillonite K10 clay (2.00 g) were combined. The mixture was purified by column chromatography using an eluent of 50 %

Experimental

EtOAc/Hexane. Imidazo[1,2-*a*]pyridine **98** was collected as a viscous brown oil (5.222 g, 66 %). R_f = 0.28 (50 % EtOAc/Hexane). $^1\text{H NMR}$ (300 MHz, CDCl_3): δ_{H} = 8.14 (1H, dt, J = 6.9 and 1.2 Hz, H-5), 7.65 (1H, dd, J = 8.0 and 1.2 Hz, H-15), 7.61 (1H, dd, J = 7.7 and 1.8 Hz, H-12), 7.53 (1H, dt, J = 9.1 and 1.1 Hz, H-8), 7.39 (1H, td, J = 7.5 and 1.3 Hz, H-13), 7.28 – 7.20 (1H, m, H-14), 7.14 (1H, ddd, J = 9.1, 6.7 and 1.3 Hz, H-7), 6.80 (1H, td, J = 6.8 and 1.2 Hz, H-6), 3.25 (1H, d, J = 7.0 Hz, H-22), 2.67 (1H, m, H-16), 1.73 – 1.61 (2H, m, H-17a and H-21a), 1.61 – 1.52 (2H, m, H-18a and H-20a), 1.46 (1H, m, H-19a), 1.15 – 0.94 (5H, m, H-17b, H-18b, H-19b, H-20b and H-21b). $^{13}\text{C NMR}$ (75 MHz, CDCl_3): δ_{C} = 141.5 (C-9), 136.8 (C-3), 136.2 (C-2), 132.9 (C-15*), 132.7 (C-12*), 129.5 (C-13), 127.5 (C-14), 126.0 (C-10), 123.9 (C-7), 123.03 (C-5), 123.00 (C-11), 117.7 (C-8), 111.8 (C-6), 56.5 (C-16), 34.0 (C-17 and C-21), 25.8 (C-19), 24.7 (C-18 and C-20). $\text{IR (v}_{\text{m}}\cdot\text{cm}^{-1})$ = 3383, 3086, 2930, 2855, 1634, 1564, 1504, 1450, 1350, 1265, 1258, 1194, 1024, 923, 733, 646. ESI-MS (m/z) calculated $[\text{M}+\text{H}]^+$ for $\text{C}_{19}\text{H}_{21}\text{N}_3\text{Br}$ 370.0919, found 370.0925.

**99**

2-Aminopyridine (2.00 g, 21.25 mmol), 2-bromobenzaldehyde (3.93 g, 21.25 mmol, 1 eq), *t*-butyl isocyanide (1.766 g, 21.25 mmol, 1 eq) and Montmorillonite K10 clay (2.00 g) were combined and the general procedure followed. The resulting mixture was purified by recrystallization from hot ether to afford **99** as cream crystals (2.919 g, 40 %). R_f = 0.57 (50 % EtOAc/Hexane). $m.p.$ = 184 - 185 °C. $^1\text{H NMR}$ (300 MHz, CDCl_3): δ_{H} = 8.28 (1H, dt, J = 6.8 and 1.3 Hz, H-5), 7.62 (2H, m, H-15 and H-12), 7.51 (1H, d, J = 9.0 Hz, H-8), 7.37 (1H, td, J = 7.5 and 1.3 Hz, H-14*), 7.19 (1H, td, J = 7.7 and 1.8 Hz, H-13*), 7.12 (1H, ddd, J = 8.7, 6.7 and 1.3 Hz, H-7), 6.76 (1H, td, J = 6.8 and 1.2 Hz, H-6), 3.19 (1H, s, H-20), 0.90 (9H, s, H-17, H-18 and H-19). $^{13}\text{C NMR}$ (75 MHz, CDCl_3): δ_{C} = 142.1 (C-9), 139.3 (C-3), 137.0 (C-2), 133.1 (C-15*), 132.6 (C-12*), 129.4 (C-13), 127.5 (C-14), 124.6 (C-10), 124.2 (C-7), 123.7 (C-5), 122.7 (C-11), 117.5 (C-8), 111.4 (C-6), 55.8 (C-16), 30.0 (C-17, C-18 and C-19). $\text{IR (v}_{\text{m}}\cdot\text{cm}^{-1})$ = 3236, 2968, 1630, 1554, 1503, 1470, 1431, 1385, 1339, 1273, 1222, 1219, 1024, 947, 918, 812, 752, 700, 650, 609. ESI-MS (m/z) calculated $\text{M}+\text{H}$ for $\text{C}_{17}\text{H}_{19}\text{N}_3\text{Br}$, $[\text{M}+\text{H}]^+$, 344.0762, found 344.0770.

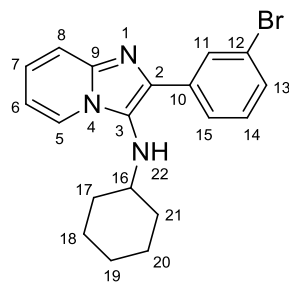
**100**

Following the general procedure 2-aminopyridine (0.717 g, 7.62 mmol), 2-bromobenzaldehyde (1.41 g, 7.62 mmol, 1 eq), xylyl isocyanide (1.00 g, 7.62 mmol, 1 eq) and Montmorillonite K10 clay (1.00 g) were

Experimental

combined. The mixture was purified by column chromatography using an eluents of 30-80 % EtOAc/Hexane to afford **100** which was collected as a bottle green powder (1.768 g, 59 %). $R_f = 0.31$ (50 % EtOAc/Hexane). $m.p.$ = 60 °C. $^1\text{H NMR}$ (300 MHz, CDCl_3): $\delta_H = 7.70$ (1H, dt, $J = 6.9$ and 1.2 Hz, H-5), 7.63 – 7.60 (1H, m, H-12), 7.58 (1H, q, $J = 1.3$ Hz, H-8), 7.40 (1H, dd, $J = 7.6$, 1.9 Hz, H-15), 7.30 – 7.23 (1H, m, H-14), 7.21 – 7.12 (2H, m, H-7 and H-13), 6.85 (2H, d, $J = 7.4$ Hz, H-18 and H-20), 6.73 (2H, m, $J = 8.3$, 6.8 Hz, H-6 and H-19), 5.50 (1H, s, H-24), 1.91 (6H, s, H-22 and H-23). $^{13}\text{C NMR}$ (75 MHz, CDCl_3): $\delta_C = 141.1$ (C-9), 140.3 (C-3), 137.9 (C-16), 135.3 (C-2), 132.3 (C-12), 132.0 (C-15), 129.6 (C-13), 129.3 (C-18 and C-20), 127.2 (C-14), 126.6 (C-17 and C-21), 123.8 (C-10), 123.8 (C-13), 122.6 (C-11), 122.4 (C-5), 121.4 (C-19), 117.9 (C-8), 112.3 (C-6), 18.3 (C-22 and C-23). $\text{IR } (\nu_{\text{m}}, \text{cm}^{-1}) = 3209, 2945, 1634, 1572, 1499, 1474, 1466, 1421, 1350, 1269, 1222, 1152, 1099, 1024, 918, 840, 839, 762, 745, 648$. $\text{ESI-MS } (m/z)$ calculated $[\text{M}+\text{H}]^+$ for $\text{C}_{21}\text{H}_{19}\text{N}_3\text{Br}$ 392.0762, found 392.0769.

2-Aminopyridine (1.50 g, 15.94 mmol), 3-bromobenzaldehyde (2.95 g, 15.94 mmol, 1 eq), cyclohexyl isocyanide (1.74 g, 15.94 mmol, 1 eq)

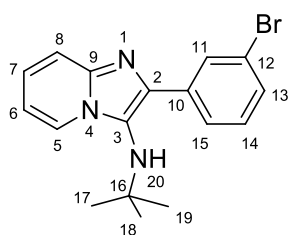


101

and Montmorillonite K10 clay (2.00 g) were combined and the general procedure followed. The mixture was purified by recrystallization from hot ether, resulting in a white powder that was found to be **101** (2.188 g, 37 %). $R_f = 0.34$ (50 % EtOAc/Hexane). $m.p.$ = 139 – 140 °C. $^1\text{H NMR}$ (300 MHz, CDCl_3): $\delta_H = 8.29$ (1H, t, $J = 1.8$ Hz, H-11), 8.07 (1H, dt, $J = 6.9$ and 1.2 Hz, H-5), 8.00

(1H, dt, $J = 7.8$, 1.4 Hz, H-15), 7.52 (1H, dt, $J = 9.1$ and 1.1 Hz, H-8), 7.43 (1H, ddd, $J = 8.0$, 2.0 and 1.1 Hz, H-13), 7.30 (1H, t, $J = 7.9$ Hz, H-14), 7.13 (1H, ddd, $J = 9.1$, 6.7 and 1.3 Hz, H-7), 6.78 (1H, td, $J = 6.7$ and 1.2 Hz, H-6), 3.03 (1H, d, $J = 4.9$ Hz, H-22), 3.01 – 2.90 (1H, m, H-16), 1.82 (2H, d, $J = 11.2$ Hz, H-17a and H-21a), 1.70 (2H, d, $J = 6.9$ Hz, H-18a and H-20a), 1.58 (1H, s, H-19a), 1.21 (5H, m, H-17b, H-18b, H-19b, H-20b and H-21b). $^{13}\text{C NMR}$ (75 MHz, CDCl_3): $\delta_C = 141.7$ (C-9), 136.7 (C-3), 135.2 (C-2), 130.1 (C-11), 131.0 (C-13 and C-14), 130.0 (C-10), 125.4 (C-15), 125.3, 124.2 (C-7), 122.8 (C-12), 122.7 (C-5), 117.6 (C-8), 111.8 (C-6), 57.0 (C-16), 34.3 (C-17 and C-21), 25.7 (C-19), 24.8 (C-18 and C-20). $\text{IR } (\nu_{\text{m}}, \text{cm}^{-1}) = 3258, 2922, 2851, 1634, 1595, 1572, 1508, 1447, 1362, 1335, 1225, 1219, 1070, 995, 970, 889, 851, 783, 735, 681$. $\text{ESI-MS } (m/z)$ calculated $[\text{M}+\text{H}]^+$ for $\text{C}_{19}\text{H}_{21}\text{N}_3\text{Br}$ 370.0919, found 370.0928.

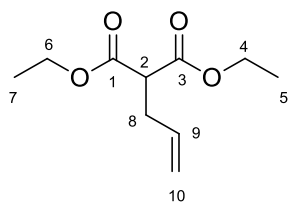
Experimental

**102**

Following the general procedure, 2-aminopyridine (1.00 g, 10.627 mmol), 3-bromobenzaldehyde (1.97 g, 10.627 mmol, 1 eq), *t*-butyl isocyanide (1.16 g, 10.627 mmol, 1 eq) and Montmorillonite K10 clay (1.00 g) were combined in ethanol. The resulting mixture was purified by recrystallization from hot ether. The

product was collected as yellow crystals and found to be **102** (2.301 g, 63 %). $R_f = 0.40$ (50 % EtOAc/Hexane). **m.p.** = 153 – 155 °C. $^1\text{H NMR}$ (300 MHz, CDCl_3): $\delta_{\text{H}} = 8.21$ (1H, t, $J = 1.8$ Hz, H-11), 8.15 (1H, dt, $J = 6.9$ and 1.2 Hz, H-5), 7.90 (1H, dt, $J = 7.7$, 1.3 Hz, H-15), 7.50 (1H, dt, $J = 9.0$ and 1.1 Hz, H-8), 7.41 (1H, ddd, $J = 8.0$, 2.1 and 1.1 Hz, H-13), 7.25 (1H, t, $J = 7.9$ Hz, H-14), 7.11 (1H, ddd, $J = 9.0$, 6.7, 1.3 Hz, H-7), 6.74 (1H, td, $J = 6.8$ and 1.2 Hz, H-6), 3.02 (1H, s, H-20), 1.04 (9H, s, H-17, H-18 and H-19). $^{13}\text{C NMR}$ (75 MHz, CDCl_3): $\delta_{\text{C}} = 142.2$ (C-9), 138.0 (C-3), 137.4 (C-2), 131.0 (C-11), 130.2 (C-13), 129.7 (C-14), 126.5 (C-15), 124.4 (C-7), 123.8 (C-10), 123.4 (C-5), 122.4 (C-12), 117.4 (C-8), 111.6 (C-6), 56.5 (C-16), 30.5 (C-17, C-18 and C-19). **IR** ($\nu_{\text{m}}\cdot\text{cm}^{-1}$) = 3305, 2972, 2922, 1629, 1595, 1560, 1541, 1504, 1471, 1442, 1386, 1190, 1068, 993, 929, 891, 856, 781, 754, 734, 719, 673, 605. **ESI-MS** (m/z) calculated $[\text{M}+\text{H}]^+$ for $\text{C}_{17}\text{H}_{19}\text{N}_3\text{Br}$ 344.0762, found 344.0770.

7.2.2. Tether synthesis

**103**

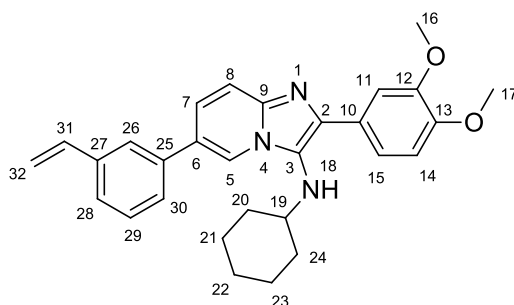
Diethyl malonate (5.00g, 31.217 mmol) was dissolved in 50 ml THF in a dry 2-necked round bottomed flask under and inert atmosphere. The solution was cooled to 0 °C in an ice bath before NaH (1.373 g, 34.339 mmol, 1.1 eq) was added portionwise. The solution was left stirring for 40 min at 0 °C before allyl bromide (5.665 g, 46.826 mmol, 1.5 eq) was added dropwise. The solution was allowed to warm to room temperature and stirred overnight. The resulting opaque yellow solution was extracted using brine, washed with ether (3 x 30 ml) and dried over anhydrous Na₂SO₄ before being concentrated *in vacuo*. The crude product was purified by distillation under reduced pressure and **103** was collected as a colourless oil (4.187 g, 67 %). ¹H NMR (300 MHz, CDCl₃): δ_H = 5.87 – 5.58 (1H, m, H-9), 5.19 – 5.02 (2H, m, H-10), 4.27 – 4.14 (4H, m, H-4 and H-6), 3.49 – 3.34 (1H, m, H-2), 2.64 (2H, m, H-8), 1.34 – 1.19 (6H, m, H-5 and H-7). ¹³C NMR (75 MHz, CDCl₃): δ_C = 168.9 (C-1 and C-3), 134.2 (C-9), 117.5 (C-10), 61.4 (C-4 and C-6), 51.7 (C-2), 32.9 (C-8), 14.1 (C-5 and C-7). IR (ν_m.cm⁻¹) = 3086, 2986, 2941, 1730, 1643, 1447, 1369, 1286, 1215, 1194, 1144, 1128, 1036, 1024, 920, 858, 642. ESI-MS (m/z) calculated for C₁₀H₁₇O₄, [M+H]⁺, 201.1127, found 201.1121.

7.2.3. Suzuki-Miyaura Cross Coupling reactions

Both the use of conventional heating and microwave irradiation was used to perform the Suzuki-Miyaura cross coupling reactions. Two general procedures are described that detail each method of reaction. The general procedure is described followed by the characterisation for the compounds synthesized using that method.

7.2.3.1. General Procedure for the Microwave assisted Suzuki-Miyaura coupling reactions

In a clean, unscratched microwave tube, the bromine-containing imidazo[1,2-*a*]pyridine (1 eq), 3-vinylphenylboronic acid (1.5 eq), CsF (2.5 eq) and Pd(PPh₃)₄ (10 mol %) were added and diluted with DME (3 ml). After adding a microwave stirrer bar and sealing the microwave tube, the mixture was reacted in a CEM Discover microwave oven at 150 °C, 150 W for 20 minutes. Once cooled, the contents were extracted with water and washed with EtOAc (3 x 30 ml). The organic layer was dried over anhydrous Na₂SO₄, concentrated *in vacuo* and purified by column chromatography with an appropriate eluent and the structure confirmed by ¹H NMR, ¹³C NMR, infrared and mass spectrophotometry.



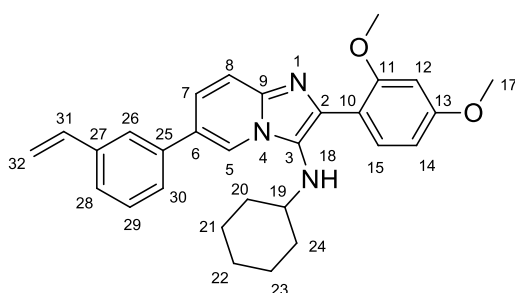
106

Imidazo[1,2-*a*]pyridine **85** (0.250 g, 0.581 mmol), 3-vinylphenylboronic acid (0.129 g, 0.871 mmol, 1.5 eq), Pd(PPh₃)₄ (0.0671 g, 0.0581 mmol, 10 mol %) and CsF (0.220 g, 1.452 mmol, 2.5 eq) were combined in a microwave tube and reacted using the microwave assisted general procedure. The product was purified by column chromatography with an eluent mixture

of 50-80 % EtOAc/Hexane. After concentration *in vacuo*, the yellow solid collected was found to be **106** (0.258 g, 97 %). *R_f* = 0.41 (50 % EtOAc/Hexane). *m.p.* = 142-143 °C. ¹H NMR (300 MHz, CDCl₃): δ_H = 8.28 (1H, dd, *J* = 1.8 and 1.0 Hz, H-5), 7.78 (1H, d, *J* = 8.5 Hz, H-14), 7.66 – 7.57 (2H, m, H-8 and H-26), 7.50 (1H, m, H-28*), 7.48 – 7.42 (2H, m, H-29* and H-30*), 7.37 (1H, dd, *J* = 9.3, 1.9 Hz, H-7), 6.81 (1H, dd, *J* = 17.6 and 10.9 Hz, H-31), 6.68 (1H, dd, *J* = 8.5 and 2.4 Hz, H-15), 6.59 (1H, d, *J* = 2.4 Hz, H-11), 5.91 – 5.79 (1H, m, H-32_{trans}), 5.33 (1H, d, *J* = 10.9 Hz, H-32_{cis}), 3.89 (3H, s, H-16[#]), 3.87 (3H, s, H-17[#]), 2.65 (1H, m, H-19), 1.71 (2H, dd, *J* = 10.5 and 4.2 Hz, H-20a and H-24a), 1.59 (2H, q, *J* = 4.4, 3.7 Hz, H-21a and H-23a), 1.54 – 1.44 (1H, m, H-22a), 1.06 (5H, m, H-20b, H-21b, H-22b, H-23b and H-24a). ¹³C NMR (75 MHz, CDCl₃): δ_C = 160.8 (C-12'), 157.0 (C-13'), 141.2

Experimental

(C-9), 138.7 (C-3), 138.5 (C-27), 136.7 (C-31), 134.30 (C-2), 132.4 (C-14), 129.4 (C-29*), 127.2 (C-25), 126.6 (C-28*), 125.6 (C-10), 125.4 (C-30*), 125.1 (C-26), 123.8 (C-7), 120.0 (C-5), 117.2 (C-8), 114.8 (C-32), 105.9 (C-15), 99.4 (C-11), 56.7 (C-16), 56.2 (C-16[#]), 55.6 (C-17[#]), 34.3 (C-20 and C-24), 25.8 (C-22), 24.9 (C-21 and C-23). **IR** ($\nu_{\text{m}} \cdot \text{cm}^{-1}$) = 3298, 2928, 2853, 1585, 1510, 1464, 1418, 1409, 1325, 1244, 1180, 1138, 1109, 1026, 908, 885, 798, 760, 721, 709, 627. **ESI-MS** (**m/z**) calculated for $\text{C}_{29}\text{H}_{32}\text{N}_3\text{O}_2$, $[\text{M}+\text{H}]^+$, 454.2495, found 454.2517.

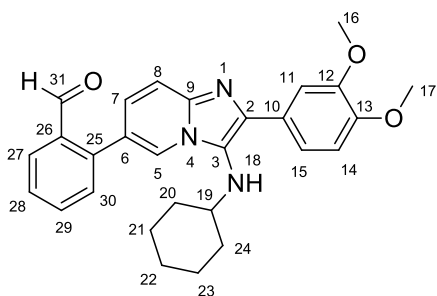
**107**

89 (0.250 g, 0.581 mmol), 3-vinylphenylboronic acid (0.129 g, 0.871 mmol, 1.5 eq), $\text{Pd}(\text{PPh}_3)_4$ (0.0671 g, 0.0581 mmol, 10 mol %) and CsF (0.220 g, 1.452 mmol, 2.5 eq) were combined and reacted according to the general procedure for microwave assisted reactions. The product was purified by column chromatography

with an eluent mixture of 80 % EtOAc/Hexane. After concentration *in vacuo*, the yellow solid that was collected was found to be **107** (0.215 g, 82 %). $R_f = 0.75$ (50 % EtOAc/Hexane). **m.p.** = 107 °C. **¹H NMR** (500 MHz, CDCl_3) $\delta_{\text{H}} = 8.30$ (1H, t, $J = 1.3$ Hz, H-5), 7.78 (1H, d, $J = 8.5$ Hz, H-15), 7.64 (1H, d, $J = 9.3$ Hz, H-8), 7.60 (1H, d, $J = 2.0$ Hz, H-26), 7.50 – 7.45 (1H, m, H-28[#]), 7.45 – 7.40 (2H, m, H-29[#] and H-30[#]), 7.38 (1H, dd, $J = 9.2$ and 1.8 Hz, H-7), 6.78 (1H, dd, $J = 17.6$ and 10.9 Hz, H-31), 6.65 (1H, dd, $J = 8.5$ and 2.4 Hz, H-14), 6.57 (1H, d, $J = 2.4$ Hz, H-12), 5.87 – 5.78 (1H, m, H-32_{trans}), 5.31 (1H, d, $J = 10.9$ Hz, H-32_{cis}), 3.92 (1H, d, $J = 7.78$ Hz, H-18), 3.85 (3H, s, H-16*), 3.83 (3H, s, H-17*), 2.74 – 2.65 (1H, m, H-19), 1.76 – 1.67 (2H, m, H-20a and H-24a), 1.62 – 1.54 (2H, m, H-21a and H-23a), 1.50 – 1.43 (1H, m, H-22a), 1.07 (5H, m, H-20b, H-21b, H-22b, H-23b, H-24b). **¹³C NMR** (126 MHz, CDCl_3) $\delta_{\text{C}} = 160.6$ (C-11'), 156.8 (C-13'), 140.5 (C-9), 138.2 (C-3), 138.1 (C-25), 136.4 (C-31), 133.5 (C-27), 132.1 (C-15), 129.1 (C-29[#]), 127.0 (C-2), 126.3 (C-28[#]), 125.7 (C-6), 125.2 (C-30[#]), 124.8 (C-26), 124.1 (C-7), 119.7 (C-5), 116.6 (C-8), 116.1 (C-10), 114.5 (C-32), 105.6 (C-14), 99.1 (C-12), 56.3 (C-19), 55.9 (C-16*), 55.2 (C-17*), 33.9 (C-20 and C-24), 25.5 (C-22), 24.6 (C-21 and C-23). **IR** ($\nu_{\text{m}} \cdot \text{cm}^{-1}$) = 3346, 2930, 2855, 1738, 1614, 1599, 1504, 1452, 1394, 1327, 1304, 1258, 1207, 1155, 1150, 1078, 1030, 1018, 918, 833, 800, 716, 632. **ESI-MS** (**m/z**) calculated for $\text{C}_{29}\text{H}_{32}\text{N}_3\text{O}_2$, $[\text{M}+\text{H}]^+$, 453.2495, found 454.2495.

7.2.3.2. General Procedure for the Conventional Suzuki-Miyaura Cross Coupling Reactions

The boronic acid (1.5 eq), Pd(PPh₃)₄ (10 mol %) and brominated imidazo[1,2-*a*]pyridine (1 eq) was added to a 2-neck round bottomed flask with a stirrer bar. To this a condenser was fitted to one neck and a rubber septum to the other neck and the set up evacuated and filled with N₂. This evacuation process was repeated 3 times, followed by the addition of DME and freshly prepared Na₂CO₃ (2M, 5 eq). The mixture was heated to reflux and stirred under a N₂ atmosphere overnight. After cooling, the reaction was filtered through Celite, washed with EtOAc, extracted with water and washed further with EtOAc. The organic layer was dried over anhydrous Na₂SO₄ and concentrated *in vacuo*. The product was then purified by column (or flash column) chromatography using EtOAc/Hexane as the eluent.



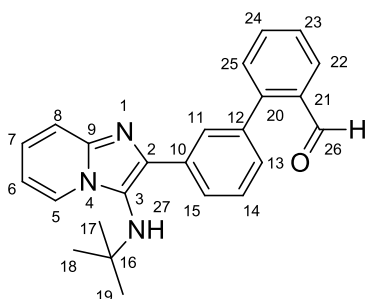
108

Using the general procedure for the conventionally heated Suzuki-Miyaura coupling reactions, **85** (0.250 g, 0.581 mmol), 2-formylphenylboronic acid (0.131 g, 0.871 mmol, 1.5 eq), Pd(PPh₃)₄ (0.0671 g, 0.0581 mmol, 10 mol %) and CsF (0.220 g, 1.452 mmol, 2.5 eq) were combined and reacted. The product was purified by column chromatography with an eluent mixture of 50-80 % EtOAc/Hexane and

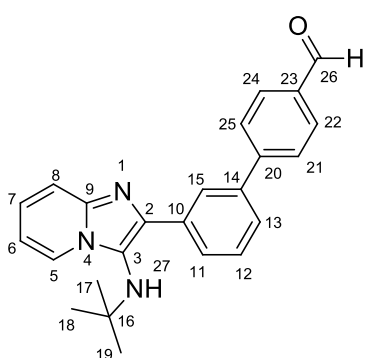
again using flash column chromatography with an eluent of 40 % EtOAc/Hexane. After concentration *in vacuo*, the green solid that was collected was found to be **108** (0.266 g, 99 %). *R_f* = 0.18 (50 % EtOAc/Hexane). *m.p.* = 170-173 °C. ¹H NMR (500 MHz, CDCl₃): δ_H = 10.09 (1H, d, *J* = 0.8 Hz, H-31), 8.09 (1H, dd, *J* = 1.8 and 1.0 Hz, H-5), 8.07 (1H, dd, *J* = 7.9 and 1.4 Hz, H-27), 7.73 – 7.68 (2 H, m, H-11 and H-29), 7.61 (1 H, dd, *J* = 9.2 and 1.0 Hz, H-8), 7.60 – 7.58 (1H, m, H-15), 7.56 (1 H, dt, *J* = 7.8 and 1.1 Hz, H-28), 7.52 (1H, dd, *J* = 7.7 and 1.1 Hz, H-30), 7.19 (1H, dd, *J* = 9.1 and 1.8 Hz, H-7), 6.97 (1H, d, *J* = 8.4 Hz, H-14), 4.01 (3H, s, H-16*), 3.95 (3H, s, H-17*), 3.16 – 3.09 (1H, m, H-18), 3.01 (1H, s, H-19), 1.82 (2H, dt, *J* = 12.2 and 3.0 Hz, H-20a and H-24a), 1.70 (2H, dt, *J* = 10.5 and 3.0 Hz, H-21a and H-23a), 1.58 (1H, dd, *J* = 10.8 and 4.1, H-22a), 1.24 – 1.10 (5H, m, H-20b, H-21b, H-22b, H-23b and H-24b). ¹³C NMR (125 MHz, CDCl₃): δ_C = 191.5 (C-31), 149.1 (C-12'), 148.7 (C-13'), 141.9 (C-25), 140.6 (C-9), 137.8 (C-3), 134.3 (C-2), 133.9 (C-11*), 131.0 (C-30), 128.4 (C-28), 128.3 (C-27), 127.2 (C-10), 126.1 (C-7), 124.6 (C-6), 122.6 (C, 122.2 (C-5), 119.4 (C-15), 116.8 (C-8), 111.1 (C-14), 110.5 (C-29*), 57.0 (C-19), 56.0 (C-16[#]), 55.9 (C-17[#]), 34.2 (C-20 and C-24), 25.7 (C-22), 24.8 (C-21 and C-23). IR (ν_m, cm⁻¹) = 3316, 2936, 2857, 1691, 1589, 1508, 1464,

Experimental

1408, 1404, 1323, 1252, 1225, 1130, 1020, 883, 812, 764, 716, 638. **ESI-MS (m/z)** calculated for $C_{28}H_{30}N_3O_3$, $[M+H]^+$, 456.2287, found 456.2289.

**109**

The general procedure was followed using **102** (1.00 g, 2.91 mmol), 2-formylphenyl boronic acid (0.653 g, 4.357 mmol, 1.5 eq), $Pd(PPh_3)_4$ (0.336 g, 0.291 mmol, 10 mol %) and Na_2CO_3 (2M, 7.26 ml, 5 eq). The reaction was heated under reflux for 18 hours and the product was purified by column chromatography using 50-60 % EtOAc/Hexane as the eluent. The product, **109**, was collected as a golden foam (1.109 g, 99 %). $R_f = 0.47$ (50 % EtOAc/Hexane). **m.p.** = 76-78 °C. 1H NMR (300 MHz, $CDCl_3$): $\delta_H = 10.04$ (1H, s, H-26), 8.22 (1H, d, $J = 6.9$ Hz, H-5), 8.06 – 8.02 (1H, m, H-11), 8.01 (2H, dd, $J = 3.5, 1.7$ Hz, H-22 and H-25), 7.68 – 7.60 (1H, m, H-14), 7.56 – 7.46 (4H, m, H-8, H-15, H-23 and H-24), 7.33 – 7.28 (1H, m, H-13), 7.17 – 7.09 (1H, m, H-7), 6.78 (1H, td, $J = 6.8$ Hz and $J = 1.0$ Hz, H-6), 3.08 (1H, s, N-H), 1.06 (9H, s, H-17, H-18 and H-19). ^{13}C NMR (75 MHz, $CDCl_3$): $\delta_C = 192.5$ (C-26), 146.1 (C-21), 142.2 (C-9), 139.0 (C-3), 137.9 (C-12), 135.8 (C-2), 133.8 (C-20), 133.5 (C-14), 130.9 (C-23*), 129.6 (C-10), 129.2 (C-13), 128.3 (C-25[#]), 127.9 (C-22[#]), 127.8 (C-24*), 127.4 (C-11), 124.2 (C-7), 123.8 (C-15), 123.5 (C-5), 117.4 (C-8), 111.5 (C-6), 56.5 (C-16), 30.4 (C-17, C-18 and C-19). **IR (v_m, cm⁻¹)** = 3367, 3055, 2968, 2843, 2754, 1681, 1593, 1546, 1504, 1473, 1444, 1390, 1365, 1340, 1284, 1218, 1197, 1093, 1026 906, 829, 808, 760, 706, 676, 640, 615, 607. **ESI-MS (m/z)** calculated for $C_{24}H_{24}N_3O$, $[M+H]^+$, 370.1919, found 370.1929.

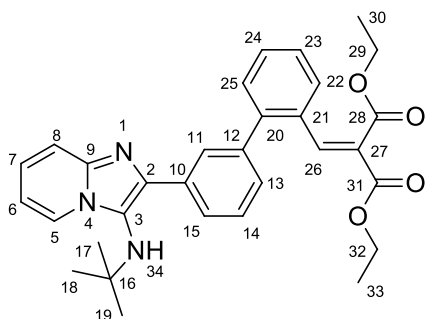
**110**

Compound **102** (1.00 g, 2.91 mmol), 4-formylphenyl boronic acid (0.653 g, 4.357 mmol, 1.5 eq), $Pd(PPh_3)_4$ (0.336 g, 0.291 mmol, 10 mol %) and Na_2CO_3 (2M, 7.26 ml, 5 eq) were combined according to the general conventional heating procedure. The reaction was purified by flash column chromatography using 0-60 % EtOAc/Hexane as the eluent. **110** was collected as a yellow powder (0.931 g, 87 %). $R_f = 0.4$ (50 % EtOAc/Hexane). **m.p.** = 73-76°C. 1H NMR (500 MHz, $CDCl_3$): $\delta_H = 10.03$ (1H, s, H-26), 8.32 (1H, 1H, s, H-15), 8.19 (1H, d, $J = 6.8$ Hz, H-5), 8.00 (1H, d, $J = 7.6$ Hz, H-8), 7.93 (2H, d, $J = 8.1$ Hz, H-21 and H-25), 7.82 (1H, d, $J = 8.1$ Hz, H-22 and H-24), 7.54 (1H, t, $J = 7.7$ Hz, H-11 and H-13), 7.48 (1H, t, $J = 7.7$ Hz, H-7), 7.14 – 7.08 (1H, m, H-12), 6.74 (1H,

Experimental

t, $J = 6.7$ Hz, H-6), 1.05 (s, 9H). $^{13}\text{C NMR}$ (126 MHz, CDCl_3): $\delta_{\text{C}} = 191.9$ (C-26), 147.2 (C-20), 142.1 (C-9), 139.6 (C-3), 139.0 (C-14), 136.1 (C-23), 135.1 (C-2), 130.2 (C-22 and C-24), 128.8 (C-12), 128.1 (C-13), 127.7 (C-21 and C-25), 127.1 (C-11), 126.2 (C-7), 124.1 (C-5), 123.7 (C-10), 123.4 (C-15), 117.3 (C-8), 111.4 (C-6), 56.4 (C-16), 30.4 (C-17, C-18 and C-19). **IR** ($\text{v}_{\text{m}}\cdot\text{cm}^{-1}$) = 3362, 2972, 2926, 1711, 1632, 1605, 1504, 1476, 1445, 1366, 1356, 1259, 1209, 1186, 1065, 1026, 910, 835, 799, 754, 748, 702. **ESI-MS** (m/z) calculated for $\text{C}_{24}\text{H}_{24}\text{N}_3\text{O}$, $[\text{M}+\text{H}]^+$, 370.1919, found 370.1924.

7.2.4. Knoevenagel condensation reaction



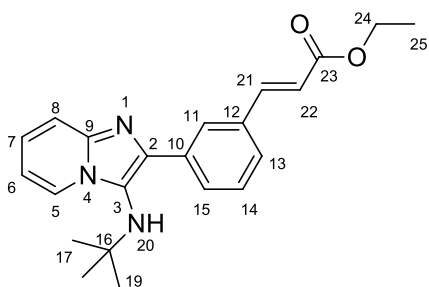
111

The general reaction for the Knoevenagel condensation was adapted from work by Gu and Holland.¹⁰⁶ In a 50 ml round bottomed flask, the imidazo[1,2-*a*]pyridine containing an aldehyde **109** (1.109g, 3.010 mmol), diethyl malonate (0.271 g, 0.258 ml, 4.515 mmol, 1.5 eq), piperidine (0.051 g, 0.060 ml, 0.602 mmol, 0.2 eq) and benzoic acid (0.037 g, 0.301 mmol, 0.1 eq) were combined and a Dean-Stark apparatus was fitted. To this set up

toluene (25 ml) was added and the system was heated under reflux under an N₂ atmosphere overnight. After cooling the reaction mixture was washed with water, 1M HCl, saturated NaHCO₃ and brine sequentially. The organic layer was then dried over anhydrous Na₂SO₄, concentrated *in vacuo* and purified by flash column chromatography using flash column chromatography using 80 % EtOAc/Hexane as the eluent. The product was collected as a yellow oil (1.06 g, 69 %). *R_f* = 0.72 (80 % EtOAc/Hexane). ¹H NMR (300 MHz, CDCl₃): δ_H = 8.19 (1H, d, *J* = 6.8 Hz, H-5), 8.00 (1H, s, H-26), 7.97 (1H, d, *J* = 3.8 Hz, H-25), 7.79 – 7.65 (1H, m, H-15), 7.53 – 7.19 (7H, m, H-8, H-11, H-13, H-14, H-22, H-23 and H-24), 7.08 (1H, t, *J* = 7.4 Hz, H-7), 6.71 (1H, t, *J* = 6.5 Hz, H-6), 4.28 (2H, q, *J* = 7.1 Hz, H-29*), 4.23 – 4.12 (2H, m, H-32*), 3.19 (1H, s, N-H), 1.27 – 1.14 (6H, m, H-30 and H-33), 1.04 (9H, d, *J* = 2.1 Hz, H-17, H-18 and H-19). ¹³C NMR (75 MHz, CDCl₃): δ_C = 166.4 (C-28[#]), 163.8 (C-31[#]), 143.4 (C-26), 142.7 (C-9), 142.0 (C-3), 139.8 (C-12), 139.1 (C-2), 135.7 (C-10), 132.1 (C-21), 130.1 (C-14*), 129.9 (C-24*), 129.1 (C-13*), 128.9 (C-23*), 128.3 (C-22*), 128.1 (C-15), 127.6 (C-27), 127.4 (C-11*), 127.3 (C-21), 124.0 (C-7), 123.8 (C-20), 123.5 (C-5), 117.2 (C-8), 111.3 (C-6), 61.4 (C-29'), 61.3 (C-32'), 56.3 (C-16), 30.3 (C-17, C-18 and C-19), 14.0 (C-30[~]), 13.9 (C-33[~]). IR (ν_m.cm⁻¹) = 3364, 2976, 2872, 1726, 1632, 1618, 1599, 1506, 1472, 1445, 1366, 1248, 1198, 1113, 1065, 1026, 920, 862, 808, 756, 706, 671, 623. ESI-MS (m/z) calculated for C₃₁H₃₄N₃O₄, [M+H]⁺, 512.2549, found 512.2550.

7.2.5. General Procedure for Heck Reactions

The Heck reaction was adapted from Riaan Petersen's thesis.¹⁰⁷ A 2-necked round bottom flask, fitted with a condenser and a dropping funnel, containing Pd(OAc)₂ (0.4 eq) and P(*o*-tolyl)₃ (1.6 eq) and a stirrer bar was evacuated and charged with N₂ repeatedly. Following this, a mixture of DMF (3 ml), MeCN (4 ml) and H₂O (2 ml) was added. The solution was stirred at 40 °C for approximately 30 min until the solution formed the catalyst complex (a yellow precipitate). The imidazo[1,2-*a*]pyridine (1 eq) was dissolved in 4 ml MeCN and added to the dropping funnel along with ethyl acrylate (1.5 eq) and NEt₃ (10 eq) and added to the catalyst solution. The dropping funnel was washed with 3 ml of DMF to ensure that all the starting materials had been successfully transferred to the dropping funnel removed from the flask and stoppered. The reaction mixture was heated to 78 °C and stirred under these conditions overnight. The mixture was extracted with water (30 ml) and washed with ether (30 ml). The organic phase was then washed with 6M HCl (2 x 30 ml). The acid layers were combined and neutralised with solid NaHCO₃ and, after being placed in a separating funnel, extracted with ether (2 x 30 ml) before being dried over anhydrous Na₂SO₄ and concentrated *in vacuo*.

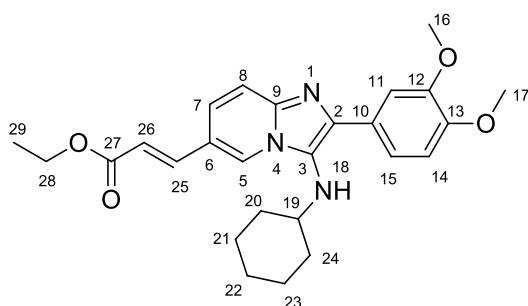


113

The catalyst was formed from Pd(OAc)₂ (0.078g, 0.350 mmol, 0.4 eq) and P(*o*-tolyl)₃ (0.426 g, 1.340 mmol, 1.6 eq). To this **102** (0.300 g, 0.874 mmol), ethyl acrylate (0.131 g, 1.311 mmol, 1.5 eq) and NEt₃ (0.944 g, 9.264 mmol, 10 eq) were added. After extraction and concentration *in vacuo*, the product **113** was collected as a yellow solid (0.297 g, 94 %). **R_f** = 0.5 (50 % EtOAc/Hexane). **m.p.** = 135 – 136 °C.

¹H NMR (300 MHz, CDCl₃): δ_H = 8.21 (1H, d, *J* = 1.8 Hz, H-11), 8.16 (1H, dt, *J* = 6.9 and 1.3 Hz, H-5), 7.99 (1H, dt, *J* = 7.3 and 1.7 Hz, H-15), 7.76 (1H, d, *J* = 16.0 Hz, H-21), 7.51 (1H, dt, *J* = 9.1 and 1.1 Hz, H-8), 7.46 – 7.34 (2H, m, H-13 and H-14), 7.09 (1H, ddd, *J* = 9.1, 6.6 and 1.3 Hz, H-7), 6.72 (1H, td, *J* = 6.8 and 1.2 Hz, H-6), 6.54 (1H, d, *J* = 16.0 Hz, H-22), 4.27 (2H, q, *J* = 7.1 Hz, H-24), 3.17 (1H, s, H-20), 1.33 (3H, t, *J* = 7.1 Hz, H-25), 1.02 (9H, s, H-17, H-18 and H-19). **¹³C NMR** (75 MHz, CDCl₃): δ_C = 167.0 (C-23), 144.7 (C-21), 142.1 (C-9), 138.6 (C-3), 136.1 (C-12), 134.4 (C-2), 129.9 (C-15), 128.6 (C-13*), 127.8 (C-11), 126.8 (C-14*), 124.1 (C-7), 123.7 (C-10), 123.4 (C-5), 118.3 (C-22), 117.3 (C-8), 111.4 (C-6), 60.4 (C-24), 56.3 (C-16), 30.4 (C-17, C-18 and C-19), 14.3 (C-25). **IR** (ν_m.cm⁻¹) = 3300, 3067, 2974, 1709, 1636, 1449, 1366, 1275, 1275, 1086, 1038, 986, 910, 868, 806, 754, 731, 689, 567. **ESI-MS** (**m/z**) calculated [M+H]⁺ for C₂₂H₂₆N₃O₂ 364.2025, found 364.2033.

Experimental

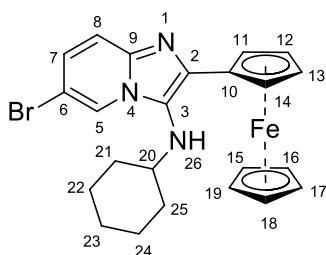
**114**

Imidazo[1,2-*a*]pyridine **85** (0.250 g, 0.581 mmol), ethyl acrylate (0.0582 g, 0.581 mmol, 1 eq) were added to the freshly formed catalyst from Pd(OAc)₂ (0.0521, 0.232 mmol, 0.4 eq) and P(*o*-tolyl)₃ (0.283 g, 0.930 mmol, 1.6 eq) with Et₃N (0.627 g, 6.159 mmol, 10.6 eq). After purification using the

acid extraction method, **114** was collected as a sticky red oil (0.143 g, 55 %). *R_f* = 0.36 (50 % EtOAc/Hexane). ¹H NMR (500 MHz, CDCl₃): δ_H = 8.18 – 8.14 (1H, m, H-5), 7.70 – 7.65 (2H, m, H-11 and H-25), 7.56 (1H, dd, *J* = 8.3 and 2.0 Hz, H-15), 7.51 – 7.48 (1H, m, H-8), 7.33 (1H, dd, *J* = 9.4 and 1.8 Hz, H-7), 6.94 (1H, d, *J* = 8.4 Hz, H-14), 6.40 (1H, d, *J* = 15.8 Hz, H-26), 4.29 (2H, q, *J* = 7.1 Hz, H-28), 3.99 (3H, s, H-16*), 3.93 (3H, s, H-17*), 3.11 (1H, s, H-18), 3.03 – 2.94 (1H, m, H-19), 1.86 – 1.77 (2H, m, H-20a and H-24a), 1.70 (2H, m, H-21a and H-23), 1.64 – 1.56 (1H, m, H-22a), 1.36 (3H, t, *J* = 7.1 Hz, H-29), 1.30 – 1.10 (5H, m, H-20b, H-21b, H-22b, H-23b and H-24b). ¹³C NMR (126 MHz, CDCl₃): δ_C = 166.8 (C-27), 149.0 (C-12[#]), 148.7 (C-13[#]), 141.22 (C-9), 141.17 (C-25), 137.7 (C-2), 127.0 (C-10), 124.9 (C-3), 124.6 (C-5), 121.0 (C-7), 119.8 (C-6), 119.4 (C-15), 117.8 (C-8), 117.4 (C-26), 111.1 (C-14), 110.4 (C-11), 60.7 (C-28), 56.9 (C-19), 56.0 (C-16*), 55.9 (C-17*), 34.2 (C-20 and C-24), 25.7 (C-22), 24.8 (C-21 and -23), 14.4 (C-29). IR (ν_m·cm⁻¹) = 3339, 2928, 2851, 2363, 1707, 1634, 1508, 1462, 1418, 1312, 1256, 1235, 1174, 1140, 1032, 979, 852, 806, 764, 733. ESI-MS (*m/z*) calculated for C₂₆H₃₂N₃O₄, [M+H]⁺, 450.2393, found 450.2400.

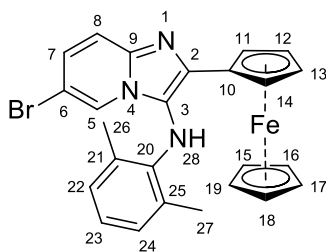
7.2.6. Synthesis of ferrocene-containing imidazo[1,2-*a*]pyridines

The synthesis of ferrocene-containing imidazo[1,2-*a*]pyridines **115** to **117** were synthesized according to the general procedure for Groebke-Blackburn-Bienaymé Multicomponent Reactions (Section 7.2.1.) using ferrocenecarbaldehyde.



115

2-Amino-5-bromopyridine (1.5 g, 8.67 mmol), ferrocenecarboxaldehyde (1.86 g, 8.67 mmol, 1 eq), cyclohexyl isocyanide (0.945 g, 8.67 mmol, 1 eq) and Montmorillonite K10 clay (1.5 g) were combined and the general procedure followed. The product purified by recrystallization in an ether/methanol mixture. Orange crystals and salmon powder were collected and found to be **115** (2.42 g, 55 %). $R_f = 0.77$ (50 % EtOAc/Hexane), **m.p.** = 197-199 °C, $^1\text{H NMR}$ (300 MHz, CDCl_3): $\delta_H = 8.19$ (1H d, $J = 1.1$ Hz, H-5), 7.38 (1H, d, $J = 9.4$ Hz, H-8), 7.14 (1H, dd, $J = 9.4$ and $J = 1.8$ Hz, H-7), 4.92 – 4.87 (2H, m, H-11 and H-14), 4.38 – 4.34 (2H, m, H-12 and H-13), 4.08 (5H, s, H-15, H-16, H-17, H-18 and H-19), 3.14 (1H, d, $J = 3.7$ Hz, H-20), 2.92 (1H, d, $J = 4.0$ Hz, H-26), 1.88 (2H, d, $J = 9.7$ Hz, H-21a and H-25a), 1.79 (2H, d, $J = 6.5$ Hz, H-22a and H-24a), 1.67 (1H, d, $J = 6.5$ Hz, H-23a), 1.42 – 1.16 (5H, m, H-21b, H-22b, H-23b, H-24b and H-25b). $^{13}\text{C NMR}$ (75 MHz, CDCl_3): $\delta_C = 140.0$ (C-9), 137.7 (C-3), 126.6 (C-7), 124.0 (C-2), 122.5 (C-5), 117.3 (C-8), 106.1 (C-6), 78.3 (C-10), 69.3 (C-15, C-16, C-17, C-18, C-19), 68.8 (C-12 and C-13), 66.9 (C-11 and C-14), 57.2 (C-20), 34.2 (C-21 and C-25), 25.7 (C-23), 25.0 (C-22 and C-24). **IR** ($\nu_{\text{m.cm}^{-1}}$) = 3315, 3099, 2922, 2852, 1573, 1446, 1392, 1340, 1315, 1236, 1176, 1120, 1103, 1001, 943, 823, 783, 732, 667. **ESI-MS** (**m/z**) calculated for $\text{C}_{23}\text{H}_{25}\text{FeN}_3\text{Br}$, $[\text{M}+\text{H}]^+$, 478.0581, found 478.0592.

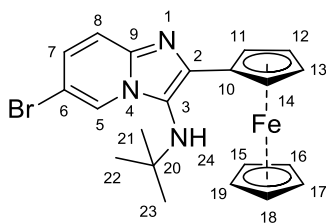


116

The general procedure was followed using 2-amino-5-bromopyridine (2.00 g, 11.56 mmol), ferrocenecarboxaldehyde (2.47 g, 11.56 mmol, 1 eq), xylyl isocyanide (1.52 g, 11.56 mmol, 1 eq) and Montmorillonite K10 clay (2.00 g). The product purified by recrystallization from hot EtOAc. Brown crystals were collected and found to be **116** (0.17 g, 3 %). $R_f = 0.62$ (50 % EtOAc/Hexane). **m.p.** = >300 °C. $^1\text{H NMR}$ (300 MHz, CDCl_3): $\delta_H = 7.93$ (1H, s, H-5), 7.46 (1H, d, $J = 9.5$ Hz, H-8), 7.20 (1H, d, $J = 9.1$ Hz, H-7), 7.06 (2H, d, $J = 7.3$ Hz, H-22 and H-24), 6.87 (1H, t, $J = 7.4$ Hz, H-23), 5.12 (1H, s, H-28), 4.70 (2H, s, H-11 and H-14), 4.27 (2H, s, H-12 and H-13), 4.03

Experimental

(5H, s, H-15, H-16, H-17, H-18 and H-19), 2.06 (6H, s, H-26 and H-27). ^{13}C NMR not available due to a lack of solubility. IR ($\nu_{\text{m}}\cdot\text{cm}^{-1}$) = 3315, 3099, 2922, 2852, 1573, 1446, 1392, 1340, 1315, 1236, 1176, 1120, 1103, 1001, 943, 823, 783, 732, 667. ESI-MS (m/z) calculated for $\text{C}_{25}\text{H}_{23}\text{FeN}_3\text{Br}$, $[\text{M}+\text{H}]^+$, 500.0425, found 500.0428.

**117**

Following the general procedure 2-Amino-5-bromopyridine (1.50 g, 8.67 mmol), ferrocenecarboxaldehyde (1.86 g, 8.67 mmol, 1 eq), *t*-butyl isocyanide (0.72 g, 8.67 mmol, 1 eq) and Montmorillonite K10 clay (1.50 g) were combined, reacted and then purified by recrystallization from hot ether. Beige crystals were collected and found to be **117**

(3.01 g, 72 %). R_f = 0.69 (50 % EtOAc/Hexane). **m.p.** = 201 - 202 °C. ^1H NMR (300 MHz, CDCl_3): δ_{H} = 8.28 (1H, d, J = 1.2 Hz, H-5), 7.40 (1H, d, J = 9.4 Hz, H-8), 7.14 (1H, dd, J = 9.4 and 1.9 Hz, H-7), 4.92 – 4.80 (2H, m, H-11 and H-14), 4.38 – 4.29 (2H, m, H-12 and H-13), 4.10 (5H, s, H-15, H-16, H-17, H-18 and H-19), 2.89 (1H, s, H-24), 1.13 (9H, s, H-21, H-22 and H-23). ^{13}C NMR (75 MHz, CDCl_3): δ_{C} = 140.5 (C-9), 139.6 (C-3), 126.7 (C-7), 123.3 (C-5), 123.1 (C-2), 117.4 (C-8), 105.7 (C-6), 79.3 (C-10), 69.4 (C-15, C-16, C-17, C-18 and C-19), 68.4 (C-12 and C-13), 68.0 (C-11 and C-14), 56.2 (C-20), 30.5 (C-21, C-22 and C-23). IR ($\nu_{\text{m}}\cdot\text{cm}^{-1}$) = 3315, 3103, 2972, 2950, 2895, 1573, 1469, 1402, 1388, 1323, 1224, 1124, 1105, 1022, 939, 819, 796, 717, 671, 628. ESI-MS (m/z) calculated for $\text{C}_{21}\text{H}_{23}\text{N}_3\text{FeBr}$, $[\text{M}+\text{H}]^+$, 452.0425, found 452.0443.

7.2.7. General procedure for the synthesis of isocyanides used in the Groebke-Blackburn-Bienaymé multicomponent coupling reaction

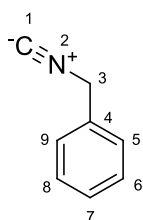
General procedure for involves a two-step synthesis where the desired amine is formylated and then dehydrated resulting in the formation of the substituted isocyanide.

7.2.7.1. Step One: formylation of the amine

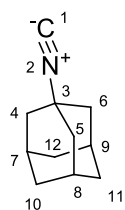
The appropriate amine is stirred in excess acetic anhydride in a round bottomed flask with 2 equivalents of formic acid under an inert atmosphere for 18 hours. Following which the contents of the flask were emptied into a 100 ml beaker and washed with water. The solution was neutralized by a slow addition of solid NaHCO_3 before being washed with EtOAc three times in a separation funnel. The organic layer was dried over anhydrous Na_2SO_4 , concentrated *in vacuo* and continued to the next step without further purification.

7.2.7.2. Step Two: dehydration to form the isocyanide

In a large two necked round bottomed flask fitted with a dropping funnel, the formylated amine was dissolved in dry DCM under an inert atmosphere. To this 10 equivalents of NEt_3 was added and the solution cooled to 0 °C in an ice bath. POCl_3 (3 eq) was added dropwise to this solution at 0 °C. The solution was then allowed to warm to room temperature and stirred under N_2 for a further 2 hours. The reaction was quenched by the slow addition of saturated NaHCO_3 , transferred to a separating funnel and washed three times with DCM. The organic layer was dried over anhydrous Na_2SO_4 , concentrated *in vacuo* and purified by column chromatography. It was noted that some decomposition occurs with the isocyanide on silica so purification methods need to be highly optimised to obtain the maximum yield.



The general procedure was followed using benzyl amine (3.00 g, 28.00 mmol), formic acid (2.58 g, 56.00 mmol, 2 eq), NEt_3 (24.66 g, 0.244 mol, 10 eq) and POCl_3 (11.21 g, 73.11 mmol 3 eq). Following purification by column chromatography with 0 – 50 % EtOAc/Hexane as the eluent, benzyl isocyanide was collected as a pungent yellow oil (1.56 g, 55 %). $^1\text{H NMR}$ (300 MHz, CDCl_3) δ_{H} = 7.44 – 7.27 (5H, m, H-5, H-6, H-7, H-8 and H-9), 4.74 – 4.45 (2H, m, H-3). $^{13}\text{C NMR}$ (75 MHz, CDCl_3) δ_{C} = 157.7 (t, C-1), 132.4 (C-4), 129.0 (C-5 and C-9), 128.4 (C-6 and C-8), 126.6 (C-7), 45.6 (t, C-3).

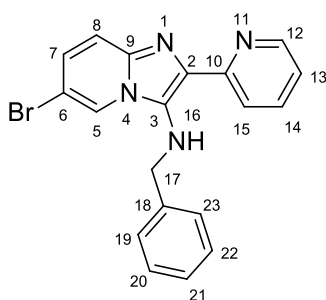
Experimental

Adamantylamine (1.00 g, 6.61 mmol), formic acid (0.608 g, 13.22 mmol, 2 eq), NEt_3 (6.21 g, 61.4 mmol, 10 eq) and POCl_3 (2.82 g, 5.94 mmol, 3 eq) were used following the general procedure. The adamantyl isocyanide was collected as a white powder (0.696 g, 97 %) after purification by column chromatography with 10 %

EtOAc/Hexane as the eluent and concentration *in vacuo*. $^1\text{H NMR}$ (300 MHz, MeOD) $\delta_{\text{H}} = 3.32$ (3H, p, $J = 1.6$ Hz, H-7, H-8 and H-9), 1.78 – 1.61 (12H, m, H-4, H-5, H-6, H-10, H-11 and H-12). $^{13}\text{C NMR}$ (75 MHz, MeOD) $\delta_{\text{C}} = 184.8$ (C-1), 49.1 (C-3), 45.3 (C-4, C-5 and C-6), 37.2 (C-10, C-11 and C-12), 31.0 (C-7, C-8 and C-9).

7.2.8. Synthesis of pyridyl-containing imidazo[1,2-*a*]pyridines for metal complexation reactions

The general procedure for the Groebke-Blackburn-Bienaymé multicomponent reactions (section 7.2.1) to synthesize the pyridyl-containing imidazo[1,2-*a*]pyridines. Reactions were performed in ethanol under reflux conditions overnight. The compounds were purified by recrystallization or column chromatography as appropriate. Spectroscopic characterisation for these compounds is outlined below.

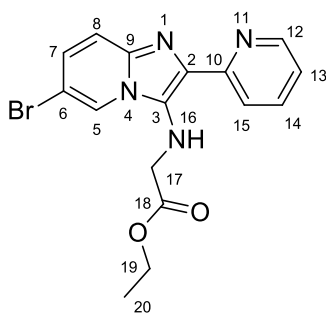


124

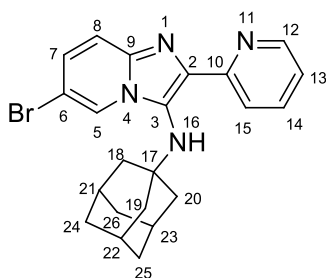
Combining 5-bromo-2-aminopyridine (2.304 g, 13.317 mmol), benzyl isocyanide (1.56 g, 13.317 mmol, 1 eq) and pyridinecarbaldehyde (1.27 ml, 13.317 mmol, 1 eq) with Montmorillonite K10 clay (2.30 g) and following the general procedure with EtOH as the solvent resulted in **124** (2.037 g, 40 %), which was collected as a mustard yellow powder after recrystallization from ether. $R_f = 0.57$ (50 % EtOAc/Hexane). **m.p.** = 121 °C. $^1\text{H NMR}$ (500

MHz, CDCl_3) δ 8.53 – 8.48 (1H, m, H-12), 8.13 (1H, d, $J = 8.0$ Hz, H-15), 8.10 (1H, d, $J = 1.0$ Hz, H-5), 7.74 (1H, td, $J = 7.8$ and 1.8 Hz, H-14), 7.41 (1H, dd, $J = 9.5$ and 0.9 Hz, H-8), 7.40 – 7.36 (2H, m, H-19 and H-23), 7.33 – 7.28 (2H, m, H-20 and H-22), 7.28 – 7.23 (1H, m, H-21), 7.16 – 7.11 (2H, m, H-7 and H-13) 6.53 (1H, t, $J = 7.1$ Hz, H-16), 4.24 (2H, d, $J = 6.8$ Hz, H-17). $^{13}\text{C NMR}$ (126 MHz, CDCl_3) δ 154.5 (C-10), 148.6 (C-12), 140.1 (C-9), 136.6 (C-14), 131.9 (C-3), 131.3 (C-2), 128.5 (C-20 and C-22), 128.1 (C-19 and C-23), 127.5 (C-7*), 126.9 (C-18), 122.8 (C-5), 121.5 (C-13*), 120.3 (C-15), 118.5 (C-8), 106.8 (C-6), 51.4 (C-17). **IR** ($\nu_{\text{m}} \cdot \text{cm}^{-1}$) = 3302, 3028, 2930, 2856, 1589, 1516, 1477, 1429, 1396, 1352, 1317, 1290, 1251, 1226, 1110, 1037, 995, 931, 790, 733, 798, 663, 628, 617. **ESI-MS** (**m/z**) calculated $[\text{M}+\text{H}]^+$ for $\text{C}_{19}\text{H}_{16}\text{N}_4\text{Br}$ 379.0558, found 379.0544.

Experimental

**125**

2-Amino-5-bromopyridine (1.835 g, 10.609 mmol), 2-pyridinecarboxaldehyde (1.01 ml, 10.609 mmol, 1 eq), ethyl isocyanoacetate (1.20 g, 10.609 mmol, 1 eq) and Montmorillonite K10 clay (1.80 g) were combined and the general procedure followed. The resulting mixture was purified by recrystallization from a DCM/Hexane mixture to afford **125** as mustard flakes (1.763 g, 44 %). $R_f = 0.23$ (50 % EtOAc/Hexane). **m.p.** = 142 - 144 °C. $^1\text{H NMR}$ (300 MHz, CDCl_3): $\delta_H = 8.59$ (1H, ddd, $J = 4.9$ Hz, $J = 1.8$ Hz and $J = 0.9$ Hz, H-12), 8.23 (1H, dd, $J = 1.9$ Hz and $J = 0.9$ Hz, H-15), 8.15 (1H, dt, $J = 8.0$ Hz and $J = 1.1$ Hz, H-5), 7.80 – 7.72 (1H, m, H-7), 7.43 (1H, dd, $J = 9.5$ Hz and $J = 0.8$ Hz, H-14), 7.21 – 7.12 (2H, m, H-8 and H-13), 6.50 (1H, t, $J = 6.5$ Hz, N-H), 4.18 (2H, q, $J = 7.2$ Hz, H-19), 3.89 (2H, d, $J = 6.6$ Hz, H-17), 1.25 – 1.19 (3H, m, H-20). $^{13}\text{C NMR}$ (75 MHz, CDCl_3): $\delta_C = 170.6$ (C-18), 154.2 (C-10), 148.8 (C-12), 139.3 (C-9), 136.7 (C-7), 131.9 (C-3), 130.5 (C-2), 127.1 (C-13*), 122.8 (C-15), 121.7 (C-8*), 120.5 (C-5), 118.6 (C-14), 107.0 (C-6), 61.2 (C-17), 48.6 (C-19), 14.1 (C-20). **IR** (ν_{max} , cm^{-1}) = 3199, 3087, 2976, 2927, 2904, 1735, 1591, 1548, 1481, 1431, 1396, 1371, 1340, 1317, 1238, 1207, 1110, 1097, 1024, 995, 958, 871, 794, 746, 696, 632. **ESI-MS** (m/z) calculated for $\text{C}_{16}\text{H}_{16}\text{N}_4\text{O}_2\text{Br}$, $[\text{M}+\text{H}]^+$, 375.0458, found 375.0449.

**126**

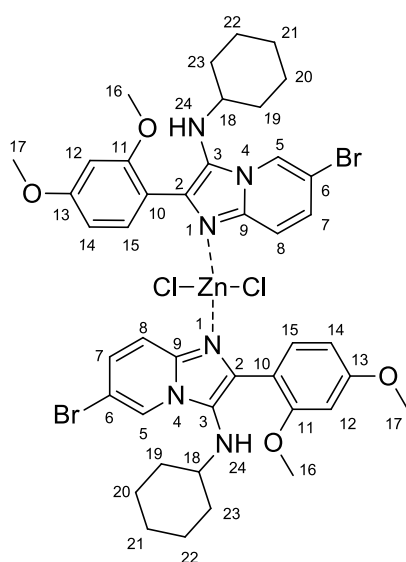
The general procedure was followed using 2-amino-5-bromopyridine (0.322 g, 1.863 mmol), 2-pyridinecarboxaldehyde (0.177 ml, 1.863 mmol, 1 eq), adamantyl isocyanide (0.300 g, 1.863 mmol, 1 eq) and Montmorillonite K10 clay (0.50 g). The resulting mixture was purified by flash column chromatography using 30-50 % EtOAc/Hexane as an eluent. The product, **126** was collected as a yellow powder (0.738 g, 94 %). $R_f = 0.50$ (50 % EtOAc/Hexane). **m.p.** = 159 - 162 °C. $^1\text{H NMR}$ (500 MHz, CDCl_3): $\delta_H = 8.57$ (1H, ddd, $J = 4.9$ Hz, $J = 1.8$ Hz and $J = 1.0$ Hz, H-12), 8.44 (1H, dd, $J = 1.9$ Hz and $J = 0.9$ Hz, H-5), 8.16 – 8.12 (1H, m, H-15), 7.76 (1H, td, $J = 7.7$ Hz and $J = 1.8$ Hz, H-14), 7.40 (1H, dd, $J = 9.5$ Hz and $J = 0.9$ Hz, H-8), 7.18 (1H, ddd, $J = 7.6$ Hz, $J = 4.9$ and $J = 1.2$ Hz, H-13), 7.14 (1H, dd, $J = 9.5$ Hz and $J = 1.9$ Hz, H-7), 5.39 (1H, s, N-H), 2.00 – 1.96 (3H, m, H-21, H-22 and H-23), 1.71 (6H, d, $J = 2.9$ Hz, H-18, H-19 and H-20), 1.58 (3H, d, $J = 12.7$ Hz, H-24, H-25a), 1.55 – 1.49 (3H, m, H-25b and H-26). $^{13}\text{C NMR}$ (126 MHz, CDCl_3) $\delta_C = 154.7$ (C-10), 148.3 (C-12), 140.0 (C-9), 136.5 (C-14), 135.7 (C-3), 128.2 (C-2), 127.2 (C-7), 124.4 (C-5), 121.9 (C-13), 121.3 (C-15), 118.1 (C-8), 106.2 (C-6), 57.7 (C-17), 43.5 (C-

Experimental

18, C-19 and C-20), 36.2 (C-24, C-25 and C-26), 29.8 (C-21, C-22 and C-23). **IR** ($\nu_{\text{m.cm}^{-1}}$) = 3303, 2904, 2849, 1591, 1568, 1476, 1425, 1395, 1321, 1288, 1229, 1199, 1103, 1088, 1045, 920, 842, 787, 743, 696, 603. **ESI-MS** (**m/z**) calculated for $\text{C}_{22}\text{H}_{24}\text{N}_4\text{Br}$, $[\text{M}+\text{H}]^+$, 423.1184, found 423.1180.

7.2.9. General procedure for the synthesis of metal-imidazo[1,2-*a*]pyridine complexes

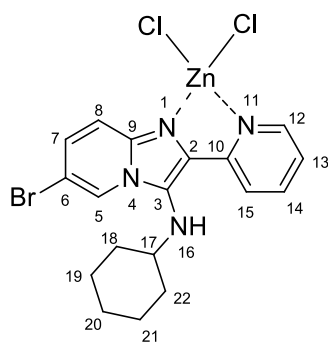
The general procedure for metal co-ordination was loosely based off of a procedure by Steffen and Palenik.¹¹² This procedure initially was performed in ethanol, however the copper-containing complexes were too soluble in ethanol so this procedure was adapted accordingly. In an appropriately sized round bottom flask, the relevant imidazo[1,2-*a*]pyridine was dissolved in ether. Metal salt (1 eq) was added to the solution and the reaction stirred overnight at room temperature. With time a precipitate forms and is collected by gravity filtration and washed with ether and recrystallized using an appropriate method. This method was used unless otherwise stated.



119

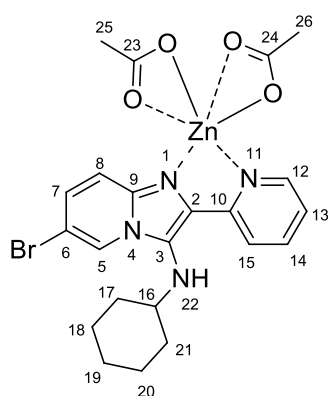
89 (0.100 g, 0.232 mmol), zinc(II) chloride (0.015 g, 0.116 mmol, 1 eq) and triethyl orthoformate (0.138 g, 0.929 mmol, 4 eq) were combined and refluxed in ethanol overnight resulting in the formation of a cream powder that was collected by gravity filtration and dried. After vapour diffusion recrystallization from EtOAc/hexane, the structure of **119** was confirmed by single crystal X-ray crystallography (0.117 g, 99 %). IR ($\nu_{\text{m}}\cdot\text{cm}^{-1}$) = 3289, 3090, 2932, 2855, 1603, 1528, 1503, 1474, 1412, 1331, 1294, 1238, 1092, 1049, 843, 789, 758, 712, 648, 546.

Experimental

**120**

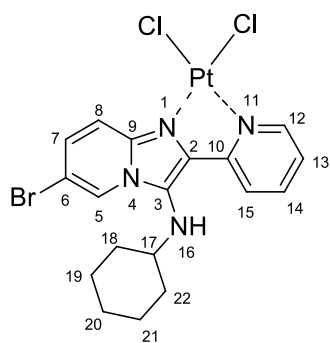
1144, 1097, 1047, 1042, 843, 789, 806, 758, 711, 685, 648, 546.

* The complex was not significantly soluble in $CDCl_3$ or d_4 -MeOD to obtain a good NMR. The complex was soluble in d_6 -DMSO however, significant exchange occurred between the d_6 -DMSO and the complex so the NMR could not be sufficiently resolved.

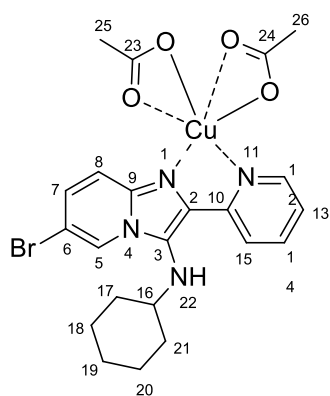
**121**

Using the general procedure, **88** (0.200 g, 0.539 mmol) and zinc(II) acetate monohydrate (0.099g, 0.539 mmol, 1 eq) were combined in ether with a few drops of EtOH resulting in a white powder. After recrystallization by slow evaporation from isopropyl alcohol, the structure of the complex **121** was confirmed by single crystal X-ray crystallography and NMR spectroscopy (0.149 g, 50 %). 1H NMR (500 MHz, $CDCl_3$) δ_H = 8.87 (1H, d, J = 5.1 Hz, H-12), 8.22 (1H, s, H-5), 8.01 (1H, d, J = 8.0 Hz, H-15), 7.93 (1H, d, J = 9.0 Hz, H-8), 7.89 (1H, t, J = 7.8 Hz, H-14), 7.40 (1H, t, J = 6.4 Hz, H-13), 7.31 (1H, d, J = 9.5 Hz, H-7), 3.80 (1H, s, H-22), 2.82 (1H, s, H-16), 2.10 (6H, s, H-25 and H-26), 1.85 – 1.70 (5H, m, H-17a, H-18a, H-19a, H-20a and H-21a), 1.32 (2H, q, J = 11.1 Hz, H-18b and H-20b), 1.17 (3H, t, J = 9.8 Hz, H-17b, H-19b and H-21b). ^{13}C NMR (126 MHz, $CDCl_3$) δ_C = 180.6 (C-23 and C-24), 149.8 (C-12), 147.2 (C-9), 139.6 (C-3), 139.4 (C-14), 131.9 (C-7), 130.4 (C-10), 127.8 (C-2), 124.3 (C-13), 123.3 (C-5), 121.2 (C-15), 118.5 (C-8), 109.4 (C-6), 57.8 (C-16), 34.4 (C-18 and C-20), 25.4 (C-19), 25.0 (C-17 and C-21), 22.1 (C-25 and C-26). IR ($\nu_m \cdot cm^{-1}$) = 3259, 3074, 2923, 2854, 1581, 1406, 1332, 1236, 1092, 1047, 1015, 822, 798, 758, 674, 618.

Experimental

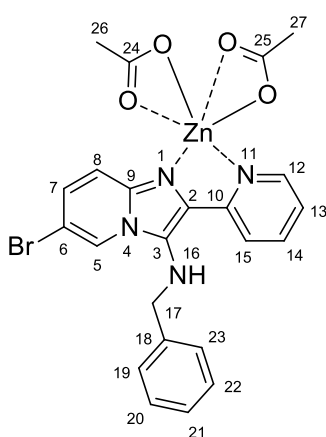
**122**

In a 10 ml round bottomed flask, **88** (0.100 g, 0.269 mmol, 1.1 eq) and PtCl_2 (0.065 g, 0.245 mmol) were combined with 2 ml DMF and triethyl orthoformate (0.199 g, 1.345 mmol, 5 eq) and refluxed overnight. This resulted in the formation of a mustard yellow powder that following characterisation by NMR spectroscopy was determined to be **122** (0.190 g, 99 %). $^1\text{H NMR}$ (500 MHz, $\text{DMSO-}d_6$) $\delta_{\text{H}} = 9.39$ (1H, d, $J = 6.0$ Hz, H-12), 8.82 (1H, d, $J = 2.0$ Hz, H-5), 8.77 – 8.71 (1H, m, H-8), 8.31 (1H, td, $J = 7.7$ and 1.7 Hz, H-14), 8.15 (1H, d, $J = 8.0$ Hz, H-15), 7.73 (1H, dd, $J = 9.8$ and 2.0 Hz, H-7), 7.58 (1H, td, $J = 6.9$, 6.2 and 1.7 Hz, H-13), 5.59 (1H, d, $J = 8.0$ Hz, H-16), 3.04 – 2.91 (1H, m, H-17), 1.88 (2H, d, $J = 12.1$ Hz, H-18a and H-22a), 1.68 (2H, $J = 12.1$ Hz, H, H-19a and H-21a), 1.55 (1H, d, $J = 10.7$ Hz, H-20a), 1.38 (2H, q, $J = 11.7$ Hz, H-18b and H-22b), 1.16 (3H, h, $J = 12.7$ Hz, H-19b, H-20b and H-21b). $^{13}\text{C NMR}$ (126 MHz, DMSO) $\delta_{\text{C}} = 152.6$ (C-9), 148.2 (C-12), 141.4 (C-3), 139.9 (C-14), 134.0 (C-10), 132.9 (C-7), 130.5 (C-2), 125.1 (C-5), 124.4 (C-13), 121.8 (C-15), 116.3 (C-8), 108.5 (C-6), 57.7 (C-17), 33.5 (C-18 and C-22), 25.1 (C-20), 24.7 (C-19 and C-21).

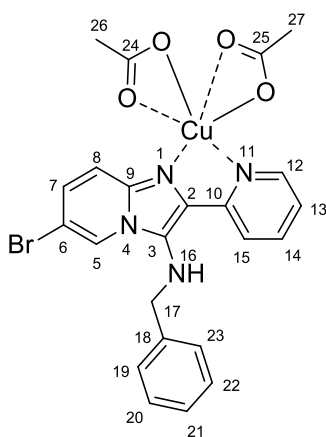
**123**

88 (0.200 g, 0.539 mmol) and copper(II) acetate monohydrate (0.106g, 0.539 mmol, 1 eq) were combined following the general procedure. The product purified by recrystallization from DCM to afford **123**. The structure of the complex was confirmed by single crystal X-ray crystallography (0.708 g, 99 %). IR ($\nu_{\text{m}}, \text{cm}^{-1}$) = 3444, 3252, 3076, 2925, 2856, 1571, 1500, 1389, 1329, 1245, 1098, 1047, 1020, 784, 755, 674, 619.

Experimental

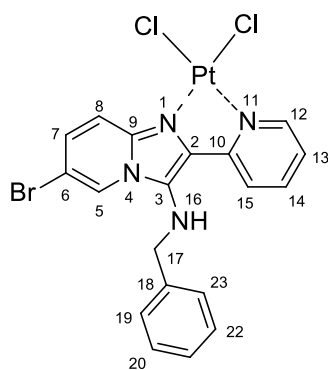
**127**

124 (0.500 g, 1.319 mmol) and zinc(II) acetate monohydrate (0.290 g, 1.319 mmol, 1 eq) were combined according to the general procedure with the addition of a few drops of EtOH. The complex **127** was collected as a light yellow powder. After vapour diffusion recrystallization from *d*₄-MeOD and ether, the structure of the complex was confirmed by single crystal X-ray crystallography (0.483 g, 65 %). ¹H NMR (500 MHz, CDCl₃) δ_H = 8.80 (1H, s, H-12), 7.90 – 7.80 (2H, m, H-5 and H-15), 7.75 (1H, s, H-8), 7.70 (1H, td, *J* = 7.8, 1.7 Hz, H-14), 7.30 (1H, d, *J* = 6.5 Hz, H-13), 7.26 – 7.22 (3H, m, H-7, H-19 and H-23), 7.16 (3H, td, *J* = 9.1, 3.5 Hz, H-20, H-21 and H-22), 4.88 (1H, s, N-H), 4.07 (2H, d, *J* = 6.1 Hz, H-17), 2.06 (6H, s, H-26 and H-27). ¹³C NMR (126 MHz, CDCl₃) δ_C = 180.7 (C-24 and C-25), 149.5 (C-12), 146.7 (C-9), 139.4 (C-14), 138.3 (C-3), 131.9 (C-18 and C-10), 129.9 (C-17), 128.9 (C-19 and C-23), 128.8 (C-21), 128.1 (C-20 and C-22), 124.2 (C-13), 123.5 (C-8), 121.0 (C-5*), 118.0 (C-15*), 109.0 (C-6), 52.6 (C-17), 22.1 (C-26 and C-27). IR (ν_m, cm⁻¹) = 3271, 3072, 3018, 1577, 1407, 1329, 1232, 1038, 1016, 810, 781, 740, 675, 619.

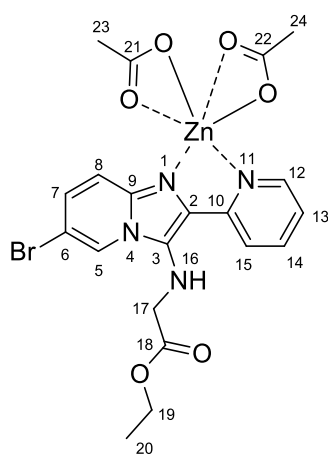
**128**

The general procedure was followed using **124** (0.200 g, 0.527 mmol) and copper(II) acetate monohydrate (0.116 g, 0.570 mmol, 1.1 eq). After collection of the green powder, the product **128** (0.320 g, 99 %) was recrystallized by vapour diffusion from CDCl₃ and ether. The structure of the complex was confirmed by single crystal X-ray crystallography. IR (ν_m, cm⁻¹) = 3428, 3246, 3084, 3029, 2999, 2925, 1577, 1564, 1526, 1498, 1482, 1391, 1330, 1244, 1204, 1166, 1124, 1096, 1045, 1018, 975, 930, 842, 813, 785, 750, 704, 675, 647, 617.

Experimental

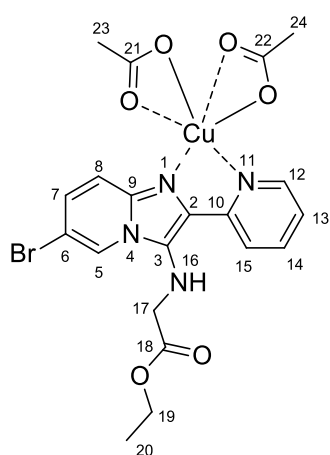
**129**

In a 25 ml round bottomed flask, **123** (0.300 g, 0.791 mmol, 2 eq) and PtCl_2 (0.105 g, 0.396 mmol) were combined in 10 ml DMF and refluxed for 18 hours. A yellow solid precipitated out of solution and this was collected by filtration and washed with MeOH. The yellow solid was characterised by NMR spectroscopy and SCXRD and determined to be **129** (0.170 g, 67 %). $^1\text{H NMR}$ (500 MHz, *d*-DMSO) $\delta_{\text{H}} = 9.37$ (1H, dd, $J = 6.0$ and 1.6 Hz, H-12), 8.71 (1H, d, $J = 9.8$ Hz, H-5), 8.51 (1H, d, $J = 1.7$ Hz, H-8), 8.18 (1H, td, $J = 7.8$ and 1.6 Hz, H-14), 8.03 (1H, dd, $J = 8.2$ and 1.5 Hz, H-15), 7.70 (1H, dd, $J = 9.8$ and 1.9 Hz, H-7), 7.56 (1H, ddd, $J = 7.5$, 6.0 and 1.5 Hz, H-13), 7.34 – 7.21 (5H, m, H-19, H-20, H-21, H-22, H-23), 6.18 (1H, t, $J = 6.3$ Hz, H-16), 4.26 (2H, d, $J = 6.3$ Hz, H-17).

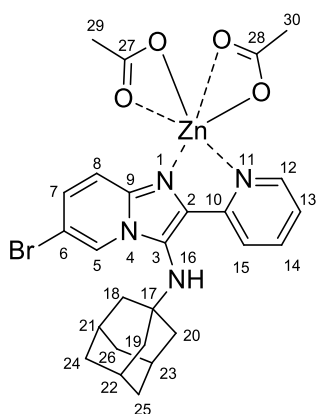
**130**

Zinc (II) acetate monohydrate (0.108 g, 0.108 mmol, 1.1 eq) and **125** (0.200 g, 0.533 mmol) were combined according to the general procedure with additional EtOH added. **130** was collected as a mustard powder (0.226 g, 76 %). After vapour diffusion recrystallization from CDCl_3 and ether, the structure of the complex was confirmed by SCXRD. $^1\text{H NMR}$ (500 MHz, CDCl_3) $\delta_{\text{H}} = 8.85$ (1H, d, $J = 5.1$ Hz, H-12), 8.54 – 8.50 (1H, m, H-5), 8.08 (1H, d, $J = 8.0$ Hz, H-15), 8.01 (1H, s, H-8), 7.90 (1H, td, $J = 7.8$, 1.7 Hz, H-14), 7.45 – 7.40 (1H, m, H-13), 7.38 (1H, d, $J = 9.5$ Hz, H-7), 4.20 (2H, q, $J = 7.2$ Hz, H-19), 3.83 (2H, d, $J = 5.8$ Hz, H-17), 2.09 (6H, s, H-23 and H-24), 1.89 (1H, s, N-H), 1.25 (3H, t, $J = 7.1$ Hz, H-20). $^{13}\text{C NMR}$ (126 MHz, CDCl_3) $\delta = 180.6$ (C-21 and C-22), 171.3 (C-18), 149.5 (C-12), 146.5 (C-9), 139.8 (C-10), 139.6 (C-14), 132.2 (C-13), 127.5 (C-2 and C-3), 124.5 (C-7), 124.1 (C-5), 121.2 (C-15), 118.3 (C-8), 109.3 (C-6), 61.9 (C-19), 49.1 (C-17), 22.7 (C-23 and C-24), 14.1 (C-20). IR ($\text{v}_{\text{m}}\cdot\text{cm}^{-1}$) = 3273, 3080, 2980, 2922, 2845, 1730, 1582, 1474, 1416, 1337, 1296, 1238, 1198, 1105, 1028, 928, 820, 792, 727, 677, 673, 619.

Experimental

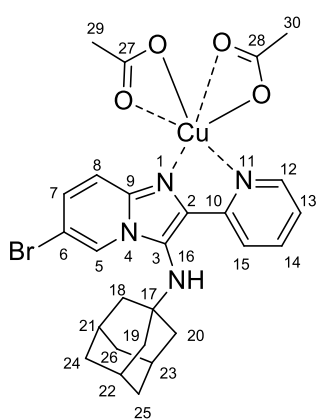
**131**

The general procedure was followed using **125** (0.200 g, 0.533 mmol) and copper(II) acetate monohydrate (0.106 g, 0.533 mmol, 1 eq). In order to confirm the structure of the collected green powder **131**, the product (0.271 g, 91 %) was recrystallized by vapour diffusion from d_4 -MeOD and ether. IR ($\nu_{\text{m}} \cdot \text{cm}^{-1}$) = 3443, 3269, 3082, 2907, 2851, 1572, 1528, 1503, 1481, 1389, 1358, 1334, 1242, 1159, 1121, 1090, 1047, 1018, 928, 860, 829, 792, 760, 738, 706, 673, 619.

**132**

126 (0.161 g, mmol) and zinc(II) acetate monohydrate (0.077 g, 0.419 mmol, 1.1 eq) were combined following the general procedure with an additional few drops of EtOH. A white powder was collected (0.161 g, 70 %). After recrystallization by vapour diffusion from CDCl_3 and ether, the structure of the white powder was found to be **132** by single crystal X-ray crystallography. ^1H NMR (500 MHz, CDCl_3) δ_{H} = 8.93 – 8.88 (1H, m, H-12), 8.43 (1H, d, J = 8.0 Hz, H-15), 8.37 (1H, s, H-5), 8.01 (1H, d, J = 9.5 Hz, H-8), 7.88 (1H, t, J = 7.8 Hz, H-14), 7.44 – 7.36 (2H, m, H-7 and H-13), 3.34 (1H, s, N-H), 2.09 (6H,

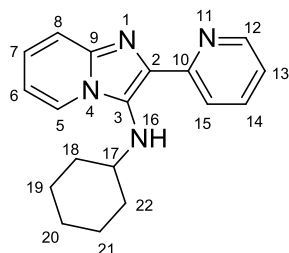
s, H-29 and H-30), 2.06 (3H, s, H-21, H-22 and H-23), 1.77 – 1.72 (6H, m, H-18, H-19 and H-20), 1.66 – 1.51 (6H, m, H-24, H-25 and H-26). ^{13}C NMR (126 MHz, CDCl_3) δ = 180.6 (C-27 and C-28), 149.8 (C-12), 147.5 (C-9), 140.3 (C-10), 138.9 (C-14), 133.3 (C-3), 132.2 (C-7*), 125.0 (C-2), 124.6 (C-13*), 124.1 (C-5), 121.9 (C-15), 118.6 (C-8), 109.2 (C-6), 58.2 (C-17), 44.3 (C-18, C-19 and C-20), 35.9 (C-24, C-25 and C-26), 29.7 (C-21, C-22 and C-23), 22.1 (C-29 and C-30). IR ($\nu_{\text{m}} \cdot \text{cm}^{-1}$) = 3271, 3074, 3018, 2907, 2855, 1585, 1530, 1503, 1472, 1412, 1393, 1323, 1234, 1088, 1049, 1013, 922, 824, 797, 760, 706, 671, 617.

Experimental**133**

The general procedure was followed using **126** (0.150 g, 0.355 mmol) and copper(II) acetate monohydrate (0.078 g, 0.390 mmol, 1.1 eq). The product was collected as a turquoise solid (0.144 g, 67 %) and after recrystallization from MeOD and ether was found to be **133** from SCXRD. IR ($\nu_{\text{m}}, \text{cm}^{-1}$) = 3257, 3086, 2905, 2845, 1585, 1558, 1530, 1506, 1476, 1412, 1385, 1360, 1327, 1250, 1186, 1151, 1117, 1088, 1047, 1018, 924, 853, 806, 791, 762, 735, 706, 675, 646, 619.

7.2.10. Synthesis of pyridyl imidazo[1,2-*a*]pyridines for the SAR study

The synthesis of the following imidazo[1,2-*a*]pyridines were synthesized according to the general procedure outlined in Section 7.2.1 by heating the reactants under reflux conditions in ethanol overnight. The products were purified by recrystallization or flash column chromatography.

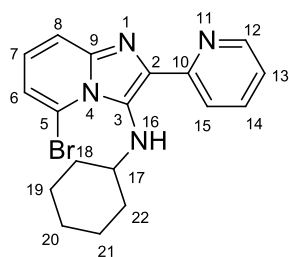


134

2-Aminopyridine (1.00 g, 10.626 mmol), 2-pyridinecarboxaldehyde (1.14 g, 10.626 mmol, 1 eq), cyclohexyl isocyanide (1.16 g, 10.626 mmol, 1 eq) and Montmorillonite K10 clay (1.2 g) were combined and the general procedure followed. The resulting mixture was purified by recrystallization from an ether/DCM mixture to afford imidazo[1,2-*a*]pyridine **134** as yellow crystals (2.31 g, 74 %). R_f = 0.40 (50% EtOAc/Hexane),

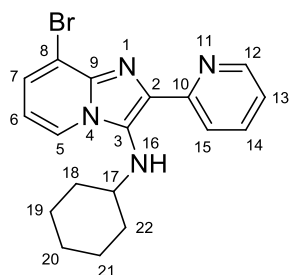
$m.p.$ = 123 - 124 °C, $^1\text{H NMR}$ (300 MHz, CDCl_3): δ_{H} = 8.54 (1H, ddd, J = 5.0 Hz, J = 1.8 Hz and J = 0.9 Hz, H-12), 8.18 (1H, dt, J = 8.1 Hz and J = 1.1 Hz, H-15), 8.01 – 7.94 (1H, m, H-5), 7.73 (1H, td, J = 7.7 and J = 1.7 Hz, H-14), 7.52 (1H, d, J = 9.1 Hz, H-8*), 7.18 – 6.98 (2H, m, H-13 and H-7), 6.73 (1H, td, J = 6.7 Hz and J = 1.1 Hz, H-6), 6.25 (1H, s, H-16), 3.10 (1H, d, J = 9.9 Hz, H-17), 1.89 (2H, dd, J = 10.2 Hz and J = 4.5 Hz, H-18), 1.77 – 1.65 (2H, m, H-19), 1.55 (1H, d, J = 3.9 Hz, H-20a), 1.39 – 1.14 (5H, m, H-20b, H-21, H-22). $^{13}\text{C NMR}$ (75 MHz, CDCl_3): δ_{C} = 155.1 (C-10), 148.3 (C-12), 140.7 (C-9), 136.4 (C-14), 131.2 (C-3), 130.2 (C-2), 123.2 (C-7), 123.0 (C-5), 121.0 (C-13), 120.2 (C-15), 117.8 (C-8*), 111.6 (C-6), 55.5 (C-17), 34.0 (C-18 and C-22), 25.8 (C-20), 25.0 (C-19 and C-21). IR ($\nu_{\text{m}}\cdot\text{cm}^{-1}$) = 3262, 2925, 2848, 1590, 1555, 1477, 1403, 1346, 1229, 1095, 1073, 892, 792, 760, 734, 694, 639. ESI-MS (m/z) calculated for $\text{C}_{18}\text{H}_{21}\text{N}_4$, $[\text{M}+\text{H}]^+$, 293.1766, found 293.1765.

Experimental

**135**

2-Amino-6-bromopyridine (2.00 g, 11.56 mmol), 2-pyridinecarboxaldehyde (1.238 g, 11.56 mmol, 1 eq), cyclohexyl isocyanide (1.262 g, 11.65 mmol, 1 eq) and Montmorillonite K10 clay (1.0 g) were combined and the general procedure followed. The resulting mixture was purified by column chromatography with 20 % EtOAc/Hexane as an eluent to afford a sticky golden oil, **135** (2.976 g, 69 %). $R_f = 0.54$ (50 % EtOAc/Hexane). ^1H

NMR (500 MHz, CDCl_3) $\delta = 8.56$ (1H, ddd, $J = 4.9, 1.9$ and 0.9 Hz, H-12), 8.18 (1H, dt, $J = 8.0$ and 1.1 Hz, H-15), 7.73 (1H, td, $J = 7.7$ and 1.8 Hz, H-14), 7.48 (1H, dd, $J = 8.9$ and 1.2 Hz, H-8), 7.14 (1H, ddd, $J = 7.5, 4.8$ and 1.2 Hz, H-13), 6.93 (1H, dd, $J = 7.1$ and 1.1 Hz, H-6), 6.87 (1H, dd, $J = 8.8$ and 7.1 Hz, H-7), 4.96 (1H, s, H-16), $3.15 - 3.02$ (1H, m, H-17), 1.92 (2H, dt, $J = 8.8$ and 3.1 Hz, H-18a and H-22a), 1.64 (2H, dt, $J = 6.8$ and 3.3 Hz, H-19a and H-21a), $1.58 - 1.50$ (1H, m, H-20a), $1.20 - 1.03$ (5H, m, H-18b, H-19b, H-20b, H-21b and H-22b). ^{13}C **NMR** (126 MHz, CDCl_3) $\delta = 158.8, 154.5$ (C-10), 148.1 (C-12), 142.8 (C-9), $139.6, 136.5$ (C-14), 133.1 (C-3), 132.9 (C-2), 123.6 (C-6), 121.5 (C-13), 121.0 (C-15), 118.8 (C-7), 117.2 (C-8), 112.2 (C-5), 60.2 (C-17), 32.7 (C-18 and C-22), 25.9 (C-20), 25.5 (C-19 and C-21). **IR** ($\nu_{\text{m}} \cdot \text{cm}^{-1}$) = 3268, 2928, 2852, 1589, 1552, 1470, 1428, 1400, 1298, 1225, 1144, 1074, 976, 891, 768, 721. **EIS-MS** (m/z) calculated for $\text{C}_{18}\text{H}_{20}\text{BrN}_4$, $[\text{M}+\text{H}]^+$, 371.0871, found 371.0866.

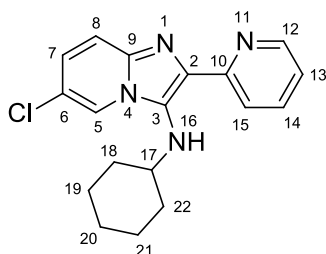
**136**

Following the general procedure, 2-amino-3-bromopyridine (1.00 g, 5.78 mmol), 2-pyridinecarboxaldehyde (0.619 g, 5.78 mmol, 1 eq), cyclohexyl isocyanide (0.631 g, 5.78 mmol, 1 eq) and Montmorillonite K10 clay (1.0 g) were combined in ethanol. The resulting mixture was purified by flash column chromatography with 20 % EtOAc/Hexane as yellow crystals, **136** (1.00 g, 47 %). $R_f = 0.45$ (50 %

EtOAc/Hexane). **m.p.** = 136 - 137 °C. ^1H **NMR** (300 MHz, CDCl_3): $\delta_{\text{H}} = 8.54$ (1H, dt, $J = 4.8$ Hz and $J = 1.8$ Hz, H-12), 8.29 (1H, dt, $J = 8.0$ Hz and $J = 1.4$ Hz, H-15), 7.96 (1H, dd, $J = 6.9$ Hz and $J = 2.7$ Hz, H-5), 7.74 (1H, tq, $J = 7.9$ Hz and $J = 1.8$ Hz, H-14), 7.34 (1H, dt, $J = 7.2$ Hz and $J = 2.2$ Hz, H-7), 7.14 (1H, m, H-13), 6.63 (1H, td, $J = 7.1$ Hz and $J = 4.7$ Hz, H-6), 6.29 (s, 1H), 3.07 (1H, s, H-17), 1.87 (2H, d, $J = 12.8$ Hz, H-18), 1.71 (2H, s, H-19), 1.55 (1H, s, H-20a), 1.25 (5H, m, H-20b, H-21, H-22). ^{13}C **NMR** (75 MHz, CDCl_3): $\delta_{\text{C}} = 154.7$ (C-10), 151.5 (C-9), 148.2 (C-12), 138.2 (C-10), 136.4 (C-14), 132.5 (C-3), 131.1 (C-2), 125.4 (C-7), 122.5 (C-5), 121.3 (C-13), 120.9 (C-15), 112.1 (C-8), 111.5 (C-6), 55.6 (C-17), 34.0 (C-18 and C-22), 25.8 (C-19 and C-21), 24.9 (C-20). **IR** ($\nu_{\text{m}} \cdot \text{cm}^{-1}$) = 3262, 2926,

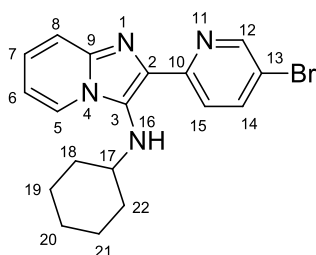
Experimental

2849, 1591, 1573, 1475, 1436, 1370, 1349, 1293, 1251, 1236, 1209, 1143, 1071, 992, 936, 895, 836, 791, 758, 722, 662. **ESI-MS (m/z)** calculated for $C_{18}H_{20}N_4Br$, $[M+H]^+$, 371.0871, found 371.0869.

**137**

Following the general procedure, 2-amino-5-chloropyridine (1.00 g, 7.78 mmol), 2-pyridinecarboxaldehyde (0.833 g, 7.78 mmol, 1 eq), cyclohexyl isocyanide (0.857 g, 7.78 mmol, 1 eq) and Montmorillonite K10 clay (1.0 g) were combined in ethanol. Column chromatography was used to purify the compound with 20 % EtOAc/Hexane as an eluent to afford a yellow powder, **137** (2.27 g, 89 %). $R_f = 0.57$ (50 % EtOAc/Hexane).

m.p. = 118 - 119 °C. 1H NMR (300 MHz, $CDCl_3$): $\delta_H = 8.60 - 8.52$ (1H, m, H-12), 8.15 (1H, dt, $J = 8.0$ Hz and $J = 1.1$ Hz, H-15), 7.98 (1H, dd, $J = 2.0$ Hz and $J = 0.9$ Hz, H-5), 7.74 (1H, dd, $J = 8.7$ Hz and $J = 6.8$ Hz, H-14), 7.46 (1H, d, $J = 9.5$ Hz, H-8), 7.13 (1H, ddd, $J = 8.6$ Hz, $J = 4.1$ Hz and $J = 2.7$ Hz, H-13), 7.08 - 6.91 (1H, m, H-7), 6.21 (1H, s, H-16), 3.07 (1H, s, H-17), 1.88 (2H, d, $J = 11.1$ Hz, H-18), 1.78 - 1.62 (2H, m, H-19), 1.56 (1H, d, $J = 6.0$ Hz, H-20a), 1.45 - 1.13 (5H, m, H-20b, H-21 and H-22). ^{13}C NMR (75 MHz, $CDCl_3$): $\delta_C = 154.7$ (C-10), 148.3 (C-12), 139.0 (C-9), 136.5 (C-14), 131.5 (C-3), 131.5 (C-2), 124.5 (C-7), 121.3 (C-6), 120.7 (C-13), 120.3 (C-5), 120.0 (C-15), 118.2 (C-8), 55.4 (C-17), 34.0 (C-18 and C-22), 25.8 (C-20), 24.9 (C-19 and C21). **IR (v_m.cm⁻¹)** = 3305, 2930, 2853, 1590, 1476, 1400, 1324, 1287, 1232, 1201, 1184, 1115, 1085, 1046, 943, 891, 807, 786, 740, 702, 626. **ESI-MS (m/z)** calculated for $C_{18}H_{20}ClN_4$, $[M+H]^+$, 327.1376, found 327.1369.

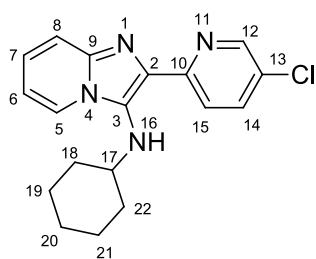
**138**

2-Aminopyridine (0.253 g, 2.688 mmol), 5-bromo-2-pyridinecarboxaldehyde (0.500 g, 2.688 mmol, 1 eq), cyclohexyl isocyanide (0.293 g, 2.688 mmol, 1 eq) and Montmorillonite K10 clay (0.500 g) were combined and the general procedure followed. The resulting mixture was purified by column chromatography with 20 % EtOAc/Hexane as an eluent to afford **138** as a yellow solid (0.816 g, 82 %). $R_f = 0.63$ (50 % EtOAc/Hexane).

m.p. = 144 °C. 1H NMR (300 MHz, $CDCl_3$): $\delta_H = 8.60$ (1H, dt, $J = 2.4$ and 0.8 Hz, H-12), 8.08 (1H, dt, $J = 8.6$ and 0.8 Hz, H-15), 7.96 (1H, dq, $J = 6.9$ and 1.1 Hz, H-5), 7.85 (1H, ddd, $J = 8.6$, 2.4 and 0.9 Hz, H-14), 7.50 (1H, dq, $J = 9.1$ and 1.1 Hz, H-8), 7.09 (1H, ddt, $J = 9.1$, 6.6 and 1.1 Hz, H-7), 6.76

Experimental

(1H, tt, $J = 6.8$ and 1.0 Hz, H-6), 5.93 (1H, d, $J = 9.8$ Hz, H-16), 3.14 – 3.00 (1H, m, H-17), 1.89 (2H, d, $J = 11.7$ Hz, H-18a and H-19a), 1.72 (2H, q, $J = 5.2$ Hz, H-19a and H-21a), 1.57 (1H, s, H-20a), 1.40 – 1.15 (5H, m, H-18a, H-19a, H-20a, H-21a and H-22a). $^{13}\text{C NMR}$ (75 MHz, CDCl_3): $\delta_{\text{C}} = 153.6$ (C-9), 149.3 (C-12), 140.9 (C-3), 139.1 (C-14), 131.3 (C-10), 129.5 (C-2), 123.6 (C-7), 123.1 (C-5), 121.6 (C-15), 117.9 (C-8), 117.4 (C-13), 111.8 (C-6), 55.6 (C-17), 34.1 (C-18 and C-22), 25.8 (C-20), 25.0 (C-19 and C-21). $\text{IR (v}_{\text{m}}, \text{cm}^{-1}) = 3302, 2922, 2848, 1580, 1537, 1471, 1444, 1413, 1359, 1292, 1265, 1230, 1197, 1139, 1120, 1086, 1047, 1002, 922, 889, 841, 752, 702, 636, 617$. ESI-MS (m/z) calculated for $\text{C}_{18}\text{H}_{20}\text{BrN}_4$, $[\text{M}+\text{H}]^+$, 371.0871, found 371.0855.



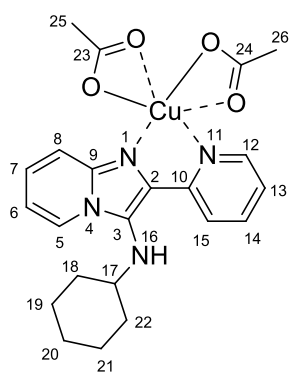
139

The combination of 2-aminopyridine (0.332 g, 3.532 mmol), 5-chloro-2-pyridinecarboxaldehyde (0.500 g, 3.532 mmol, 1 eq), cyclohexyl isocyanide (0.386 g, 3.532 mmol, 1 eq) and Montmorillonite K10 clay (0.500 g) according to the general procedure resulted in the formation of **139** (0.997 g, 86 %) as a yellow powder following purification by column chromatography with a 20 % EtOAc/Hexane eluent. $R_f = 0.54$ (50 %

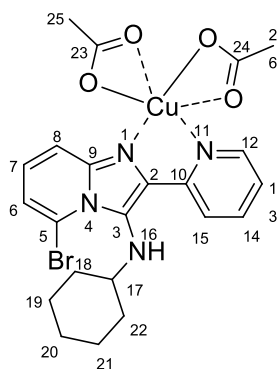
EtOAc/Hexane). $\text{m.p.} = 139 - 140$ °C. $^1\text{H NMR}$ (300 MHz, CDCl_3): $\delta_{\text{H}} = 8.50$ (1H, dt, $J = 2.5$ and 0.8 Hz, H-12), 8.13 (1H, dt, $J = 8.6$ and 0.8 Hz, H-15), 7.96 (1H, dq, $J = 6.9$ and 1.1 Hz, H-5), 7.71 (1H, ddd, $J = 8.6, 2.5$ and 0.8 Hz, H-14), 7.50 (1H, dq, $J = 9.1$ and 1.0 Hz, H-8), 7.09 (1H, ddt, $J = 9.0, 6.6$ and 1.1 Hz, H-7), 6.75 (1H, tt, $J = 6.8$ and 1.0 Hz, H-6), 5.93 (1H, d, $J = 9.8$ Hz, H-16), 3.06 (1H, m, H-17), 1.94 – 1.83 (2H, m, H-18a and H-22b), 1.73 (2H, d, $J = 7.8$ Hz, H-19a and H-21a), 1.57 (1H, s, H-20), 1.40 – 1.15 (5H, m, H-18b, H-19b, H-20b, H-21b and H-22b). $^{13}\text{C NMR}$ (75 MHz, CDCl_3): $\delta_{\text{C}} = 153.5$ (C-9), 147.3 (C-12), 141.0 (C-3), 136.4 (C-14), 131.4 (C-13), 129.7 (C-2), 129.1 (C-10), 123.7 (C-7), 123.2 (C-5), 121.3 (C-15), 118.0 (C-8), 111.9 (C-6), 55.8 (C-17), 34.3 (C-18 and C-22), 25.9 (C-20), 25.1 (C-19 and C-21). $\text{IR (v}_{\text{m}}, \text{cm}^{-1}) = 3303, 2925, 2850, 1579, 1541, 1471, 1446, 1363, 1346, 1288, 1230, 1199, 1139, 1107, 1089, 1008, 923, 891, 842, 798, 752, 738, 704, 638, 621$. ESI-MS (m/z) calculated for $\text{C}_{18}\text{H}_{20}\text{ClN}_4$, $[\text{M}+\text{H}]^+$, 327.1376, found 327.1379.

7.2.11. Synthesis of Copper Complexes

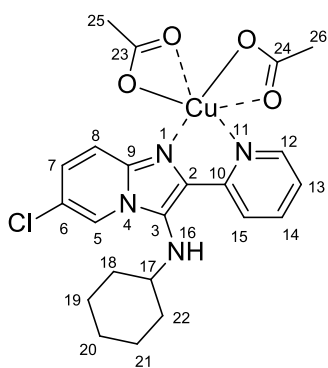
Following the general procedure outlined in Section 7.2.9. the following copper complexes were synthesized in diethyl ether, the resulting powders collected by gravity filtration and recrystallized from acetone unless otherwise stated. Crystals suitable for SCXRD were grown from appropriate solvents.

**140**

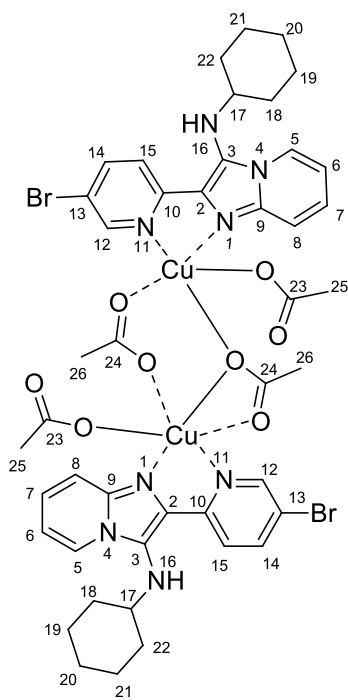
Combining **134** (0.300 g, 1.074 mmol) and $\text{Cu}(\text{OAc})_2 \cdot \text{H}_2\text{O}$ (0.214 g, 1.074 mmol, 1 eq) according to the general procedure resulted in the formation of a green powder (0.455 g, 89 %). After vapour diffusion recrystallization from d_4 -MeOD and ether and characterisation by SXCRD the green powder was found to be **140**. IR ($\nu_{\text{m}} \cdot \text{cm}^{-1}$) = 3302, 3265, 3107, 3082, 3049, 2930, 2857, 1582, 1506, 1479, 1381, 1327, 1292, 1247, 1151, 1091, 1047, 1010, 941, 926, 850, 775, 758, 673, 646, 621.

**141**

The general procedure was followed using **135** (1.776 g, 4.784 mmol) and $\text{Cu}(\text{OAc})_2 \cdot \text{H}_2\text{O}$ (0.955 g, 4.784 mmol, 1 eq). A green powder, **141** resulted. The structure of the complex was confirmed by single crystal X-ray crystallography (2.238 g, 85 %) following suitable crystal formation by slow evaporation from d_4 -MeOD. IR ($\nu_{\text{m}} \cdot \text{cm}^{-1}$) = 3414, 3287, 3080, 2924, 2855, 1576, 1485, 1391, 1334, 1306, 1256, 1159, 1099, 1047, 1022, 964, 930, 785, 758, 679, 648, 621.

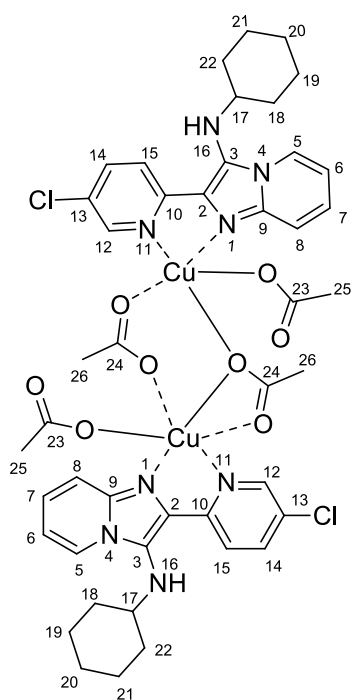
Experimental
**142**

137 (0.500 g, 1.530 mmol) and $\text{Cu}(\text{OAc})_2 \cdot \text{H}_2\text{O}$ (0.305 g, 1.530 mmol, 1 eq) were combined following the general procedure. A dark green powder precipitated from the reaction and this was collected by gravity filtration and washed with ether to afford **142**. The structure of the complex was confirmed by single crystal X-ray crystallography (0.789 g, 99 %). IR ($\nu_{\text{m}} \cdot \text{cm}^{-1}$) = 3379, 3282, 3282, 3067, 2930, 2858, 1610, 1568, 1528, 1502, 1477, 1400, 1331, 1292, 1242, 1151, 1128, 1097, 1078, 1047, 1022, 877, 822, 787, 756, 725, 679, 621.

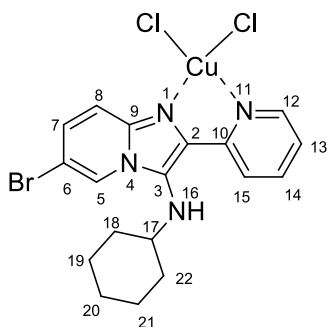
**147**

The combination of **138** (0.300 g, 0.808 mmol) with $\text{Cu}(\text{OAc})_2 \cdot \text{H}_2\text{O}$ (0.161 g, 0.808 mmol, 1 eq) according to the general procedure resulted in the formation of a green solid (0.408 g, 35 %). Following slow evaporation recrystallization from isopropyl alcohol the structure of **147** was confirmed. IR ($\nu_{\text{m}} \cdot \text{cm}^{-1}$) = 3294, 3250, 3105, 3043, 2928, 2855, 1570, 1508, 1479, 1389, 1377, 1331, 1248, 1146, 1105, 1030, 1013, 949, 928, 841, 779, 752, 673, 619.

Experimental

**148**

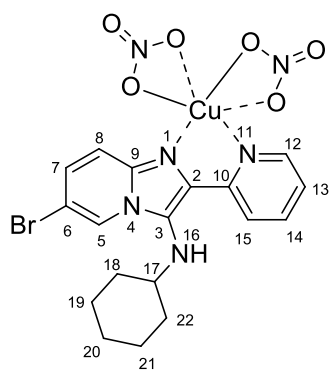
The general procedure was followed using **139** (0.300 g, 0.918 mmol) and $\text{Cu}(\text{OAc})_2 \cdot \text{H}_2\text{O}$ (0.183 g, 0.918 mmol, 1 eq). The resulting green powder (0.408 g, 47 %) was found to be **148** following recrystallization by slow evaporation from d_4 -MeOD. IR ($\nu_{\text{m}} \cdot \text{cm}^{-1}$) = 3510, 3221, 3111, 3053, 2930, 2855, 1595, 1504, 1483, 1423, 1375, 1325, 1246, 1146, 1121, 1097, 1069, 1032, 1013, 928, 854, 826, 756, 681, 667, 617.

**145**

The general procedure was followed using **88** (0.300 g, 0.808 mmol) and $\text{CuCl}_2 \cdot \text{H}_2\text{O}$ (0.138 g, 0.808 mmol, 1 eq) in ether resulting in the formation of a light green solid, **145** (0.215 g, 53 %) after filtration. The structure of the green solid was confirmed by SCXRD following recrystallization from a MeOH/ H_2O solution (although this structure could not be solved satisfactorily). IR ($\nu_{\text{m}} \cdot \text{cm}^{-1}$) = 3283, 3101, 3067, 2928, 2849, 1628, 1605, 1582, 1522, 1497, 1450, 1408, 1367, 1333, 1300, 1258,

1238, 1167, 1128, 1096, 1016, 947, 870, 804, 787, 752, 706, 671, 642, 602.

* Acetone could not be used to recrystallize this compound – it exchanges with the counterion

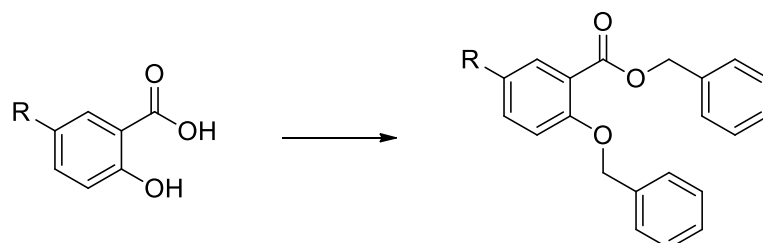
Experimental**146**

708, 675, 652.

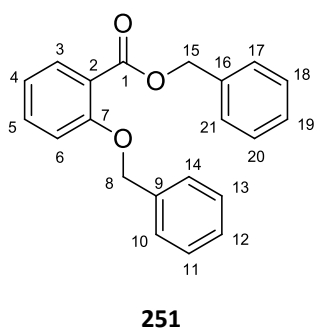
The combination of an ethereal solution of **88** (0.300 g, 0.808 mmol) with $\text{Cu}(\text{NO}_3)_2$ (0.188 g, 0.808 mmol, 1 eq) according to the general procedure resulted in the formation of a lime green powder (0.439 g, 97 %) that was collected by filtration. A slow evaporation recrystallization from a MeOH/DCM solution provided suitable crystals for SCXRD which confirmed the structure of **146**. IR ($\nu_{\text{m}}, \text{cm}^{-1}$) = 3327, 3094, 2924, 2854, 1610, 1568, 1479, 1452, 1410, 1302, 1275, 1246, 1161, 1113, 1097, 1069, 1009, 970, 893, 872, 808, 783, 750,

7.3. Experimental Procedures for the preparation of xanthenes and related compounds.

7.3.1. General procedure for the benzyl protection of salicylic acids and salicylaldehyde

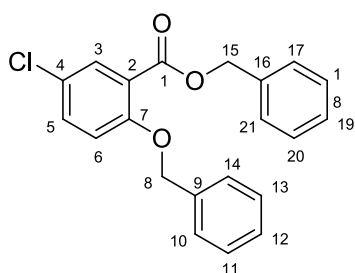


To a solution containing the relevant salicylic acid or aldehyde (1 eq) in dry acetone, K_2CO_3 (3 eq) was added and the mixture heated under reflux for 15 minutes. Benzyl bromide (2.1 eq for salicylic acids or 1.1 eq for salicylaldehyde) was added to the resulting cloudy solution and the reaction left to reflux overnight. On completion of the reaction, the K_2CO_3 was filtered off and concentrated *in vacuo*. The products were purified by column chromatography.



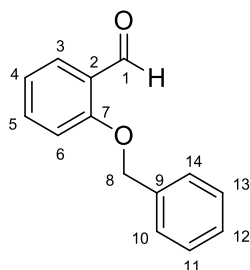
Salicylic acid (5.00g, 56.20 mmol), K_2CO_3 (15.00 g, 0.108 mol, 3 eq) and benzyl bromide (18.57 g, 0.108 mol, 3 eq) were combined according to the general procedure in acetone (120 ml). Following purification, **251** was collected as a white solid (11.36 g, 99 %). $R_f = 0.77$ (10 % EtOAc/Hexane). **m.p.** = 49-51 °C, lit 48-50 °C. ^{191}H NMR (300 MHz, $CDCl_3$): $\delta_H = 7.84$ (1H, dd, $J = 7.6$ and 1.8 Hz, H-3), 7.45 – 7.34 (6H, m, H-5, H-10, H-12, H-14, H-17 and H-21), 7.29 (5H, m, H-11, H-13, H-18, H-19 and H-20), 7.00 – 6.90 (2H, m, H-4 and H-6), 5.32 (2H, s, H-15), 5.10 (2H, s, H-8). ^{13}C NMR (75 MHz, $CDCl_3$): $\delta_C = 166.2$ (C-1), 158.2 (C-7), 136.6 (C-9), 136.1 (C-16), 133.4 (C-5), 131.8 (C-3), 128.6 (C-2), 128.5 (C-10* and C-14*), 128.4 (C-17* and C-21*), 128.1 (C-11* and C-13*), 128.0 (C-12*), 127.7 (C-19*), 127.0 (C-18* and C-20*), 120.5 (C-4'), 113.7 (C-6'), 70.6 (C-8), 66.6 (C-15).

Experimental

**301**

5-chlorosalicylic acid (10.00 g, 58.29 mmol), benzyl bromide (20.94 g, 0.1224 mol, 2.1 eq) and K_2CO_3 (24.17 g, 0.1749 mol, 3 eq) were combined following the general procedure. The product (**301**) was purified by column chromatography in 10 % EtOAc/Hexane and collected as a white solid (20.10 g, 99 %). $R_f = 0.65$ (20 % EtOAc/Hex). **m.p.** = 63-64 °C; 64-66 °C. ^{191}H NMR (300 MHz, $CDCl_3$) $\delta_H = 7.79$ (1H, d, $J = 2.8$ Hz, H-3), 7.45 – 7.22

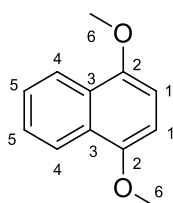
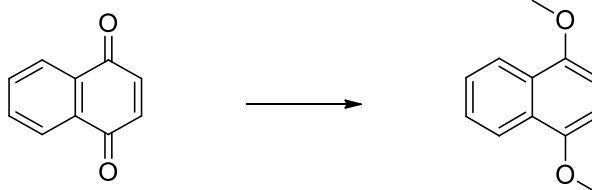
(11H, m, H-5, H-10, H-11, H-12, H-13, H-14, H-17, H-18, H-19, H-20 and H-21), 6.87 (1H, d, $J = 8.9$ Hz, H-6), 5.31 (2H, s, H-15), 5.07 (2H, s, H-8). ^{13}C NMR (75 MHz, $CDCl_3$) $\delta_C = 164.9$ (C-1), 156.7 (C-7), 136.1 (C-9*), 135.7 (C-16*), 133.0 (C-11#, C-12# and C-13#), 131.4 (C-18#, C-19# and C-20#), 128.5 (C-17~ and C-21~), 128.2 (C-3), 127.9 (C-5), 127.0 (C-10~ and C-14~), 125.5 (C-4), 122.0 (C-2), 115.2 (C-6), 70.9 (C-8), 67.0 (C-15).

**309**

Salicylaldehyde (2.00 g, 16.38 mmol), K_2CO_3 (2.49 g, 18.02 mmol, 1.1 eq) and benzyl bromide (3.08 g, 18.02 mmol, 1.1 eq) were combined as outlined in the general procedure. Following purification by column chromatography using 10 % EtOAc/Hexane and the resulting viscous colourless oil was found to be **309** (2.73 g, 73 %). $R_f = 0.44$ (10 % EtOAc/Hexane). 1H NMR (300 MHz, $CDCl_3$): $\delta_H = 10.55$ (1H, d, $J = 0.7$ Hz, H-1),

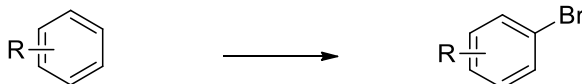
7.88 – 7.82 (1H, m, H-3), 7.54 – 7.49 (1H, m, H-5), 7.46 – 7.29 (1H, m, H-10, H-11, H-12, H-13 and H-14), 7.05 (1H, s, H-6), 7.01 (1H, d, $J = 7.1$ Hz, H-4), 5.17 (1H, s, H-8). ^{13}C NMR (75 MHz, $CDCl_3$): $\delta_C = 189.65$ (C-1), 161.05 (C-7), 136.09 (C-9), 135.86 (C-5), 128.71 (C-11 and C-13), 128.43 (C-3), 128.25 (C-6), 127.27 (C-10 and C-14), 125.24 (C-2), 121.00 (C-4), 113.07 (C-6), 70.49 (C-8). **IR** ($\nu_m \cdot cm^{-1}$) = 3071, 3034, 2867, 1685, 1597, 1470, 1452, 1379, 1286, 1237, 1188, 1159, 1102, 1004, 852, 832, 756, 733, 696, 659.

7.3.2. Reduction of naphthoquinone

**150**

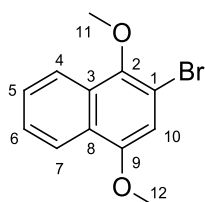
This procedure was modified from work originally done by Johnson.¹²⁸ Naphthoquinone **151** (1 eq) was dissolved in 250 ml of THF in a 1 litre round bottomed flask. Water (50 ml) was added to the flask along with sodium dithionite (16.51 g, 94.9 mmol, 3 eq) and TBAI (1.051 g, 2.85 mmol, 0.09 eq) and the reaction stirred under a nitrogen atmosphere for 30 minutes. During this time KOH (17.74 g, 0.316 mol, 10 eq) was dissolved in 100 ml of water and allowed to cool. The basic solution was added to the reaction mixture and stirred for a further 1 hour. Finally dimethyl sulfate (39.86 g, 0.316 mol, 10 eq) was added to the reaction mixture and the reaction stirred for 18 hours. Ammonia solution was added to quench the reaction and the organic layer extracted with EtOAc. This layer was then washed sequentially with water, 5 % HCl and brine in a separation funnel. The organic layer was then dried over MgSO₄, concentrated *in vacuo* and purified by column chromatography using 10 % EtOAc/Hexane as the eluent. The product **150** was collected as white crystals (4.76 g, 80 %). *R_f* = 0.70 (10 % EtOAc/Hexane). *m.p.* = 88-90 °C, lit 86-88 °C.²⁰⁷ ¹H NMR (300 MHz, CDCl₃) δ_H = 8.20 (2H, dd, *J* = 6.4 and 3.3 Hz, H-4), 7.49 (2H, dd, *J* = 6.4 and 3.3 Hz, H-5), 6.68 (2H, s, H-1), 3.94 (6H, s, H-6). ¹³C NMR (75 MHz, CDCl₃) δ_C = 149.5 (C-2), 126.4 (C-3), 125.8 (C-4), 121.8 (C-5), 103.2 (C-1), 55.7 (C-6). IR (ν_m·cm⁻¹) = 3078, 3046, 2947, 2849, 1690, 1614, 1489, 1464, 1414, 1389, 1288, 1263, 1238, 1163, 1088, 1013, 962, 912, 837, 812, 787, 762, 738, 712, 687, 662, 611.

7.3.3. General procedure for the bromination of substituted benzenes and naphthalenes



Freshly recrystallized N-Bromosuccinimide* (NBS) (1 eq) was weighed out in a 100 ml round bottomed flask and 50 ml of DCM added to this with a stirrer bar. To this the appropriate methoxy-substituted benzene (1 eq) was added. Depending on the nature of the substituted benzene the reaction was either stirred at room temperature for 30 minutes or heated under reflux conditions for 2 hours (or longer). Once the reaction was deemed complete (as determined by TLC) the reaction mixture was poured into a separation funnel and the reaction quenched with saturated sodium sulfite. After a further two washes with the saturated sodium sulfite (Na_2SO_3) and a wash with brine, the DCM layer was dried over anhydrous Na_2SO_4 and concentrated *in vacuo*. The product was then purified by column chromatography with a 0-10 % EtOAc/Hexane eluent mixture and characterised by NMR Spectroscopy.

* NBS was recrystallized from boiling water. On cooling white crystals precipitated out of the solution which were collected by filtration and dried in a desiccator overnight. The recrystallized NBS was stored in the fridge in a container that blocked out light.



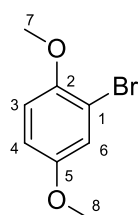
250

Previously prepared 1,4-dimethoxynaphthalene **150** (3.00 g, 15.94 mmol, 1 eq) was added to NBS (2.84 g, 15.94 mmol, 1 eq) in CHCl_3 (30 ml). The reaction was heated under reflux for 2 hours before being quenched as described by the general procedure. Following purification, **250** was collected as a colourless oil (2.13 g, 50 %). $R_f = 0.65$ (10 % EtOAc/Hexane). $^1\text{H NMR}$ (300

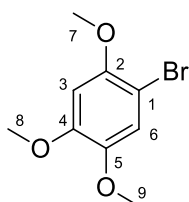
MHz, CDCl_3) $\delta_H = 8.18 - 8.11$ (1H, m, H-4), 8.05 – 7.97 (1H, m, H-7), 7.45 (2H, m, H-5 and H-6), 6.81 (1H, d, $J = 2.0$ Hz, H-10), 3.90 (3H, d, $J = 2.2$ Hz, H-11*), 3.84 (3H, d, $J = 2.2$ Hz, H-12*). $^{13}\text{C NMR}$ (75 MHz, CDCl_3) $\delta_C = 152.2$ (C-2*), 146.7 (C-9*), 128.9 (C-8), 127.3 (C-5[#]), 125.7 (C-3), 125.7 (C-6[#]), 122.5 (C-7[~]), 121.7 (C-4[~]), 111.9 (C-1), 107.8 (C-10), 61.3 (C-11'), 55.7 (C-12').

*This compound was found to be unstable and so was used immediately after purification in the next step.

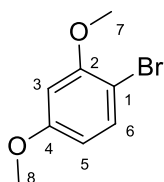
Experimental

**289**

Following the general procedure, 1,4-dimethoxybenzene (10.00 g, 72.38 mmol) and NBS (12.90 g, 72.38 mmol, 1 eq) were combined and heated under reflux in CHCl_3 (60 ml) for 3 days. After purification, a light brown oil resulted and determined to be **289** (12.05 g, 77 %). $R_f = 0.51$ (10 % EtOAc/Hexane). $^1\text{H NMR}$ (300 MHz, CDCl_3) $\delta_{\text{H}} = 7.11$ (1H, dd, $J = 2.3$ and 0.9 Hz, H-6), 6.83 – 6.78 (2H, m, H-3 and H-4), 3.81 (3H, s, H-7*), 3.73 (3H, s, H-8*). $^{13}\text{C NMR}$ (75 MHz, CDCl_3) $\delta_{\text{C}} = 154.1$ (C-2*), 150.3 (C-5*), 119.0 (C-6), 114.6 (C-1), 113.6 (C-4), 113.0 (C-3), 56.8 (C-7[#]), 55.9 (C-8[#]).

**246**

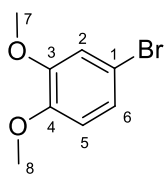
On the slow addition of 1,2,4-trimethoxybenzene (5.00 g, 29.73 mmol) to the stirring NBS (5.30 g, 29.73 mmol) DCM suspension, the reaction heated up significantly, dissolving the NBS. After 20 minutes the reaction had cooled and the NBS crashed out of solution. No starting material could be visualised on the TLC plate and so the reaction was quenched and purified. The white crystals that resulted were determined to be **246** (6.40 g, 87 %). $R_f = 0.32$ (10 % EtOAc/Hex). **m.p.** 52-54 °C; lit 51-52 °C. $^{208}\text{H NMR}$ (300 MHz, CDCl_3) $\delta_{\text{H}} = 7.04$ (1H, s, H-6), 6.56 (1H, s, H-3), 3.89 (3H, s, H-7), 3.87 (3H, s, H-8), 3.83 (3H, s, H-9). $^{13}\text{C NMR}$ (75 MHz, CDCl_3) $\delta_{\text{C}} = 150.4$ (C-2*), 149.2 (C-4*), 143.9 (C-5*), 116.6 (C-6), 101.2 (C-1), 99.0 (C-3), 57.3 (C-8), 56.7 (C-9), 56.3 (C-3). **IR** ($\text{v}_{\text{m}}\cdot\text{cm}^{-1}$) = 2990, 2955, 2851, 1593, 1512, 1458, 1431, 1377, 1323, 1269, 1215, 1161, 1053, 1026, 945, 864, 837, 783, 702.

**314**

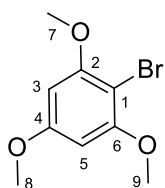
1,3-Dimethoxybenzene (10.00 g, 72.38 mmol, 1 eq) and NBS (12.90 g, 72.38 mmol, 1 eq) were reacted according to the general procedure. The product **314** was collected after purification as a dark liquid (15.14 g, 96 %). $R_f = 0.67$ (20 % EtOAc/Hex). $^1\text{H NMR}$ (300 MHz, CDCl_3) $\delta_{\text{H}} = 7.37$ (1H, d, $J = 8.7$ Hz, H-6), 6.46 (1H, d, $J = 2.7$ Hz, H-3), 6.36 (1H, dd, $J = 8.7$ and 2.7 Hz, H-5), 3.83 (3H, s, H-7*), 3.76 (3H, s, H-8*). $^{13}\text{C NMR}$ (75 MHz, CDCl_3) $\delta_{\text{C}} = 160.3$ (C-2*), 156.5 (C-4*), 133.1 (C-6), 106.2 (C-1), 106.0 (C-5), 100.0 (C-3), 56.1 (C-7[#]), 55.5 (C-8[#]). **IR** ($\text{v}_{\text{m}}\cdot\text{cm}^{-1}$) = 3009, 2947, 2824,

Experimental

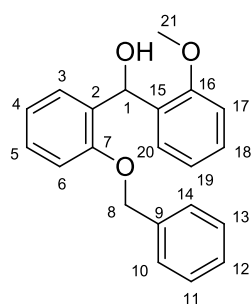
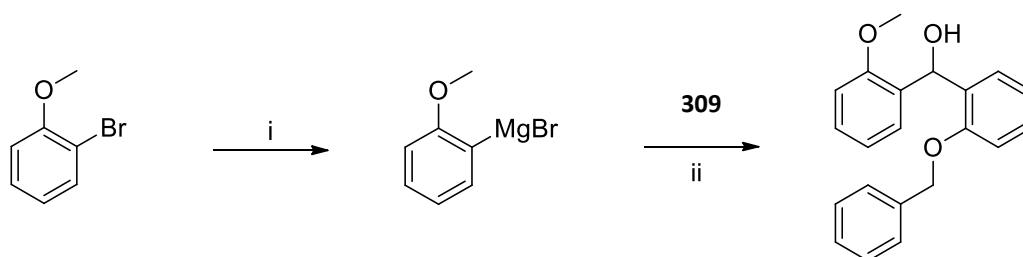
1589, 1464, 1439, 1414, 1313, 1288, 1263, 1138, 1113, 1063, 1038, 1012, 937, 912, 837, 812, 786, 762, 687, 636.

**316**

Veratrole (10.00 g, 72.38 mmol, 1 eq) was added to a NBS (12.90 g, 72.38 mmol, 1 eq)/DCM slurry. Following purification by column chromatography resulted in a dark oil that was determined to be **316** (13.65 g, 87 %) by NMR spectroscopy. $R_f = 0.69$ (20 % EtOAc/Hex) $^1\text{H NMR}$ (300 MHz, CDCl_3) $\delta_H = 6.99$ (1H, dd, $J = 8.5$ and 2.3Hz, H-6), 6.94 (1H, d, $J = 2.3$ Hz, H-2), 6.68 (1H, d, $J = 8.5$ Hz, H-5), 3.81 (3H, s, H-7*), 3.80 (3H, s, H-8*). $^{13}\text{C NMR}$ (75 MHz, CDCl_3) $\delta_C = 149.7$ (C-3*), 148.3 (C-4*), 123.3 (C-6), 120.8 (C-5), 114.8 (C-1), 112.5 (C-2), 56.0 (C-7[#]), 55.9 (C-8[#]). **IR** ($\nu_{\text{m}}, \text{cm}^{-1}$) = 3040, 2980, 2920, 2860, 1605, 1577, 1498, 1466, 1435, 1404, 1323, 1242, 1215, 1161, 1134, 1026, 864, 810, 756, 729, 621. **ESI-MS** (m/z) calculated $[\text{M}+\text{H}]^+$ for $\text{C}_8\text{H}_{10}\text{O}_2\text{Br}$ 216.9864, found 216.9860.

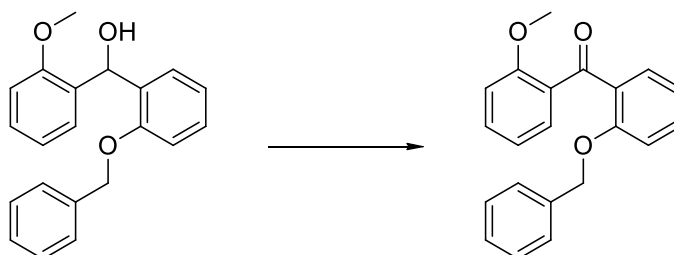
**318**

The reaction between 1,3,5-trimethoxybenzene (10.00 g, 59.46 mmol, 1 eq) and NBS (10.60 g, 59.46 mmol, 1 eq) resulted in the brominated compound **318** (11.71 g, 80 %) as white crystals. $R_f = 0.50$ (20 % EtOAc/Hexane). **m.p.** = 90-92 °C, lit 93-95 °C. $^1\text{H NMR}$ (300 MHz, CDCl_3) $\delta_H = 6.17$ (2H, s, H-3 and H-5), 3.87 (6H, s, H-7 and H-9), 3.81 (3H, s, H-8). $^{13}\text{C NMR}$ (75 MHz, CDCl_3) $\delta_C = 160.5$ (C-4), 157.5 (C-2 and C-6), 92.1 (C-1), 91.7 (C-3 and C-5), 56.4 (C-7 and C-9), 55.5 (C-8). **IR** ($\nu_{\text{m}}, \text{cm}^{-1}$) = 2970, 2933, 2824, 1578, 1468, 1431, 1395, 1321, 1219, 1190, 1161, 1132, 1074, 1016, 959, 930, 814, 785, 669, 640. **ESI-MS** (m/z) calculated $[\text{M}+\text{H}]^+$ for $\text{C}_9\text{H}_{12}\text{O}_3\text{Br}$ 246.9970, found 246.9972.

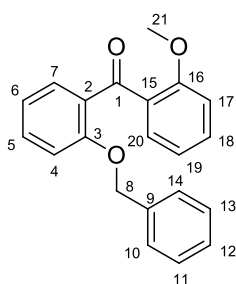
7.3.4. Grignard Reaction for the synthesis of **310****310**

In a 2-neck round bottomed flask, dry magnesium (0.183g, 7.54 mmol, 1.6 eq) was weighed out and a stirrer bar added, followed by a rubber septum and condenser. The entire chamber was then evacuated, further dried under evacuation and the chamber filled with nitrogen. This process was repeated a further 3 times. Once filled with nitrogen for the final time, THF (5 ml) was injected followed by the 2-bromoanisole (1.32 g, 7.07 mmol, 1.5 eq). Heat was applied as necessary to initiate the Grignard reagent formation and then the reaction left to stir until all the magnesium was consumed (approximately 30 min) under a nitrogen atmosphere. To the brown solution, a further 5 ml of THF was added and cooled to 0 °C. The protected salicylaldehyde **309** (1.00 g, 4.71 mmol) was dissolved in THF (5 ml) and injected dropwise into the cooled Grignard solution. An immediate colour change is observed and a bright yellow colour developed while the reaction was left to stir at 0 °C for 2 hours. 1M HCl (10 ml) was added to the reaction with vigorous stirring for 10 min, the suspension transferred to a separation funnel and the aqueous layer removed. The organic layer was further washed with brine before being dried with anhydrous MgSO₄ and concentrated *in vacuo*. The product was then purified by column chromatography with using 10-20 % EtOAc/Hexane as the eluent and **310** was collected as a yellow oil (1.48 g, 99 %). $R_f = 0.31$ (10 % EtOAc/Hexane). ¹H NMR (300 MHz, CDCl₃): $\delta_H = 7.38 - 7.20$ (7H, m, H-3, H-6, H-10, H-11, H-12, H-13 and H-14), 7.18 (1H, dd, $J = 7.5$ and 1.7 Hz, H-20), 7.00 – 6.90 (2H, m, H-4 and H-5), 6.87 (2H, d, $J = 7.7$ Hz, H-18 and H-19), 6.43 (1H, d, $J = 5.5$ Hz, H-1), 5.05 (2H, d, $J = 3.8$ Hz, H-8), 3.77 (3H, s, H-21), 3.35 (d, $J = 5.4$ Hz, 1H). ¹³C NMR (75 MHz, CDCl₃): $\delta_C = 156.91$ (C-7), 155.82 (C-16), 136.91 (C-9), 131.57 (C-2), 131.21 (C-15), 128.47 (C-11 and C-13), 128.30 (C-20), 127.94 (C-5), 127.85 (C-18), 127.79 (C-12), 127.33 (C-10 and C-14), 120.83 (C-4), 120.56 (C-19), 111.72 (C-6*), 110.50 (C-17*), 70.07 (C-8), 67.25 (C-1), 55.38 (C-21). IR ($\nu_{m.cm^{-1}}$) = 3560, 3442, 3030, 2940, 2839, 1601, 1488, 1449, 1381, 1287, 1238, 1105, 1015, 870, 745, 695, 651. ESI-MS (m/z) calculated [M+H]⁺ for C₂₁H₂₀O₃Na 343.1310, found 343.1302.

7.3.5. Method for Pyridinium Chlorochromate (PCC) oxidation



In a round bottomed flask, alcohol **310** (1.00 g, 4.71 mmol, 1 eq) was dissolved in 20 ml DCM. To this solution 1.00 g of flash chromatography silica was added followed by PCC (1.49 g, 6.92 mmol, 1.5 eq) in portions. This reaction mixture was stirred under nitrogen for 2 hours, a thick brown by product results as the reaction progresses. Once the reaction is completed (as determined by TLC) the reaction was filtered through a glass fritted funnel lined with Celite and flash silica and this plug washed with EtOAc. The filtrate was concentrated *in vacuo* and the resulting product **311** collected as a viscous yellow oil (1.131 g, 77 %) used with no further purification.



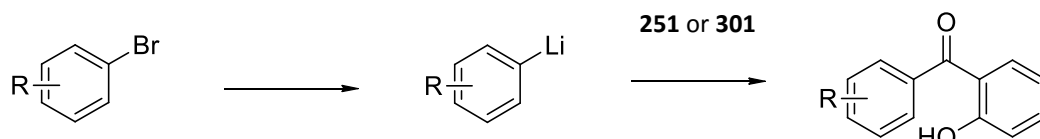
311

$R_f = 0.22$ (10 % EtOAc/Hexane). $^1\text{H NMR}$ (300 MHz, CDCl_3): $\delta_{\text{H}} = 7.60$ (1H, dd, $J = 7.6, 1.8$ Hz, H-7), 7.52 (1H, dd, $J = 7.6, 1.8$ Hz, H-20), 7.40 (2H, m, H-5 and H-18), $7.22 - 7.17$ (3H, m, H-11, H-12 and H-13), $7.07 - 7.00$ (1H, m, H-6), $7.00 - 6.90$ (4H, m, H-4, H-10, H-14 and H-19), 6.82 (1H, dd, $J = 8.4$ and 0.9 Hz, H-17), 4.93 (2H, s, H-8), 3.59 (3H, d, $J = 0.6$ Hz, H-21). $^{13}\text{C NMR}$ (75 MHz, CDCl_3): $\delta_{\text{C}} = 195.5$ (C-1), 158.3 (C-3[#]), 157.2 (C-

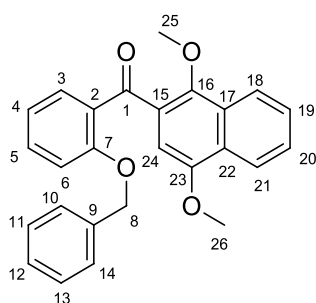
16[#]), 136.4 (C-9), 132.6 (C-18*), 132.5 (C-5*), 130.9 (C-2[~]), 130.6 (C-15[~]), 130.4 (C-7), 130.3 (C-20), 128.2 (C-11 and C-13), 127.4 (C-12), 126.7 (C-10 and C-14), 120.8 (C-6), 120.3 (C-4'), 112.4 (C-19'), 111.6 (C-17), 70.1 (C-8), 55.6 (C-21). IR ($\nu_{\text{m}} \cdot \text{cm}^{-1}$) = 3027, 2944, 2837, 1642, 1596, 1484, 1446, 1382, 1308, 1248, 1161, 1103, 1022, 924, 853, 750, 695, 638. ESI-MS (m/z) calculated $[\text{M}+\text{H}]^+$ for $\text{C}_{21}\text{H}_{19}\text{O}_3$ 319.1334, found 319.1340.

* Care should be taken when disposing of the silica plug as PCC contains toxic chromium.

7.3.6. General procedure for the lithiation reactions to form benzophenones



After drying a 2-necked flask and stirrer bar in an oven overnight, a rubber septum was fitted to one neck of the flask and a nitrogen line attached to the other. The flask was evacuated, heated and filled with nitrogen several times before the addition of the relevant substituted bromobenzene (1.1 eq) and dry THF. Once the substituted bromobenzene had completely dissolved, the solution was cooled to $-78\text{ }^{\circ}\text{C}$ and *n*-BuLi (1.1 eq) added dropwise with high stirring. This solution was left to stir for 30 min at $-78\text{ }^{\circ}\text{C}$. During this time, the protected salicylic acid (**251** or **301**) (1 eq) was added to another dry 2-necked flask also fitted with a stirrer bar, rubber septum and nitrogen line. This flask was then evacuated and filled with nitrogen repeatedly before the addition of dry THF injected through the rubber septum. Once the ester had completely dissolved, it was cooled to $-78\text{ }^{\circ}\text{C}$ with high stirring. The lithiated solution was added to the ester solution dropwise over several minutes. The mixture was left to react at $-78\text{ }^{\circ}\text{C}$ for 1-2 hours under nitrogen, saturated NH_4Cl added to quench the solution and warmed to room temperature. The suspension was extracted with water and brine and washed with EtOAc, dried over anhydrous Na_2SO_4 and concentrated *in vacuo*. The resulting products were purified by flash column chromatography with 10-20 % EtOAc/Hexane as the eluent and characterised by NMR spectroscopy.

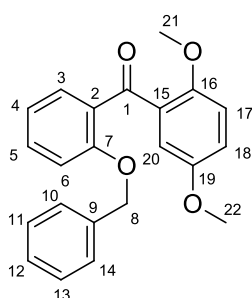


252

Following the general procedure, brominated dimethoxynaphthalene **250** (1.964 g, 7.353 mmol, 1.1 eq), *n*-BuLi (5.74 ml, 7.353 mmol, 1.28 M, 1.1 eq) and ester **251** (2.128 g, 6.685 mmol, 1 eq) were reacted. Following purification by flash column chromatography, the product **252** (1.541 g, 58 %) was collected as a green oil. $R_f = 0.56$ (20 % EtOAc/Hexane). $^1\text{H NMR}$ (300 MHz, CDCl_3) $\delta_{\text{H}} = 8.28 - 8.21$ (1H, m, H-18), 8.11 – 8.03 (1H, m, H-21), 7.72 – 7.65 (1H, m, H-3), 7.59 – 7.51 (2H, m, H-19 and H-20), 7.50 – 7.41 (1H, m, H-5), 7.13 – 7.04 (2H, m, H-4 and H-6), 7.03 – 6.97 (1H, m, H-12), 6.96 – 6.86 (3H, m, H-10, H-14 and H-24), 6.79 – 6.72 (2H, m, H-11 and H-13), 4.90 (2H, s, H-

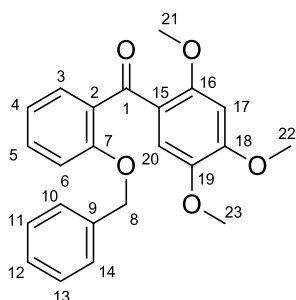
Experimental

8), 3.92 (3H, s, H-25*), 3.59 (3H, s, H-26*). $^{13}\text{C NMR}$ (75 MHz, CDCl_3) δ_{C} = 196.2 (C-1), 157.5 (C-7*), 151.7 (C-16*), 150.3 (C-23*), 135.9 (C-9), 132.9 (C-5), 130.2 (C-3), 128.8 (C-17), 128.4 (C-2), 127.9 (C-10 and C-24), 127.5 (C-4[#]), 127.2 (C-22), 126.8 (C-11, C-13, C-19 and C-20), 123.1 (C-21), 122.4 (C-18), 120.7 (C-6[#]), 112.4 (C-12), 103.1 (C-24), 96.8 (C-15), 70.3 (C-8), 63.6 (C-26'), 55.8 (C-25').



296

2-Bromo-1,4-dimethoxybenzene **289** (2.50 g, 11.5 mmol, 1 eq), *n*-BuLi (8.2 ml, 11.5 mmol, 1.4 M, 1 eq) and ester **251** (3.66 g, 11.5 mmol, 1 eq) were reacted following the general procedure. The product, **296**, was collected as a yellow oil (2.83 g, 71 %) after purification by flash column chromatography. R_f = 0.17 (10 % EtOAc/Hexane). $^1\text{H NMR}$ (300 MHz, CDCl_3) δ_{H} = 7.58 (1H, dd, J = 7.6 and 1.8 Hz, H-7), 7.41 (1H, ddd, J = 8.3, 7.4 and 1.8 Hz, H-5), 7.35 – 7.31 (1H, m, H-12), 7.23 – 7.17 (2H, m, H-10 and H-14), 7.08 (1H, d, J = 3.2 Hz, H-20), 7.02 (1H, td, J = 7.5 and 1.0 Hz, H-6), 6.98 – 6.89 (4H, m, H-4, H-18, H-11 and H-13), 6.74 (1H, d, J = 9.0 Hz, H-17), 4.92 (2H, s, H-8), 3.73 (3H, s, H-21*), 3.50 (3H, s, H-22*). $^{13}\text{C NMR}$ (75 MHz, CDCl_3) δ_{C} = 195.3 (C-1), 157.2 (C-3*), 153.5 (C-16*), 152.7 (C-19*), 136.4 (C-5), 132.6 (C-7), 131.2 (C-9), 130.8 (C-15[#]), 130.3 (C-2[#]), 128.2 (C-10 and C-14), 127.5 (C-12), 126.9 (C-6), 126.7 (C-11 and C-13), 120.7 (C-4), 118.5 (C-18), 114.5 (C-17), 112.3 (C-20), 70.1 (C-8), 56.4 (C-21'), 55.8 (C-22').

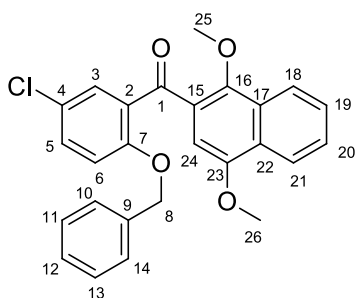


299

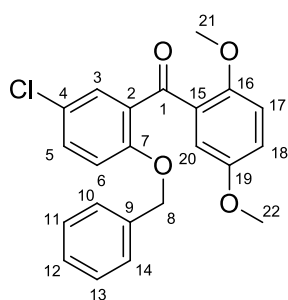
Following the general procedure, 1-bromo-2,4,5-trimethoxybenzene **246** (0.500 g, 2.023 mmol, 1.1 eq) and *n*-BuLi (1.84 ml, 2.208 mmol, 1.2 M, 1.2 eq) were reacted, with a yellow colour observed on the formation of the lithiated species. This was further reacted with ester **251** (0.586 g, 1.840 mmol, 1 eq) and the resulting product **299** collected as a yellow liquid (0.404 g, 58 %) after purification by flash column chromatography. R_f = 0.20 (20 % EtOAc/Hexane). $^1\text{H NMR}$ (500 MHz, CDCl_3): δ_{H} = 7.50 (1H, dd, J = 7.5 and 1.8 Hz, H-3), 7.39 (1H, ddd, J = 8.3, 7.4 and 1.8 Hz, H-5), 7.26 (1H, s, H-20), 7.21 (3H, dt, J = 4.4 and 1.6 Hz, H-10, and H-12 H-14), 7.03 (1H, td, J = 7.5 and 1.0 Hz, H-4), 7.01 – 6.98 (2H, m, H-11 and H-13), 6.95 (1H, dd, J = 8.3 and 0.9 Hz, H-6), 6.34 (1H, s, H-17), 4.98 (2H, s, H-8), 3.87 (3H, s, H-21), 3.86 (3H, s, H-22), 3.50 (3H, s, H-23). $^{13}\text{C NMR}$ (75 MHz, CDCl_3): δ_{C} = 194.0 (C-1), 156.5 (C-7[#]), 155.1 (C-16[#]), 153.4 (C-19[#]), 143.2 (C-18),

Experimental

136.6 (C-9), 132.4 (C-2), 131.6 (C-5), 129.6 (C-3), 128.1 (C-10 and C-14), 127.5 (C-12), 126.5 (C-11 and C-13), 121.6 (C-15), 120.8 (C-4), 113.3 (C-20), 112.1 (C-6), 97.3 (C-17), 70.1 (C-8), 56.7 (C-21*), 56.5 (C-22*), 56.0 (C-23*).

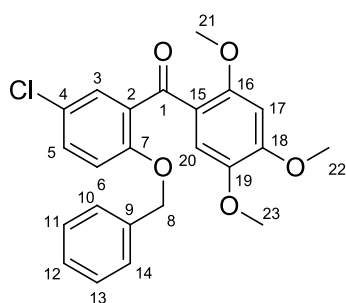
**302**

Brominated **250** (2.94 g, 10.99 mmol, 1.1 eq) was lithiated using *n*-BuLi (8.6 ml, 1.28 M, 10.99 mmol, 1.1 eq) and combined with ester **301** (3.53 g, 9.99 mmol) following the general procedure. The product was collected as a cream solid (1.54 g, 32 %). $R_f = 0.53$ (20 % EtOAc/Hexane). **m.p.** = 165-167 °C, lit 160-162 °C.¹⁹¹ **¹H NMR** (300 MHz, CDCl₃): $\delta_H = 8.29 - 8.21$ (1H, m, H-18), 8.11 – 8.03 (1H, m, H-21), 7.69 (1H, dd, $J = 7.5$ and 1.8 Hz, H-5), 7.58 – 7.50 (2H, m, H-19 and H-20), 7.50 – 7.45 (1H, m, H-3), 7.09 (1H, dt, $J = 8.0$ and 1.4 Hz, H-12), 7.07 – 6.97 (1H, m, H-6), 6.95 – 6.87 (3H, m, H-10, H-14 and H-24), 6.78 – 6.72 (2H, m, H-11 and H-13), 4.90 (2H, s, H-8), 3.92 (3H, s, H-25*), 3.59 (3H, s, H-26*). **¹³C NMR** (75 MHz, CDCl₃): $\delta_C = 196.2$ (C-1), 157.5 (C-7*), 151.7 (C-16*), 150.3 (C-23*), 135.9 (C-9), 132.9 (C-3), 130.2 (C-5), 129.0 (C-4'), 128.4 (C-17'), 127.9 (C-10 and C-14), 127.5 (C-2), 127.2 (C-22), 126.8 (C-11, C-13, C-19 and C-20), 123.1 (C-21), 122.4 (C-18), 120.7 (C-6), 112.4 (C-12), 103.0 (C-24), 100.0 (C-15) 70.3 (C-8), 63.6 (C-26[#]), 55.8 (C-25[#]).

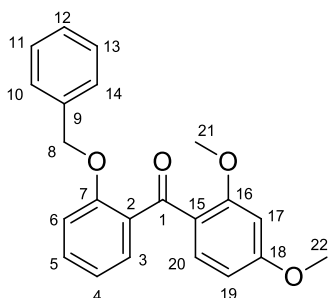
**303**

Following the general procedure, ester **301** (1.343 g, 3.807 mmol), brominated **289** (0.909 g, 4.188 mmol, 1.1 eq) and *n*-BuLi (3.35 ml, 4.188 mmol, 1.25 M, 1.1 eq) were combined at -78 °C. The product **303** was collected as a yellow solid after purification by column chromatography (1.103 g, 76 %). $R_f = 0.37$ (20 % EtOAc/Hexane). **m.p.** = 76-78 °C, lit 70-72 °C.¹⁹¹ **¹H NMR** (300 MHz, CDCl₃): $\delta_H = 7.52$ (1H, d, $J = 2.7$ Hz, H-3), 7.39 – 7.32 (1H, m, H-5), 7.21 (3H, dd, $J = 5.0$ and 1.9 Hz, H-11, H-12 and H-13), 7.11 (1H, d, $J = 3.2$ Hz, H-20), 6.94 (3H, m, H-10, H-14 and H-18), 6.88 (1H, d, $J = 8.8$ Hz, H-6), 6.76 (1H, d, $J = 9.0$ Hz, H-17), 4.91 (2H, s, H-8), 3.76 (3H, s, H-21*), 3.52 (3H, s, H-22*). **¹³C NMR** (75 MHz, CDCl₃): $\delta_C = 193.8$ (C-1), 155.6 (C-7[#]), 153.6 (C-16[#]), 152.9 (C-19[#]), 136.0 (C-9), 132.4 (C-4), 131.8 (C-5), 130.2 (C-15), 129.7 (C-3), 128.3 (C-11 and C-13), 127.7 (C-12), 126.7 (C-10 and C-14), 125.9 (C-2), 119.2 (C-18), 114.4 (C-20), 113.7 (C-6), 113.4 (C-17), 70.5 (C-8), 56.3 (C-21*), 55.9 (C-22*).

Experimental

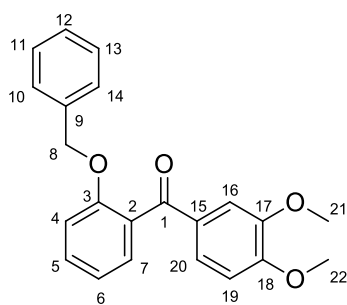
**304**

Combining brominated **246** (5.00 g, 20.23 mmol, 1.1 eq), *n*-BuLi (15.8 ml, 1.28 M, 20.23 mmol, 1.1 eq) and ester **301** (5.99 g, 18.39 mmol, 1 eq) according to the general procedure resulted in the formation of a yellow oil that was determined to be **304** (5.08g, 61 %). $R_f = 0.21$ (10 % EtOAc/Hexane). $^1\text{H NMR}$ (500 MHz, CDCl_3): $\delta_{\text{H}} = 7.42$ (1H, d, $J = 2.7$ Hz, H-7), 7.30 (1H, dd, $J = 8.7$ and 2.7 Hz, H-5), 7.26 (1H, s, H-20), 7.22 – 7.18 (3H, m, H-11, H-12 and H-13), 6.99 – 6.94 (2H, m, H-10 and H-14), 6.86 (1H, d, $J = 8.8$ Hz, H-4), 6.32 (1H, s, H-17), 4.92 (2H, s, H-8), 3.86 (3H, s, H-21*), 3.84 (3H, s, H-22*), 3.48 (3H, s, H-23). $^{13}\text{C NMR}$ (125 MHz, CDCl_3): $\delta_{\text{C}} = 192.3$ (C-1), 155.4 (C-7), 154.9 (C-16[#]), 154.0 (C-19[#]), 143.3 (C-18[#]), 136.1 (C-9), 133.9 (C-4), 130.9 (C-5), 128.9 (C-3), 128.2 (C-11 and C-13), 127.6 (C-12), 126.5 (C-10 and C-14), 125.8 (C-2), 120.5 (C-15), 113.5 (C-6), 113.1 (C-20), 96.9 (C-17), 70.4 (C-8), 56.4 (C-21*), 56.3 (C-22*), 56.0 (C-23*).

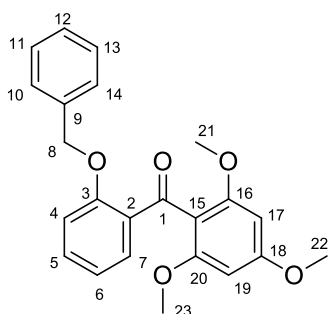
**319**

Combining brominated **314** (3.77 g, 17.30 mmol, 1.1 eq), *n*-BuLi (13.5 ml, 17.30 mmol, 1.28 M, 1.1 eq) and ester **251** (5.00 g, 15.73 mmol, 1 eq) according to the general procedure resulted in the formation of a yellow oil that was determined to be **319** (5.03 g, 92 %). $R_f = 0.44$ (20 % EtOAc/Hexane). $^1\text{H NMR}$ (300 MHz, CDCl_3): $\delta_{\text{H}} = 7.58$ (1H, dd, $J = 8.7$ and 1.3 Hz, H-17), 7.50 (1H, dd, $J = 7.5$ and 1.8 Hz, H-3), 7.42 – 7.34 (1H, m, H-5), 7.24 – 7.17 (3H, m, H-10, H-12 and H-14), 7.06 – 6.96 (3H, m, H-4, H-11 and H-13), 6.94 (1H, dd, $J = 8.4$ and 1.0 Hz, H-6), 6.48 (1H, dd, $J = 8.6$ and 2.3, H-19), 6.33 (1H, d, $J = 2.2$ Hz, H-20), 4.95 (2H, s, H-8), 3.81 (3H, s, H-21*), 3.57 (3H, s, H-22*). $^{13}\text{C NMR}$ (75 MHz, CDCl_3): $\delta_{\text{C}} = 194.1$ (C-1), 164.1 (C-7*), 160.7 (C-16*), 156.6 (C-18*), 136.6 (C-9), 133.0 (C-17), 132.0 (C-2'), 131.7 (C-5), 129.8 (C-3), 128.1 (C-10 and C-14), 127.4 (C-12), 126.6 (C-11 and C-13), 123.2 (C-15'), 120.8 (C-4), 112.3 (C-6), 104.7 (C-19), 98.6 (C-20), 70.1 (C-8), 55.6 (C-21[#]), 55.4 (C-22[#]). $\text{IR (}\nu_{\text{m}}\text{.cm}^{-1}\text{)} = 3013, 2947, 2843, 1624, 1601, 1504, 1483, 1433, 1333, 1306, 1285, 1242, 1209, 1150, 1144, 1030, 945, 826, 758$. ESI-MS (m/z) calculated $[\text{M}+\text{H}]^+$ for $\text{C}_{22}\text{H}_{21}\text{O}_4$ 349.1140, found 349.1438.

Experimental

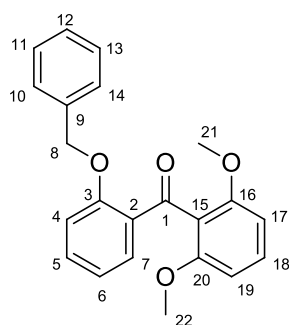
**320**

Combining brominated **316** (3.78 g, 17.30 mmol, 1.1 eq), *n*-BuLi (13.5 ml, 17.30 ml, 1.1 eq) and ester **251** (5.00 g, 15.73 mmol, 1 eq) according to the general procedure resulted in the formation of a yellow oil that was determined to be **320** (2.41 g, 44 %). $R_f = 0.36$ (20 % EtOAc/Hexane). $^1\text{H NMR}$ (300 MHz, CDCl_3): $\delta_{\text{H}} = 7.58$ (1H, d, $J = 8.6$ Hz, H-19), 7.50 (1H, dd, $J = 7.5$ and 1.8 Hz, H-4*), 7.43 – 7.32 (1H, m, H-7*), 7.23 – 7.16 (3H, m, H-10, H-12 and H-14), 7.05 – 6.93 (4H, m, H-5*, H-6*, H-11 and H-13), 6.48 (1H, dd, $J = 8.6$ and 2.3 Hz, H-20), 6.33 (1H, d, $J = 2.3$ Hz, H-16), 4.95 (2H, s, H-8), 3.81 (3H, s, H-21'), 3.57 (3H, s, H-22'). $^{13}\text{C NMR}$ (125 MHz, CDCl_3): $\delta_{\text{C}} = 194.1$ (C-1), 164.0 (C-3[#]), 160.7 (C-18[#]), 156.6 (C-17[#]), 136.6 (C-9), 133.0 (C-19), 132.0 (C-15[~]), 131.7 (C-7*), 129.8 (C-4*), 128.1 (C-10 and C-14), 127.4 (C-12), 126.6 (C-11 and C-13), 123.2 (C-2[~]), 120.8 (C-5*), 112.3 (C-6*), 104.7 (C-20), 98.5 (C-16), 70.1 (C-8), 55.6 (C-21'), 55.4 (C-22'). IR ($\nu_{\text{m}}\cdot\text{cm}^{-1}$) = 3024, 2943, 2862, 2376, 1647, 1593, 1521, 1485, 1458, 1431, 1296, 1269, 1107, 1053, 1026, 918, 729, 702. ESI-MS (m/z) calculated $[\text{M}+\text{H}]^+$ for $\text{C}_{22}\text{H}_{21}\text{O}_4$ 349.1140, found 349.1441.

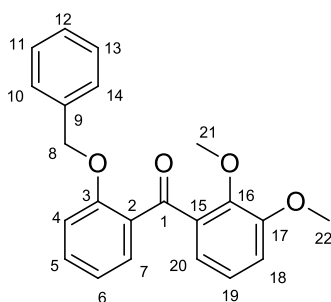
**321**

Combining brominated **318** (4.27 g, 17.28 mmol, 1.1 eq), *n*-BuLi (13.5 ml, 17.28 mmol, 1.28 M, 1.1 eq) and ester **251** (5.00 g, 15.71 mmol, 1 eq) according to the general procedure resulted in the formation of a yellow oil that was determined to be **321** (2.65 g, 45 %). $R_f = 0.18$ (20 % EtOAc/Hexane). $^1\text{H NMR}$ (300 MHz, CDCl_3): $\delta_{\text{H}} = 7.72$ (1H, dd, $J = 7.7$ and 1.9 Hz, H-7), 7.35 (1H, ddd, $J = 8.3, 7.3$ and 1.9 Hz, H-5), 7.24 (3H, dd, $J = 5.0$ and 1.9 Hz, H-10, H-12 and H-14), 7.12 (2H, dd, $J = 6.7$ and 2.9 Hz, H-11 and H-13), 7.00 – 6.88 (2H, m, H-4 and H-6), 5.96 (2H, s, H-17 and H-19), 4.89 (2H, s, H-8), 3.72 (3H, s, H-22), 3.52 (6H, s, H-21 and H-23). $^{13}\text{C NMR}$ (75 MHz, CDCl_3): $\delta_{\text{C}} = 193.3$ (C-1), 162.1 (C-3), 158.8 (C-16 and C-20), 157.9 (C-18), 136.5 (C-9), 133.1 (C-5), 131.3 (C-7), 130.3 (C-2), 128.1 (C-10 and C-14), 127.5 (C-12), 127.3 (C-11 and C-13), 120.5 (C-4*), 114.8 (C-15), 113.0 (C-6*), 90.8 (C-17 and C-19), 70.3 (C-8), 55.8 (C-21 and C-23), 55.2 (C-22). IR ($\nu_{\text{m}}\cdot\text{cm}^{-1}$) = 3001, 2978, 2931, 2862, 2839, 1659, 1485, 1458, 1431, 1377, 1296, 1242, 1161, 1107, 1026, 999, 918, 891, 849, 802, 779, 756, 733, 687, 640, 617. ESI-MS (m/z) calculated $[\text{M}+\text{H}]^+$ for $\text{C}_{23}\text{H}_{23}\text{O}_5$ 379.1545, found 379.1546.

Experimental

**322**

A directed ortho-metalation was performed using 1,3-dimethoxybenzene **313** (2.39 g, 17.30 mmol, 1.1 eq) and *n*-BuLi (13.5 ml, 1.28 M, 17.30 mmol, 1.1 eq) at -78 °C in dry THF. This solution was added to ester **251** (5.00 g, 15.73 mmol, 1 eq) also at -78 °C and the reaction mixture stirred for 2 hours. The reaction was quenched and purified as outlined in the general procedure and **322** was collected as a peach solid (4.41 g, 81 %). $R_f = 0.26$ (20 % EtOAc/Hexane). **m.p.** = 85-87 °C. $^1\text{H NMR}$ (300 MHz, CDCl_3): $\delta_{\text{H}} = 7.77$ (1H, dd, $J = 7.7$ and 1.8 Hz, H-7), 7.37 (1H, ddd, $J = 8.4$, 7.3 and 1.9 Hz, H-5), 7.30 (2H, d, $J = 4.6$ Hz, H-10 and H-14), 7.24 (2H, dd, $J = 5.2$ and 1.8 Hz, H-11 and H-13), 7.15 (1H, d, $J = 8.5$ Hz, H-18), 7.13 – 7.09 (1H, m, H-12), 6.96 (1H, dd, $J = 7.6$ and 1.0 Hz, H-4*), 6.94 – 6.87 (1H, m, H-6*), 6.42 (2H, d, $J = 8.4$ Hz, H-17 and H-19), 4.90 (2H, s, H-8), 3.55 (6H, s, H-21 and H-22). $^{13}\text{C NMR}$ (75 MHz, CDCl_3): $\delta_{\text{C}} = 194.1$ (C-1), 158.3 (C-3), 157.3 (C-16 and C-20), 136.4 (C-9), 133.6 (C-5), 131.7 (C-7), 130.1 (C-18), 128.2 (C-10 and C-14), 127.4 (C-2), 127.2 (C-11 and C-13), 126.9 (C-12), 120.5 (C-18), 113.2 (C-15), 104.2 (C-17 and C-19), 70.3 (C-8), 55.8 (C-21 and C-22). **IR** ($\nu_{\text{m}} \cdot \text{cm}^{-1}$) = 2943, 2889, 2835, 2376, 1674, 1593, 1485, 1458, 1431, 1296, 1269, 1242, 1161, 1107, 1026, 999, 945, 918, 864, 783, 756, 729, 702, 621. **ESI-MS** (m/z) calculated $[\text{M}+\text{H}]^+$ for $\text{C}_{22}\text{H}_{21}\text{O}_4$ 349.1140, found 349.1440.

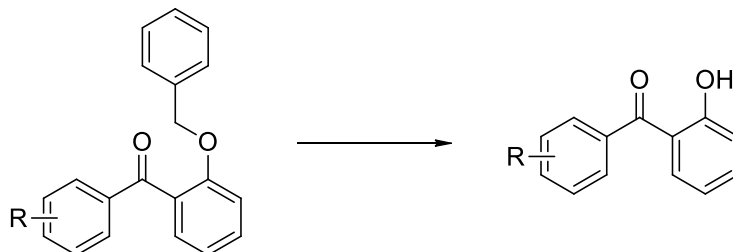
**323**

A directed ortho-metalation reaction was performed in order to synthesize **323**. Veratrole **315** (2.39 g, 17.30 mmol, 1.1 eq) was lithiated using *n*-BuLi (13.5 ml, 1.28M, 17.30 mmol, 1.1 eq) at -78 °C in dry THF. This solution was added to ester **251** (5.00 g, 15.73 mmol, 1 eq) and the general procedure followed. After purification by flash column chromatography, **323** was collected as a liquid (2.35 g, 43 %). $R_f = 0.38$ (20 % EtOAc/Hexane). $^1\text{H NMR}$ (500 MHz, CDCl_3): $\delta_{\text{H}} = 7.62$ (1H, dd, $J = 7.6$ and 1.8, H-7), 7.43 (1H, ddd, $J = 8.3$, 7.4 and 1.8 Hz, H-5), 7.19 (3H, dd, $J = 5.1$ and 2.0 Hz, H-10, H-12 and H-14), 7.07 (1H, dd, $J = 7.7$ and 1.7 Hz, H-19), 7.03 (2H, t, $J = 7.8$ Hz, H-6 and H-20), 6.96 (4H, ddd, $J = 7.9$, 5.2 and 1.2 Hz, H-4, H-11, H-13 and H-18), 4.93 (2H, s, H-8), 3.80 (3H, s, H-21*), 3.52 (3H, s, H-22*). $^{13}\text{C NMR}$ (125 MHz, CDCl_3): $\delta_{\text{C}} = 195.7$ (C-1), 157.4 (C-3), 152.7 (C-16*), 148.0 (C-17*), 136.3 (C-9), 135.8 (C-2), 132.9 (C-5), 130.5 (C-7), 130.3 (C-15), 128.2 (C-10 and C-14), 127.5, 126.8 (C-11 and H-13), 123.6 (C-6'), 121.1 (C-19), 120.7 (C-20'), 115.1 (C-4#),

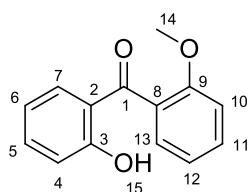
Experimental

112.5 (C-18[#]), 70.1 (C-8), 61.3 (C-21'), 56.0 (C-22'). **IR** ($\nu_{\text{m}} \cdot \text{cm}^{-1}$) = 2943, 2889, 2835, 1647, 1593, 1566, 1485, 1458, 1431, 1377, 1296, 1269, 1242, 1161, 1107, 1080, 1053, 1026, 999, 972, 837, 756, 702, 621. **ESI-MS** (**m/z**) calculated $[\text{M}+\text{H}]^+$ for $\text{C}_{22}\text{H}_{21}\text{O}_4$ 349.1140, found 349.1442.

7.3.7. General procedure for the debenzylation of organic compounds using palladium on carbon



10 % Palladium on activated carbon (10 mass %) was added to the desired benzylated ketone and dissolved in MeOH (30 ml). The resulting suspension was then exposed to a H₂ atmosphere at ambient pressure, stirring at room temperature for 12 hours and then filtered through a Celite/flash silica plug, washed with EtOAc and concentrated *in vacuo*. If all the palladium was successfully removed the product was used with no further purification, if not the product was cleaned using column chromatography.

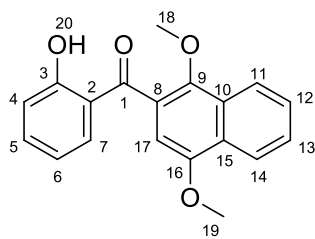


312

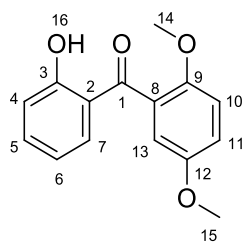
Following the general procedure for debenzylation, ketone **311** (1.131 g, 3.716 mmol) and 10 % Pd/C (0.113 g, 10 mass %) in 30 ml of MeOH resulted in the formation of **312** (0.717 g, 85 %) as a yellow solid after filtration and concentration was used with no further purification. *R_f* = 0.42 (10 % EtOAc/Hexane). *m.p.* = 74-75 °C. ¹H NMR (300 MHz, CDCl₃): δ_H = 12.19 (1H, s, H-

15), 7.51 – 7.41 (2H, m, H-7 and H-13), 7.33 (1H, dd, *J* = 8.0 and 1.8 Hz, H-11), 7.28 (1H, dd, *J* = 7.5 and 1.8 Hz, H-5), 7.08 – 6.98 (3H, m, H-6, H-10 and H-12), 6.79 (1H, ddd, *J* = 8.1, 7.2 and 1.2 Hz, H-4), 3.76 (3H, s, H-14). ¹³C NMR (75 MHz, CDCl₃): δ_C = 202.10 (C-1), 162.90 (C-3), 156.55 (C-9), 136.44 (C-5), 133.75 (C-11), 131.85 (C-7), 128.79 (C-13), 127.83 (C-8), 120.52 (C-6), 120.22 (C-2), 118.68 (C-12), 118.03 (C-4), 111.48 (C-10), 55.64 (C-14). IR (ν_m.cm⁻¹) = 3026, 2968, 2939, 2835, 1601, 1483, 1463, 1447, 1333, 1306, 1279, 1244, 1146, 1117, 1101, 1020, 932, 824, 793, 748, 698, 640. ESI-MS (*m/z*) calculated [M+H]⁺ for C₁₄H₁₃O₃ 229.0865, found 229.0866.

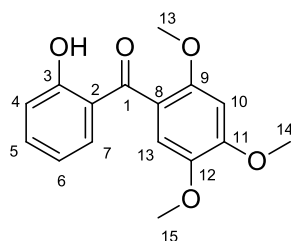
Experimental

**253**

Protected ketone **134** (0.610 g, 1.53 mmol) and 5 % Pd/C (0.031 g, 10 mass %) were reacted according to the general procedure under a hydrogen atmosphere. After purification by column chromatography in 10 % EtOAc/Hexane, **253** was collected as yellow crystals (0.349 g, 74 %). $R_f = 0.22$ (10 % EtOAc/Hexane). **m.p.** = 117-119 °C, lit 116-118 °C. $^{191}\text{H NMR}$ (500 MHz, CDCl_3): $\delta_{\text{H}} = 12.22$ (1H, s, H-20), 8.35 – 8.27 (1H, m, H-11), 8.20 – 8.12 (1H, m, H-14), 7.60 (2H, td, $J = 6.5, 5.9$ and 3.4 Hz, H-12 and H-13), 7.53 – 7.43 (2H, m, H-5 and H-7), 7.06 (1H, dd, $J = 8.3$ and 1.1 Hz, H-4), 6.81 (1H, ddd, $J = 8.3, 7.1$ and 1.2 Hz, H-6), 6.68 (1H, s, H-17), 3.97 (3H, s, H-18*), 3.82 (3H, s, H-19*). $^{13}\text{C NMR}$ (125 MHz, CDCl_3): $\delta_{\text{C}} = 202.4$ (C-1), 163.0 (C-3), 151.8 (C-9), 147.5 (C-16), 136.8 (C-5*), 134.1 (C-7*), 128.4 (C-2), 127.7 (C-10), 127.3 (C-12[#]), 127.1 (C-13[#]), 126.3 (C-15), 122.7 (C-14), 122.6 (C-11), 119.9 (C-8), 119.0 (C-17), 118.1 (C-6), 102.3 (C-17), 63.7 (C-18'), 55.8 (C-19').

**258**

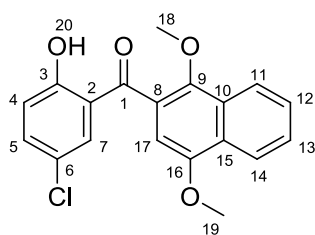
Benzophenone **296** (2.00 g, 5.74 mmol) and 5 % Pd/C (0.100 g, 10 mass %) were reacted according to the general procedure and collected as a white solid (**258**) after purification (1.12 g, 76 %). $R_f = 0.33$ (10 % EtOAc/Hexane). **m.p.** = 86-87 °C, lit 96-98 °C. $^{191}\text{H NMR}$ (300 MHz, CDCl_3): $\delta_{\text{H}} = 12.12$ (1H, s, H-16), 7.47 (1H, ddd, $J = 8.6, 7.1$ and 1.7 Hz, H-5), 7.36 (1H, dd, $J = 8.0, 1.7$, H-3), 7.06 – 6.99 (2H, m, H-6 and H-11), 6.94 (1H, d, $J = 9.0$ Hz, H-10), 6.85 (1H, d, $J = 3.0$ Hz, H-13), 6.81 (1H, ddd, $J = 8.2, 7.2$ and 1.2, H-4), 3.79 (3H, s, H-14*), 3.72 (3H, s, H-15*). $^{13}\text{C NMR}$ (75 MHz, CDCl_3): $\delta_{\text{C}} = 201.7$ (C-1), 162.9 (C-7), 153.5 (C-9), 150.6 (C-12'), 136.5 (C-5), 133.8 (C-3), 128.4 (C-2), 120.1 (C-8), 118.7 (C-4), 118.1 (C-6*), 117.1 (C-11*), 114.0 (C-13), 113.0 (C-10), 56.4 (C-14[#]), 55.9 (C-15[#]).

**261**

Following the general procedure, **299** (0.404 g, 1.067 mmol) and 5 % Pd/C (0.080 g, 20 mass %) was dissolved in methanol under a hydrogen atmosphere. The product **261** was collected as a yellow oil that solidified on standing (3.04 g, 99 %). $R_f = 0.23$ (20 % EtOAc/Hexane). **m.p.** = 105-107 °C, lit 107-110 °C. $^{191}\text{H NMR}$ (500 MHz, CDCl_3): $\delta_{\text{H}} = 12.16$ (1H, s, H-16), 7.46

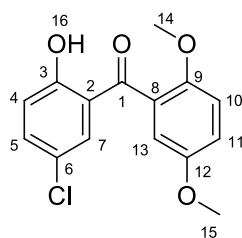
Experimental

(1H, ddd, $J = 8.6, 7.2$ and 1.7 Hz, H-5), 7.42 (1H, dd, $J = 8.0$ and 1.7 Hz, H-7), 7.03 (1H, dd, $J = 8.4$ and 1.2 Hz, H-4), 6.89 (1H, s, H-13), 6.82 (1H, ddd, $J = 8.1, 7.1$ and 1.1 Hz, H-6), 6.59 (1H, s, H-10), 3.97 (3H, s, H-13*), 3.85 (3H, s, H-14*), 3.75 (3H, s, H-15*). $^{13}\text{C NMR}$ (125 MHz, CDCl_3): $\delta_{\text{C}} = 201.0$ (C-1), 162.8 (C-3*), 152.2 (C-9*), 152.0 (C-11*), 143.1 (C-12*), 136.2 (C-5), 133.8 (C-7), 120.4 (C-2'), 119.0 (C-8'), 118.5 (C-6), 118.0 (C-4), 112.7 (C-13), 97.4 (C-10), 56.6 (C-13[#]), 56.6 (C-14[#]), 56.2 (C-15[#]).



263

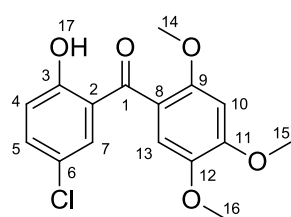
The general procedure was followed by combining **302** (1.54 g, 3.548 mmol) and 5 % Pd/C (0.152 g, 10 mass %) in 20 ml EtOAc for 1 hour under a hydrogen atmosphere. The product **263** was purified as outlined in the general procedure (0.511 g, 42 %) and collected as a yellow solid. $R_f = 0.71$ (20 % EtOAc/Hexane). $m.p. = 165$ -167 °C, lit 109-111 °C. $^{191}\text{H NMR}$ (500 MHz, CDCl_3): $\delta_{\text{H}} = 12.12$ (1H, s, H-20), 8.37 – 8.27 (1H, m, H-11), 8.21 – 8.12 (1H, m, H-14), 7.69 – 7.58 (2H, m, H-12 and H-13), 7.49 – 7.40 (2H, m, H-7 and H-5), 7.03 (1H, dd, $J = 8.5$ and 0.8 Hz, H-4), 6.65 (1H, s, H-17), 4.00 (3H, s, H-18*), 3.83 (3H, s, H-19*). $^{13}\text{C NMR}$ (126 MHz, CDCl_3): $\delta_{\text{C}} = 201.6$ (C-1), 161.5 (C-3), 158.6 (C-9[~]), 152.0 (C-16[~]), 136.7 (C-5*), 132.9 (C-7*), 128.5 (C-10), 127.9 (C-15), 127.5 (C-12'), 127.4 (C-13'), 125.7 (C-6), 123.8 (C-8), 122.8 (C-14), 122.7 (C-11), 120.6 (C-2), 119.8 (C-4), 102.0 (C-17), 63.8 (C-18[#]), 55.9 (C-19[#]).



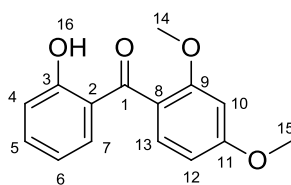
265

Following the general procedure, protected benzophenone **303** (1.013 g, 2.646 mmol) and 5 % Pd/C (0.100 g, 10 mass %) were combined in EtOAc (50 ml) for 4 hours. Following purification by flash column chromatography with an eluent consisting of 20 % EtOAc/Hexane, the product **265** was collected as a yellow solid (0.664 g, 79 %) $R_f = 0.56$ (20 % EtOAc/Hexane). $m.p. = 96$ -98 °C, lit 74-76 °C. $^{191}\text{H NMR}$ (300 MHz, CDCl_3): $\delta_{\text{H}} = 12.02$ (1H, s, H-16), 7.41 (1H, dd, $J = 8.9$ and 2.7 Hz, H-5), 7.31 (1H, d, $J = 2.6$ Hz, H-7), 7.04 (1H, dd, $J = 9.0$ and 3.0 Hz, H-11), 6.97 (2H, t, $J = 8.7$ Hz, H-4 and H-10), 6.84 (1H, d, $J = 3.0$ Hz, H-13), 3.80 (3H, s, H-14*), 3.74 (3H, s, H-15*). $^{13}\text{C NMR}$ (75 MHz, CDCl_3): $\delta_{\text{C}} = 200.8$ (C-1), 161.3 (C-16*), 153.6 (C-9*), 150.6 (C-12*), 136.4 (C-5), 132.6 (C-7), 127.6 (C-6'), 123.4 (C-2'), 120.7 (C-8'), 119.7 (C-4*), 117.7 (C-11), 114.0 (C-13), 113.1 (C-10*), 56.3 (C-16[#]), 55.9 (C-15[#]).

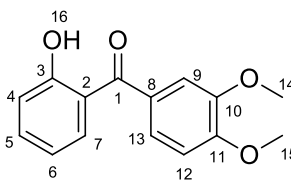
Experimental

**270**

When exposed to 5 % Pd/C (0.490 g, 10 % mass eq) under a hydrogen atmosphere, **304** (4.90 g, 10.87 mmol) was reduced to **270** (2.67 g, 70 %) as a yellow solid. $R_f = 0.17$ (10 % EtOAc/Hexane). **m.p.** = 158-160 °C, lit 161-163 °C.¹⁹¹ $^1\text{H NMR}$ (300 MHz, CDCl_3): $\delta_{\text{H}} = 12.18$ (1H, s, H-17), 7.48 – 7.40 (1H, m, H-4), 7.03 – 6.97 (1H, m, H-7), 6.90 (1H, s, H-10), 6.81 (1H, td, $J = 7.3$ Hz, 1.2 = H-5), 6.60 (1H, s, H-13), 3.96 (3H, s, H-14*), 3.83 (3H, s, H-15*), 3.73 (3H, s, H-16*). $^{13}\text{C NMR}$ (75 MHz, CDCl_3): $\delta_{\text{C}} = 201.0$ (C-1), 162.7 (C-3'), 152.3 (C-9'), 152.0 (C-12'), 143.1 (C-11'), 136.2 (C-6), 133.8 (C-7), 120.3 (C-2), 119.0 (C-8), 118.5 (C-5), 117.9 (C-7), 112.7 (C-10), 97.5 (C-13), 56.5 (C-14*), 56.5 (C-15*), 56.2 (C-16*).

**324**

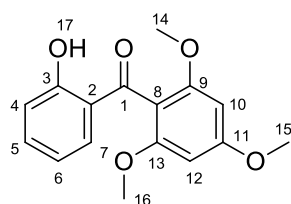
Ketone **319** (4.86 g, 13.99 mmol) and 5 % Pd/C (0.486 g, 10 mass %) were combined according to the general procedure. A yellow oil was collected after purification and confirmed to be **324** (2.58 g, 71 %). $R_f = 0.46$ (20 % EtOAc/Hexane). $^1\text{H NMR}$ (300 MHz, CDCl_3): $\delta_{\text{H}} = 12.24$ (1H, s, H-16), 7.42 (2H, m, $J = 8.3, 7.9, 1.7$, H-7 and H-5), 7.27 (1H, d, $J = 8.1$ Hz, H-13), 7.00 (1H, dd, $J = 8.4$ and 1.2 Hz, H-12), 6.79 (1H, ddd, $J = 8.1, 7.2$ and 1.1 Hz, H-6), 6.59 – 6.46 (2H, m, H-4 and H-10), 3.86 (3H, s, H-14*), 3.74 (3H, s, H-15*). $^{13}\text{C NMR}$ (125 MHz, CDCl_3): $\delta_{\text{C}} = 201.2$ (C-1), 163.2 (C-3*), 162.8 (C-9*), 158.6 (C-11*), 136.1 (C-5), 133.8 (C-7), 131.0 (C-13), 120.7 (C-2'), 120.5 (C-8'), 118.5 (C-6), 118.0 (C-4), 104.6 (C-12), 98.9 (C-10), 55.6 (C-14[#]), 55.5 (C-15[#]). **IR** ($\nu_{\text{m},\text{cm}^{-1}}$) = 2936, 2839, 1605, 1508, 1470, 1412, 1335, 1315, 1277, 1238, 1200, 1161, 1123, 1026, 949, 910, 833, 795, 756, 737, 698, 640, 621. **ESI-MS** (m/z) calculated $[\text{M}+\text{H}]^+$ for $\text{C}_{15}\text{H}_{15}\text{O}_4$ 259.0970, found 259.0974.

**325**

Benzyl protected benzophenone **320** (2.21 g, mmol) was reduced using 5 % Pd/C (0.221 g, 10 mass %) under a hydrogen atmosphere. After purification by flash column chromatography, **325** was collected as a yellow solid (1.01 g, 62 %). $R_f = 0.35$ (20 % EtOAc/Hexane). **m.p.** = 86-89 °C, 76-78 °C.²⁰⁹ $^1\text{H NMR}$ (300 MHz, CDCl_3): $\delta_{\text{H}} = 11.97 - 11.82$ (1H, s, H-16), 7.70 – 7.64 (1 H, m, H-7), 7.50 (1H, ddd, $J = 8.6, 7.1$ and 1.6 Hz, H-5), 7.36 – 7.30 (2H, m, H-13 and H-9), 7.10 – 7.05 (1H, m, H-4), 6.94 (1H, d, $J = 7.9$ Hz, H-12), 6.92

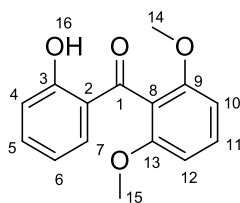
Experimental

– 6.85 (1H, m, H-6), 3.97 (3H, d, $J = 1.1$ Hz, H-14*), 3.94 (3H, d, $J = 1.1$ Hz, H-15*). ^{13}C NMR (75 MHz, CDCl_3): $\delta_{\text{C}} = 199.9$ (C-1), 162.9 (C-16), 152.7 (C-10*), 149.1 (C-11*), 135.8 (C-5), 133.3 (C-7), 130.5 (C-8), 124.3 (C-9[#]), 119.5 (C-2), 118.5 (C-6), 118.4 (C-4), 112.2 (C-13[#]), 110.1 (C-12), 56.1 (C-14'), 56.1 (C-5'). IR ($\nu_{\text{m}}\cdot\text{cm}^{-1}$) = 3424, 3007, 2972, 2936, 2833, 1618, 1584, 1514, 1479, 1462, 1447, 1410, 1358, 1323, 1306, 1254, 1219, 1167, 1132, 1115, 1063, 1028, 976, 889, 854, 820, 802, 768, 750, 698, 646, 611. ESI-MS (m/z) calculated $[\text{M}+\text{H}]^+$ for $\text{C}_{15}\text{H}_{15}\text{O}_4$ 259.0970, found 259.0974.

**326**

The benzyl group on **321** (2.342 g, 6.19 mmol) was removed using 5 % Pd/C (0.234 g, 10 mass %) under a hydrogen atmosphere as described in the general procedure. After filtration the product was recrystallized from isopropyl alcohol resulting in the collection of light yellow crystals of **326** (1.322 g, 74 %).

$R_f = 0.32$ (20 % EtOAc/Hexane). **m.p.** = 144-146 °C. ^1H NMR (300 MHz, CDCl_3): $\delta_{\text{H}} = 12.23$ (1H, s, H-17), 7.44 (1H, ddd, $J = 8.6, 7.1$ and 1.8 Hz, H-5), 7.32 (1H, dd, $J = 8.0$ and 1.8, H-7), 7.00 (1H, dd, $J = 8.4$ and 1.2 Hz, H-4), 6.78 (1H, ddd, $J = 8.2, 7.2$ and 1.1 Hz, H-6), 6.17 (2H, s, H-12 and H-10), 3.86 (3H, s, H-15), 3.71 (6H, s, H-14 and H-16). ^{13}C NMR (75 MHz, CDCl_3): $\delta_{\text{C}} = 201.1$ (C-1), 162.8 (C-17*), 162.6 (C-11*), 158.4 (C-9 and C-13), 136.2 (C-5), 133.2 (C-7), 121.4 (C-2), 118.7 (C-6), 117.8 (C-4), 109.7 (C-8), 90.7 (C-10 and C-12), 55.9 (C-14 and C-16), 55.5 (C-15). IR ($\nu_{\text{m}}\cdot\text{cm}^{-1}$) = 3686, 2970, 2943, 2930, 2862, 2862, 2849, 1607, 1580, 1485, 1404, 1337, 1296, 1242, 1229, 1202, 1188, 1148, 1121, 1053, 1026, 1013, 959, 932, 824, 797, 756, 716. ESI-MS (m/z) calculated $[\text{M}+\text{H}]^+$ for $\text{C}_{16}\text{H}_{17}\text{O}_5$ 289.1076, found 289.1082.

**327**

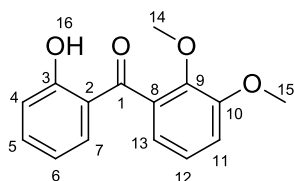
Following the general procedure, benzophenone **322** (4.08 g, 11.71 mmol) and 5 % Pd/C (0.41 g, 10 mass %) was used to remove the benzyl group resulting in the collection of a yellow solid that was confirmed to be **327** (1.82 g, 60 %). $R_f = 0.41$ (20 % EtOAc/Hexane). **m.p.** = 104-107°C. ^1H NMR (300 MHz, CDCl_3): $\delta_{\text{H}} = 12.15$ (1H, s, H-16), 7.44 (1H, ddd, $J = 8.7, 7.2$ and 1.8 Hz, H-5), 7.36

(1H, t, $J = 8.4$ Hz, H-11), 7.28 (1H, dd, $J = 7.9$ and 1.7 Hz, H-7), 7.01 (1H, dd, $J = 8.4$ and 1.1 Hz, H-4), 6.77 (1H, ddd, $J = 8.1, 7.2$ and 1.1 Hz, H-6), 6.62 (2H, d, $J = 8.4$ Hz, H-10 and H-12), 3.71 (6H, s, H-14 and H-15). ^{13}C NMR (75 MHz, CDCl_3): $\delta_{\text{C}} = 201.3$ (C-1), 162.5 (C-3), 157.3 (C-9 and C-13), 136.4 (C-5), 133.0 (C-7), 131.3 (C-11), 121.0 (C-2), 118.9 (C-6), 117.9 (C-4), 116.5 (C-8), 104.0 (C-10 and C-12), 55.9 (C-14 and C-15). IR ($\nu_{\text{m}}\cdot\text{cm}^{-1}$) = 3699, 2978, 2936, 2851, 1620, 1578, 1472,

Experimental

1450, 1366, 1344, 1302, 1281, 1238, 1132, 1111, 1069, 1026, 941, 835, 793, 772, 750, 729, 623.

ESI-MS (m/z) calculated $[M+H]^+$ for $C_{15}H_{15}O_4$ 259.0970, found 259.0571.



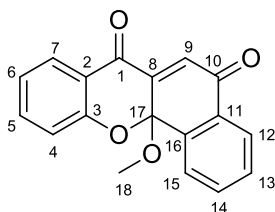
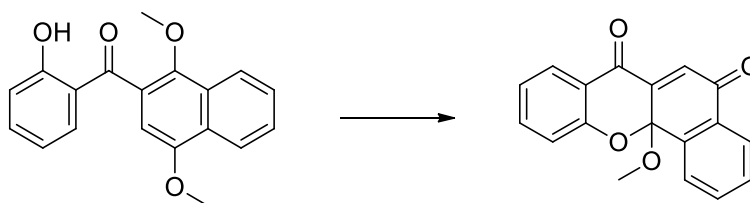
328

Methanol was used to dissolve benzylated **323** (2.35 g, 6.76 mmol) and 5 % Pd/C (0.24 g, 10 mass %) added. After stirring under a hydrogen atmosphere and purification according to the general procedure, **328** was collected as a white solid (1.16 g, 66 %). R_f = 0.56 (10 % EtOAc/Hexane). **m.p.** = 75-77 °C. 1H NMR (300 MHz, $CDCl_3$): δ_H = 12.16 (1H, s, H-16), 7.45 (1H, ddd, J =

8.7, 7.2 and 1.8 Hz, H-5), 7.35 (1H, dd, J = 8.0 and 1.7 Hz, H-7), 7.11 (1H, d, J = 7.5 Hz, H-12), 7.03 (2H, m, H-6 and H-13), 6.85 (1H, dd, J = 7.4 and 1.7 Hz, H-11), 6.79 (1H, ddd, J = 8.2, 7.2 and 1.2 Hz, H-4), 3.90 (3H, s, H-14*), 3.77 (3H, s, H-15*). ^{13}C NMR (75 MHz, $CDCl_3$): δ_C = 201.8 (C-1), 162.9 (C-3), 152.8 (C-9*), 146.2 (C-10*), 136.7 (C-5), 133.9 (C-3), 133.0 (C-2), 124.1 (C-12), 120.1 (C-8), 119.8 (C-11), 118.8 (C-6), 118.0 (C-4[#]), 114.4 (C-13[#]), 61.7 (C-14'), 55.9 (C-15'). **IR** ($\nu_{m\cdot cm^{-1}}$) = 3678, 2984, 2868, 2839, 2810, 1624, 1595, 1566, 1479, 1450, 1422, 1335, 1306, 1248, 1161, 1074, 1045, 1016, 959, 843, 814, 785, 756, 698, 669, 611. **ESI-MS (m/z)** calculated $[M+H]^+$ for $C_{15}H_{15}O_4$ 259.0970, found 259.0972.

7.3.8. General Procedure for the novel CAS-mediated ring closure

A CHCl_3 and MeCN solution in a 1:4 ratio was used to dissolve the hydroxy-containing benzophenone derivatives. Once the benzophenone had completely dissolved, water (double the volume than that of the CHCl_3) was added and a suspension resulted. Ceric Ammonium Sulfate (4 eq) was added slowly and the suspension stirred at room temperature overnight. The mixture was then transferred to a separating funnel and EtOAc and water added. The water layer was run off and the organic layer was washed further with sat NaHCO_3 and brine, dried over anhydrous Na_2SO_4 concentrated *in vacuo* and purified by column chromatography. In some cases several products resulted from the reaction and so the reaction schemes as well as the products are given for each reaction below.

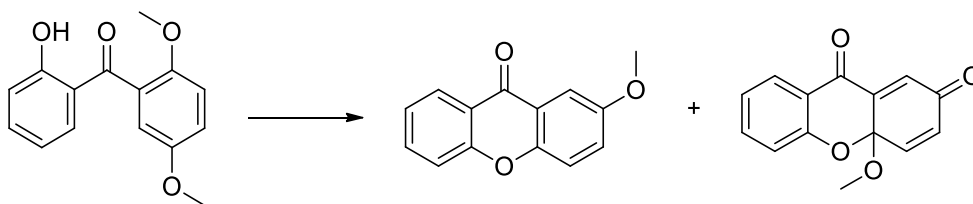


257

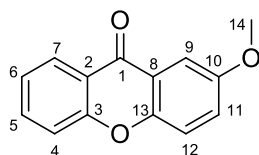
Benzophenone **253** (0.120 g, 0.434 mmol, 1 eq) in a 4:2:1 MeCN:H₂O:CHCl₃ solvent mixture was exposed to CAS (0.824 g, 1.303 mmol, 3 eq) overnight. After purification by flash column chromatography in 20 % EtOAc/Hexane, an orange solid resulted. NMR spectroscopy was used to confirm the identity of **257** (0.092 g, 73 %). *R_f* = 0.46 (20 % EtOAc/Hexane). **m.p.** =

139-140 °C, lit 162-165 °C. ¹⁹¹ **¹H NMR** (500 MHz, CDCl₃): δ_H = 8.15 (1H, dd, *J* = 7.9 and 1.4 Hz, H-12), 8.03 (2H, m, H-7 and H-15), 7.80 (1H, td, *J* = 7.6 and 1.4 Hz, H-14), 7.62 (2H, m, H-5 and H-13), 7.19 (1H, d, *J* = 1.4 Hz, H-9), 7.19 – 7.16 (2H, m, H-4 and H-6), 3.03 (3H, s, H-18). **¹³C NMR** (75 MHz, CDCl₃): δ_C = 184.0 (C-1[#]), 180.9 (C-10[#]), 157.7 (C-3), 143.7 (C-8), 137.0 (C-5*), 136.6 (C-16), 133.9 (C-14), 130.8 (C-11), 130.6 (C-9'), 130.2 (C-13*), 127.5 (C-15[~]), 126.9 (C-12), 126.5 (C-7[~]), 123.2 (C-4'), 121.5 (C-2), 118.6 (C-6'), 96.4 (C-17), 51.3 (C-18). **IR** (ν_m.cm⁻¹) = 3069, 2936, 2833, 1726, 1691, 1666, 1607, 1458, 1387, 1294, 1267, 1219, 1134, 1103, 1067, 1016, 943, 870, 756, 737, 702, 660. **ESI-MS** (*m/z*) calculated [M+H]⁺ for C₁₈H₁₃O₄ 293.0814, found 293.0811.

Experimental

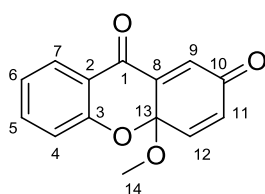


The general procedure was followed using benzophenone **258** (0.400 g, 1.688 mmol, 1 eq) and CAS (3.350 g, 5.296 mmol, 3 eq). Purification using flash column chromatography 10-20 % EtOAc/Hexane resulted in a white solid and yellow crystals being collected. Using NMR spectroscopy, the white powder was determined to be **260** (0.142 g, 36 %) and the yellow crystals to be **259** (0.153 g, 36 %).

**260**

$R_f = 0.33$ (10 % EtOAc/Hexane). **m.p.** = 127-128 °C, lit 131-133 °C. $^{191}\text{H NMR}$ (300 MHz, CDCl_3): $\delta_{\text{H}} = 8.36$ (1H, dd, $J = 8.0$ and 1.7 Hz, H-7), 7.76 – 7.68 (2H, m, H-5 and H-9), 7.49 (1H, dd, $J = 8.5$ and 1.2 Hz, H-11), 7.45 (1H, d, $J = 9.1$ Hz, H-12), 7.41 – 7.37 (1H, m, H-6), 7.37 – 7.33 (1H, m, H-4), 3.93 (3H, s, H-14). $^{13}\text{C NMR}$ (75 MHz,

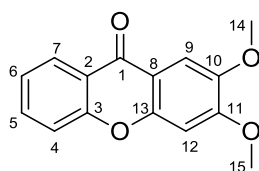
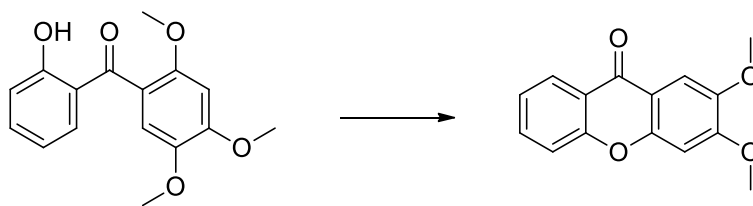
CDCl_3): $\delta_{\text{C}} = 177.1$ (C-1), 156.1 (C-10*), 156.0 (C-13*), 151.0 (C-3*), 134.6 (C-5), 126.7 (C-7), 124.9 (C-6), 123.7 (C-2[#]), 122.2 (C-8[#]), 121.3 (C-11), 119.4 (C-12), 118.0 (C-4), 105.9 (C-9), 55.9 (C-14). **IR** ($\nu_{\text{m}}\cdot\text{cm}^{-1}$) = 2972, 2938, 2868, 2851, 1670, 1636, 1601, 1462, 1288, 1236, 1219, 1202, 1150, 1097, 1045, 1028, 1011, 959, 941, 854, 820, 785, 750, 698, 629. **ESI-MS** (m/z) calculated $[\text{M}+\text{H}]^+$ for $\text{C}_{14}\text{H}_{11}\text{O}_3$ 227.0708, found 227.0708.

**259**

$R_f = 0.19$ (10 % EtOAc/Hexane). **m.p.** = 108-110 °C, 110-112 °C. $^{191}\text{H NMR}$ (300 MHz, CDCl_3): $\delta_{\text{H}} = 8.02$ (1H, dd, $J = 7.9$ and 1.8 Hz, H-7), 7.60 (1H, ddd, $J = 8.3$, 7.3 and 1.7 Hz, H-5), 7.18 (1H, ddd, $J = 8.0$, 7.3 and 1.1 Hz, H-6), 7.14 – 7.07 (2H, m, H-4 and H-12), 6.89 (1H, d, $J = 2.0$ Hz, H-9), 6.44 (1H, dd, $J = 10.4$ and 2.0 Hz, H-11), 3.35 (3H, s, H-14). $^{13}\text{C NMR}$ (75 MHz, CDCl_3): $\delta_{\text{C}} = 185.0$ (C-10),

180.9 (C-1), 157.0 (C-3), 144.5 (C-8), 140.1 (C-12*), 137.0 (C-5), 130.7 (C-11), 128.5 (C-9), 127.5 (C-7), 123.3 (C-6), 121.7 (C-2), 118.5 (C-4*), 95.1 (C-13), 51.3 (C-14). **IR** ($\nu_{\text{m}}\cdot\text{cm}^{-1}$) = 2972, 2938, 2868, 2851, 1670, 1636, 1601, 1462, 1288, 1236, 1219, 1202, 1150, 1097, 1045, 1028, 1011, 959, 941, 854, 820, 785, 750, 698, 629. **ESI-MS** (m/z) calculated $[\text{M}+\text{H}]^+$ for $\text{C}_{14}\text{H}_{11}\text{O}_4$ 243.0657, found 247.1680.

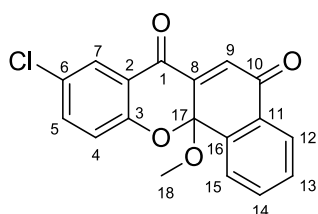
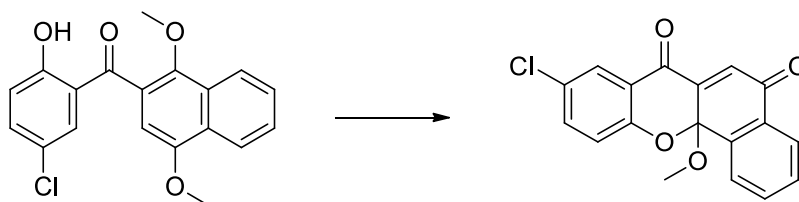
Experimental

**262**

Following the general procedure, benzophenone **261** (0.167 g, 0.579 mmol, 1 eq) exposed to CAS (1.466 g, 2.317 mmol, 4 eq) resulted in a single product that was determined to be **262**. This was collected as yellow crystals (0.122 g, 69 %). R_f = 0.43 (20 % EtOAc/Hexane). **m.p.** = 153-155 °C, lit 170-172 °C. $^{191}\text{H NMR}$ (300 MHz, CDCl_3): δ_{H} = 8.35 (1H, ddd, J = 8.0,

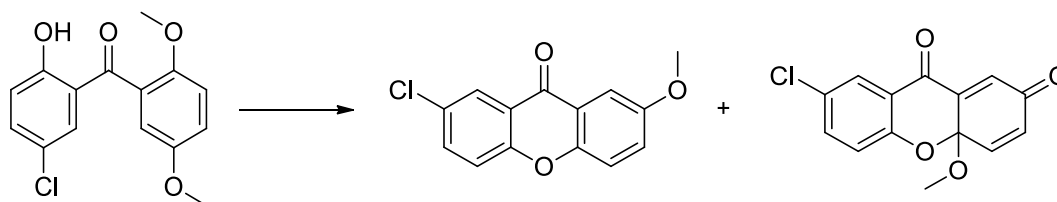
1.8 and 0.5 Hz, H-7), 7.74 – 7.65 (2H, m, H-5 and H-9), 7.47 (1H, ddd, J = 8.5, 1.1 and 0.5 Hz, H-4), 7.38 (1H, ddd, J = 8.2, 7.1 and 1.1 Hz, H-6), 6.93 (1H, s, H-12), 4.03 (3H, s, H-14*), 4.01 (3H, s, H-15*). $^{13}\text{C NMR}$ (75 MHz, CDCl_3): δ_{C} = 176.1 (C-1), 156.1 (C-3[#]), 155.5 (C-13[#]), 152.5 (C-10[#]), 146.8 (C-11[#]), 134.0 (C-5), 126.6 (C-7), 123.8 (C-6), 121.6 (C-2), 117.7 (C-4), 115.0 (C-8), 105.5 (C-9), 99.7 (C-12), 56.5 (C-14*), 56.4 (C-15*). **IR** ($\nu_{\text{m}}\cdot\text{cm}^{-1}$) = 2972, 2938, 2868, 2833, 1653, 1601, 1514, 1462, 1427, 1306, 1271, 1236, 1201, 1132, 1063, 1028, 1011, 941, 854, 820, 785, 750, 698, 646. **ESI-MS** (**m/z**) calculated $[\text{M}+\text{H}]^+$ for $\text{C}_{15}\text{H}_{13}\text{O}_4$ 257.0814, found 257.0816.

Experimental

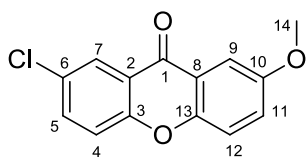
**264**

The general procedure was followed using **263** (0.183 g, 0.534 mmol) and CAS (1.351 g, 2.136 mmol) resulting in the formation of **264**. This was collected as a yellow solid (0.146 g, 84 %). $R_f = 0.65$ (20 % EtOAc/Hexane). **m.p.** = 158-160 °C, lit 162-165 °C. $^{191}\text{H NMR}$ (300 MHz, CDCl_3): $\delta_{\text{H}} = 8.16$ (1H, ddd, $J = 7.8, 1.4$ and 0.6 Hz, H-12), $8.03 - 7.97$ (2H, m, H-7 and H-15), 7.81 (1H, ddd, $J = 7.9, 7.4$ and 1.4 Hz, H-13*), 7.63 (1H, td, $J = 7.6$ and 1.3 Hz, H-14*), 7.56 (1H, dd, $J = 8.8$ and 2.7 Hz, H-5), 7.21 (1H, s, H-9), $7.19 - 7.13$ (1H, m, H-4), 3.02 (H, s, C-18). $^{13}\text{C NMR}$ (75 MHz, CDCl_3): $\delta_{\text{C}} = 183.7$ (C-10), 180.1 (C-1), 156.2 (C-3), 143.0 (C-8), 136.7 (C-5), 136.2 (C-16), 134.0 (C-13*), 131.1 (C-9), 130.8 (C-11), 130.4 (C-14*), 128.9 (C-6), 127.0 (C-12'), 126.9 (C-7'), 126.5 (C-15'), 122.4 (C-2), 120.2 (C-4), 96.7 (C-17), 51.4 (C-18). **IR** ($\nu_{\text{m.cm}^{-1}}$) = 3109, 2974, 2936, 2820, 1682, 1663, 1624, 1605, 1470, 1412, 1258, 1200, 1142, 1123, 1065, 1026, 987, 949, 891, 833, 775, 737, 718, 679, 660, 621. **ESI-MS** (m/z) calculated $[\text{M}+\text{H}]^+$ for $\text{C}_{18}\text{H}_{12}\text{O}_4\text{Cl}$ 327.0424, found 327.0415.

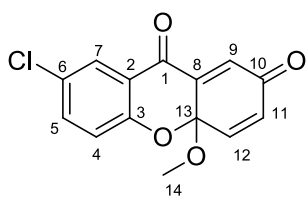
Experimental



When exposed to CAS (2.644 g, 4.180 mmol, 4 eq), benzophenone **265** (0.306 g, 1.045 mmol, 1 eq) was transformed into two products. The two products were separated by flash column chromatography and collected as a light pink solid that was found to be **267** (0.027 g, 26 %) and a yellow solid that was found to be **266** (0.114 g, 40 %).

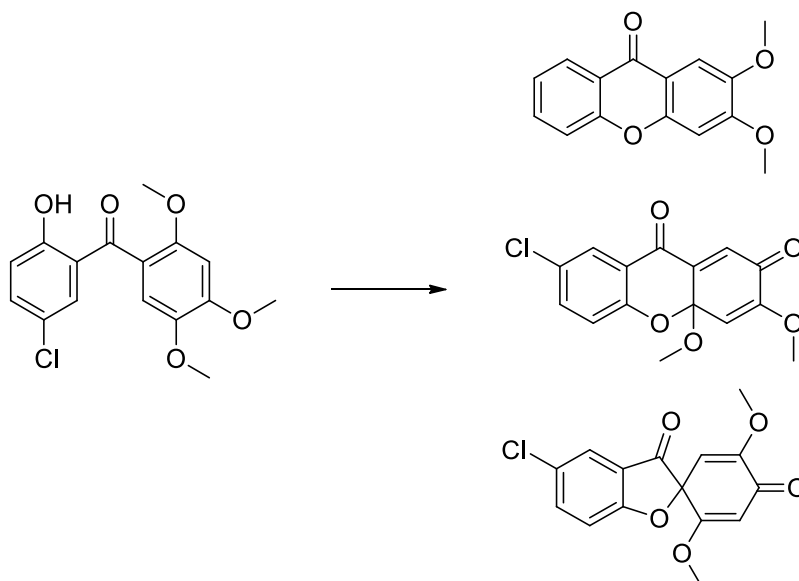
**267**

$R_f = 0.59$ (20 % EtOAc/Hexane). **m.p.** = 171-172 °C, lit 130-133 °C. $^{191}\text{H NMR}$ (300 MHz, CDCl_3): $\delta_H = 8.31$ (1H, d, $J = 2.6$ Hz, H-7), 7.69 (1H, d, $J = 3.2$ Hz, H-9), 7.65 (1H, dd, $J = 8.9$ and 2.6 Hz, H-5), 7.45 (2H, dd, $J = 9.0, 6.2$, H-4 and H-12), 7.35 (1H, dd, $J = 9.1$ and 3.1 Hz, H-11), 3.92 (3H, s, H-14). $^{13}\text{C NMR}$ (75 MHz, CDCl_3): $\delta_C = 176.0$ (C-1), 156.3 (C-10[#]), 154.4 (C-3), 150.9 (C-13[#]), 134.7 (C-5), 129.5 (C-6), 126.0 (C-7), 125.3 (C-11), 122.1 (C-2'), 121.8 (C-8'), 119.7 (C-4*), 119.5 (C-12*), 105.8 (C-9), 56.0 (C-14). **IR** ($\nu_{\text{m.cm}^{-1}}$) = 3071, 2980, 2953, 2853, 1655, 1612, 1485, 1462, 1445, 1364, 1292, 1242, 1209, 1144, 1123, 1107, 1024, 993, 904, 872, 814, 785, 719, 687, 629. **ESI-MS** (**m/z**) calculated $[\text{M}+\text{H}]^+$ for $\text{C}_{14}\text{H}_{10}\text{O}_3\text{Cl}$ 261.0318, found 261.0318.

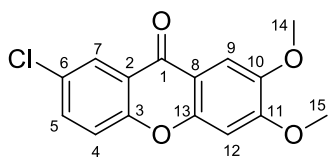
**266**

$R_f = 0.29$ (20 % EtOAc/Hexane). **m.p.** = 143-144 °C, 122-124 °C. $^{191}\text{H NMR}$ (300 MHz, CDCl_3): $\delta_H = 7.97$ (1H, d, $J = 2.7$ Hz, H-7), 7.54 (1H, dd, $J = 8.7$ and 2.7 Hz, H-5), 7.08 (2H, dd, $J = 9.5$ and 8.7 Hz, H-4 and H-12), 6.89 (1H, d, $J = 2.0$ Hz, H-9), 6.45 (1H, dd, $J = 10.4$ and 2.0 Hz, H-11), 3.35 (3H, s, H-14). $^{13}\text{C NMR}$ (75 MHz, CDCl_3): $\delta_C = 184.7$ (C-10[#]), 180.0 (C-1[#]), 155.4 (C-3), 143.8 (C-8), 139.7 (C-12*), 136.7 (C-5), 130.9 (C-11), 129.0 (C-6), 129.0 (C-9), 126.9 (C-7), 122.6 (C-2), 120.2 (C-4*), 95.3 (C-13), 51.4 (C-14). **IR** ($\nu_{\text{m.cm}^{-1}}$) = 3071, 3005, 2945, 2831, 1668, 1643, 1603, 1468, 1422, 1288, 1267, 1203, 1142, 1099, 1003, 945, 837, 821, 779, 714, 677. **ESI-MS** (**m/z**) calculated $[\text{M}+\text{H}]^+$ for $\text{C}_{14}\text{H}_{10}\text{O}_4\text{Cl}$ 277.0268, found 277.0268.

Experimental



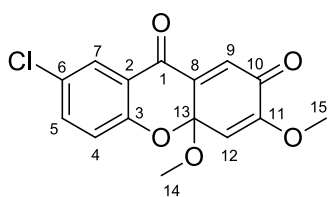
Following the general procedure, when **270** (0.265 g, 0.821 mmol, 1 eq) was exposed to CAS (2.078 g, 3.284 mmol, 4 eq) three new spots were observed on the TLC plate. The three spots were successfully separated using flash column chromatography and found to be **269** as white crystals (0.097 g, 41 %), **268** as bright yellow crystals (0.045 g, 18 %) and **271** (0.014 g, 4 %) as a dark yellow solid.

**269**

R_f = 0.26 (20 % EtOAc/Hexane). **m.p.** = 204-206 °C, lit 202-204 °C.¹⁹¹ $^1\text{H NMR}$ (300 MHz, CDCl_3): δ_{H} = 8.24 (1H, d, J = 2.6 Hz, H-7), 7.62 – 7.55 (2H, m, H-5 and H-9), 7.36 (1H, d, J = 8.9 Hz, H-4), 6.85 (1H, s, H-12), 4.01 (3H, s, H-14*), 3.98 (3H, s, H-15*). $^{13}\text{C NMR}$ (75 MHz, CDCl_3): δ_{C} = 174.8 (C-1), 155.7 (C-13[#]), 154.3 (C-3), 152.3 (C-11[#]),

147.0 (C-10[#]), 134.0 (C-5*), 129.5 (C-6), 125.8 (C-7), 122.3 (C-2), 119.4 (C-4), 114.5 (C-8), 105.3 (C-9*), 99.6 (C-12), 56.5 (C-14'), 56.3 (C-15'). **IR** ($\nu_{\text{m}}, \text{cm}^{-1}$) = 3076, 2990, 2972, 2920, 2833, 1636, 1618, 1566, 1514, 1479, 1462, 1427, 1288, 1271, 1236, 1184, 1167, 1132, 1063, 1028, 1011, 959, 906, 871, 820, 785, 698, 611. **ESI-MS** (m/z) calculated $[\text{M}+\text{H}]^+$ for $\text{C}_{15}\text{H}_{12}\text{O}_4\text{Cl}$ 291.0424, found 291.0426.

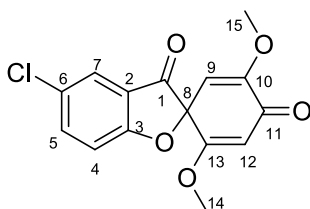
Experimental



268

R_f = 0.17 (20 % EtOAc/Hexane). **m.p.** = 142-144 °C, lit 118-120 °C. $^{191}\text{H NMR}$ (300 MHz, CDCl_3): δ_H = 7.94 (1H, d, J = 2.7 Hz, H-7), 7.58 – 7.48 (1H, m, H-5), 7.04 (1H, d, J = 8.7 Hz, H-4), 6.86 (1H, d, J = 1.1 Hz, H-12), 5.95 (1H, s, H-9), 3.82 (3H, s, H-15), 3.33 (3H, d, J = 1.3 Hz, H-14). $^{13}\text{C NMR}$ (75 MHz, CDCl_3): δ_C = 180.2 (C-1*), 179.9 (C-10*), 156.0 (C-3[#]), 152.5 (C-11[#]), 144.3 (C-8), 136.6 (C-5),

128.8 (C-6), 128.1 (C-12), 126.9 (C-7), 122.6 (C-2), 120.1 (C-4), 106.8 (C-9), 98.2 (C-13), 55.7 (C-15), 51.2 (C-14). **IR** ($\nu_{\text{m}}\cdot\text{cm}^{-1}$) = 3013, 2974, 2936, 2839, 1682, 1643, 1604, 1470, 1412, 1373, 1296, 1258, 1238, 1200, 1180, 1123, 1045, 988, 968, 910, 833, 775, 737, 718, 698, 640. **ESI-MS** (m/z) calculated $[\text{M}+\text{H}]^+$ for $\text{C}_{15}\text{H}_{12}\text{O}_5\text{Cl}$ 307.0373, found 307.0370.

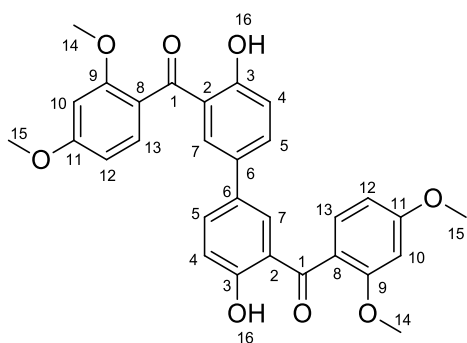
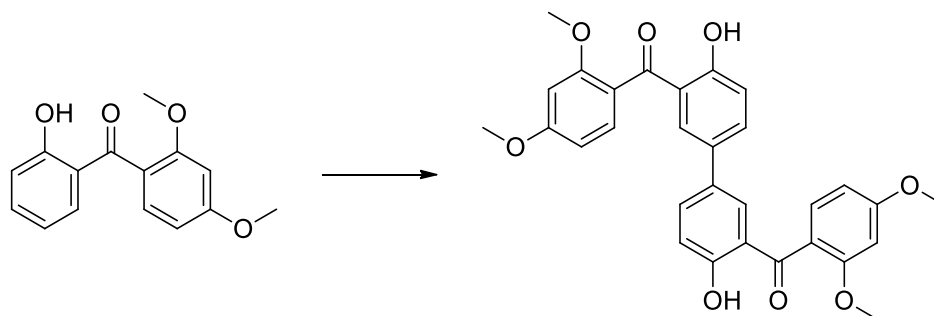


271

R_f = 0.09 (20 % EtOAc/Hexane). **m.p.** = 200-202 °C, lit 223-225 °C. $^{191}\text{H NMR}$ (300 MHz, CDCl_3): δ_H = 7.67 (2H, m, H-7 and H-4), 7.19 (1H, dd, J = 8.4 and 1.0 Hz, H-5), 5.76 (1H, s, H-9), 5.18 (1H, s, H-12), 3.69 (3H, s, H-15), 3.68 (3H, s, H-14). $^{13}\text{C NMR}$ (75 MHz, CDCl_3): δ_C = 194.3 (C-1), 181.1 (C-11), 170.8 (C-3), 167.5 (C-13[#]), 153.4 (C-10[#]), 138.8 (C-5), 128.3 (C-6), 124.8 (C-7), 121.1 (C-2),

115.1 (C-4), 104.0 (C-9), 102.4 (C-12), 87.0 (C-8), 56.7 (C-14*), 55.6 (C-15*). **IR** ($\nu_{\text{m}}\cdot\text{cm}^{-1}$) = 3076, 3042, 2938, 2851, 1740, 1670, 1618, 1462, 1358, 1288, 1236, 1184, 1080, 1011, 993, 872, 820, 768, 698, 663, 629. **ESI-MS** (m/z) calculated $[\text{M}+\text{H}]^+$ for $\text{C}_{15}\text{H}_{12}\text{O}_5\text{Cl}$ 307.0373, found 307.0373.

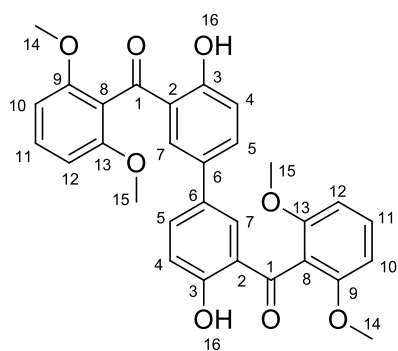
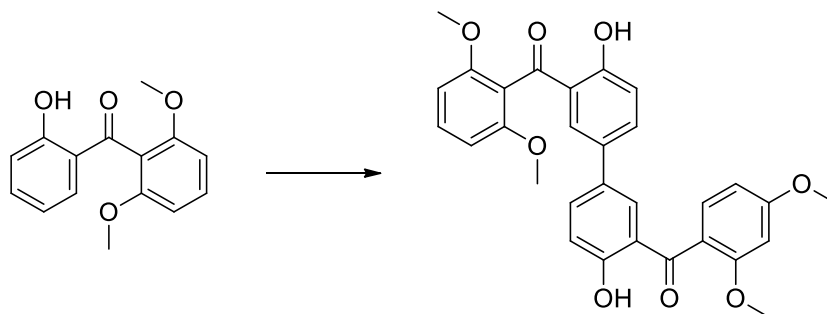
Experimental

**329**

The mixture of **324** (0.521 g, 2.017 mmol, 1 eq) and CAS (2.552 g, 4.035 mmol, 2 eq) resulted multiple spots visualized on the TLC plate. After purification by flash column chromatography, the only product that could be successfully isolated and characterised was a white solid determined to be **329** (0.082 g, 24 %) from NMR spectroscopy and SCXRD. R_f = 0.32 (30 % EtOAc/Hexane). **m.p.** = 171-175 °C. $^1\text{H NMR}$ (300 MHz, CDCl_3): δ_{H} = 12.15 (1H,

s, H-16), 7.51 (1H, dd, J = 8.6 and 2.4 Hz, H-5), 7.42 (1H, d, J = 2.4 Hz, H-3), 7.28 (1H, d, J = 8.4 Hz, H-13), 7.04 (1H, d, J = 8.6 Hz, H-6), 6.55 (1H, dd, J = 8.4 and 2.3 Hz, H-12), 6.51 (1H, d, J = 2.2 Hz, H-10), 3.91 (3H, s, H-14*), 3.61 (3H, s, H-15*). $^{13}\text{C NMR}$ (75 MHz, CDCl_3): δ_{C} = 201.1 (C-1), 163.3 (C-11[#]), 162.0 (C-9[#]), 158.5 (C-7[#]), 134.4 (C-5), 131.3 (C-4), 131.1 (C-3), 130.8 (C-13), 120.7 (C-5'), 120.5 (C-2'), 118.5 (C-6), 104.7 (C-12), 99.1 (C-10), 55.6 (C-14*), 55.5 (C-15*). **IR** ($\nu_{\text{m}} \cdot \text{cm}^{-1}$) = 2972, 2938, 2851, 1601, 1584, 1514, 1462, 1410, 1323, 1288, 1236, 1202, 1167, 1132, 1115, 1028, 976, 941, 820, 785, 768, 611. **ESI-MS** (m/z) calculated $[\text{M}+\text{H}]^+$ for $\text{C}_{30}\text{H}_{27}\text{O}_8$ 515.1706, found 515.1702.

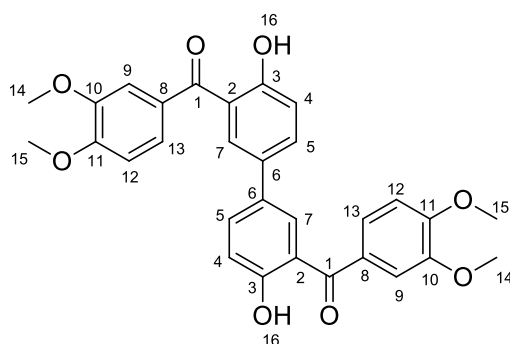
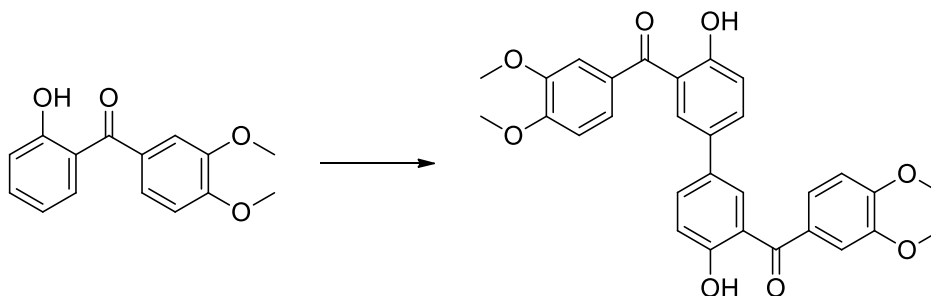
Experimental

**330**

Following the general procedure, benzophenone **327** (0.291 g, 1.127 mmol, 1 eq) and CAS (2.138 g, 3.380 mmol, 3 eq) were combined. Multiple spots were visualized on the TLC plate, however after purification by flash column chromatography only a single spot could be successfully isolated. The yellow oil collected and this was determined to be **330** by NMR spectroscopy (0.052 g, 18 %). $R_f = 0.44$ (30 % EtOAc/Hexane). $^1\text{H NMR}$ (300 MHz, CDCl_3): $\delta_{\text{H}} = 12.13$ (1H, s, H-16), 7.50 (1H, dd, $J = 8.7$ and 2.4 Hz, H-5), 7.42

– 7.33 (1H, m, H-11), 7.22 (1H, d, $J = 2.4$ Hz, H-7), 7.04 (1H, d, $J = 8.6$ Hz, H-4), 6.59 (2H, d, $J = 8.4$, H-10 and H-12), 3.63 (6H, s, H-14 and H-15). $^{13}\text{C NMR}$ (75 MHz, CDCl_3): $\delta_{\text{C}} = 201.1$ (C-1), 161.8 (C-3), 157.3 (C-9 and C-13), 134.9 (C-5), 131.3 (C-11), 131.2 (C-6), 130.5 (C-3), 120.9 (C-2), 118.4 (C-4), 116.3 (C-8), 104.1 (C-10 and C-12), 55.9 (C-14 and C-15). IR ($\nu_{\text{m}}\cdot\text{cm}^{-1}$) = 3009, 2978, 2947, 2839, 1636, 1589, 1466, 1435, 1327, 1281, 1250, 1219, 1157, 1111, 1049, 1034, 941, 833, 787, 756, 725, 632. ESI-MS (m/z) calculated $[\text{M}+\text{H}]^+$ for $\text{C}_{30}\text{H}_{27}\text{O}_8$ 515.1706, found 515.1707.

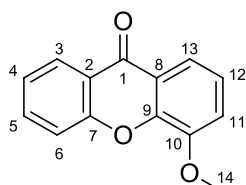
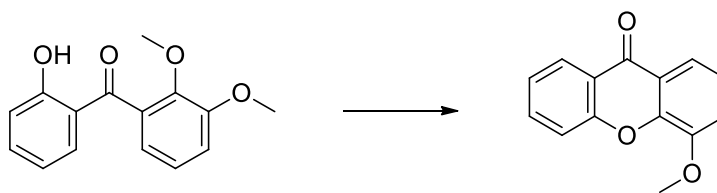
Experimental

**331**

Benzophenone **325** (0.409 g, 1.584 mmol, 1 eq) and CAS (2.00 g, 3.167 mmol) were combined following the general procedure. Multiple spots were visualized on the TLC plate as the reaction was monitored, however only one of the compounds isolated could be successfully characterised. This spot was collected as a yellow solid and determined to be product **331** (0.062 g,

15 %). $R_f = 0.21$ (30 % EtOAc/Hexane). $m.p.$ = 148-150 °C. $^1\text{H NMR}$ (300 MHz, CDCl_3): $\delta_{\text{H}} = 11.78$ (1H, s, H-16), 7.78 (1H, d, $J = 2.4$ Hz, H-7), 7.64 (1H, dd, $J = 8.6$ and 2.4 Hz, H-5), 7.35 (1H, d, $J = 2.0$ Hz, H-9), 7.32 (1H, dd, $J = 8.2$ and 2.0 Hz, H-13), 7.13 (1H, d, $J = 8.6$ Hz, H-4), 6.86 (1H, d, $J = 8.2$ Hz, H-12), 3.96 (3H, s, H-15), 3.90 (3H, s, H-14). $^{13}\text{C NMR}$ (75 MHz, CDCl_3): $\delta_{\text{C}} = 199.5$ (C-1), 162.1 (C-3), 153.0 (C-11), 149.2 (C-10), 133.9 (C-5), 130.9 (C-7), 130.6 (C-6), 130.2 (C-8), 124.5 (C-13), 119.6 (C-2), 119.0 (C-4), 112.1 (C-9), 109.9 (C-12), 56.1 (C-15), 56.0 (C-14). IR ($\nu_{\text{m}}, \text{cm}^{-1}$) = 3013, 2974, 2974, 2936, 2858, 2839, 1624, 1566, 1508, 1470, 1412, 1335, 1258, 1238, 1200, 1180, 1142, 1065, 1026, 872, 814, 795, 756, 698, 660, 621. ESI-MS (m/z) calculated $[\text{M}+\text{H}]^+$ for $\text{C}_{30}\text{H}_{27}\text{O}_8$ 515.1706, found 515.1704.

Experimental

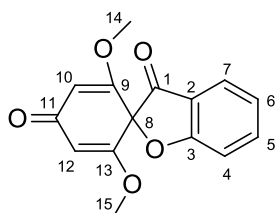
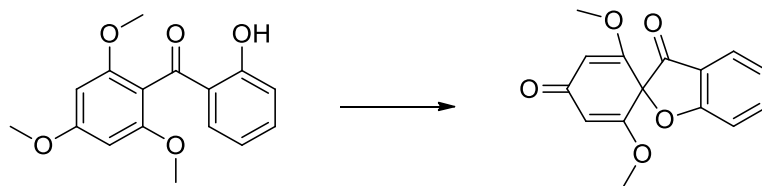
**332**

After dissolving **328** (0.117 g, 0.453 mmol, 1 eq) as outlined in the general procedure, CAS (1.433 g, 2.265 mmol, 5 eq) was added and the reaction mixture stirred overnight. Only a single spot was visualized on the TLC plate. This product was characterised by NMR spectroscopy and determined to be **332** (0.061 g, 60 %).

R_f = 0.37 (20 % EtOAc/Hexane). **m.p.** = 178 °C, 175-176

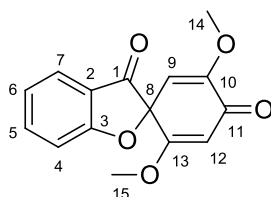
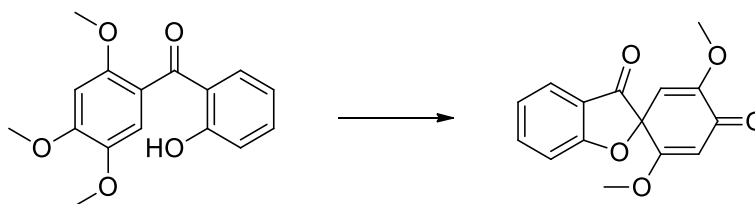
°C. $^{210}\text{H NMR}$ (300 MHz, CDCl_3): δ_{H} = 8.35 (1H, ddd, J = 7.9, 1.7 and 0.5 Hz, H-7), 7.92 (1H, dd, J = 7.8 and 1.8 Hz, H-13), 7.74 (1H, ddd, J = 8.7, 7.0 and 1.8 Hz, H-6), 7.62 (1H, ddd, J = 8.5, 1.1 and 0.5 Hz, H-4), 7.40 (1H, ddd, J = 8.1, 7.1 and 1.2 Hz, H-5), 7.32 (2H, m, H-11 and H-12), 4.04 (3H, s, H-14). $^{13}\text{C NMR}$ (75 MHz, CDCl_3): δ_{C} = 177.2 (C-1), 156.0 (C-3), 148.7 (C-9[#]), 146.6 (C-10[#]), 134.8 (C-6), 126.7 (C-7), 124.1 (C-5), 123.4 (C-11*), 122.8 (C-2'), 121.7 (C-8'), 118.3 (C-4), 117.7 (C-13), 115.4 (C-12*), 56.5 (C-14). **IR** ($\nu_{\text{m}}\cdot\text{cm}^{-1}$) = 2993, 2955, 2916, 2858, 2839, 1663, 1605, 1566, 1489, 1470, 1450, 1354, 1335, 1277, 1258, 1238, 1200, 1142, 1065, 1026, 968, 891, 853, 814, 756, 718, 679, 621. **ESI-MS** (m/z) calculated $[\text{M}+\text{H}]^+$ for $\text{C}_{14}\text{H}_{11}\text{O}_3$ 227.0708, found 227.0704.

Experimental

**333**

To a solution of **326** (0.300 g, 1.041 mmol, 1 eq), CAS (2.634 g, 4.164 mmol, 4 eq) was added and stirred overnight. After purification by flash column chromatography, white crystals were collected and found to be **333** (0.166 g, 59 %). $R_f = 0.50$ (30 % EtOAc/Hexane). **m.p.** = 194-196 °C. $^1\text{H NMR}$ (300 MHz, CDCl_3): $\delta_{\text{H}} = 7.75 - 7.63$ (2H, m, H-7 and H-5), 7.26 – 7.20 (1H, m, H-4), 7.17 (1H, ddd, $J = 7.9, 7.2$ and 0.8 Hz, H-6), 5.64 (2H, d, $J = 1.0$ Hz, H-10 and H-12), 3.64 (6H, s, H-14 and H-15). $^{13}\text{C NMR}$ (75 MHz, CDCl_3): $\delta_{\text{C}} = 194.4$ (C-1*), 186.8 (C-11*), 173.8 (C-3), 164.8 (C-9 and C-13), 138.6 (C-5), 125.3 (C-7), 122.7 (C-6), 120.1 (C-2), 113.5 (C-4), 103.5 (C-10 and C-12), 84.3 (C-8), 56.5 (C-14 and C-15). **IR** ($\nu_{\text{m}\cdot\text{cm}^{-1}}$) = 2972, 2938, 2920, 2868, 2816, 1722, 1670, 1636, 1601, 1462, 1358, 1323, 1306, 1236, 1219, 1184, 1150, 1097, 1063, 993, 924, 889, 854, 768, 716, 629. **ESI-MS** (m/z) calculated $[\text{M}+\text{H}]^+$ for $\text{C}_{15}\text{H}_{13}\text{O}_5$ 273.0763, found 273.0764.

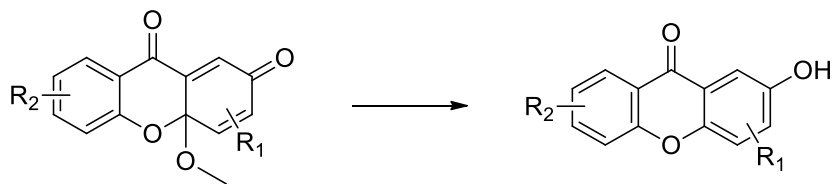
7.3.9. CAN-mediated formation of spirofuran 300

**300**

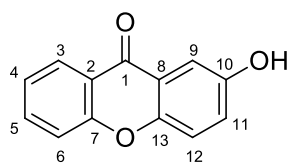
To a rapidly stirring solution of benzophenone **261** (0.260 g, 0.902 mmol) in MeCN (15 ml), CAN (1.711 g, 2.706 mmol, 3 eq) dissolved in H₂O (6 ml) was added dropwise. The yellow solution immediately turned black and after 10 minutes no more starting material was observed on the TLC plate and a new spot was evident.

The reaction mixture was transferred to a separation funnel, water (20 ml) and EtOAc (50 ml) added to the mixture and the water layer removed. Following this, the organic layer was further washed with saturated NaHCO₃ and brine. After drying over anhydrous Na₂SO₄ and concentration *in vacuo* the product was purified by flash column chromatography with 10-20 % EtOAc/Hexane as the eluent. A white solid was collected (0.036 g, 13 %) and determined to be **300** following characterisation by NMR spectroscopy. **R_f** = 0.20 (20 % EtOAc/Hexane). **m.p.** = 103-105 °C. **¹H NMR** (300 MHz, CDCl₃): δ_H = 7.77 – 7.67 (2H, m, H-5 and H-7), 7.26 – 7.21 (1H, m, H-4), 7.18 (1H, ddd, *J* = 7.9, 7.2 and 0.8 Hz, H-6), 5.77 (1H, s, H-12), 5.20 (1H, s, H-9), 3.69 (3H, s, H-14*), 3.68 (3H, s, H-15*). **¹³C NMR** (75 MHz, CDCl₃): δ_C = 195.4 (C-1[#]), 181.3 (C-11[#]), 172.5 (C-13[~]), 168.0 (C-3[~]), 153.3 (C-10[~]), 139.0 (C-5*), 125.7 (C-7*), 122.7 (C-6), 119.9 (C-2), 113.9 (C-4), 104.0 (C-12), 103.0 (C-9), 86.1 (C-8), 56.6 (C-14'), 55.6 (C-15'). **IR** (**v_m**.cm⁻¹) = 3063, 2938, 2852, 1719, 1666, 1643, 1601, 1506, 1456, 1402, 1337, 1261, 1205, 1171, 1099, 1084, 1032, 991, 924, 887, 850, 750, 706, 629. **ESI-MS** (**m/z**) calculated [M+CH₃+2H⁺]⁺ for C₁₆H₁₇O₅ 289.1076, found 289.1072.

7.3.10. General procedure for the conversion of diones to xanthenes



In a 25 ml round bottomed flask, dione (1 eq) was dissolved in freshly distilled THF (5 ml). To this 5 ml of water was added and 3 equivalents of sodium dithionite was added to the solution while being stirred at a high speed. Just after the addition of the sodium dithionite a colour change of the mixture was noted and the solution was stirred for a further 15 minutes. A TLC of the reaction mixture confirmed that no more starting material was present and the mixture was transferred to a separation funnel and diluted by the addition of 15 ml water and 15 ml diethyl ether. The water layer was removed and washed with a further 15 ml of water and this layer extracted. Concentrated sodium hydroxide (15 ml) was added, the separation funnel stoppered and shaken vigorously. A notable change in colour was observed during shaking. The aqueous layer (now highly coloured) was collected. Further additions of conc. NaOH along with vigorous shaking was repeated until no further colour change was observed in the aqueous layer. The basic aqueous layers that were collected and combined were neutralized by the slow addition of solid ammonium chloride. Ammonium chloride was added until a solid precipitated out of solution, the solid collected by filtration and dried in a desiccator overnight. The solids were characterised by NMR, Infrared and Mass spectroscopy.

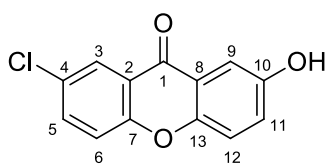


305

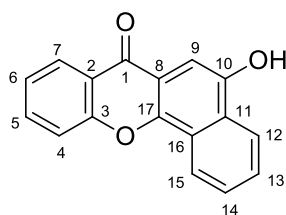
Dione **259** (0.100 g, 0.413 mmol, 1 eq) was reduced to **305** with sodium dithionite (0.216 g, 1.239 mmol, 3 eq). **305** was collected as a cream coloured powder (0.079 g, 90 %). **M.p.** = >310 °C. **¹H NMR** (300 MHz, MeOD): δ_{H} = 8.25 (1H, dd, J = 8.1 and 1.7 Hz, H-7), 7.81 (1H, ddd, J = 8.7, 7.1 and 1.7 Hz, H-5), 7.60 – 7.54 (2 H, m, H-4 and H-

9), 7.49 (1H, d, J = 9.1 Hz, H-12), 7.43 (1H, ddd, J = 8.1, 7.0 and 1.1 Hz, H-6), 7.33 (1H, dd, J = 9.1 and 3.0 Hz, H-11). **¹³C NMR** (75 MHz, MeOD): δ_{C} = 179.0 (C-1), 157.7 (C-3[#]), 155.4 (C-13[#]), 151.6 (C-10[#]), 136.3 (C-5), 127.2 (C-7), 125.9 (C-11), 125.0 (C-6), 123.2 (C-8'), 122.0 (C-2'), 120.5 (C-12), 119.2 (C-4*), 109.8 (C-9*). **IR** (ν_{m} , cm^{-1}) = 3302, 3069, 2947, 2872, 1651, 1614, 1597, 1460, 1342, 1302, 1223, 1146, 1190, 1130, 871, 816, 787, 748, 711, 619. **ESI-MS** (m/z) calculated [M-H]⁻ for C₁₃H₉O₃ 211.0395, found 211.0395.

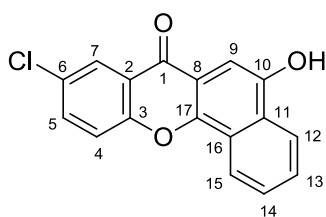
Experimental

**306**

The reduction of dione **266** (0.257 g, 0.929 mmol, 1 eq) was performed using sodium dithionite (0.485 g, 2.786 mmol) resulting in the formation of a beige powder **306** (0.171 g, 75 %) after the work up given in the general procedure. **m.p.** = 250 °C, lit 221-222 °C. ¹H NMR (500 MHz, d-DMSO): δ_{H} = 7.85 (1H, d, J = 2.6 Hz, H-3), 7.45 (1H, dd, J = 9.0 and 2.7 Hz, H-5), 7.26 (1H, d, J = 8.9 Hz, H-12), 7.21 (1H, d, J = 3.0 Hz, H-9), 7.17 (1H, d, J = 9.1 Hz, H-6), 7.01 (1H, dd, J = 9.0 and 3.0 Hz, H-11). ¹³C NMR (126 MHz, d-DMSO): δ_{C} = 180.3 (C-1), 158.6 (C-7*), 158.4 (C-10*), 154.0 (C-13*), 138.7 (C-5), 133.0 (C-4), 128.83 (C-3 and C-11), 128.76 (C-2[#]), 125.5 (C-8[#]), 124.0 (C-12), 123.1 (C-6), 112.4 (C-9). IR ($\nu_{\text{m}}, \text{cm}^{-1}$) = 3312, 2984, 2959, 2878, 1651, 1616, 1476, 1375, 1285, 12238, 1150, 1059, 1034, 1030, 891, 889, 820, 795, 733, 689, 629. ESI-MS (m/z) calculated $[\text{M}+\text{H}]^+$ for C₁₃H₈O₃Cl 247.0162, found 247.0157.

**307**

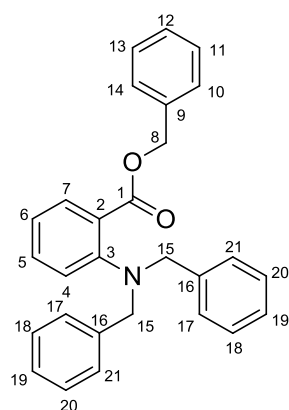
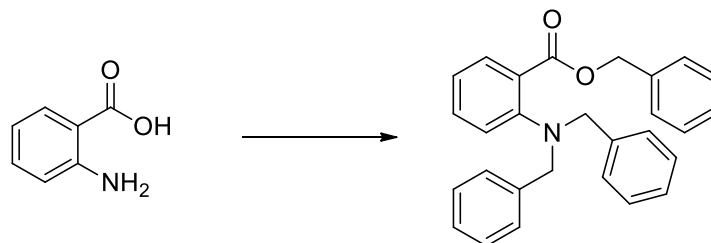
In the presence of sodium dithionite (0.179 g, 1.026 mmol, 3 eq), dione **257** (0.100 g, 0.342 mmol, 1 eq) was reduced to **307** following the general procedure resulting in the formation of a yellow solid (0.057 g, 64 %). **m.p.** = decomposed at 260 °C. ¹H NMR (300 MHz, CDCl₃): δ_{H} = 8.64 (1H, dt, J = 6.8 and 3.4 Hz, H-12), 8.34 (1H, dt, J = 7.0 and 3.5 Hz, H-15), 8.27 – 8.19 (1H, m, H-7), 7.94 – 7.84 (2H, m, H-4 and H-5), 7.80 (2H, dt, J = 6.4 and 3.5 Hz, H-13 and H-14), 7.50 (1H, ddd, J = 8.1, 5.8 and 2.3 Hz, H-6), 7.42 (1H, s, H-9). ¹³C NMR (75 MHz, CDCl₃): δ_{C} = 175.5 (C-1), 155.1 (C-3[#]), 151.4 (C-10[#]), 146.1 (C-17[#]), 134.4 (C-4*), 129.4 (C-11), 128.7 (C-13'), 127.4 (C-14'), 125.6 (C-12), 124.5 (C-16), 124.2 (C-6), 123.0 (C-15), 122.4 (C-12), 121.1 (C-2), 118.3 (C-5*), 117.9 (C-8), 99.1 (C-9). IR ($\nu_{\text{m}}, \text{cm}^{-1}$) = 3329, 3074, 1624, 1607, 1581, 1470, 1420, 1286, 1265, 1234, 1130, 1076, 1022, 889, 858, 842, 771, 745, 698, 661, 635. ESI-MS (m/z) calculated $[\text{M}+\text{H}]^+$ for C₁₇H₁₁O₃ 263.0708, found 263.0708.

Experimental**308**

Following the general procedure, dione **264** (0.146 g, 0.447 mmol, 1 eq) was reduced by sodium dithionite (0.233 g, 1.341 mmol, 3 eq). The product was collected as a yellow solid and determined to be **308** (0.090 g, 68 %). **m.p.** = decomposed >270 °C. **¹H NMR** (500 MHz, *d*-DMSO): δ_{H} = 8.63 – 8.56 (1H, m, H-12), 8.29 – 8.24 (1H, m, H-15), 8.08 (1H, d, *J* = 1.5 Hz, H-7), 7.88 (2H, d, *J* = 1.6 Hz, H-4 and H-5), 7.83 – 7.77 (2H, m, H-13 and H-14), 7.38 (1H, s, H-9). **¹³C NMR** (126 MHz, *d*-DMSO): δ_{C} = 175.0 (C-1), 154.2 (C-17[#]), 150.6 (C-3[#]), 147.4 (C-10), 134.9 (C-5*), 129.9 (C-6), 129.2 (C-13'), 128.3 (C-14'), 124.9 (C-7), 123.2 (C-15), 123.15 (C-11 and C-16), 123.09 (C-12), 122.6 (C-2), 121.4 (C-4*), 117.8 (C-8), 99.7 (C-9). **IR** (ν_{m} , cm^{-1}) = 3323, 2981, 2924, 2868, 1626, 1601, 1685, 1452, 1402, 1267, 1117, 1057, 1034, 1016, 893, 585, 812, 766, 710, 665, 615. **ESI-MS** (*m/z*) calculated $[\text{M}+\text{H}]^+$ for $\text{C}_{17}\text{H}_{10}\text{O}_3\text{Cl}$ 297.0318, found 297.0312.

7.4. Experimental Procedures for the preparation of acridones.

7.4.1. Benzyl Protection of Anthranilic acid

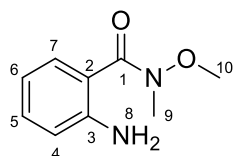
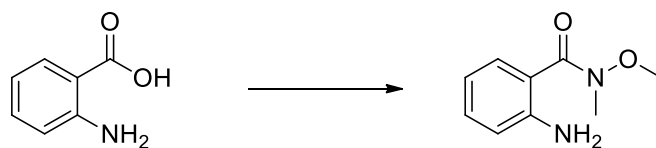


290

Anthranilic acid (10.0 g, 72.9 mmol) and K_2CO_3 (38.3 g, 0.277 mol, 3.8 eq) were dissolved in a 5:1 MeOH:H₂O solution (250 ml MeOH and 50 ml H₂O). Benzyl bromide (47.4 g, 0.277 mol, 3.8 eq) was added slowly to the rapidly stirring solution. The reaction mixture was heated under reflux for 2 hours. The methanol was removed *in vacuo*, EtOAc added to dissolve the organic content and extracted with water. The organic layer was dried over anhydrous Na_2SO_4 and concentrated *in vacuo*. The product **290** was purified by column chromatography with an eluent containing 0-10 % EtOAc/Hexane and collected as a colourless oil that

formed white crystals on standing (21.29 g, 72 %). R_f = 0.51 (10 % EtOAc/Hexane). **m.p.** = 60-62 °C; 53-55 °C. ^{199}H NMR (500 MHz, $CDCl_3$): δ_H = 7.71 (1H, dd, J = 8.0 and 1.7 Hz, H-4), 7.46 – 7.41 (2H, m, H-10 and H-14), 7.37 – 7.30 (3H, m, H-11, H-12 and H-13), 7.27 – 7.15 (11H, m, H-7, H-16, H-17, H-18, H-19, H-20 and H-21), 6.93 – 6.88 (2H, m, H-5 and H-6), 5.34 (2H, s, H-8), 4.18 (4H, s, H-15). ^{13}C NMR (126 MHz, $CDCl_3$): δ_C = 168.2 (C-1), 150.8 (C-3), 137.9 (C-16), 136.0 (C-2), 131.8 (C-7), 131.3 (C-4), 128.5 (C-10, C-11, C-12, C-13 and C-14), 128.3 (C-18 and C-20), 128.22 (C-9), 128.17 (C-17 and C-21), 126.9 (C-19), 121.3 (C-5*), 120.8 (C-6*), 66.8 (C-8), 56.9 (C-15). IR ($\nu_{m,cm^{-1}}$) = 3069, 3028, 2955, 2926, 2853, 1703, 1595, 1489, 1450, 1377, 1290, 1256, 1217, 1117, 1078, 1049, 1026, 959, 907, 887, 745, 694. ESI-MS (m/z) calculated $[M+H]^+$ for $C_{28}H_{26}NO_2$ 408.1964, found 408.1964.

7.4.2. Synthesis of Weinreb amide

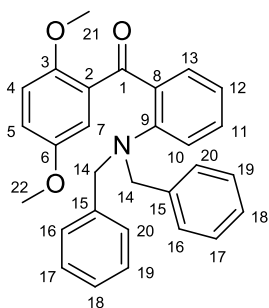
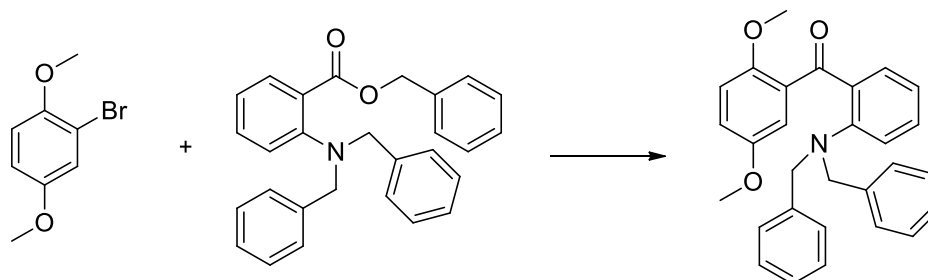
**339**

Using the methodology established in our laboratory,¹¹³ anthranilic acid (1.00 g, 7.292 mmol) was dissolved in CHCl_3 (50 ml). DMF was added to the reaction dropwise to ensure everything had completely dissolved. CDI (1.419 g, 8.750 mmol, 1.2 eq) was added portion-wise to the reaction – if necessary more DMF was added to

ensure the CDI complex remained in solution. Bubbles of CO_2 were generated as the CDI was added and when the bubbles stopped forming (after about 20 minutes) *N,O*-dimethylhydroxylamine.HCl (0.854 g, 8.750 mmol, 1.2 eq) was added and the solution left to stir overnight at room temperature. The product - **339** – was collected as a brown oil (1.257 g, 96 %). $R_f = 0.31$ (30 % EtOAc/Hexane). $^1\text{H NMR}$ (500 MHz, CDCl_3): $\delta_{\text{H}} = 7.33$ (1H, dd, $J = 7.8$ and 1.6 Hz, H-4), 7.15 (1H, ddd, $J = 8.4$, 7.2 and 1.6 Hz, H-6), 6.71 – 6.62 (2H, m, H-5 and H-7), 4.80 – 4.51 (2H, m, H-8), 3.62 – 3.53 (3H, s, H-10), 3.31 (3H, s, H-9). $^{13}\text{C NMR}$ (126 MHz, CDCl_3): $\delta_{\text{C}} = 170.0$ (C-1), 146.8 (C-3), 131.3 (C-6), 129.1 (C-4), 117.2 (C-2), 116.7 (C-5*), 116.6 (C-7*), 61.0 (C-10), 34.3 (C-9). IR ($\nu_{\text{m}} \cdot \text{cm}^{-1}$) = 3466, 3358, 2978, 2938, 1670, 1618, 1605, 1493, 1452, 1381, 1313, 1263, 1215, 1159, 1096, 1061, 995, 976, 885, 750, 690, 632. **ESI-MS** (m/z) calculated $[\text{M}+\text{H}]^+$ for $\text{C}_9\text{H}_{13}\text{N}_2\text{O}_2$ 181.0977, found 181.0972.

7.4.3. Lithium mediated coupling reactions

7.4.3.1. The lithiation reaction with benzyl protected anthranilic acid



291

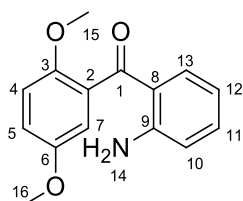
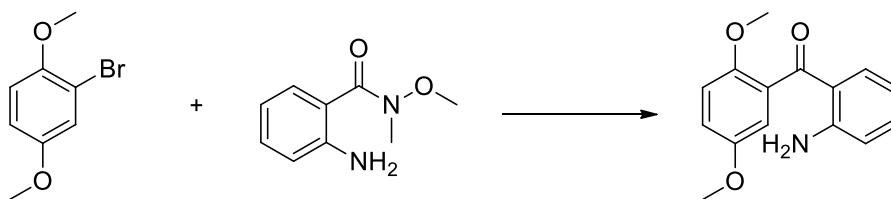
Brominated aromatic **250** (0.500 g, 2.304 mmol, 1.2 eq) was weighed out into a two-necked round bottomed flask. A stirrer bar was added, a rubber septum placed on one neck and the other neck connected to the gas line. The chamber was evacuated and filled with N₂ in triplicate before the addition of THF and the contents of the flask cooled to -78 °C in an acetone/liquid N₂ bath. *n*-BuLi (1.66 ml, 2.496 mmol, 1.5 M, 1.3 eq) was added dropwise to the stirring cold solution and the reaction

stirred for 30 min at -78 °C. In a single necked round bottomed flask ester **290** (0.782 g, 1.919 mmol, 1 eq) was weighed out, a dropping funnel fitted and the system evacuated and filled with N₂. THF was added to dissolve **290** and once dissolved, the solution was cooled to -78 °C. The lithiated mixture was transferred from the two necked flask into the dropping funnel above the ester solution and introduced to the solution dropwise. This was left to react at -78 °C for a further 2 hours and allowed to warm to room temperature. The rapidly stirring reaction was quenched by the addition of sat NH₄Cl once the mixture had warmed to room temperature and the quenched mixture transferred to a separation funnel. Additional water and EtOAc was added to the separation funnel and the aqueous layer removed. The organic layer was washed sequentially with sat NaHCO₃ and brine before being dried over anhydrous Na₂SO₄ and concentrated *in vacuo*. Following purification by flash column chromatography resulted in the collection of product **291** as a thick yellow oil (0.308 g, 31 %) which was characterised primarily by NMR spectroscopy. *R_f* = 0.71 (30 % EtOAc/Hexane). ¹H NMR (300 MHz, CDCl₃): δ_H = 7.41 (1H, dd, *J* = 7.6 and 1.7 Hz, H-10), 7.27 (1H, ddd, *J* = 8.2, 7.3 and 1.7 Hz, H-11), 7.20 – 7.14 (6H, m, H-17, H-18 and H-19), 7.11 (1H, d, *J* = 3.2 Hz, H-7), 7.06 (1H, dd, *J* = 8.9 and 3.2 Hz, H-5), 6.97 (1H, dd, *J* = 7.5 and 1.0, H-13), 6.94 – 6.82 (6H, m, H-4, H-12, H-16 and H-20), 4.10 (4H, s, H-14), 3.73 (3H, s, H-21*), 3.49 (3H, s, H-22*). ¹³C NMR (75 MHz, CDCl₃): δ_C = 197.4 (C-1), 153.5, 153.0, 150.2,

Experimental

137.4, 134.4, 131.1 (C-11), 130.5 (C-10), 130.1, 128.5 (C-16 and C-20), 128.0 (C-17 and C-19), 126.9 (C-18), 120.8 (C-13), 120.4 (C-4'), 118.7 (C-5), 115.3 (C-7), 113.6 (C-12'), 56.3 (C-15), 56.3 (C-21*), 55.8 (C-22*). **IR** ($\nu_{\text{m}}\cdot\text{cm}^{-1}$) = 3063, 300, 2939, 2833, 1649, 1591, 1493, 1445, 1412, 1275, 1217, 1151, 1042, 959, 847, 813, 732, 696, 638. **ESI-MS** (**m/z**) calculated $[\text{M}+\text{H}]^+$ for $\text{C}_{29}\text{H}_{28}\text{NO}_3$ 438.2069, found 438.2069.

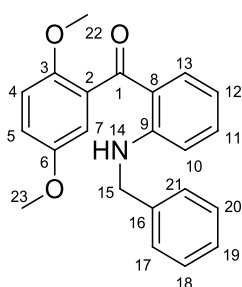
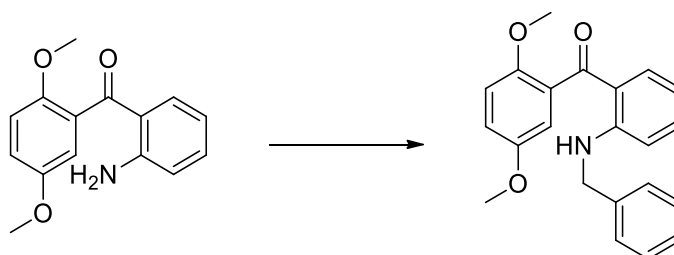
7.4.3.2. Lithiation reactions with Weinreb amide

**292**

Using a procedure described by Frye *et al.*²⁰⁰ brominated **289** (2.409 g, 11.10 mmol, 1 eq) and Weinreb amide **339** (2.00 g, 11.10 mmol, 1 eq) were combined in a round bottomed flask with a magnetic stirrer bar and fitted with a dropping funnel. The entire system was evacuated and charged with nitrogen in triplicate before the addition of THF to dissolve the

compounds. The solution was then cooled to $-78\text{ }^{\circ}\text{C}$ in an acetone/liquid N_2 bath. While stirring vigorously, $n\text{-BuLi}$ (18.5 ml, 22.20 mmol, 1.2 M, 2 eq) was added to the solution dropwise at a rate of 0.5 ml/min and the reaction stirred at $-78\text{ }^{\circ}\text{C}$ for a further 20 minutes. The reaction was quenched by the addition of 1M HCl and the solution warmed slowly to room temperature. After transferring the reaction mixture to a separation funnel and EtOAc added, the organic layer was washed further with 1M HCl followed by brine before being dried over anhydrous Na_2SO_4 and concentrated *in vacuo*. The reaction mixture was purified by flash column chromatography with a 20 % EtOAc/Hexane eluent and the product **292**, collected as a viscous yellow oil (1.57 g, 55 %). $R_f = 0.44$ (30 % EtOAc/Hexane). $^1\text{H NMR}$ (300 MHz, CDCl_3): $\delta_{\text{H}} = 7.32 - 7.22$ (2H, m, H-11 and H-13), 6.97 – 6.88 (2H, m, H-4 and H-5), 6.81 (1H, d, $J = 2.7$ Hz, H-7), 6.68 (1H, d, $J = 8.3$ Hz, H-10), 6.56 – 6.50 (1H, m, H-12), 6.39 (2H, s, H-14), 3.77 (3H, s, H-15*), 3.71 (3H, s, H-16*). $^{13}\text{C NMR}$ (75 MHz, CDCl_3): $\delta_{\text{C}} = 198.4$ (C-1), 153.4 (C-3 \sim), 151.0 (C-6 \sim), 150.4 (C-9 \sim), 135.0 (C-11*), 134.7 (C-13*), 131.0 (C-8), 118.3 (C-2), 116.8 (C-10), 116.0 (C-4'), 115.5 (C-12), 113.7 (C-7), 112.8 (C-5'), 56.4 (C-15 $\#$), 55.8 (C-16 $\#$). IR ($\nu_{\text{m}}\cdot\text{cm}^{-1}$) = 3470, 3344, 3005, 2959, 2833, 1616, 1580, 1545, 1493, 1449, 1408, 1300, 1275, 1215, 1159, 1042, 959, 860, 816, 750, 727, 700, 648. ESI-MS (m/z) calculated $[\text{M}+\text{H}]^+$ for $\text{C}_{15}\text{H}_{16}\text{NO}_3$ 258.1130, found 258.1134.

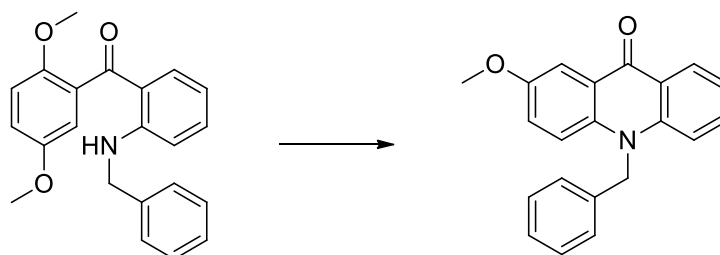
7.4.4. Benzyl protection of 2-aminobenzophenone derivative

**297**

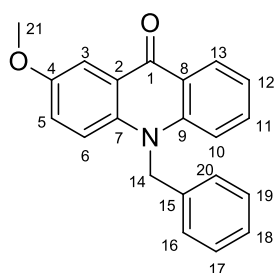
In a microwave tube, 2-aminobenzophenone **292** (0.313 g, 0.901 mmol) and benzaldehyde (0.91 ml, 0.901 mmol, 1 eq) were combined with 3 ml EtOH and a small amount of anhydrous Na_2SO_4 (0.050 g). After the addition of a microwave stirrer bar and sealing the reaction was microwaved for 10 min at 100 °C for 150 W. NaCNBH_4 (0.113 g, 1.802 mmol, 2 eq) was added and the reaction returned to the microwave under the same conditions for a further 50 min (until no more benzaldehyde was present on the TLC plate). Following

this, the reaction was concentrated *in vacuo*, extracted with EtOAc and washed with sat NaHCO_3 . The organic layer was washed further with water, 1M HCl and brine before being dried over anhydrous Na_2SO_4 and concentration *in vacuo*. Following purification by flash column chromatography using a 10-30 % EtOAc/Hexane eluent solution product **297** (0.424 g, 99 %) was collected as a viscous yellow oil. $R_f = 0.46$ (20 % EtOAc/Hexane). $^1\text{H NMR}$ (500 MHz, CDCl_3): $\delta_{\text{H}} = 9.40$ (1H, d, $J = 5.9$ Hz, H-14), 7.41 (2H, d, $J = 7.7$ Hz, H-17 and H-21), 7.38 – 7.33 (3H, m, H-18, H-19 and H-20), 7.32 – 7.26 (2H, m, H-11 and H-13), 6.93 (2H, td, $J = 9.1$ and 6.6 Hz, H-4 and H-5), 6.82 (1H, d, $J = 2.7$ Hz, H-7), 6.70 (1H, d, $J = 8.4$ Hz, H-10), 6.49 (1H, t, $J = 7.6$ Hz, H-12), 4.53 (2H, d, $J = 5.3$ Hz, H-15), 3.77 (3H, s, H-22*), 3.72 (3H, s, H-23*). $^{13}\text{C NMR}$ (126 MHz, CDCl_3): $\delta_{\text{C}} = 198.5$ (C-1), 153.3 (C-3*), 151.7 (C-9*), 150.4 (C-6*), 138.5, 135.9 (C-19), 135.4 (C-11[#]), 131.1, 128.7 (C-18 and C-20), 127.2 (C-13[#]), 127.1 (C-17 and C-21), 117.9, 115.9 (C-4'), 114.3 (C-12), 113.7 (C-7), 112.8 (C-5'), 111.8 (C-10), 56.4 (C-22[~]), 55.8 (C-23[~]), 46.9 (C-15). IR ($\nu_{\text{m}}, \text{cm}^{-1}$) = 3319, 3030, 2943, 2831, 1620, 1570, 1514, 1493, 1452, 1420, 1277, 1217, 1163, 1040, 959, 853, 812, 733, 696, 648. ESI-MS (m/z) calculated $[\text{M}+\text{H}]^+$ for $\text{C}_{22}\text{H}_{22}\text{NO}_3$ 348.1600, found 348.1601.

7.4.4. CAS mediated ring closure



A solution containing 20 ml of MeCN and 5 ml CHCl_3 was used to dissolve benzophenone **297** (0.176 g, 0.507 mmol). Water (10 ml) was added to this solution followed by CAS (1.282 g, 2.027 mmol, 4 eq) in small portions. The reaction was stoppered and stirred at room temperature overnight. The mixture was extracted into EtOAc and washed sequentially with sat NaHCO_3 and brine, the solution was dried over anhydrous Na_2SO_4 . After concentration *in vacuo*, the reaction mixture was purified by flash column chromatography, resulting in the collection of both starting material **297** and yellow crystals that were determined to be **298** (0.13 g, 8 %).

**298**

$R_f = 0.26$ (20 % EtOAc/Hexane). **m.p.** = 215-216 °C, lit 210-212 °C.²¹² **$^1\text{H NMR}$** (300 MHz, CDCl_3): $\delta_{\text{H}} = 8.62$ (1H, dd, $J = 8.1$ and 1.7 Hz, H-13), 8.01 (1H, d, $J = 2.9$ Hz, H-3), 7.63 (1H, ddd, $J = 8.7$, 6.9 and 1.7 Hz, H-11), 7.41 – 7.28 (6H, m, H-5, H-6, H-10, H-12, H-16, H-18 and H-20), 7.22 – 7.17 (2H, m, H-17 and H-19), 5.61 (2H, s, H-14), 3.95 (3H, s, H-21). **$^{13}\text{C NMR}$** (75 MHz, CDCl_3): $\delta_{\text{C}} = 177.7$ (C-1), 154.7 (C-4), 142.2 (C-9[#]), 137.4 (C-7[#]), 135.6 (C-8), 133.8

(C-11), 129.3 (C-16* and C-20*), 127.8 (C-13 and C-18*), 125.6 (C-17* and C-19*), 124.7 (C-5*), 123.3 (C-2), 121.3 (C-6*), 117.0 (C-10*), 115.0 (C-12*), 106.8 (C-3), 55.8 (C-21), 50.8 (C-14). **IR** ($\text{v}_{\text{m}}\cdot\text{cm}^{-1}$) = 3072, 2949, 2843, 1634, 1597, 1557, 1489, 1462, 1450, 1340, 1286, 1271, 1244, 1207, 1180, 1130, 1051, 1028, 1001, 970, 908, 841, 804, 752, 719, 687. **ESI-MS** (m/z) calculated $[\text{M}+\text{H}]^+$ for $\text{C}_{21}\text{H}_{18}\text{NO}_2$ 316.1338, found 316.1347.

At the End of My Tether

Appendices

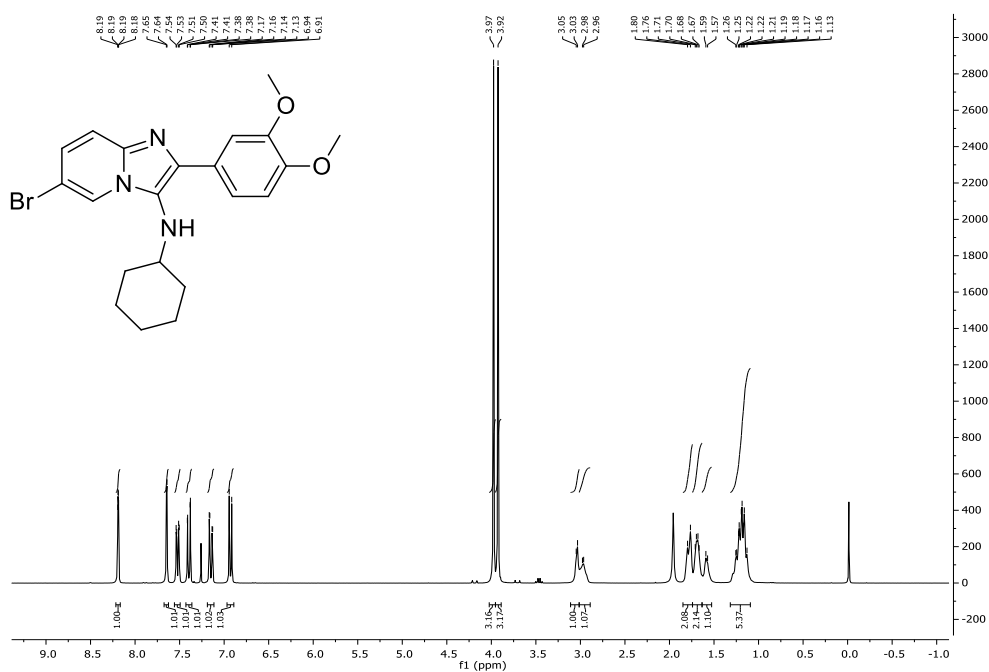
A1 – ^1H and ^{13}C NMR spectra for selected imidazo[1,2-*a*]pyridines

A2 – Crystallographic Information for selected imidazo[1,2-*a*]pyridine examples

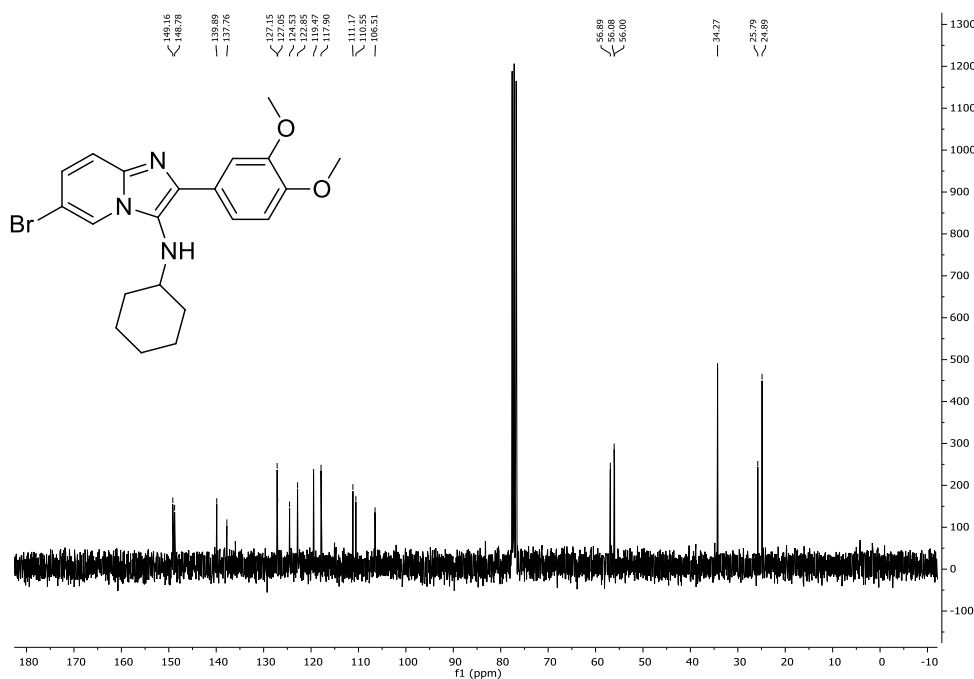
A3 – An example of the UV-vis spectra and Data Analysis obtained in this project

A1 - ^1H and ^{13}C NMR Spectra for selected imidazo[1,2-*a*]pyridines

All the NMR spectroscopic data is available in the Digital Appendix. Below are the spectra for selected compounds that may be of interest to the reader.

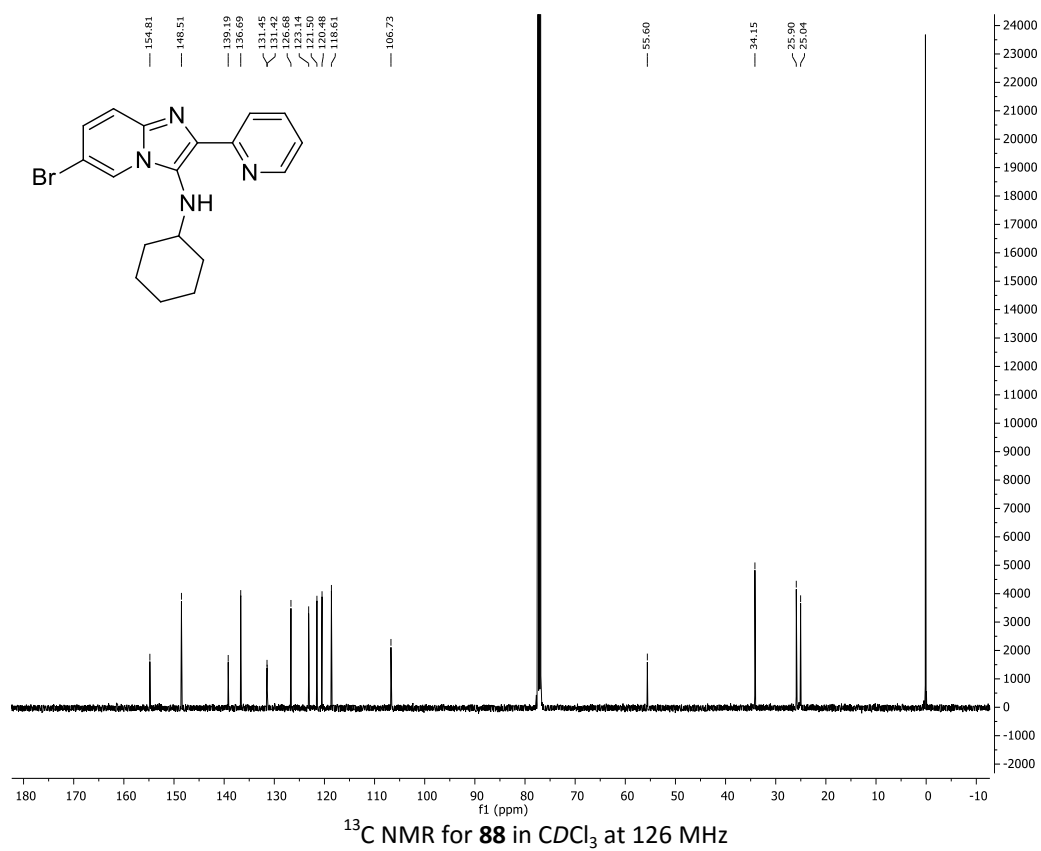
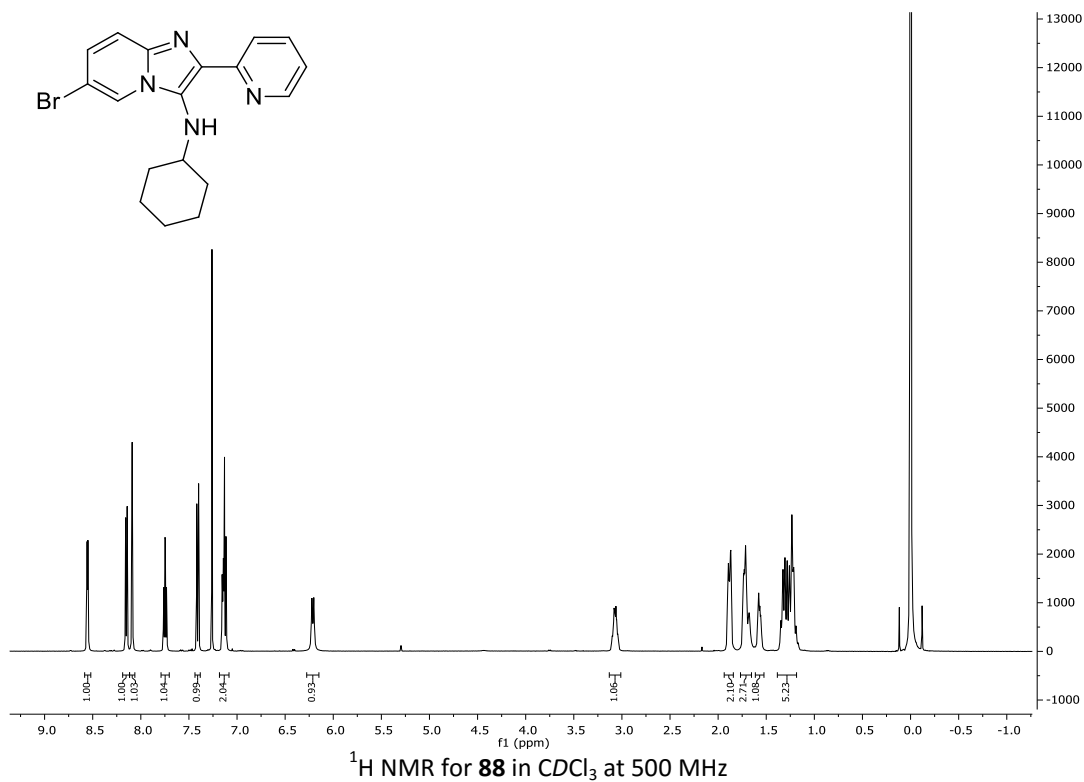


^1H NMR for **85** in CDCl_3 at 300 MHz

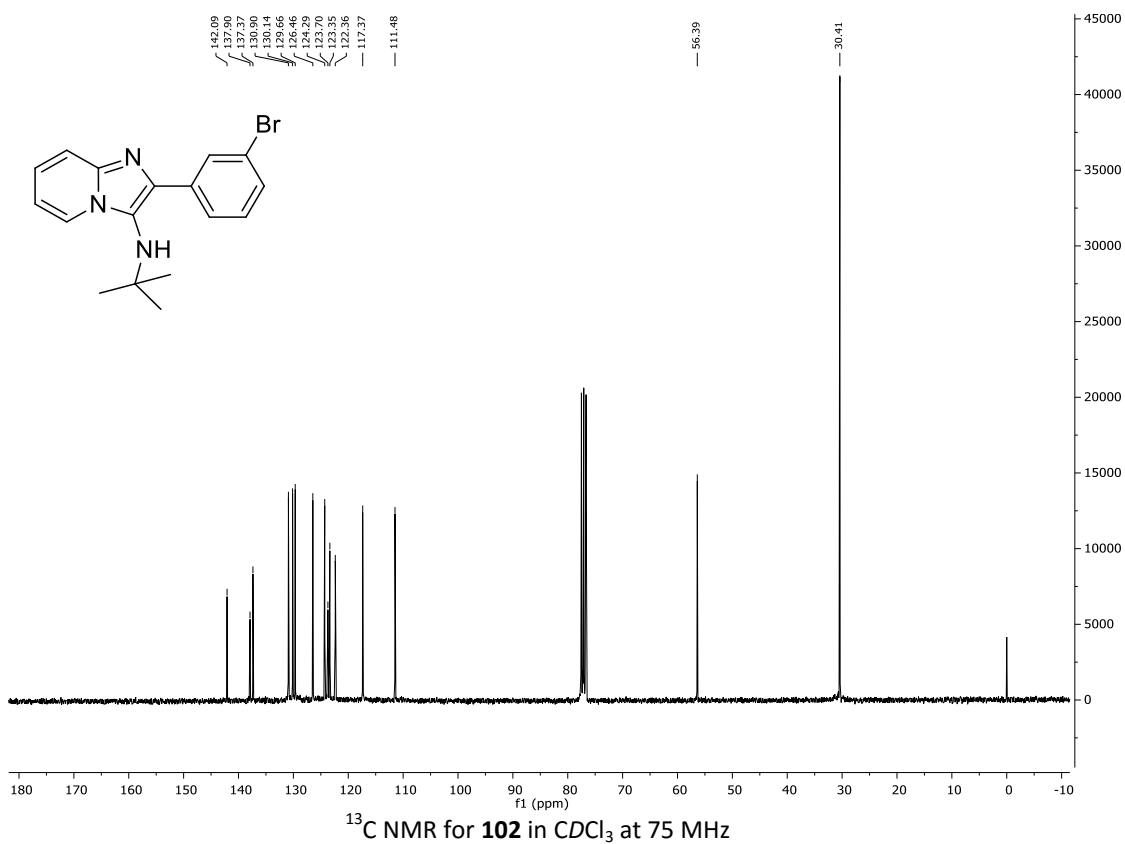
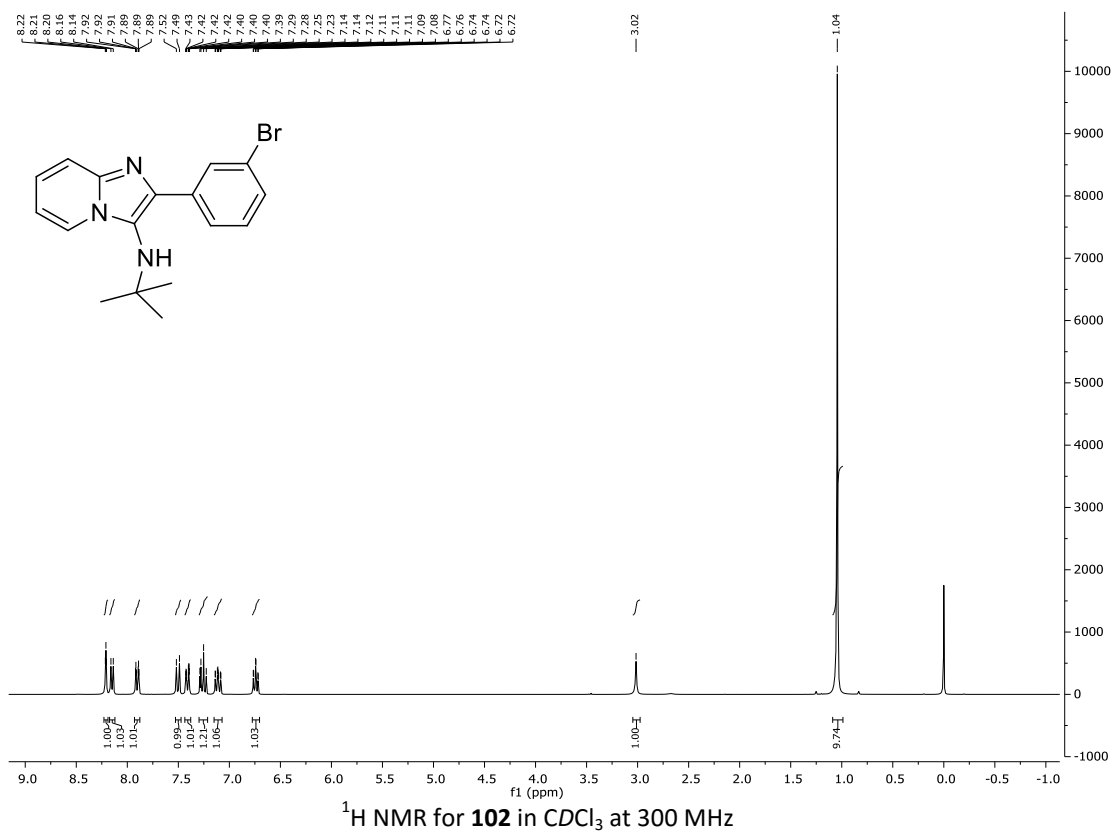


^{13}C NMR for **85** in CDCl_3 at 75 MHz

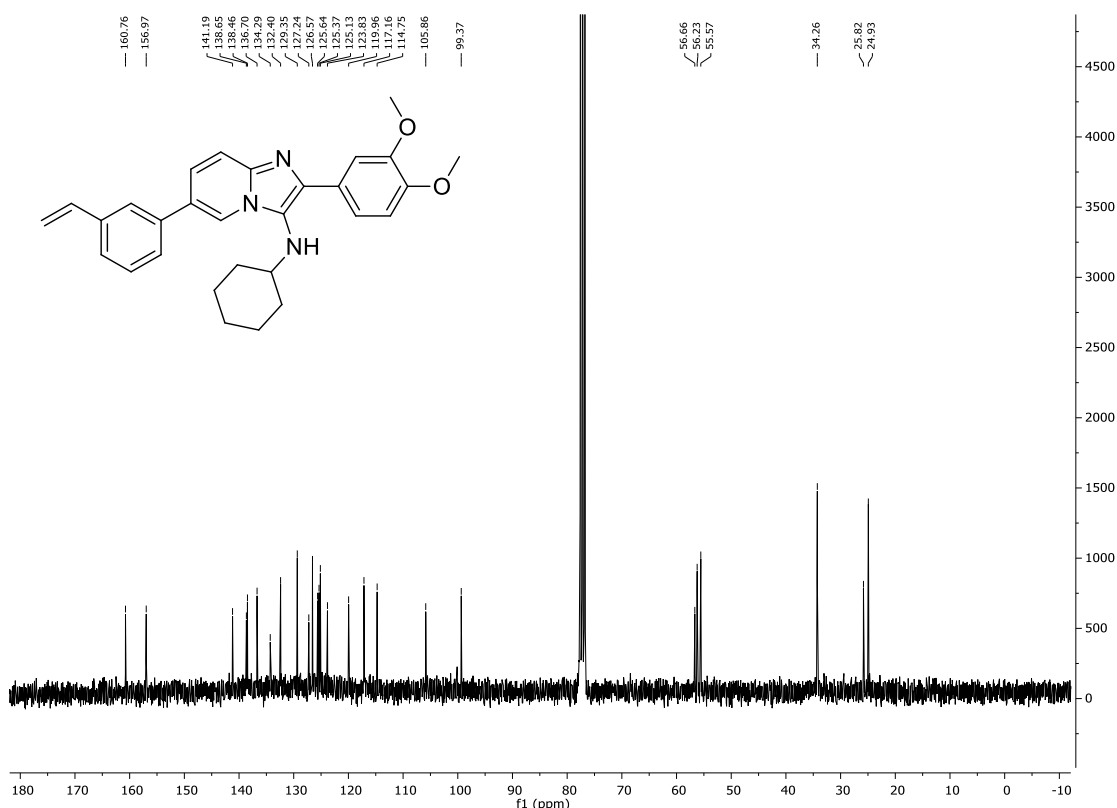
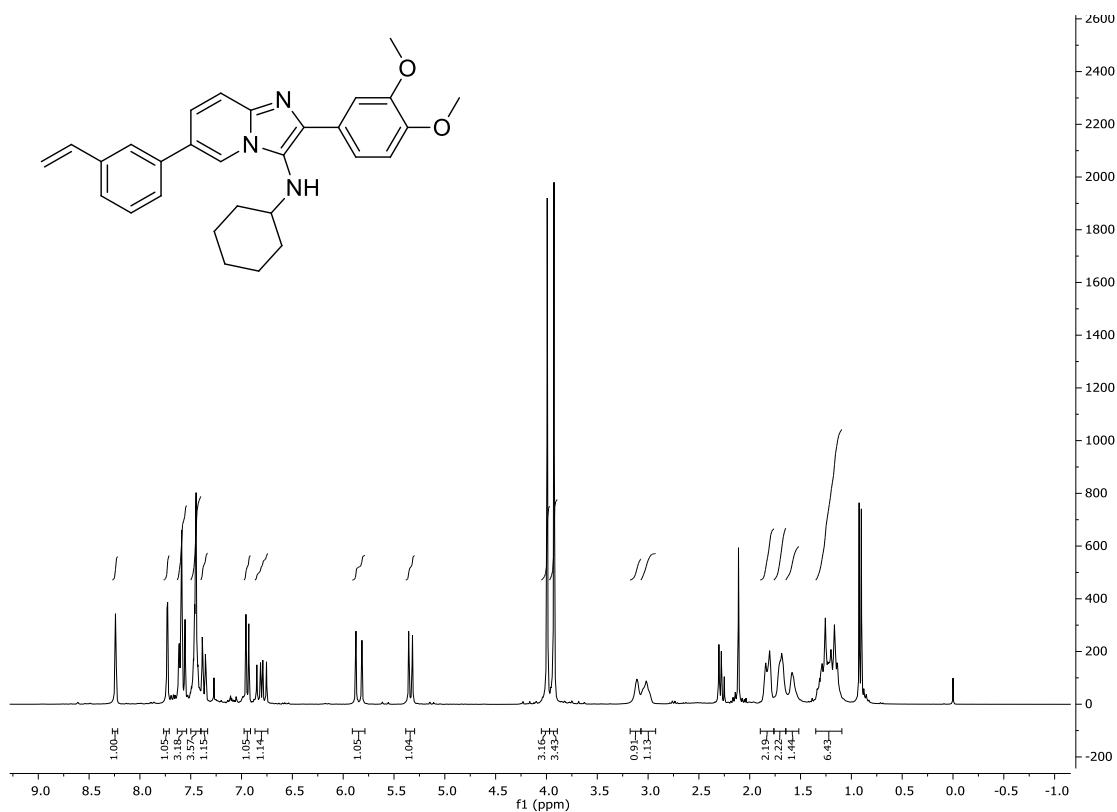
General
Appendices



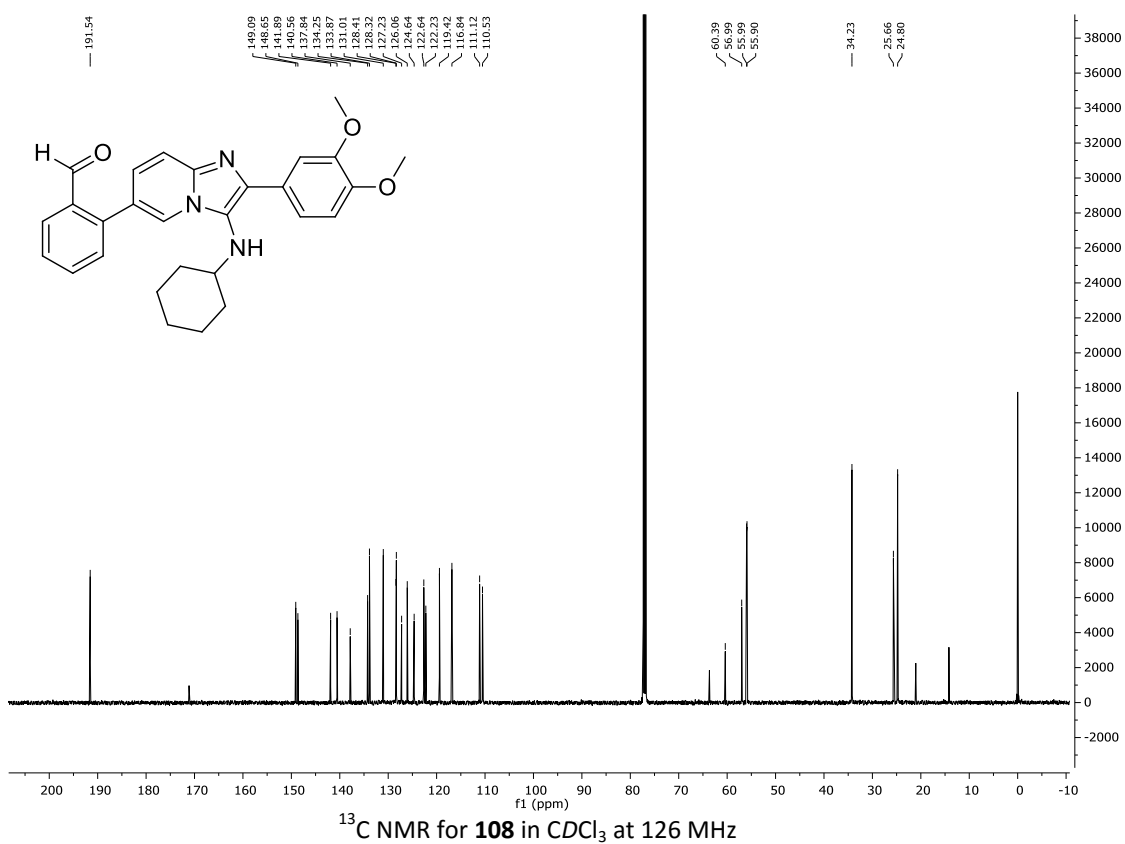
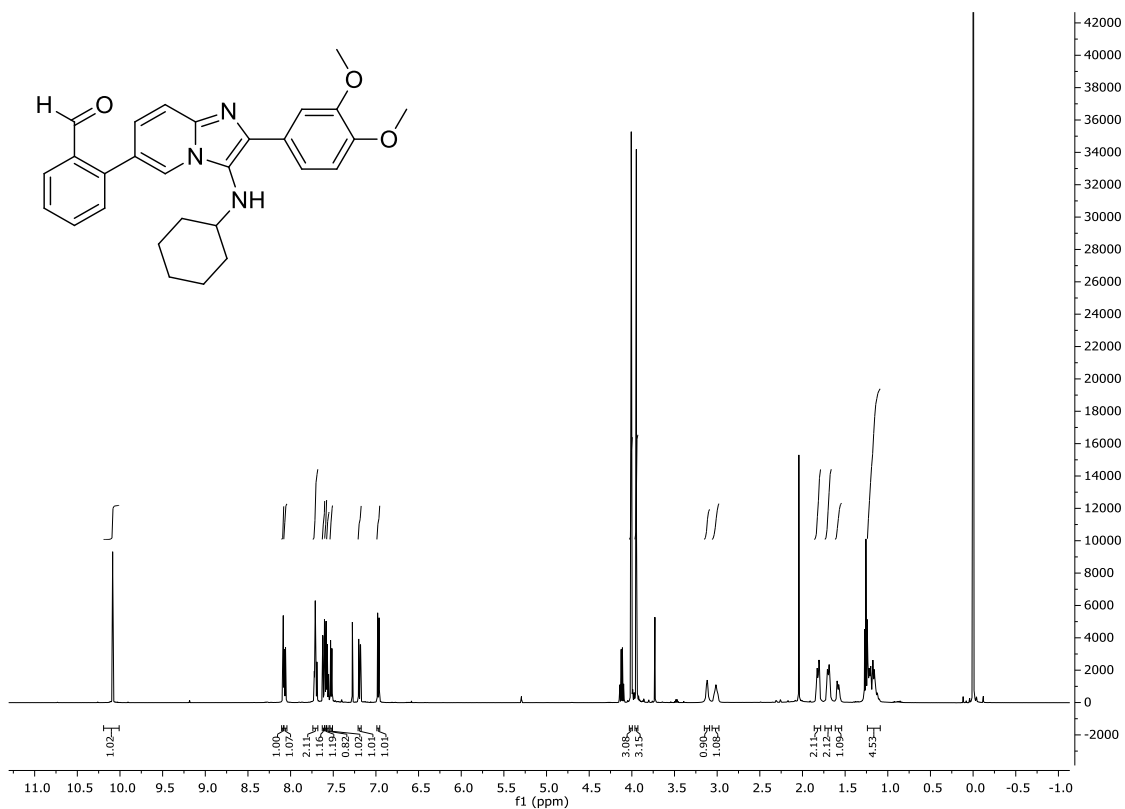
General
Appendices



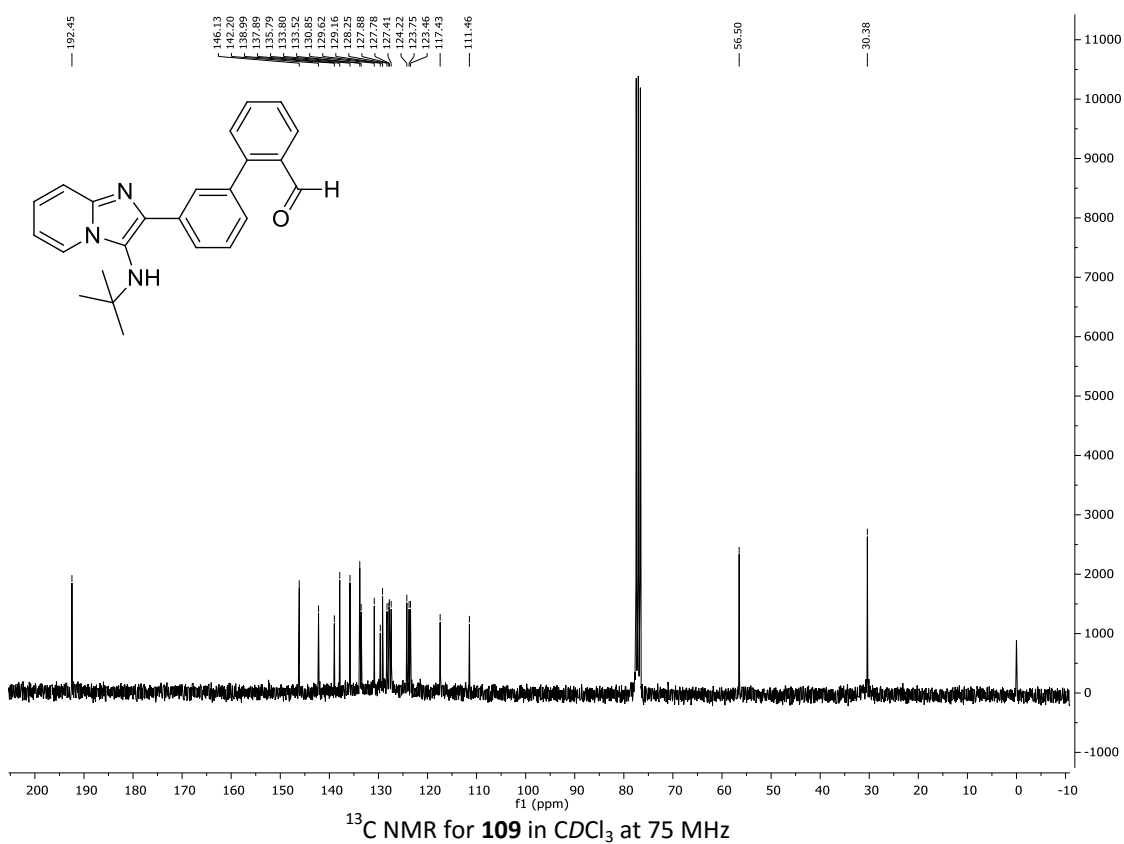
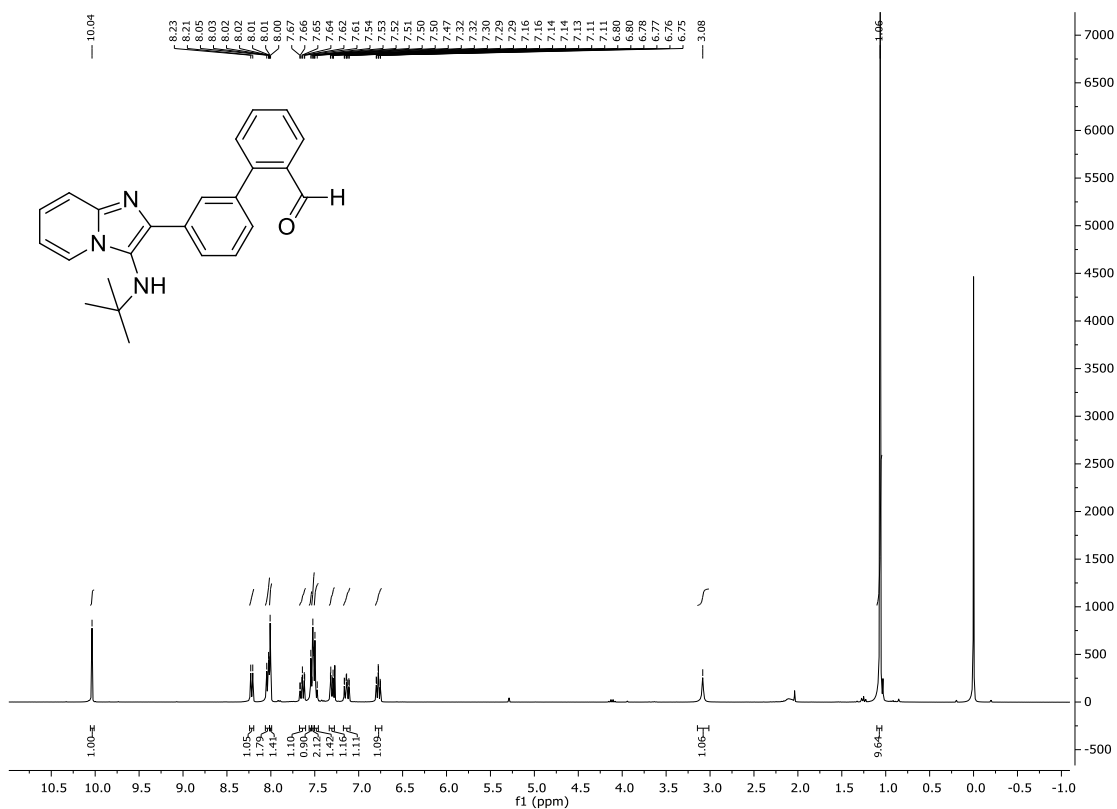
General
Appendices



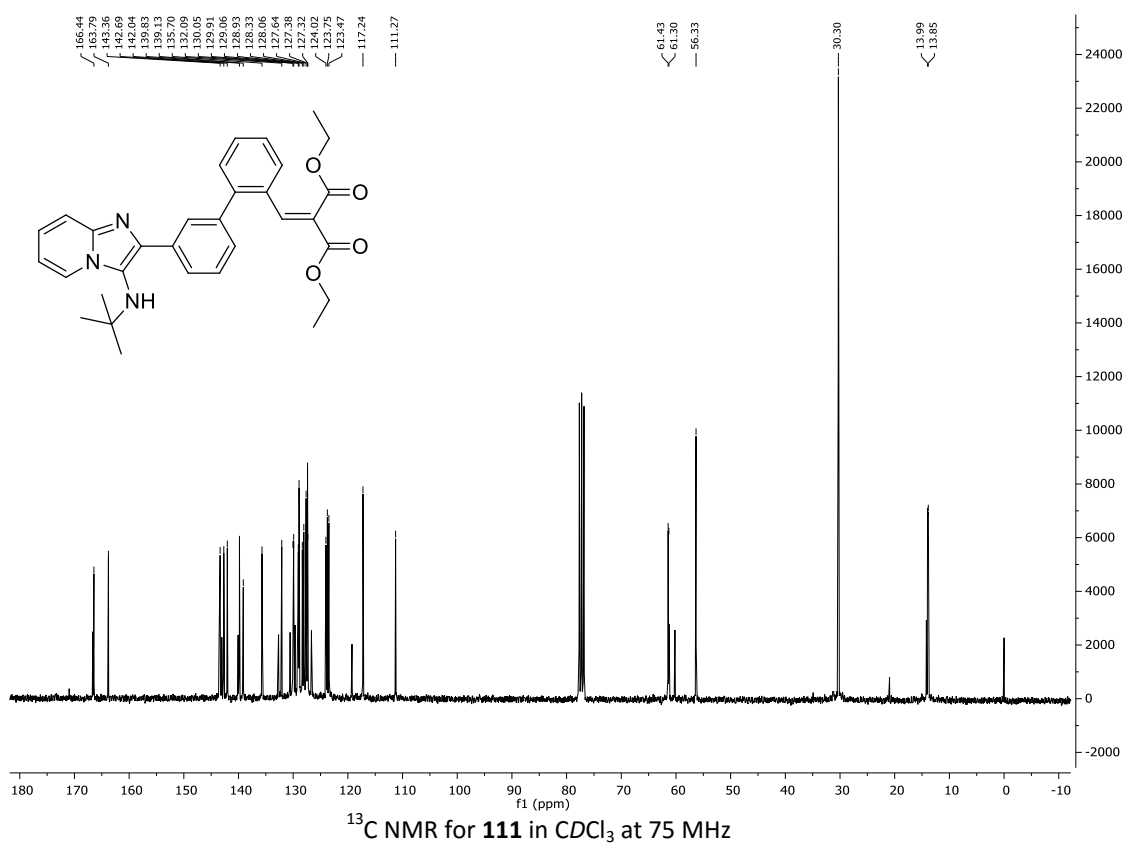
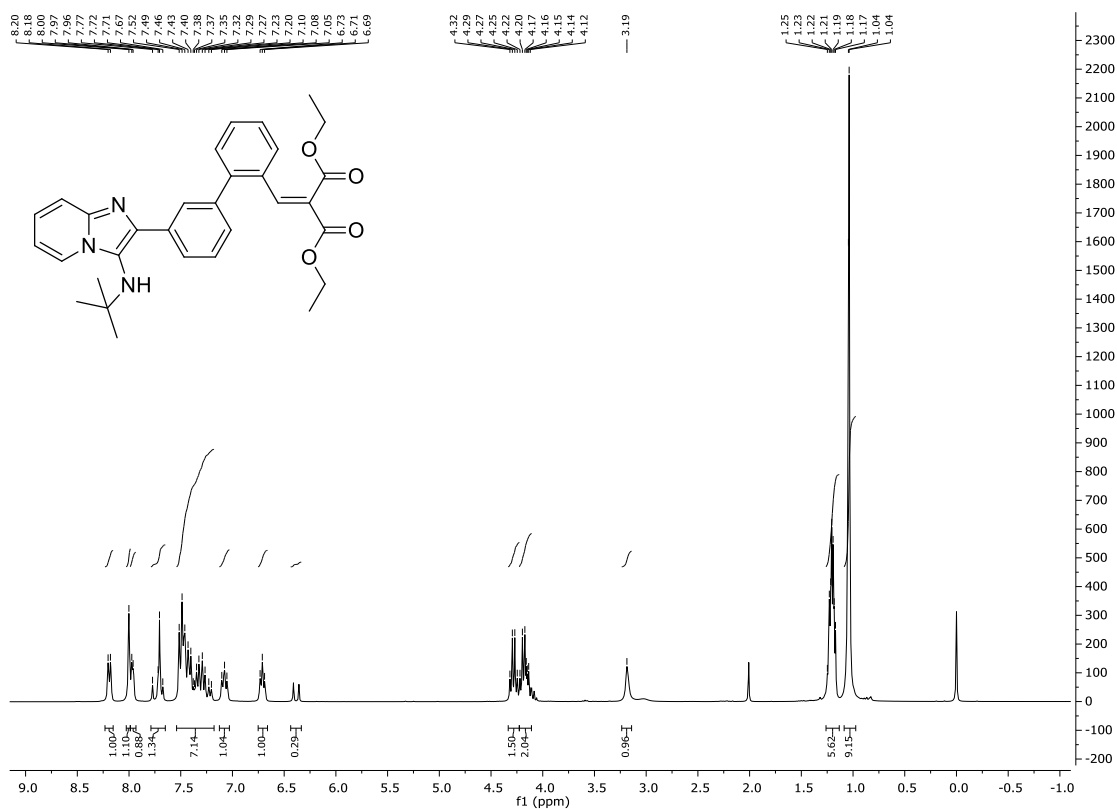
General
Appendices



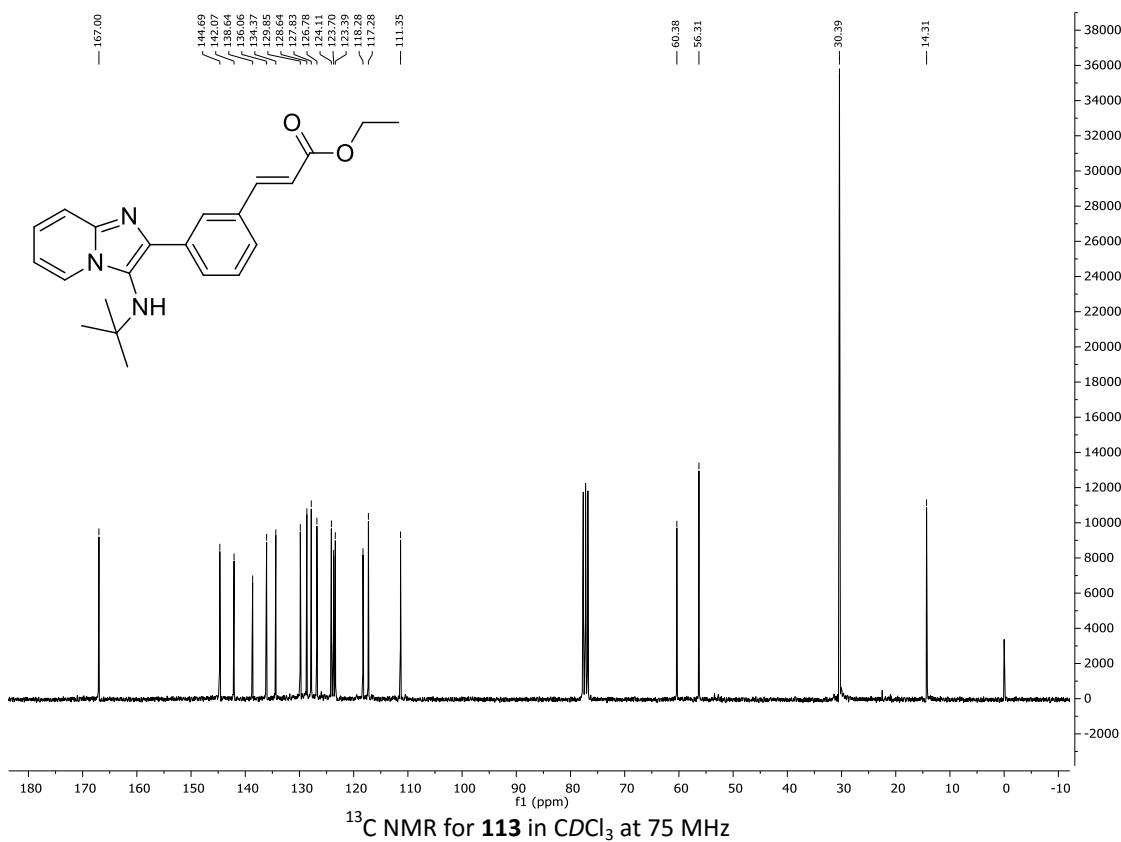
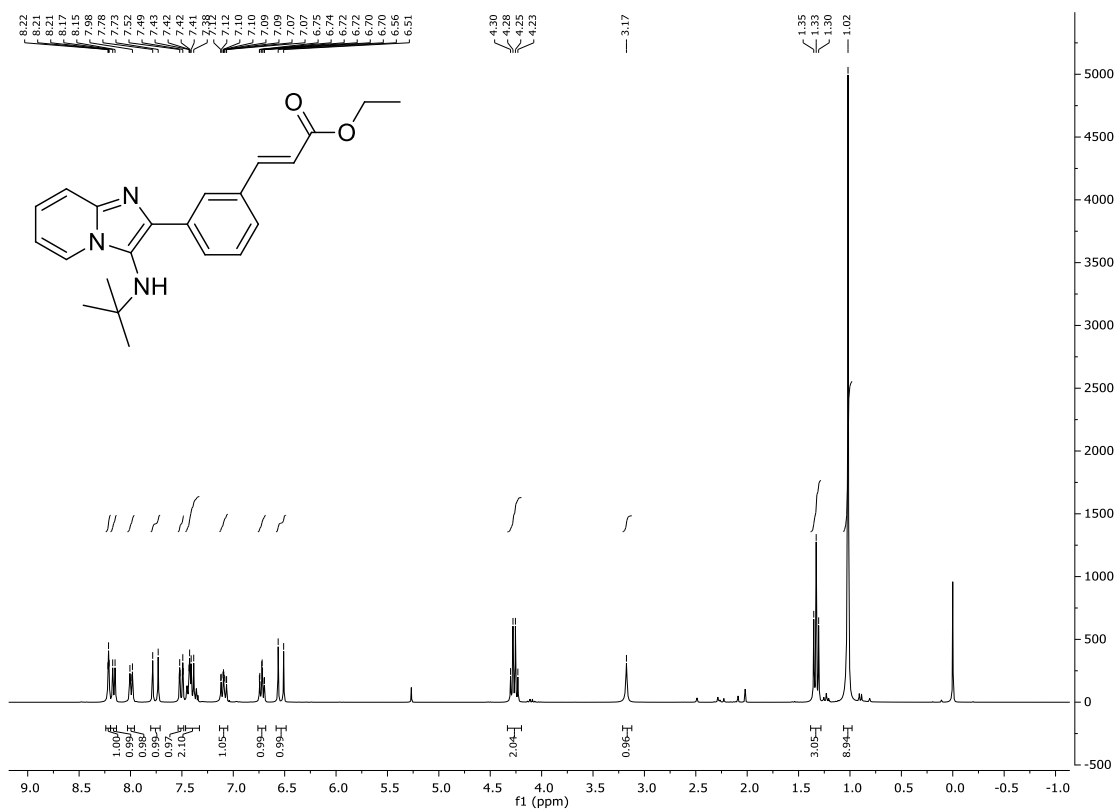
General
Appendices



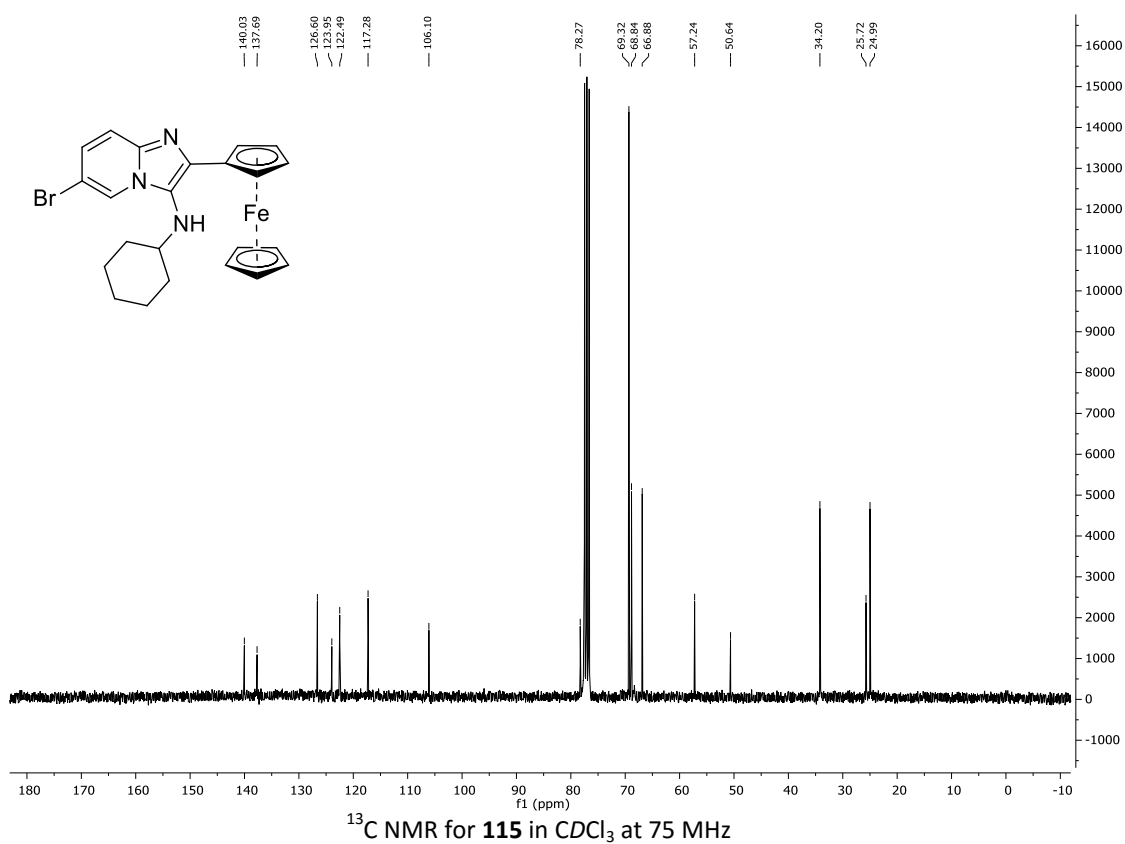
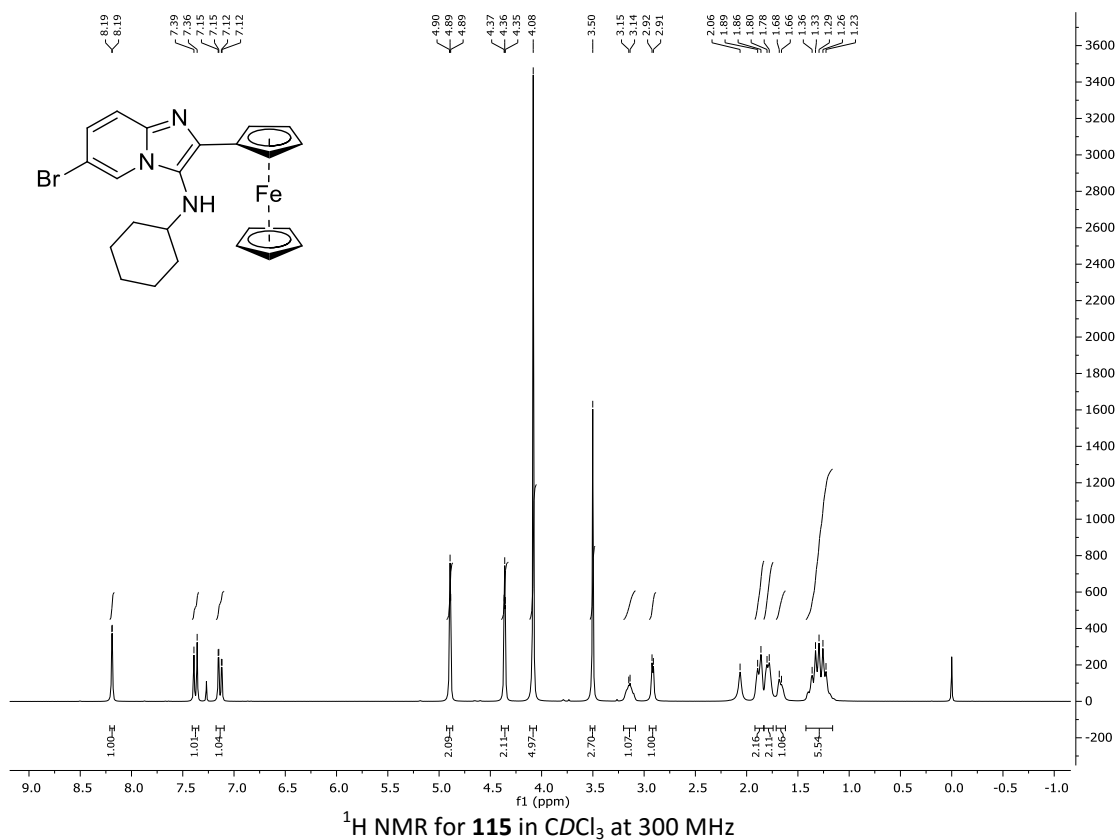
General
Appendices



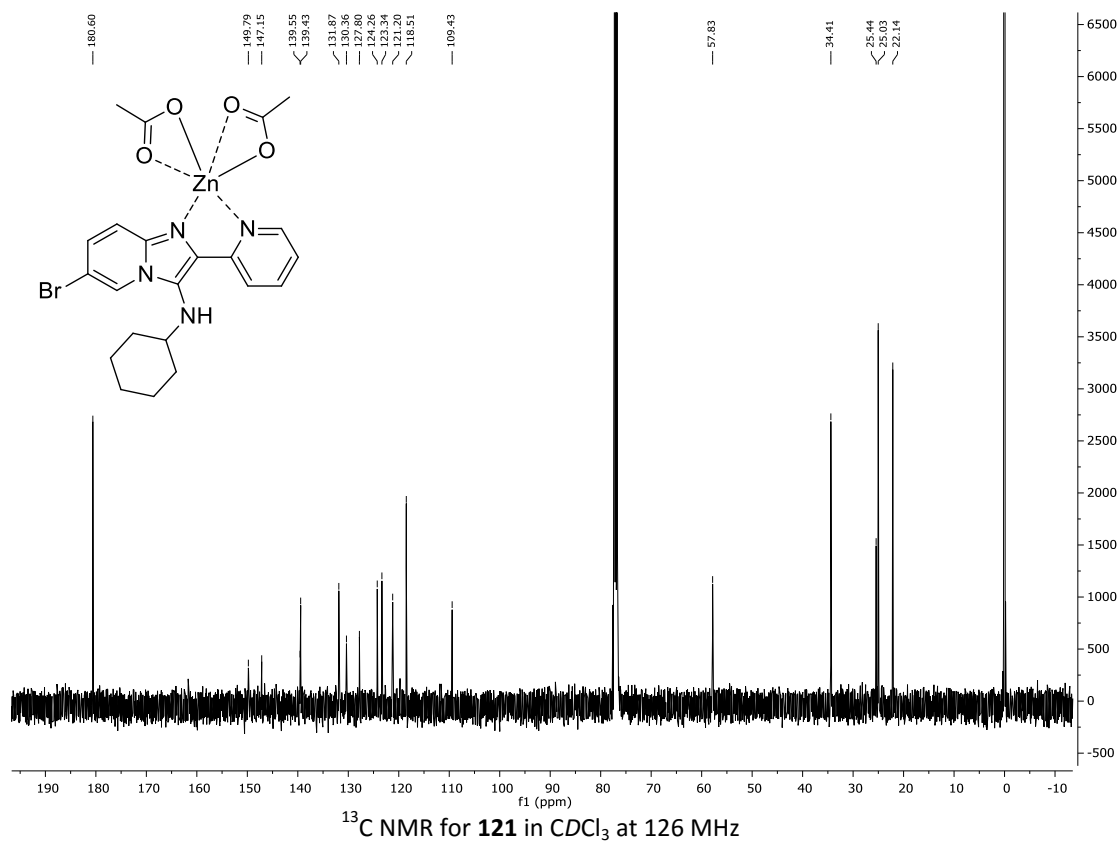
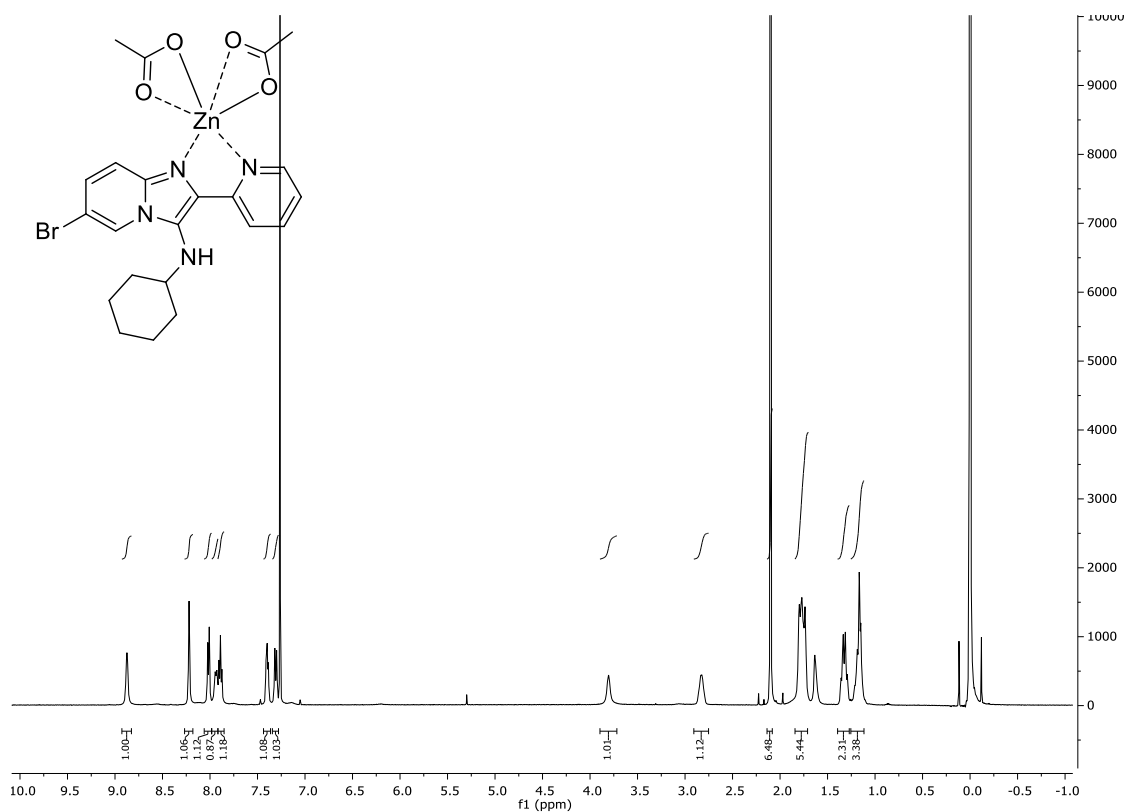
General
Appendices



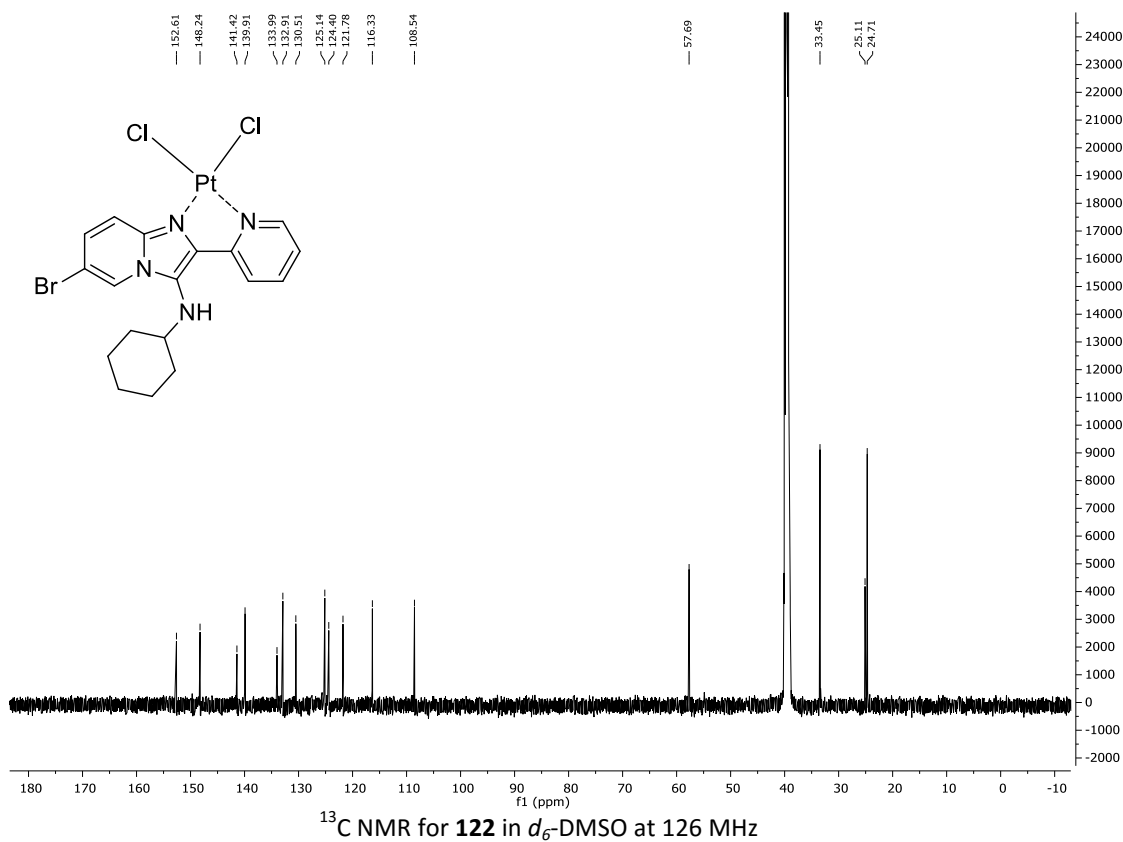
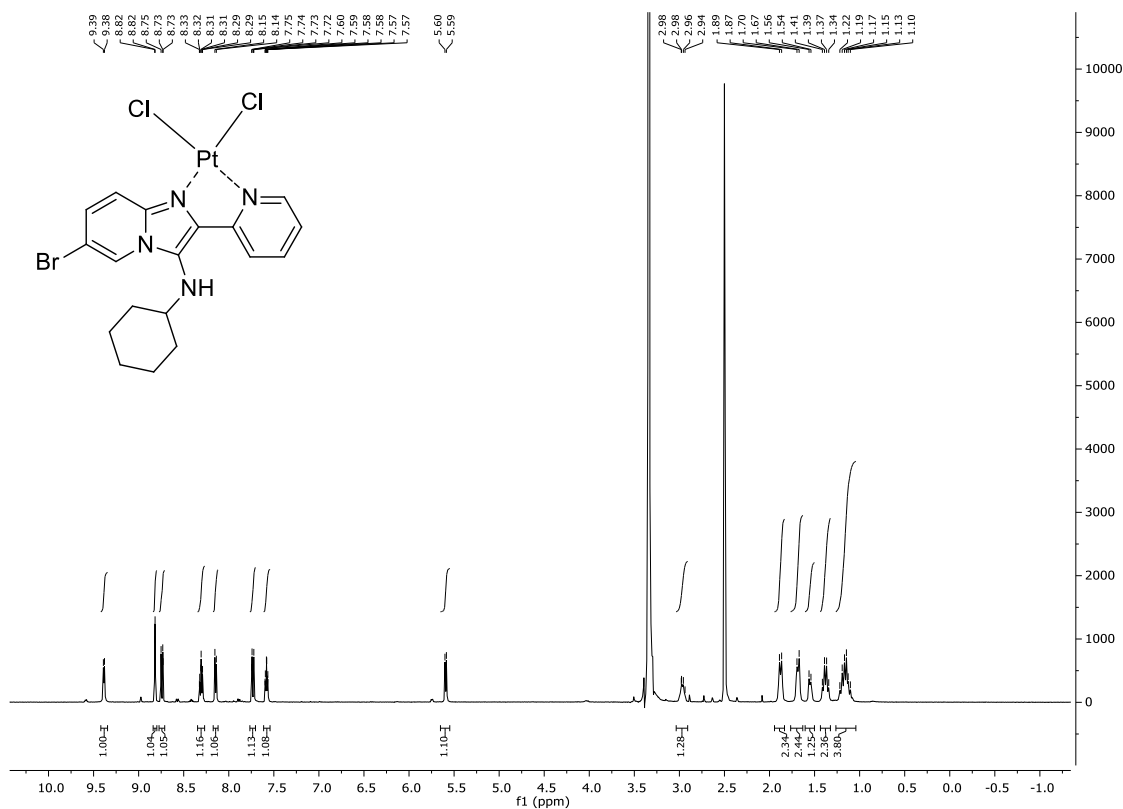
General
Appendices



General
Appendices



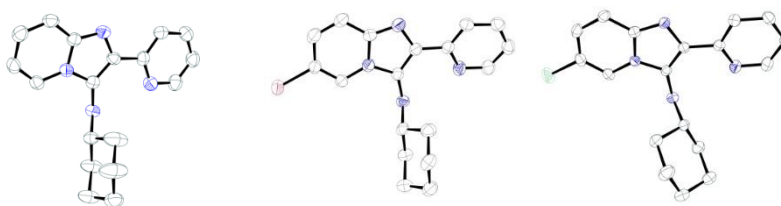
General
Appendices



A2 - Crystallographic Information for selected imidazo[1,2-*a*]pyridines

The crystallographic information for selected compounds can be found below. All the relevant crystallographic information for all the crystal structures included in this thesis can be found in the digital appendix.

Crystallographic Information for selected imidazo[1,2-*a*]pyridines 134, 88 and 137

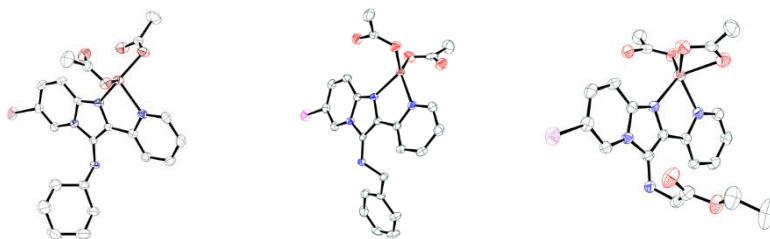


Compound	134	88	137
Identification code	15j_cdkjd12_40r_0p	12j_cdkjd4_ba601_0a	15j_cdkjd15_34r
Empirical formula	C ₁₈ H ₂₀ N ₄	C ₁₈ H ₁₉ Br N ₄	C ₁₈ H ₁₉ Cl N ₄
Formula weight	292.38	371.28	326.82
Temperature	173(2) K	173(2) K	173(2) K
Wavelength	0.71073 Å	0.71073 Å	0.71073 Å
Crystal system	Monoclinic	Triclinic	Monoclinic
Space group	P2(1)/c	P-1	P 21/c
Unit cell dimensions	a = 11.6462(4) Å b = 11.2952(4) Å c = 11.9410(5) Å α = 90° β = 92.805(2)° γ = 90°	a = 6.13550(10) Å b = 16.1046(3) Å c = 17.9030(4) Å α = 67.9870(10)° β = 89.8320(10)° γ = 84.8620(10)°	a = 5.7798(2) Å b = 25.3590(8) Å c = 22.5801(7) Å α = 90° β = 94.090(2)° γ = 90°
Volume	1568.91(10) Å ³	1632.54(5) Å ³	3301.14(19) Å ³
Z	4	4	8
Density (calculated)	1.238 Mg/m ³	1.511 Mg/m ³	1.315 Mg/m ³
Absorption coefficient	0.076 mm ⁻¹	2.523 mm ⁻¹	0.236 mm ⁻¹
F(000)	624	760	1376
Crystal size	0.31 x 0.19 x 0.04 mm ³	0.44 x 0.11 x 0.08 mm ³	0.35 x 0.15 x 0.13 mm ³
Theta range for data collection	1.75 to 25.56°	1.23 to 28.00°	1.61 to 28.00°
Index ranges	-14<=h<=14, -13<=k<=13, -14<=l<=13	-8<=h<=8, -21<=k<=21, -23<=l<=23	-7<=h<=7, -33<=k<=33, -29<=l<=29
Reflections collected	13628	23748	46161
Independent reflections	2936 [R(int) = 0.0713]	7850 [R(int) = 0.0977]	7976 [R(int) = 0.0828]
Completeness to theta = 28.00°	100.00%	99.90%	99.80%
Absorption correction	None	Integration	Integration
Max. and min. transmission		0.8237 and 0.4032	0.9699 and 0.9218

General
Appendices

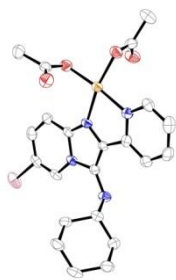
Refinement method	Full-matrix least-squares on F^2	Full-matrix least-squares on F^2	Full-matrix least-squares on F^2
Data / restraints / parameters	2936 / 0 / 203	7850 / 50 / 409	7976 / 0 / 423
Goodness-of-fit on F^2	1.062	1.017	0.974
Final R indices [$I > 2\sigma(I)$]	$R_1 = 0.0695, wR_2 = 0.1730$	$R_1 = 0.0583, wR_2 = 0.1769$	$R_1 = 0.0461, wR_2 = 0.0916$
R indices (all data)	$R_1 = 0.0942, wR_2 = 0.1900$	$R_1 = 0.0864, wR_2 = 0.1896$	$R_1 = 0.0912, wR_2 = 0.1049$
Largest diff. peak and hole	0.555 and -0.425 e. \AA^{-3}	2.577 and -0.807 e. \AA^{-3}	0.271 and -0.251 e. \AA^{-3}

Crystallographic Information for selected Zinc Complexes 121, 127 and 130

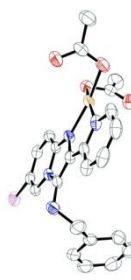


Compound	121	127	130
Identification code	14j_cdkjd8_96_0a	13j_cdkjd10_0a	14j_cdkjd9_257_0a
Empirical formula	C ₂₃ H ₂₆ Br Cl ₃ N ₄ O ₄ Zn	C ₂₃ H ₂₁ Br N ₄ O ₄ Zn	C ₂₃ H ₂₄ Br Cl ₉ N ₄ O ₆ Zn
Formula weight	674.12	562.72	916.79
Temperature	173(2) K	173(2) K	173(2) K
Wavelength	0.71073 Å	0.71073 Å	0.71073 Å
Crystal system	Monoclinic	Triclinic	Triclinic
Space group	P 21/c	P-1	P-1
Unit cell dimensions	a = 16.2492(4) Å b = 14.9187(4) Å c = 24.1221(6) Å α = 90° β = 102.5450(10) ° γ = 90°	a = 8.7640(2) Å b = 10.9349(3) Å c = 13.0299(3) Å α = 96.7010(10)° β = 108.0900(10)° γ = 106.1080(10)°	a = 8.6355(3) Å b = 13.0380(4) Å c = 17.7337(6) Å α = 106.916(2)° β = 93.724(2)° γ = 108.358(2)°
Volume	5708.0(3) Å ³	1111.89(5) Å ³	1785.86(10) Å ³
Z	8	2	2
Density (calculated)	1.569 Mg/m ³	1.681 Mg/m ³	1.705 Mg/m ³
Absorption coefficient	2.576 mm ⁻¹	2.940 mm ⁻¹	2.521 mm ⁻¹
F(000)	2720	568	912
Crystal size	0.424 x 0.293 x 0.13 mm ³	0.59 x 0.09 x 0.08 mm ³	0.34 x 0.29 x 0.07 mm ³
Theta range for data collection	1.28 to 25.24	1.69 to 27.93°	1.22 to 26.34°
Index ranges	-21<=h<=21, -19<=k<=19, -31<=l<=31	-11<=h<=11, -14<=k<=14, -17<=l<=17	-10<=h<=10, -15<=k<=16, -22<=l<=21
Reflections collected	106686	26092	19317
Independent reflections	13793 [R(int) = 0.0948]	5334 [R(int) = 0.1140]	7246 [R(int) = 0.0979]
Completeness to theta = 28.00°	100%	99.90%	99.50%
Absorption correction	Integration	Integration	Integration
Max. and min. transmission	0.7903 and 0.4128	0.7988 and 0.2759	0.8433 and 0.4810
Refinement method	Full-matrix least-squares on F ²	Full-matrix least-squares on F ²	Full-matrix least-squares on F ²
Data / restraints / parameters	13793 / 0 / 653	5334 / 0 / 304	7246 / 1 / 404
Goodness-of-fit on F2	0.993	0.921	0.926
Final R indices [I>2σ(I)]	R ₁ = 0.0499, wR ₂ = 0.1349	R ₁ = 0.0352, wR ₂ = 0.0726	R ₁ = 0.0580, wR ₂ = 0.1449
R indices (all data)	R ₁ = 0.0938, wR ₂ = 0.1464	R ₁ = 0.0612, wR ₂ = 0.0783	R ₁ = 0.1203, wR ₂ = 0.1648
Largest diff. peak and hole	2.335 and -2.034 e.Å ⁻³	0.439 and -0.476 e.Å ⁻³	1.729 and -0.976 e.Å ⁻³

Crystallographic Information for selected Copper Complexes 123, 128 and 133



123



128



133

Identification code	12j_cdkjd8_bacuac_0a	14j_cdkjd10_253_0a	mo_14a_cdkjd9_cu_0a
Empirical formula	C ₂₄ H ₂₉ Br Cl ₄ Cu N ₄ O ₄	C ₂₃ H ₂₁ Br Cu N ₄ O ₄	C ₂₈ H ₃₄ Br Cu N ₄ O ₆
Formula weight	722.76	560.89	666.04
Temperature	173(2) K	173(2) K	173(2) K
Wavelength	0.71073 Å	0.71073 Å	0.71073 Å
Crystal system	Triclinic	Orthorhombic	Triclinic
Space group	P -1	P 2/c	P-1
Unit cell dimensions	a = 10.0655(7) Å b = 12.1779(8) Å c = 12.8618(8) Å a = 94.595(4)° b = 104.690(4)° g = 101.168(4)°	a = 10.3293(5) Å b = 9.6968(5) Å c = 25.3960(12) Å a = 90° b = 91.8710(10)° g = 90°	a = 9.8245(8) Å b = 11.1441(9) Å c = 13.7793(11) Å a = 76.226(3)° b = 82.809(3)° g = 85.641(3)°
Volume	1482.21(17) Å ³	2542.3(2) Å ³	1452.0(2) Å ³
Z	2	4	2
Density (calculated)	1.620 Mg/m ³	1.465 Mg/m ³	1.523 Mg/m ³
Absorption coefficient	2.482 mm ⁻¹	2.465 mm ⁻¹	2.176 mm ⁻¹
F(000)	730	1132	684
Crystal size	0.719 x 0.272 x 0.212 mm ³	0.31 x 0.193 x 0.156 mm ³	0.30 x 0.24 x 0.14 mm ³
Theta range for data collection	1.65 to 24.91°	1.60 to 26.45°	2.75 to 28.00°
Index ranges	-11<=h<=11, -14<=k<=14, -15<=l<=15	-12<=h<=12, -12<=k<=12, -31<=l<=31	-12<=h<=12, -14<=k<=14, -18<=l<=18
Reflections collected	14786	27558	55868
Independent reflections	5004 [R(int) = 0.0892]	5226 [R(int) = 0.0543]	6986 [R(int) = 0.0366]
Completeness to theta = 28.00°	96.70%	99.80%	99.80%
Absorption correction	Integration	Integration	Integration
Max. and min. transmission	0.7382 and 0.3243	0.7637 and 0.6402	0.7504 and 0.5614
Refinement method	Full-matrix least-squares on F ²	Full-matrix least-squares on F ²	Full-matrix least-squares on F ²
Data / restraints / parameters	5004 / 1 / 348	5226 / 0 / 300	6986 / 0 / 370
Goodness-of-fit on F ²	0.967	1.023	1.029
Final R indices [I>2sigma(I)]	R ₁ = 0.0447, wR ₂ = 0.1025	R ₁ = 0.0442, wR ₂ = 0.1106	R ₁ = 0.0331, wR ₂ = 0.0896
R indices (all data)	R ₁ = 0.0935, wR ₂ = 0.1207	R ₁ = 0.0614, wR ₂ = 0.1148	R ₁ = 0.0373, wR ₂ = 0.0935
Largest diff. peak and hole	1.025 and -0.623 e.Å ⁻³	1.123 and -0.422 e.Å ⁻³	1.274 and -0.800 e.Å ⁻³

A3 - An example of the UV-vis spectra and Data Analysis obtained in this project

All the data for compounds studied using UV-vis spectroscopy can be found in the Digital Appendix. The derivation for the equations used to model the pK data can also be found in the Digital Appendix. Below is an example of the data obtained from one of the out-of-cell pK titration performed on imidazo[1,2-*a*]pyridine **124**. Table 11 outlines the changes in absorbance for the imidazo[1,2-*a*]pyridine at the specific wavelengths monitored (270, 317, 327, 340 and 380 nm) as well as the pK value for each data set as determined by a single pK model using SigmaPlot. An example of the spectral changes seen is outlined in Figure 111A and a graphical example of the single pK model fitted to the data (Figure 111B).

Table 11 – An example of the changes in absorbance of 124 monitored at various wavelengths at a 2.030 - 8.044 pH range and the pK value determined by the fit of the absorption data in SigmaPlot with a single pK model

pH	Absorbance at selected wavelengths (nm)				
	A270	A317	A327	A340	A380
2.030	0.428	0.3292	0.3398	0.2914	0.1345
2.547	0.4366	0.3271	0.3379	0.2913	0.1366
2.676	0.438	0.3259	0.3371	0.2913	0.1371
2.913	0.446	0.3205	0.3319	0.2891	0.1373
3.233	0.4679	0.3104	0.3228	0.2867	0.14
3.543	0.5017	0.2958	0.3092	0.2824	0.1441
3.737	0.5273	0.2801	0.295	0.2799	0.1466
4.063	0.5894	0.2523	0.2691	0.2681	0.1533
4.232	0.6221	0.2372	0.2555	0.2638	0.157
4.524	0.6739	0.212	0.2319	0.2548	0.1624
4.842	0.7149	0.1954	0.2162	0.2502	0.1676
5.111	0.7366	0.1828	0.2042	0.245	0.1681
5.525	0.7611	0.1811	0.2027	0.2476	0.1731
6.036	0.7723	0.1733	0.1951	0.243	0.1749
7.074	0.7837	0.1686	0.1903	0.2398	0.1765
8.044	0.784	0.1661	0.1882	0.238	0.178
pK	4.1420	4.0826	4.0943	4.1420	4.1896
Std. Error	0.0138	0.0163	0.0172	0.0435	0.0412

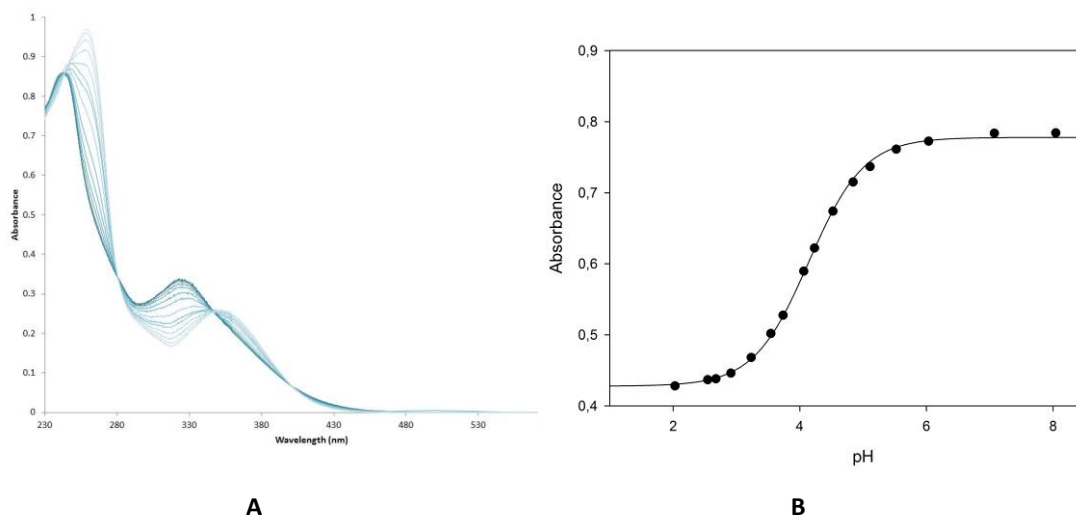


Figure 111 – Changes in the absorbance spectra for 124 over a 2-8 pH range (A) and a graphical fit of the changes in absorbance at a wavelength of 270 nm (B)

Along with each graphical fit, a report is generated for each run. Below is an example of the report generated from the single pK model applied to the changes in absorbance at a wavelength of 270 nm. Similar reports were generated for each wavelength that was monitored for each compound observed.

Nonlinear Regression

Data Source: Data 1 in Notebook1

Equation: User-Defined, One pKa

$H=10^{-x}$;

$K1=10^{-pK1}$;

$Den=H+K1$

$f=(H*A0 + K1*A1)/Den$;

R	Rsqr	Adj Rsqr	Standard Error of Estimate
0.9997	0.9993	0.9992	0.0039

	Coefficient	Std. Error	t	P
A0	0.4278	0.0020	215.3814	<0.0001
A1	0.7778	0.0018	420.5552	<0.0001
pK1	4.1420	0.0138	300.2776	<0.0001

Analysis of Variance:

	DF	SS	MS
Regression	3	6.1598	2.0533
Residual	13	0.0002	1.5139E-005
Total	16	6.1600	0.3850

Corrected for the mean of the observations:

	DF	SS	MS	F	P
Regression	2	0.2992	0.1496	9880.7578	<0.0001
Residual	13	0.0002	1.5139E-005		
Total	15	0.2994	0.0200		

Statistical Tests:

Normality Test (Shapiro-Wilk) Passed (P = 0.8776)

W Statistic= 0.9725 Significance Level = 0.0500

Constant Variance Test Passed (P = 0.0517)

Fit Equation Description:

[Variables]

x = col(5) ' {{prevmin: 0.000000}} {{prevmax: 10.000000}} }

y = col(6)

[Parameters]

A0 = col(6,2) ' {{previous: 0.427761}} }

A1 = col(6,17) ' {{previous: 0.777842}} }

pK1 = 7 ' {{previous: 4.14203}} }

[Equation]

H=10^(-x);

K1=10^(-pK1);

Den=H+K1

f=(H*A0 + K1*A1)/Den;

fit f to y

[Constraints]

[Options]

tolerance=1e-010

stepsize=1

iterations=200

Number of Iterations Performed = 9

The pK value(s) with a standard error below 1 were taken from each report and analysed in Microsoft Excel as shown in Table 12 to determine the average *K* value and hence the average pK value for each compound.

General
Appendices

Table 12 – pK values determined by a single pK model from SigmaPlot for all the fits made and the average pK for compound 124

pK	Std Dev	K
4.1413	0.0536	7.223E-05
4.1011	0.0135	7.923E-05
4.1420	0.0138	7.211E-05
4.0234	0.0311	9.475E-05
4.0766	0.0136	8.383E-05
4.0826	0.0163	8.268E-05
4.0314	0.0329	9.303E-05
4.0869	0.0176	8.187E-05
4.0943	0.0172	8.048E-05
4.0938	0.0912	8.057E-05
4.1819	0.0384	6.578E-05
4.1420	0.0435	7.211E-05
4.2328	0.0883	5.851E-05
4.1474	0.0528	7.122E-05
4.1896	0.0412	6.462E-05
	Ave K	7.687E-05
	Std Dev	1.010E-05
	pK	4.11
	Error	0.05

This process was repeated for each of the compounds analysed using either the single pK model or the two pK model as appropriate. The reports for the two pK model generate two pK values and the average pK was determined independently for each pK.

Plot Twist

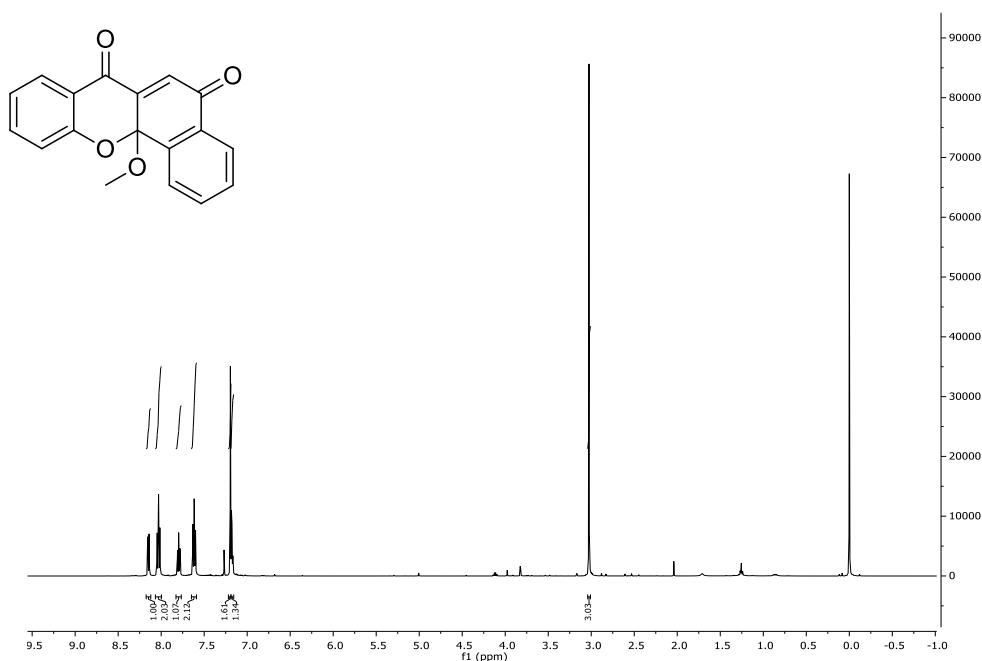
Appendices

A4 – ^1H and ^{13}C NMR spectra for selected compounds

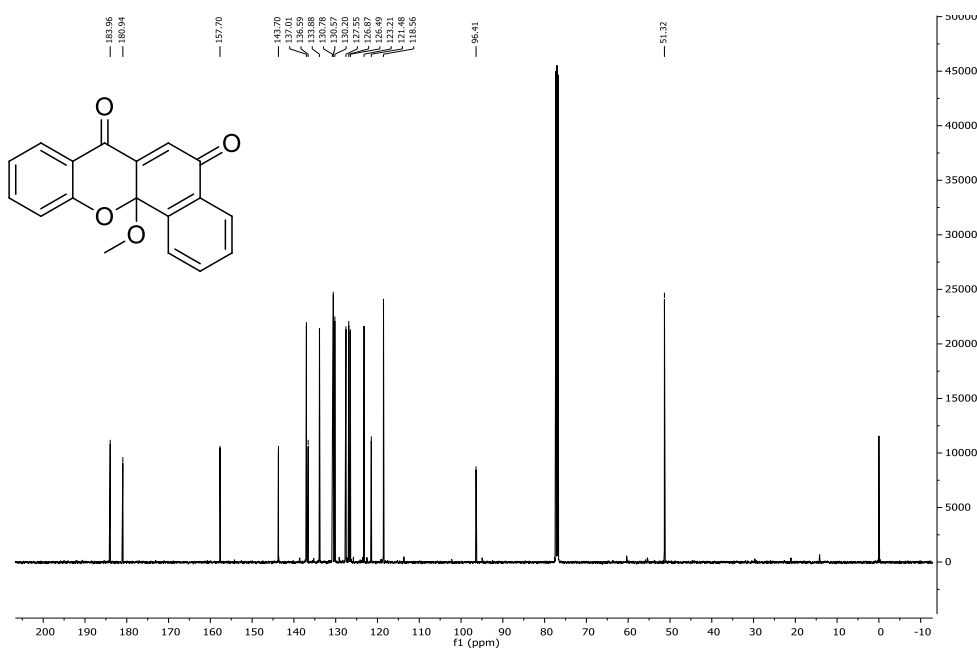
A5 – Crystallographic Data obtained for Plot Twist crystal structures

A4 - ^1H and ^{13}C NMR Spectra for selected compounds

Below are the ^1H and ^{13}C NMR spectra for a selection of the final compounds obtained from the CAS reactions and other novel xanthenes and acridones generated in the course of this project. Spectroscopic data for the synthetic precursors are available in the Digital Appendix.

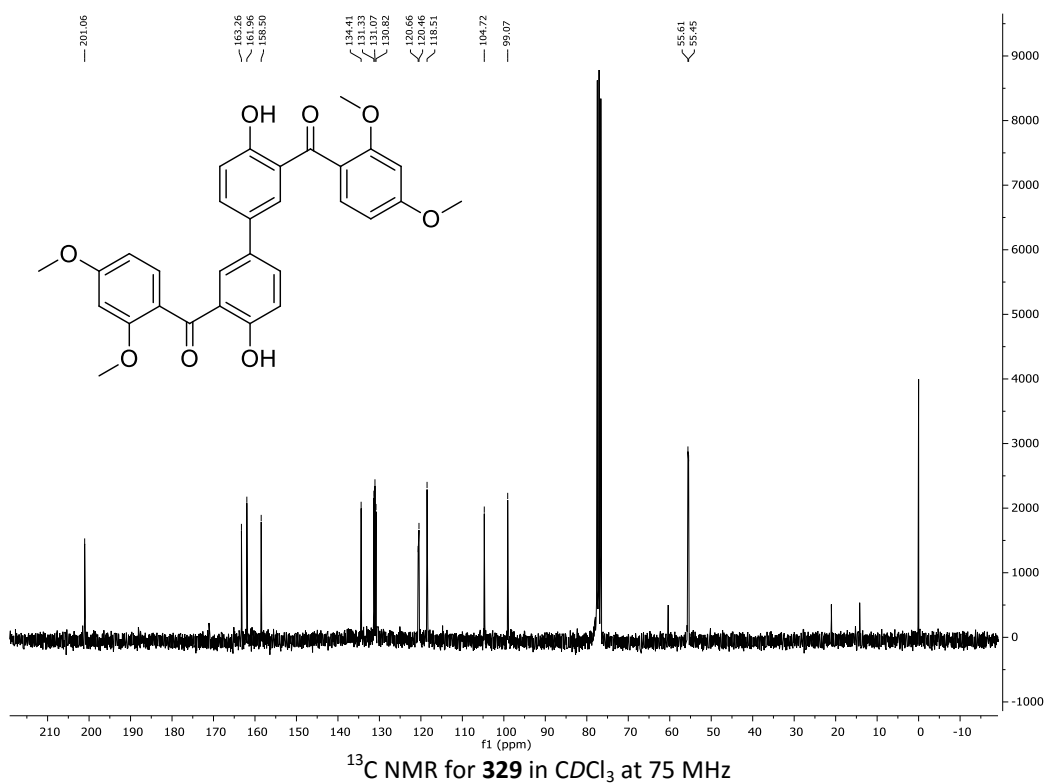
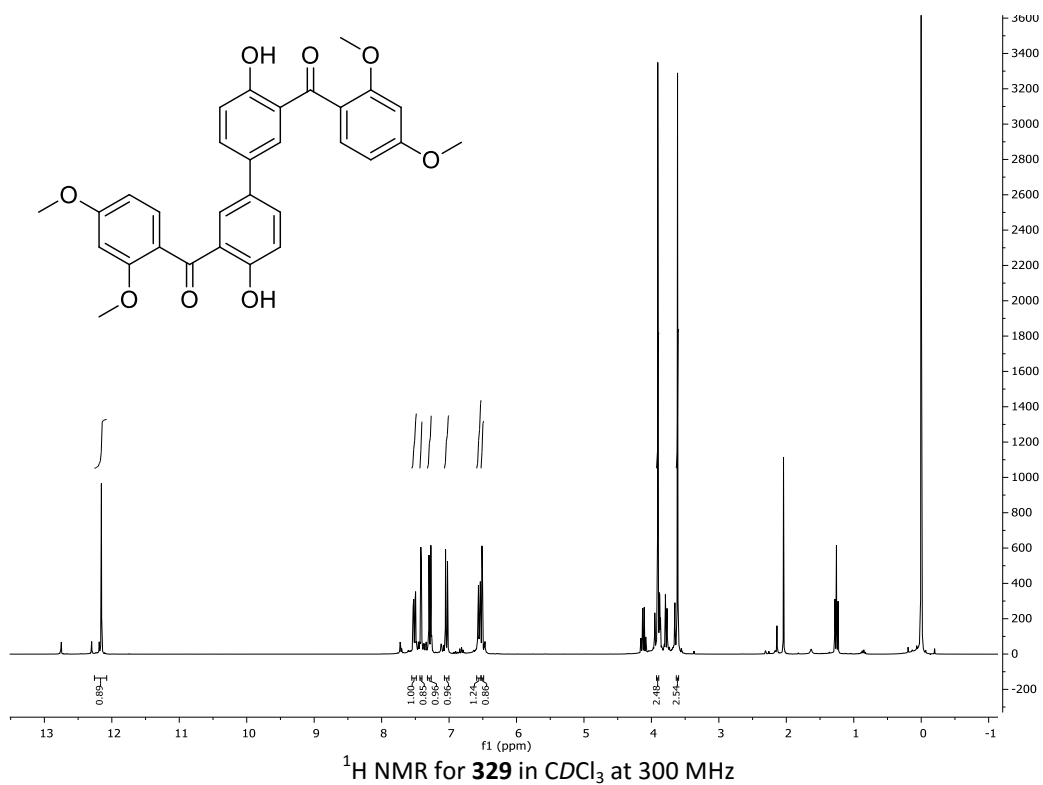


^1H NMR for **257** in CDCl_3 at 300 MHz

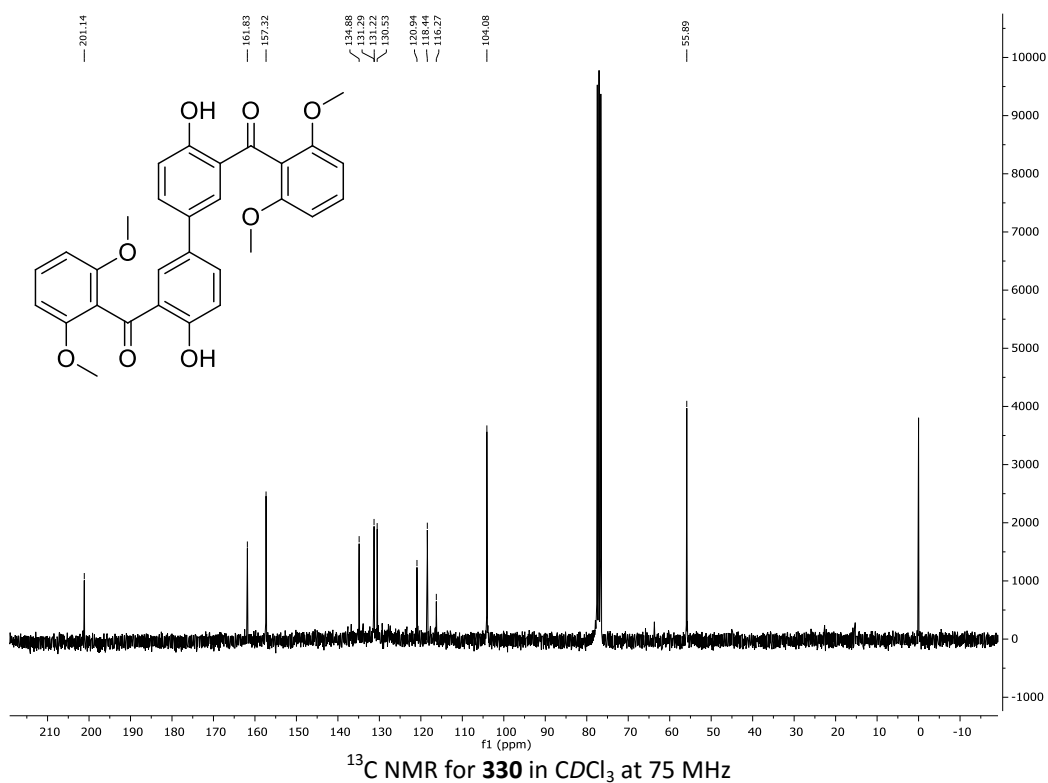
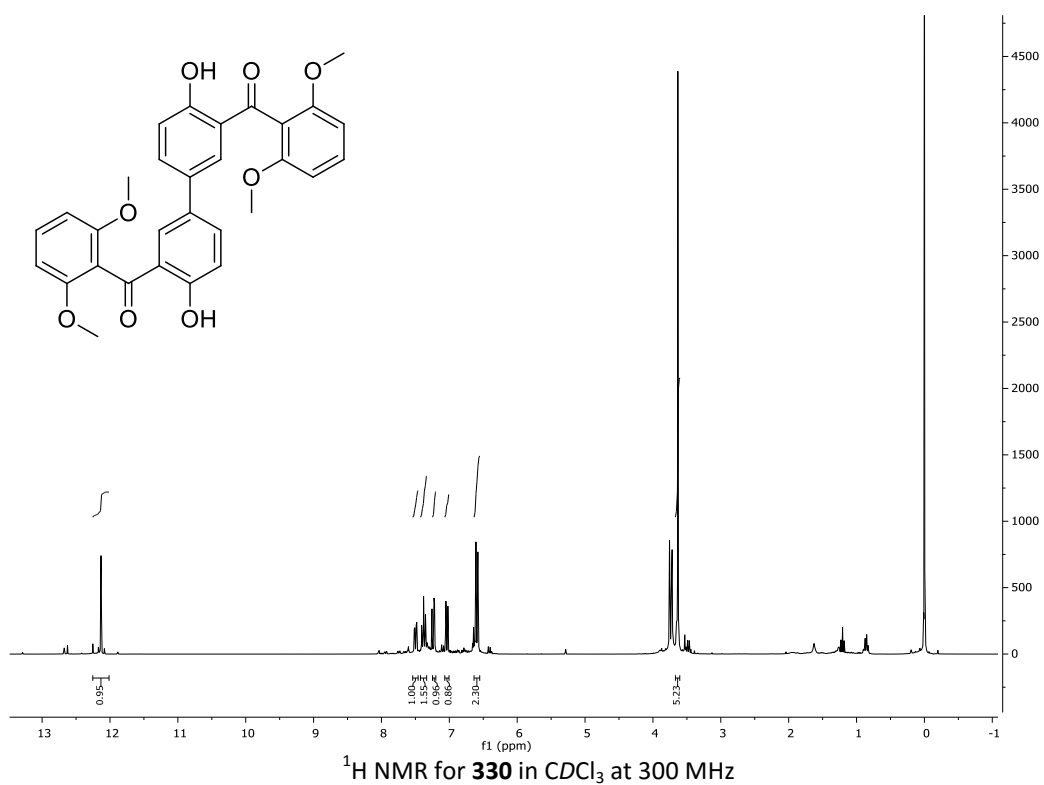


^{13}C NMR for **257** in CDCl_3 at 75 MHz

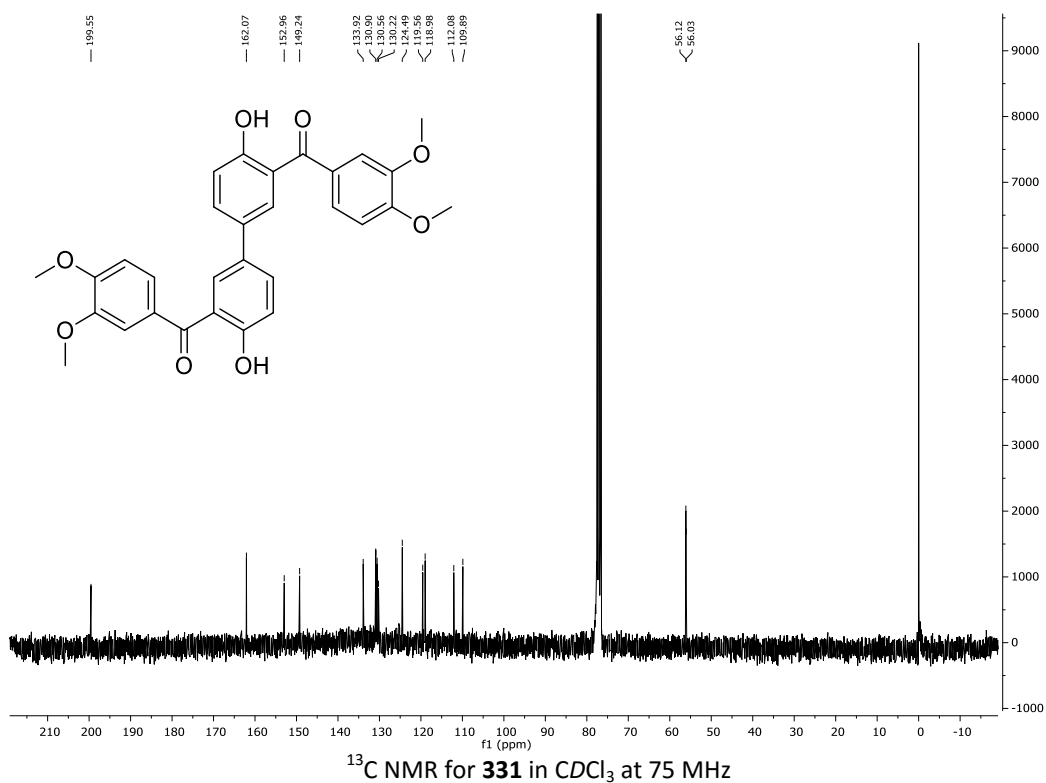
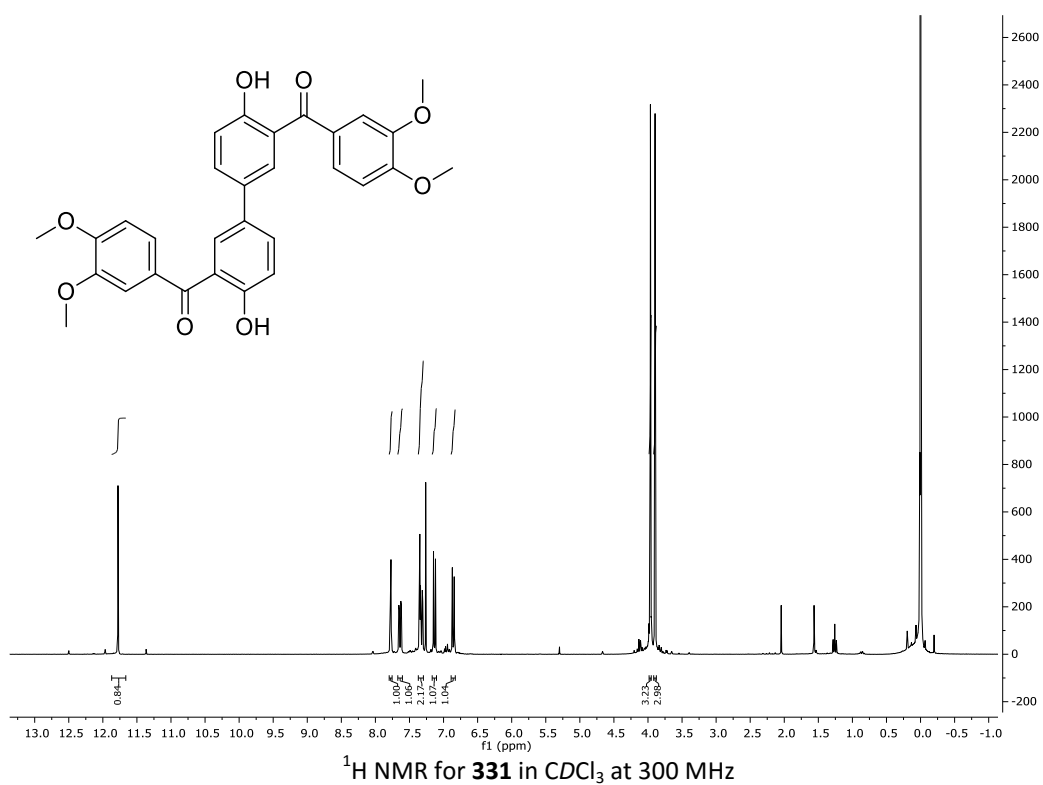
General
Appendices



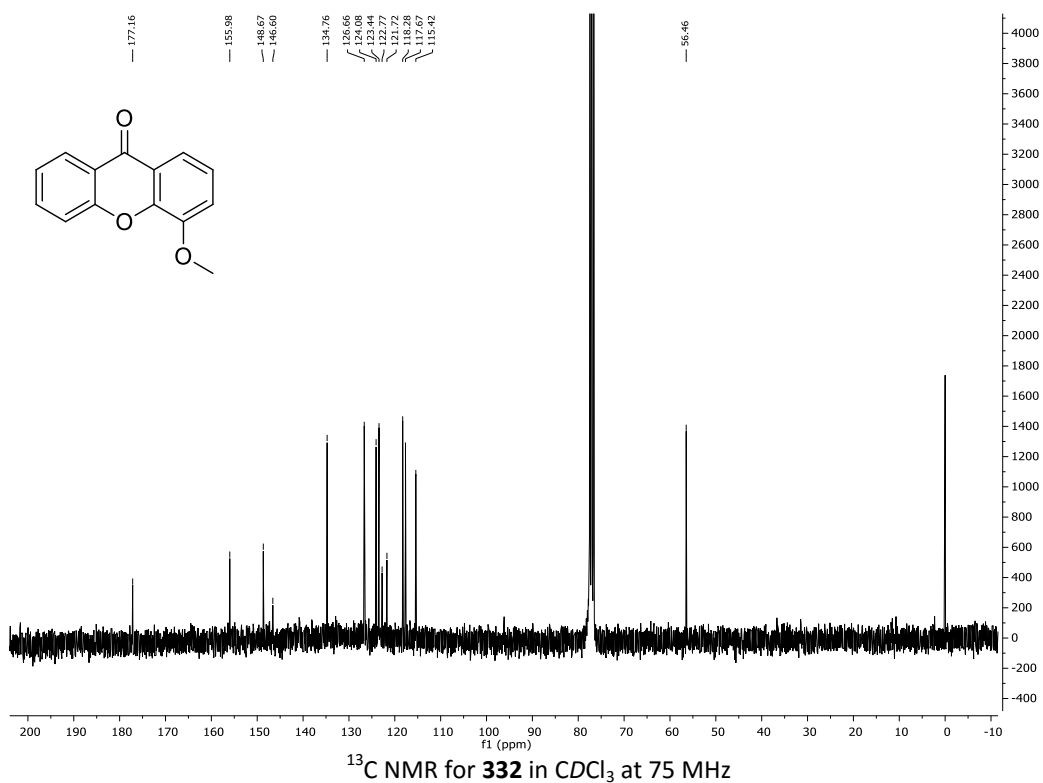
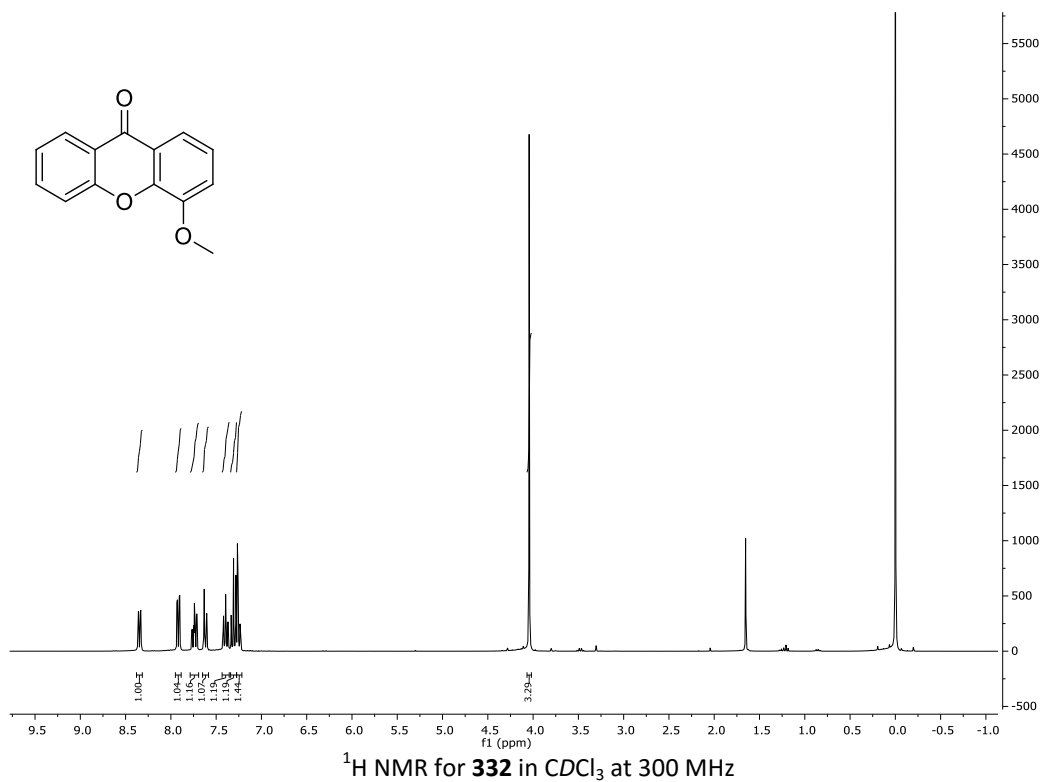
General
Appendices



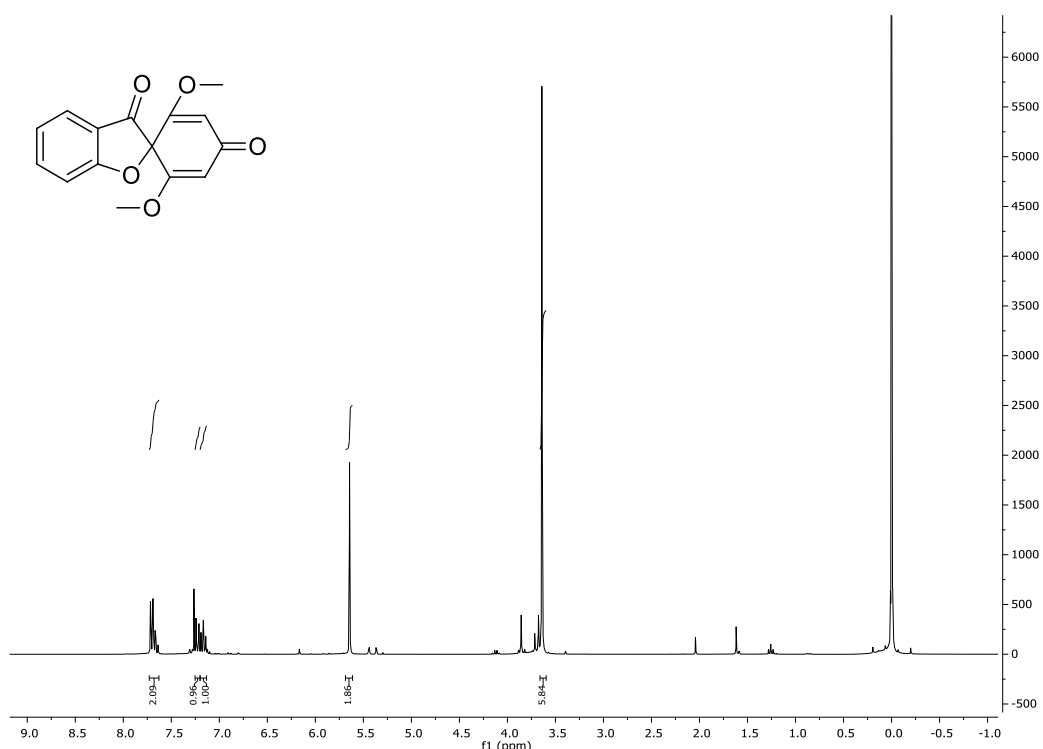
General
Appendices



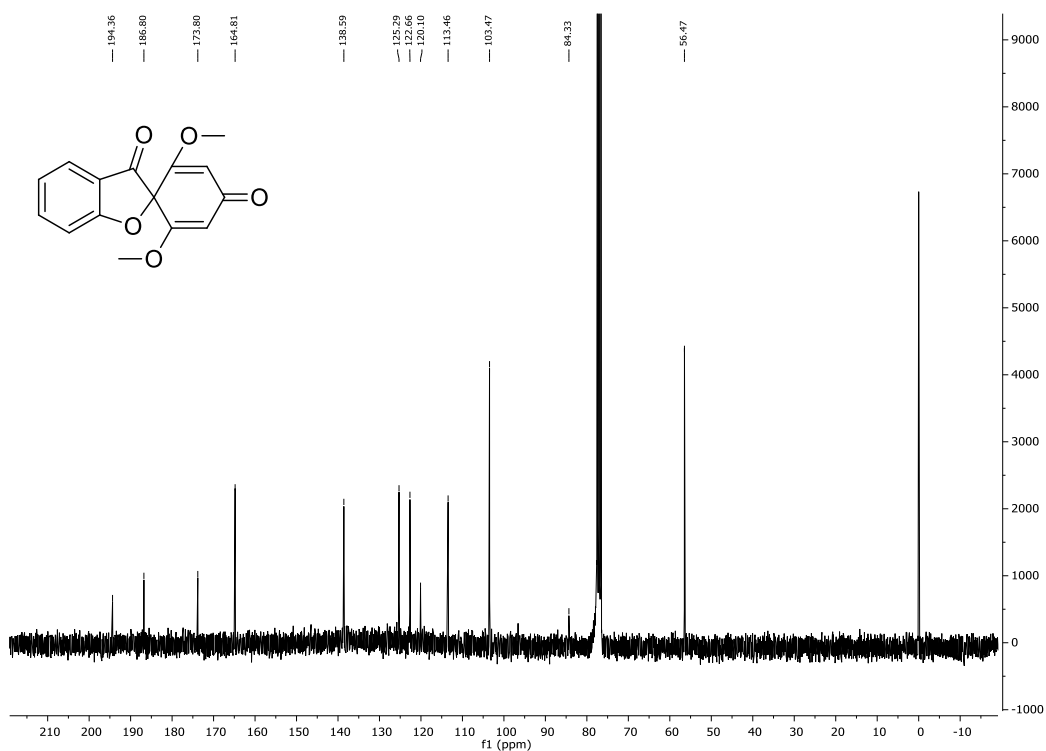
General
Appendices



General
Appendices

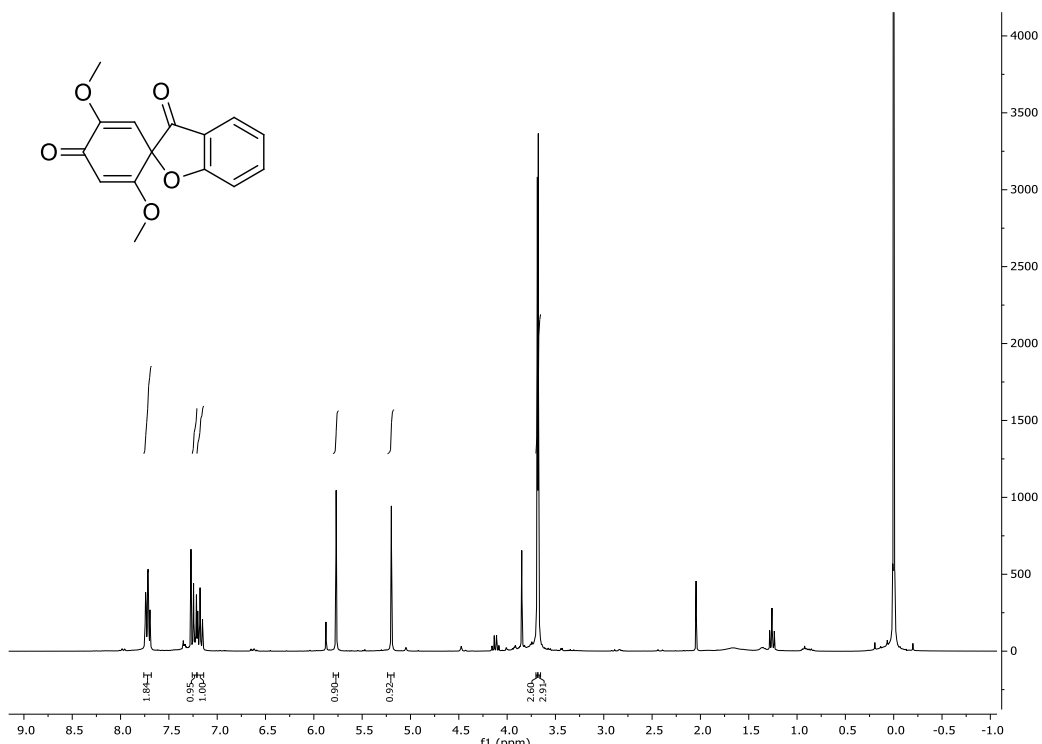


^1H NMR for **333** in CDCl_3 at 300 MHz

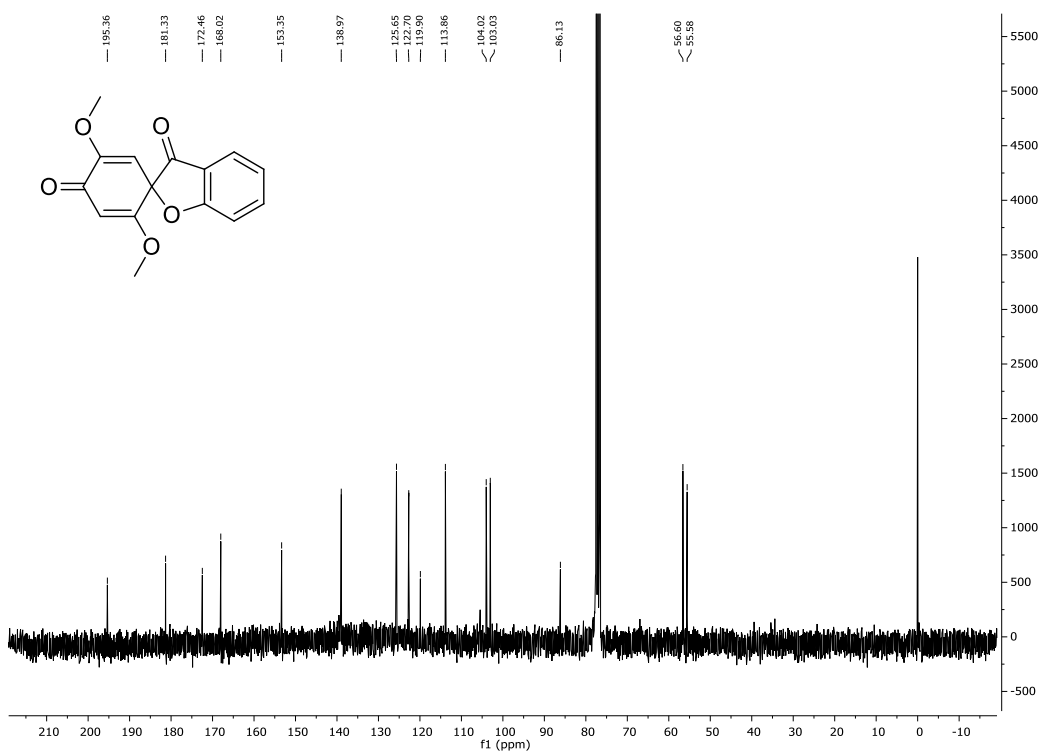


^{13}C NMR for **333** in CDCl_3 at 75 MHz

General
Appendices

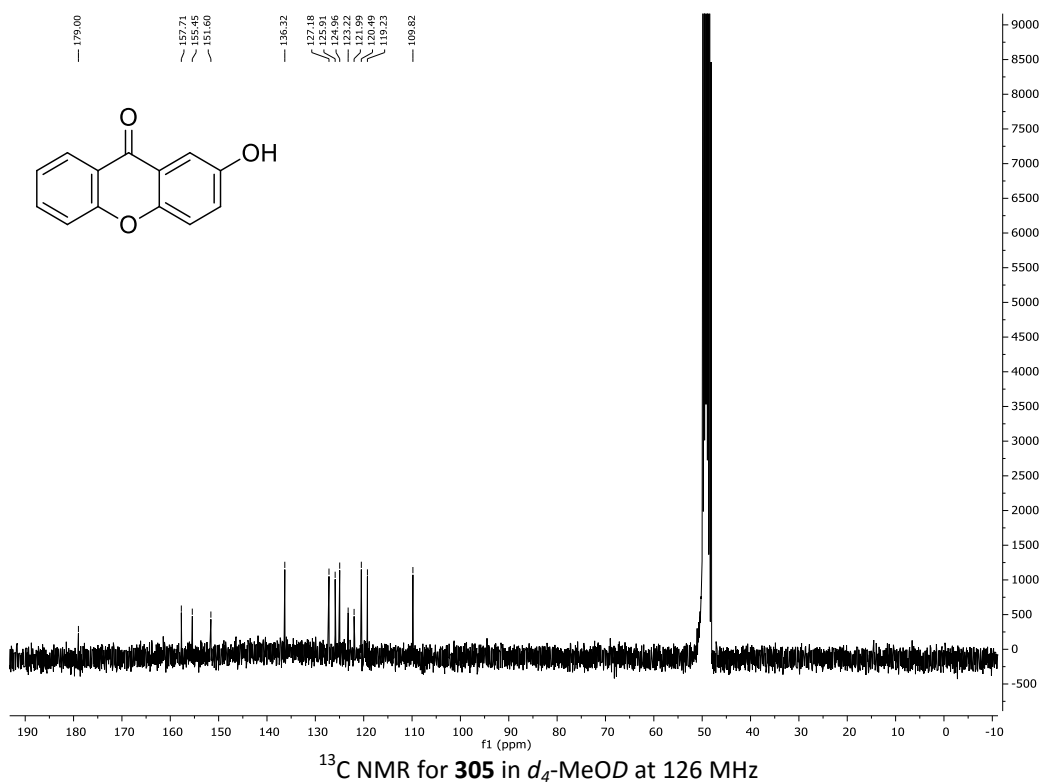
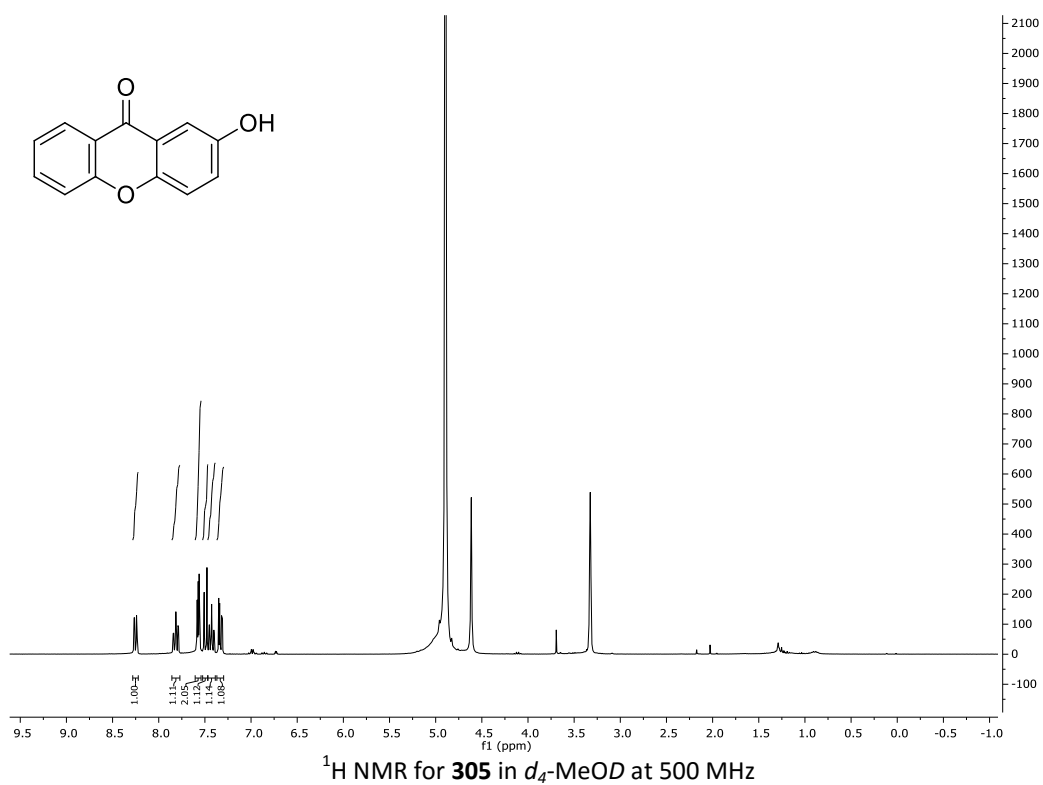


^1H NMR for **300** in CDCl_3 at 300 MHz

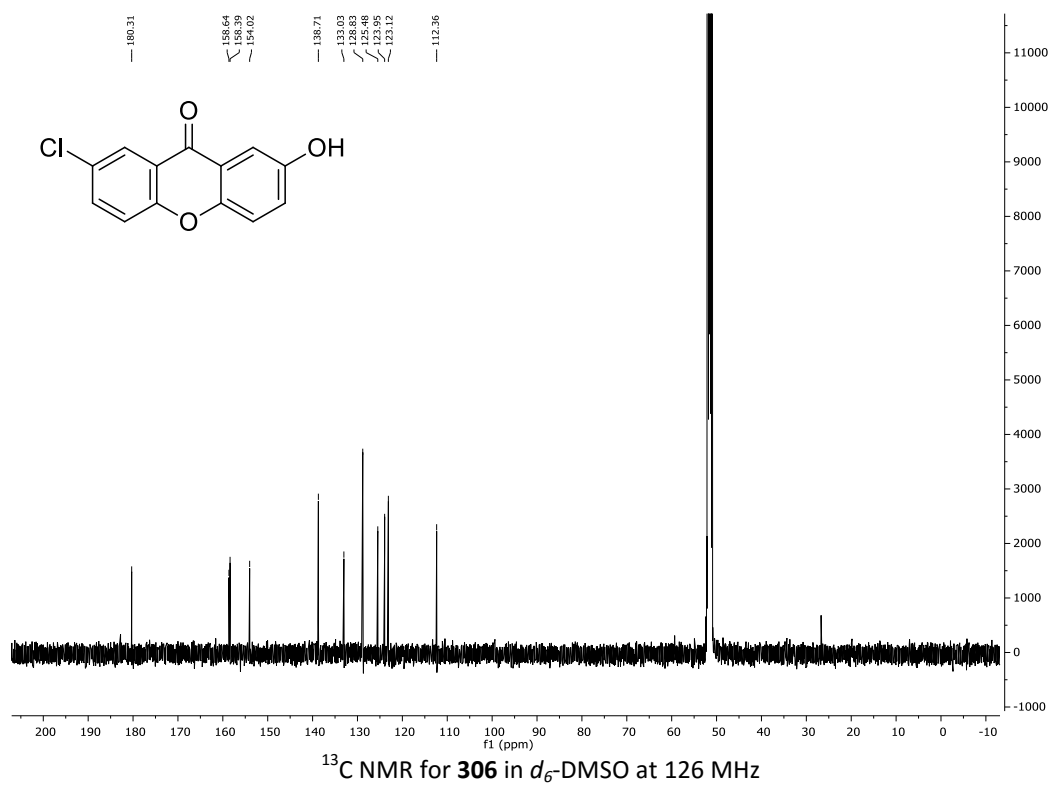
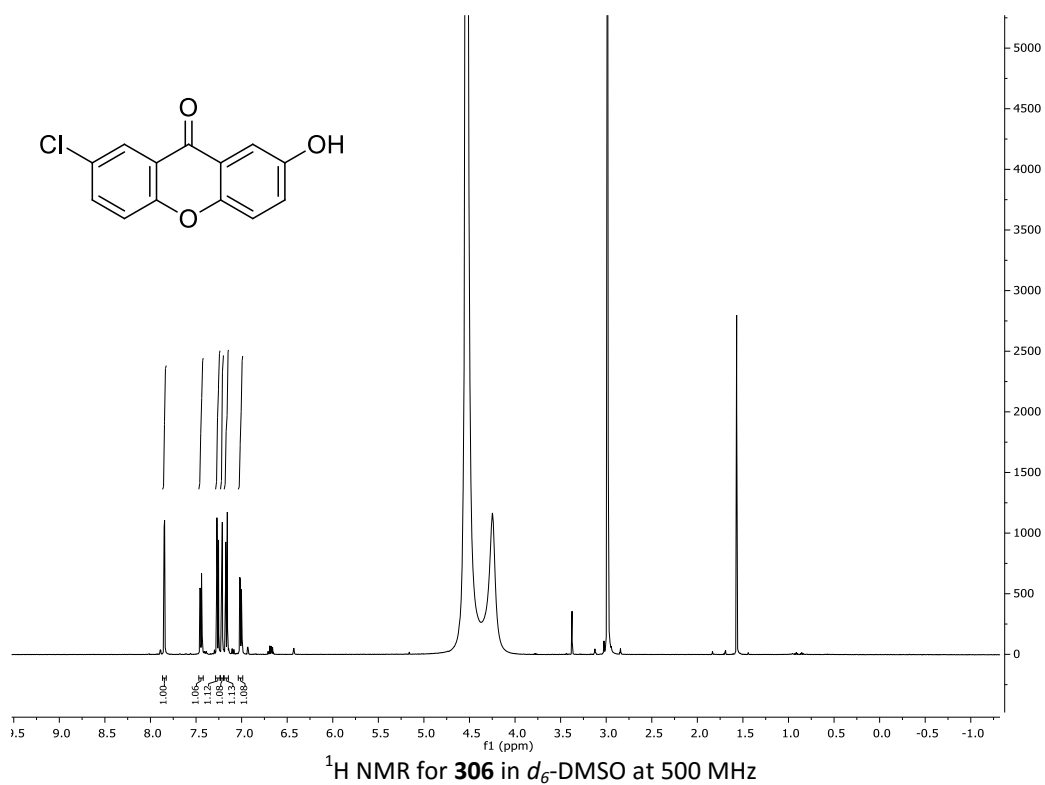


^{13}C NMR for **300** in CDCl_3 at 75 MHz

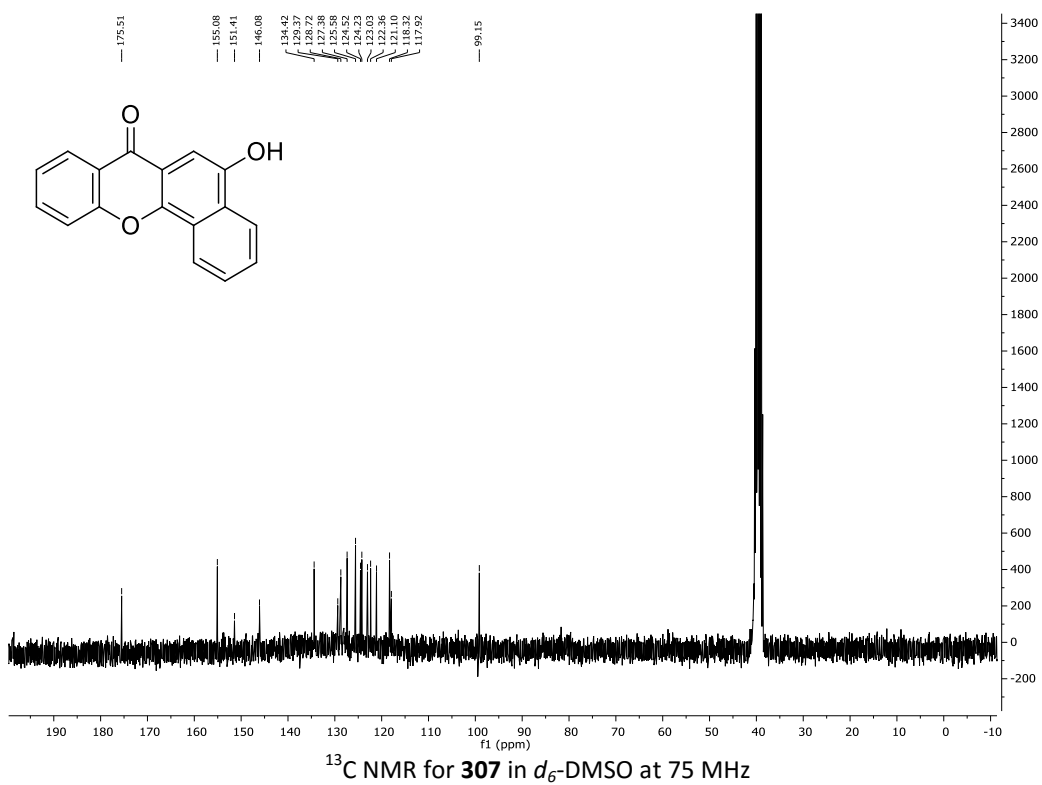
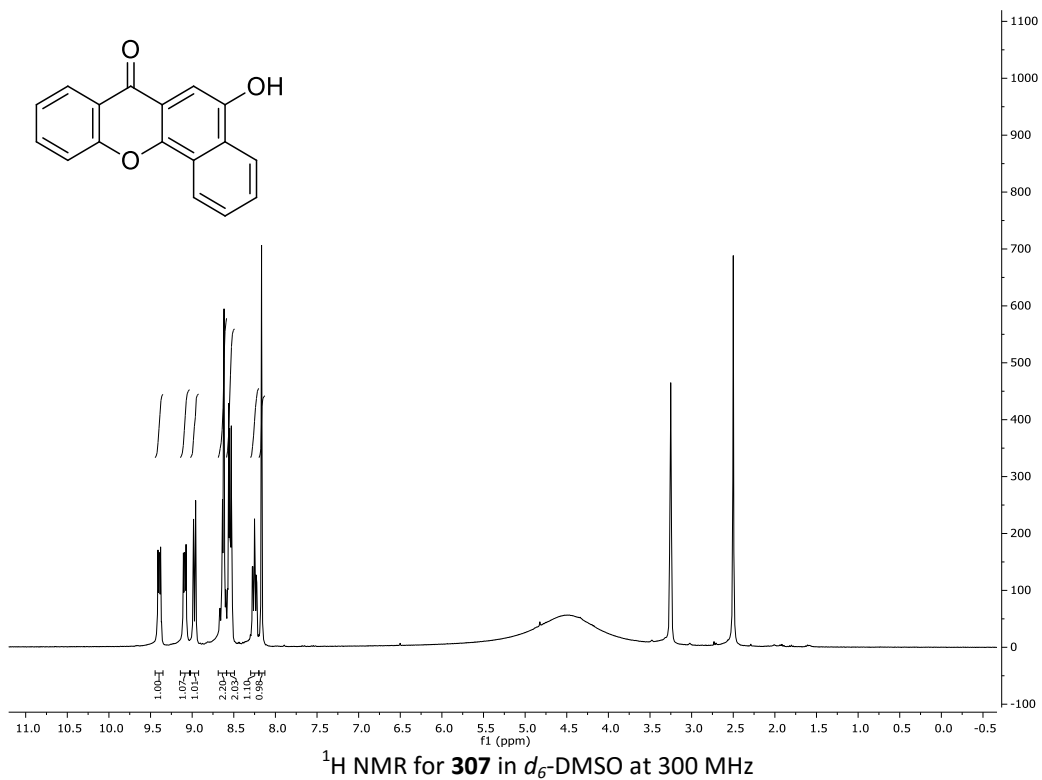
General
Appendices



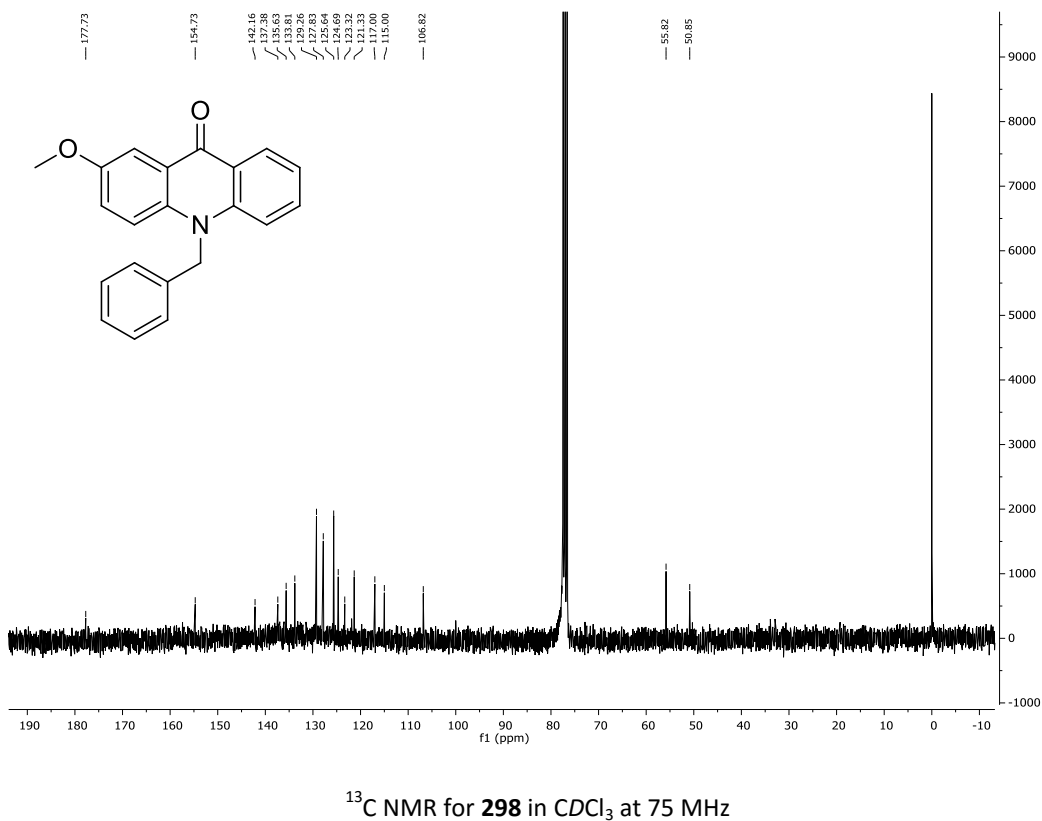
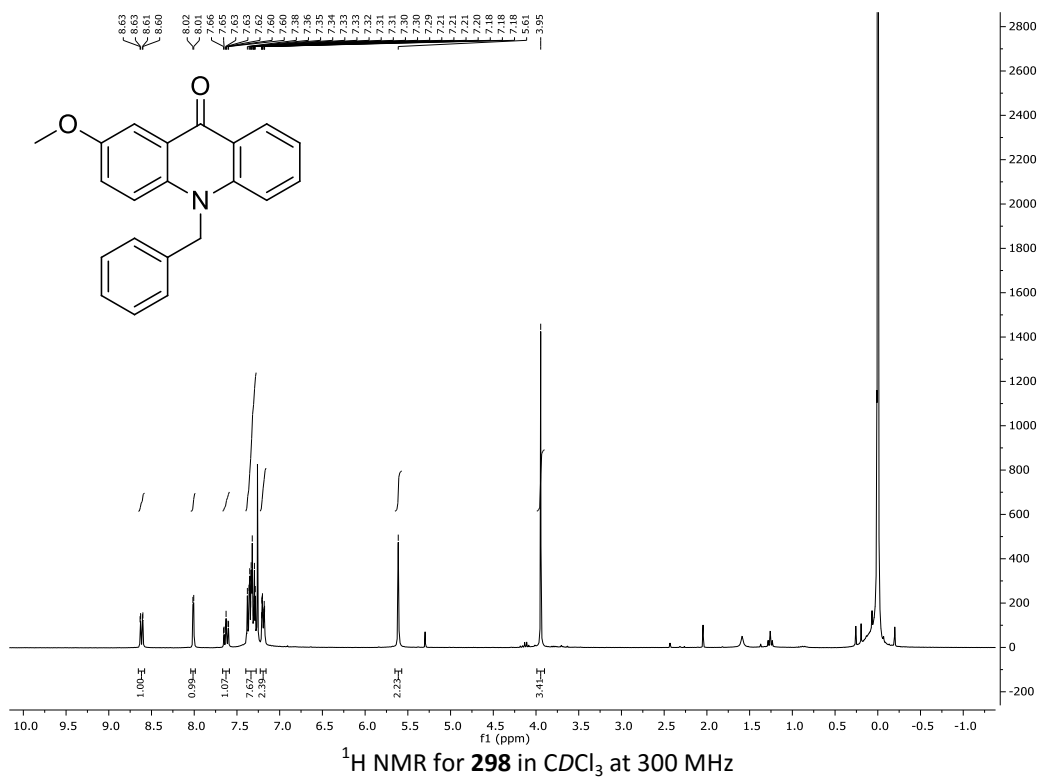
General
Appendices



General
Appendices

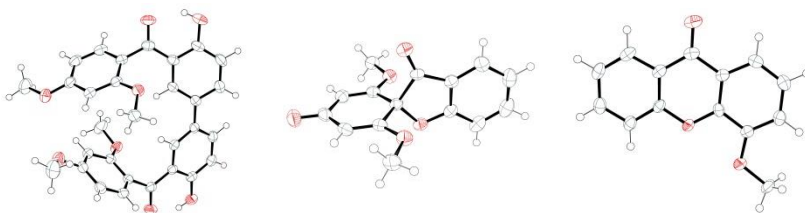


General
Appendices



A5 - Crystallographic Data obtained for Plot Twist crystal structures

The crystallographic information for the crystal structures obtained during this thesis can be outlined below. All the relevant crystallographic information for these crystal structures is included in the digital appendix.



Compound	329	333	332
Identification code	15j_cdkjd16_406-0s	16j_cdkjd5_438_0s	16j_cdkjd6_0s
Empirical formula	C30 H26 O8	C15 H12 O5	C14 H10 O3
Formula weight	514.51	272.25	226.22
Temperature	173(2) K	173(2) K	173(2) K
Wavelength	0.71073 Å	0.71073 Å	0.71073 Å
Crystal system	Triclinic	Monoclinic	Orthorhombic
Space group	P -1	P 21/c	P 21 21 21
Unit cell dimensions	a = 11.0122(2) Å b = 12.6075(2) Å c = 20.4557(3) Å $\alpha = 75.1000(10)^\circ$ $\beta = 81.5690(10)^\circ$ $\gamma = 64.9630(10)^\circ$	a = 10.2735(5) Å b = 9.9848(4) Å c = 12.4392(5) Å $\alpha = 90^\circ$ $\beta = 95.832(2)^\circ$ $\gamma = 90^\circ$	a = 3.90060(10) Å b = 16.2669(5) Å c = 16.3196(6) Å $\alpha = 90^\circ$ $\beta = 90^\circ$ $\gamma = 90^\circ$
Volume	2484.30(7) Å ³	1269.39(10) Å ³	1035.49(6) Å ³
Z	4	4	4
Density (calculated)	1.376 Mg/m ³	1.424 Mg/m ³	1.451 Mg/m ³
Absorption coefficient	0.100 mm ⁻¹	0.108 mm ⁻¹	0.102 mm ⁻¹
F(000)	1080	568	472
Crystal size	0.21 x 0.20 x 0.15 mm ³	0.16 x 0.14 x 0.12 mm ³	0.38 x 0.07 x 0.05 mm ³
Theta range for data collection	1.031 to 26.328°	1.993 to 27.997°	1.768 to 25.999°
Index ranges	-13<=h<=13, -15<=k<=15, -24<=l<=25	-13<=h<=13, -13<=k<=13, -16<=l<=16	-4<=h<=4, -20<=k<=20, -19<=l<=20
Reflections collected	27570	14390	10718
Independent reflections	10069 [R(int) = 0.0453]	3067 [R(int) = 0.3669]	2028 [R(int) = 0.0917]
Completeness to theta = 25.242°	99.80%	100.00%	100.00%
Absorption correction	None	None	None
Refinement method	Full-matrix least-squares on F ²	Full-matrix least-squares on F ²	Full-matrix least-squares on F ²

General
Appendices

Data / restraints / parameters	10069 / 0 / 697	3067 / 0 / 183	2028 / 0 / 155
Goodness-of-fit on F^2	1.061	0.861	0.964
Final R indices [$I > 2\sigma(I)$]	$R_1 = 0.0390, w_{R2} = 0.0999$	$R_1 = 0.0586, w_{R2} = 0.1243$	$R_1 = 0.0456, w_{R2} = 0.0779$
R indices (all data)	$R_1 = 0.0658, w_{R2} = 0.1128$	$R_1 = 0.0957, w_{R2} = 0.1419$	$R_1 = 0.0857, w_{R2} = 0.0891$
Extinction coefficient	n/a	n/a	n/a
Largest diff. peak and hole	0.204 and -0.172 e.Å ⁻³	0.308 and -0.377 e.Å ⁻³	0.151 and -0.175 e.Å ⁻³

References

1. Campbell, N. A.; Reece, J. B., *Biology*. Seventh Edition ed.; Pearson Education, Inc.: San Francisco, **2005**.
2. *Cancer Facts and Figures 2015*; American Cancer Society: Atlanta, **2015**.
3. Lawrence, E., *Henderson's Dictionary of Biology*. Pearson Education Limited: Harlow, 2005.
4. DeVita, V. T., Jr.; Rosenberg, S. A., Two hundred years of cancer research. *N. Engl. J. Med.* **2012**, *366* (23), 2207-14.
5. Siegel, R. L.; Miller, K. D.; Jemal, A., Cancer statistics, 2015. *CA: Cancer J* **2015**, *65* (1), 5-29.
6. Ferlay, J.; Soerjomataram, I.; Ervik, M.; Dikshit, R.; Eser, S.; Mathers, C.; Rebelo, M.; Parkin, D. M.; Forman, D.; Bray, F. Cancer Incidence and Mortality Worldwide: IARC CancerBase No. 11 [Internet]. <http://globocan.iarc.fr>, (accessed 09/08/2015).
7. Torre, L. A.; Bray, F.; Siegel, R. L.; Ferlay, J.; Lortet-Tieulent, J.; Jemal, A., Global cancer statistics, 2012. *CA: Cancer J* **2015**, *65* (2), 87-108.
8. Siegel, R.; DeSantis, C.; Jemal, A., Colorectal cancer statistics, 2014. *CA: Cancer J* **2014**, *64* (2), 104-117.
9. Herbst, M. C., Fact Sheet on Colorectal Cancer. Africa, Cancer Association of South Africa: **2013**.
10. Wils, J., Adjuvant treatment of colon cancer: past, present and future. *J Chemother* **2007**, *19* (2), 115-22.
11. American Cancer Society, Breast Cancer. Society, **2014**.
12. DeSantis, C.; Ma, J.; Bryan, L.; Jemal, A., Breast cancer statistics, 2013. *CA: Cancer J* **2014**, *64* (1), 52-62.
13. Richie, R. C.; Swanson, J. O., Breast cancer: a review of the literature. *J Insur Med* **2003**, *35* (2), 85-101.
14. Breast Cancer Warning Signs, Myths & Facts. Cancer Association of South Africa: CANSA website, **2012**; Vol. 138 KB.
15. National Cancer Institute, What You Need To Know About Leukemia. Institute, National Cancer Institute website, **2013**.
16. Ward, E.; DeSantis, C.; Robbins, A.; Kohler, B.; Jemal, A., Childhood and adolescent cancer statistics, 2014. *CA: Cancer J.* **2014**, *64* (2), 83-103.
17. American Cancer Society, Leukemia—Acute Myeloid (Myelogenous). In *American Cancer Society website*, **2014**.
18. Chu, E., Clinical Colorectal Cancer: "Ode to 5-Fluorouracil". *Clin. Colorectal Cancer* **2007**, *6* (9), 609.
19. Roche Pharmaceuticals, Xeloda Medical Professional Information Booklet. In *Food and Drug Administration*, Food and Drug Administration website, **2000**.
20. Ehrsson, H.; Wallin, I.; Yachnin, J., Pharmacokinetics of oxaliplatin in humans. *Med Oncol* **2002**, *19* (4), 261-265.
21. Pfiser, Camptosar Medical Professional Information Booklet. Food and Drug Administration: **2010**.
22. Wall, M. E., Camptothecin and taxol: Discovery to clinic. *Med. Res. Rev.* **1998**, *18* (5), 299-314.
23. GlaxoSmithKline, Highlights of Prescribing Information for Hycamtin. In *Food and Drug Administration*, **2007**.
24. Wheate, N. J.; Walker, S.; Craig, G. E.; Oun, R., The status of platinum anticancer drugs in the clinic and in clinical trials. *Dalton Trans.* **2010**, *39* (35), 8113-8127.

25. Rosenberg, B.; Van Camp, L.; Grimley, E. B.; Thomson, A. J., The inhibition of growth or cell division in *Escherichia coli* by different ionic species of platinum(IV) complexes. *J. Biol. Chem.* **1967**, *242* (6), 1347-52.
26. Prestayko, A. W.; D'Aoust, J. C.; Issell, B. F.; Crooke, S. T., Cisplatin (cis-diamminedichloroplatinum II). *Cancer Treat Rev* **1979**, *6* (1), 17-39.
27. Thayer, A. M., Platinum Drugs Take Their Toll. *Chem. Eng. News* **2010**, *88* (26), 24-28.
28. Galanski, M.; Yasemi, A.; Jakupec, M. A.; Graf v. Keyserlingk, N.; Keppler, B. K., Synthesis, Cytotoxicity, and Structure-Activity Relationships of New Oxaliplatin Derivatives. *Monatsh. Chem.* **2005**, *136* (5), 693-700.
29. Tyagi, P.; Gahlot, P.; Kakkar, R., Structural aspects of the anti-cancer drug oxaliplatin: A combined theoretical and experimental study. *Polyhedron* **2008**, *27* (18), 3567-3574.
30. Ben Venue Laboratories, Highlights of Prescribing Information for Eloxatin. Food and Drug Administration: Food and Drug Administration website, **2011**.
31. Brown, D. B.; Khokhar, A. R.; Hacker, M. P.; McCormack, J. J.; Stalick, W. M., Synthesis and Antitumor Activity of Platinum Complexes Containing Neutral and Protonated Amino-olefin Ligands *Inorg. Chim. Acta* **1982**, *87*, 45-52.
32. Kostova, I., Platinum Complexes as Anticancer Agents. *Recent Pat Anticancer Drug Discov* **2006**, *1*, 1-22.
33. American Cancer Society, Colorectal Cancer. In *American Cancer Society*, Society, American Cancer Society website, **2014**.
34. Sanofi-Aventis, Highlights of Prescribing Information for Taxotere. In *Food and Drug Administration*, Food and Drug Administration website, **2010**.
35. Bristol-Meyers Squibb Company, Taxol (Paclitaxel) Injection Patient Information. In *Food and Drug Administration*, Food and Drug Administration website, **2011**.
36. Centocor Ortho Biotech Products, L. P., Leustatin (cladribine) Injection. In *Food and Drug Administration*, Food and Drug Administration website, **2012**.
37. Ben Venue Laboratories, Fludara (fludarabine phosphate). In *Food and Drug Administration*, Food and Drug Administration website, **2008**.
38. Bristol-Meyers Squibb Company, Etopophos for Injection. In *Food and Drug Administration*, Food and Drug Administration website, **2010**.
39. Gagnon, V.; St-Germain, M. E.; Descoteaux, C.; Provencher-Mandeville, J.; Parent, S.; Mandal, S. K.; Asselin, E.; Berube, G., Biological evaluation of novel estrogen-platinum(II) hybrid molecules on uterine and ovarian cancers-molecular modeling studies. *Bioorg. Med. Chem. Lett.* **2004**, *14* (23), 5919-24.
40. Meunier, B., Hybrid Molecules with a Dual Mode of Action: Dream or Reality? *Acc. Chem. Res.* **2007**, *41* (1), 69-77.
41. Burger, R. M., Cleavage of Nucleic Acids by Bleomycin. *Chem. Rev.* **1998**, *98* (3), 1153-1170.
42. Zou, Y.; Fahmi, N. E.; Vialas, C.; Miller, G. M.; Hecht, S. M., Total Synthesis of Deamido Bleomycin A2, the Major Catabolite of the Antitumor Agent Bleomycin. *J. Am. Chem. Soc.* **2002**, *124* (32), 9476-9488.
43. Nakagawa-Goto, K.; Nakamura, S.; Bastow, K. F.; Nyarko, A.; Peng, C. Y.; Lee, F. Y.; Lee, F. C.; Lee, K. H., Antitumor agents. 256. Conjugation of paclitaxel with other antitumor agents: evaluation of novel conjugates as cytotoxic agents. *Bioorg. Med. Chem. Lett.* **2007**, *17* (10), 2894-8.
44. Dos Santos, J. L.; Lanaro, C.; Chelucci, R. C.; Gambero, S.; Bosquesi, P. L.; Reis, J. S.; Lima, L. M.; Cerecetto, H.; Gonzalez, M.; Costa, F. F.; Chung, M. C., Design, synthesis, and pharmacological evaluation of novel hybrid compounds to treat sickle cell disease symptoms. part II: furoxan derivatives. *J. Med. Chem.* **2012**, *55* (17), 7583-92.
45. Saadeh, H. A.; Mosleh, I. M.; Mubarak, M. S., Synthesis of novel hybrid molecules from precursors with known antiparasitic activity. *Molecules* **2009**, *14* (4), 1483-94.
46. Burgess, S. J.; Selzer, A.; Kelly, J. X.; Smilkstein, M. J.; Riscoe, M. K.; Peyton, D. H., A Chloroquine-like Molecule Designed to Reverse Resistance in *Plasmodium falciparum*. *J. Med. Chem.* **2006**, *49* (18), 5623-5625.

47. Graham, L. A.; Suryadi, J.; West, T. K.; Kucera, G. L.; Bierbach, U., Synthesis, aqueous reactivity, and biological evaluation of carboxylic acid ester-functionalized platinum-acridine hybrid anticancer agents. *J. Med. Chem.* **2012**, *55* (17), 7817-27.
48. Gianferrara, T.; Bratsos, I.; Alessio, E., A categorization of metal anticancer compounds based on their mode of action. *Dalton Trans* **2009**, (37), 7588-98.
49. Neuse, E., Macromolecular Ferrocene Compounds as Cancer Drug Models. *J Inorg Organomet Polym* **2005**, *15* (1), 3-31.
50. Sava, G.; Bergamo, A.; Dyson, P. J., Metal-based antitumour drugs in the post-genomic era: what comes next? *Dalton Trans* **2011**, *40* (36), 9069-75.
51. Nguyen, A.; Vessieres, A.; Hillard, E. A.; Top, S.; Pigeon, P.; Jaouen, G., Ferrocifens and Ferrocifenols as New Potential Weapons against Breast Cancer. *Chimia* **2007**, *61* (11), 716-724.
52. Marks, R.; Pearse, A. D.; Walker, A. P., The effects of a shampoo containing zinc pyrithione on the control of dandruff. *Br. J. Dermatol.* **1985**, *112* (4), 415-422.
53. Carraway, R. E.; Dobner, P. R., Zinc pyrithione induces ERK- and PKC-dependent necrosis distinct from TPEN-induced apoptosis in prostate cancer cells. *Biochim. Biophys. Acta* **2012**, *1823* (2), 544-57.
54. Liguori, P. F.; Valentini, A.; Palma, M.; Bellusci, A.; Bernardini, S.; Ghedini, M.; Panno, M. L.; Pettinari, C.; Marchetti, F.; Crispini, A.; Pucci, D., Non-classical anticancer agents: synthesis and biological evaluation of zinc(II) heteroleptic complexes. *Dalton Trans* **2010**, *39* (17), 4205-12.
55. Zhao, P.; Huang, J.-W.; Ji, L.-N., Metal complexes of porphyrin-anthraquinone hybrids: DNA binding and photocleavage specificities. *J. Coord. Chem.* **2011**, *64* (11), 1977-1990.
56. Ma, D.-L.; He, H.-Z.; Leung, K.-H.; Chan, D. S.-H.; Leung, C.-H., Bioactive Luminescent Transition-Metal Complexes for Biomedical Applications. *Angew. Chem. Int. Ed.* **2013**, *52* (30), 7666-7682.
57. Alzeer, J.; Vummidi, B. R.; Roth, P. J. C.; Luedtke, N. W., Guanidinium-modifizierte Phthalocyanine als Fluoreszenzsonden mit hoher G-Quadruplex-Affinität und als Transkriptionsregulatoren. *Angew. Chem.* **2009**, *121* (49), 9526-9529.
58. Tisato, F.; Marzano, C.; Porchia, M.; Pellei, M.; Santini, C., Copper in diseases and treatments, and copper-based anticancer strategies. *Med Res Rev* **2010**, *30* (4), 708-49.
59. Stern, B. R., Essentiality and toxicity in copper health risk assessment: overview, update and regulatory considerations. *J. Toxicol. Environ. Health. Part A* **2010**, *73* (2), 114-27.
60. Iakovidis, I.; Delimaris, I.; Piperakis, S. M., Copper and its complexes in medicine: a biochemical approach. *Mol. Bol. Int.* **2011**, *2011*, 594529.
61. Santini, C.; Pellei, M.; Gandin, V.; Porchia, M.; Tisato, F.; Marzano, C., Advances in Copper Complexes as Anticancer Agents. *Chem. Rev.* **2014**, *114* (1), 815-862.
62. Belicchi-Ferrari, M.; Bisceglie, F.; Pelosi, G.; Tarasconi, P., Heterocyclic substituted thiosemicarbazones and their Cu(II) complexes: Synthesis, characterization and studies of substituent effects on coordination and DNA binding. *Polyhedron* **2008**, *27* (5), 1361-1367.
63. Palanimuthu, D.; Shinde, S. V.; Somasundaram, K.; Samuelson, A. G., In Vitro and in Vivo Anticancer Activity of Copper Bis(thiosemicarbazone) Complexes. *J. Med. Chem.* **2013**, *56* (3), 722-734.
64. Dallavalle, F.; Gaccioli, F.; Franchi-Gazzola, R.; Lanfranchi, M.; Marchiò, L.; Pellinghelli, M. A.; Tegoni, M., Synthesis, molecular structure, solution equilibrium, and antiproliferative activity of thioxotriazoline and thioxotriazole complexes of copper(II) and palladium(II). *J. Inorg. Biochem.* **2002**, *92* (2), 95-104.
65. Tardito, S.; Bussolati, O.; Gaccioli, F.; Gatti, R.; Guizzardi, S.; Uggeri, J.; Marchiò, L.; Lanfranchi, M.; Franchi-Gazzola, R., Non-apoptotic programmed cell death induced by a copper(II) complex in human fibrosarcoma cells. *Histochem Cell Biol* **2006**, *126* (4), 473-482.
66. Ranford, J. D.; Sadler, P. J.; Tocher, D. A., Cytotoxicity and antiviral activity of transition-metal salicylato complexes and crystal structure of Bis(diisopropylsalicylato)(1,10-phenanthroline)copper(II). *J. Chem. Soc., Dalton Trans.* **1993**, (22), 3393-3399.
67. Bhat, S. S.; Kumbhar, A. A.; Heptullah, H.; Khan, A. A.; Gobre, V. V.; Gejji, S. P.; Puranik, V. G., Synthesis, Electronic Structure, DNA and Protein Binding, DNA Cleavage, and Anticancer Activity of Fluorophore-Labeled Copper(II) Complexes. *Inorg. Chem.* **2011**, *50* (2), 545-558.

68. Pitié, M.; Burrows, C. J.; Meunier, B., Mechanisms of DNA cleavage by copper complexes of 3-Clip-Phen and of its conjugate with a distamycin analogue. *Nucleic Acids Res* **2000**, *28* (24), 4856-4864.
69. de Hoog, P.; Boldron, C.; Gamez, P.; Sliedregt-Bol, K.; Roland, I.; Pitié, M.; Kiss, R.; Meunier, B.; Reedijk, J., New Approach for the Preparation of Efficient DNA Cleaving Agents: Ditopic Copper–Platinum Complexes Based on 3-Clip-Phen and Cisplatin. *J. Med. Chem.* **2007**, *50* (13), 3148-3152.
70. Trávníček, Z.; Maloň, M.; Šindelář, Z.; Doležal, K.; Rolčík, J.; Kryštof, V. r.; Strnad, M.; Marek, J. r., Preparation, physicochemical properties and biological activity of copper(II) complexes with 6-(2-chlorobenzylamino)purine (HL₁) or 6-(3-chlorobenzylamino)purine (HL₂). The single-crystal X-ray structure of [Cu(H+L₂)₂Cl₃]Cl·2H₂O. *J. Inorg. Biochem.* **2001**, *84* (1–2), 23-32.
71. Zhang, H.; Liu, C.-S.; Bu, X.-H.; Yang, M., Synthesis, crystal structure, cytotoxic activity and DNA-binding properties of the copper (II) and zinc (II) complexes with 1-[3-(2-pyridyl)pyrazol-1-ylmethyl]naphthalene. *J. Inorg. Biochem.* **2005**, *99* (5), 1119-1125.
72. Gasser, G.; Ott, I.; Metzler-Nolte, N., Organometallic anticancer compounds. *J. Med. Chem.* **2011**, *54* (1), 3-25.
73. Kalyanasundaram, K.; Grätzel, M., Applications of functionalized transition metal complexes in photonic and optoelectronic devices. *Coord. Chem. Rev.* **1998**, *177* (1), 347-414.
74. Che, C. M.; Siu, F. M., Metal complexes in medicine with a focus on enzyme inhibition. *Curr. Opin. Chem. Biol.* **2010**, *14* (2), 255-61.
75. van Rijt, S. H.; Peacock, A. F.; Johnstone, R. D.; Parsons, S.; Sadler, P. J., Organometallic osmium(II) arene anticancer complexes containing picolinate derivatives. *Inorg Chem* **2009**, *48* (4), 1753-62.
76. Gueffier, A.; Mavel, S.; Lhassani, M.; Elhakmaoui, A.; Snoeck, R.; Andrei, G.; Chavignon, O.; Teulade, J. C.; Witvrouw, M.; Balzarini, J.; De Clercq, E.; Chapat, J. P., Synthesis of imidazo[1,2-*a*]pyridines as antiviral agents. *J. Med. Chem.* **1998**, *41* (25), 5108-12.
77. Dömling, A.; Ugi, I., Multicomponent Reactions with Isocyanides. *Angew. Chem. Int. Ed.* **2000**, *39* (18), 3168-3210.
78. Bagdi, A. K.; Santra, S.; Monir, K.; Hajra, A., Synthesis of imidazo[1,2-*a*]pyridines: a decade update. *Chem. Commun.* **2015**, *51* (9), 1555-1575.
79. Martínez, R.; Ramón, D. J.; Yus, M., Catalyst-free multicomponent Strecker reaction in acetonitrile. *Tetrahedron Lett.* **2005**, *46* (49), 8471-8474.
80. Ugi, I.; Meyr, R.; Fetzer, U., Versammlungsberichte. *Angew. Chem.* **1959**, *71* (11), 386.
81. Groebke, K.; Weber, L.; Mehlin, F., Synthesis of Imidazo[1,2-*a*] annulated Pyridines, Pyrazines and Pyrimidines by a Novel Three-Component Condensation. *Synlett* **1998**, *1998* (06), 661-663.
82. Langer, S. Z.; Arbilla, S.; Benavides, J.; Scatton, B., Zolpidem and Necopidem: two imidazopyridines with selectivity for omega 1 and omega 3 receptor subtypes. *Psychopharmacol.* **1990**, *46*, 61-72.
83. Boerner, R. J.; Moller, H. J., The importance of new antidepressants in the treatment of anxiety/depressive disorders. *Pharmacopsychiatry* **1999**, *32* (4), 119-26.
84. Almirante, L.; Polo, L.; Mugnaini, A.; Provinciali, E.; Rugarli, P.; Biancotti, A.; Gamba, A.; Murmann, W., Derivatives of Imidazole. I. Synthesis and Reactions of Imidazo[1,2-*a*]pyridines with Analgesic, Antiinflammatory, Antipyretic, and Anticonvulsant Activity. *J. Med. Chem.* **1965**, *8* (3), 305-312.
85. Mizushige, K.; Ueda, T.; Yukiiri, K.; Suzuki, H., Olprinone: a phosphodiesterase III inhibitor with positive inotropic and vasodilator effects. *Cardiovasc Drug Rev* **2002**, *20* (3), 163-74.
86. Gudmundsson, K.; Boggs, S. D. Chemical Compounds. 16 March 2006, WO 2006/028896A2.
87. Rousseau, A. L.; Matlaba, P.; Parkinson, C. J., Multicomponent synthesis of imidazo[1,2-*a*]pyridines using catalytic zinc chloride. *Tetrahedron Lett.* **2007**, *48* (23), 4079-4082.
88. Mandair, G. S.; Light, M.; Russell, A.; Hursthouse, M.; Bradley, M., Re-evaluation of the outcome of a multiple component reaction—2- and 3-amino-imidazo[1,2-*a*]pyrimidines? *Tetrahedron Lett.* **2002**, *43* (23), 4267-4269.

89. Varma, R. S.; Kumar, D., Microwave-accelerated three-component condensation reaction on clay: solvent-free synthesis of imidazo[1,2-*a*] annulated pyridines, pyrazines and pyrimidines. *Tetrahedron Lett.* **1999**, *40* (43), 7665-7669.
90. Ireland, S. M.; Tye, H.; Whittaker, M., Microwave-assisted multi-component synthesis of fused 3-aminoimidazoles. *Tetrahedron Lett.* **2003**, *44* (23), 4369-4371.
91. Dahan-Farkas, N.; Langley, C.; Rousseau, A. L.; Yadav, D. B.; Davids, H.; de Koning, C. B., 6-Substituted imidazo[1,2-*a*]pyridines: Synthesis and biological activity against colon cancer cell lines HT-29 and Caco-2. *Eur. J. Med. Chem.* **2011**, *46* (9), 4573-4583.
92. Dahan-Farkas, N.; Davids, H.; Langley, C.; De Koning, C. B. Imidazo[1,2-*a*]pyridine-6-carboxamide Derivatives, their use for the treatment of Colon Cancer and their method of manufacture. 14 October 2010, WO 2010/116302A1.
93. Odell, L. R.; Nilsson, M. T.; Gising, J.; Lagerlund, O.; Muthas, D.; Nordqvist, A.; Karlen, A.; Larhed, M., Functionalized 3-amino-imidazo[1,2-*a*]pyridines: a novel class of drug-like Mycobacterium tuberculosis glutamine synthetase inhibitors. *Bioorg. Med. Chem. Lett.* **2009**, *19* (16), 4790-3.
94. Dimauro, E. F.; Kennedy, J. M., Rapid synthesis of 3-amino-imidazopyridines by a microwave-assisted four-component coupling in one pot. *J. Org. Chem.* **2007**, *72* (3), 1013-6.
95. Koubachi, J.; El Kazzouli, S.; Bousmina, M.; Guillaumet, G., Functionalization of Imidazo[1,2-*a*]pyridines by Means of Metal-Catalyzed Cross-Coupling Reactions. *Eur. J. Org. Chem.* **2014**, *2014* (24), 5119-5138.
96. Forniés, J.; Sicilia, V.; Larraz, C.; Camerano, J. A.; Martín, A.; Casas, J. M.; Tsipis, A. C., One-Pot and Step-by-Step N-Assisted CPh-H Activation in 2-(4-Bromophenyl)imidazo[1,2-*a*]pyridine: Synthesis of a New C,N-Cyclometalated Compound $[Pt(C^{\wedge}N)(\mu-Cl)_2]$ as Precursor of Luminescent Platinum(II) Compounds. *Organometallics* **2010**, *29* (6), 1396-1405.
97. Yong, G.-P.; Qiao, S.; Wang, Z.-Y., A One-Dimensional Coordination Polymer Based on Novel Radical Anion Ligand Generated In Situ: Notable Magnetic and Luminescence Properties. *Cryst. Growth Des.* **2008**, *8* (5), 1465-1467.
98. Yong, G.-P.; Li, Y.-Z.; Li, C.-F.; Zhang, Y.-M.; She, W.-L., New metal-anion radical framework materials: Coll compounds showing ferromagnetic to antiferromagnetic phase transition at about 344 K, and ZnII compounds exhibiting terminal anion ligand induced direct white-light-emission. *Dalton Trans.* **2011**, *40* (16), 4131-4139.
99. Liu, S.-D.; Kuo, B.-C.; Liu, Y.-W.; Lee, J.-Y.; Wong, K. Y.; Lee, H. M., Tuning of net architectures of Ni(ii) and Zn(ii) coordination polymers using isomeric organic linkers. *CrystEngComm* **2014**, *16* (37), 8874-8884.
100. Małeck, J. G., Spectroscopic, structure, and DFT studies of cationic palladium(II) complexes with imidazole derivative ligands. *J. Coord. Chem.* **2013**, *66* (9), 1561-1573.
101. Li, K.; Niu, J.-L.; Yang, M.-Z.; Li, Z.; Wu, L.-Y.; Hao, X.-Q.; Song, M.-P., New Type of 2,6-Bis(imidazo[1,2-*a*]pyridin-2-yl)pyridine-Based Ruthenium Complexes: Active Catalysts for Transfer Hydrogenation of Ketones. *Organometallics* **2015**, *34* (7), 1170-1176.
102. Liu, S.-F.; Wu, Q.; Schmider, H. L.; Aziz, H.; Hu, N.-X.; Popović, Z.; Wang, S., Syntheses, Structures, and Electroluminescence of New Blue/Green Luminescent Chelate Compounds: Zn(2-py-in)₂(THF), BPh₂(2-py-in), Be(2-py-in)₂, and BPh₂(2-py-aza) [2-py-in = 2-(2-pyridyl)indole; 2-py-aza = 2-(2-pyridyl)-7-azaindole]. *J. Am. Chem. Soc.* **2000**, *122* (15), 3671-3678.
103. Wanka, L.; Iqbal, K.; Schreiner, P. R., The Lipophilic Bullet Hits the Targets: Medicinal Chemistry of Adamantane Derivatives. *Chem. Rev.* **2013**, *113* (5), 3516-3604.
104. Ahmed, N.; Brahmabhatt, K. G.; Singh, I. P.; Bhutani, K. K., Efficient chemoselective alkylation of quinoline 2,4-diol derivatives in water. *J. Heterocyclic Chem.* **2011**, *48* (1), 237-240.
105. Pelly, S. C.; Parkinson, C. J.; van Otterlo, W. A. L.; de Koning, C. B., Metathesis Reactions for the Synthesis of Ring-Fused Carbazoles. *J. Org. Chem.* **2005**, *70* (25), 10474-10481.
106. Gu, J. X.; Holland, H. L., A Convenient Synthesis of 3-Arylbutanolides and 3-Arylbutenolides. *Synth. Commun.* **1998**, *28* (18), 3305-3315.
107. Petersen, R. L. Routes to Advanced Intermediates in the Asymmetric Synthesis of Aziridinomitosenes. PhD Thesis. University of the Witwatersrand, **2004**.
108. Zeevaart, J. G. Homogenous Transition Metal Catalysis in Enolate Arylation. PhD Thesis. University of the Witwatersrand, **2000**.

109. Ragie, S. The effect of novel compounds, imidazo[1,2-*a*]pyridines and azaindoles on colon cancer cell lines. MSc Dissertation. University of the Witwatersrand, **2016**.
110. Kurebwa, T. F. The Effect of imidazo[1,2-*a*]pyridine amines on MCF-7 and MDA-MB231 Breast Cancer Cells. MSc Dissertation. University of the Witwatersrand, **2015**.
111. Ismail, Z. The effect of novel compounds: imidazo[1,2-*a*]pyridines and azaindoles, on leukaemic cell lines. MSc Dissertation. University of the Witwatersrand, Johannesburg, **In Progress**.
112. Steffen, W. L.; Palenik, G. J., Infrared and crystal structure study of .sigma. vs. .pi. bonding in tetrahedral zinc(II) complexes. Crystal and molecular structures of dichlorobis(4-substituted pyridine)zinc(II) complexes. *Inorg. Chem.* **1977**, *16* (5), 1119-1127.
113. Zimuwandeyi, M. Synthesis of peptidomimetic compounds as potential anti HIV and malaria agents. MSc Dissertation. University of the Witwatersrand, Johannesburg, **2015**.
114. Gravestock, D.; Rousseau, A. L.; Lourens, A. C. U.; Hoppe, H. C.; Nkabinde, L. A.; Bode, M. L., Novel branched isocyanides as useful building blocks in the Passerini-amine deprotection-acyl migration (PADAM) synthesis of potential HIV-1 protease inhibitors. *Tetrahedron Lett.* **2012**, *53* (26), 3225-3229.
115. Paudler, W. W.; Blewitt, H. L., Ten π Electron Nitrogen Heterocyclic Compounds. V. The Site of Protonation and N-Methylation of Imidazo[1,2-*a*]pyridines and the Planarity of the Ring System. *J. Org. Chem.* **1966**, *31* (4), 1295-1298.
116. Catalán, J.; Elguero, J., Basicity of azoles. IV. Empirical relationships between basicity and ionization potential for aromatic five membered rings containing nitrogen or oxygen. *J. Heterocyclic Chem.* **1984**, *21* (1), 269-270.
117. Humphries, A. C.; Gancia, E.; Gilligan, M. T.; Goodacre, S.; Hallett, D.; Merchant, K. J.; Thomas, S. R., 8-Fluoroimidazo[1,2-*a*]pyridine: synthesis, physicochemical properties and evaluation as a bioisosteric replacement for imidazo[1,2-*a*]pyrimidine in an allosteric modulator ligand of the GABA A receptor. *Bioorg. Med. Chem. Lett.* **2006**, *16* (6), 1518-22.
118. Software, S. *SigmaPlot*, San Jose, CA, **2008**.
119. Smith, G. F.; Sullivan, V. R.; Frank, G., Hexanitrate ammonium cerate as a proposed reference standard in oxidimetry. *Ind. Eng. Chem. Res. Analytical Edition* **1936**, *8* (6), 449-451.
120. Beineke, T. A.; Delgaudio, J., Crystal structure of ceric ammonium nitrate. *Inorg. Chem.* **1968**, *7* (4), 715-721.
121. Molander, G. A., Application of lanthanide reagents in organic synthesis. *Chem. Rev.* **1992**, *92* (1), 29-68.
122. Shorter, J., 672. The kinetics of the oxidation of organic compounds by ceric sulphate. Part II. The reactivities of aliphatic ketones and acetaldehyde. *J. Chem. Soc. (Resumed)* **1950**, (0), 3425-3431.
123. Trahanovsky, W. S.; Young, L. B., Controlled Oxidations of Organic Compounds with Cerium(IV). The oxidation of benzyl alcohols to benzaldehydes. *J. Chem. Soc. (Resumed)* **1965**, (0), 5777-5778.
124. Young, L. B.; Trahanovsky, W. S., Cerium(IV) oxidation of Organic Compounds. III. Preparation of cyclopropanecarbaldehyde from cyclopropanemethanol. *J. Am. Chem. Soc.* **1966**, 2349-2350.
125. Ho, T.-L., Ceric Ion Oxidation in Organic Chemistry. *Synthesis* **1973**, *1973* (06), 347-354.
126. Kurz, M. E.; Steele, E. M.; Vecchio, R. L., Ceric ammonium nitrate promoted aromatic substitution with peroxydicarbonates. *J. Org. Chem.* **1974**, *39* (23), 3331-3336.
127. Jacob, P.; Callery, P. S.; Shulgin, A. T.; Castagnoli Jnr, N., A convenient synthesis of quinones from hydroquinone dimethyl ethers. Oxidative demethylation with Ceric Ammonium Nitrate. *J. Org. Chem.* **1976**, *41* (22), 3627-3628.
128. Johnson, M. M. The Development of Novel Synthetic Methodology for the synthesis of Oxygenated Heterocycles. MSc Dissertation. University of the Witwatersrand, **2014**.
129. Butler, R. N.; Hanniffy, J. M.; Stephens, J. C.; Burke, L. A., A Ceric Ammonium Nitrate N-Dearylation of N-p-Anisylazoles Applied to Pyrazole, Triazole, Tetrazole, and Pentazole Rings: Release of Parent Azoles. Generation of Unstable Pentazole, HN₅/N₅⁻, in Solution. *J. Org. Chem.* **2008**, *73* (4), 1354-1364.

130. Doyle, M. P.; Zuidema, L. J.; Bade, T. R., Cyclic ether formation in oxidations of primary alcohols by cerium(IV). Reactions of 5-phenyl-1-pentanol, 4-phenyl-1-butanol, and 3-phenyl-1-propanol with ceric ammonium nitrate. *J. Org. Chem.* **1975**, *40* (10), 1454-1456.
131. Baciocchi, E.; Ruzziconi, R., 1,2- And 1,4-addition in the reactions of carbonyl compounds with 1,3-butadiene induced by cerium(IV) ammonium nitrate. *J. Org. Chem.* **1986**, *51* (10), 1645-1649.
132. Bekkaye, M.; Masson, G., Cerium(IV) Ammonium Nitrate Mediated Three-Component α -Allylation of Imine Surrogates. *Org. Lett.* **2014**, *16* (5), 1510-1513.
133. Citterio, A.; Sebastiano, R.; Caceres Carvayal, M., Oxidation of diethyl (pyridylmethyl)malonates with manganese(III) acetate, cerium(IV) ammonium nitrate, and iron(III) perchlorate in the presence of alkenes and alkynes. *J. Org. Chem.* **1991**, *56* (18), 5335-5341.
134. Mehdi, H.; Bodor, A.; Lantos, D.; Horváth, I. T.; De Vos, D. E.; Binnemans, K., Imidazolium Ionic Liquids as Solvents for Cerium(IV)-Mediated Oxidation Reactions. *J. Org. Chem.* **2007**, *72* (2), 517-524.
135. Olah, G. A.; Balam Gupta, B. G., Synthetic Methods and Reactions; 751. Facile Conversion of Nitro Compounds and Silyl Nitronates into Carbonyl Compounds by Ceric Ammonium Nitrate. *Synthesis* **1980**, *1980* (01), 44-45.
136. Evans, D. A.; Nagorny, P.; Xu, R., Ceric Ammonium Nitrate Promoted Oxidation of Oxazoles. *Org. Lett.* **2006**, *8* (24), 5669-5671.
137. Dincturk, S.; Ridd, J. H., Reactions of cerium(IV) ammonium nitrate with aromatic compounds in acetonitrile. Part 2. Nitration; comparison with reactions of nitric acid. *J. Chem. Soc., Perkin Trans. 2* **1982**, (8), 965-969.
138. Chawla, H. M.; Mittal, R. S., Oxidative Nitration by Silica Gel-Supported Cerium(IV) Ammonium Nitrate. *Synthesis* **1985**, *1985* (01), 70-72.
139. Hwu, J. R.; Chen, K.-L.; Ananthan, S., A new method for nitration of alkenes to [small alpha],[small beta]-unsaturated nitroalkenes. *J. Chem. Soc., Chem. Commun.* **1994**, (12), 1425-1426.
140. Hwu, J. R.; Chen, K.-L.; Ananthan, S.; Patel, H. V., Ultrasonic Nitration of Allylsilanes by Use of Sodium Nitrite and Ceric Ammonium Nitrate. *Organometallics* **1996**, *15* (2), 499-505.
141. Deleersnyder, K.; Schaltin, S.; Fransaer, J.; Binnemans, K.; Parac-Vogt, T. N., Ceric ammonium nitrate (CAN) as oxidizing or nitrating reagent for organic reactions in ionic liquids. *Tetrahedron Lett.* **2009**, *50* (32), 4582-4586.
142. Maulide, N.; Vanherck, J.-C.; Gautier, A.; Markó, I. E., Mild and Neutral Deprotections Catalyzed by Cerium(IV) Ammonium Nitrate. *Acc. Chem. Res.* **2007**, *40* (6), 381-392.
143. Jih Ru, H.; Jain, M. L.; Tsay, S.-C.; Hakimelahi, G. H., New detritylation method for nucleosides and nucleotides by ceric ammonium nitrate. *Chem. Commun.* **1996**, (4), 545-546.
144. Jih Ru, H.; Jain, M. L.; Shwu-Chen, T.; Hakimelahi, G. H., Ceric ammonium nitrate in the deprotection of *tert*-butoxycarbonyl group. *Tetrahedron Lett.* **1996**, *37* (12), 2035-2038.
145. Markó, I. E.; Ates, A.; Gautier, A.; Leroy, B.; Plancher, J.-M.; Quesnel, Y.; Vanherck, J.-C., Cerium(IV)-Catalyzed Deprotection of Acetals and Ketals under Mildly Basic Conditions. *Angew. Chem. Int. Ed.* **1999**, *38* (21), 3207-3209.
146. Markó, I. E.; Ates, A.; Augustyns, B.; Gautier, A.; Quesnel, Y.; Turet, L.; Wiaux, M., Remarkable deprotection of THP and THF ethers catalysed by cerium ammonium nitrate (CAN) under neutral conditions. *Tetrahedron Lett.* **1999**, *40* (30), 5613-5616.
147. Ates, A.; Gautier, A.; Leroy, B.; Plancher, J.-M.; Quesnel, Y.; Vanherck, J.-C.; Markó, I. E., Mild and chemoselective catalytic deprotection of ketals and acetals using cerium(IV) ammonium nitrate. *Tetrahedron* **2003**, *59* (45), 8989-8999.
148. Cotellet, P.; Catteau, J.-P., Deprotection of benzaldehyde diacetates by ceric ammonium nitrate coated on silica. *Tetrahedron Lett.* **1992**, *33* (27), 3855-3858.
149. Yoshimura, J.; Yamaura, M.; Suzuki, T.; Hashimoto, H., Oxidative removal of *N*-(*p*-methoxybenzyl) group on diketopiperazine skeleton with ceric ammonium nitrate. *Chem. Soc. Jpn.* **1983**, 1001-1002.

150. Yamaura, M.; Suzuki, T.; Hashimoto, H.; Yoshimura, J.; Okamoto, T.; Shin, C.-g., Oxidative Removal of *N*-(4-Methoxybenzyl) Group on 2,5-Piperazinediones with Cerium(IV) Diammonium Nitrate. *Bull. Chem. Soc. Jpn.* **1985**, *58* (5), 1413-1420.
151. Bull, S. D.; Davies, S. G.; Fenton, G.; Mulvaney, A. W.; Prasad, R. S.; Smith, A. D., Chemoselective debenzoylation of *N*-benzyl tertiary amines with ceric ammonium nitrate. *J. Chem. Soc., Perkin Trans. 1* **2000**, (22), 3765-3774.
152. Davies, S. G.; Ichihara, O., Selective deprotection strategies to *N*-(α -methylbenzyl)- β -amino esters and derived β -lactams. *Tetrahedron Lett.* **1998**, *39* (33), 6045-6048.
153. Wright, J. A.; Yu, J.; Spencer, J. B., Sequential removal of the benzyl-type protecting groups PMB and NAP by oxidative cleavage using CAN and DDQ. *Tetrahedron Lett.* **2001**, *42* (24), 4033-4036.
154. Williams, B. D.; Smith, A. B., Total Synthesis of (+)-18-*epi*-Latrunculol A. *Organic Lett.* **2013**, *15* (17), 4584-4587.
155. Gu, W.; Silverman, R. B., Stereospecific Total Syntheses of Proteasome Inhibitors Omuralide and Lactacystin. *J. Org. Chem.* **2011**, *76* (20), 8287-8293.
156. Fujitani, M.; Tsuchiya, M.; Okano, K.; Takasu, K.; Ihara, M.; Tokuyama, H., Total Synthesis of (\pm)-Lepadiformine A via Radical Translocation-Cyclization Reaction. *Synlett* **2010**, *2010* (05), 822-826.
157. Fürstner, A.; Turet, L., Concise and Practical Synthesis of Latrunculin A by Ring-Closing Enyne-Yne Metathesis. *Angew. Chem. Int. Ed.* **2005**, *44* (22), 3462-3466.
158. Mandal, P. K.; Roy, S. C., Ceric ammonium nitrate as a convenient catalyst for chemoselective thioacetalisation. *Tetrahedron* **1995**, *51* (28), 7823-7828.
159. Pachamuthu, K.; Vankar, Y. D., Ceric Ammonium Nitrate-Catalyzed Tetrahydropyranylation of Alcohols and Synthesis of 2-Deoxy-O-Glycosides. *J. Org. Chem.* **2001**, *66* (22), 7511-7513.
160. Sridharan, V.; Ribelles, P.; Ramos, M. T.; Menéndez, J. C., Cerium(IV) Ammonium Nitrate Is an Excellent, General Catalyst for the Friedländer and Friedländer-Borsche Quinoline Syntheses: Very Efficient Access to the Antitumor Alkaloid Luotonin A. *J. Org. Chem.* **2009**, *74* (15), 5715-5718.
161. Clark, A. J.; Dell, C. P.; McDonagh, J. M.; Geden, J.; Mawdsley, P., Oxidative 5-Endo Cyclization of Enamides Mediated by Ceric Ammonium Nitrate. *Org. Lett.* **2003**, *5* (12), 2063-2066.
162. Tale, R. H., Novel Synthesis of 2-Arylbenzothiazoles Mediated by Ceric Ammonium Nitrate (CAN). *Org. Lett.* **2002**, *4* (10), 1641-1642.
163. Nair, V.; Augustine, A., Novel Synthesis of 2-Arylbenzothiazoles Mediated by Ceric Ammonium Nitrate (CAN): A Rebuttal. *Org. Lett.* **2003**, *5* (4), 543-544.
164. Ho, T.-L.; Wong, C. M., Ceric Ammonium Nitrate Oxidation of Diaryl Sulfides. *Synthesis* **1972**, *1972* (10), 561-562.
165. Hajipour, A. R.; Khazdooz, L.; Ruoho, A. E., Selective and Efficient Oxidation of Sulfides to Sulfoxides Using Ceric Ammonium Nitrate (CAN)/Brønsted Acidic Ionic Liquid. *Phosphorus Sulfur Silicon Rel. Elem.* **2009**, *184* (3), 705-711.
166. Nair, V.; Mathew, J., Facile synthesis of dihydrofurans by the cerium(IV) ammonium nitrate mediated oxidative addition of 1,3-dicarbonyl compounds to cyclic and acyclic alkenes. Relative superiority over the manganese(III) acetate mediated process. *J. Chem. Soc., Perkin Trans. 1* **1995**, (3), 187-188.
167. Sarac, A. S., Redox polymerization. *Prog. Polym. Sci.* **1999**, *24* (8), 1149-1204.
168. Seim, K. L.; Obermeyer, A. C.; Francis, M. B., Oxidative Modification of Native Protein Residues Using Cerium(IV) Ammonium Nitrate. *J. Am. Chem. Soc.* **2011**, *133* (42), 16970-16976.
169. Sridharan, V.; Menéndez, J. C., Cerium(IV) Ammonium Nitrate as a Catalyst in Organic Synthesis. *Chem. Rev.* **2010**, *110* (6), 3805-3849.
170. Nair, V.; Balagopal, L.; Rajan, R.; Mathew, J., Recent Advances in Synthetic Transformations Mediated by Cerium(IV) Ammonium Nitrate. *Acc. Chem. Res.* **2004**, *37* (1), 21-30.
171. Hwu, J. R.; King, K.-Y., Versatile reagent ceric ammonium nitrate in modern chemical synthesis. *Curr. Sci.* **2001**, *81* (8), 1043-1053.

172. Mino, G.; Kaizerman, S.; Rasmussen, E., The Oxidation of Pinacol by Ceric Sulfate. *J. Am. Chem. Soc.* **1959**, *81* (6), 1494-1496.
173. Subramanian, S. V.; Santappa, M., Vinyl polymerization initiated by ceric ion reducing agent systems in sulfuric acid medium. *J. Polym. Sci. Part A-1* **1968**, *6* (3), 493-504.
174. Chowdhury, P.; Samui, S.; Kundu, T.; Nandi, M. M., Graft polymerization of methyl methacrylate onto guar gum with ceric ammonium sulfate/dextrose redox pair. *J. Appl. Polym. Sci.* **2001**, *82* (14), 3520-3525.
175. Shan, Y.; Huang, S. D., $(\text{NH}_4)_8[\text{Ce}_2(\text{SO}_4)_8] \cdot 4\text{H}_2\text{O}$. *Acta Cryst. C* **1998**, *54* (12), 1744-1745.
176. Abrahams, B. F.; Coleiro, J.; Hoskins, B. F.; Robson, R., Gas hydrate-like pentagonal dodecahedral $\text{M}_2(\text{H}_2\text{O})_{18}$ cages (M = lanthanide or Y) in 2,5-dihydroxybenzoquinone-derived coordination polymers. *Chem. Commun.* **1996**, (5), 603-604.
177. Singh, D.; Singh, H. B., Metal complexes with Biologically Active Substituted Hydroxy Compounds. *Z. Naturforsch. B* **1977**, *32b*, 438-442.
178. Tozer, T. N.; Tuck, L. D., Substituent effects on oxidation and stabilization of phenothiazine semiquinone free radicals. *J. Pharm. Sci.* **1965**, *54* (8), 1169-1175.
179. Periasamy, M.; Bhatt, M. V., A Convenient Method for the Oxidation of Polycyclic Aromatic Hydrocarbons to Quinones. *Synthesis* **1977**, *1977* (05), 330-332.
180. Periasamy, M.; Bhatt, M. V., A new 1,2-shift in the oxidation of aromatic rings. *Tetrahedron Lett.* **1977**, *18* (27), 2357-2360.
181. Beletskaya, I. P.; Makhon'kov, D. I., Oxidation of Alkyl Derivatives of Aromatic Hydrocarbons by Transition Metal Salts. *Russ. Chem. Rev.* **1981**, *50* (6), 534.
182. Bhatt, M. V.; Periasamy, M., Rearrangements in the cerium(IV) and manganese(III) oxidations of substituted naphthalenes and the NIH shift mechanism. *Tetrahedron* **1994**, *50* (11), 3575-3586.
183. Skarzewski, J., Cerium catalyzed persulfate oxidation of polycyclic aromatic hydrocarbons to quinones. *Tetrahedron* **1984**, *40* (23), 4997-5000.
184. Balanikas, G.; Hussain, N.; Amin, S.; Hecht, S. S., A study of chemical carcinogenesis. 109. Oxidation of polynuclear aromatic hydrocarbons with ceric ammonium sulfate: preparation of quinones and lactones. *J. Org. Chem.* **1988**, *53* (5), 1007-1010.
185. Lawrence, S.; Christopher, C.; Bosco, A. J.; Easu raja, M.; Raja, S.; Xavier, N., Electro oxidation of substituted electron-donating benzylic alcohols in a biphasic medium. *J. Chem. Pharm. Res.* **2012**, *4* (2), 1296-1300.
186. de Koning, C. B.; Giles, R. G. F.; Engelhardt, L. M.; Whitet, A. H., Convenient syntheses of the naturally occurring benzo[*b*]xanthen-12-one bikaverin. X-Ray crystallographic confirmation of the product regiochemistry. *J. Chem. Soc., Perkin Trans. 1* **1988**, (12), 3209-3216.
187. Mondal, M.; Puranik, V. G.; Argade, N. P., Facile Synthesis of 1,3,7-Trihydroxyxanthone and Its Regioselective Coupling Reactions with Prenal: Simple and Efficient Access to Osajaxanthone and Nigrolineaxanthone F. *J. Org. Chem.* **2006**, *71* (13), 4992-4995.
188. Naidoo, J. M. Novel Methodology for the Synthesis of Xanthenes. MSc Dissertation, University of the Witwatersrand, Johannesburg, **2009**.
189. Franck, B.; Zeidler, U., Pilzinhaltsstoffe, 22. Oxidative Cyclisierung von Hydroxybenzophenonen. *Ber. Dtsch. Chem. Ges.* **1973**, *106* (4), 1182-1197.
190. Ellis, R. C.; Whalley, W. B.; Ball, K., The chemistry of fungi. Part LXX. Synthesis of some xanthenes. *J. Chem. Soc., Perkin Trans. 1* **1976**, (13), 1377-1382.
191. Johnson, M. M. Ceric Ammonium Nitrate Mediated Oxidations for the Synthesis of Xanthenes and Related Products. MSc Dissertation. University of the Witwatersrand, Johannesburg, **2011**.
192. Johnson, M. M.; Naidoo, J. M.; Fernandes, M. A.; Mmutlane, E. M.; van Otterlo, W. A. L.; de Koning, C. B., CAN-Mediated Oxidations for the Synthesis of Xanthenes and Related Products. *J. Org. Chem.* **2010**, *75* (24), 8701-8704.
193. Omolo, J. J. Bioassay-guided Isolation and Synthetic Studies on Natural Products obtained from Tanzanian Medicinal Plants. PhD Thesis. University of the Witwatersrand, Johannesburg, **2011**.

194. Omolo, J. J.; Johnson, M. M.; van Vuuren, S. F.; de Koning, C. B., The synthesis of xanthenes, xanthenediones, and spirobenzofurans: Their antibacterial and antifungal activity. *Bioorg. Med. Chem. Lett.* **2011**, *21* (23), 7085-7088.
195. Ahua, K. M.; Ioset, J.-R.; Ransijn, A.; Mauël, J.; Mavi, S.; Hostettmann, K., Antileishmanial and antifungal acridone derivatives from the roots of *Thamnosma rhodesica*. *Phytochemistry* **2004**, *65* (7), 963-968.
196. Van Duuren, B. L., Effects of the Environment on the Fluorescence of Aromatic Compounds in Solution. *Chem. Rev.* **1963**, *63* (4), 325-354.
197. Armarego, W. L. F.; Chai, C. L. L., Chapter 5 - Purification of Inorganic and Metal-Organic Chemicals: (Including Organic compounds of B, Bi, P, Se, Si, and ammonium and metal salts of organic acids). In *Purification of Laboratory Chemicals (Sixth Edition)*, Butterworth-Heinemann: Oxford, **2009**; pp 445-576.
198. Chawla, H. M.; Sharma, S. K.; Chakrabarty, K.; Bhanumati, S., Cerium(IV) induced hydroxylation of *c*-alkylated hydrocarbons and phenols. *Tetrahedron* **1988**, *44* (4), 1227-1234.
199. González-Morales, A.; Díaz-Coutiño, D.; Fernández-Zertuche, M.; García-Barradas, O.; Ordóñez, M., Preparation of dimethyl (*R*)- and (*S*)-2-(2-aminophenyl)-2-hydroxyethylphosphonate from anthranilic acid. *Tetrahedron: Asymmetry* **2004**, *15* (3), 457-463.
200. Frye, S. V.; Johnson, M. C.; Valvano, N. L., Synthesis of 2-aminobenzophenones via rapid halogen-lithium exchange in the presence of a 2-amino-*N*-methoxy-*N*-methylbenzamide. *J. Org. Chem.* **1991**, *56* (11), 3750-3752.
201. Mestrelab Research. *MestReNova*, 9; **2014**.
202. Bruker AXS Inc. *SAINT+*, Version 6.02 (Includes XPREP and SADABS); Madison, Wisconsin, USA, 2004.
203. Sheldrick, G. M., *Acta Cryst., Sect. A.* **2008**, *64*, 112-122.
204. Farrugia, L., WinGX suite for small-molecule single-crystal crystallography. *J. Appl. Cryst.* **1999**, *32* (4), 837-838.
205. Farrugia, L., ORTEP-3 for Windows - a version of ORTEP-III with a Graphical User Interface (GUI). *J. Appl. Cryst.* **1997**, *30* (5 Part 1), 565.
206. Varian; 3.00(182) ed.; Sax Software Corp.: Australia *Varian*, Australia, **2002**.
207. Rafiq, S. M.; Sivasakthikumar, R.; Mohanakrishnan, A. K., Lewis Acid/Brønsted Acid Mediated Benz-Annulation of Thiophenes and Electron-Rich Arenes. *Org. Lett.* **2014**, *16* (10), 2720-2723.
208. Gangjee, A.; Namjoshi, O. A.; Keller, S. N.; Smith, C. D., 2-Amino-4-methyl-5-phenylethyl substituted-7-*N*-benzyl-pyrrolo[2,3-*d*]pyrimidines as novel antitumor antimitotic agents that also reverse tumor resistance. *Bioorg. Med. Chem.* **2011**, *19* (14), 4355-4365.
209. Sharghi, H.; Tamaddon, F., BeCl₂ as a new highly selective reagent for dealkylation of aryl-methyl ethers. *Tetrahedron* **1996**, *52* (43), 13623-13640.
210. Jiang, N.; Li, S.-Y.; Xie, S.-S.; Yao, H.; Sun, H.; Wang, X.-B.; Kong, L.-Y., FeCl₃ and ether mediated direct intramolecular acylation of esters and their application in efficient preparation of xanthone and chromone derivatives. *RSC Advances* **2014**, *4* (109), 63632-63641.
211. Genovese, S.; Fiorito, S.; Specchiulli, M. C.; Taddeo, V. A.; Epifano, F., Microwave-assisted synthesis of xanthenes promoted by ytterbium triflate. *Tetrahedron Letters* **2015**, *56* (6), 847-850.
212. Xian-Feng, H.; Yulan, Z.; Hai-Liang, Z., Synthesis and Evaluation of *N*-Benzyl-Acridinone Derivatives Induced Apoptosis in Human Liver Cancer Cell-Lines. *Lett. Drug Des. Discov.* **2011**, *8* (7), 606-611.